TRANSITION METAL-MEDIATED DIASTEREOSELECTIVE SYNTHESIS OF METALLOPHOSPHINATES

ZHONGXIN ZHOU

Transition Metal-Mediated Diastereoselective Synthesis of Metallophosphinates

by

© Zhongxin Zhou

B.Sc. (Hons.), Central China Normal University, Wuhan, China, 1982

M.Sc., Hubei Research Institute of Chemistry, Wuhan, China, 1985

A thesis submitted to the School of Graduate Studies in partial fulfilment of the requirements for the degree of Doctor of Philosophy

Department of Chemistry

Memorial University of Newfoundland

August 1994

St. John's Newfoundland

Abstract

Transition metal-mediated diastereoselective synthesis is one of the most important and extensively used methods to create chirality at carbon and other heteroatom centres. This thesis focuses on chiral induction from an asymmetric, pseudo-octahedral metal centre in the Arbuzov-like dealkylation of prochiral phosphonites. A series of η^5-cyclopentadienyl, η^5-pentamethylcyclopentadienyl, and η^5-indenyl three-legged piano-stool complexes have been studied as chiral auxiliaries. The effects of ligand sphere steric and electronic properties on $M^* \rightarrow P$ optical induction have been examined.

The synthesis, structure, spectroscopic properties of a series of chiral η^5-indenyl cobalt complexes are described. X-ray crystal structure and solution conformational analysis showed that all η^5-indenyl complexes have a propensity to distort away from η^5 toward η^3 coordination, and that the indenyl ring always has certain conformational preferences with respect to the ligands on the metal. Distortion and conformational preferences of indenyl complexes are fully discussed on the basis of extended Hückel molecular orbital (EHMO) calculations, and fragment molecular orbital (FMO) analysis.

Arbuzov reactions of η^5-indenyl, η^5-cyclopentadienyl, and η^5-pentamethylcyclopentadienyl cobalt iodide auxiliaries with $PR'(OMe)_2$ (R' = OMe, Ph) proceed via an ionic mechanism to form the corresponding cobaltophosphonates or phosphinates. Ionic intermediates were observed by ^1H NMR spectroscopy at ambient temperature in

most cases and isolated in some cases.

The following conclusions can be drawn from the results presented in this thesis: (i) The chiral metal center is essential for stereoselectivity. (ii) The steric requirements of the spectator ligands is crucial in determining chiral induction. The bulkier the spectator ligands, the higher the chiral induction. (iii) The stereochemical properties of the entering phosphonites, $PR'(OMe)_2$ is also important for diastereoselectivity. Large substituent R' result in high diastereoselectivity. (iv) Intramolecular hydrogen bonding plays a significant role in controlling the stereoselectivity in the Arbuzov reaction by restricting population of solution conformations, maximizing the preference of one diastereomer over another.

Acknowledgements

I am greatly indebted to my supervisor, Professor Chet R. Jablonski, for his outstanding supervision, continuous encouragement, great help, and financial support throughout the course of this research. His assistance and patience in the preparation of this thesis are also gratefully acknowledged.

Special acknowledgement is extended to Dr. John N. Bridson for collection of X-ray crystallographic data and structural refinement, and to Ms. Nathalie Brunet for NMR spectroscopic measurements. I am grateful to Dr. Carlo Mealli (Italy) for providing the CACAO program package for EHMO calculations and orbital drawing.

I greatly appreciate Dr. D. J. Burnell and Dr. C. R. Lucas for their patience in reading through this thesis, and helpful comments and suggestions in shaping this thesis. Many thanks are also extended to the staff and faculty as well as my fellow students in the Chemistry Department for making the years in MUN enjoyable. I would like to thank Memorial University for award of a graduate fellowship.

Finally, I greatly appreciate my lovely wife, Chunxia Fan, for her understanding, patience, encouragement, support and love.

To My Wife, Chunxia Fan

and Our Parents

Table of Contents

List of Tables

List of Figures

List of Abbreviations

BDPP	2,3-bis(diphenylphosphino)-pentane
BINAP	2,2'-bis(diphenylphosphino)-1,1'-binaphthyl
BMPP	benzylmethylphenylphosphine (P*CH_2Ph(Me)Ph)
BPPFA	*N,N'*-dimethyl-1-[1',2-bis(diphenylphosphino)ferrocenyl]ethylamine
BPPM	*N*-*t*-butoxycarbonyl-4-diphenylphosphino-2-diphenylphosphinomethyl-pyrrolidine
CD	circular dichroism
CHIRAPHOS	2,3-bis(diphenylphosphino)-butane
CIP	Cahn-Ingold-Prelog
COD	1,5-cyclooctadiene
Cp	η^5-cyclopentadienyl
Cp*	η^5-pentamethylcyclopentadienyl
CYCPHOS	1,2-bis(diphenylphosphino)-1-cyclohexylethane
de	diastereomeric excess
DIOP	4,5-bis(diphenylphosphinomethyl)-2,2-dimethyl-1,3-dioxolane
DIPAMP	1,2-bis[(*o*-methoxyphenyl)phenylphosphino]-ethane
DPCP	1,2-bis(diphenylphosphino)-cyclopentane
EAC	ethyl-2-acetamidocinnamate
ee	enantiomeric excess
EHMO	extended Hückel molecular orbital

h	hour
HETCOR	^{1}H-^{13}C ^{1}J heterocorrelation
HOMO	highest occupied molecular orbital
FAB	fast atomic bombardment
FMO	fragment molecular orbital
IR	infrared
L-Dopa	(*S*)-3,4-dihydroxyphenylalanine
LUMO	lowest unoccupied molecular orbital
MBHOX	2,2'-(dimethyl)methylenebis(dihydrooxazoles)
MCPBA	*m*-chloroperoxybenzoic acid
Me/Et-DuPHOS	1,2-bis[(1,5-dimethyl/ethyl)-phospholano]-benzene
MO	molecular orbital
MOP	2-(diphenylphosphino)-2'-alkoxy-1,1'-binaphthyl
mp	melting point
Naproxen	(*S*)-2-(6-methoxy-2-naphthyl)propionic acid
NHOMO	next highest occupied molecular orbital
NM	neomenthyl
NMR	nuclear magnetic resonance
N-N*	(*S*)-Ph(Me)C*H-N=CH-$C_4H_3N^-$ ($C_4H_3N^-$ = pyrrolyl)
N-O	R-C(O)-$C_4H_3N^-$ ($C_4H_3N^-$ = pyrrolyl)
nOe	nuclear Overhauser effect
nOed	nuclear Overhauser effect difference

NORPHOS	2,3-bis(diphenylphosphino)bicyclo[2.2.1]hept-5-ene
Np^{α}	α-naphthyl
PEtNH	$PEt_2NHC^*H(Me)Ph$ ((*S*)-diethyl-((1-phenylethyl)amino)phosphine)
PNH	$PPh_2NHC^*H(Me)Ph$ ((*S*)-diphenyl-((1-phenylethyl)amino)-phosphine)
PNNP	*N,N'*-bis(diphenylphosphino)-N,N'-bis[(2-phenyl)ethyl]-ethylenediamine
PPEI	pyridine-2-carbaldehyde-(1-phenyl)ethylimine (Schiff base)
ProNOP	*N*-diphenylphosphino-1-diphenylphosphinooxymethyl-pyrrolidine
Pybox	2,6-bis(oxazolinyl)pyridine
PYRPHOS	3,4-bis(diphenylphosphino)-pyrrolidine
Pythia	pyridine-2-thiazolidines
rect	rectangular
s	second
THF	tetrahydrofuran
TFA	trifluoroacetic acid
TLC	thin layer chromatography

Chapter 1

Transition Metal-Mediated Asymmetric Synthesis And The Arbuzov Reaction

1.1. Introduction

The biological world, including its human component, can be regarded as a chiral world from both the macroscopic and microscopic points of view. The need for chiral specificity in bio-active products reflects the fact that most enzymes have an inherent chirality, which expresses different responses toward two enantiomers. Thus, the desired biological activity is usually associated with only one of the two stereoisomers of a chiral compound. In the extreme case, exemplified by the tragic case of the well-known drug, thalidomide, shown in Scheme 1-1, one optical isomer (*R*) is a very effective sedative and hypnotic, however the other (*S*) has serious undesired biological consequences.[1,2] More examples[3, 4] with different biological activity within enantiomeric pairs illustrated in Scheme 1-2, emphasize the importance

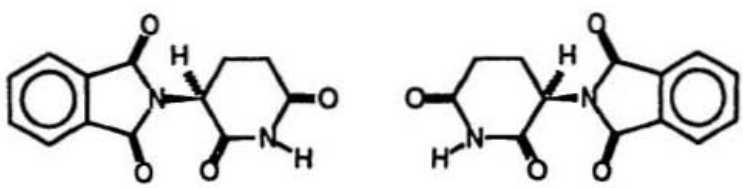

S– thalidomide
Teratogenic

R– thalidomide
Sedative, hypnotic

Scheme 1-1

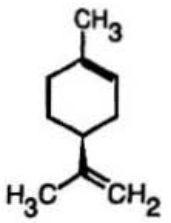

R– limonene
lemon taste

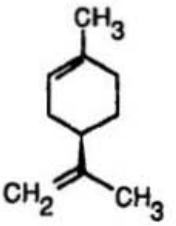

S– limonene
orange taste

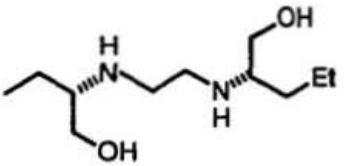

S,S — ethambutol
Tuberculostatic

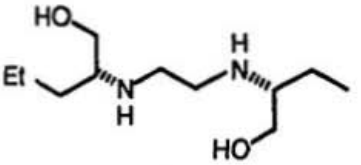

R,R— ethambutol
Blindness

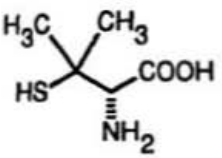

S– Penicillamine
Antiarthritic

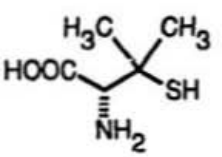

R– Penicillamine
Toxic

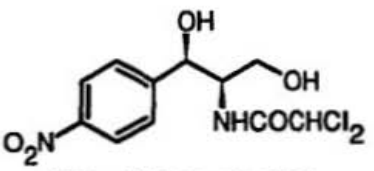

R,R— Chloramphenicol
Antibacterial

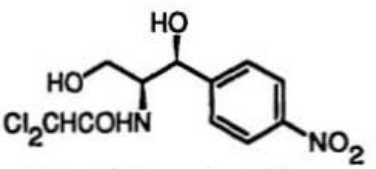

S,S – Chloramphenicol
Inactive

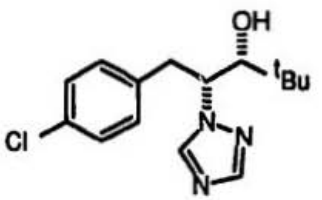

2R,3R— Paclobutrazol
Fungicide

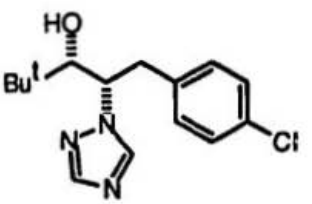

2S,3S— Paclobutrazol
Plant growth regulator

Scheme 1-2. Differences in Biological Activity

and necessity of searching for highly efficient and reliable methods to produce the desired enantiomerically pure compounds. Recent regulations of the Food and Drug Administration (FDA) in the United States clearly reflect the significance of isomerically pure chiral drugs: pharmaceutical industries will have to provide rigorous justification to obtain the FDA's approval of racemates.

There are several ways to obtain enantiomerically pure materials.[4] These are, synthesis from a chiral compound,[1,4-6] resolution by diastereomeric crystallization,[4] chromatographic separation,[4,7] chemical kinetic resolution,[4,8] and finally asymmetric chemical synthesis.[1,9-12] Although large amounts of relatively inexpensive, optically active natural products are available from the chiral pool, these still do not meet the ever-growing requirements of the pharmaceutical, agricultural, and chemical reagent industries. Many new chiral sources wait to be exploited. Substances from the chiral pool are often used as building blocks to afford the desired biological active products,[1] although some are directly used as medicinal drugs, food additives, and agricultural chemicals.

The technique of resolving enantiomeric pairs of molecules by conversion to diastereomers has been used for well over a century, since Louis Pasteur mechanically separated crystals of each optical isomer of sodium ammonium tartrate in 1848.[13] This method obviously is not suitable as a general resolution technique; however the idea of forming tartrate salts of a racemate and selectively crystallizing

one desired enantiomer is still used today as a method of resolution. Consequently, this dictates that the compound to be separated contain either an acid or amine functional group. One must then find a suitable compound containing an amine or acid fragment to act as a resolving agent that will produce different solubility in the resulting diastereomeric salts in order to effect efficient separation. Other methods of resolution involve the formation of a covalent bond between the racemic substrate and a chirally pure molecule. The resulting pair of diastereomers, in many instances, can be separated by chromatographic techniques, and the desired enantiomer regenerated from the appropriate diastereomer by chemical manipulation. This again requires that the substrate possess some functional groups to react with the resolving agent. In some cases, the reaction rate of the resolving reagent with one enantiomer may be very different from that with the other. These racemates may be kinetically resolved.

Each of the resolution methods described above suffers from the major disadvantage that half of the mixture is the wrong enantiomer. A quantitative separation in the resolution step at best recovers only half of the synthesized material. The remaining undesired enantiomer is usually discarded, which might cause both serious environmental problems and high costs. The situation would become much worse if more than two chiral centers exist in the molecule.

These difficulties can be avoided by using asymmetric synthesis, which has been

fully acknowledged by chemists in synthetic organic chemistry, medicinal chemistry, agricultural chemistry, natural product chemistry, the pharmaceutical industries, and the agricultural industries.

Strategically, there are mainly two basic approaches for asymmetric synthesis. First is incorporation of a chiral fragment of known absolute configuration into the target molecule. In this case, a compound from the natural chiral pool, such as an amino acid,[1, 4] has served as the major source. Second is the creation of a new chiral centre using an external chiral auxiliary either stoichiometrically or catalytically. This approach has attracted a great deal of attention in the last decade.[10-12, 14-20] Transition metal chiral auxiliaries are among the most intensively used chiral-induction reagents to afford enantiomerically pure or enriched compounds.[10-12, 14, 15]

1.2. Transition Metal-Mediated Asymmetric Synthesis

In principle, transition metal-mediated asymmetric synthesis can be grouped into the following two categories, as shown in Scheme 1-3. The first involves a chiral source in the ligand sphere by binding a chiral ligand to the metal. In this case the chiral center is "distal" to the prochiral target. The second category involves a chiral center on the metal atom itself. In this case the chiral center is "proximal" to the prochiral target and would have greater potential for stereocontrol than that in the first

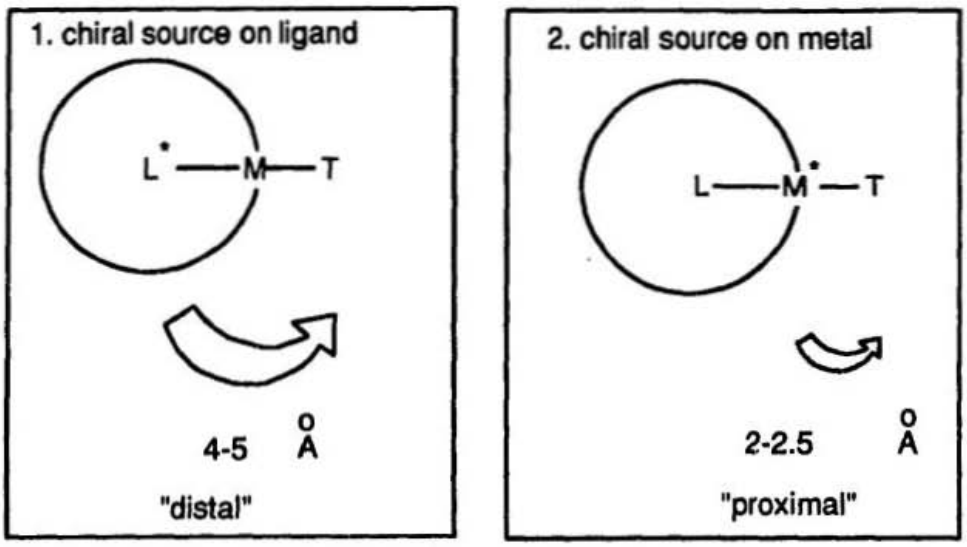

Scheme 1-3

category. Both methods have been used in organic synthesis to create chirality at carbon and heteroatoms. Commercial processes have been developed in pharmaceutical, food additive, and agrochemical industries.[9, 21, 22]

1.2.1. Catalytic Asymmetric Synthesis with Chiral Ligand Auxiliaries. Of the types of asymmetric reactions, the most desirable and successful applications of transition metal complexes in catalytic asymmetric synthesis incorporate phosphine-, nitrogen-, or oxygen-containing chiral ligands for hydrogenation,[23-35] hydrosilylation,[23, 25, 36-38] hydroformylation,[23, 25, 37, 39, 40] epoxidation,[41-47] cyclopropanation,[30, 48, 49] and coupling reactions.[14, 50, 51] These cases have been thoroughly reviewed, and a few examples are presented here to highlight the achievements in these fields.

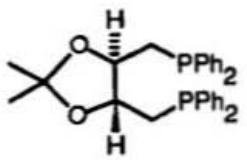

(H,R)- DIOP

1-1

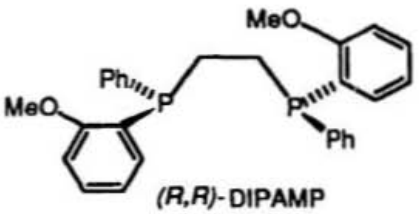

(R,R)- DIPAMP

1-2

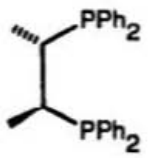

(S,S)- CHIRAPHOS

1-3

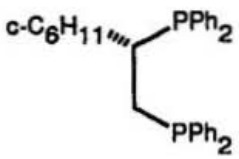

(S)- CYCPHOS

1-4

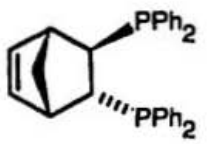

(R,R)- NORPHOS

1-5

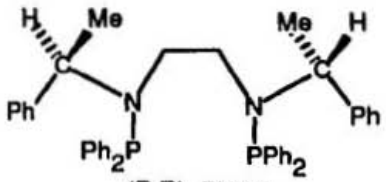

(R,R)- PNNP

1-6

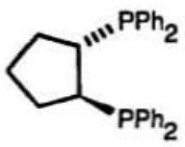

(S,S)- DPCP

1-7

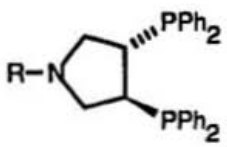

(S,S)- PYRPHOS

1-8

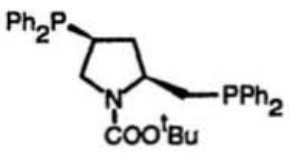

(S,S)- BPPM

1-9

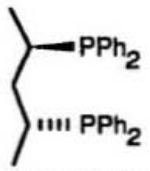

(R,R)- BDPP

1-10

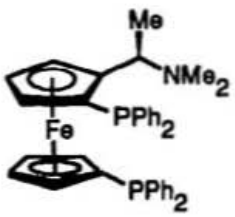

(R,S)- BPPFA

1-11

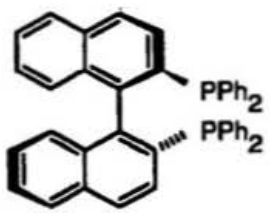

(R)- BINAP

1-12

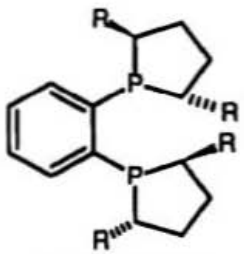

Me/Et-DuPHOS

1-13a/1-13b

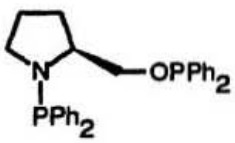

ProNOP

1-14

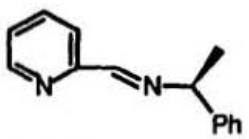

(S)- PPEI

1-15

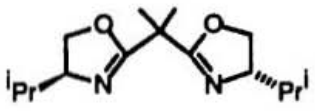

(S,S)- MBHOX

1-16

Scheme 1-4. Selected Chiral Ligands

1.2.1.1. Hydrogenation, Hydrosilylation and Hydroformylation. Since Horner[52] and Knowles[53] independently reported Rh(I) complexes bearing chiral tertiary phosphines for homogeneous asymmetric hydrogenation in 1968, a number of optically pure chelating chiral diphosphines and dinitrogen ligands, which have been shown[14, 54] to have greater optical induction than the monodentate ligands, have been synthesized.[25, 55-60] Some typical examples are illustrated in Scheme 1-4. The rhodium, ruthenium, iridium, and other transition metal complexes of these ligands have been employed as catalysts for asymmetric hydrogenation of C=C, C=O, and C=N bonds to give the corresponding chiral alkyl, alcohol, and amine compounds with up to 90-100 %ee. Some recent examples of catalytic asymmetric hydrogenation of olefins are shown in Scheme 1-5.[29, 33] Analysis of the results reported in the literature shows that:

(1) Chelating chiral phosphine-Rh (generally formed *in situ*), and -Ru complexes are the most successful giving high percent ee. The best chiral phosphine ligands are those containing aromatic rings on the coordinating phosphorus atoms.

(2) Substrate plays an important role in determining the stereoselectivity.[14, 29, 33, 34] In general, olefins that produce the highest enantioselectivity upon hydrogenation are those capable of a secondary interaction with the metal center in addition to the primary coordination of the olefinic double bond. Thus, the substrates are limited to *N*-acylaminoacrylic acid derivatives, carboxylic acids, enamides, enol derivatives, allylic alcohols, and α,β-unsaturated esters, amides and ketones as shown in

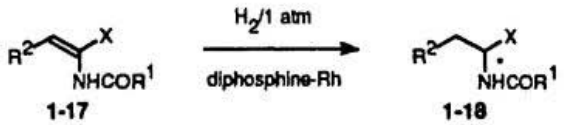

Substrate			% ee with diphosphine-Rh				
R^1	R^2	X	(R,R)- DIOP	(R,R)-DIPAMP	(S,S)- NORPHOS	(S,S)- BPPM	(S,R)- BPPFA
Me	H	COOH	*73(R)*	*90(S)*	*95(R)*	*99(R)*	*76(S)*
Me	Ph	COOH	*85(R)*	*96(S)*	*95(R)*	*91(R)*	*93(R)*
Me	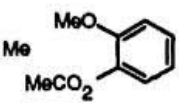	COOH	*84(R)*	*94(S)*	*94(R)*	*86(R)*	*86(S)*
Me	Ph	COOMe		*95(S)*			
Me	Ph	$CONH_2$		*94(S)*			
Me	Ph	COPh		*85(S)*			
Me	Ph	CN		*89(S)*			
Me	Me	Ph	*92(S) ((S,S)- DIOP)*				
^{i}-Pr	Me	Ph	*90(S) ((S,S)- DIOP)*				
Me		Ph	*90(S) ((S,S)- DIOP)*				

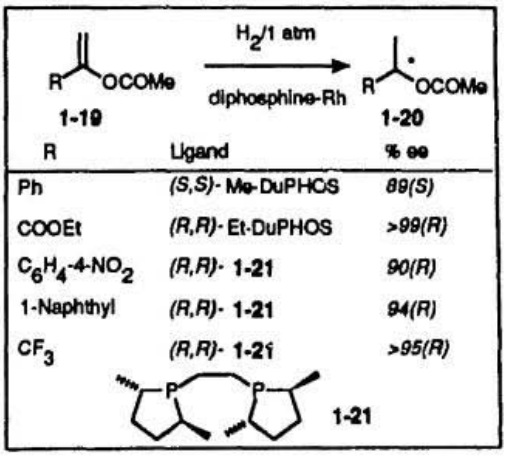

R	Ligand	% ee
Ph	(S,S)- Me-DuPHOS	*89(S)*
COOEt	(R,R)- Et-DuPHOS	*>99(R)*
C_6H_4-4-NO_2	(R,R)- **1-21**	*90(R)*
1-Naphthyl	(R,R)- **1-21**	*94(R)*
CF_3	(R,R)- **1-21**	*>95(R)*

1-21

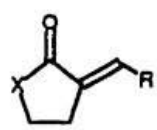

X = O	R = H	*95% ee*
X = O	R = Et	*95% ee*
X = CH_2	R = n-Bu	*98% ee*

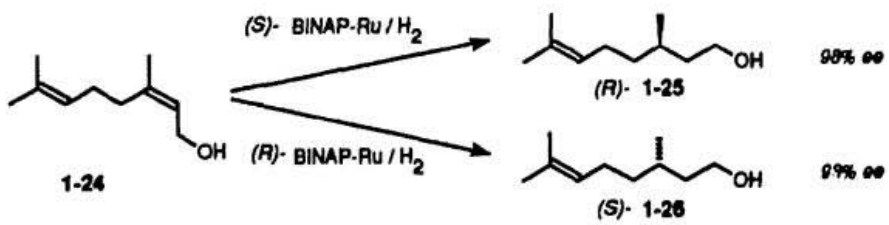

Scheme 1-5. Enantioselective Hydrogenations of C=C

Scheme 1-6A. All of these olefins contain an oxygen function that can coordinate

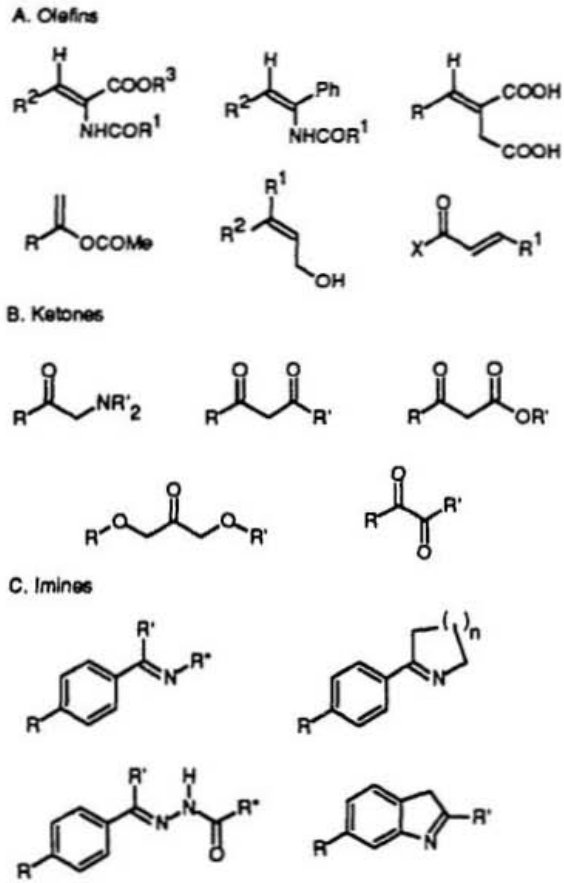

Scheme 1-6. Most Successful Substrates for Asymmetric Hydrogenation

with the metal center (cf. Scheme 1-7)[26] and help orient the chiral induction. Olefins incapable of this secondary interaction show lower asymmetric induction. Therefore, asymmetric hydrogenation of simple olefins with high enantiomeric excess has not been attained using chiral Rh and Ru catalysts.[29] However, chiral cyclopentadienyl complexes of titanium and lanthanide elements have opened a way for high enantioselective hydrogenation of simple olefins as shown in Scheme 1-8.[29, 61]

(3) The enantioselectivity is highly dependent on the reaction conditions, particularly

the hydrogen pressure.

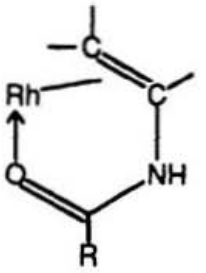

Scheme 1-7

(4) Halpern's detailed mechanism studies,[26] based on the x-ray crystal structure of a key intermediate and systematic kinetic measurements, showed that the enantioselectivity in asymmetric hydrogenation is related to the conformational rigidity of the diastereomeric intermediate and the dissymmetric arrangement of phenyl rings on phosphorus atoms. In the asymmetric hydrogenation of ethyl 2-acetamidocinnamate (EAC), the minor diastereomeric catalyst-substrate adduct is more reactive (at least 10^3 times) toward H_2 than the major one and thus gives the predominant product (**(*R*)-1-29**) as shown in Scheme 1-9.[26, 29]

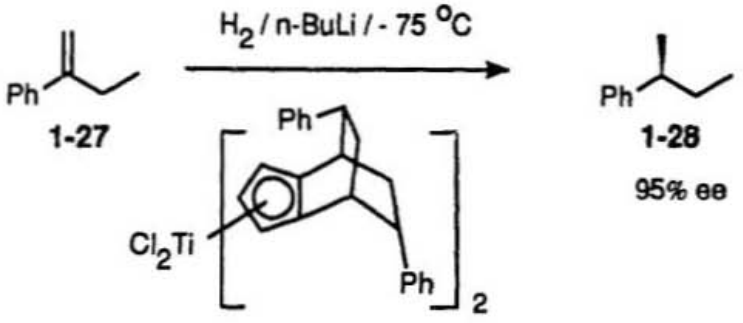

Scheme 1-8

(5) It was interesting that the Rh and Ru catalysts have opposite chiral orientations toward the same substrate. This provides an excellent choice for us to achieve the desired enantiomers. The case of chiral phosphine-Rh as catalyst is opposite to the result with chiral phosphine-Ru as catalyst. High ee's are obtained for (*Z*)-α-acylaminoacrylic acids and esters, but the asymmetric hydrogenation of the

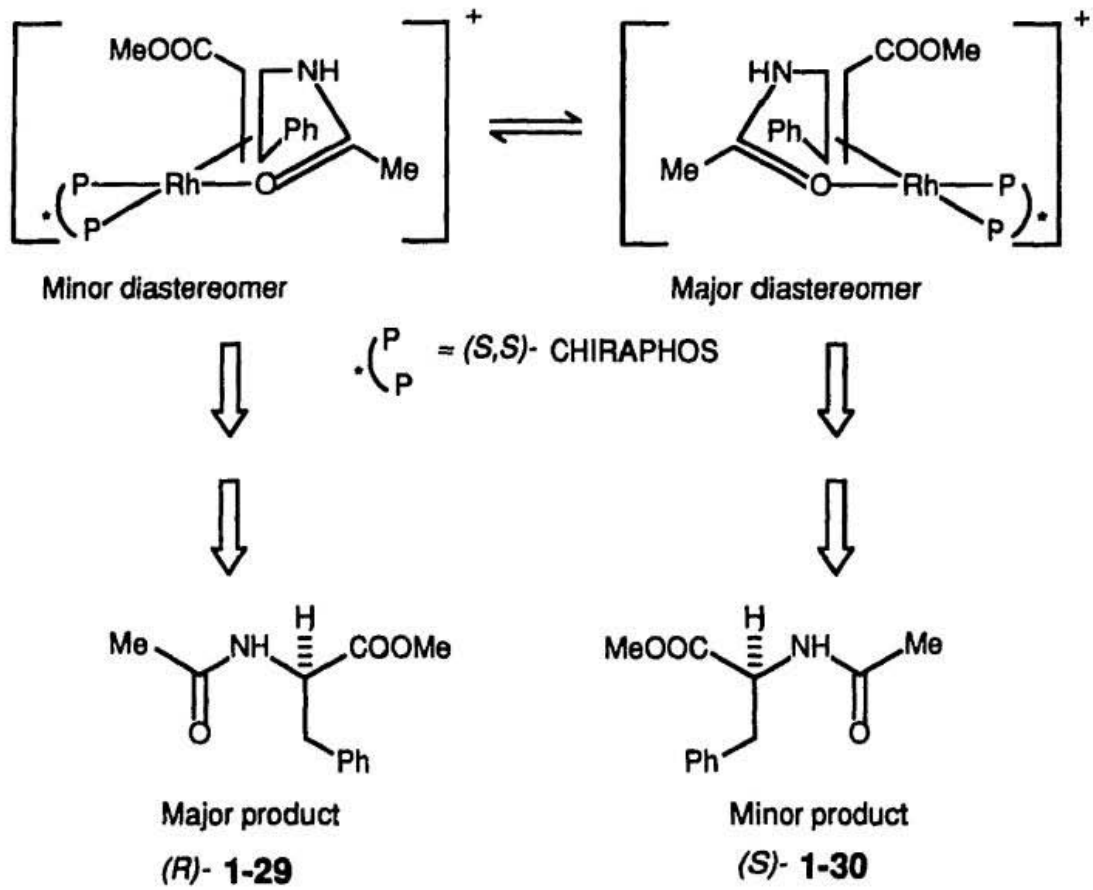

Scheme 1-9

corresponding (*E*)-isomers usually proceeds very slowly and with poor enantioselectivity.[29, 33] For example (cf. Scheme 1-10), compound **1-31** was hydrogenated to (*S*)-**1-32** with 92-100% ee by using Rh complexes bearing (*R*)-BINAP, while the (*R*)-BINAP-Ru complexes catalyze the same reaction to give the opposite enantiomer (*R*)-**1-33**. (*E*)-β-N-Acylaminoacrylic acid derivatives were hydrogenated with BINAP-Ru(II) complexes to give the products with up to 96% ee.[62] The (*Z*)-isomers are more reactive, but enantioselectivities are poor. BINAP-Rh(I)

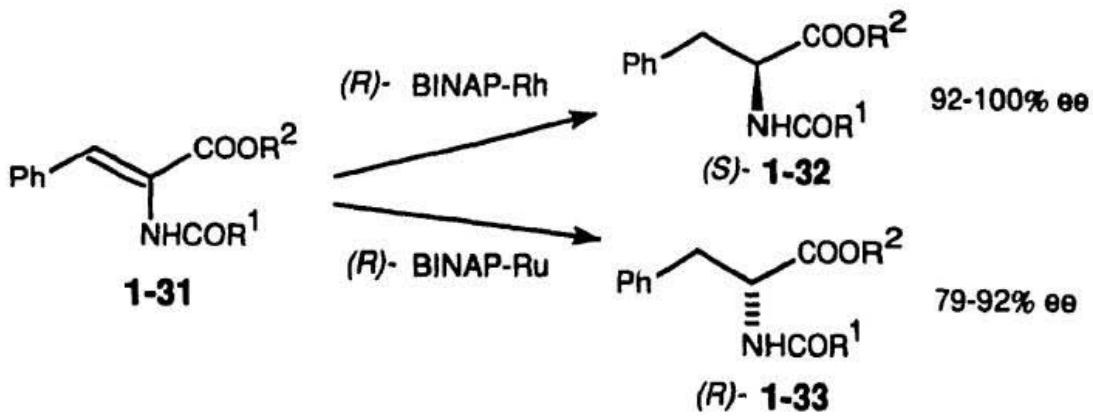

Scheme 1-10

complexes again have opposite enantiofacial selection toward these derivatives.

Similarly, a great number of functionalized ketones (*cf.* Scheme 1-6B) have been hydrogenated to the corresponding optically active secondary alcohols (cf. Scheme 1-11) catalyzed by chiral diphosphine-Rh and Ru complexes with enantioselectivity up to 100% ee.[29] It has also been shown that high enantioselectivity for the hydrogenation of simple ketones is difficult to achieve with conventional chiral diphosphine complexes as observed in the hydrogenation of simple olefins. Although systematic mechanistic studies for the hydrogenation of ketones are absent, it seems reasonable to assume that similar secondary interactions between functional groups on the ketones and the metal center, in addition to the primary interaction with the carbonyl lone pair, produces

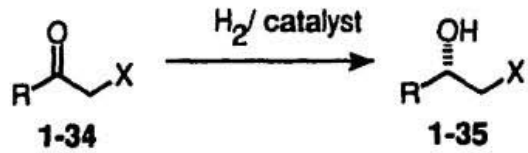

Scheme 1-11

chelating rigidity like that in the catalytic hydrogenation of olefins and leads to high enantioselectivity.

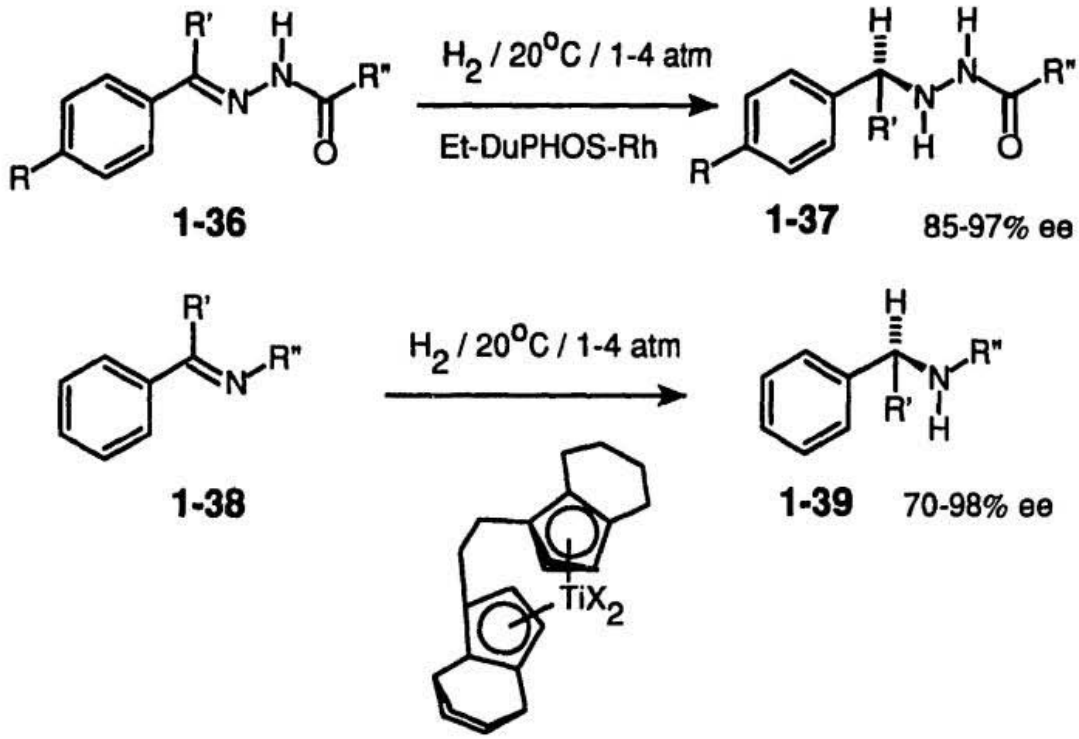

Scheme 1-12

Although the resulting optically active amines are synthetically important, a relatively small number of examples have been reported for the enantioselective hydrogenation of imines (cf. Scheme 1-6C), Hydrogenation of a C=N double bond often leads to low enantioselectivities. However, Burk[60] and Buchwald[63] recently showed that (*R,R*-Et-DuPHOS)-Rh and chiral titanocene are highly enantioselective catalysts for hydrogenation of conjugated imines to form chiral amines with up to 98% ee under

the mild conditions shown in Scheme 1-12.[59]

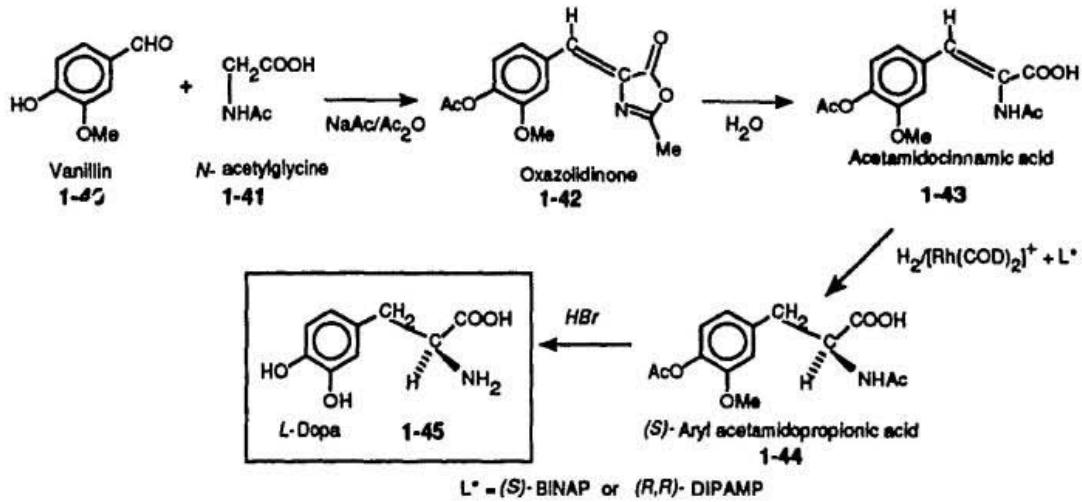

Scheme 1-13

The asymmetric hydrogenation of olefins has been successfully applied to the production of *L*-Dopa, *L*-phenylalanine, and Naproxen in the pharmaceutical and food additive industries. *L*-Dopa (cf. Scheme 1-13), a natural neurotransmitter used in the treatment of Parkinson's disease, was the first commercialized enantioselective process (Monsanto 1971[9]) using a rhodium complex incorporating with a chiral diphosphine catalyst. Either (*S*)-BINAP[33] or (*R,R*)-DIPAMP[64] can be employed as the chiral source in this process. Vanillin (**1-40**) is converted to an oxazolidinone (**1-42**) by reaction with *N*-acetylglycine (**1-41**) in the presence of sodium acetate and acetic anhydride. The heterocyclic ring in **1-42** is then hydrolyzed with aqueous acetone to give enamide (**1-43**). This acetamidocinnamic acid is the prochiral substrate in the enantioselective hydrogenation, which is the key step in the overall process. The hydrogenation of **1-43** is carried out at 50 °C/3 atm H_2 by adding the solid substrate

1-43 to the catalyst solution. The chiral aryl acetamidopropionic acid (**1-44**) is obtained with 95% ee and in 90% yield. Subsequent hydrolysis of the hydrogenation product (**1-44**) gives *L*-Dopa ((*S*)-3,4-dihydroxyphenylalanine, **1-45**).

Similar technology to that used in the synthesis of *L*-Dopa has been employed commercially to produce phenylalanine in Europe. The demand for this amino acid has increased substantially as a result of the commercial success of the synthetic

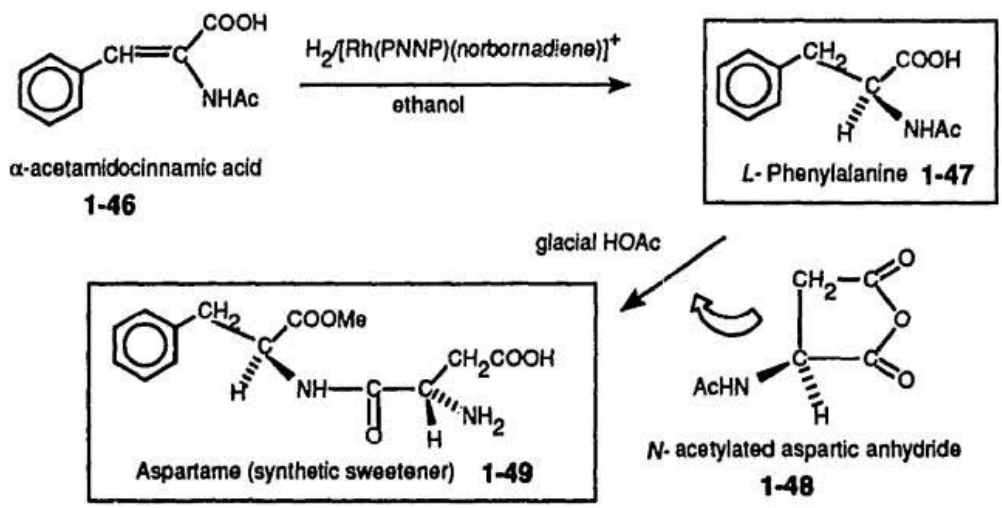

Scheme 1-14

sweetener aspartame. As shown in Scheme 1-14, hydrogenation of α-acetamidocinnamic acid (**1-46**) in ethanol with the cationic rhodium catalyst, [Rh(PNNP)(norbornadiene)]$^+$, gives *L*-phenylalanine (**1-47**) which then reacts with *N*-acetylated aspartic anhydride (**1-48**) in glacial acetic acid to form the desired aspartame (**1-49**) after removal of the acetyl protecting group followed by conversion to the methyl ester.

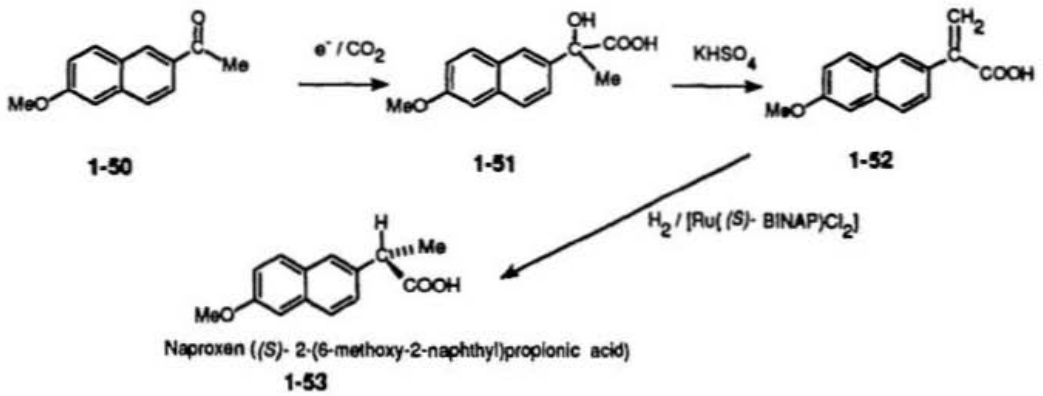

Scheme 1-15

Naproxen is one of the world's largest-selling prescription anti-inflammatory drugs. It is sold as the pure *S*-isomer because the *R*-isomer is a liver toxin. Currently the desired isomer is obtained by conventional optical resolution of the racemate.[21] Enantioselective hydrogenation (cf. Scheme 1-15) provides a good commercial opportunity for the production of Naproxen, especially since the original patent on the drug expired in 1993. Electrochemical reduction (aluminum anode, lead cathode) of acetylnaphthalene derivative (**1-50**) in the presence of CO_2 gives the corresponding α-hydroxy-naphthyl-propionic acid (**1-51**) which is then dehydrated over an acidic catalyst to produce the α-naphthylacrylic acid (**1-52**). Enantioselective hydrogenation of **1-52** with (*S*)-BINAP-Ru(II)Cl_2 complex catalyst at low temperatures and high hydrogen pressure in the presence of excess triethylamine gives Naproxen ((*S*)-2-(6-methoxyl-2-naphthyl)propionic acid, **1-53**) with 96-98% ee.

Studies on asymmetric hydrosilylation[23, 25, 36, 37] parallel asymmetric hydrogenation. Asymmetric hydrosilylation shares a number of common transition metal chiral

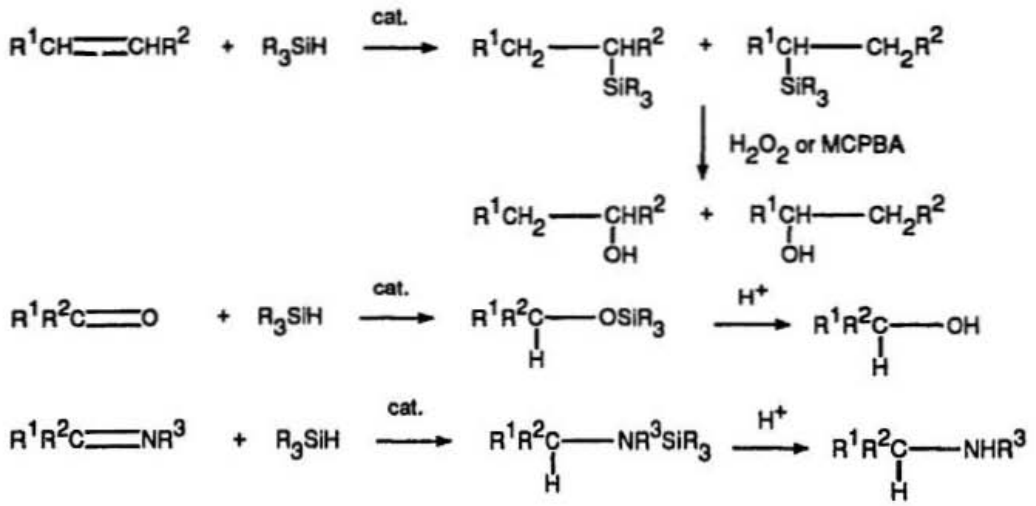

MCPBA = *m*- chloroperoxybenzoic acid

Scheme 1-16

catalysts and similar types of substrates, which include prochiral ketones, imines, and olefins, have been catalytically hydrosilylated with asymmetric hydrogenation, as shown in Scheme 1-16. In the hydrosilylation of ketones and imines, silyl ethers and silyl amines are formed, which may be hydrolyzed to give the corresponding alcohols and amines, respectively. The discovery of the oxidative cleavage of carbon-silicon bonds with hydrogen peroxide or *m*-chloroperoxybenzoic acid (MCPBA) suggests that asymmetric hydrosilylation of olefins will be a valuable synthetic route to optically active secondary alcohols and other functionalized compounds.[65, 66] Among these three types of substrates, prochiral ketones are the most successful and most studied systems. Although nickel, palladium, platinum and rhodium complexes have been used as the catalysts for hydrosilylations, rhodium complexes have received the most attention.

It is generally believed that asymmetric induction in hydrosilylation is somewhat lower than that achieved in hydrogenation.[14] Although the enantioselectivities attained in asymmetric hydrosilylation of prochiral ketones, imines, and olefins with mono- or bidenate chiral phosphines as chiral sources were moderate (50-85% ee)[36, 37] in most cases, better optical yields were achieved in hydrosilylations compared to asymmetric hydrogenations, when unfunctionalized substrates lacking secondary interactions with metal centers were employed.

Several interesting features exist in the asymmetric hydrosilylation reactions:[14, 36, 37] (1) Contrary to hydrogenation, both mono- and bidentate chiral phosphine ligands incorporated in the transition metal show comparable chiral induction in hydrosilylations. (2) Selectivity increases when there exists a possible secondary interaction of an ancillary carbonyl functionality with the metal center. However, this effect is not as dramatic as that in hydrogenation. (3) Both the configuration and the optical yield of products depend markedly on the structure of the silanes employed. Several examples are shown in Scheme 1-17.

Remarkable progress has been made in the rhodium-catalyzed asymmetric hydrosilylation of ketones with the application of chiral chelating nitrogen ligands (Scheme 1-18, **1-60 - 1-68**),[36, 67-71] and with simple olefins using a palladium-MOP

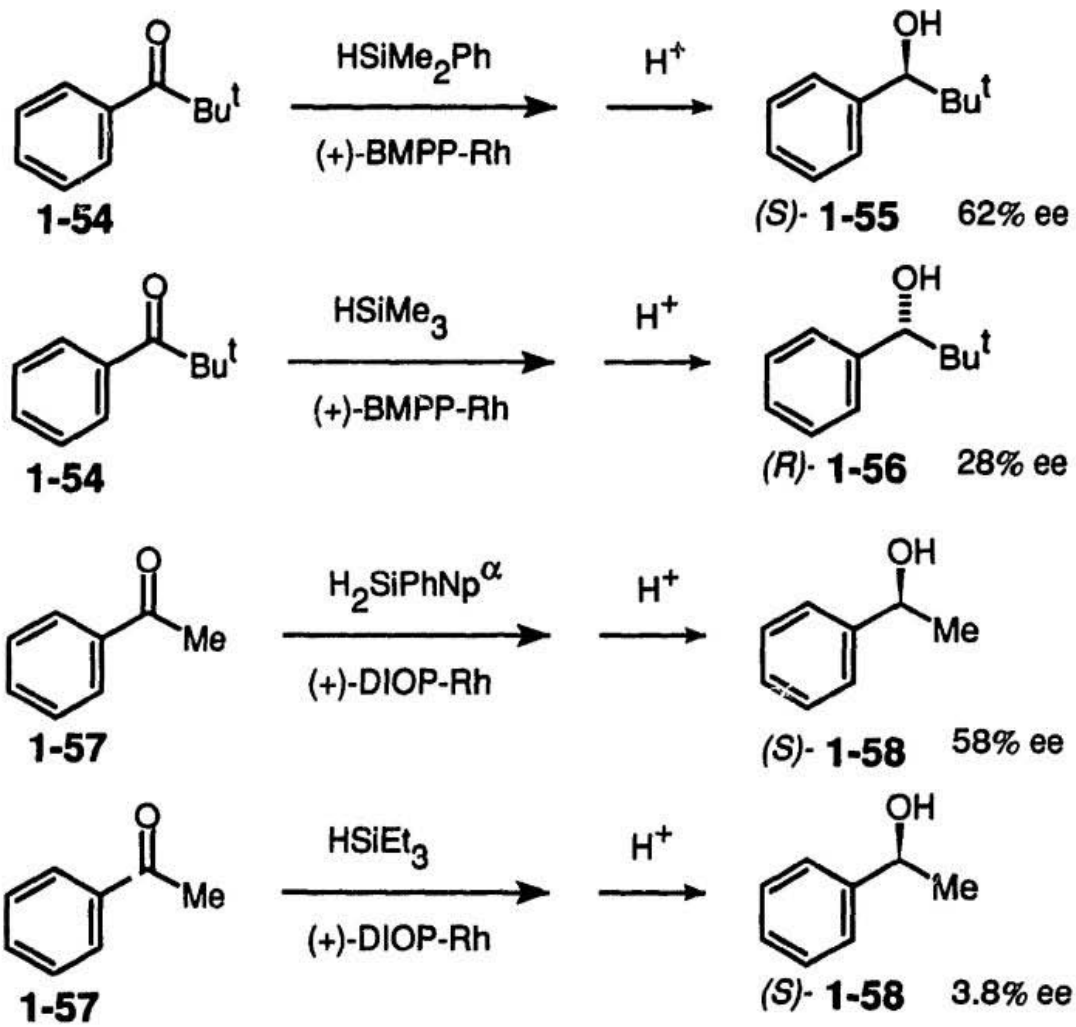

BMPP = P*CH_2Ph(Me)Ph; Np^{α} = α-naphthyl

Scheme 1-17

(**1-59**)[36,72] catalyst. For example, catalytic hydrosilylation of acetophenone (**1-57**) with [Rh(COD)Cl)]$_2$/(*R*)-Pythia-(Et,H) (**1-62**), which has proved to be the best nitrogen ligand to date for asymmetric hydrosilylation, gave (*R*)-1-phenylethanol (**1-70**) with 98% ee as shown in Scheme 1-19.[67,69] Pythia-(Me,H) (**1-60**) and Pythia-(Me,Me) (**1-**

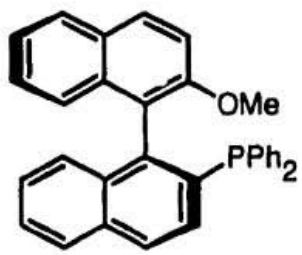

(S)- (-)-MOP

1-59

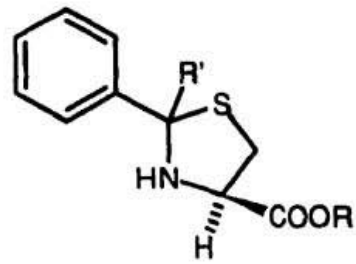

(R)- Pythia

R, R' = Me, H **(1-60)**

R, R' = Me, Me **(1-61)**

R, R' = Et, H **(1-62)**

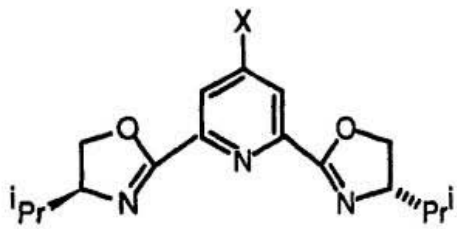

(S,S)- 4-X-Pybox

X = Me_2N **(1-63)**

X = MeO **(1-64)**

X = Cl **(1-65)**

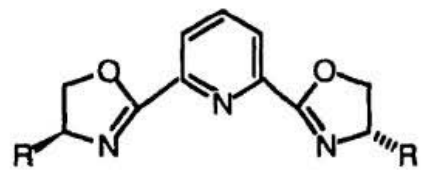

(S,S)- Pybox

R = ^{i}Pr **(1-66)**

R = ^{t}Bu **(1-67)**

R = CH_2Ph **(1-68)**

Scheme 1-18. Recently Designed Chiral Ligands

61) also promote high enantioselectivies, 87% and 84% ee, respectively, in this reaction. Excellent enantioselectivity toward (*S*)-1-phenylethanol (**1-58**, 95% ee)[70,71] was also obtained for the hydrosilylation of acetophenone (**1-57**) using [((*S,S*)-Pybox-^{i}Pr)$RhCl_3$] (**1-71**) as the catalyst in the presence of excess (*S,S*)-Pybox-^{i}Pr (**1-66**). This catalyst (**1-71**) also hydrosilylates α-tetralone (**1-72**) to the corresponding alcohol ((*S*)-**1-73**) with almost complete enantioselectivity (99% ee).[71] One common feature for all these systems is the application of a 4-15 fold excess of the ligand to promote

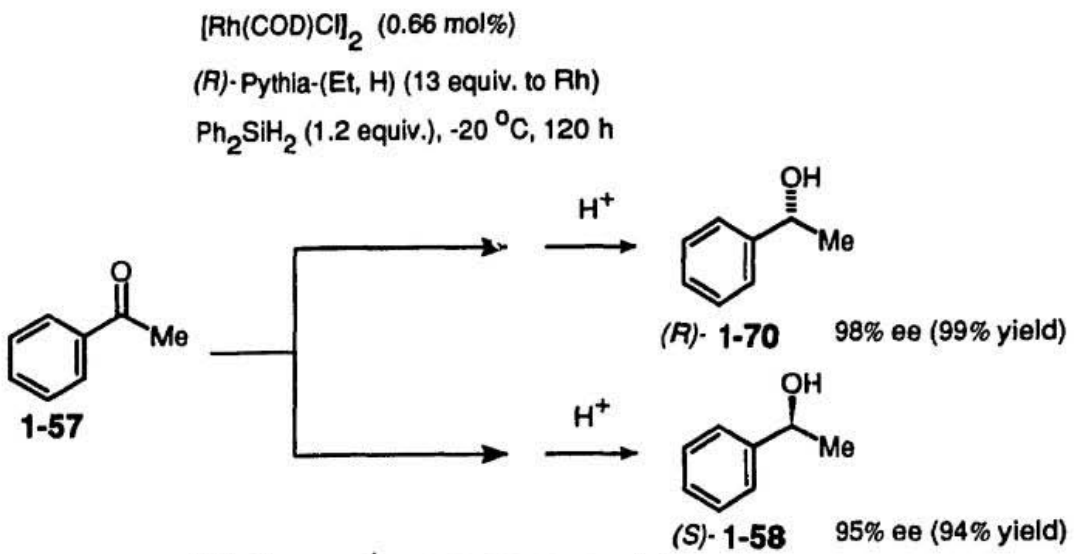

Scheme 1-19

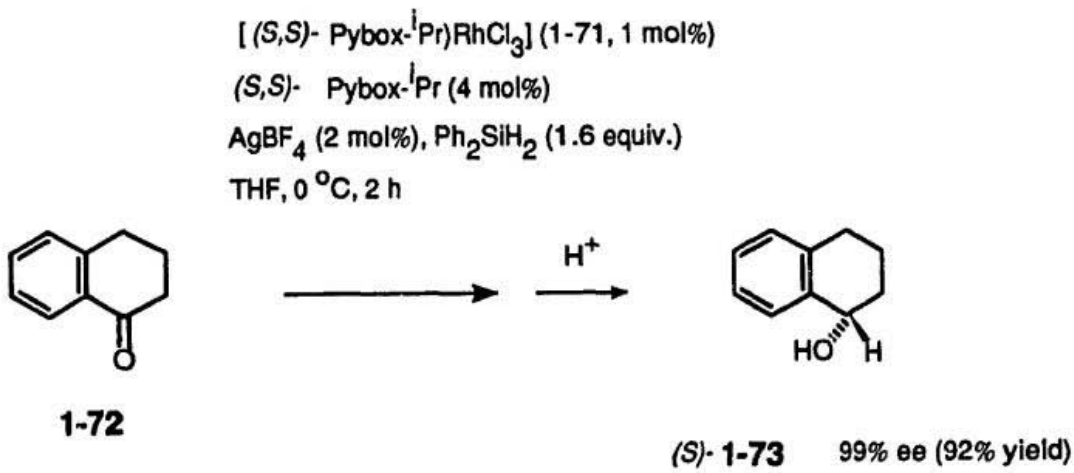

Scheme 1-20

high enantioselectivity.

A breakthrough in the asymmetric hydrosilylation of olefins was achieved using a palladium catalyst with the chiral monodentate phosphine ligand (*S*)-MOP (**1-59**)[73] obtained from binaphthol.[72] As shown in Scheme 1-21, simple 1-alkenes were converted to optically active 2-alkanols with more than 95% ee via (*S*)-MOP-Pd

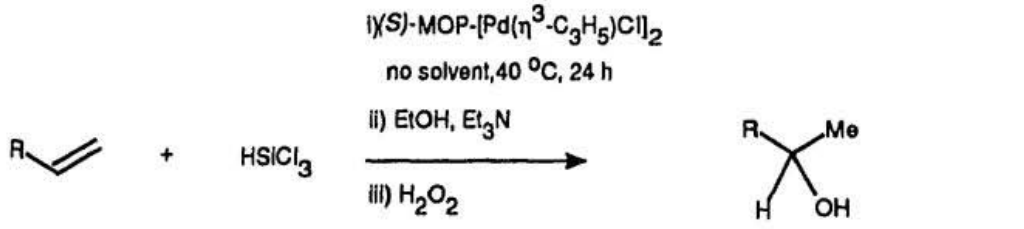

R = $^{n}C_6H_{13}$-, *(R)*- **1-74** 95% ee (71% yield)

R = $PhCH_2CH_2$-, *(S)*- **1-75** 97% ee (68% yield)

Scheme 1-21

catalysed hydrosilylation followed by oxidation with hydrogen peroxide.

Compared to asymmetric hydrogenation and hydrosilylation, asymmetric hydroformylation of olefins (cf. Scheme 1-22) has been much less satisfactory.[23, 25, 37, 39, 40] In addition to regioselectivity problems, hydroformylation is often accompanied by hydrogenation and isomerization (where applicable). Catalysts useful for asymmetric

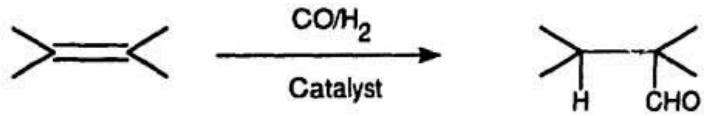

Scheme 1-22

synthesis must possess high enantioselectivity, regioselectivity, and chemoselectivity. None of the catalysts investigated so far filfills these requirements. Rhodium and platinum incorporating chiral phosphines have been the most intensively studied catalyst systems. High enantioselectivities coupled with high regioselectivities have been achieved only in the case of chiral platinum catalyzed hydroformation of vinyl aromatics.[40, 74-77] However, these catalysts are normally much less chemoselective than the corresponding rhodium catalysts.

1.2.1.2. Epoxidation. If we accept that the development of the Monsanto process for asymmetric hydrogenation was an epoch-making success in asymmetric synthesis in the 1970s, the establishment of the Arco process for asymmetric epoxidation of a range of allylic alcohols (Sharpless epoxidation) in the 1980s becomes a significant milestone in asymmetric synthesis. In this process, chiral titanium-tartrate complexes are employed as the catalysts for enantioselective epoxidation of allylic alcohols to the corresponding epoxy alcohols with up to >99% ee.[41-45] The addition of activated Molecular Sieves to the asymmetric epoxidation system has been demonstrated to increase the reaction efficiency greatly such that nearly all epoxidations are completed efficiently with only 5-10 mol% of the catalyst.[78, 79] Enantioselective olefin epoxidation may, simultaneously, create two chiral centers, which has also been applied intensively in laboratory organic synthesis.[41, 44, 45, 80]

Scheme 1-23 illustrates the four essential components for the titanium-catalyzed asymmetric epoxidation of allylic alcohols:[41, 42] an allylic alcohol substrate, a titanium(IV) alkoxide, a chiral tartrate ester, and an alkyl hydroperoxide. The chirality

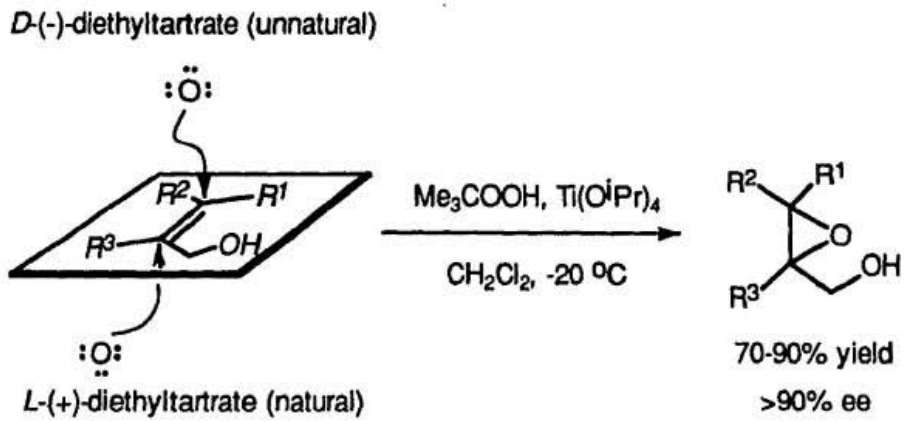

Scheme 1-23. Asymmetric Epoxidation of Prochiral Allylic Alcohols

of the epoxy product depends on the chirality of tartrate used. To date, no exception has been found among *prochiral* substrates to the enantiofacial selection rule. When *D*-(-)-tartrate is used, oxygen attacks the allylic alcohol from the top face as shown in Scheme 1-23. When *L*-(+)-tartrate is used, oxygen attacks the double bond from the bottom face. However, epoxidation of allylic alcohols with *chiral* substituents at C1, C2, and/or C3 does not always follow this rule. Nevertheless, enantioselectivities for the epoxidation of prochiral allylic alcohols and diastereoselectivities for the chiral allylic alcohols are normally very high with 90-100 % ee (or % de).[41-43] The key point in the epoxidation reactions is that the chiral tartrate ligand creates an asymmetric environment abou the titanium center.[41, 42] When the allylic alcohol and the *t*-butyl hydroperoxide bind through displacement of alkoxide from the metal, they are

disposed in such a way as to direct oxygen transfer to a specific face of the C=C double bond as shown in Scheme 1-24.

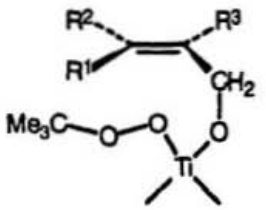

Scheme 1-24

The best known commercial application of the Sharpless chemistry is the synthesis of a chiral epoxide that is an intermediate to disparlure, the sex pheromone of the gypsy moth, as shown in Scheme 1-25. (+)-Disparlure, the active component of sex attractant emitted by the female gypsy moth, can be used to lure male moths. Alternatively, it can be used to

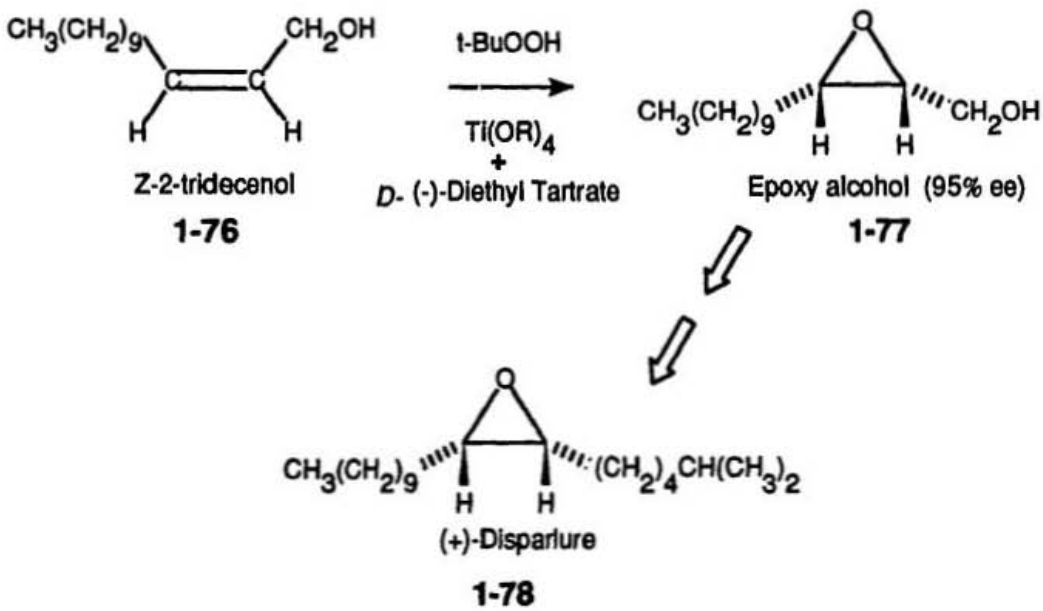

Scheme 1-25

confuse males and prevent them from finding females, which is quite successful in reducing mating. The key step in the Upjohn process[61] is the enantioselective epoxidation of the *Z*-2-tridecenol (**1-76**) using a complex of $Ti(OR)_4$ and *D*-(-)-diethyl

tartrate as the catalyst. The epoxy alcohol (**1-77**) is produced in 90-95% enantiomeric purity before recrystallization. Conversion of **1-77** to (+)-disparlure requires three conventional organic steps.

The requirement of an anchoring functional group (cf. Scheme 1-24) to control the stereoselectivity largely limited the application of Sharpless epoxidation to the epoxidation of allylic alcohols. Epoxidation of simple olefins shows little enantioselectivity. Significant achievements have been made most recently, with chiral salen-Mn(III) oxo transfer catalysts as shown in Scheme 1-26.[46, 82-88] These catalysts were employed to enantioselectively epoxidize unfunctionalized olefins using aqueous sodium hypochlorite (NaOCl) as oxidant (cf. Scheme 1-27) with up to 98% ee.[82-84] Among all the salen-Mn(III) complexes, **1-80** is the most selective catalyst developed to date for the epoxidation of a wide range of unfunctionalized olefins, especially conjugated olefins and cyclic ketal derivatives.[83, 89, 90] Remarkably high enantioselectivities are observed in the epoxidation of 2,2-dimethylchromene derivatives by **1-80** as shown in Scheme 1-28.[89]

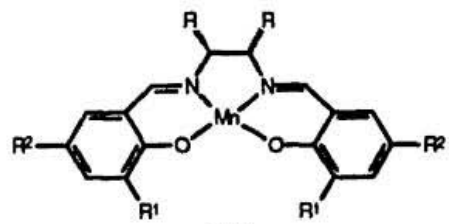

1-79

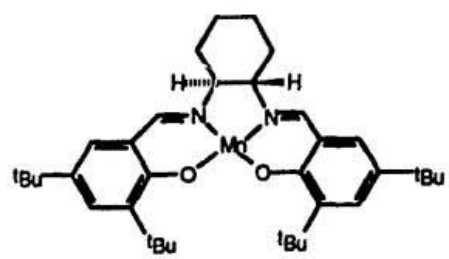

1-80

Scheme 1-26

This method was applied to highly efficient syntheses of the antihypertensive agent Cromakalim and a related compound (cf. Scheme 1-29).[89]

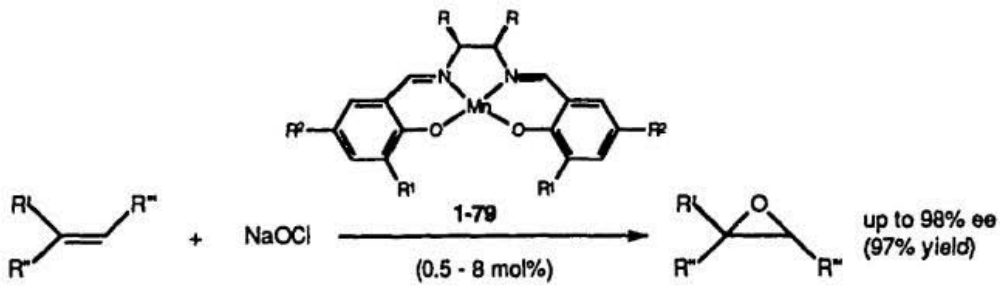

Scheme 1-27

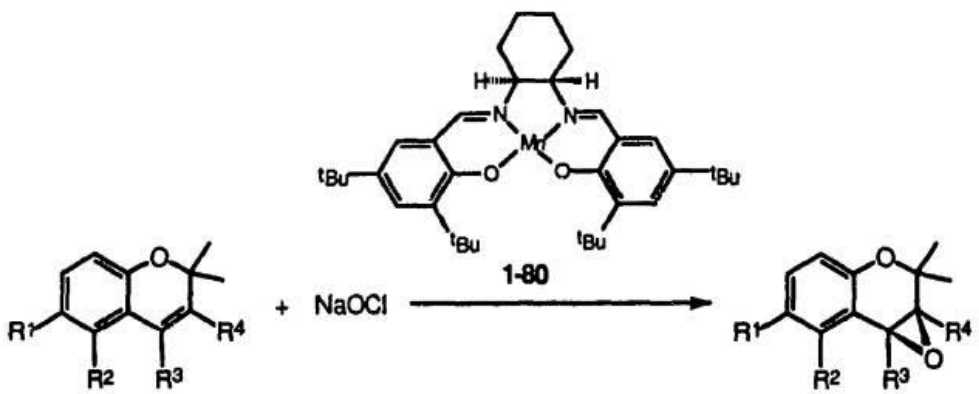

R1	R2	R3	R4		% ee	% yield	Product
CN	H	H	H	**1-81**	97	96	(3*R*,4*R*)-(+)-**1-86**
NO_2	H	H	H	**1-82**	94	76	(3*R*,4*R*)-(+)-**1-87**
MeCO	OMe	H	H	**1-83**	98	75	(3*R*,4*R*)-(+)-**1-88**
H	H	Me	H	**1-84**	97	51	(3*R*,4*R*)-(+)-**1-89**
CN	H	H	Me	**1-85**	>98	82	(3*R*,4*R*)-(+)-**1-90**

Scheme 1-28

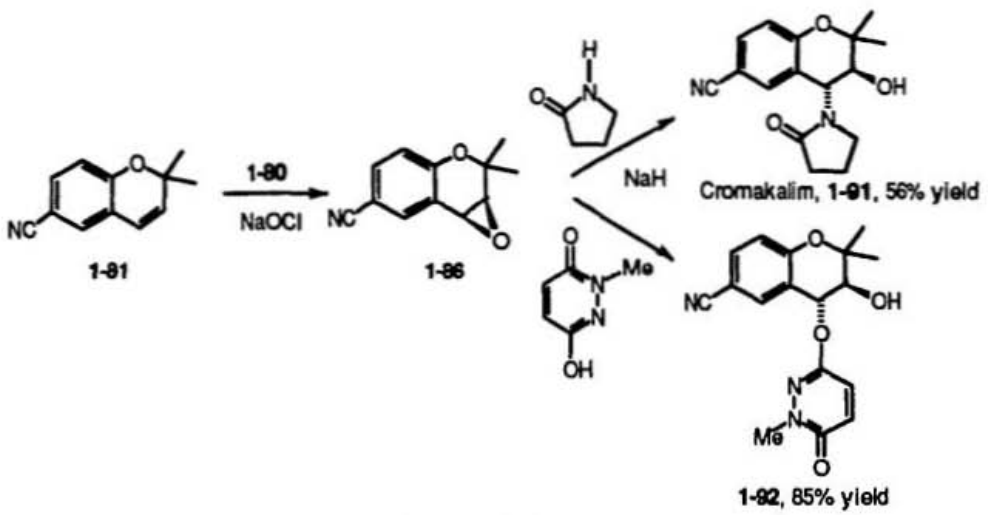

1-91 1-86

Scheme 1-29

In addition, transition-metal complexes incorporating chiral ligand auxiliaries have also been successfully applied in catalytic asymmetric dihydroxylation,[91-95] cyclopropanation,[30, 48, 49] cross-coupling,[14, 50, 51] and allylic substitution.[14, 50, 58, 96, 97] A variety of catalysts involving transition metals and chiral chelating phosphines and nitrogen donors possessing similar skeletons to those illustrated in Schemes 1-4 and 1-18 were used to promote chiral induction in these reaction systems. The catalysts shown in Scheme 1-30 are among the best investigated so far, and give up to >90-99% ee in selected examples.

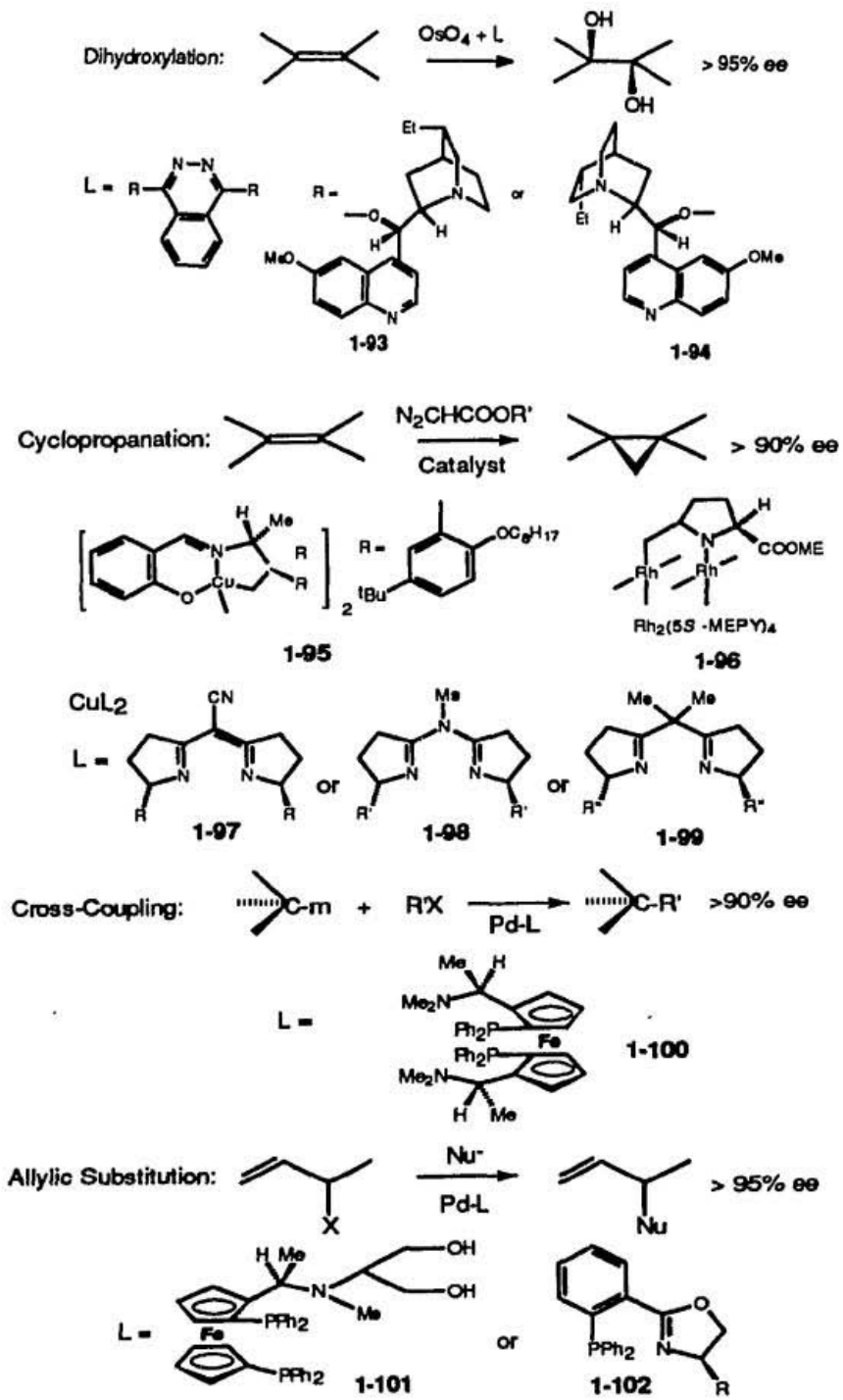
Dihydroxylation:
OsO4 + L
> 95% ee
L =
R =
or
1-93
1-94
Cyclopropanation:
N2CHCOOR'
Catalyst
> 90% ee
1-95
Rh2(5S -MEPY)4
1-96
CuL2
L =
or
or
1-97
1-98
1-99
Cross-Coupling:
C-m + R'X
Pd-L
C-R'
>90% ee
L =
1-100
Allylic Substitution:
Nu-
Pd-L
> 95% ee
L =
or
1-101
1-102

Scheme 1-30

1.2.2. Stoichiometric Asymmetric Synthesis with Chiral Metal Auxiliaries. Among the applications of chiral-at-metal complexes in asymmetric organic synthesis, the most famous systems are the piano-stool chiral auxiliaries developed by Liebeskind, Davies (chiral Fe auxiliary), Gladysz (chiral Re auxiliary) and Faller (chiral Mo auxiliaries), as shown in Scheme 1-31. These auxiliaries have been successfully applied to create stereoselectively, new chiral carbon centres in transition-metal-mediated alkylation and aldol condensation. Some examples presented here highlight the achievements of these chiral-at-metal complexes in stoichiometric organic synthesis. Excellent results have also been obtained with other chiral metal auxiliaries, such as chiral titanium complexes,[15] but are not discussed here.

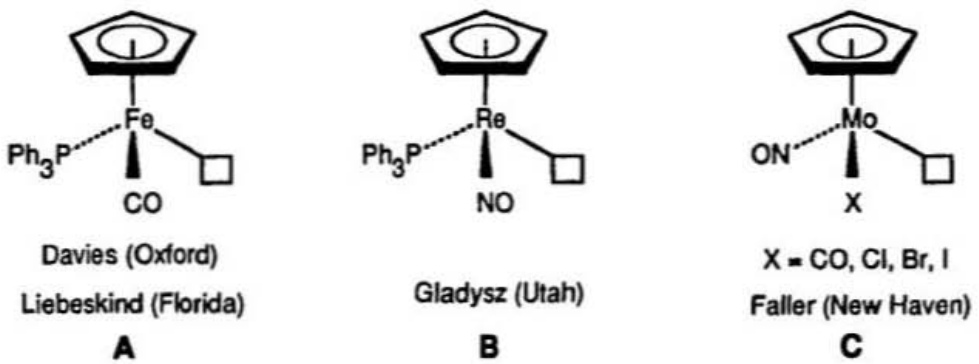

Scheme 1-31. Piano-stool Chiral Auxiliaries

1.2.2.1. Chiral Iron Auxiliary. The chiral iron auxiliary [(η^5-Cp)Fe(CO)(PPh_3)-][14, 96-128] is one of the most intensively studied chiral-at-metal systems for the asymmetric synthesis of organic compounds. High stereochemical selectivities have been achieved in a wide variety of reactions of this chiral-iron auxiliary mediated acyl

ligands (cf. Scheme 1-32), including alkylations,[101, 109-112, 129] aldol reactions,[102, 103, 114-118, 124] as well as tandem Michael additions and alkylations.[119-122, 130]

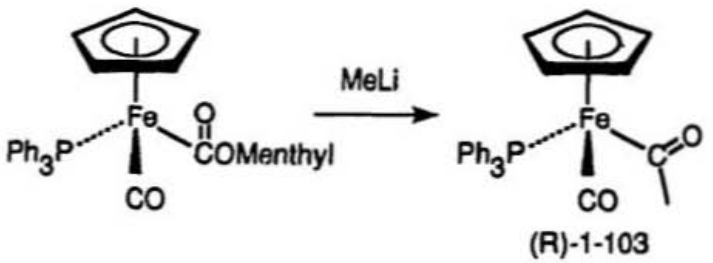

Scheme 1-32

The homochiral iron-acyl complex (**1-103**) was first prepared and resolved by Brunner[131, 132] from the diastereomerically pure menthyl esters by the addition of methyllithium (cf. Scheme 1-32), which was the conventionally applied method to achieve **1-103**. Recently, another method has been reported by Davies,[133] using a chiral thiolsulphonate resolving reagent.

This air-stable complex (**1-103**) and most of its derivatives are configurationally stable and easy to handle. As demonstrated by their crystal structures, this complex and its derivatives adopt a pseudooctahedral geometry placing the η^5-cyclopentadienyl ligand

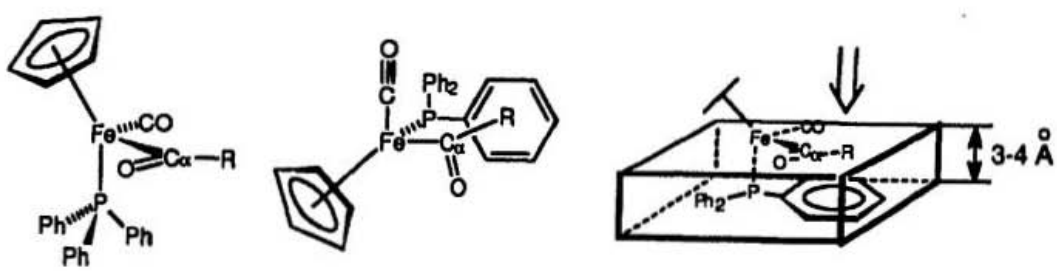

Scheme 1-33

at the three *fac* positions with triphenylphosphine, carbonyl, and acyl ligands occupying the remaining coordination sites.[106, 134, 135] Crystal structure and conformational analysis[107, 108, 134-141] showed that these complexes prefer a conformation with acyl oxygen *anti* to the carbonyl ligand both in the solid state and in solution (cf. Scheme 1-33). Both steric[108, 134] and stereoelectronic[142, 143] interactions may be important in determining this conformational preference. Rotation of the triphenylphosphine leaves one of the phenyl groups under the acyl ligand plane at a distance of 3-4 Å,[106, 134, 135] effectively blocking one face of the acyl ligand. Reagent approach is thus directed to the top side of the acyl plane as shown in Scheme 1-33 resulting in high selectivity.

As shown in Scheme 1-34,[96-101, 109-112, 129] deprotonation of the acyl complex **1-103** quantitatively gives the corresponding enolate **1-104**, which then reacts with primary alkyl halides or sulphonate esters cleanly forming another acyl complex **1-105** in 90-

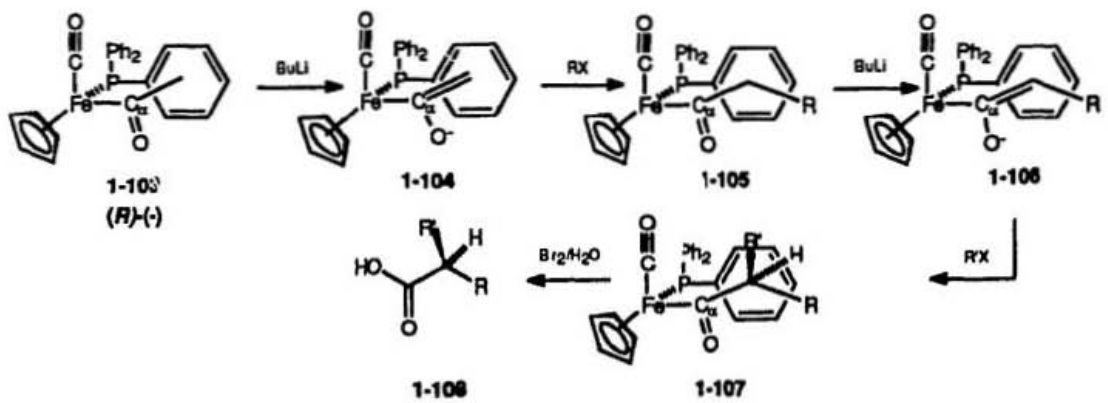

Scheme 1-34

98% yield. The hydrogens on the β-carbon are now diastereotopic and deprotonation from the less hindered direction stereospecifically generates the *E*-enolates **1-106** (Fe *trans* to R) in most cases. Approach of another electrophile from the unshielded face again results in a single alkylated diastereomer **1-107**. Further deprotonation of the dialkylated complex **1-107** does not occur since the remaining proton on the β-carbon is buried in the chiral auxiliary and is therefore inaccessible to base. Oxidative cleavage of the Fe-C bond by Br_2 in the presence of water, alcohols or amines gives the corresponding acids, esters or amides (**1-108**) respectively.[98-100] The chirality at the β-carbon is controlled by the chirality at the iron center.[98-100, 106]

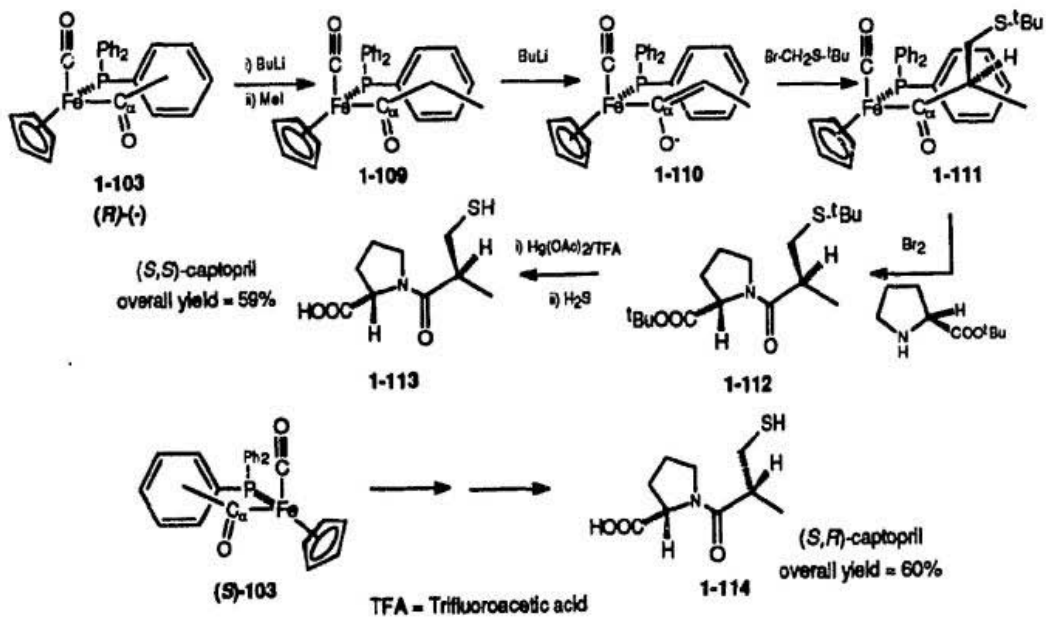

Scheme 1-35

This alkylation methodology was applied successfully to the synthesis of the anti-hypertensive drug (*S,S*)-(-)-Captopril (*cf.* Scheme 1-35)[100, 144] and other biologically

active products, such as (-)-actinonin.[100, 145] The opposite chirality at the α-carbon in **1-113** and **1-114** coming from **(*R*)-1-103** and **(*S*)-1-103**, respectively, clearly demonstrates that the chirality at the newly formed chiral carbon center is controlled by the chirality of the iron atom.

The diethyl aluminum chiral-iron enolate **1-104** can undergo aldol condensations with aldehydes to form the corresponding chiral alcohols (**1-115**) with high percent de (cf. Scheme 1-36).[14, 98, 115, 118] However, the same enolate with lithium as the counterion reacts with aldehydes with little stereoselectivity.[14, 98, 115, 118] The same enolate with a tin containing counterion reacts with aldehydes with high percent de, but generates the opposite chirality at the γ-carbon.[14, 103, 124] Although a similar counterion effect was also observed in the reaction between enolate **1-104** and (*E*)-imine, the diastereoselectivity toward the chiral amines **1-116** (cf. Scheme 1-37) is counterion independent.[14, 125] The counterion effect was maximized in the reactions between chiral-iron associated enolate **1-106** (cf. Scheme 1-38) and aldehydes. Enolate **1-106** with either $AlEt_2^+$ or $CuCN^+$ counterion reacts with aldehydes with high diastereoselectivities, but the major products generated by these two counterions possess opposite configurations at the hydroxy bonded carbon.[14, 116]

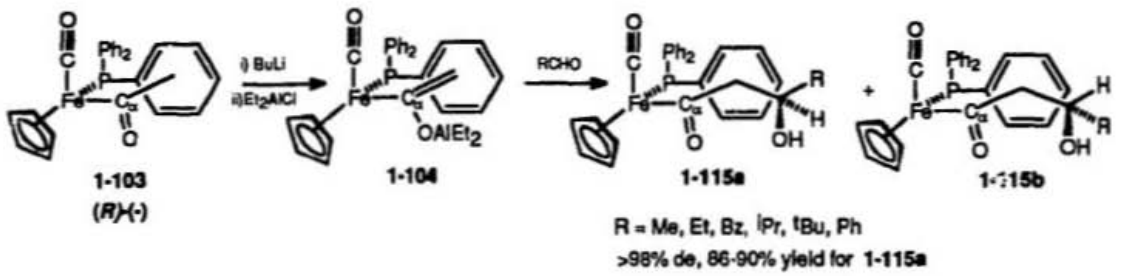

R = Me, Et, Bz, ^{i}Pr, ^{t}Bu, Ph

>98% de, 86-90% yield for **1-115a**

Scheme 1-36

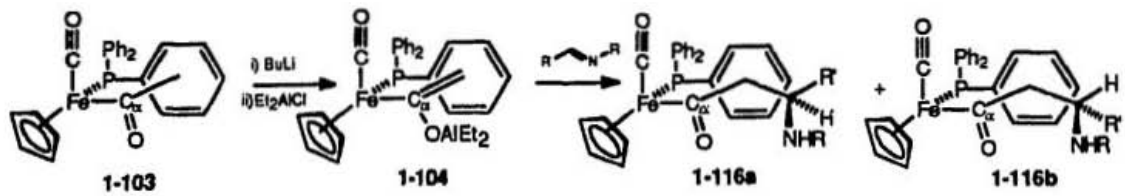

R'	R	%de (a major)
Ph	Ph	70
Ph	nPr	90
iPr	nPr	90

Scheme 1-37

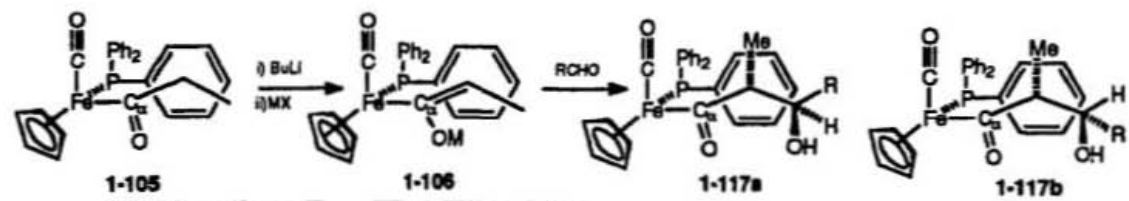

R	M	a	b	c	d
Me	$AlEt_2$	100	-	7	3
Et	$AlEt_2$	100	-	14	-
^{i}Pr	$AlEt_2$	100	-	10	<1
^{t}Bu	$AlEt_2$	100	-	-	-
Me	CuCN	14	100	<1	-
Et	CuCN	10	100	<1	-
^{i}Pr	CuCN	7	100	<1	-
^{t}Bu	CuCN	4	100	-	-
Ph	CuCN	4	100	<1	-

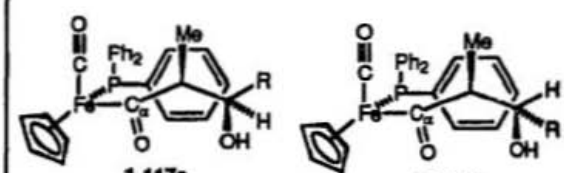

Scheme 1-38

Similar steric interaction models have been proposed by Davies[106, 108, 139] and Liebeskind[124, 125, 127] to account for the stereoselectivity in the enolate-aldehyde and -imine reactions with $AlEt_2^+$ as the counterion (cf. Scheme 1-39).[14] Davies assumes

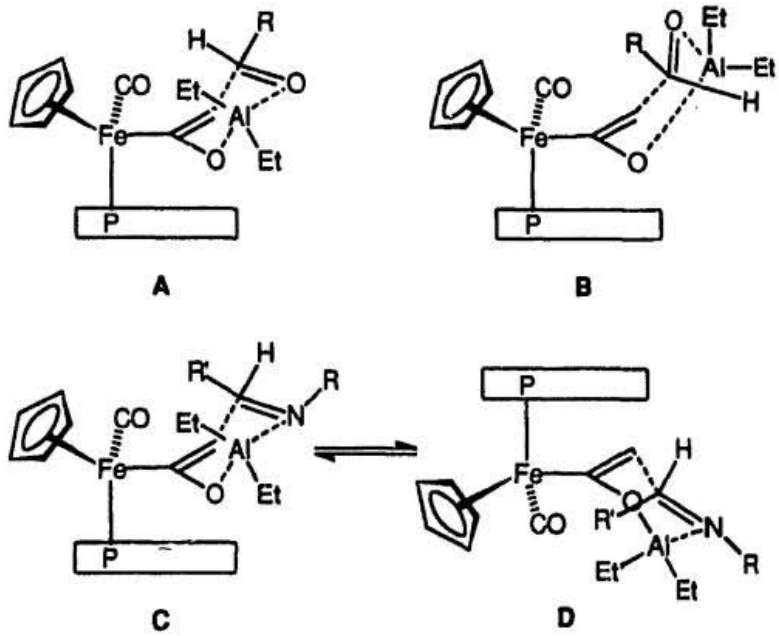

Scheme 1-39

that the 1,3-diaxial interactions between Al-*Et* and C(O)-*R* in the six-membered *quasi*-chair or -boat transition-state as well as the steric interactions between Al-*Et* and η^5-Cp would control the stereoselectivities of aldol condensations. Thus, the C(O)-*R* group in both conformations prefers the *pseudo*-equatorial position (Scheme 1-39A,B). However, since the *quasi*-chair conformation (cf. Scheme 1-39A) puts the Al-*Et* group toward the Cp ring resulting in a steric interaction, which is diminished in the *quasi*-boat conformation (cf. Scheme 1-39B), conformer B becomes the preferred

transition state for aldol condensations.

Liebeskind, however, emphasized that the steric interactions between the η^5-Cp and R' group on the imine carbon may be the controlling factor in determining the stereoselectivity of enolate-imine reactions. Therefore, he proposed that the equilibrium between the *syn-* and *anti- quasi*-chair transition states (Scheme 1-39C,D) is controlled by the relative size of the R' group, which governs the conformational preference and in turn determines the stereoselectivity.

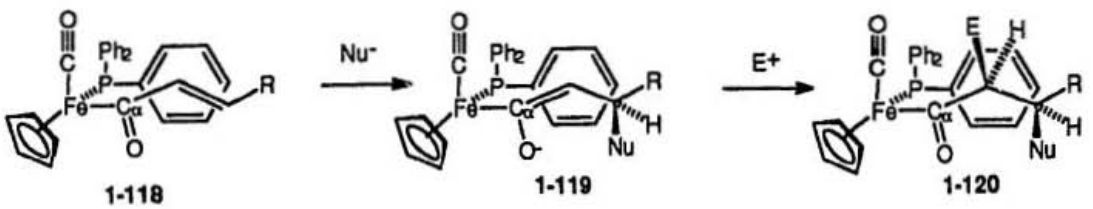

Scheme 1-40

Similar to the chiral-iron mediated alkylation and aldol condensation, tandem Michael addition-alkylation on the (*E*)-α,β-unsaturated acyl ligands (**1-118**) also proceeds with high stereoselectivity as shown in Scheme 1-40.[98-100, 119-122, 130] Generally, only a single diastereomer of the product **1-120** is detectable, indicating complete stereocontrol over both carbon centers. This methodology has been successfully applied to the synthesis of β-lactams.[98-100, 105, 122, 125, 130, 146]

1.2.2.2. Chiral Rhenium Auxiliary. The chiral-at-rhenium auxiliary, [(η^5-

Cp)Re(NO)(PPh_3)-] (cf. Scheme 1-31), has been studied by Gladysz and coworkers.[14, 147-164] As with the iron complexes, the rhenium analogues, (η^5-Cp)Re(NO)(PPh_3)(R), adopt a pseudooctahedral geometry with η^5-cyclopentadienyl occupying three *fac* positions and the remaining three coordination sites occupied by PPh_3, NO and ligand R, respectively.[106, 147, 148, 152, 157] The conformational preference of ligand R with respect to the (η^5-Cp)Re(NO)(PPh_3)- template is nearly the same as that in the iron template.[108, 157] Therefore, it is reasonable that the stereoselectivities observed for reactions of ligands attached to the rhenium chiral auxiliary parallel those observed for the corresponding iron complexes. For example, high enantioselectivities are observed for alkylations of chiral-rhenium attached acyl moieties.[148, 152-154, 156]

In addition, this chiral-rhenium auxiliary has been used to promote stereoselective reactions on attached ketones,[161-165] alkenes,[155, 166], acetylides[167, 168], and carbenes.[158, 160] For example,[14, 161-164] reaction of hydride with chiral rhenium-ketone complexes gives optically active alcohols in high enantiomeric excess as shown in Scheme 1-41.

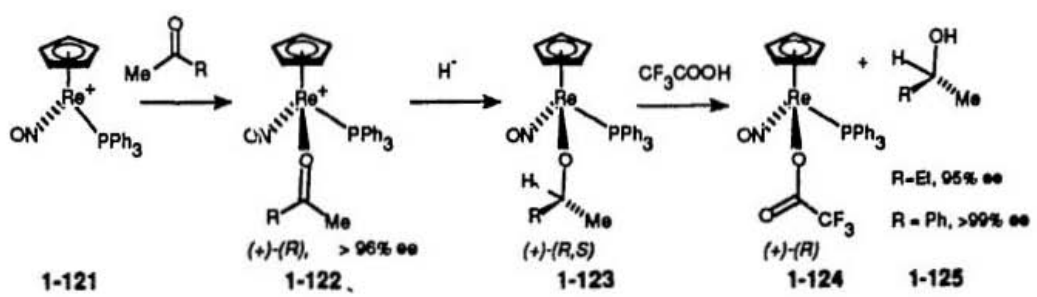

Scheme 1-41

1.2.2.3. Chiral Molybdenum Auxiliaries. Chiral induction from the asymmetric metal center to the newly formed chiral carbon is usually dominated by steric effects (cf. discussion above). Examples of electronic control in enantioselective synthesis are not common. This section presents several examples of stereoselectivity promoted by electronic asymmetry in the ligand sphere.

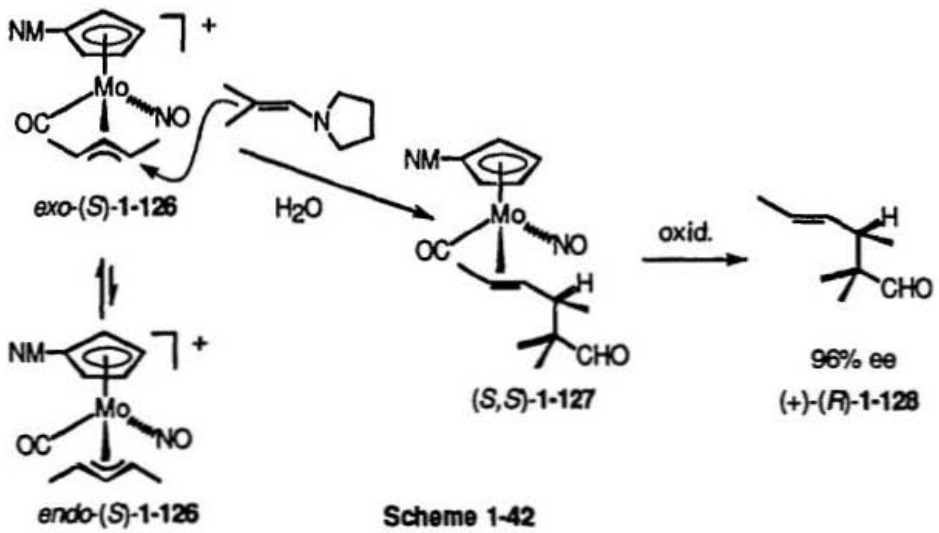

Scheme 1-42

Faller and coworkers have developed chiral molybdenum templates (cf. Scheme 1-31C) to promote enantioselective reactions on coordinated allyl moieties.[169-175] Three different ligands, η^5-cyclopentadienyl, nitrosyl, and carbonyl (or Cl, Br, or I), are introduced into the η^3-allyl molybdenum complex to form an asymmetric molybdenum center, which is resolved as a pair of neomenthyl (NM) diastereomers (Scheme 1-42).[170, 176] Reaction of enantiomerically pure *exo*- and *endo*-(*S*)-**1-126** with 1-pyrrolidino-2-methylpropene gave essentially a single product, (+)-(*R*)-2,2,3-

trimethylhex-4-enal (**1-128**) after decomplexation via air oxidation (cf. Scheme 1-42).[170] This high enantioselectivity was attributed to a much faster nucleophilic addition to the *exo* isomer combined with a nucleophile-catalyzed interconversion from the *endo* to *exo* isomer. The nucleophile approaches the coordinated allylic moiety from the less hindered side opposite to the metal template. Preferential attack occurs on the allylic carbon *cis* to the NO ligand,[170] which indicates that chiral induction in this system comes mainly from electronic asymmetry of the ligand sphere, since the steric bulk of CO and NO ligands are nearly the same.

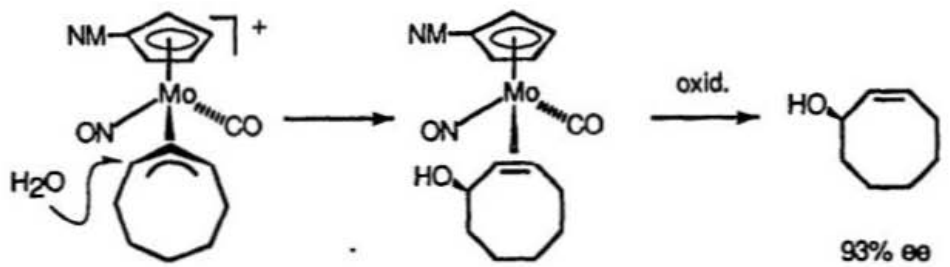

exo-(*R*)-**1-129** (*R,R*)-**1-130** (-)-(*R*)-**1-131**

Scheme 1-43

Electronically orientated asymmetric addition of hydroxide at the allylic carbon *cis* to the nitrosyl ligand in (*R*)-**1-129** afforded (-)-(*R*)-3-hydroxycyclooctene with high enantioselectivity (93% ee), as shown in Scheme 1-43.[171]

Several halide substituted chiral-at-molybdenum templates have been applied to

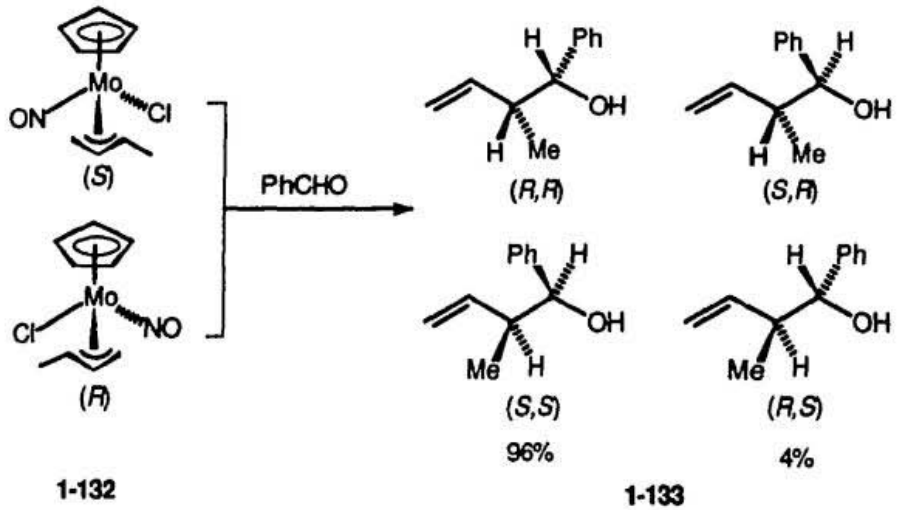

Scheme 1-44

asymmetric aldol reactions to give optically active secondary homoallylic alcohols.[172, 174, 175] The electronic asymmetry-promoted chiral induction is clearly demonstrated in these examples. Treatment of racemic (η^5-Cp)Mo(Cl)(NO)(η^3-crotyl) (**1-132**) with benzaldehyde in methanol/CH_2Cl_2 yields the chiral secondary alcohols in a (*R,R;S,S*):(*R,S;S,R*) ratio of 22:1, as shown in Scheme 1-44. Use of the neomenthylcyclopentadienyl analogue of **1-132** provides a resolved chiral metal and a route to nonracemic chiral condensation products. Reaction of (-)-(*S*)-(NM-Cp)Mo(NO)(Cl)(η^5-Crotyl) ((*S*)-**1-134**) with benzaldehyde yields (+)-(*R,R*)-2-methyl-phenyl-3-buten-1-ol ((*R,R*)-**1-133**) in > 98% ee.[174] The origin of this extraordinary selectivity with this molybdenum reagent lies in the electronic asymmetry created by the different backbonding capabilities of the nitrosyl and halide ligands. NO is a much better electron acceptor than Cl. Thus, RCHO is directed *trans* to the NO group and

crotyl therefore forms a σ-bond *cis* to the NO group. A chair-like transition state is generated, in which an antiperiplanar arrangement of the phenyl relative to the Cp ring is expected in order to minimize steric interactions with the Cp ring. This provides for the ultimate control of the high stereoselectivity as shown in Scheme 1-45.[174]

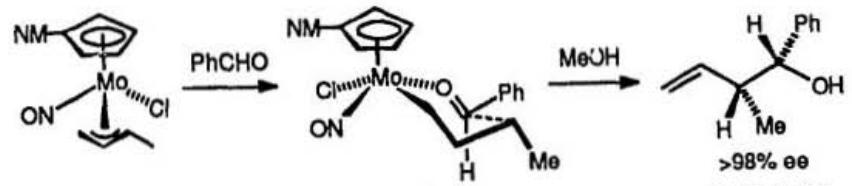

(*S*)-1-134 1-135 (*R,R*)-1-133

Scheme 1-45

Similarly, reactions of PhCHO with resolved (+)-(*R*)-(η^5-Cp)Mo(NO)(X)(η^3-methylallyl) (X = Cl, Br, I, (*R*)-**1-136**) in the presence of methanol gives (-)-(*S*)-3-methyl-1-phenyl-3-buten-1-ol ((*S*)-**1-138**) in 88 - 98% ee (cf. Scheme 1-46) via the same chair-like transition state.[175]

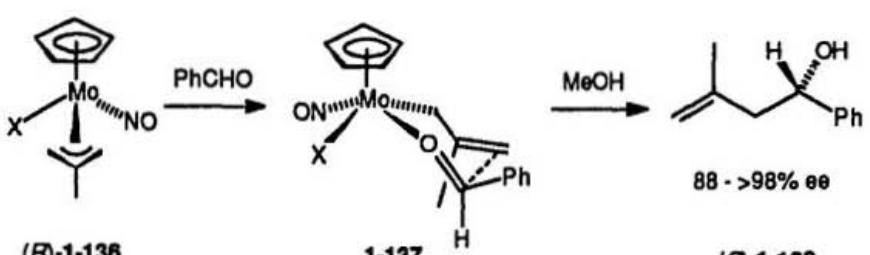

(*R*)-1-136 1-137 (*S*)-1-138

Scheme 1-46

1.3. Transition Metal-Mediated Arbuzov Reactions

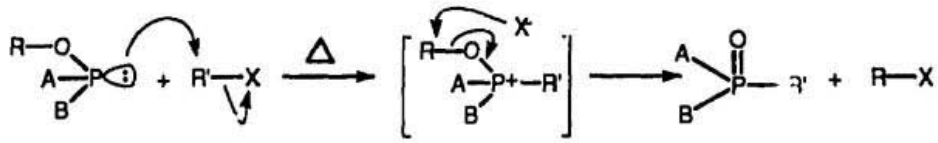

Phosphites (A, B = OR)
Phosphonites (A = R, B = OR)
Phosphinites (A, B = R)

Phosphonates (A, B = OR)
Phosphinates (A = R, B = OR)
Phosphine Oxide (A, B = R)

R, R' = alkyl, aryl; X = I, Br, Cl

Scheme 1-47

1.3.1. Classical and Transition Metal-Mediated Arbuzov Reactions. The Arbuzov reaction[177] is one of the most versatile pathways for the formation of carbon-phosphorus bonds.[178] It involves the reaction of an ester of trivalent phosphorus with alkyl halides, as shown in Scheme 1-47. In this reaction, the phosphorus ester may be a phosphite (A, B = OR), phosphonite (A = R, B = OR) or phosphinite (A, B = R). Numerous investigations have shown that this reaction proceeds via an ionic mechanism involving a quasi-phosphonium intermediate, although other mechanisms, such as autocatalytic, and radical, have been reported.[177, 178] This reaction is initiated by the attack of the phosphorus lone pair on the alkyl halide producing an unstable phosphonium ion (cf. Scheme 1-47).[179] The released halide then attacks the α-carbon of the ester resulting in the formation of the P=O bond with the loss of a new alkyl halide. The overall reaction is the conversion of trivalent phosphorus into pentavalent phosphorus. The driving force for this reaction can be attributed to the formation of a very stable phosphoryl P=O bond which provides a thermodynamic

sink in the order of 134-272 kJ/mol.[177]

Normally, prolonged heating is required to promote this reaction, which is sensitive to the substituents on phosphorus and the alkyl halide employed. For example, for the case R'X = MeI, the reactivity for phosphonites and phosphinites follows the order of electron-donor ability of substituent A and B: alkyamino > alkyl > aryl > alkoxy > aryloxy.[180] The reactivity order when phosphite reacts with R'X decreases in the order:[181] H_2CO-X > RCH_2-X > R_2CH-X >> RR'R"C-X, with R-I > R-Br > R-Cl, consistent with an S_N2 mechanism, as shown in Scheme 1-47. In accordance with these observations, the reactivity of R'I decreases toward the reaction with phosphites in the order Me > Et > ^iPr.[178, 180, 181]

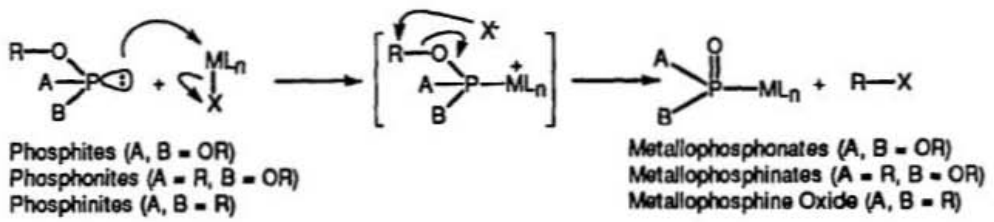

R, R' = alkyl, aryl; X = I, Br, Cl; M = transition metal; L = ligand

Scheme 1-48

By analogy with the classical Arbuzov chemistry, reaction of a transition-metal halide (L_nM-X) instead of R'X in Scheme 1-47 with phosphites, phosphonites, or phosphinites leads to the corresponding metallophosphonates, phosphinates, or phosphine oxides (L_nM-P(O)(A)(B)), respectively, as shown in Scheme 1-48. This

provides one of the most versatile pathways for the synthesis of L_nM-P(O)(A)(B) complexes.[182-208] Among these reports, alkyl phosphites are the prevailing phosphorus esters employed in transition metal-mediated Arbuzov reactions. Unlike the classical Arbuzov reactions (Scheme 1-47), transition metal-mediated Arbuzov reactions (Scheme 1-48) generally proceed readily under mild conditions, which facilitates mechanistic studies.

Although both ionic and radical mechanisms have been claimed in the literature,[182] the majority of mechanistic studies have shown that transition metal Arbuzov-like dealkylation reactions proceed via an ionic mechanism,[182, 184, 188, 192, 194-201, 203-206, 209] (cf. Scheme 1-48). Initial substitution of the L_nM-X halide by a phosphorus ester, such as phosphite, forms a cationic phosphite intermediate complex as an ion pair, $[L_nM(P(OR)_3)]^+X^-$. Subsequent collapse via halide attack at the α-carbon of the coordinated phosphite releases alkyl halide and the metallophosphonate. Cationic $18e^-$ ion-pair phosphite complexes of the form $[L_nM(P(OR)_3)]^+X^-$ (R=alkyl) are extremely labile with respect to Arbuzov-like dealkylation, hence only a few of these have been isolated.[184, 195-197, 209, 210] The first structurally characterized organometallic trimethylphosphite Arbuzov intermediate was isolated by Brill[182, 204] as a stable PF_6^- salt. Addition of iodide to the solution of this ionic intermediate results in the formation of the corresponding metallophosphonate.

In addition, other nucleophiles, such as $Mn(CO)_5^-$, $Co(CO)_4^-$, and $[(\eta^5\text{-Cp})Mo(CO)_3]^-$,

can also attack the α-carbon of coordinated phosphite to give the corresponding phosphonate and organometallic alkyl compound via the ionic mechanism.[182, 211-213] However, in many similar systems a radical mechanism is operative.[182, 214-216]

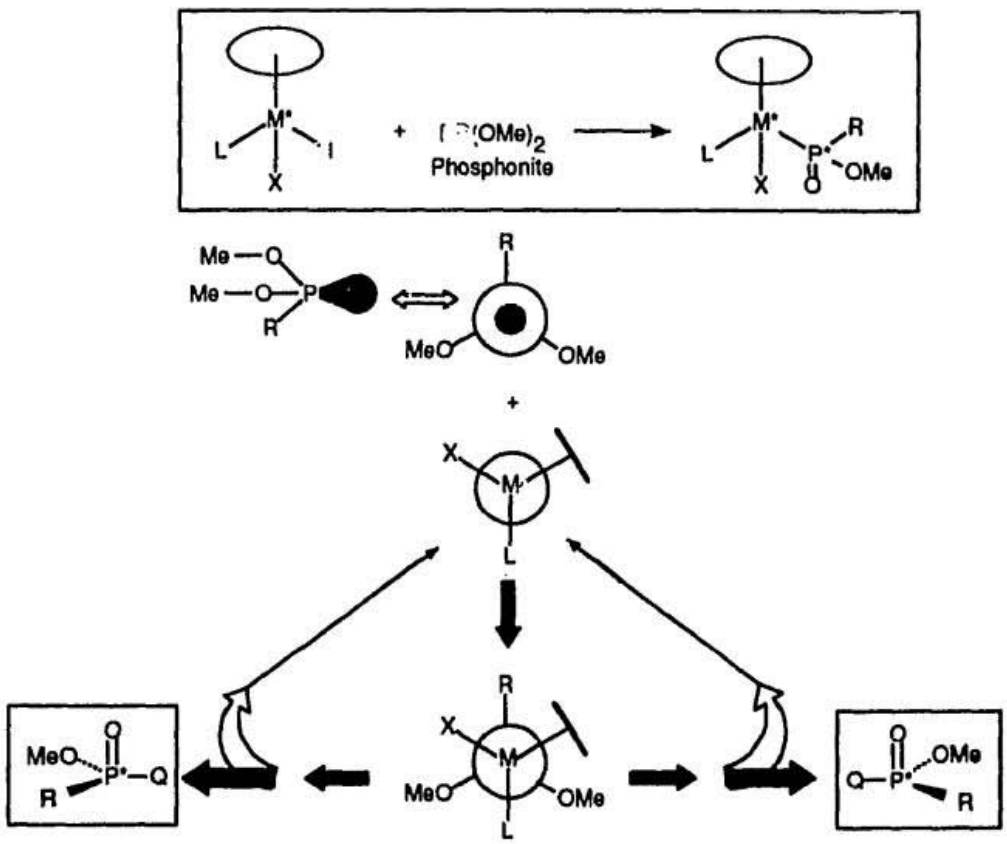

Scheme 1-49

1.3.2. Chiral Induction in Transition Metal-Mediated Arbuzov Reactions. The research undertaken in this thesis focused on using the Arbuzov reaction between an asymmetric pseudooctahedral, piano-stool iodide and phosphonite as a model to

investigate metal to phosphorus chiral induction. In this chemistry (cf. Scheme 1-49), a prochiral phosphonite is converted to a chiral metallophosphinate. This metallophosphinate could be converted to chiral organic phosphorus compounds via metal-phosphorus bond cleavage. This kind of organic phosphorus compound possesses both commercial and synthetic significance.[178]

Previous studies[206, 217, 218] showed that reaction of organometallic iodides with phosphonite in aminophosphine-substituted complexes gave cationic intermediates (cf. Scheme 1-50). Chiral induction from the asymmetric Co center to prochiral phosphorus was facilitated by the P-N-H•••O=P hydrogen bonding, which restricted population of solution conformations, maximized the preference of one diastereomer over another, and in turn dominated the diastereoselectivity.

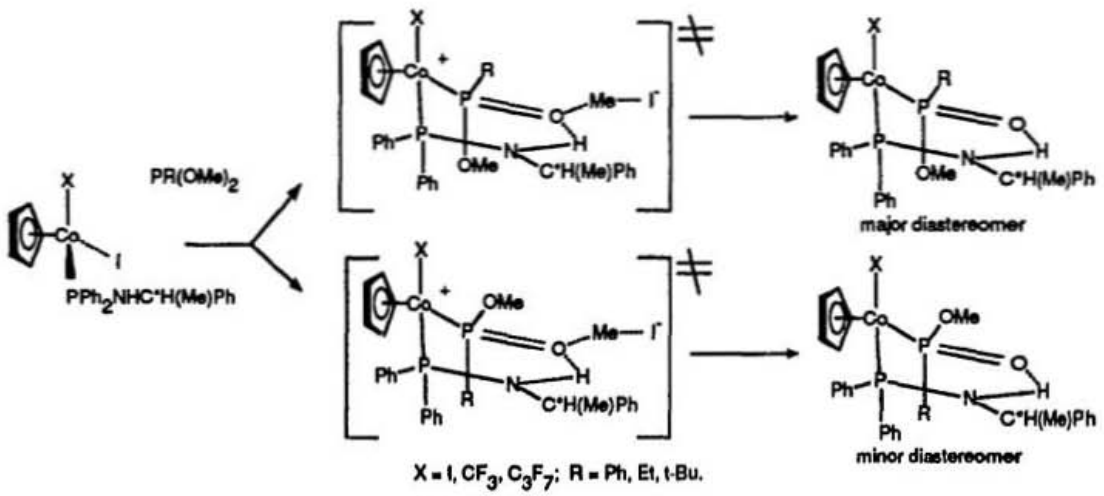

X = I, CF_3, C_3F_7; R = Ph, Et, t-Bu.

Scheme 1-50

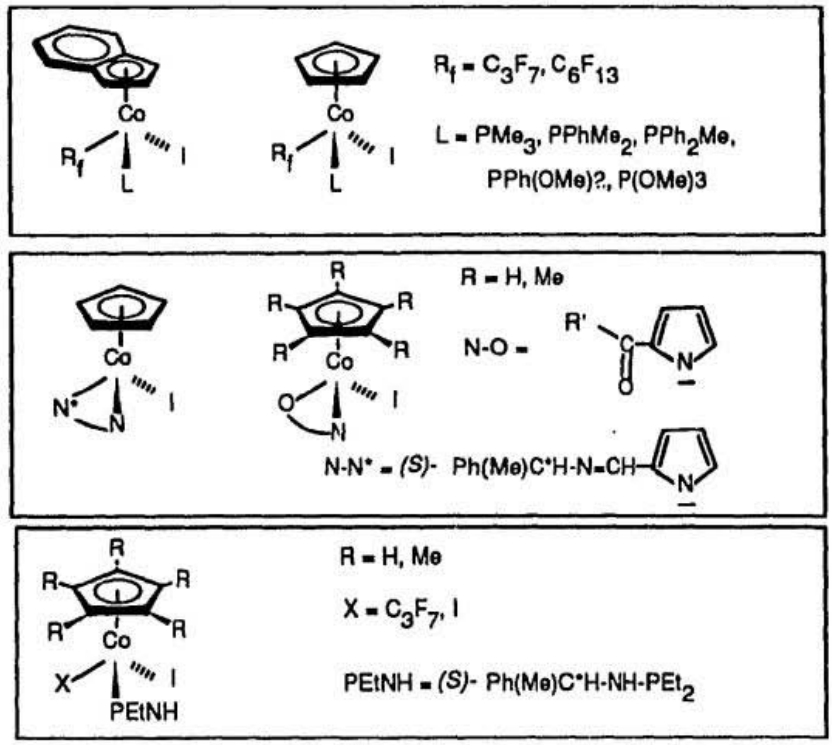

Scheme 1-51. Chiral Cobalt Auxiliaries

To further investigate this idea and to reveal which factors are important in determining the Co* → P chiral induction, systems with or without the potential to form the P-N-H•••O=P hydrogen bonding have been examined. A series of η^5-cyclopentadienyl, η^5-pentamethylcyclopentadienyl, η^5-indenyl three-legged piano-stool metal complexes (cf. Scheme 1-51) have been studied as the chiral templates for the Arbuzov reaction. The electronic and stereochemical properties of the ligand sphere were varied from simple phosphines and chiral aminophosphines to chelating N-N and N-O coordinated ligands, and the results are discussed in the following chapters.

Chapter 2

Synthesis, Structure and Solution Conformation of $[(\eta^5\text{-Indenyl})Co(R_f)(I_{2-n})(L_n)]^{(n-1)+}$ ($n = 1, 2$; R_f = Perfluoroalkyl; L = CO, P-donor) Complexes.

2.1. Introduction

During the course of our search for efficient chiral templates for the Arbuzov reaction, we have focused our attention to the η^5-indenyl cobalt complexes with different simple phosphine ligands as shown in Scheme 1-51. Presumably these complexes could serve as non-hydrogen bonding templates for diastereoselective Arbuzov reaction to prove the significance of intramolecular P=O•••H-N hydrogen bonding in controlling the stereoselectivity in the Arbuzov dealkylation step, as shown in Scheme 1-50. Before examining this feature of Arbuzov reactions with these complexes, it is worthwhile to demonstrate the properties of the η^5-indenyl cobalt iodide complexes.

Transition metal π-indenyl complexes have attracted a great deal of attention in recent years[219-246] since they characteristically display enhanced reactivity in ligand substitution and related reactions[221, 224, 230, 247-261] and catalysis [237, 262-265] compared to their isostructural cyclopentadienyl derivatives. The enhanced reactivity or "indenyl effect" has been interpreted on the basis of the ability of the π-indenyl ligand to undergo facile $\eta^5 \leftrightarrow \eta^3$ "ring-slippage", which was believed to be stabilized by the

aromatization of the indenyl 6-ring.[223, 252, 255-257, 259, 266-274] This hypothesis has been reinforced by crystal structures of several η^3-indenyl complexes.[257, 268, 269, 272]

Compared to other transition metals, the π-indenyl chemistry of cobalt remains relatively underdeveloped. π-Indenyl complexes are known for cobalt in formal oxidation states III, II and I with the most numerous being the very air sensitive Co(I) derivatives (η^5-indenyl)CoL_2 (L = ethylene,[235, 237] CO,[233, 275] PPh_3,[244, 245] PMe_3,[276] $P(OR)_3$,[277] or L_2 = cyclo- or acyclo- dienes[235, 264, 265] or vinylketenes[244, 245]). Fewer Co(III) complexes have been reported,[234, 236, 244, 245, 276] and only one crystal structure ((η^5-indenyl)Co($C_2B_9H_{11}$)) has been determined.[236] The homoleptic examples bis(indenyl)$CoPF_6$[234] and bis(indenyl)Co[278] serve to delineate bonding extrema observed for cobalt and to illustrate the dependence of indene distortion and hapticity on electronic configuration.[279] Structural studies[279] established that the 19e$^-$ Co(II) indenyl complex significantly distorts towards an η^3 bonding mode, while ^{13}C NMR data[234, 238, 279] confirmed that the 18e$^-$ Co(III) complex, bis(indenyl)$CoPF_6$, is a slightly distorted η^5-indenyl species.

A series of $[(\eta^5\text{-indenyl})Co(I_{2-n})(R_f)(L_n)]^{(n-1)+}$ (n = 1, 2; R_f = perfluoroalkyl; L = CO, P-donor) complexes, which will be used as templates for Arbuzov reactions as shown later in Chapter 3, was prepared in order to search for organometallic chiral auxiliaries with efficient chiral induction to coordinated phosphorus and to clearly define the relationship of reactivity and optical selectivity with the ligand properties in the Arbuzov dealkylation reaction as discussed in Chapter 1. This chapter presents

the synthesis, structure and analysis of the solution conformation of these complexes.[280-282]

2.2. Results and Discussion

2.2.1. Synthesis and Properties. Preparation of the title complexes was carried out according to Scheme 2-1. The known complex **2-1** was prepared[280] using a modification of the methods originally described by Bönnemann[265] and Salzer,[275] which represent the most convenient route to **2-1**, the precursor for preparation of the new π-indenyl cobalt complexes. Oxidative additions of R_fI (R_fI = C_3F_7, C_6F_{13}) to **2-1** are slow but afford complexes **2-2** and **2-3** in good yield. Facile, ambient temperature CO substitution of **2-2** and **2-3** in non-polar solvents by a stoichiometric amount of phosphorus donor ligands provided *rac*-$[(\eta^5\text{-indenyl})Co(I_{2-n})(R_f)(L_n)]^{(n-1)+}$ (n = 1, **2-4** to **2-18**) in excellent (>80%) yield. Low conversions were realized in the case of bulky PPh_3, **2-18**.

In contrast, the small, strongly nucleophilic phosphorus donor ligand PMe_3 leads to stepwise disubstitution of CO and I^- in **2-2**. Reaction with two equivalents of PMe_3 gave $[(\eta^5\text{-indenyl})Co(I_{2-n})(R_f)(L_n)]^{(n-1)+}$ (n = 2, **2-19**) as a red crystalline salt in 94% isolated yield. Except for **2-7**, which decomposes at room temperature in the solid state within several days, all the π-indenyl cobalt(III) complexes prepared in this study are air stable in the solid state, but they decompose gradually over a period of days

in solution at room temperature. They have been characterized by elemental analysis, infrared, and multinuclear NMR spectroscopy, and in the case of **2-3**, **2-6**, **2-8a** and **2-19**, by x-ray diffraction. Their physical properties are summarized in Table 2-1. NMR spectra are discussed in more detail below.

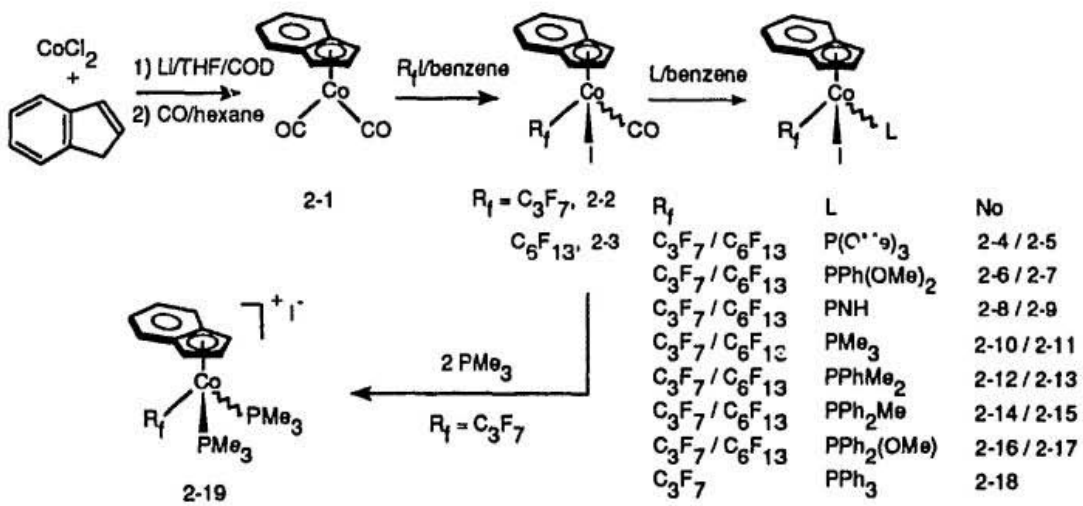

R_f	L	No
C_3F_7 / C_6F_{13}	$P(OMe)_3$	2-4 / 2-5
C_3F_7 / C_6F_{13}	$PPh(OMe)_2$	2-6 / 2-7
C_3F_7 / C_6F_{13}	PNH	2-8 / 2-9
C_3F_7 / C_6F_{13}	PMe_3	2-10 / 2-11
C_3F_7 / C_6F_{13}	$PPhMe_2$	2-12 / 2-13
C_3F_7 / C_6F_{13}	PPh_2Me	2-14 / 2-15
C_3F_7 / C_6F_{13}	$PPh_2(OMe)$	2-16 / 2-17
C_3F_7	PPh_3	2-18

Scheme 2-1

2.2.2. (η⁵-Indenyl)Co(C₃F₇)(I)(PPh₂NHC*H(Me)Ph) (2-8), An Easily Resolvable Chiral-at-Metal Complex. As described above, a Co-epimeric mixture of the title complex **2-8a,b** was initially obtained when CO in racemic **2-2** was substituted by the chiral aminophosphine L = (*S*)-(-)diphenyl-((1-phenylethyl)amino)phosphine (PNH)[283] at room temperature in benzene solution. Sublimation of benzene solvent at 0 °C/0.1 Torr afforded the crude product as a dark red-brown powder in 95% yield. TLC and ^{1}H NMR analysis showed that the crude product was almost a single diastereomer

(>99.8% **2-8a** and <0.2% **2-8b** by integration of ^{1}H NMR doublets for C*-Me at 1.25 and 0.90 ppm). Thus, in this synthesis the optical yield was equal to the chemical yield. However, the similar resolution of **2-9a** and **2-9b** was not observed when R_f was changed to C_6F_{13}.

That spontaneous resolution occurred during workup was established by three independent experiments: (i) NMR reactions at ambient temperature in benzene-d_6 established that the reaction of **2-2** with PNH was very rapid and complete conversion to **2-8** occurred during mixing to afford **2-8b:2-8a** in a kinetic product ratio of 46:54 at 22 °C; (ii) variable temperature equilibrium concentration measurements of **2-8b:2-8a** by ^{1}H NMR in benzene-d_6 (cf. Scheme 2-2) gave ΔH=2.6±0.2 kJ·mol^{-1} and ΔS=7.2±0.7 J·K^{-1}·mol^{-1} for K_{eq} = **2-8b/2-8a** leading to a calculated equilibrium ratio for **2-8b/2-8a** of 44:56 at +5 °C; and (iii) workup of the reaction by sublimation of benzene solvent at low temperature (-11 °C) afforded a 34:66 Co-epimeric mixture of **2-8b:2-8a**. Isolation of a single diastereomer by sublimation at 0 °C was therefore the result of a second order asymmetric transformation,[284] which occurred during workup. Freezing point depression from the dissolved epimeric mixture **2-8a,b** provided for the presence of a small volume of liquid phase benzene at 0 °C in which fractional crystallization of the less soluble diastereomer **2-8a**

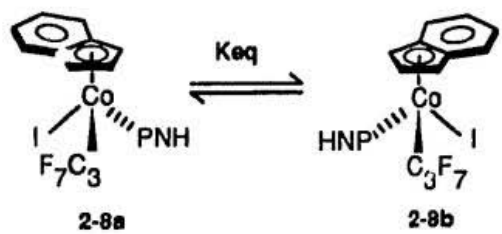

PNH = $PPh_2NHC^*H(Me)Ph$

Scheme 2-2

occurred, replenished by shifting the Co epimerization equilibrium **2-8b**⇌**2-8a**.

The facile preparation of resolved **2-8a** and the presence of a reactive Co-I bond suggested use as an organometallic chiral synthon. However, such applications of **2-8a** were severely limited by facile Co epimerization. Preliminary kinetic studies indicated that diastereomerically pure **2-8a,** like the related $CpCo^{\bullet}(L\text{-}L^{\bullet})X$ containing labile X reported by Brunner,[285] epimerized readily via a dissociative mechanism to give an 46:54 equilibrium mixture of **2-8b:2-8a**. The approach to equilibrium in benzene solution follows clean first order kinetics at 22-80 °C. However, the first order rate constants measured by NMR are irreproducible with values ranging from 10^{-6} to 10^{-4} s^{-1} at 22 °C. A single electron mechanism involving homolysis of the Co-halide bond may be responsible.

2.2.3. Crystal structures of (η⁵-Indenyl)Co(C_6F_{13})(I)(CO) (2-3), (η⁵-Indenyl)Co(C_3F_7)(I)(PPh(OMe)₂) (2-6), (S_{Co},S_C)-(η⁵-Indenyl)Co(C_3F_7)(I)(PPh2NHC*H(Me)Ph) (2-8a), and [(η⁵-Indenyl)Co(C_3F_7)(PMe_3)2]I·0.5CH_2Cl_2 (2-19). The crystal structures of complexes **2-3**, **2-6**, **2-8a** and **2-19**·0.5CH_2Cl_2 were determined using crystals grown by slow diffusion of hexane into dichloromethane solutions of these complexes at -20 °C. In the cases of **2-3** and **2-6**, the selected crystals proved to be twinned and the precision of the determined structures was therefore limited. For **2-8a**, attempts made to model a disorder involving two conformations of the C_3F_7 group which became

apparent on refinement were unsuccessful. Although giving a reduced R value, unreasonable thermal parameters throughout the molecule resulted. Therefore the structure was refined assuming the presence of a single, major conformation for the C_3F_7 group. This approach resulted in large B(eq) values for several atoms in C_3F_7 and a final Fourier difference map which showed significant peaks in the area of C_3F_7. In the case of **2-19**, ^1H and ^{13}C NMR characterization of the product, obtained by reaction of **2-2** with 2 equivalents of PMe_3, revealed the presence of a symmetry plane bisecting the indenyl ring consistent with formulation as $[(\eta^5\text{-indenyl})Co(C_3F_7)(PMe_3)_2]I$. A single crystal X-ray study confirmed the structure as $[(\eta^5\text{-indenyl})Co(C_3F_7)(PMe_3)_2]I\cdot 0.5CH_2Cl_2$, **2-19**. The solid state structure shows two chemically identical but crystallographically distinct molecules (**2-19**, **2-19'**) which share a CH_2Cl_2 solvent molecule. Although we can anticipate unequal population of both rotamers in solution, rapid rotation of $Co(PMe_3)_2(C_3F_7)$ established the time-averaged symmetry plane revealed in the NMR data.

As shown in Figures 2-1 to 2-4, the coordination sphere of cobalt in each case is best described as a distorted octahedral with η^5-indenyl occupying three *fac* coordination sites. Interligand bond angles (I-Co-CO, I-Co-C(R_t), OC-Co-C(R_t) for **2-3** ; I-Co-P, I-Co-C(R_t), P-Co-C(R_t) for **2-6** and **2-8a**; P(1)-Co-P(2), P(1)-Co-C(R_t), P(2)-Co-C(R_t) for **2-19** and **2-19'**) are all close to 90°. Atomic coordinates, selected bond lengths and bond angles are given in Tables 2-2 to 2-9. Consistent with their 18e$^-$ configurations the indenyl ring is η^5 bonded in all these complexes (**2-3, 2-6, 2-8a,**

2-19) but shows a characteristic displacement of the metal away from the C_{3a}-C_{7a} ring junction and distortions of the 5-membered ring from planarity as observed in other formally η-indenyl complexes.[238, 269, 270, 279, 286] As shown in Table 2-10, Co displacement towards C_1-C_3 (Δ(M-C) = [average of d(M-C_{3a},C_{7a})] - [average of d(M-C_1,C_3)]) is 0.16 Å for **2-3**, 0.17 Å for **2-6**, 0.20 Å for **2-8a**, 0.15 Å for **2-19** and 0.18 Å for **2-19'**. Hinge angles, defined by the intersection of the planes C_1-C_2-C_3 and C_1-C_3-C_{3a}-C_{7a}, of 5.8° for **2-3**, 4.6° for **2-6**, 10.8° for **2-8a**, 6.8° for **2-19** and 6.6° for **2-19'** as well as fold angles between the plane C_1-C_2-C_3 and the best plane containing C_{3a}-C_4-C_5-C_6-C_7-C_{7a} of 7.0° for **2-3**, 9.3° for **2-6**, 14.9° for **2-8a**, 12.4° for **2-19** and 13.6° for **2-19'** are consistent with a moderate distortion compared to a range of reported indenyl complexes.[238, 269, 270, 279, 286]

The solid state conformations of the pseudooctahedral molecules **2-3**, **2-6**, **2-8a**, **2-19** and **2-19'** are remarkably distinct with respect to rotation about the metal-indenyl centroid. Complex **2-3** adopts a conformation with the perfluoroalkyl (C_6F_{13}) group *trans* to the indenyl 6-ring, as shown in Figure 2-1. However, the solid state conformation adopted by complex **2-6** puts the $PPh(OMe)_2$ group *trans* to the indenyl 6-ring (cf. Figure 2-2), which is different from the solution conformation adopted by **2-6** (cf. later discussion). Figure 2-3 shows that **2-8a** adopts a solid state conformation which places the PNH *syn* to the ring junction carbon (C_{7a}) and the C_3F_7 group *trans* to the indenyl 6-ring. In addition, the two ligand phenyl rings "stack"[287-289] with the indenyl aromatic ring. The mean distance between the best plane defined

by the phenyl rings C(9)-C(14) and C(24)-C(29) is 3.28(2) Å with a dihedral angle of 3.0° defined by a slight tilt of C(24)-C(26) toward the plane of C(9)-C(14). The mean interplanar distances from C(3)-C(8) to the best plane of C(9)-C(14) is 3.43(2) Å with a dihedral angle of 15.4°. The measured interplanar distances are comparable to graphite (3.35 Å). This conformation is retained in solution. Reference to the crystal structure of Figure 2-3 shows that the absolute configuration of **2-8a** is S_{Co} based on the modified CIP[290-293] preference I>η^5-indenyl>PNH>R_f.

The crystal structure of **2-19** shows the presence of two chemically identical but crystallographically distinct molecules adopting different conformations in the unit cell. Conformer **2-19** (Figure 2-4a) has the C_3F_7 group *trans* to the indenyl 6-ring, but **2-19'** (Figure 2-4b) prefers a conformation in which one PMe_3 group is *trans* to the indenyl 6-ring while the C_3F_7 group is *trans* to C(3).

2.2.4. Spectroscopic Characterization of the Monosubstituted Complexes (η^5-Indenyl)Co(R_f)(I)(L) 2-2 - 2-18. The structures of the monosubstituted complexes (η^5-indenyl)Co(R_f)(I)(L), **2-2 - 2-18** prepared in this study were confirmed by ^{31}P, ^{1}H, and ^{13}C NMR spectroscopy (cf. Tables 2-11 and 2-12). ^{31}P NMR spectra (Table 2-11) show a characteristic singlet corresponding to coordinated phosphine. The ^{31}P complexation shifts ($\Delta(\delta_{complex}-\delta_{free})$) increase with increasing (positive) chemical shift of the free ligand.[294] Comparison of the isostructural pairs **2-4/2-5**, **2-6/2-7**, **2-8/2-9**, **2-10/2-11**, **2-12/2-13**, **2-14/2-15**, **2-16/2-17** shows that the perfluoroalkyl ligand has no effect on the ^{31}P chemical shift.

The presence of a chiral Co centre in (η^5-indenyl)Co(R_l)(I)(L) requires that the indenyl ring atoms (1,3; 4,7; 5,6, cf. Scheme 2-3 for indenyl ring numbering) be diastereotopic, and, in general, well resolved resonances were observed in both ^{1}H and ^{13}C NMR spectra. ^{1}H NMR assignments (cf. Table 2-11) are based on nuclear Overhauser effect difference (nOed) spectra shown in Figure 2-5 for the representative case of complex **2-10** and are supported by 2-D ^{1}H/^{13}C ^{1}J heterocorrelation spectra. Irradiation of the proton resonance at δ=5.11 ppm (Figure 2-5g) results in a 1.6% enhancement of the signal at δ=5.83 ppm and a 1.2% enhancement of the signal at δ=7.37 ppm, but no enhancement to the signal at 6.67 ppm. Irradiation of the proton resonance at δ=5.83 ppm (Figure 2-5f) shows a 1.8% enhancement at δ=5.11 ppm and a 2.8% enhancement at δ=6.67 ppm, respectively. Irradiation of the proton at δ=6.67 ppm (Figure 2-5e) results in 1.6% enhancement of the proton at δ=5.83ppm and 2.0% enhancement of the proton at δ=7.67 ppm, respectively. Accordingly, the three indenyl signals in the region of 5.0-7.0 ppm are assigned to H_1 (5.11 ppm), H_2 (5.83 ppm), H_3 (6.67 ppm), respectively. The higher field doublet (δ=7.37 ppm) is assigned to H_7 while the lower field doublet (δ=7.67 ppm) corresponds to H_4. The assignment of H_5 (7.32 ppm) and H_6 (7.52 ppm) follows from Figure 2-5a,b and is confirmed by the 2-D ^{1}H/^{13}C heterocorrelation spectrum. ^{1}H NMR spectra for the remaining complexes were assigned similarly or by comparison with complex **2-10** with

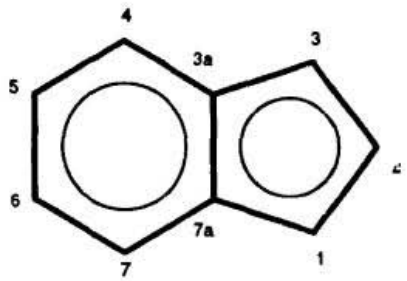

Scheme 2-3. Indenyl Ring Numbering

confirmation for some well resolved phenyl protons resonances from nOed data.

The ^{13}C NMR spectra of these complexes (cf. Table 2-12) were unambiguously assigned on the basis of 2-D $^{1}H/^{13}C$ ^{1}J heterocorrelation spectra (cf. Figure 2-6). In the case of complex **2-10** the correlations ^{13}C (96.47 ppm) with H_2 (δ=5.83 ppm), ^{13}C (81.08 ppm) with H_3 (δ=6.67 ppm), and ^{13}C (65.36 ppm) with H_1 (δ=5.11 ppm) assign the indenyl carbon atoms as C_1 (δ=65.36 ppm), C_2 (δ=96.47 ppm), and C_3 (δ=81.08 ppm), respectively. Correlations of H_4-H_7 with C_4-C_7 were also clearly observed so that the assignments of the remaining indenyl carbons presented in Table 2-12 are unambiguous. Assignments for the remaining complexes in the series were made analogously. Characteristic chemical shift patterns were observed for the phenyl ring carbons hence assignments were based on a combination of 2-D $^{1}H/^{13}C$ heterocorrelations and comparison of their $^{13}C\{^{1}H\}$ spectra.

The ^{19}F chemical shifts and coupling constants for the complexes investigated in this study are reported in Table 2-13. All complexes showed well-separated C_α-C_γ and C_α-C_ζ resonances for the perfluoropropyl and perfluorohexyl groups. The presence of the chiral Co centre and typically small vicinal couplings ($^{3}J_{FF}$=5-10 Hz) allows approximation of the diastereotopic $(CF_2)_n$ groups as a series of isolated AB spin systems. Table 2-14 collects the coupling constants $^{2}J_{F_aF_b}$ and diastereotopic chemical shift differences $\Delta\delta(F_b\text{-}F_a)$ for F_a-C_f-F_b for the (η^5-indenyl)Co(R_f)(I)(L) complexes prepared in this study. Geminal coupling $^{2}J_{F_aF_b}$ shows a marked increase

on passing from C_α to C_β but remains relatively constant further along the perfluoroalkyl chain (cf. Figure 2-7) consistent with a weakening of the C_α-F bond.[295] The diastereotopic chemical shift difference $\Delta\delta(F_b\text{-}F_a)$ for those complexes with strongly anisotropic substituents (L=CO or PPh_nR_{3-n}, n=1,2,3, entries A-K) shows a maximum at C_β (Figure 2-8a) except for the case with L = $PPh_2(OMe)$ (**2-17**, entry H). However the trimethylphosphite or trimethylphosphine derivatives show a monatomic decrease for $\Delta\delta(F_b\text{-}F_a)$ (Figure 2-8b) with increasing distance from the chiral cobalt centre.

2.2.5. Solution Conformation of the Monosubstituted Complexes (η⁵-Indenyl)Co(R$_f$)(I)(L) 2-4 - 2-18. The solution conformation shown in Scheme 2-4 for the monosubstituted derivatives **2-4** - **2-18** was derived using ^{1}H nOed. The nOed spectra of complexes **2-4** (Figure 2-9), **2-6** (Figure 2-10), **2-8a** (Figure 2-11), **2-10** (Figure 2-5) and **2-13** (Figure 2-12) are representative. The data of Figure 2-5 unambiguously show that the PMe_3 ligand is proximal to the indenyl H_1 and H_7 protons.

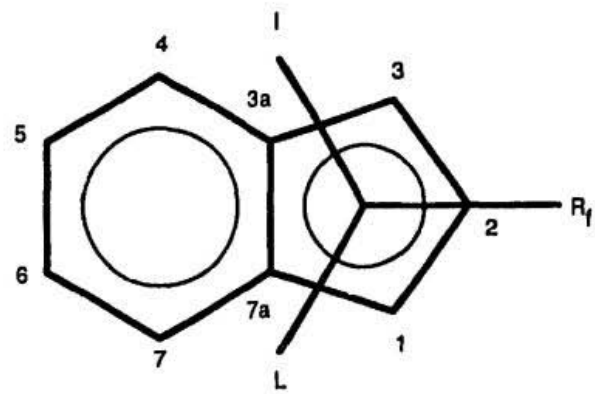

Scheme 2-4. Solution Conformation

Irradiation of the P-Me groups results in a moderate enhancement of H_1 (1.7%) and H_7 (3.0%), and a very weak enhancement of H_2 (0.5%), H_3 (0.4%) and H_4 (0.3%) (cf. Figure 2-5h). The nOed spectra of complex **2-4** (cf. Figure 2-9) are also in accord with the conformational arguments presented above. Irradiation of the P-OMe groups results in a moderate enhancement of H_1 (1.1%) and H_7 (2.3%) and a very weak enhancement to H_2 (0.3%), but no enhancement of H_3 (cf. Figure 2-9f). Successive irradiation of H_3, H_2 and H_1 reveal the proximal protons (Figure 2-9c, d, e). Consistent with the nOed results above, irradiation of the *ortho*-proton resonances of the $PPhMe_2$ ligand in complex **2-13** results in enhancements for H_7 (2.6%), H_1 (3.7%), and the diastereotopic PMe_2 groups (2.0% and 2.3%) (cf. Figure 2-12a). Irradiation of H_7 results in enhancement of the *ortho*-protons (1.8%), H_1 (4.9%), and the diastereotopic Me groups (0.9% and 1.2%), respectively (cf. Figure 2-12f). The diastereotopic PMe_2 groups could not be saturated with complete selectivity, however, Figure 2-12i,j shows that irradiation of the higher and lower field diastereotopic resonances (cf. Figure 2-12i,j) led to enhancements of H_1 (2.7%, 3.4%) and H_7 (3.4%, 2.4%) but weaker enhancement to H_2 (1.5%, 1,3%) and H_3 (0.7%, 0.4%).

The nOed spectra pattern of complex **2-6** shown in Figure 2-10 reveals that **2-6** also adopts the same solution conformation as the complexes discussed above. The solution conformation is different from the solid state conformation, which may be due to crystal packing effects. The solid state conformation of **2-8a** persists in solution as

shown in Figure 2-11, which is the nOed spectra of **2-8a** obtained at -30° on a sample containing about 20% isomer **2-8b**. Spectra f and g (cf. Figure 2-11f, g) locate nonisochronous C*H(Me)Ph ortho protons in the multiplets at 6.76 ppm (integration 3H, overlapped with H_3 and an unassigned phenyl proton) and 7.87 ppm (integration 2H, overlapped with H_7) implying a restricted C*-Ph phenyl rotation. Restricted rotation of one of the diastereotopic PPh_2 rings which is "sandwiched" between the indenyl ligand and C*-Ph is also apparent from spectrum e (Figure 2-11e) which correlates H_1 (4.50 ppm) with the doublet at 6.42 ppm (integration 1H) and the multiplet at 7.87 ppm assigned to H_7. Assignment of the 6.42 ppm signal to one nonisochronous ortho proton of a diastereotopic PPh_2 group is consistent with restricted phenyl rotation arguments presented above and suggests a solution conformation which places PNH syn to the ring junction (C_{7a}), similar to that observed in the solid state (cf. Figure 2-3). Variable temperature NMR experiments on **2-8a** were carried out to search for phenyl rotation leading to coalescence behaviour of the nonequivalent o-C_6H_5 resonances of P-Ph at 6.42 and C-Ph at 7.87 ppm. These experiments were limited by facile Co epimerization leading to an equilibrium mixture **2-8a,b** and sample deterioration at the upper temperature limit. Examination of ^1H NMR spectra recorded at 25-80 °C in C_6D_6 showed no line broadening associated with site exchange.

Two-bond phosphorus/carbon coupling constant data support the same conformational preference. The indenyl ^{13}C resonances of C_3 which are *trans* to

phosphorus (cf. Table 2-12) for all complexes with the formula (η^5-indenyl)Co(R_f)(L)(I) (**2-4** - **2-18**) are doublets with $^2J_{PC}$ equal to 10.0±2.5 Hz. No coupling was observed for C_1 which is *cis* to the phosphorus atom. In some cases coupling of C_2 to phosphorus was also detected.

2.2.6. Indenyl Distortions of the Monosubstituted Complexes (η^5-Indenyl)Co(R_f)(I)(L) 2-2 - 2-18. Literature evidence suggests that NMR chemical shift parameters are reliable indicators of distortion for transition metal organometallic π-indenyl complexes.[234, 238, 268, 271, 280-282, 296-298] The parameter $\Delta\delta^{13}C_{3a,7a}$ ($\Delta\delta^{13}C_{3a,7a}$ = $\delta^{13}C_{3a,7a}$(indenyl) - $\delta^{13}C_{3a,7a}$(Na^+indenyl$^-$)) is diagnostic of indene hapticity[234, 238, 279, 286, 299] with values in the range -10 to -40 ppm and +5 to +30 indicating η^5 and η^3 bonding, respectively.[238] The calculated $\Delta\delta^{13}C_{3a,7a}$ parameters, determined as the value for the diastereotopic ring junction carbons of all the chiral complexes **2-2** - **2-18** (cf. Table 2-15), are in the range of -23 to -15 ppm consistent with their description as moderately distorted η^5 complexes.[238, 279]

Both electronic[270, 300] and steric[243, 296, 298, 301] factors of the ancillary ligands appear to influence the extent of η^5-indenyl ring distortion as well as the preferred conformation of the ligands relative to indenyl ring in solution. Tables 2-11 and 2-12 show that ^1H and ^{13}C chemical shifts of η^5-indenyl are relatively insensitive to the perfluoroalkyl ligand for the complexes prepared in this study. The observed diastereotopic

chemical shifts for the η^5-indenyl H_1/H_3 and C_1/C_3 resonances in complexes **2-2** - **2-18**, however, are a function of the stereoelectronic parameters ($\theta(°)$ and $\chi(cm^{-1})$)[302, 303] of the phosphorus ligand. Comparative data tabulating $\Delta\delta(H_3\text{-}H_1)$ and $\Delta\delta(C_3\text{-}C_1)$ for the (η^5-indenyl)Co(R_f)(I)(L) complexes are given in Table 2-15 and Figure 2-13.

Faller and Crabtree[270, 300] have convincingly argued that preferential weakening of the Co-C_{3a} and Co-C_{7a} bonds will facilitate more significant stabilization via aromatization, hence strong *trans*-influence ligands will prefer a site *trans* to the indenyl 6-ring regardless of steric consequences. This rationale predicts that strong *trans*-influence perfluoroalkyl ligands in complexes **2-2** - **2-18** will select a conformation placing L between H_1 and H_7, *trans* to H_3 of the indenyl ring as shown in Scheme 2-4. As a consequence, the chemical shifts of H_2/C_2 are relatively insensitive to P-donor stereoelectronic parameters whereas the chemical shifts of H_1/C_1 and H_3/C_3, which are *cis* and *trans* to L respectively, correlate with P-donor steric and electronic parameters as shown in Figure 2-13 and demonstrate that a preferred rotamer is adopted by these chiral complexes in solution.

The preferred conformation of the high *trans*-influence of perfluoroalkyl ligands in this series of η^5-indenyl complexes results in weakening of the cobalt-ring junction carbon bond. The latter causes distortion of the η^5-indenyl ring and the former renders the diastereotopic chemical shifts for indenyl ^1H and ^{13}C sensitive to the ligands. Accordingly, the diastereotopic chemical shift differences $\Delta\delta(H_3\text{-}H_1)$ and $\Delta\delta(C_3\text{-}C_1)$

may provide an internal measurement of indenyl distortion in chiral complexes. Figure 2-14 shows good empirical correlations of both $\Delta\delta(H_3\text{-}H_1)$ and $\Delta\delta(C_3\text{-}C_1)$ with $\Delta\delta^{13}C_{3a,7a}$ and suggests that the diastereotopic chemical shift differences are an alternative indicator of indenyl ring distortion.

2.3. Summary

The preparation and spectroscopic and crystallographic characterization of a series of η^5-indenyl cobalt(III) iodide complexes are described. Consistent with their 18e$^-$ configurations, the indenyl ring in these complexes is η^5-bonded but both crystal and NMR parameters suggest a characteristic distortion towards η^3. ^{1}H nuclear Overhauser effect difference spectra show that all of the monosubstituted complexes prefer a solution conformation placing the perfluoroalkyl ligand *trans* to the indenyl 6-ring and the P-donor ligand *trans* to C_3.

Table 2-1. Physical Properties of η^5-Indenyl Co(III) Complexes.

Cpd.	Complex	Yield[a] (%)	Appearance	mp[b] (°C)	Anal. (C, H, N %) Calc.(Found)
2-2	$(C_9H_7)Co(C_3F_7)(I)(CO)$[c]	80	Black microcrystal	dec. >120	31.35(31.71), 1.42(1.83)
2-3	$(C_9H_7)Co(C_6F_{13})(I)(CO)$[c]	75	Black rect. plate	dec. >120	29.65(29.64), 1.09(0.88)
2-4	$(C_9H_7)Co(C_3F_7)(I)(P(OMe)_3)$	99	Black rect. plate	141-143	30.32(30.01), 2.71(2.36)
2-5	$(C_9H_7)Co(C_6F_{13})(I)(P(OMe)_3)$	82	Black rect. plate	137-140	29.05(29.23), 2.17(2.04)
2-6	$(C_9H_7)Co(C_3F_7)(I)(PPh(OMe)_2)$	93	Black prism	144-146	37.52(37.14), 2.83(2.39)
2-7	$(C_9H_7)Co(C_6F_{13})(I)(PPh(OMe)_2)$	84	Red-brown powder	110-113	[d]
2-8[e]	$(C_9H_7)Co(C_3F_7)(I)(PNH)$[f]	95	Black rect. plate	dec. 132	49.57(49.21), 3.51(3.23), 1.81(1.82)
2-9[e]	$(C_9H_7)Co(C_6F_{13})(I)(PNH)$[f]	25	Red-brown powder	102-104	45.42(45.14), 2.94(2.83), 1.51(1.53)
2-10	$(C_9H_7)Co(C_3F_7)(I)(PMe_3)$	81	Black rect. plate	128-129	32.99(32.59), 2.95(2.89)
2-11	$(C_9H_7)Co(C_6F_{13})(I)(PMe_3)$	86	Black rect. plate	153-154	31.06(31.18), 2.32(2.15)
2-12	$(C_9H_7)Co(C_3F_7)(I)(PPhMe_2)$	92	Black rect. plate	120-122	39.50(39.48), 2.98(2.99)
2-13	$(C_9H_7)Co(C_6F_{13})(I)(PPhMe_2)$	88	Black rect. plate	135-136	36.44(36.40), 2.33(2.31)
2-14	$(C_9H_7)Co(C_3F_7)(I)(PPh_2Me)$	94	Black rect. plate	111-112	44.80(45.21), 3.01(3.09)
2-15	$(C_9H_7)Co(C_6F_{13})(I)(PPh_2Me)$	95	Black rect. plate	105-106	41.00(41.44), 2.46(2.20)
2-16	$(C_9H_7)Co(C_3F_7)(I)(PPh_2(OMe))$	92	Deep-red powder	106-107	43.76(44.06), 2.94(3.15)
2-17	$(C_9H_7)Co(C_6F_{13})(I)(PPh_2(OMe))$	87	Deep-red powder	82-84	40.22(40.26), 2.41(2.58)
2-18	$(C_9H_7)Co(C_3F_7)(I)(PPh_3)$	23	Brown powder	115-117	49.20(49.19), 3.03(2.94)
2-19	$[(C_9H_7)Co(C_3F_7)(PMe_3)_2]^+I^-$	94	Deep-red prism	138-140	33.43(33.17), 3.94(3.98)[g]

[a] Yield before crystallization. [b] Sealed (N_2) capillary. [c] ν (*CO, in* CH_2Cl_2) = 2081 cm^{-1}. [d] *Decomposed at room temp. over a period of several days and was not analyzed.* [e] High R_f isomer. [f] PNH = (*S*)-(-)-$PPh_2NHC^*H(Me)Ph$. [g] Analyzed as $[(C_9H_7)Co(C_3F_7)(PMe_3)_2]_2^+I^-\cdot 0.5\ CH_2Cl_2$.

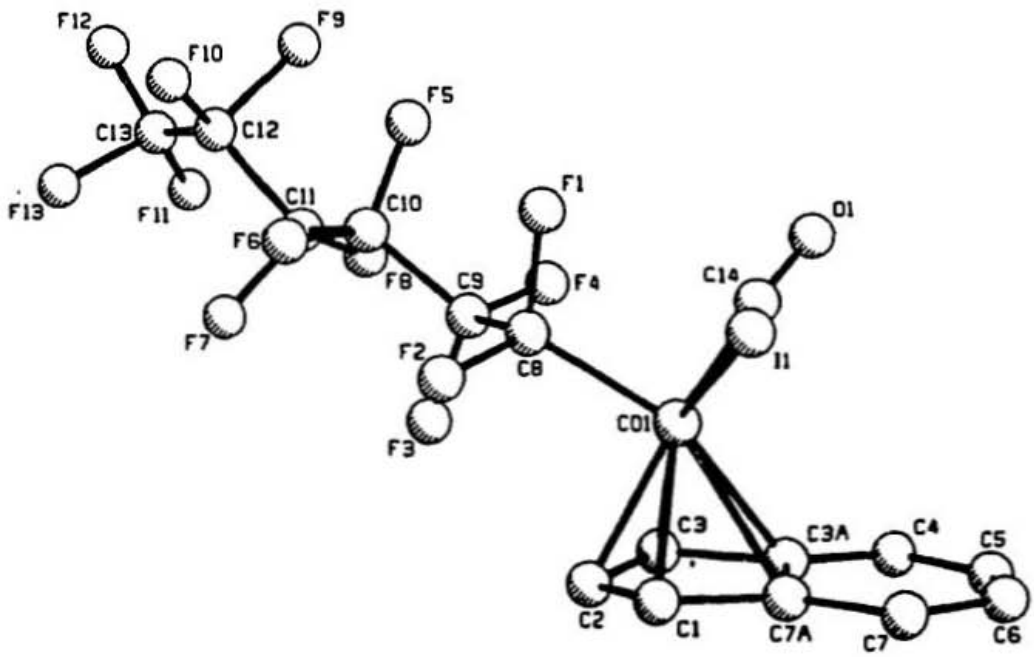

Figure 2-1. Molecular Structure of (η^5-Indenyl)Co(C_6F_{13})(I)(CO) (**2-3**)

Table 2-2. Atomic Coordinates for (η^5-Indenyl)Co(C_6F_{13})(I)(CO) (**2-3**)

atom	x	y	z	B(eq)
I(1)	0.11052(8)	0.9679(1)	0.70408(7)	4.92(5)
Co(1)	0.1679(1)	0.8382(2)	0.5736(1)	3.8(1)
F(1)	0.2493(6)	1.1103(8)	0.6159(6)	5.2(4)
F(2)	0.1478(5)	1.1103(8)	0.4793(6)	5.7(4)
F(3)	0.2423(6)	0.959(1)	0.3868(6)	7.5(5)
F(4)	0.3337(6)	0.919(1)	0.5239(7)	8.0(6)
F(5)	0.366(1)	1.204(2)	0.550(1)	13(1)
F(6)	0.2674(8)	1.269(1)	0.436(1)	10.7(8)
F(7)	0.327(1)	1.167(2)	0.3027(9)	14(1)
F(8)	0.410(1)	1.033(2)	0.397(1)	13(1)
F(9)	0.505(1)	1.258(3)	0.484(1)	16(1)
F(10)	0.405(1)	1.421(2)	0.423(1)	13(1)
F(11)	0.497(2)	1.192(2)	0.298(2)	17(2)
F(12)	0.530(1)	1.406(2)	0.351(1)	17(2)
F(13)	0.426(2)	1.380(3)	0.254(1)	19(2)
O(1)	0.3204(8)	0.774(1)	0.728(1)	7.7(7)
C(1)	0.048(1)	0.787(2)	0.488(1)	5.1(8)
C(2)	0.102(2)	0.794(2)	0.432(1)	7(1)
C(3)	0.166(1)	0.685(2)	0.465(1)	7(1)
C(3A)	0.147(1)	0.596(2)	0.541(1)	4.7(8)
C(4)	0.181(1)	0.471(2)	0.596(1)	5.3(8)
C(5)	0.141(2)	0.418(2)	0.657(1)	7(1)
C(6)	0.069(1)	0.477(2)	0.673(1)	5.4(8)
C(7)	0.034(1)	0.597(2)	0.623(1)	4.9(8)
C(7A)	0.071(1)	0.661(2)	0.553(1)	5.0(8)
C(8)	0.2106(9)	1.022(1)	0.5343(9)	3.5(6)
C(9)	0.277(1)	1.014(2)	0.476(1)	4.8(8)
C(10)	0.320(1)	1.157(2)	0.464(1)	6(1)
C(11)	0.373(1)	1.159(2)	0.397(1)	6(1)
C(12)	0.430(2)	1.296(3)	0.399(3)	12(2)
C(13)	0.477(2)	1.309(5)	0.330(3)	11(2)
C(14)	0.264(1)	0.803(2)	0.668(1)	5(1)

Table 2-3. Selected Bond Distances (Å) and Bond Angles (°) for **2-3**

Bond Distance	
I-Co	2.584(2)
Co-C14	1.83(2)
Co-C1	2.11(2)
Co-C2	2.05(1)
Co-C3	2.05(1)
Co-C3a	2.22(1)
Co-C7a	2.25(2)
Co-C8	1.94(1)
C1-C2	1.36(2)
C1-C7a	1.44(2)
C2-C3	1.44(2)
C3-C3a	1.45(2)
C3a-C4	1.39(2)
C4-C5	1.32(2)
C5-C6	1.40(3)
C6-C7	1.33(2)
C7a-C3a	1.46(2)
C7a-C7	1.43(2)
Bond Angles	
I-Co-C8	93.9(4)
I-Co-C14	89.7(5)
C8-Co-C14	91.4(6)
Co-C8-C9	119(1)
Co-C14-O1	175(2)

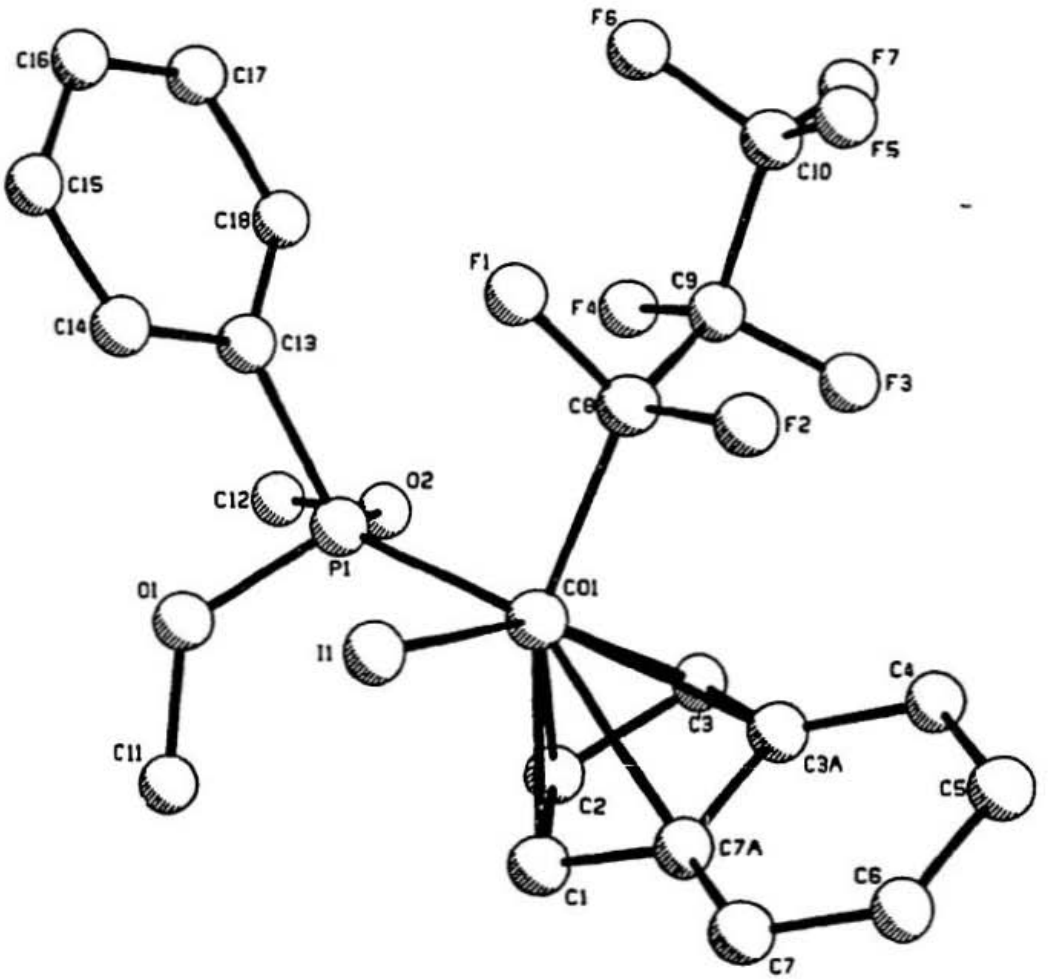

Figure 2-2. Molecular Structure of (η^5-Indenyl)Co(C_3F_7)(I)(PPh(OMe)$_2$) (**2-6**)

Table 2-4. Atomic Coordinates for (η^5-Indenyl)Co(C_3F_7)(I)(PPh(OMe)$_2$) (**2-6**)

atom	x	y	z	B(eq)
I(1)	0.10348(8)	0.0929(2)	0.24440(7)	3.93(6)
Co(1)	0.1834(1)	0.2986(3)	0.1673(1)	2.2(1)
P(1)	0.2731(3)	0.3577(6)	0.2669(2)	2.5(2)
F(1)	0.2760(5)	-0.023(1)	0.1918(5)	3.0(4)
F(2)	0.1895(5)	-0.012(1)	0.0841(5)	3.3(5)
F(3)	0.2883(6)	0.195(2)	0.0227(6)	5.6(7)
F(4)	0.3686(6)	0.246(1)	0.1288(6)	5.0(6)
F(5)	0.324(1)	-0.166(2)	0.047(1)	11(1)
F(6)	0.4129(8)	-0.083(2)	0.1407(9)	10(1)
F(7)	0.4216(8)	0.011(2)	0.0320(8)	9(1)
O(1)	0.2405(7)	0.435(2)	0.3395(5)	3.6(6)
O(2)	0.3336(6)	0.507(1)	0.2454(6)	3.2(6)
C(1)	0.095(1)	0.508(2)	0.1569(9)	2.9(8)
C(2)	0.169(1)	0.571(2)	0.1507(9)	3.1(9)
C(3)	0.194(1)	0.486(2)	0.085(1)	4(1)
C(3A)	0.126(1)	0.377(2)	0.048(1)	2.8(9)
C(4)	0.108(1)	0.284(3)	-0.023(1)	4(1)
C(5)	0.033(2)	0.208(3)	-0.043(1)	5(1)
C(6)	-0.025(1)	0.218(3)	0.003(2)	5(1)
C(7)	-0.011(1)	0.304(3)	0.071(1)	4(1)
C(7A)	0.064(1)	0.392(3)	0.094(1)	2.9(8)
C(8)	0.244(1)	0.093(2)	0.1369(9)	2.5(7)
C(9)	0.318(1)	0.125(3)	0.091(1)	3(1)
C(10)	0.369(2)	-0.035(4)	0.073(1)	6(2)
C(11)	0.179(1)	0.565(3)	0.340(1)	5(1)
C(12)	0.385(1)	0.617(3)	0.302(1)	6(1)
C(13)	0.342(1)	0.196(2)	0.3198(9)	3.1(9)
C(14)	0.318(1)	0.092(3)	0.377(1)	4(1)
C(15)	0.373(1)	-0.020(3)	0.421(1)	5(1)
C(16)	0.449(1)	-0.044(3)	0.408(1)	5(1)
C(17)	0.475(1)	0.058(3)	0.354(1)	5(1)
C(18)	0.422(1)	0.176(2)	0.309(1)	3(1)

Table 2-5. Selected Bond Distances (Å) and Bond Angles (°) for **2-6**

Bond Distance	
I-Co	2.593(3)
Co-P	2.152(5)
Co-C1	2.15(2)
Co-C2	2.08(2)
Co-C3	2.07(2)
Co-C3a	2.26(2)
Co-C7a	2.29(2)
Co-C8	1.97(2)
C1-C2	1.35(2)
C1-C7a	1.44(2)
C2-C3	1.46(2)
C3-C3a	1.45(2)
C3a-C4	1.43(2)
C4-C5	1.35(3)
C5-C6	1.39(3)
C6-C7	1.35(3)
C7a-C3a	1.45(2)
C7a-C7	1.40(2)
P-O1	1.61(1)
P-O2	1.60(1)
P-C13	1.82(2)
O1-C11	1.41(2)
O2-C12	1.46(2)
Bond Angles	
I-Co-C8	90.7(5)
I-Co-P	91.7(1)
P-Co-C8	94.6(4)
Co-P-O1	117.3(5)
Co-P-O2	108.6(4)
Co-P-C13	124.3(6)

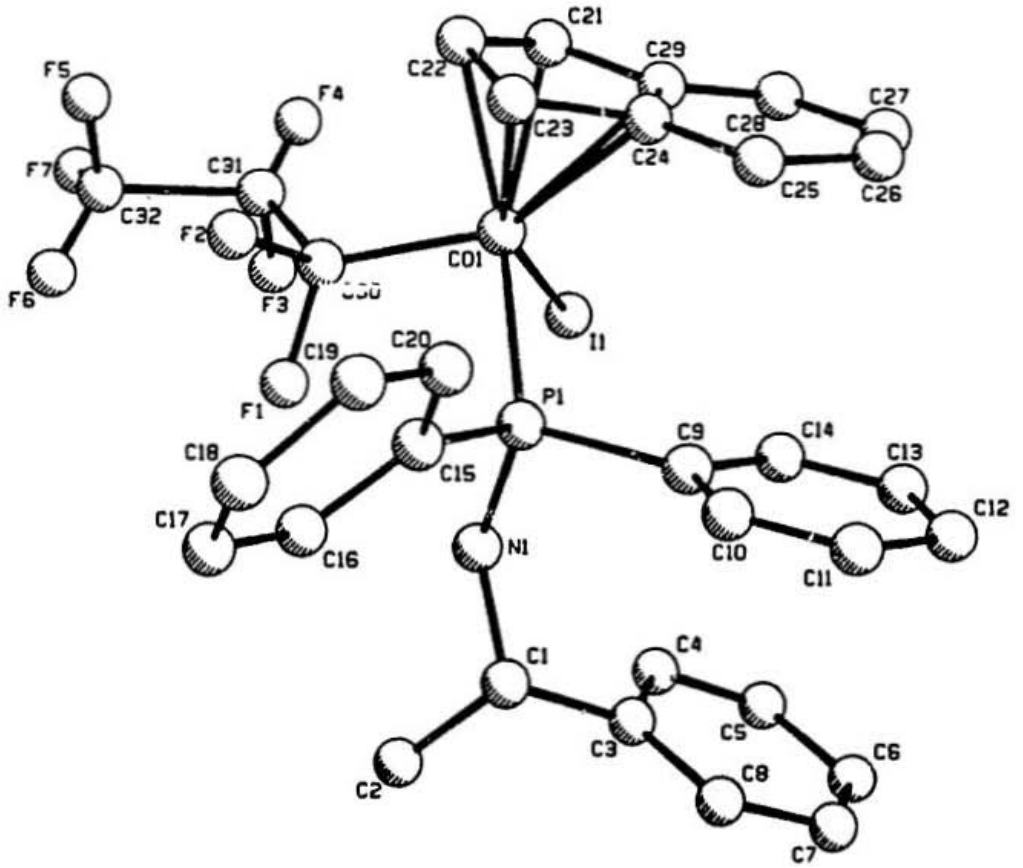

Figure 2-3. Molecular Structure of (S_{Co},S_C)-(η^5-Indenyl)Co(C_3F_7)(I)(PNH) (**2-8a**)

Table 2-6. Atomic Coordinates for (S_{Co},S_C)-(η^5-Indenyl)Co(C_3F_7)(I)(PNH) (**2-8a**)

Atom	x	y	z	B(eq)
I(1)	0.24379(7)	0.20943(7)	0.1436(1)	5.37(6)
Co(1)	0.1131(1)	0.2751(1)	0.0713(2)	3.6(1)
P(1)	0.1242(2)	0.2544(2)	-0.1655(5)	3.2(2)
F(1)	0.2252(7)	0.3660(6)	-0.054(1)	9.9(4)
F(2)	0.1120(7)	0.4151(5)	-0.009(1)	8.6(3)
F(3)	0.272(1)	0.375(1)	0.158(2)	22.9(8)
F(4)	0.1855(8)	0.3808(6)	0.263(1)	9.6(4)
F(5)	0.151(1)	0.497(1)	0.183(2)	21.1(8)
F(6)	0.242(1)	0.4951(8)	0.051(2)	13.6(5)
F(7)	0.275(1)	0.489(1)	0.246(3)	22.4(8)
N(1)	0.2213(6)	0.2540(6)	-0.223(1)	3.1(6)
C(1)	0.2494(9)	0.2279(7)	-0.359(2)	3.6(7)
C(2)	0.3201(9)	0.2689(9)	-0.413(2)	6(1)
C(3)	0.2722(8)	0.1526(8)	-0.354(2)	3.8(8)
C(4)	0.318(1)	0.130(1)	-0.236(2)	5(1)
C(5)	0.340(1)	0.062(1)	-0.231(2)	5(1)
C(6)	0.311(1)	0.017(1)	-0.335(3)	6(1)
C(7)	0.264(2)	0.040(1)	-0.446(3)	9(2)
C(8)	0.243(1)	0.109(1)	-0.461(2)	5(1)
C(9)	0.0825(8)	0.1735(8)	-0.228(2)	2.9(8)
C(10)	0.031(1)	0.1647(9)	-0.334(2)	4(1)
C(11)	0.004(1)	0.105(1)	-0.376(2)	5(1)
C(12)	0.034(1)	0.048(1)	-0.301(2)	6(1)
C(13)	0.087(1)	0.057(1)	-0.190(2)	5(1)
C(14)	0.116(1)	0.1164(9)	-0.148(2)	4.5(9)
C(15)	0.0699(9)	0.3153(7)	-0.280(2)	3.0(8)
C(16)	0.1131(8)	0.3623(8)	-0.364(2)	4.1(9)
C(17)	0.075(1)	0.4097(8)	-0.447(2)	5(1)
C(18)	-0.008(1)	0.4089(9)	-0.455(2)	5(1)
C(19)	-0.053(1)	0.366(1)	-0.366(2)	6(1)
C(20)	-0.017(1)	0.320(1)	-0.286(2)	5(1)
C(21)	0.064(1)	0.268(1)	0.278(2)	6(1)
C(22)	0.028(1)	0.320(1)	0.202(3)	7(2)
C(23)	-0.010(1)	0.297(1)	0.083(2)	5(1)
C(24)	-0.0142(8)	0.227(1)	0.092(2)	4(1)
C(25)	-0.058(1)	0.178(1)	0.006(2)	5(1)
C(26)	-0.053(1)	0.113(1)	0.057(2)	6(1)
C(27)	0.000(1)	0.094(1)	0.168(3)	7(1)
C(28)	0.040(1)	0.143(2)	0.244(2)	9(2)
C(29)	0.036(1)	0.209(1)	0.213(2)	5(1)
C(30)	0.1697	0.3612	0.0489	7.8(6)
C(31)	0.2072	0.3936	0.1792	-
C(32)	0.2119	0.4788	0.1440	39(5)

Table 2-7. Selected Bond Distances (Å) and Bond Angles (°) for **2-8a**

Bond	Distances		
I-Co	2.599(2)	C21-C22	1.39(3)
Co-P	2.275(5)	C21-C29	1.41(3)
Co-C21	2.11(2)	C22-C23	1.36(2)
Co-C22	2.07(2)	C23-C24	1.42(2)
Co-C23	2.06(1)	C24-C25	1.45(2)
Co-C24	2.30(2)	C24-C29	1.44(2)
Co-C29	2.26(2)	C25-C26	1.38(2)
Co-C30	1.962(2)	C26-C27	1.41(3)
P-N	1.68(1)	C27-C28	1.38(3)
N-C1	1.46(2)	C28-C29	1.35(3)

Bond	Angles
I-Co-P	95.7(1)
I-Co-C21	92.3(6)
I-Co-C22	128.3(8)
I-Co-C23	153.8(5)
I-Co-C24	120.7(5)
I-Co-C29	90.7(5)
I-Co-C30	94.61(8)
P-Co-C21	157.2(6)
P-Co-C22	135.8(8)
P-Co-C23	99.8(6)
P-Co-C24	94.5(4)
P-Co-C29	121.1(6)
P-Co-C30	90.9(1)
C21-Co-C30	109.8(7)
C22-Co-C30	90.3(6)
C23-Co-C30	106.1(6)
C24-Co-C30	143.4(5)
C29-Co-C30	146.9(5)

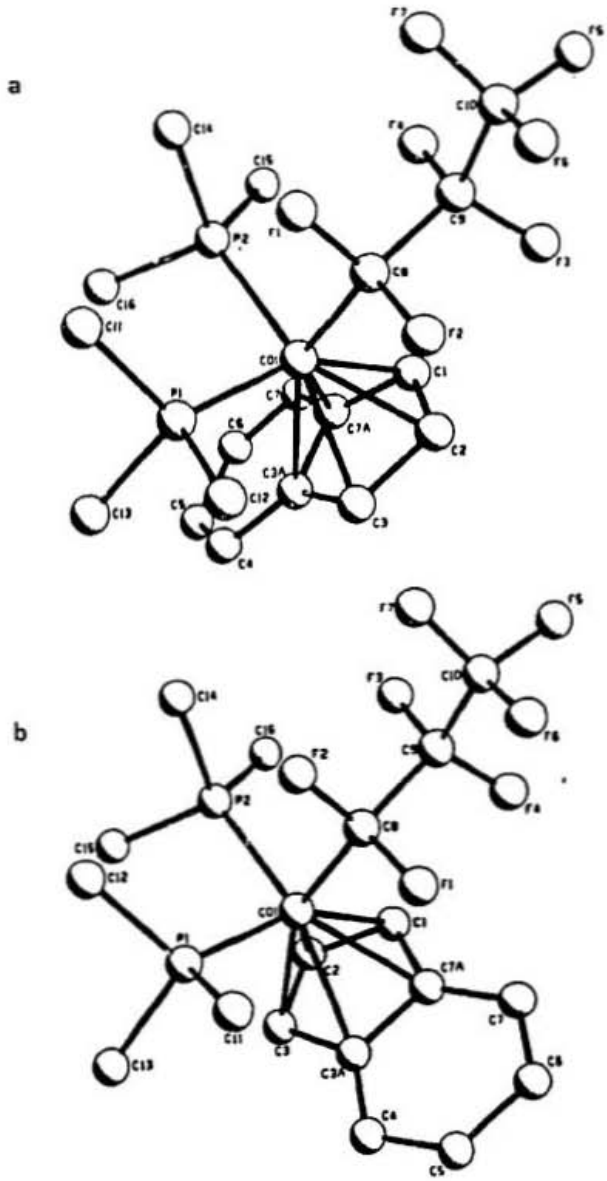

Figure 2-4. Molecular Structure of $[(\eta^5\text{-Indenyl})Co(C_3F_7)(PMe_3)_2)]^+I^-\bullet 0.5CH_2Cl_2$ (a: **2-19**, b: **2-19'**, I^- and CH_2Cl_2 omitted for clarity).

Table 2-8. Atomic Coordinates for [(η^5-Indenyl)(C_3F_7)(PMe_3)$_2$Co]$^+$I$^-$·0.5 CH_2Cl_2, **2-19** and **2-19'**

atom	x	y	z	B(eq)
I(1)	0.38906(4)	0.15836(6)	0.74481(2)	3.71(3)
I(2)	0.10274(4)	0.24785(7)	0.47472(3)	5.88(4)
Co(1)	0.68633(7)	0.2084(1)	0.40045(4)	2.73(5)
Co(1')	0.40499(6)	0.2533(1)	0.19398(4)	2.56(5)
Cl(1)	0.8305(2)	0.0961(4)	0.8765(1)	9.9(2)
Cl(2)	0.8587(2)	0.3609(4)	0.8935(1)	9.4(2)
P(1)	0.8193(1)	0.2335(2)	0.42483(8)	3.3(1)
P(1')	0.4242(1)	0.0986(2)	0.14141(8)	3.2(1)
P(2)	0.6772(2)	0.0082(2)	0.42089(9)	3.6(1)
P(2')	0.3951(1)	0.4143(2)	0.14271(8)	3.2(1)
F(1)	0.6701(3)	0.4094(5)	0.4602(2)	4.3(3)
F(1')	0.2541(3)	0.2040(5)	0.1427(2)	4.0(2)
F(2)	0.7076(3)	0.2395(5)	0.4999(2)	4.4(3)
F(2')	0.2749(3)	0.1007(5)	0.2092(2)	4.6(3)
F(3)	0.5488(3)	0.1454(6)	0.4739(2)	6.3(3)
F(3')	0.2431(3)	0.2993(6)	0.2589(2)	6.0(3)
F(4)	0.5195(3)	0.3288(6)	0.4444(2)	5.4(3)
F(4')	0.2469(3)	0.4286(5)	0.2000(2)	5.7(3)
F(5)	0.4800(4)	0.3127(7)	0.5291(2)	8.0(4)
F(5')	0.1005(4)	0.3636(8)	0.2234(2)	9.3(5)
F(6)	0.5827(5)	0.4314(8)	0.5310(3)	10.8(6)
F(6')	0.1180(4)	0.1737(8)	0.2048(3)	9.9(5)
F(7)	0.5935(5)	0.241(1)	0.5569(2)	11.7(6)
F(7')	0.1189(4)	0.3190(8)	0.1545(2)	8.9(4)
C(1)	0.5801(5)	0.2251(9)	0.3547(3)	3.7(3)
C(1')	0.4230(5)	0.3442(9)	0.2592(3)	3.4(4)
C(2)	0.6353(6)	0.1465(8)	0.3346(3)	3.5(4)
C(2')	0.4108(5)	0.214(1)	0.2650(3)	3.5(5)
C(3)	0.7043(5)	0.2151(8)	0.3291(3)	3.3(4)
C(3A)	0.6901(5)	0.3445(9)	0.3411(3)	3.0(4)
C(3')	0.4728(5)	0.1488(8)	0.2466(3)	3.2(4)
C(3A')	0.5292(5)	0.2401(9)	0.2338(3)	3.1(4)
C(4)	0.7346(6)	0.457(1)	0.3366(3)	4.4(5)
C(4')	0.6074(6)	0.232(1)	0.2202(3)	4.1(5)
C(5)	0.7009(7)	0.568(1)	0.3454(4)	5.4(6)
C(5')	0.6520(6)	0.338(1)	0.2171(3)	5.5(6)
C(6)	0.6223(8)	0.575(1)	0.3593(4)	5.2(6)
C(6')	0.6204(8)	0.457(1)	0.2267(4)	5.3(6)
C(7)	0.5777(6)	0.471(1)	0.3657(3)	4.3(5)
C(7A)	0.6114(5)	0.3511(8)	0.3561(3)	2.9(4)
C(7')	0.5461(7)	0.472(1)	0.2388(3)	4.4(5)
C(7A')	0.4983(5)	0.3636(9)	0.2424(3)	3.3(5)
C(8)	0.6583(5)	0.2792(8)	0.4598(3)	3.3(5)
C(8')	0.2891(5)	0.2170(8)	0.1896(3)	3.3(4)
C(9)	0.5721(6)	0.267(1)	0.4750(3)	4.1(5)
C(9')	0.2314(6)	0.309(1)	0.2114(3)	4.1(5)
C(10)	0.5587(8)	0.315(1)	0.5239(4)	6.4(8)

Table 2-8. cont'd

C(10')	0.1409(7)	0.290(1)	0.1985(5)	5.9(7)
C(11)	0.8459(6)	0.389(1)	0.4482(3)	4.7(5)
C(11')	0.3745(6)	0.1057(9)	0.0813(3)	4.5(5)
C(12)	0.8684(5)	0.134(1)	0.4712(3)	4.6(5)
C(12')	0.3959(6)	-0.0574(8)	0.1594(3)	5.0(5)
C(13)	0.8861(5)	0.214(1)	0.3794(3)	4.5(5)
C(13')	0.5270(6)	0.072(1)	0.1307(4)	5.6(6)
C(14)	0.6959(6)	-0.0387(8)	0.4020(3)	4.2(5)
C(14')	0.3126(5)	0.4214(9)	0.0957(3)	4.0(5)
C(15)	0.7454(6)	-0.0909(9)	0.3921(3)	5.0(5)
C(15')	0.3919(6)	0.5740(8)	0.1663(3)	4.9(5)
C(16)	0.5813(6)	-0.0670(9)	0.4027(4)	5.4(6)
C(16')	0.4832(6)	0.4216(9)	0.1100(3)	4.5(5)
C(17)	0.8205(7)	0.220(1)	0.9146(4)	8.9(9)

Table 2-9. Selected Bond Distances (Å) and Bond Angles (°) for [(η^5-Indenyl)(C_3F_7)(PMe_3)$_2$Co]$^+$I$^-$ •CH_2Cl_2, **2-19** and **2-19'**

2-19		**2-19'**	
	Distances		
Co(1)-P(1)	2.273(3)	Co(1')-P(1')	2.274(3)
Co(1)-P(2)	2.214(3)	Co(1')-P(2')	2.245(3)
Co(1)-C(1)	2.092(8)	Co(1')-C(1')	2.091(8)
Co(1)-C(2)	2.082(8)	Co(1')-C(2')	2.065(8)
Co(1)-C(3)	2.099(9)	Co(1')-C(3')	2.097(8)
Co(1)-C(3A)	2.235(8)	Co(1')-C(3A')	2.259(8)
Co(1)-C(7A)	2.261(8)	Co(1')-C(7A')	2.288(8)
Co(1)-C(8)	1.961(9)	Co(1')-C(8')	1.971(9)
C(1)-C(2)	1.41(1)	C(1')-C(2')	1.41(1)
C(1)-C(7A)	1.44(1)	C(1')-C(7A')	1.42(1)
C(2)-C(3)	1.39(1)	C(2')-C(3')	1.40(1)
C(3)-C(3A)	1.44(1)	C(3')-C(3A')	1.43(1)
C(3A)-C(7A)	1.43(1)	C(3A')-C(7A')	1.44(1)
	Angles		
P(1)-Co(1)-P(2)	97.3(1)	P(1')-Co(1')-P(2')	97.1(1)
P(1)-Co(1)-C(1)	156.3(3)	P(1')-Co(1')-C(1')	155.0(3)
P(1)-Co(1)-C(2)	126.9(3)	P(1')-Co(1')-C(2')	120.6(3)
P(1)-Co(1)-C(3)	92.8(3)	P(1')-Co(1')-C(3')	89.2(3)
P(1)-Co(1)-C(3A)	92.5(2)	P(1')-Co(1')-C(3A')	95.5(2)
P(1)-Co(1)-C(7A)	123.7(2)	P(1')-Co(1')-C(7A')	129.1(3)
P(1)-Co(1)-C(8)	90.8(3)	P(1')-Co(1')-C(8')	91.8(3)
P(2)-Co(1)-C(1)	99.6(3)	P(2')-Co(1')-C(1')	102.9(3)
P(2)-Co(1)-C(2)	84.4(3)	P(2')-Co(1')-C(2')	142.1(3)
P(2)-Co(1)-C(3)	108.1(3)	P(2')-Co(1')-C(3')	149.9(3)
P(2)-Co(1)-C(3A)	146.1(2)	P(2')-Co(1')-C(3A')	111.8(2)
P(2)-Co(1)-C(7A)	137.8(2)	P(2')-Co(1')-C(7A')	90.0(2)
P(2)-Co(1)-C(8)	96.2(3)	P(2')-Co(1')-C(8')	96.3(3)
C(1)-Co(1)-C(8)	103.7(4)	C(1')-Co(1')-C(8')	100.7(4)
C(2)-Co(1)-C(8)	142.0(4)	C(2')-Co(1')-C(8')	87.5(4)
C(3)-Co(1)-C(8)	154.7(3)	C(3')-Co(1')-C(8')	113.0(4)
C(3A)-Co(1)-C(8)	116.1(3)	C(3A')-Co(1')-C(8')	149.8(3)
C(7A)-Co(1)-C(8)	93.2(3)	C(7A')-Co(1')-C(8')	137.6(3)

Table 2-10. Solid State Distortion Parameters of $[(\eta^5\text{-Indenyl})Co(I_{2-n})(R_t)(L_n)]^{(n-1)+}$ Complexes.

cpd.	Hinge angle (°)[a]	Fold angle (°)[a]	Δ(M-C) (Å)[b]
2-3	5.8	7.0	0.16(3)
2-6	4.6	9.3	0.17(4)
2-8a	10.8	14.9	0.20(3)
2-19	6.8	12.4	0.15(2)
2-19'	6.6	13.6	0.18(2)

[a] Hinge angle = the angle between plane C_1-C_2-C_3 and plane C_1-C_3-C_{3a}-C_{7a}; Fold angle = the angle between plane C_1-C_2-C_3 and plane C_{3a}-C_4-C_5-C_6-C_7-C_{7a}. [b] Δ(M-C)= [average of d(M-$C_{3a,7a}$)] - [average of d(M-$C_{1,3}$)].

Table 2-11. ^{1}H and ^{31}P NMR for η^5-Indenyl Co(III) Complexes[a,b,c,d,e]

Cpd	H_1	H_2	H_3	H_4	H_5	H_6	H_7	C_6H_5	Me	^{31}P	$\Delta(\delta_{MP}-\delta_P)$
2-2	5.80	5.90	6.84	7.74 (d,8.5)	7.62 (t,8.4)	7.43 (t,8.3)	7.53 (d,8.5)				
2-3	5.80	5.90	6.85	7.74 (d,8.3)	7.63 (t,8.2)	7.42 (t,8.3)	7.52 (d,8.3)				
2-4	5.27	5.79	6.38	7.51 (d,8.0)	7.28-7.40		7.42		3.62 (d,10.3)	138.89	-2.84
2-5	5.28	5.78	6.37	7.50 (d,8.0)	7.27-7.41		7.42		3.62 (d,10.4)	138.90	-2.83
2-6	4.88	5.68	6.47	7.53 (d,7.8)	7.26/7.48(m)[f]		7.16 (d,7.8)	7.26(m)[g] 7.48(m)[g] 7.77(m)[h]	3.56 (d,10.8)	170.50	9.43
2-7	4.91	5.68	6.46	7.53 (d,7.8)	7.25/7.48(m)[f]		7.17 (d,7.8)	7.25(m)[g] 7.48(m)[g] 7.78(m)[h]	3.56 (d,10.9)	170.67	9.60
2-8a	4.50	5.65	6.63[f]		6.40-7.90[f]		7.87(m)			73.29	36.65
2-8b	4.64	5.65			6.40-7.90[f]		7.88(m)			74.96	38.32
2-9[k]	4.52	5.65	6.63[f]		6.40-7.90						
2-10	5.11	5.83	6.67	7.67 (d, 8.4)	7.32 (t, 8.5)	7.52 (t, 8.4)	7.37 (d, 8.4)		1.38 (d, 12.2)	8.35	68.89
2-11	5.12	5.83	6.67	7.67 (d, 8.4)	7.32 (t, 8.3)	7.52 (t, 8.4)	7.37 (d, 8.4)		1.39 (d, 10.8)	8.39	68.93
2-12	4.57	5.61	6.55	7.50[f]	7.22 (t, 8.3)	7.06 (t, 8.2)	6.35 (d, 8.4)	7.50 (m)[g] 7.75 (m)[h]	1.81 (d, 9.7) 1.73 (d, 9.9)	12.33	57.27

Table 2-11. cont'd

2-13	4.58	5.60	6.56	7.50[f]	7.21 (t, 7.6)	7.06 (t, 7.8)	6.33 (d, 7.8)	7.50 (m)[g] 7.76 (m)[h]	1.83 (d, 10.7) 1.75 (d, 10.6)	12.21	57.15
2-14	4.94	5.70	6.68	7.40[f]	7.26 (t, 7.5)	6.96 (t, 7.6)	6.30 (d, 7.8)	[m]	2.02 (d, 10.1)	23.71	50.07
2-15	4.96	5.69	6.67	7.40[f]	7.26 (t, 7.6)	6.95 (t, 7.6)	6.29 (d, 7.8)	[m]	2.03 (d, 10.2)	23.84	50.20
2-16	4.74	5.67	6.47	[f]	[f]	[f]	6.85 (m)	7.06-7.52 (m)	3.29 (d, 10.8)	141.98	24.60
2-17	4.85	5.75	6.55	[f]	[f]	[f]	6.94 (m)	7.14-7.60 (m)	3.37 (d, 9.9)	141.74	24.36
2-18	4.40	6.02	6.75	7.82 (d, 8.2)	[f]	[f]	6.22 (d, 8.3)	7.10-7.53 (m)		34.73	39.66
2-19[n]	6.34 (d,2.7)[o]	6.09	6.34 (d,2.7)[o]	7.90 (m)	7.77 (m)	7.77 (m)	7.90 (m)		1.71 (t, 5.6)	12.50	73.04

[a] ^{1}H (300.1 MHz) NMR chemical shifts in ppm relative to TMS. [b] ^{31}P (121.5 MHz) NMR chemical shifts in ppm relative to external 85% H_3PO_4. [c] ^{31}P NMR of free ligands in $CDCl_3$: PMe_3, -60.54; $PPhMe_2$, -44.94; PPh_2Me, -26.36; PPh_3, -4.93; $PPh_2(OMe)$, 117.38; $PPh(OMe)_2$, 161.07; $P(OMe)_3$, 141.73; $PPh_2NHC^*H(Me)Ph$ (PNH), 36.64. [d] Solvent = $CDCl_3$; m = multiplet; d = doublet; t = triplet; J values in Hz are given in brackets. [e] Coupling constants of indenyl protons (H_4-H_7) are $^3J_{HH}$; Coupling constants for Me are J_{PH}; All indenyl proton peaks show further small, unresolved coupling (0.3-1.5 Hz). [f] Overlapped with phenyl resonances. [g] H_{meta}, H_{para}. [h] H_{ortho}. [i] Phenyl protons: 6.40-7.90; 6.63 (m, 2H, H_3 and H_{ortho} (C*-Ph)), 6.42 (d, 1H, H_{ortho} (P-Ph)), 7.87 (m, 2H, H_7 and H_{ortho} (C*-Ph)). [j] **2-8a** C*H: 3.66 (m), C*-Me: 1.25 (d, 6.5), NH: 2.98 (m); **2-8b** C*H: 3.66 (m), C*-Me: 0.90 (d, 6.5), NH: 2.82 (m). [k] High R_f isomer. [l] C*H: 3.65 (m), C*-Me: 1.25 (d, 6.8), NH: 3.00 (m). [m] Two phenyl signals appear as two multiplets at 7.36-7.51 and 7.54-7.64 ppm, respectively. [n] Solvent = acetone-d_6. [o] J_{PH}.

Table 2-12. ^{13}C NMR for η^5-Indenyl Co(III) Complexes[a].

Cpd	C_1	C_2	C_3	C_{3a}/C_{7a}	C_4	C_5	C_6	C_7	$\underline{C}_6H_5$[a]	Me and others
2-2	71.79	95.34	87.88	111.63, 109.45	128.69	133.07	132.25	124.04		CO: 197.86
2-3	71.94	95.37	87.95	111.65, 109.46	128.72	133.12	132.31	124.12		CO: 197.78
2-4	68.94	94.67 (d,5.9)	82.05 (d,12.4)	112.34, 110.19	127.79	130.64	130.53	126.33		55.64 (d, 9.5)
2-5	69.07	94.63	81.92 (d,11.9)	112.28, 110.22	127.81	130.63	130.55	126.33		55.64 (d, 7.8)
2-6	70.72	94.82	79.82 (d,11.3)	113.70, 109.92	127.46	130.08	128.00	125.79	134.94[c], 131.35[d], 131.06[d] 128.13[e], 131.48[f], 131.17[f]	56.73 (d, 9.0) 55.34 (d, 9.0)
2-7	70.80	94.65	79.64 (d,11.2)	113.65, 109.93	-	-	-	-	125.79-135.30	56.68 (d, 9.2) 55.41 (d, 11.2)
2-8a	72.52	94.74 (d,8.8)	78.16 (d,8.2)	112.78, 111.27	-	-	-	-	124.32-145.37	27.21 (d, 4.0) CH: 54.71(d,12.4)
2-9a	72.56	94.82 (d,8.1)	78.57 (d,9.4)	112.53, 111.71	-	-	-	-	124.35-145.63	27.24 (d, 3.2) CH: 54.69(d,12.4)
2-10	65.36	96.47 (d,6.2)	81.08 (d,7.6)	111.32, 110.89	130.04	131.70	129.81	123.43		16.99 (d, 32.4)
2-11	65.46	96.47 (d,8.3)	81.10 (d,7.7)	111.35, 110.81	130.06	131.70	129.82	123.43		17.01 (d, 32.2)
2-12	70.50	93.65 (d,6.4)	77.65 (d,9.2)	113.30, 108.20	127.65	131.00	130.19	124.08	136.10[c], 130.58[d], 130.48[d] 130.19[e], 128.53[f], 128.41[f]	17.95 (d, 34.8) 16.97 (d, 27.9)
2-13	70.69	93.73 (d,7.5)	77.54 (d,9.6)	113.63, 108.32	127.69	131.10	130.21	124.18	136.10[c], 130.65[d], 130.55[d] 130.21[e], 128.60[f], 128.49[f]	18.16 (d, 35.2) 17.03 (d, 29.9)

Table 2-12. cont'd

2-14	70.85	93.21	79.09 (d,8.4)	113.23, 110.04	130.24	131.20	130.98	124.21	133.37[c], 133.30[c], 132.98[d] 132.85[d], 132.80[d], 132.67[d] 130.43[e], 128.29[f], 128.14[f]	18.91 (d,33.1)
2-15	70.95	93.16	78.98 (d,6.9)	113.26, 109.90	130.24	131.24	130.96	124.27	134.03[c], 133.47[c], 132.93[d] 132.80[d], 132.68[d], 130.41[e] 128.16[f], 128.04[f]	19.00 (d,33.1)
2-16	71.36	95.07	80.37 (d,9.4)	113.97, 111.84	130.92	131.37	131.11	125.27	134.[illegible][c], 134.16[c], 133.20[d] 133.06[d], 132.80[d], 132.66[d] 131.11[e], 127.80[f], 127.64[f] 127.50[f]	56.61 (d,10.5)
2-17	71.36	95.12	80.25 (d,10.2)	113.93, 111.79	130.86	131.32	131.03	125.27	134.65[c], 134.20[c], 133.20[d] 133.07[d], 132.70[d], 132.56[d] 131.03[e], 127.73[f], 127.57[f] 127.43[f]	56.54 (d,5.2)
2-18	72.84	95.76 (d,9.4)	78.37 (d,9.5)	114.96, 112.24	128.05	132.03	131.27	124.44	134.90[c], 133.05, 132.90 131.50, 130.31, 129.15 127.65, 127.53	
2-19[b]	76.80	99.64	76.80	112.40	127.19	133.50	133.50	127.19		18.61 (t, 16.3)

[a] ^{13}C (75.47 MHz) NMR chemical shifts in ppm relative to solvent $CDCl_3$ = 77.00; d = doublet; J values in Hz given in brackets, J_{PC}; perfluoroalkyl carbons distributed in the chemical shift range of 105-140 ppm with very weak intensity. [b] solvent = acetone-d_6 (29.80, 206.00 ppm). [c] $C_{\alpha\text{-}\beta}$ (d, $^1J_{PC}$ = 45-52 Hz). [d] C_{ortho}. [e] C_{para}. [f] C_{meta}.

Table 2-13. ^{19}F NMR for η^5-Indenyl Co(III) Complexes[a].

Cpd	$C_\alpha F_2$	$C_\beta F_2$	$C_\gamma F_2$	$C_\delta F_2$	$C_\varepsilon F_2$	CF_3
	F_a, F_b	F_a, F_b	F_a, F_b	F_a, F_b	F_a, F_b	
2-2	-47.59, -51.15 (d, 208.1)	-111.94, -115.70 (d, 278.0)				-79.73
2-3	-47.16, -49.32 (d, 210.6)	-106.32, -112.39 (d, 286.6)	-120.63, -122.38 (d, 298.8)	-122.55, -123.62 (d, 301.0)	-126.06, -127.17 (d, 294.5)	-81.32
2-4	-56.21, -63.29 (d, 228.3)	-112.95, -114.60 (d, 281.2)				-79.58
2-5	-54.97, -63.25 (d, 230.6)	-107.78, -111.33 (d, 284.0)	-120.96, -122.18 (d, 295.3)	-122.48, -123.49 (d, 307.8)	-126.07, -127.07 (d, 294.6)	-81.31
2-6	-57.02, -57.58 (d, 230.0)	-109.75, -112.70 (d, 279.1)				-79.73
2-8a	-58.17, -58.57 (d, 247.6)	-107.86, -112.19 (d, 277.3)				-79.96
2-10	-55.76, -65.68 (d, 233.8)	-112.95, -115.24 (d, 280.5)				-79.31 (t,12.4)
2-11	-54.42, -65.57 (d, 234.2)	-107.74, -111.87 (d, 288.0)	-120.63, -122.01 (d, 299.32)	-122.48, -123.60 (d, 306.5)	-126.09, -127.04 (d, 293.3)	-81.32 (t, 9.5)
2-12	-58.94, -58.94	-108.29, -113.82 (d, 277.9)				-79.59 (t,10.5)
2-13	-57.77, -58.58 (d, 227.9)	-103.56, -110.23 (d, 284.5)	-120.90, -122.06 (d, 292.9)	-122.89, -122.89	-126.53, -126.53	-81.27 (t,10.8)
2-14	-57.35, -58.16 (d, 227.7)	-109.18, -112.86 (d, 276.87)				-79.76 (t,10.8)

Table 2-13. cont'd

2-15	-56.67, -57.21 (d, 229.2)	-104.80, -108.97 (d, 283.5)	-121.62, -121.62	-122.95, -122.95	-126.60, -126.60	-81.30 (t, 9.9)
2-16	-55.71, -57.33 (d, 228.4)	-109.81, -111.65 (d, 278.0)				-79.88
2-17	-54.22, -56.99 (d, 222.5)	-106.71, -106.71	-121.13, -122.40 (d, 295.0)	-122.57, -123.34 (d, 290.1)	-126.22, -127.01 (d, 293.6)	-81.30
2-18	-54.05, -54.73 (d, 224.9)	-108.47, -111.62 (d, 274.5)				-80.02
2-19[b]	-71.09	-112.84				-78.16 (t,12.32)

[a] 282.4 MHz, chemical shifts in ppm relative to $CFCl_3$; solvent = $CDCl_3$; $^2J_{FaFb}$, and $^3J_{FF}$ in the case of CF_3, in Hz given in brackets; all CF_2 peaks show further unresolved coupling of ca. 5-10 Hz (^3J and ^4J). [b] solvent = acetone-d_6.

Table 2-14. Correlation of ^{19}F NMR Parameters with Ligand Properties for (η^5-indenyl)Co(R_f)(I)(L) Complexes.[a]

L	R	$C_\alpha F_a F_b$		$C_\beta F_a F_b$		$C_\gamma F_a F_b$		$C_\delta F_a F_b$		$C_\varepsilon F_a F_b$		[b]
		$\Delta\delta(F_b\text{-}F_a)$	$^2J_{FaFb}$	$\Delta\delta(F_b\text{-}F_a)$	$^2J_{FaFb}$	$\Delta\delta(F_b\text{-}F_a)$	$^2J_{FaFb}$	$\Delta\delta(F_b\text{-}F_a)$	$^2J_{FaFb}$	$\Delta\delta(F_b\text{-}F_a)$	$^2J_{FaFb}$	
CO	C_3F_7	3.56	208.1	3.76	278.0							A
CO	C_6F_{13}	2.16	210.6	6.07	286.6	1.75	298.8	1.07	300.9	1.11	294.5	B
$PPh(OMe)_2$	C_3F_7	0.56	229.9	2.95	279.1							C
PNH[c]	C_3F_7	0.40	247.6	4.33	277.3							D
PPh_2Me	C_3F_7	0.81	227.7	3.68	276.9							E
PPh_2Me	C_6F_{13}	0.54	229.2	4.17	283.5	0	-	0	-	0	-	F
$PPh_2(OMe)$	C_3F	1.62	228.4	1.84	278.0							G
$PPh_2(OMe)$	$C_{\cdot}$	2.77	222.5	0	-	1.27	295.0	0.77	290.1	0.79	293.6	H
$PPhMe_2$	C_3F_7	0	-	4.91	277.9							I
$PPhMe_2$	C_6F_{13}	0.81	227.8	6.67	284.5	1.16	292.9	0	-	0	-	J
PPh_3	C_3F_7	0.70	224.9	3.15	274.5							K
$P(OMe)_3$	C_3F_7	7.08	228.3	1.65	281.2							M
$P(OMe)_3$	C_6F_{13}	8.28	230.6	3.55	284.0	1.22	295.3	1.01	307.8	1.00	294.6	N
PMe_3	C_3F_7	9.92	233.8	2.29	280.9							O
PMe_3	C_6F_{13}	11.15	234.2	4.13	288.0	1.38	299.3	1.12	306.5	0.95	293.3	P

[a] $\Delta\delta(F_b\text{-}F_a) = \delta_{Fb} - \delta_{Fb}$ in ppm; $^2J_{FaFb}$ in Hz. [b] Legend used in Figures 2-7 & 2-8. [c] PNH = (*S*)-$PPh_2NHC^*H(Me)Ph$.

Table 2-15. Distortion, Electronic and Stereochemical Parameters for the (η^5-Indenyl)Co(R_f)(I)(L) Complexes.

L	R	$\Delta\delta(H_3\text{-}H_1)$[a]	$\Delta\delta(C_3\text{-}C_1)$[b]	$\Delta\delta(C_{3a,7a})$[c] (Ave.)	θ(°)[d]	χ (cm^{-1})[d]
PMe_3	C_3F_7	1.56	15.72	-19.38, -19.81 (-19.60)	118	8.55
PMe_3	C_6F_{13}	1.55	15.64	-19.35, -19.89 (-19.62)	118	8.55
$PPhMe_2$	C_3F_7	1.98	7.15	-17.40, -22.50 (-19.95)	122	10.60
$PPhMe_2$	C_6F_{13}	1.98	6.85	-17.07, -22.38 (-19.73)	122	10.60
PPh_2Me	C_3F_7	1.74	8.24	-17.47, -20.66 (-19.07)	136	12.10
PPh_2Me	C_6F_{13}	1.71	8.03	-17.44, -20.80 (-19.12)	136	12.10
$PPh_2(OMe)$	C_3F_7	1.73	9.01	-16.73, -18.86 (-17.80)	132	16.30
$PPh_2(OMe)$	C_6F_{13}	1.70	8.89	-16.77, -18.91 (-17.84)	132	16.30
PPh_3	C_3F_7	2.35	5.53	-15.74, -18.46 (-17.10)	145	13.25
CO	C_3F_7	1.04	16.09	-19.05, -21.24 (-20.14)	-	-
CO	C_6F_{13}	1.05	16.01	-19.07, -21.25 (-20.16)	-	-
$PPh(OMe)_2$	C_3F_7	1.59	9.10	-17.00, -20.78 (-18.89)	120	19.45
$PPh(OMe)_2$	C_6F_{13}	1.55	8.84	-17.05, -20.77 (-18.91)	120	19.45
$P(OMe)_3$	C_3F_7	1.11	13.11	-18.36, -20.51 (-19.44)	107	24.10
$P(OMe)_3$	C_6F_{13}	1.09	12.85	-18.42, -20.48 (-19.45)	107	24.10
PNH*	C_3F_7	2.13	6.01	-18.17, -18.99 (-18.58)	140	10.50
PNH*	C_6F_{13}	2.11	5.64	-17.92, -19.43 (-18.68)	140	10.50

[a] $\Delta\delta(H_3\text{-}H_1) = \delta(H_3) - \delta(H_1)$ (ppm). [b] $\Delta\delta(C_3\text{-}C_1) = \delta(C_3) - \delta(C_1)$ (ppm). [c] $\Delta\delta(C_{3a,7a}) = \delta[C_{3a,7a}(\text{indenyl})] - \delta[C_{3a,7a}(\text{Na}^+\text{indenyl})]$, $\delta[C_{3a,7a}(\text{Na}^+\text{indenyl})] = 130.70$ ppm[238, 279]. [d] parameters obtained from references[302, 303]. * PNH = *S*-$PPh_2NHCH(Me)Ph$.

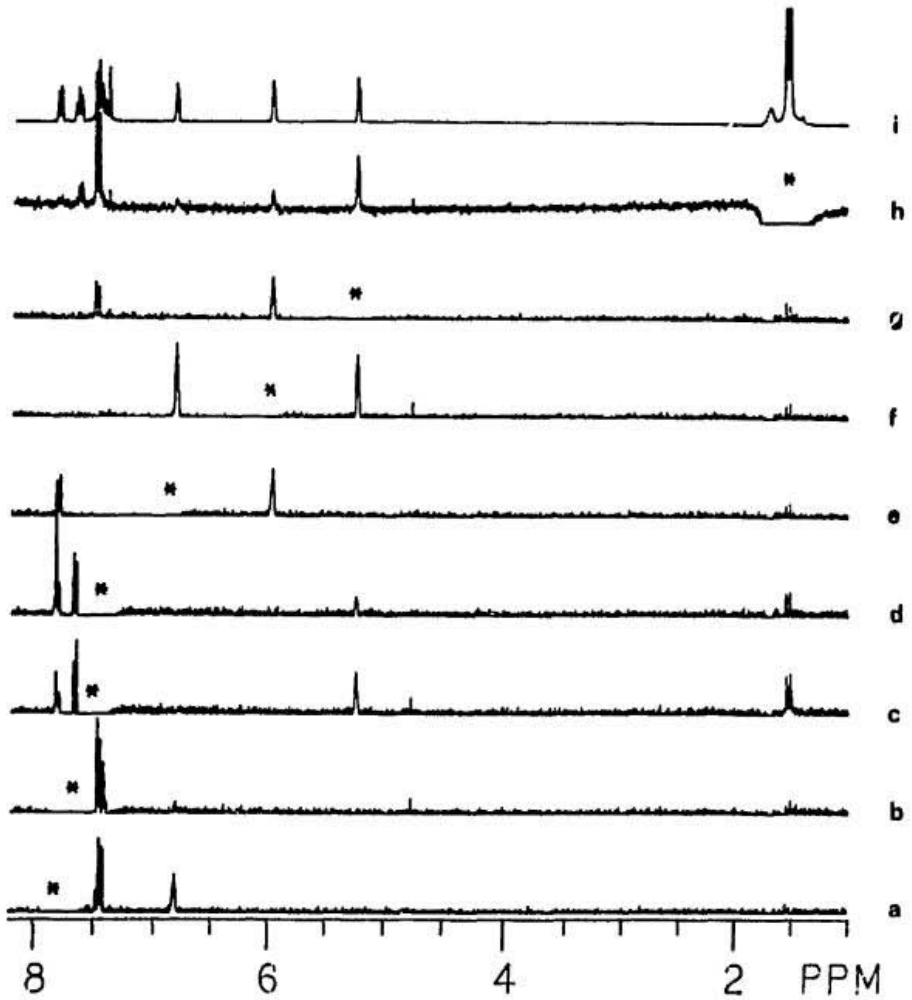

Figure 2-5. ^{1}H nOed spectra for (η^5-Indenyl)Co(C_3F_7)(I)(PMe_3), **2-10**. (i) reference spectrum; (a-h) difference spectra (64x) for irradiation at the indicated (*) frequency; (a) H_4; (b) H_6 (c & d) H_7 & H_5; (e) H_3; (f) H_2; (g) H_1; (h) Me.

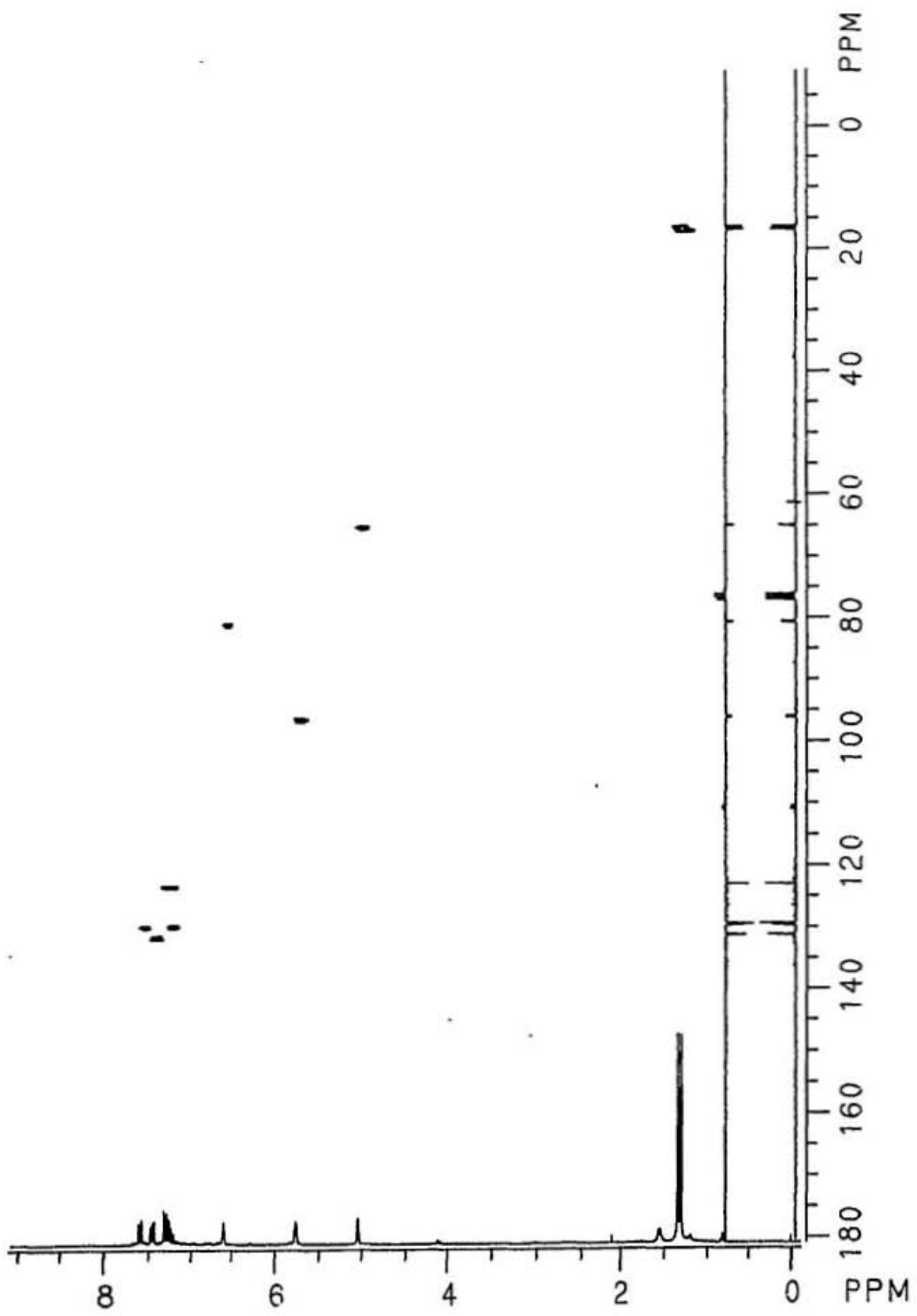

Figure 2-6. $^{1}H/^{13}C$ ^{1}J Heterocorrelation Spectrum for (η^5-Indenyl)Co(C_3F_7)(I)-(PMe_3), **2-10**.

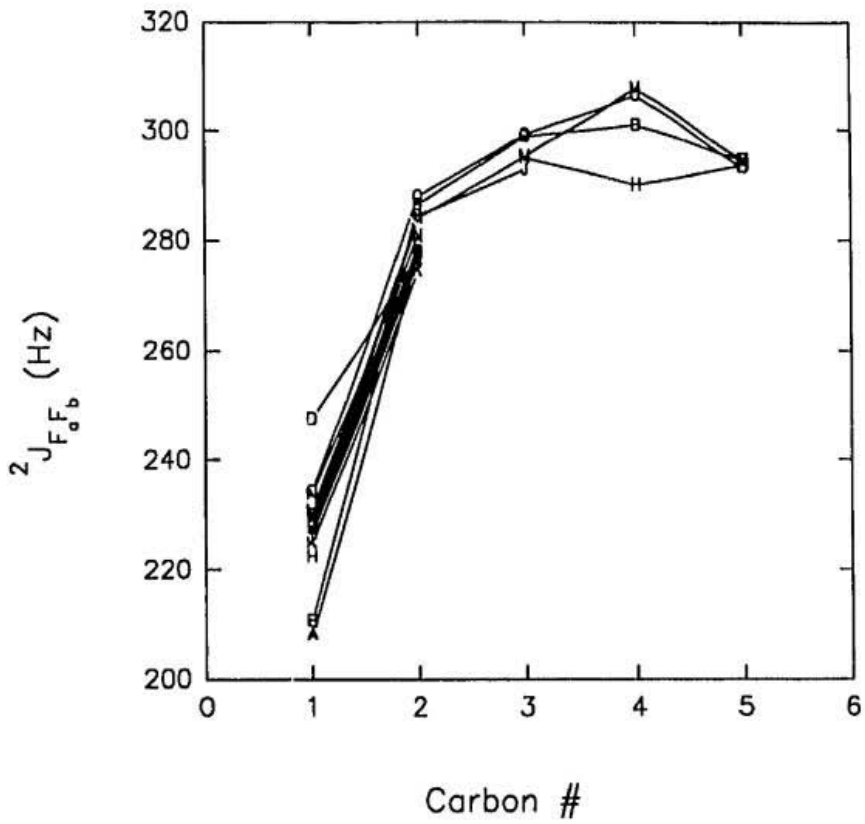

Figure 2-7. Dependence of the ^{19}F Coupling Constants on Position for (η^5-indenyl)Co(F_i)(I)(L) Complexes (cf. Table 2-14 for legend).

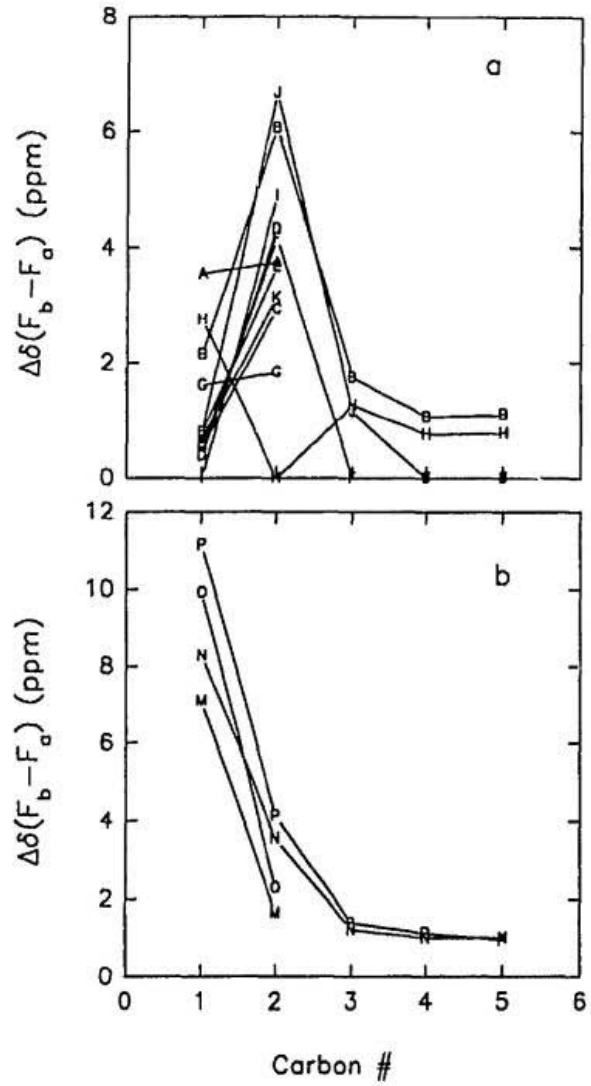

Figure 2-8. Dependence of Diastereotopic ^{19}F Chemical Shift Difference $\Delta\delta(F_b\text{-}F_a)$ on Position for (η^5-indenyl)Co(R_l)(I)(L) Complexes (cf. Table 2-14 for legend).

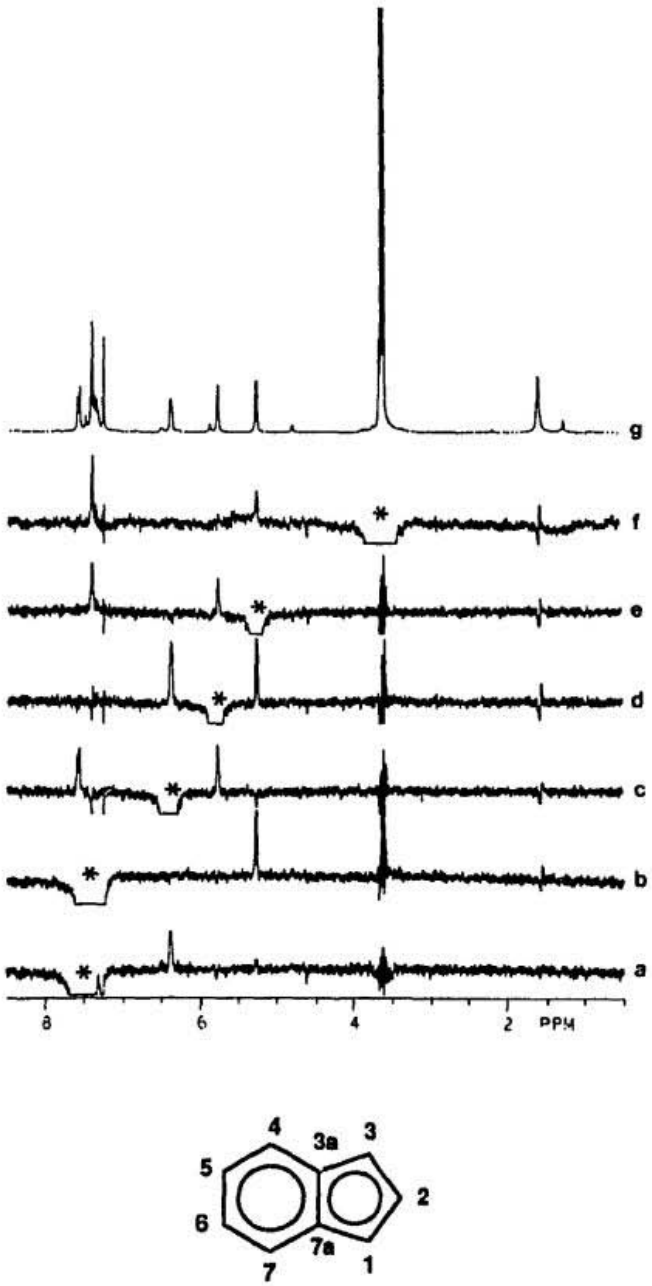

Figure 2-9. ^1H nOed Spectra for (η^5-Indenyl)Co(C_3F_7)(I)($P(OMe)_3$), **2-4**. (g) reference spectrum; (a-f) difference spectra (32x) for irradiation at the indicated (*) frequency; (a) H_4; (b) H_7; (c) H_3; (d) H_2; (e) H_1; (f) OCH_3

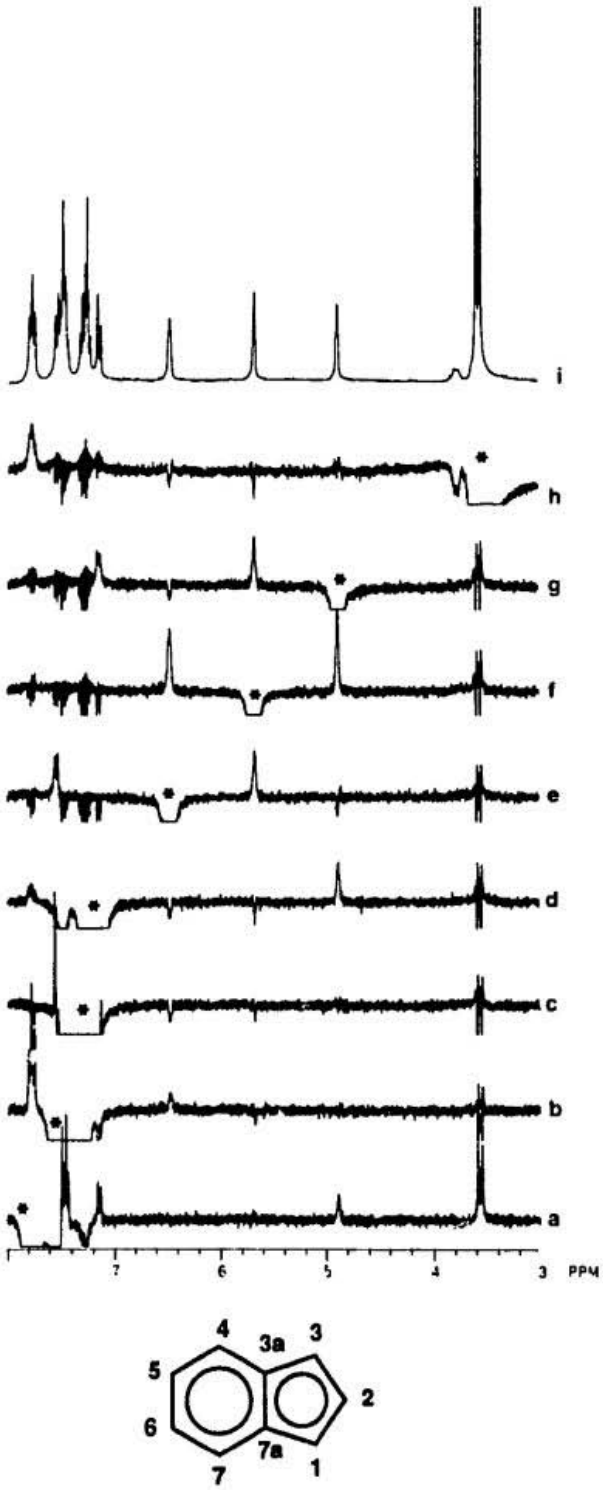

Figure 2-10. ^1H nOed Spectra for (η^5-Indenyl)Co(C_3F_7)(I)(PPh(OMe)$_2$), **2-6**. (i) reference spectrum; (a-h) difference spectra (16x) for irradiation at the indicated (*) frequency; (a) H_{ortho}; (b) H_4 & H_{meta}; (c) H_5,H_6 & H_{para}; (d) H_7; (e) H_3; (f) H_2; (g) H_1; (h) OCH_3.

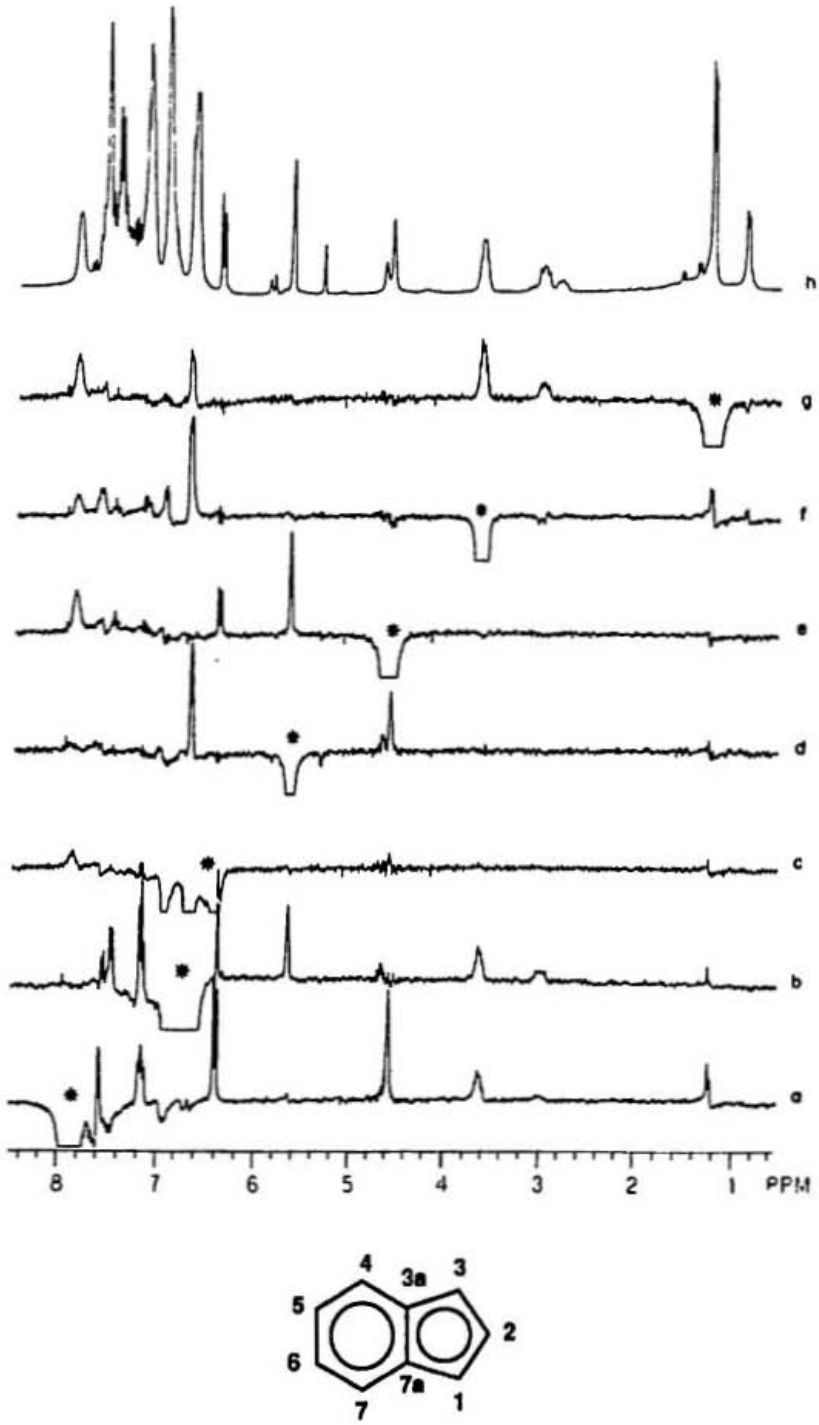

Figure 2-11. ^{1}H nOed Spectra for (η^5-Indenyl)Co(C_3F_7)(I)(PNH), **2-8a**. (h) reference spectrum; (a-g) difference spectra (16x) for irradiation at the indicated (*) frequency; (a) H_7 & H_{ortho} of C*-Ph; (b) H_3 & H_{ortho} of C*-Ph; (c) H_{ortho} of P-Ph; (d) H_2; (e) H_1; (f) C*H; (g)C*-CH_3.

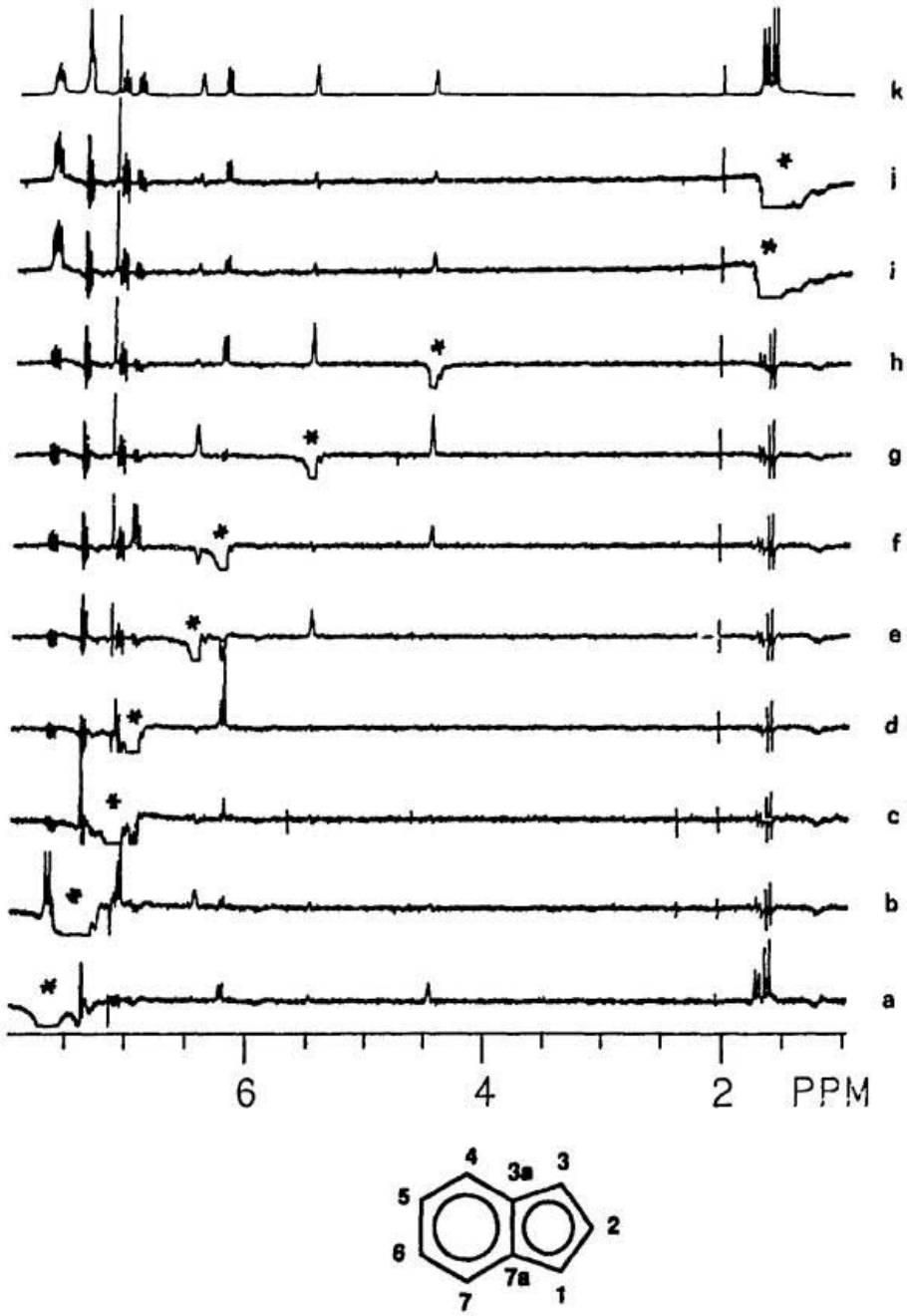

Figure 2-12. ^{1}H nOed Spectra for (η^5-indenyl)Co(C_6F_{13})(I)($PPhMe_2$)Co, **2-13**. (k) reference spectrum; (a-j) difference spectra (32x) for irradiation at the indicated (*) frequency; (a) H_{ortho}; (b) H_4, H_{meta}, & H_{para}; (c) H_5; (d) H_6; (e) H_3; (f) H_7; (g) H_2; (h) H_1; (i & j) Me.

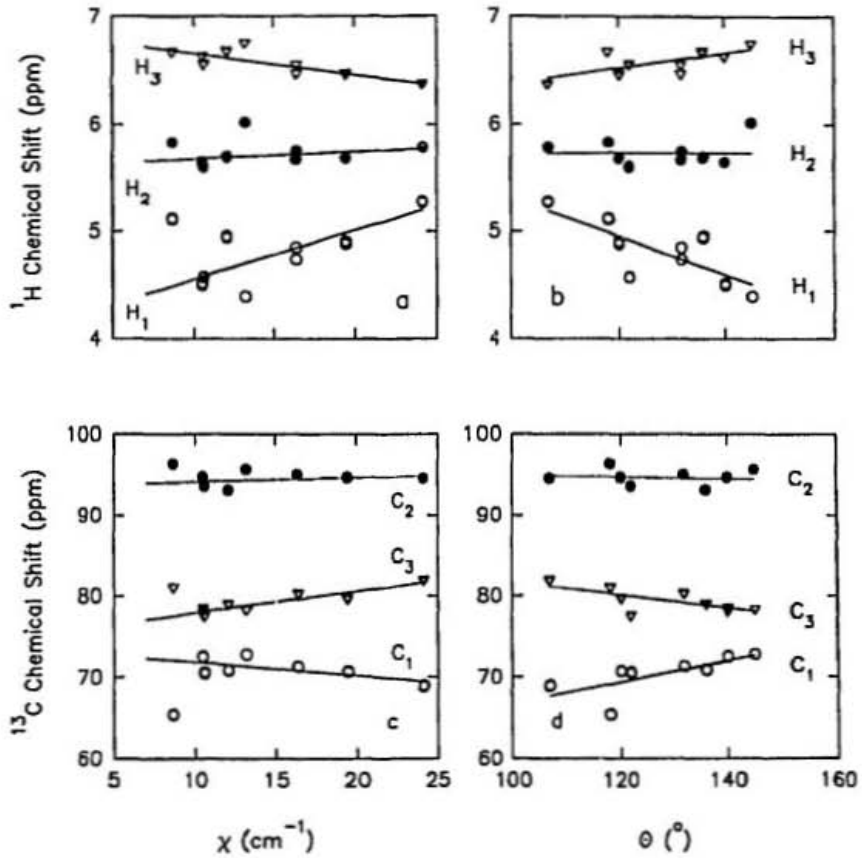

Figure 2-13. Correlation of Indenyl ^{1}H and ^{13}C Chemical Shifts with Stereoelectronic Parameters for (η^5-indenyl)Co(R_t)(I)(L) Complexes (cf. Tables 2-11, 2-12, and 2-15).

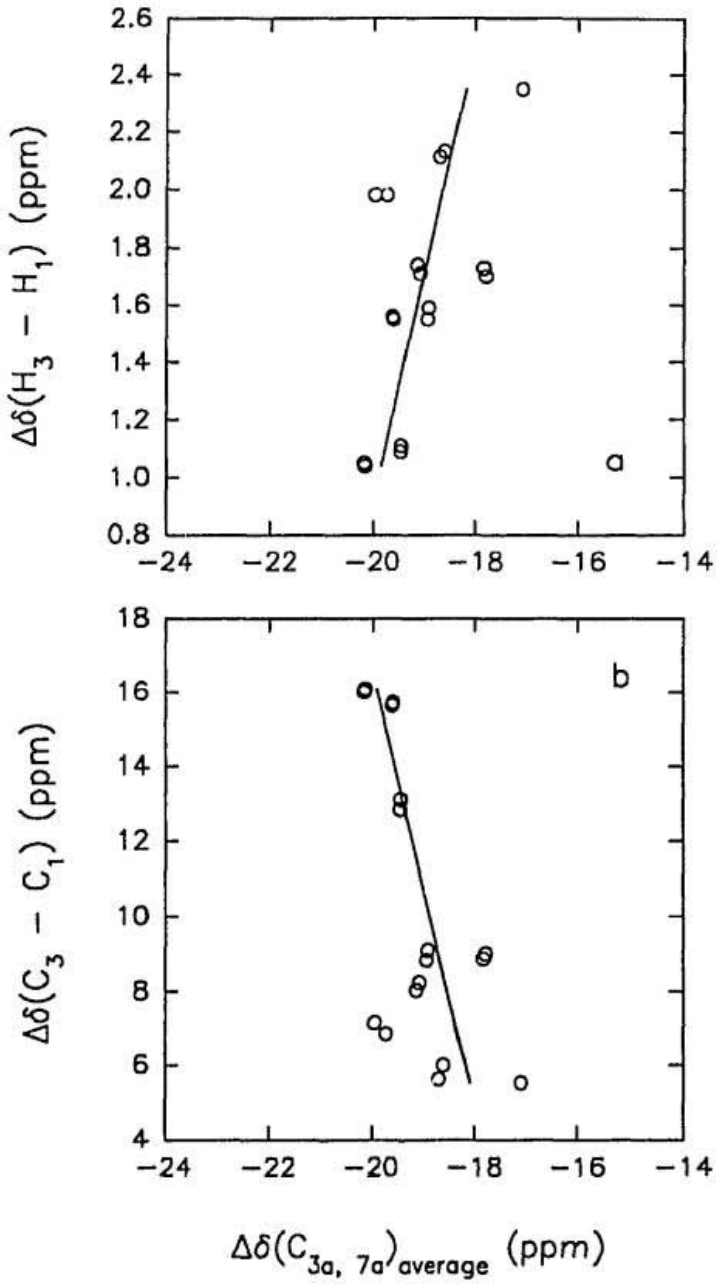

Figure 2-14. Correlation between the Indenyl Distortion Parameters for (η^5-indenyl)Co(R_l)(I)(L) Complexes (cf. Table 2-15).

2.4. Experimental Section

2.4.1. Reagents and Methods. Unless otherwise noted, all manipulations were performed under a dry, oxygen-free nitrogen atmosphere using standard Schlenk techniques. Nitrogen gas was purified by passing through a series of columns containing DEOX (Alpha) catalyst heated to 120 °C, granular P_4O_{10}, and, finally, activated 3A Molecular Sieves. THF, benzene, and hexane solvents were distilled under nitrogen from blue solutions of sodium benzophenone ketyl. Dichloromethane was distilled under nitrogen from P_4O_{10} and acetone from 4A Molecular Sieves (4-8 mesh). Anhydrous $CoCl_2$ was prepared by refluxing $CoCl_2 \cdot 6H_2O$ with thionyl chloride ($SOCl_2$, bp 77°C). Indene and 1,5-cyclooctadiene (COD) were distilled at 54°C/5 Torr and 57°C/30 Torr, respectively, before use. C_3F_7I, $C_6F_{13}I$, PMe_3, $PPhMe_2$, PPh_2Me, $PPh_2(OMe)$ and PPh_3 were purchased from Aldrich and were used as received. $P(OMe)_3$ from Strem was distilled before use. (*S*)-(-)-Diphenyl((1-phenylethyl)amino)phosphine (PNH) was prepared using the established procedure.[304] Thin layer chromatographic (TLC) analyses were performed on pre-coated analytical TLC plates (silica gel F-254, Merck). Chromatographic separations were carried out using a Chromatotron (Harrison Associates) with 1, 2, or 4 mm thick silica $gel_{60}PF_{254}$ (Merck) adsorbent. Elemental analyses were performed by Canadian Microanalytical Service Ltd. (Delta, B.C.). Melting points (mp) were determined in capillaries sealed under nitrogen and are uncorrected. Infrared spectra were measured on Mattson Polaris Fourier transform spectrometer as solutions in KBr

cells (0.1 mm) or as thin films deposited on a KBr disk. NMR spectra were recorded on a GE 300-NB Fourier transform spectrometer operating at a proton frequency of 300.12 MHz.

Proton nOed spectra were determined under steady state conditions on the GE 300-NB instrument. Data was collected at 25.0 °C using interleaved experiments of 16 or 32 transients cycled 12 to 16 times through the list of decoupling frequencies. In each experiment the decoupler was gated on in continuous wave (CW) mode for 2 s with sufficient attenuation to give an approximate 70-90% reduction in intensity of the irradiated peak. A 30 s delay preceded each frequency change. A set of four dummy scans was employed to equilibrate the spins prior to data acquisition. No relaxation delay was applied between successive scans of a given decoupling frequency. Difference spectra were obtained on 16K or zero-filled 32K data tables which had been digitally filtered with a 0.1 Hz exponential or Gaussian line broadening function. Quantitative data were obtained by integration.

2.4.2. Crystal Structure Determinations. Crystal data was collected at ambient temperature on a Rigaku AFC6S diffractometer with graphite monochromated Mo Kα radiation, λ=0.71069 Å, and a 2KW sealed tube generator using the ω scan technique to a maximum 2θ value of 50.0°. The selected crystals for both **2-3** and **2-6** proved to be twinned. Data from one crystal fragment was successfully indexed, collected and refined for **2-3**. Inspection of peak profiles from **2-6** suggested twinning

but with alignment of fragments so close as to preclude separate data collection. Indexing and collection proceeded normally. Data collection and refinement for the remaining two crystals of complexes **2-8a** and **2-19** proceeded smoothly, although disordered perfluoroalkyl was detected in **2-8a**. Cell constants and an orientation matrix for data collection were determined from least squares refinement using the setting angles of the 18 (**2-3**), 24 (**2-6**), 25 (**2-8a**) or 18 (**2-19**) carefully centered reflections in the range $40.10 < 2\theta < 43.21°$ (**2-3**), $29.43 < 2\theta < 36.56°$ (**2-6**), $31.26 < 2\theta < 40.68°$ (**2-8a**), or $29.25 < 2\theta < 34.76°$ (**2-19**) and are given in Table 2-16. The space group $P2_1/c$ (#14) (**2-3, 2-6**), $P2_12_12_1$ (#19) (**2-8a**), or $P2_1/n$ (#14) (**2-19**) was assigned on the basis of systematic absences ((h01: $h \neq 2n$ and 0k0: $k \neq 2n$) (**2-3, 2-6**), (h00: $h \neq 2n$, 0k0: $k \neq 2n$ and 00l: $l \neq 2n$) (**2-8a**), or (h01: $h+1 \neq 2n$ and 0k0: $k \neq 2n$) (**2-19**)) and on the successful solution and refinement of the structure. Omega scans of several intense reflections, made prior to data collection, had an average width at half-height of 0.43° (**2-3**), 0.29°(**2-6**), 0.27° (**2-8a**), or 0.44° (**2-19**) with a take-off angle of 6.0°. Scans of $(1.78+0.30 \tan\theta)°$ (**2-3**), $(1.63+0.30 \tan\theta)°$ (**2-6**), $(0.89+0.30 \tan\theta)°$ (**2-8a**), or $(1.13+0.30 \tan\theta)°$ were made at a speed of 8.0°/min (in omega). Weak reflections ($I<10.0\sigma(I)$) were rescanned (max 2), and the counts accumulated to assure good counting statistics. The intensities of three representative reflections were measured after every 150 reflections and these remained constant throughout the data collection hence no decay corrections were applied. The linear absorption coefficient for Mo Kα is 24.4 cm^{-1} (**2-3**), 23.1 cm^{-1} (**2-6**), 16.7 cm^{-1} (**2-8a**), or 21.7 cm^{-1} (**2-19**). An empirical absorption correction, based on

azimuthal scans of several reflections, was applied resulting in transmission factors ranging from 0.79 to 1.09 (**2-3**), 0.67 to 1.00 (**2-6**), 0.77 to 1.00 (**2-8a**) or 0.87 to 1.00 (**2-19**). The data were corrected for Lorentz and polarization effects. A correction for secondary extinction (coefficient = 0.27596 x 10^{-7}) was applied for **2-19**. The structure was solved by direct methods[305] using the Molecular Structure Corporation TEXSAN software. Non-hydrogen atoms were refined anisotropically. Idealized hydrogen atoms were included at the calculated positions and were not refined. The absolute configuration of **2-8a** was determined by refining both enantiomers to convergence on the complete data set with anomalous dispersion corrections included. The configuration of Figure 2-3 refined to a value of 0.6% lower than its enantiomer. Since the correct hand (*S*) was obtained for the chiral carbon on PNH ligand of known chirality, we are confident that the assignment of absolute configuration at cobalt is correct. Further details are given in Table 2-16.

2.4.3. Synthesis of Complexes

2.4.3.1. Synthesis of $(\eta^5\text{-}C_9H_7)Co(CO)_2$ ***(2-1).*** This complex was prepared using a modification[280] of the method originally described by Bönnemann[265] and Salzer and Taschler.[275] Finely divided lithium (1.50 g, 0.219 mol) was suspended in 250 mL of dry THF under an argon atmosphere. The mixture was heated at 65 °C in an oil bath, and a mixture of indene (30.5 g, 0.263 mol) and 1,5-cyclooctadiene (27.8 g,

0.258 mol) was slowly added with stirring. Continued stirring for 1 h resulted in a yellow solution. The oil bath was removed and anhydrous $CoCl_2$ (13.9 g, 0.107 mol) added slowly over a 25 minute period. This stage of the reaction was vigorously exothermic! The solution was stirred for an additional 30 minutes. The resulting dark red-brown solution was cooled to room temperature and filtered through a Schlenk filter fitted with a 5 cm silica gel plug. Removal of volatiles under vacuum (0.1 Torr) at 40 °C left a dark residue, which was taken up in 200 mL of hexane and stirred under an atmosphere of CO at room temperature for 90 min. Filtration through a short plug of silica gel and removal of volatiles under vacuum (0.1 Torr) gave the crude product as an air-sensitive, deep red-brown oil (22.1 g, 90%), IR ν_{CO}: 2020, 1960 cm^{-1}.

2.4.3.2. Synthesis of $(\eta^5\text{-}C_9H_7)Co(R_f)(I)(CO)$ ***(*** $R_f = C_3F_7$ ***(2-2),*** C_6F_{13} ***(2-3)).*** A slight excess (4.30 g, 14.5 mmol) of perfluoropropyl iodide (C_3F_7I) was added via syringe at room temperature to a solution of 3.30 g (14.3 mmol) of $(\eta^5\text{-}C_9H_7)Co(CO)_2$ in 100 mL benzene. Continued stirring at room temperature for 40 h resulted in the formation of a dark red-brown solution containing some black precipitate. The precipitate was collected on a glass frit, washed with a small amount of hexane and redissolved in CH_2Cl_2. Removal of the solvent under vacuum left the crude product as an air-stable black powder. Additional product was recovered by chromatography of the filtrate on a 300X35 mm silica gel column (2:1 benzene/hexane elution) to give a combined yield of 5.71 g (80%) of **2-2**. Complex **2-3** was prepared from **2-1** and

$C_6F_{13}I$ using similar conditions, and it crystallized by slow diffusion of hexane into its dichloromethane solution at -20 °C to give **2-3** as black, rectangular plates.

2.4.3.3. Synthesis of ***(η^5-C_9H_7)Co(C_3F_7)(I)(PNH) (2-8a), Method A.*** A solution of (*S*)-(-)-diphenyl((phenylethyl)amino)phosphine (PNH, 0.564 g, 1.85 mmol) in 15 mL of benzene was added slowly to a solution of **2-2** (0.921 g, 1.85 mmol) in 30 mL of benzene at room temperature. After stirring for 30 minutes, the solution was placed in an ice bath for 10 minutes, and the benzene solvent was removed by sublimation under vacuum to afford a dark red-brown powder (1.37 g, 95%). TLC (elution with THF/hexane 1:5) and ^{1}H NMR analysis revealed the presence of a single isomer, which was shown to be **2-8a**. The crude product was crystallized at -20 °C from CH_2Cl_2/hexane under a nitrogen atmosphere to give **2-8a** as well formed, rectangular black crystals. IR, ν_{NH} = 3378 cm^{-1}. Polarimetric data [α] (λ): -320° (579 nm), -670° (546 nm), -1100° (436 nm).

Method B. A solution of (*S*)-(-)-diphenyl((phenylethyl)amino)phosphine (PNH, 0.0163 g, 0.0534 mmol) in 3 mL of benzene was added slowly to a solution of **2-2** (0.0238 g, 0.0477 mmol) in 4 mL of benzene at room temperature. After stirring for 10 minutes, the solution was placed in a refrigerated bath at - 11 °C. After the solvent was frozen, benzene was removed by sublimation in oil pump vacuum over a 48 h period. ^{1}H NMR analysis showed that the crude product contained a 34:66 mixture of **2-8b:2-8a**.

2.4.3.4. Synthesis of ***(η^5-C_9H_7)Co(R_f)(I)(PMe_3) (R_f=C_3F_7 (2-10), C_6F_{13}, 2-11).*** These two complexes were synthesized using the procedure described below. A 10 mL benzene solution of PMe_3 (0.0319 g, 0.419 mmol) was added dropwise with stirring via a pressure equalised dropping funnel to a black solution of **2-3** (0.2503 g, 0.3862 mmol) in 20 mL benzene at ambient temperature. After stirring for 20 minutes, the solution was placed on an ice bath for a further 20 minutes. Removal of volatiles from the deep-red solution under oil pump vacuum left a deep-red powder. The crude product was dissolved in *ca.* 4 mL of acetone and purified chromatographically on 4 mm silica gel plates. Acetone elution moved a high R_f deep-red zone which was collected. Removal of volatiles at aspirator and then oil pump vacuum left a deep-red powder (0.2305 g, 86%). Black rectangular plates were obtained by slow diffusion of hexane into an acetone solution of **2-11** at -20°C. A low R_f yellow band was shown by ^{1}H NMR to be a bis-substituted complex with a structure similar to **2-19.**

2.4.3.5. Synthesis of ***(η^5-C_9H_7)Co(R_f)(I)(L) (2-4 - 2-7, 2-9, 2-12 - 2-17).*** These complexes were prepared following the procedure described for **2-12.** In some cases (**2-12, 2-13, 2-14, 2-15**) the crude product required no further purification. The remaining complexes were purified by preparative radial TLC (benzene eluent). Reaction yields are reported in Table 2-1. A slight excess of $PPhMe_2$ (0.0582 g, 0.421 mmol) was added slowly via syringe with stirring to a black solution of **2-2**

(0.1901 g, 0.3817 mmol) in 10 mL of benzene at room temperature. After stirring for 30 minutes the resulting deep-red solution was cooled in an ice bath for *ca.* 10 minutes. Removal of volatiles at oil pump vacuum gave the crude product as a deep red powder (0.2130 g, 92%). Black rectangular plates were obtained by slow diffusion of hexane into a CH_2Cl_2 solution of **2-12** at -20°C.

2.4.3.6. Synthesis of ***(η^5-C_9H_7)Co(C_3F_7)(I)(PPh_3) (2-18).*** A 10 mL benzene solution of PPh_3 (0.2070 g, 0.7892 mmol) was added dropwise at room temperature with stirring via a pressure equalized dropping funnel to a black solution of **2-2** (0.3215 g, 0.6456 mmol) in 20 mL of benzene. Stirring was continued for 20 minutes then the brown-red solution containing some uncharacterised green precipitate was filtered through a glass frit, and the filtrate was placed in an ice bath for *ca.* 10 minutes. Removal of volatiles at oil pump vacuum left a brown powder, which was dissolved in 4 mL of benzene and purified with chromatograph. Benzene/hexane (2/1) elution moved a brown zone which was collected. Removal of volatiles with rotary evaporator followed by oil pump vacuum afforded the product as a brown powder (0.1098 g, 23%).

2.4.3.7. Synthesis of [(η^5-C_9H_7)Co(C_3F_7)(PMe_3)$_2$]$^+$I$^-$ (2-19). Excess PMe_3 (0.0888 g, 1.17 mmol) was added slowly via syringe with stirring to a black solution of **2-2** (0.2483 g, 0.4985 mmol) in 20 mL of benzene at room temperature. The reaction mixture was stirred for 30 minutes, resulting in a red solution containing some

precipitate, and then placed in an ice bath for *ca.* 10 minutes. Removal of volatiles at oil pump vacuum left a red powder. The crude product was dissolved in *ca.* 4 mL of acetone and purified chromatographically on a 4 mm silica gel plate. Acetone elution moved a yellow-red zone which was collected. Removal of solvent at water aspirator and then oil pump vacuum left a red crystalline powder (0.2915 g, 94%). Deep-red prisms were obtained by slow diffusion of hexane into the CH_2Cl_2 solution of **2-19** at -20°C.

Table 2-16. Summary of Crystallographic Data for **2-3**, **2-6**, **2-8a** and **2-19**.

	3	**6**	**2-8a**	**2-19**
Formula	$C_{16}H_7CoF_{13}IO$	$C_{20}H_{18}CoF_7IO_2P$	$C_{32}H_{27}CoF_7INP$	$C_{37}H_{52}Co_2F_{14}I_2P_4Cl_2$
F.W.(g/mol)	648.05	640.16	775.37	1329.27
Crystal Habit	black rect.	black prism	black rect.	deep-red prism
Crystal Size (mm)	0.35x0.35x0.05	0.40x0.15x0.15	0.37x0.27x0.08	0.35x0.25x0.15
Crystal System	monoclinic	monoclinic	orthorhombic	monoclinic
No.Rflns for unit cell determination (2θ range)	18 (40.1-43.2°)	24 (29.4-36.6°)	25 (31.3-40.7°)	18 (29.3-34.8°)
Omega Scan Peak Width at Half-height	0.43	0.29	0.27	0.44
Lattice Parameters				
a (Å)	16.926(6)	16.633(5)	16.362(1)	16.760(5)
b (Å)	8.944(3)	7.530(3)	19.944(4)	10.614(7)
c (Å)	14.133(6)	17.875(3)	9.417(2)	28.595(5)
β (°)	106.04(3)	100.40(2)	-	96.61(2)
V (Å^3)	2056(1)	2201.9(9)	3073.0(8)	5053(3)
Space Group	$P2_1/c$ (#14)	$P2_1/c$ (#14)	$P2_12_12_1$ (#19)	$P2_1/n$ (#14)
Z	4	4	4	4
D_{calcd}(g/cm^3)	2.093	1.931	1.676	1.747
F_{000}	1232	1248	1536	2616
μ(MoKα)(cm^{-1})	24.36	23.09	16.66	21.73
Scan Width(°)	1.78+0.30 tanθ	1.63+0.30 tanθ	0.89+0.30 tanθ	1.13+0.30 tanθ
$2\theta_{max}$ (°)	50.0	50.0	50.0	45.0
No.Rflns measured				
Total	4045	4352	6184	7295
Unique	3876	4201	3092	7015
R_{int}	0.057	0.105	0.055	0.029
Corrections[a]	Lorentz polarization			
trans.factors:	0.79-1.09	0.67-1.00	0.77-1.00	0.87-1.00
secondary extinction coef.	-	-	-	0.27596×10^{-7}
Function Minimized	$\Sigma w(\|Fo\|-\|Fc\|)^2$			
Least-squares weights	$4Fo^2/\sigma^2(Fo^2)$			
p-factor	0.01	0.01	0.01	0.01
Anomalous Dispersion	All non-hydrogen atoms			
No.Observations (I>3.00σ(I))	1673	1792	3415	4097
No.Variables	289	289	329	551
Rfln/Param	5.79	6.20	10.38	7.44
R[b]	0.062	0.061	0.071	0.040
R_w[c]	0.048	0.058	0.064	0.036
GOF[d]	2.37	2.63	3.07	1.56
Max Shift Error in Final Cycle	0.05	0.04	2.64	0.00
Δρ final (max/min) (e$^-$/Å^3)	0.67/-0.62	0.84/-1.07	1.19/-0.78	1.09/-0.66

[a] Cf. reference[308]. [b] $R=\Sigma||Fo|-|Fc||/\Sigma|Fo|$. [c] $R_w=[(\Sigma w(|Fo|-|Fc|)^2/\Sigma wFo^2)]^{1/2}$

[d] $GOF=(\Sigma(|Fo|-|Fc|)/\sigma)/(n-m))$ where n=#reflections, m=#variables, and σ^2=variance of (|Fo|-|Fc|)

Chapter 3

Synthesis, Characterization and Conformational Aspects of Chiral Cobalt(III) η^5-Indenyl and η^5-Cyclopentadienyl Phosphonate and Phosphinate Complexes

3.1. Introduction

As discussed in Chapter 1, previous studies[206, 207, 217, 218] of Arbuzov-like dealkylations[182] using the Co-chiral aminophosphine substituted auxiliary $CpCoX(PNH^*)(I)$ (X=I, CF_3, C_3F_7; PNH^*=*S*-(-)-$Ph_2PNHC^*H(Me)Ph$) concluded that intramolecular P=O•••H-N hydrogen bonding at the nascent phosphoryl oxygen site played an important role in $Co^* \rightarrow P$ chiral induction by limiting conformational mobility. The stereochemistry of the major diastereomer was reliably predicted from the transition state which minimizes 1,3-diaxial interactions between the phosphonite substituent R and a pseudo-axial phenyl substituent of the aminophosphine (cf. Scheme 1-50).

Attempts to assess the controlling effect of intramolecular hydrogen bonding in these reactions by studying analogs containing blocked, *N*-alkylated aminophosphine $Ph_2PN(R)C^*H(CH_3)Ph$ failed.[208] This Chapter examines Arbuzov dealkylations of $P(OMe)_3$ and the prochiral phosphonite $PPh(OMe)_2$ mediated by the isostructural Co-

chiral auxiliaries [(η^5-Cp)Co(PMe_3)(C_3F_7)-]$^+$ and [(η^5-indenyl)Co(L)(R_f)-]$^+$ (L= PPh_nMe_{3-n} (n=0-2), $PR(OMe)_2$ (R=Ph, OMe); R_f = C_3F_7, C_6F_{13}) prepared in Chapter 2, which provide non-hydrogen bonding templates for diastereoselective Arbuzov dealkylation. Solid state and solution conformations are compared and evidence for restricted rotation about the cobalt-indenyl and -P(O) bonds is presented.

3.2. Results and Discussion

3.2.1. Synthesis of Cobalt η^5-Cyclopentadienyl and η^5-Indenyl Phosphonate and Phosphinate Complexes. Phosphonate and P-chiral phosphinate targets were synthesized using the transition metal Arbuzov reaction,[182] which involved sequential substitutions of the iodides **3-1** and **3-4** at cobalt and carbon (cf. Schemes 3-1 and 3-2). As presented in Chapter 2, preferential substitution of labile CO in (η^5-Cp)Co(R_f)(CO)(I) and (η^5-indenyl)Co(R_f)(CO)(I) by P-donor ligands[283, 285, 307] represents a more general synthetic route[206, 280-282, 308] to the required substrates **3-1** and **3-4** than oxidative addition of RI (R=I or R_f) to phosphine-substituted Co(I) complexes.[309] Treatment of **3-1** and **3-4** with $P(OMe)_3$ or $PPh(OMe)_2$ initially afforded the corresponding labile ionic intermediate[182, 184, 195-197, 204, 209], [(η^5-Cp)Co(C_3F_7)(L)($PR(OMe)_2$)]$^+$ and [(η^5-indenyl)Co(R_f)(L)($PR(OMe)_2$)]$^+$ **3-2** and **3-5** respectively, which rapidly dealkylated in non-polar solvents to give good yields of the orange-yellow phosphonate and phosphinate complexes, (η^5-Cp)Co(C_3F_7)(L)(P(O)(R)(OMe)) and (η^5-indenyl)Co(R_f)(L)(P(O)(R)(OMe)), **3-3** and **3-6**

(R=OMe, Ph), respectively (cf. Schemes 3-1 and 3-2). Physical and analytical data for these phosphonate and phosphinate complexes is reported in Table 3-1.

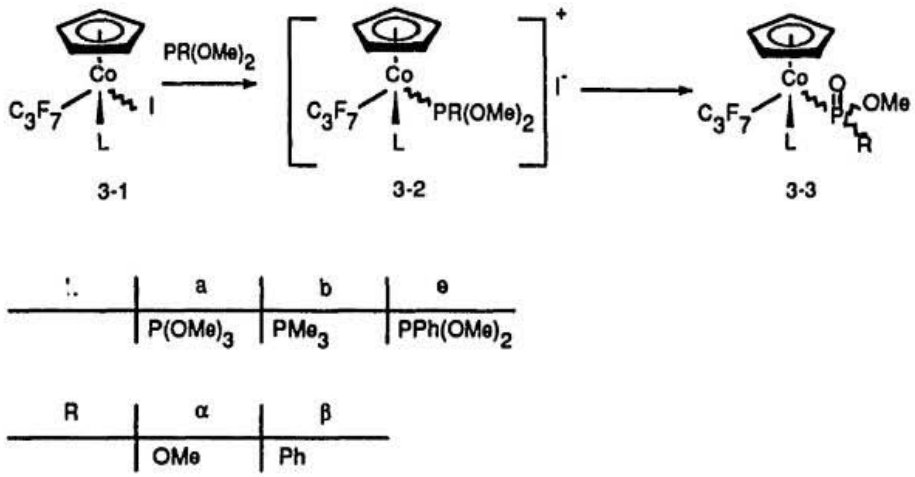

Scheme 3-1

Reactions of several η^5-Cp and η^5-indenyl complexes with $P(OMe)_3$ were followed by ^1H NMR at 25 °C in benzene-d_6 and in acetone-d_6. Only reactants (**3-1** or **3-4**) and products (**3-3** or **3-6**) were observable in benzene-d_6; however, a reaction intermediate was clearly detected for both series in acetone-d_6 (cf. Figures 3-1 and 3-2). For the reaction of **3-1a** with $P(OMe)_3$, the reactant (δ=5.40 ppm) diminishes, an intermediate **3-2a** (δ=5.81 ppm) builds and then decays, and the phosphonate product **3-3a**α increases (δ=5.27 ppm). Similarly **3-4a** (H_1, δ=5.52; H_3, δ=6.27 ppm) is rapidly consumed on treatment with $P(OMe)_3$ to form an unstable intermediate **3-5a**α (H_3, H_1, δ=6.43; H_2, δ=5.95 ppm), which subsequently collapses to form the

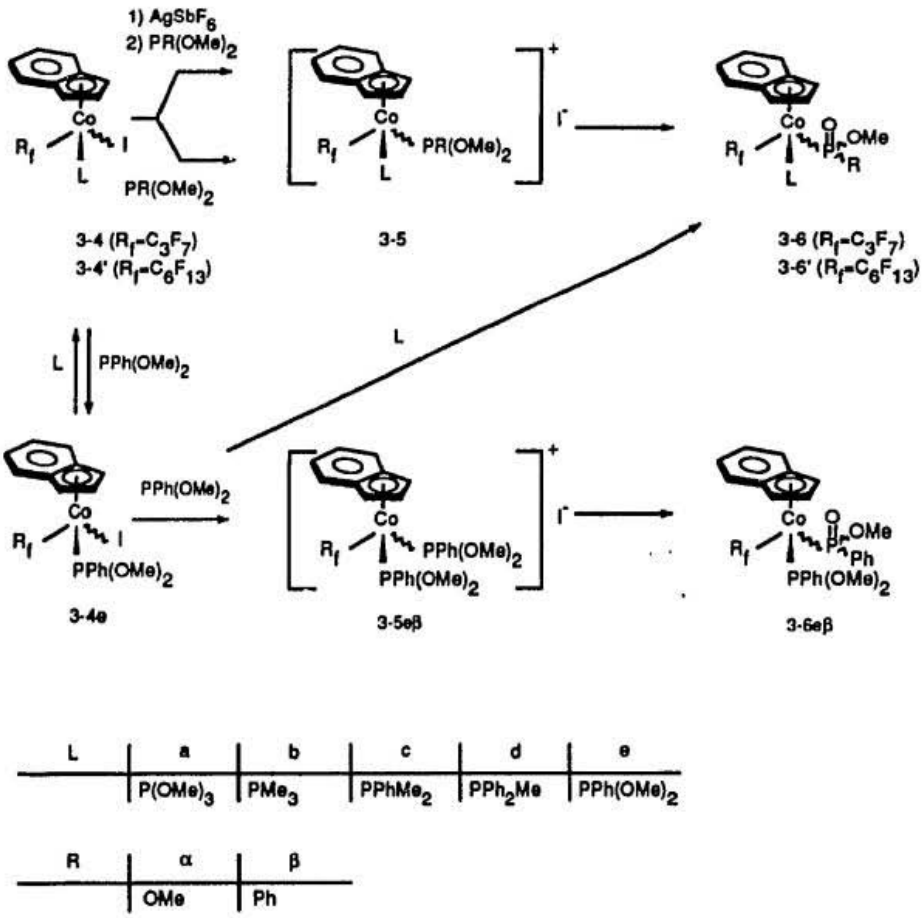

Scheme 3-2

phosphonate **3-6aα** (H_2, δ=5.85; H_1, δ=5.40 ppm).

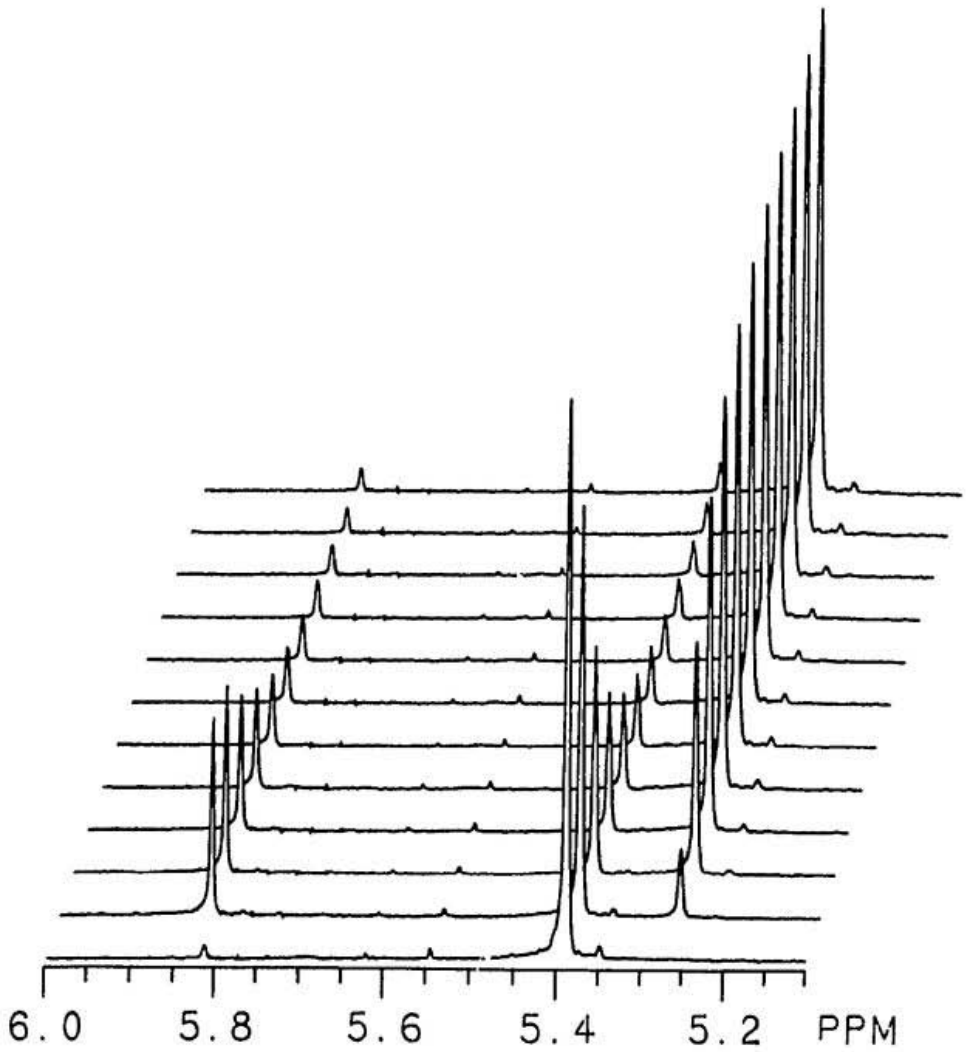

Figure 3-1. ^{1}H NMR Spectra for the Reaction between (η^5-Cp)Co(C_3F_7)(P(OMe)$_3$)(I), **3-1a**, and P(OMe)$_3$ in Acetone-d_6 at 25 °C. [**3-1a**]$_0$ = 0.01568 mol•L^{-1}, [P(OMe)$_3$]$_0$ = 0.1728 mol•L^{-1}. The first spectrum was recorded at t=550 s; Δ=1800 s for remaining spectra.

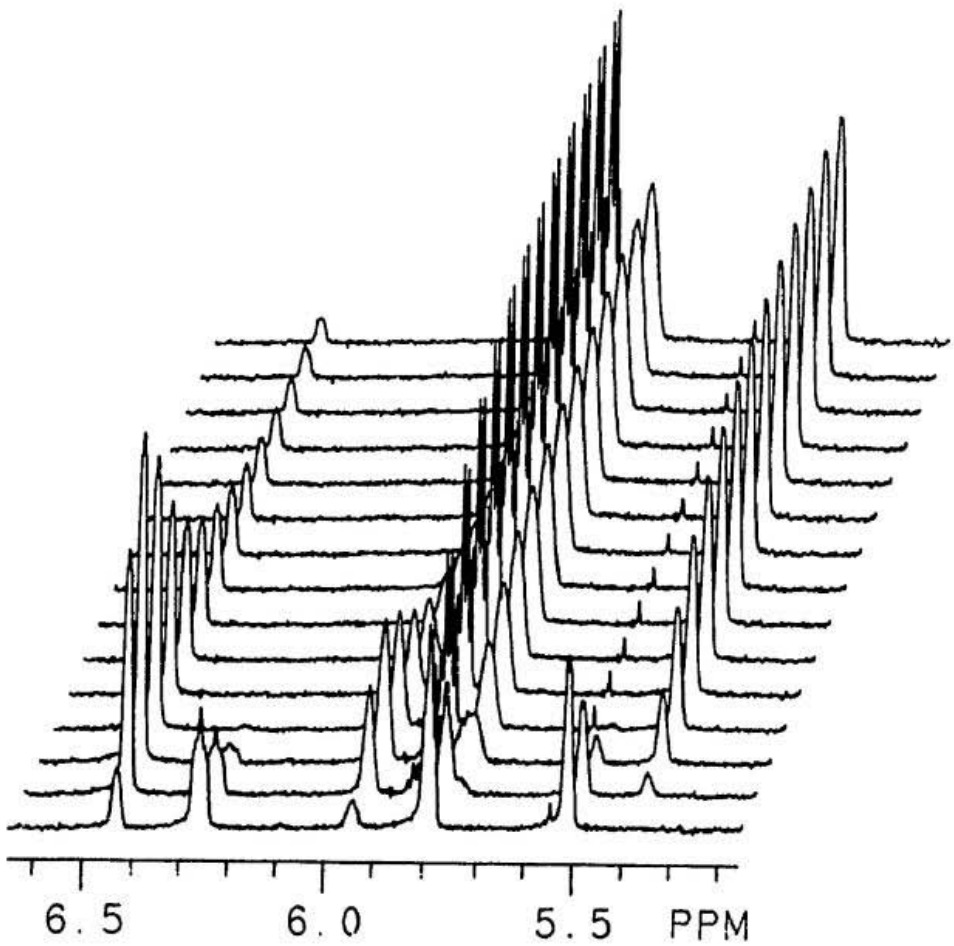

Figure 3-2. ^{1}H NMR Spectra for the Reaction between (η^5-Indenyl)Co(C_3F_7)($P(OMe)_3$)(I), **3-4a**, and $P(OMe)_3$ in Acetone-d_6 at 25 °C. $[\mathbf{3\text{-}4a}]_0$ = 0.01566 mol•L^{-1}, $[P(OMe)_3]_0$ = 0.1733 mol•L^{-1}. The first spectrum was recorded at t=425 s, Δt= 600 s for remaining spectra.

Reactions of **3-1** and **3-4** with prochiral $PPh(OMe)_2$ were more complicated since diastereomers were possible. For **3-1b**, **3-4b**, and **3-4c** (cf. Schemes 3-1 and 3-2) cationic intermediates $[(\eta^5\text{-Cp})Co(C_3F_7)(PMe_3)(PPh(OMe)_2)]^+$, **3-2bβ**, $[(\eta^5\text{-indenyl})Co(C_3F_7)(L)(PPh(OMe)_2)]^+$ (L=PMe_3, **3-5bβ**, and $PPhMe_2$, **3-5cβ**) were directly observed by ^1H NMR as a pair of diastereotopic O<u>Me</u> doublets at 4.0-4.2 ppm with $^3J_{PH} \approx 10$ Hz in acetone-d_6 at 25 °C. Displaced I^- in the ion pair subsequently attacks at carbon on coordinated $PPh(O\underline{Me})_2$ to afford two red/orange diastereomeric phosphinate complexes $(\eta^5\text{-Cp})Co(C_3F_7)(PMe_3)(P(O)Ph(OMe))$, **3-3bβ-1,2** and $(\eta^5\text{-indenyl})Co(C_3F_7)(L)(P(O)Ph(OMe))$, **3-6bβ-1,2** and **3-6cβ-1,2** respectively. (The designations **-1** and **-2** refer to diastereomers in order of decreasing chromatographic Rf values.)

The spectroscopic characterization of the cationic intermediate phosphite and phosphonite species were confirmed by isolation and X-ray crystallographic study of **3-5aα,SbF_6** prepared by an independent route. Abstraction of iodide from **3-4a** with $AgSbF_6$ in acetone followed by reaction with one equivalent of $P(OMe)_3$ gave a 95% yield of orange, crystalline $[(\eta^5\text{-indenyl})Co(C_3F_7)(P(OMe)_3)_2]^+SbF_6^-$, **3-5aα,$SbF_6$**. Treatment of **3-5aα,SbF_6** with an acetone solution of LiI afforded a phosphonate product **3-6aα** identical with that obtained by direct reaction of **3-4a** with $P(OMe)_3$ (cf. Scheme 3-2). The solid state structure **3-5aα,SbF_6** (cf. Figure 3-3) consists of an unexceptional η^5-indenyl piano stool with an approximately octahedral coordination geometry about cobalt. Interligand bond angles for (P(1)-Co(1)-P(2), P(1)-Co(1)-C(8),

P(2)-Co(1)-C(8)) are all close to 90°. Atomic coordinates and selected bond lengths and angles are given in Tables 3-2 and 3-3.

Minor amounts of mixed, diastereomeric phosphonite/phosphinate (η^5-Cp)Co(C_3F_7)(PPh(OMe)$_2$)(P(O)Ph(OMe)), **3-3eβ-1,2** and (η^5-indenyl)Co(C_3F_7)(PPh(OMe)$_2$)(P(O)Ph(OMe)), **3-6eβ-1,2**, presumably the result of stepwise disubstitution of I and L by PPh(OMe)$_2$ followed by Arbuzov dealkylation, were spectroscopically observed in the reaction of dimethyl phenylphosphonite with **3-1** and **3-4**. The source of the phosphonite/phosphinate complexes was confirmed by direct ^{1}H NMR observation of an apparent triplet at δ=3.95 assigned as a pair of overlapping doublets due to the diastereotopic phosphonite methoxy groups of [(η^5-indenyl)Co(C_3F_7)(PPh(OMe)$_2$)$_2$]$^+$, **3-5eβ**, on treatment of **3-4e** with PPh(OMe)$_2$ in acetone-d_6.

The analogous reaction of **3-4d** or [(η^5-indenyl)Co(C_3F_7)(PPh_3)(I)] with PPh(OMe)$_2$ did not afford the expected phosphinate product. Instead, a low yield (*ca.* 10%) of **3-6eβ-1,2** along with a significant amount of uncharacterized green-blue decomposition products were obtained in both cases. Presumably preferential substitution of the bulky phosphine dominates. A diastereomeric mixture of the phosphinate **3-6dβ-1,2** was successfully prepared, albeit in very low yield, by an inverse mode of reaction of **3-4e** with PPh_2Me.

Table 3-1. Physical Properties of η^5-Cyclopentadienyl and η^5-Indenyl Co(III) Complexes.

Cpd.	Formula	Appearance	mp[a] (°C)	Anal. (C, H %) Calc.(Found)
3-1b	$(C_5H_5)Co(C_3F_7)(I)(PMe_3)$	dark-blue powder	197-199	26.64(26.74), 2.84(2.74)
3-1b'	$[(C_5H_5)Co(C_3F_7)(PMe_3)_2]^+I^-$	orange plate	195-197	29.39(28.93), 4.05(3.95)
3-3aα	$(C_5H_5)Co(C_3F_7)(P(OMe)_3)(P(O)(OMe)_2)$	orange microcrystal	102-104	29.68(30.06), 3.83(3.69)
3-3bα	$(C_5H_5)Co(C_3F_7)(PMe_3)(P(O)(OMe)_2)$	yellow microcrystal	136-138	32.65(32.49), 4.22(4.45)
3-5aα	$[(C_9H_7)Co(C_3F_7)(P(OMe)_3)_2]^+SbF_6^-$	orange rect. plate	176-177	26.14(26.17), 3.05(3.00)
3-6aα	$(C_9H_7)Co(C_3F_7)(P(OMe)_3)(P(O)(OMe)_2)$	red powder	87-88	35.44(35.51), 3.85(3.96)
3-6'aα	$(C_9H_7)Co(C_6F_{13})(P(OMe)_3)(P(O)(OMe)_2)$	red powder	48-50	33.08(33.03), 3.05(2.82)
3-6bα	$(C_9H_7)Co(C_3F_7)(PMe_3)(P(O)(OMe)_2)$	deep-red prism	151-153	38.66(38.67), 4.20(4.35)
3-6cα	$(C_9H_7)Co(C_3F_7)(PPhMe_2)(P(O)(OMe)_2)$	red powder	134-135	44.76(44.63), 4.10(4.14)
3-3bβ-1	$(C_5H_5)Co(C_3F_7)(PMe_3)(P(O)Ph(OMe))$	orange prism	185-187	41.24(41.35), 4.23(4.16)
3-3bβ-2	$(C_5H_5)Co(C_3F_7)(PMe_3)(P(O)Ph(OMe))$	orange microcrystal	143-144	41.24(40.95), 4.23(4.21)
3-6bβ-1	$(C_9H_7)Co(C_3F_7)(PMe_3)(P(O)Ph(OMe))$	orange plate	160-161	46.01(45.67), 4.21(4.25)
3-6bβ-2	$(C_9H_7)Co(C_3F_7)(PMe_3)(P(O)Ph(OMe))$	red microcrystal	101-104	46.01(45.74), 4.21(4.13)
3-6cβ-1	$(C_9H_7)Co(C_3F_7)(PPhMe_2)(P(O)Ph(OMe))$	red powder	145-146	50.96(51.14), 4.12(4.23)
3-6cβ-2	$(C_9H_7)Co(C_3F_7)(PPhMe_2)(P(O)Ph(OMe))$	red prism	98-101	-
3-6dβ-1	$(C_9H_7)Co(C_3F_7)(PPh_2Me)(P(O)Ph(OMe))$	red powder	150-151	55.03(54.88), 4.04(4.15)
3-6dβ-2	$(C_9H_7)Co(C_3F_7)(PPh_2Me)(P(O)Ph(OMe))$	red powder	-	-
3-6eβ-1	$(C_9H_7)Co(C_3F_7)(PPh(OMe)_2)(P(O)Ph(OMe))$	red powder	78-81	48.52(48.45), 3.92(3.92)
3-6eβ-2	$(C_9H_7)Co(C_3F_7)(PPh(OMe)_2)(P(O)Ph(OMe))$	red powder	90-93	48.52(48.04), 3.92(3.72)

[a] Sealed (N_2) capillary.

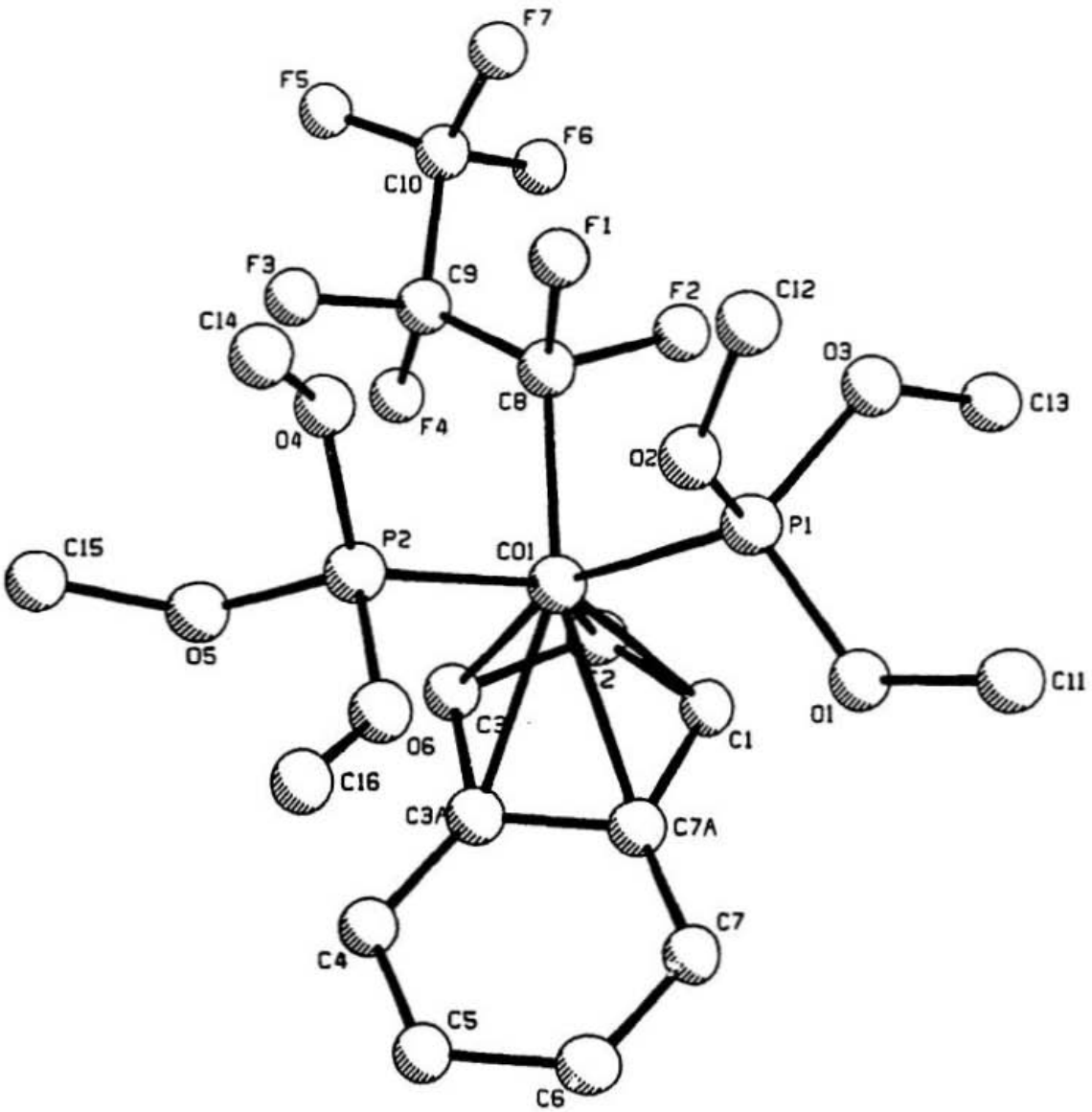

Figure 3-3. Molecular Structure of $[(\eta^5\text{-}C_9H_7)Co(C_3F_7)(P(OMe)_3)_2]^+SbF_6^-$, **3-5aα** ($SbF_6^-$ omitted for clarity).

Table 3-2. Atomic Coordinates for $[(\eta^5\text{-}C_9H_7)Co(C_3F_7)(P(OMe)_3)_2]^+SbF_6^-$, **3-5aα**.

atom	x	y	z	B(eq)
Sb(1)	0.20043(8)	0.2001(1)	0.75701(6)	6.07(6)
Co(1)	0.7568(1)	0.2758(1)	0.53760(8)	4.08(9)
P(1)	0.8081(3)	0.1053(3)	0.5681(2)	5.1(2)
P(2)	0.6799(3)	0.2352(3)	0.4280(2)	5.3(2)
F(1)	0.5846(5)	0.1485(6)	0.5674(4)	5.9(4)
F(2)	0.6585(5)	0.2525(6)	0.6574(3)	5.9(4)
F(3)	0.4834(7)	0.3194(8)	0.5008(4)	9.4(5)
F(4)	0.5644(6)	0.4373(6)	0.5781(5)	8.4(5)
F(5)	0.3652(7)	0.3763(9)	0.5924(5)	10.3(7)
F(6)	0.4859(7)	0.3553(8)	0.6825(4)	9.5(6)
F(7)	0.4244(7)	0.2155(8)	0.6258(5)	9.5(6)
F(8)	0.1129(7)	0.0790(8)	0.7630(5)	11.1(7)
F(9)	0.2896(8)	0.3167(8)	0.7533(6)	13.0(7)
F(10)	0.3106(7)	0.1028(8)	0.7578(6)	13.0(7)
F(11)	0.0881(8)	0.289(1)	0.7574(8)	18(1)
F(12)	0.2288(8)	0.204(1)	0.8540(4)	14.9(8)
F(13)	0.1744(9)	0.187(1)	0.6599(5)	15.6(8)
O(1)	0.9318(7)	0.0922(7)	0.5730(5)	6.3(6)
O(2)	0.7564(8)	0.0151(8)	0.5123(5)	7.8(6)
O(3)	0.7806(8)	0.0321(8)	0.6385(5)	7.5(6)
O(4)	0.5878(8)	0.1498(8)	0.4190(5)	6.7(6)
O(5)	0.633(1)	0.3406(8)	0.3858(5)	9.1(7)
O(6)	0.768(1)	0.186(1)	0.3863(5)	10.5(8)
C(1)	0.682(1)	0.345(1)	0.6088(7)	5.3(3)
C(2)	0.794(1)	0.413(1)	0.6026(7)	5.2(3)
C(3)	0.766(1)	0.448(1)	0.5301(7)	4.2(3)
C(3A)	0.849(1)	0.409(1)	0.4936(6)	4.2(3)
C(4)	0.868(1)	0.433(1)	0.4232(7)	5.7(3)
C(5)	0.958(1)	0.393(1)	0.4036(7)	6.1(4)
C(6)	1.028(1)	0.327(1)	0.4509(7)	6.0(3)
C(7)	1.012(1)	0.302(1)	0.5165(7)	5.8(3)
C(7A)	0.921(1)	0.344(1)	0.5404(6)	4.0(3)
C(8)	0.630(1)	0.254(1)	0.5809(7)	5.4(3)
C(9)	0.535(1)	0.331(1)	0.5703(8)	5.4(3)
C(10)	0.448(1)	0.317(1)	0.617(1)	7(1)
C(11)	0.988(1)	-0.011(1)	0.5913(8)	8(1)
C(12)	0.717(2)	-0.090(2)	0.521(1)	14(1)
C(13)	0.833(1)	0.079(1)	0.7088(8)	10(1)
C(14)	0.551(2)	0.076(2)	0.372(1)	19(2)
C(15)	0.557(1)	0.357(1)	0.328(1)	11(1)
C(16)	0.779(2)	0.157(2)	0.325(1)	13(1)

Table 3-3. Selected Bond Distances (Å) and Bond Angles (°) for [(η^5-C_9H_7)Co(C_3F_7)($P(OMe)_3$)$_2$]$^+SbF_6^-$, **3-5aα**.

	distance		angle
Co(1)-P(1)	2.205(4)	P(1)-Co(1)-P(2)	96.0(2)
Co(1)-P(2)	2.187(4)	P(1)-Co(1)-C(1)	92.5(4)
Co(1)-C(1)	2.09(1)	P(1)-Co(1)-C(2)	124.4(4)
Co(1)-C(2)	2.07(1)	P(1)-Co(1)-C(3)	158.0(4)
Co(1)-C(3)	2.09(1)	P(1)-Co(1)-C(3A)	127.9(3)
Co(1)-C(3A)	2.24(1)	P(1)-Co(1)-C(7A)	95.5(3)
Co(1)-C(7A)	2.25(1)	P(1)-Co(1)-C(8)	89.8(4)
Co(1)-C(8)	1.95(1)	P(2)-Co(1)-C(1)	150.6(4)
C(1)-C(2)	1.39(2)	P(2)-Co(1)-C(2)	139.5(4)
C(1)-C(7A)	1.45(1)	P(2)-Co(1)-C(3)	100.4(4)
C(2)-C(3)	1.42(2)	P(2)-Co(1)-C(3A)	89.6(3)
C(3)-C(3A)	1.44(1)	P(2)-Co(1)-C(7A)	111.9(3)
C(3A)-C(4)	1.42(1)	P(2)-Co(1)-C(8)	95.2(4)
C(3A)-C(7A)	1.41(1)	C(1)-Co(1)-C(8)	113.0(5)
C(4)-C(5)	1.36(2)	C(2)-Co(1)-C(8)	89.1(5)
C(5)-C(6)	1.41(2)	C(3)-Co(1)-C(8)	103.0(5)
C(6)-C(7)	1.33(1)	C(3A)-Co(1)-C(8)	141.3(5)
C(7)-C(7A)	1.41(1)	C(7A)-Co(1)-C(8)	151.5(5)
C(8)-C(9)	1.52(2)		
C(9)-C(10)	1.54(2)		
P(1)-O(1)	1.581(9)		
P(1)-O(2)	1.578(9)		
P(1)-O(3)	1.566(9)		
P(2)-O(4)	1.555(9)		
P(2)-O(5)	1.56(1)		
P(2)-O(6)	1.60(1)		

3.2.2. Molecular Structures of the Cobalt η^5-Cyclopentadienyl and η^5-Indenyl Phosphonate and Phosphinate Complexes. Single crystal X-ray diffraction structures of the η^5-indenyl phosphonate **3-6bα** and of selected diastereomers of the η^5-cyclopentadienyl (**3-3bβ-1**) and η^5-indenyl (**3-6bβ-1**, **3-6cβ-2**) phosphinates were obtained in order to confirm their structures and, in the case of the Co- and P-chiral phosphinates, to establish unequivocally their relative configurations. All structures were solved by direct methods. In each case, cobalt has an unexceptional, distorted octahedral geometry with η^5-indenyl or η^5-Cp occupying three *fac* coordination sites, as shown in Figures 3-4 - 3-7. Interligand bond angles (P(1)-Co(1)-P(2), P(1)-Co(1)-C(8), P(2)-Co(1)-C(8) for **3-6bα**, **3-6bβ-1** and **3-6cβ-2**; P(1)-Co(1)-P(2), P(1)-Co(1)-C(6), P(2)-Co(1)-C(6) for **3-3bβ-1**) are approximately 90°. Atomic coordinates, selected bond lengths and bond angles are given in Tables 3-4 to 3-11.

Consistent with their 18e⁻ configurations, all the π-indenyl complexes are η^5-bonded. However, small characteristic displacements of the metal away from the C_{3a}-C_{7a} junction and distortions of the indenyl ring from planarity as observed in other formally η^5-indenyl complexes[238, 269, 270, 279, 286] are evident. Co displacement towards C_1-C_3 (Δ(M-C) = [average of d(M-C_{3a},C_{7a})] - [average of d(M-C_1,C_3)]) is 0.16(1) Å in **3-5aα**, 0.153(4) Å in **3-6bα**, 0.19(1) Å in **3-6bβ-1** and 0.16(1) Å in **3-6cβ-2**. Hinge angles of 5.8° in **3-5aα**, 6.7° in **3-6bα**, 7.3° in **3-6bβ-1** and 7.0° in **3-6cβ-2** between the planes defined by C_1-C_2-C_3 and C_1-C_3-C_{3a}-C_{7a} as well as fold angles of 11.0° in **3-5aα**, 10.0° in **3-6bα**, 11.4° in **3-6bβ-1**, and 10.5° in **3-6cβ-2** between the plane C_1-

C_2-C_3 and the best plane containing C_{3a}-C_4-C_5-C_6-C_7-C_{7a} (Table 3-15) are consistent with moderate distortion compared to a variety of previously reported indenyl complexes.[269, 270, 279-281, 286]

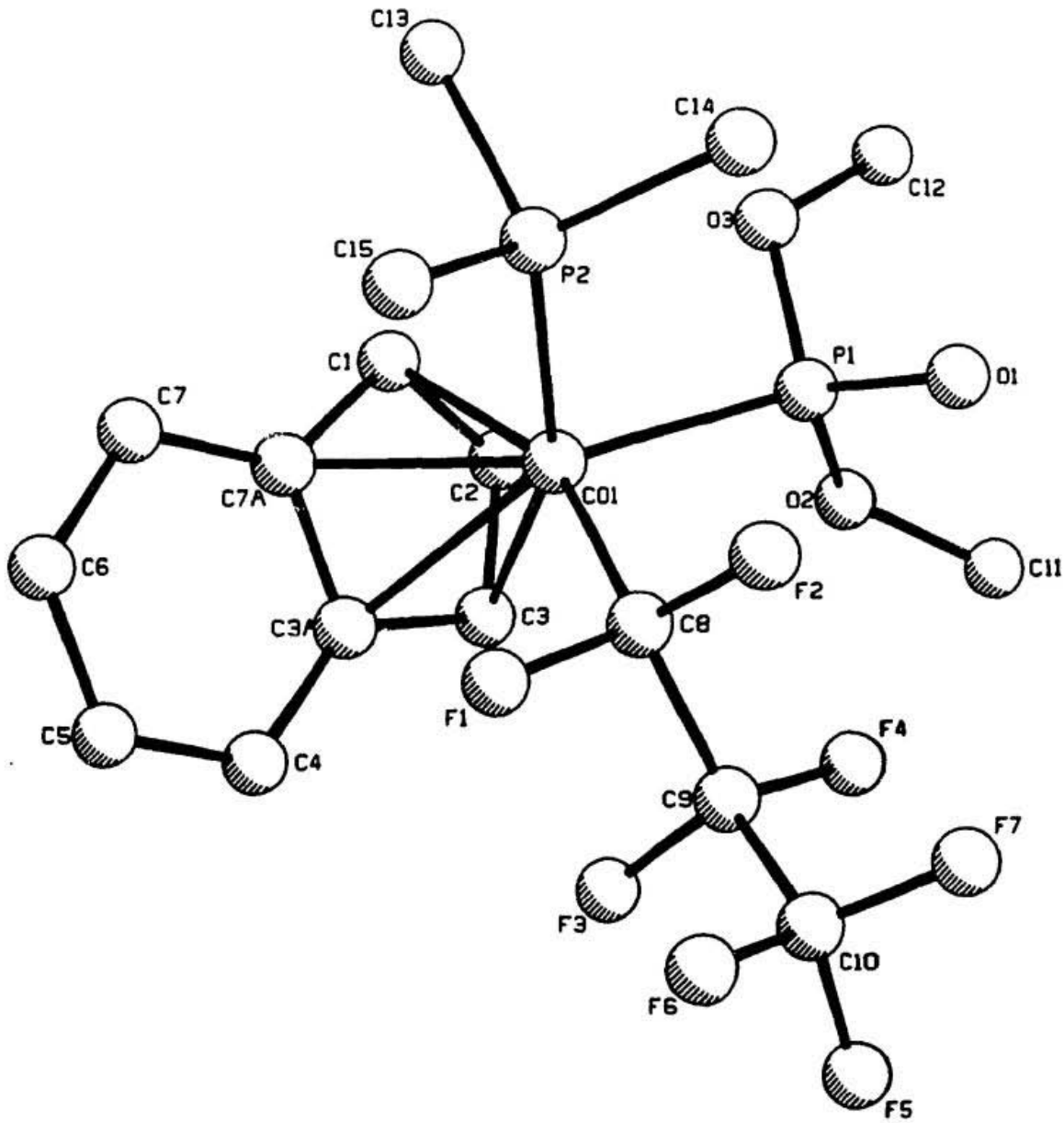

Figure 3-4. Molecular structure of (η^5-Indenyl)Co(C_3F_7)(PMe_3)(P(O)(OMe)$_2$, **3-6bα**.

Table 3-4. Atomic Coordinates for (η^5-C_9H_7)Co(C_3F_7)(PMe_3)(P(O)(OMe)$_2$), **3-6bα**.

atom	x	y	z	B(eq)
Co(1)	0.43916(7)	0.15022(3)	0.18159(4)	3.11(2)
P(1)	0.5806(2)	0.19389(8)	0.30512(8)	4.07(6)
P(2)	0.3149(2)	0.26574(7)	0.14658(8)	4.25(6)
F(1)	0.1223(3)	0.0905(2)	0.1644(1)	4.6(1)
F(2)	0.1822(3)	0.1663(2)	0.2779(2)	5.0(1)
F(3)	0.3020(4)	-0.0263(2)	0.2459(2)	6.8(2)
F(4)	0.4038(3)	0.0447(2)	0.3564(2)	6.8(2)
F(5)	0.1558(4)	-0.0553(2)	0.3719(2)	8.0(2)
F(6)	-0.0123(4)	0.0102(2)	0.2792(2)	9.5(2)
F(7)	0.1141(5)	0.0627(3)	0.3951(2)	10.3(3)
O(1)	0.4997(4)	0.2262(2)	0.3730(2)	5.3(2)
O(2)	0.7123(4)	0.1271(2)	0.3460(2)	4.7(2)
O(3)	0.6999(4)	0.2585(2)	0.2737(2)	5.6(2)
C(1)	0.5887(6)	0.1600(3)	0.0890(3)	4.0(2)
C(2)	0.6656(6)	0.1130(3)	0.1585(3)	4.4(2)
C(3)	0.5656(6)	0.0467(3)	0.1652(3)	4.0(2)
C(3A)	0.4309(5)	0.0469(3)	0.0908(3)	3.5(2)
C(4)	0.3071(6)	-0.0080(3)	0.0580(3)	4.6(2)
C(5)	0.1987(6)	0.0082(3)	-0.0175(3)	5.2(3)
C(6)	0.2113(6)	0.0784(4)	-0.0625(3)	5.4(3)
C(7)	0.3294(6)	0.1340(3)	-0.0337(3)	4.7(2)
C(7A)	0.4437(5)	0.1181(3)	0.0447(3)	3.4(2)
C(8)	0.2545(5)	0.1110(3)	0.2320(3)	3.6(2)
C(9)	0.2733(6)	0.0363(3)	0.2913(3)	4.1(2)
C(10)	0.1278(7)	0.0137(4)	0.3327(4)	5.7(3)
C(11)	0.7430(6)	0.1059(4)	0.4356(3)	6.6(3)
C(12)	0.8378(7)	0.2889(3)	0.3345(4)	7.4(3)
C(13)	0.4150(8)	0.3299(3)	0.0806(4)	6.9(3)
C(14)	0.2868(7)	0.3320(3)	0.2323(3)	5.9(3)
C(15)	0.1045(7)	0.2577(3)	0.0836(3)	6.8(3)

Table 3-5. Selected Bond Distances (Å) and Bond Angles (°) for (η^5-C_9H_7)Co(C_3F_7)(PMe_3)(P(O)($OMe)_2$), **3-6bα**.

	distance		angle
Co(1)-P(1)	2.186(1)	P(1)-Co(1)-P(2)	93.20(5)
Co(1)-P(2)	2.229(1)	P(1)-Co(1)-C(1)	108.2(1)
Co(1)-C(1)	2.104(4)	P(1)-Co(1)-C(2)	85.8(1)
Co(1)-C(2)	2.071(4)	P(1)-Co(1)-C(3)	102.0(1)
Co(1)-C(3)	2.086(4)	P(1)-Co(1)-C(3A)	140.5(1)
Co(1)-C(3A)	2.258(4)	P(1)-Co(1)-C(7A)	146.4(1)
Co(1)-C(7A)	2.238(4)	P(1)-Co(1)-C(8)	93.9(1)
Co(1)-C(8)	1.972(4)	P(2)-Co(1)-C(1)	93.6(1)
C(1)-C(2)	1.399(6)	P(2)-Co(1)-C(2)	127.5(2)
C(1)-C(7A)	1.442(6)	P(2)-Co(1)-C(3)	157.9(1)
C(2)-C(3)	1.412(6)	P(2)-Co(1)-C(3A)	125.0(1)
C(3)-C(3A)	1.441(6)	P(2)-Co(1)-C(7A)	94.2(1)
C(3A)-C(4)	1.399(6)	P(2)-Co(1)-C(8)	92.6(1)
C(3A)-C(7A)	1.426(6)	C(1)-Co(1)-C(8)	156.6(2)
C(4)-C(5)	1.362(7)	C(2)-Co(1)-C(8)	139.9(2)
C(5)-C(6)	1.402(7)	C(3)-Co(1)-C(8)	102.2(2)
C(6)-C(7)	1.366(7)	C(3A)-Co(1)-C(8)	93.9(2)
C(7)-C(7A)	1.419(6)	C(7A)-Co(1)-C(8)	118.4(2)
C(8)-C(9)	1.565(6)		
C(9)-C(10)	1.527(7)		
P(1)-O(1)	1.479(3)		
P(1)-O(2)	1.609(3)		
P(1)-O(3)	1.617(4)		
P(2)-C(13)	1.818(6)		
P(2)-C(14)	1.812(5)		
P(2)-C(15)	1.817(5)		

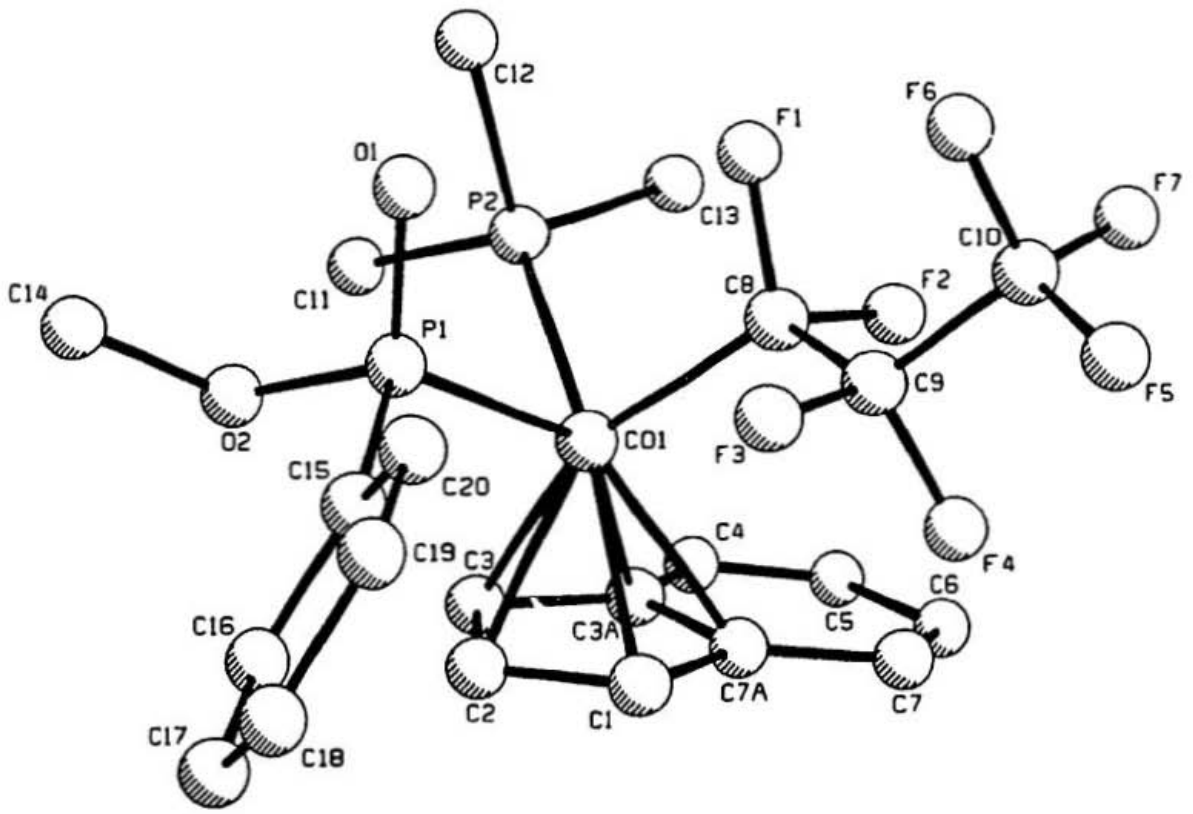

Figure 3-5. Molecular structure of [$S_{Co}, S_P / R_{Co}, R_P$]-($\eta^5$-Indenyl)Co($C_3F_7$)($PMe_3$)(P(O)Ph(OMe)), **3-6bβ-1**.($S_{Co}S_P$ enantiomer shown)

Table 3-6. Atomic Coordinates for [$S_{Co}, S_P / R_{Co}, R_P$]-($\eta^5$-$C_9H_7$)Co($C_3F_7$)($PMe_3$)(P(O)Ph(OMe)), **3-6bβ-1**.

atom	x	y	z	B(eq)
Co(1)	0.27899(7)	0.10912(7)	0.81577(6)	2.84(4)
P(1)	0.3524(1)	0.2025(2)	0.7279(1)	3.27(9)
P(2)	0.1427(1)	0.2154(2)	0.8054(1)	3.7(1)
F(1)	0.1196(3)	0.0889(3)	0.6271(3)	4.6(2)
F(2)	0.1065(3)	-0.0155(3)	0.7350(3)	4.8(2)
F(3)	0.3207(4)	-0.0065(4)	0.6291(4)	8.2(3)
F(4)	0.2725(5)	-0.1152(4)	0.7139(3)	9.3(3)
F(5)	0.2163(4)	-0.1590(4)	0.5339(3)	7.5(3)
F(6)	0.1357(5)	-0.0297(4)	0.4866(4)	9.1(3)
F(7)	0.0695(5)	-0.1215(5)	0.5686(4)	10.4(4)
O(1)	0.2801(4)	0.2346(3)	0.6316(3)	4.3(2)
O(2)	0.3929(4)	0.2913(4)	0.8018(3)	4.3(2)
C(1)	0.4035(8)	0.0137(8)	0.8836(5)	6.2(5)
C(2)	0.4322(6)	0.1034(9)	0.9187(6)	6.1(5)
C(3)	0.3592(7)	0.1361(6)	0.9640(5)	4.7(4)
C(3A)	0.2873(6)	0.0607(6)	0.9682(5)	3.6(3)
C(4)	0.2058(8)	0.0509(8)	1.0171(6)	7.0(6)
C(5)	0.157(1)	-0.034(1)	1.013(1)	10.8(9)
C(6)	0.183(1)	-0.113(1)	0.969(1)	12(1)
C(7)	0.258(1)	-0.107(1)	0.9172(7)	10.2(8)
C(7A)	0.3151(7)	-0.0187(6)	0.9190(5)	4.6(4)
C(8)	0.1849(6)	0.0351(5)	0.7034(5)	3.2(3)
C(9)	0.2352(7)	-0.0408(6)	0.6531(5)	4.3(4)
C(10)	0.1610(9)	-0.0911(7)	0.5623(7)	5.4(5)
C(11)	0.1769(6)	0.3109(6)	0.8942(6)	5.9(5)
C(12)	0.0827(7)	0.2838(6)	0.6952(6)	6.5(5)
C(13)	0.0186(6)	0.1627(7)	0.8218(7)	7.3(5)
C(14)	0.4242(7)	0.3778(6)	0.7657(7)	7.0(5)
C(15)	0.4841(5)	0.1660(5)	0.7062(5)	3.1(3)
C(16)	0.5866(6)	0.1753(6)	0.7750(5)	4.3(4)
C(17)	0.6838(6)	0.1519(6)	0.7526(6)	5.6(5)
C(18)	0.6762(7)	0.1203(7)	0.6608(7)	6.0(5)
C(19)	0.5767(7)	0.1128(7)	0.5911(6)	5.4(4)
C(20)	0.4805(6)	0.1344(6)	0.6143(5)	4.4(4)

Table 3-7. Selected Bond Distances (Å) and Bond Angles (°) for [S_{Co},S_P/R_{Co},R_P]-(η^5-C_9H_7)Co(C_3F_7)(PMe_3)(P(O)Ph(OMe)), **3-6bβ-1**.

	distance		angle
Co(1)-P(1)	2.207(2)	P(1)-Co(1)-P(2)	90.73(8)
Co(1)-P(2)	2.247(2)	P(1)-Co(1)-C(1)	105.2(3)
Co(1)-C(1)	2.072(8)	P(1)-Co(1)-C(2)	88.2(2)
Co(1)-C(2)	2.055(8)	P(1)-Co(1)-C(3)	108.5(3)
Co(1)-C(3)	2.102(7)	P(1)-Co(1)-C(3A)	145.6(2)
Co(1)-C(3A)	2.267(7)	P(1)-Co(1)-C(7A)	143.2(2)
Co(1)-C(7A)	2.283(8)	P(1)-Co(1)-C(8)	95.5(2)
Co(1)-C(8)	1.987(7)	P(2)-Co(1)-C(1)	156.6(2)
C(1)-C(2)	1.36(1)	P(2)-Co(1)-C(2)	127.6(4)
C(1)-C(7A)	1.43(1)	P(2)-Co(1)-C(3)	94.3(2)
C(2)-C(3)	1.36(1)	P(2)-Co(1)-C(3A)	94.3(2)
C(3)-C(3A)	1.41(1)	P(2)-Co(1)-C(7A)	124.3(2)
C(3A)-C(4)	1.417(9)	P(2)-Co(1)-C(8)	91.9(2)
C(3A)-C(7A)	1.42(1)	C(1)-Co(1)-C(8)	103.3(4)
C(4)-C(5)	1.34(2)	C(2)-Co(1)-C(8)	140.3(4)
C(5)-C(6)	1.37(2)	C(3)-Co(1)-C(8)	155.1(3)
C(6)-C(7)	1.37(1)	C(3A)-Co(1)-C(8)	118.2(3)
C(7)-C(7A)	1.43(1)	C(7A)-Co(1)-C(8)	94.2(3)
P(1)-O(1)	1.482(5)	Co(1)-P(1)-O(1)	118.0(2)
P(1)-O(2)	1.617(5)	Co(1)-P(1)-O(2)	100.7(2)
P(1)-C(15)	1.854(6)	Co(1)-P(1)-C(15)	119.0(2)
P(2)-C(11)	1.810(8)	O(1)-P(1)-O(2)	111.4(3)
P(2)-C(12)	1.812(8)	O(1)-P(1)-C(15)	104.9(3)
P(2)-C(13)	1.812(8)	O(2)-P(1)-C(15)	101.6(3)

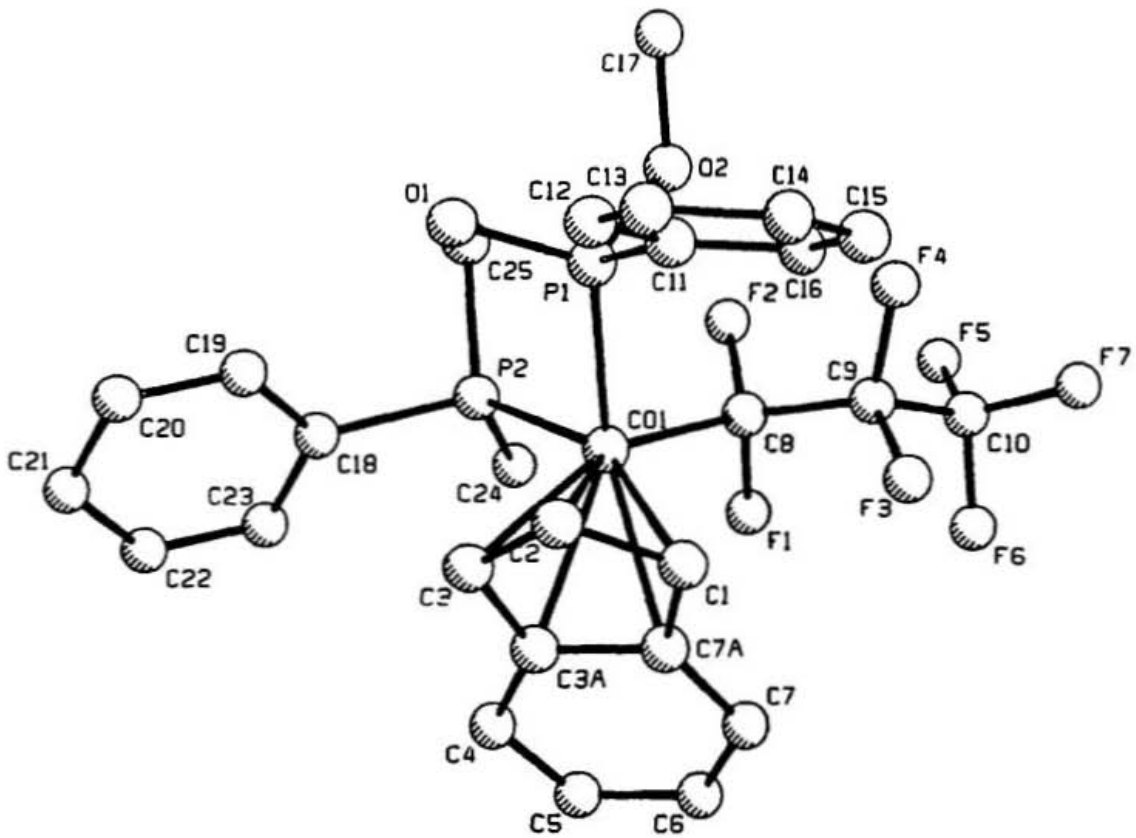

Figure 3-6. Molecular Structure of $[S_{Co}, R_P / R_{Co}, S_P]$-($\eta^5$-Indenyl)Co($C_3F_7$)($PPhMe_2$)(P(O)Ph(OMe)), **3-6cβ-2**.(S_{Co},$R_P$enantiomer shown)

Table 3-8. Atomic Coordinates for [S_{Co},R_P/R_{Co},S_P]-(η^5-C_9H_7)Co(C_3F_7)(PPhMe$_2$)(P(O)Ph(OMe)), **3-6cβ-2**.

atom	x	y	z	B(eq)	Occupancy
Co(1)	0.71137(3)	0.12953(4)	0.63195(3)	3.48(3)	
P(1)	0.67932(7)	-0.0057(1)	0.61424(7)	4.10(7)	
P(2)	0.63744(7)	0.1569(1)	0.70110(6)	4.19(7)	
F(1)	0.7886(1)	0.1892(2)	0.7275(1)	4.9(2)	
F(2)	0.7478(1)	0.0653(2)	0.7555(1)	5.1(2)	
F(3)	0.86[illegible]7(2)	0.0838(3)	0.6440(2)	8.8(2)	
F(4)	0.8264(2)	-0.0273(2)	0.6952(2)	8.4(2)	
F(5)	0.8635(2)	0.0627(4)	0.8052(2)	13.0(4)	
F(6)	0.9057(2)	0.1535(3)	0.7485(2)	12.1(4)	
F(7)	0.9311(2)	0.0220(3)	0.7425(2)	10.3(3)	
O(1)	0.6116(1)	-0.0093(2)	0.5990(2)	4.8(2)	
O(2)	0.6983(2)	-0.0637(2)	0.6752(2)	4.8(2)	
C(1)	0.7661(3)	0.1521(3)	0.5548(2)	4.4(3)	
C(2)	0.7042(3)	0.1407(3)	0.5339(2)	4.5(3)	
C(3)	0.6686(2)	0.2061(4)	0.5595(2)	4.4(3)	
C(3A)	0.7093(3)	0.2678(3)	0.5919(2)	4.0(3)	
C(4)	0.6990(3)	0.3512(4)	0.6203(3)	5.8(4)	
C(5)	0.7494(4)	0.3966(4)	0.6433(3)	7.1(4)	
C(6)	0.8090(4)	0.3633(5)	0.6399(3)	7.2(4)	
C(7)	0.8197(3)	0.2843(5)	0.6139(3)	5.7(4)	
C(7A)	0.7700(3)	0.2340(4)	0.5886(2)	4.1(3)	
C(8)	0.7714(2)	0.1059(3)	0.7027(2)	4.1(3)	
C(9)	0.8341(3)	0.0610(4)	0.6968(3)	5.4(4)	
C(10)	0.8833(4)	0.0722(6)	0.7500(4)	7.5(5)	
C(11)	0.7158(3)	-0.0636(3)	0.5498(3)	4.5(3)	
C(12)	0.6808(3)	-0.0825(4)	0.4955(3)	6.8(4)	
C(13)	0.7059(4)	-0.1226(6)	0.4440(3)	9.2(5)	
C(14)	0.7665(4)	-0.1454(5)	0.4457(4)	9.2(6)	
C(15)	0.8021(3)	-0.1284(5)	0.5000(4)	9.8(6)	
C(16)	0.7762(3)	-0.0871(5)	0.5515(3)	7.3(4)	
C(17)	0.6747(3)	-0.1508(4)	0.6805(3)	7.2(4)	
C(18)	0.5672(2)	0.2076(4)	0.6677(3)	4.8(3)	
C(19)	0.5280(3)	0.1590(4)	0.6290(3)	5.8(4)	
C(20)	0.4742(3)	0.1940(6)	0.6030(3)	7.7(5)	
C(21)	0.4586(4)	0.2807(7)	0.6163(4)	8.9(6)	
C(22)	0.4977(4)	0.3297(5)	0.6544(4)	8.5(5)	
C(23)	0.5516(3)	0.2948(5)	0.6804(3)	6.6(4)	
C(24)	0.6619(2)	0.2315(4)	0.7642(2)	5.7(3)	
C(25)	0.6059(2)	0.0657(4)	0.7456(2)	5.6(3)	
Cl(1)	0.4526(1)	0.0833(2)	0.0403(1)	12.0(2)	
Cl(2)	0.4804(1)	0.1189(2)	0.1709(1)	15.0(2)	
Cl(3)	0.5147(1)	0.2360(2)	0.0764(1)	16.6(2)	
C(26)	0.5047(3)	0.1269(5)	0.0957(3)	7.8(4)	
O(3)	0.068(1)	-0.003(2)	0.530(2)	15(1)	0.350
O(4)	-0.0453(7)	0.0329(8)	0.5449(7)	9.7(3)	0.550
O(5)	0.067(1)	-0.007(2)	0.494(2)	12.9(8)	0.350
O(6)	-0.000(1)	0.046(1)	0.497(1)	13.4(6)	0.350
O(7)	-0.0654(8)	0.075(1)	0.4996(9)	9.4(4)	0.350
O(8)	-0.000(1)	0.042(1)	0.5746(9)	9.7(5)	0.350
O(9)	0.0413(8)	0.0378(8)	0.5721(6)	10.5(3)	0.550

Table 3-9. Selected Bond Distances (Å) and Bond Angles (°) for $[S_{Co},R_P/R_{Co},S_P]$-(η^5-C_9H_7)Co(C_3F_7)(PPhMe$_2$)(P(O)Ph(OMe)), **3-6cβ-2**.

	distance		angle
Co(1)-P(1)	2.200(2)	P(1)-Co(1)-P(2)	93.01(6)
Co(1)-P(2)	2.257(2)	P(1)-Co(1)-C(1)	102.1(2)
Co(1)-C(1)	2.086(5)	P(1)-Co(1)-C(2)	84.0(1)
Co(1)-C(2)	2.078(5)	P(1)-Co(1)-C(3)	105.4(2)
Co(1)-C(3)	2.109(5)	P(1)-Co(1)-C(3A)	143.4(1)
Co(1)-C(3A)	2.266(5)	P(1)-Co(1)-C(7A)	140.5(1)
Co(1)-C(7A)	2.256(5)	P(1)-Co(1)-C(8)	98.9(2)
Co(1)-C(8)	1.979(5)	P(2)-Co(1)-C(1)	157.1(1)
C(1)-C(2)	1.414(7)	P(2)-Co(1)-C(2)	127.1(2)
C(1)-C(7A)	1.437(7)	P(2)-Co(1)-C(3)	93.5(1)
C(2)-C(3)	1.386(7)	P(2)-Co(1)-C(3A)	93.8(1)
C(3)-C(3A)	1.443(7)	P(2)-Co(1)-C(7A)	124.3(1)
C(3A)-C(4)	1.426(7)	P(2)-Co(1)-C(8)	90.7(2)
C(3A)-C(7A)	1.423(7)	C(1)-Co(1)-C(8)	103.7(2)
C(4)-C(5)	1.370(8)	C(2)-Co(1)-C(8)	140.0(2)
C(5)-C(6)	1.399(9)	C(3)-Co(1)-C(8)	155.1(2)
C(6)-C(7)	1.345(8)	C(3A)-Co(1)-C(8)	116.9(2)
C(7)-C(7A)	1.413(7)	C(7A)-Co(1)-C(8)	93.8(2)
P(1)-O(1)	1.500(3)	Co(1)-P(1)-O(1)	111.9(2)
P(1)-O(2)	1.600(3)	Co(1)-P(1)-O(2)	108.0(1)
P(1)-C(11)	1.831(5)	Co(1)-P(1)-C(11)	115.6(2)
P(2)-C(18)	1.830(6)	O(1)-P(1)-O(2)	111.9(2)
P(2)-C(24)	1.815(5)	O(1)-P(1)-C(11)	106.0(2)
P(2)-C(25)	1.825(5)	O(2)-P(1)-C(11)	103.1(2)

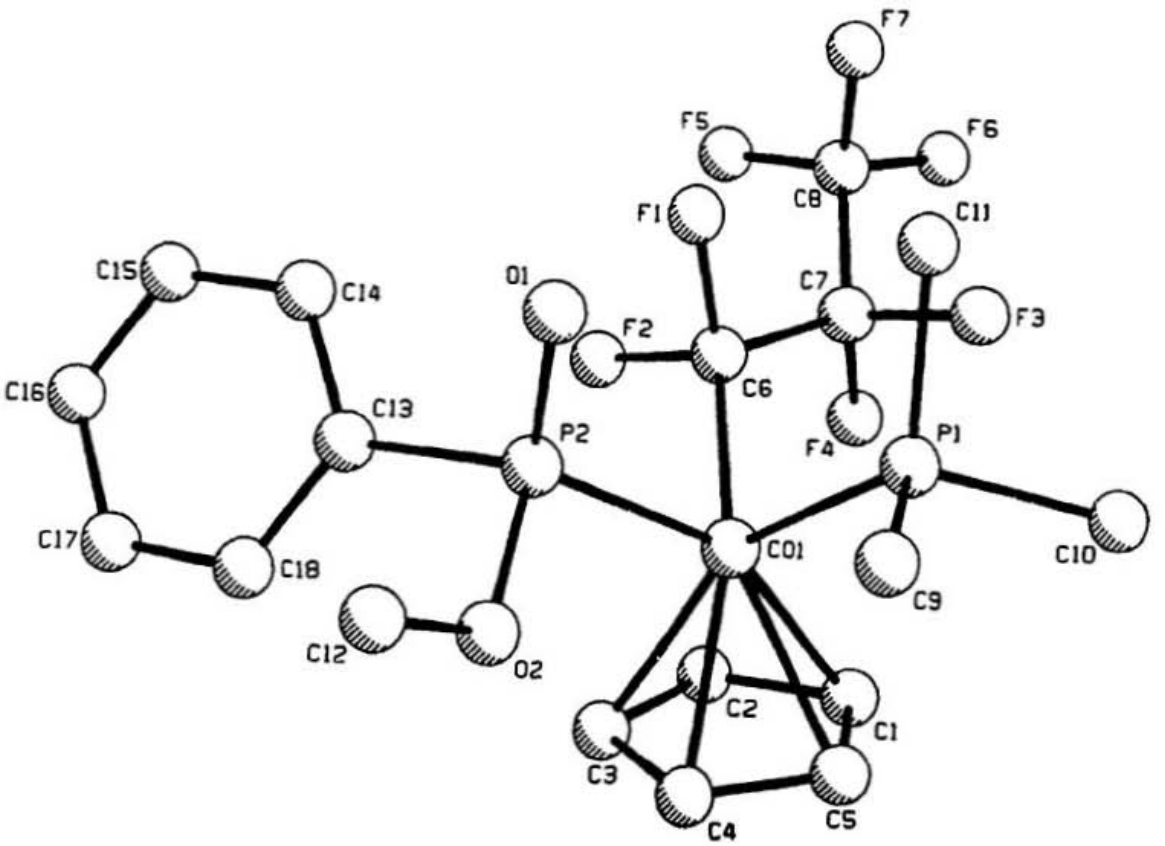

Figure 3-7. Molecular structure of $[R_{Co}R_P/S_{Co}S_P]$-$(\eta^5$-Cp)Co$(C_3F_7)(PMe_3)(P(O)Ph(OMe))$, **3-3bβ-1**. ($R_{Co}R_P$ enantiomer shown)

Table 3-10. Atomic Coordinates for [R_{Co},R_P/S_{Co},S_P]-(η^5-C_5H_5)Co(C_3F_7)(PMe_3)(P(O)Ph(OMe)), **3-3bβ-1**.

atom	x	y	z	B(eq)
Co(1)	0.82130(6)	0.13987(3)	0.14799(3)	2.91(2)
P(1)	0.6213(1)	0.21760(5)	0.11060(7)	3.52(4)
P(2)	0.8992(1)	0.20812(6)	0.27431(6)	3.42(4)
F(1)	0.6289(3)	0.1001(1)	0.2886(1)	4.5(1)
F(2)	0.8178(3)	0.0209(1)	0.2724(1)	4.6(1)
F(3)	0.4792(3)	0.0523(1)	0.1120(2)	7.3(1)
F(4)	0.6584(3)	-0.0339(1)	0.1171(2)	6.6(1)
F(5)	0.5774(4)	-0.0735(2)	0.2884(2)	10.1(2)
F(6)	0.3982(4)	-0.0818(2)	0.1768(2)	8.3(2)
F(7)	0.3938(5)	0.0037(2)	0.2723(3)	12.1(3)
O(1)	0.7759(3)	0.2456(1)	0.3230(2)	4.5(1)
O(2)	1.0189(3)	0.2688(1)	0.2378(2)	4.8(1)
C(1)	0.8424(5)	0.0808(3)	0.0239(3)	4.5(2)
C(2)	0.9481(6)	0.0517(3)	0.0972(3)	5.0(2)
C(3)	1.0518(5)	0.1081(3)	0.1318(3)	5.2(2)
C(4)	1.0128(6)	0.1725(3)	0.0785(3)	5.2(2)
C(5)	0.8858(6)	0.1549(3)	0.0127(3)	4.9(2)
C(6)	0.7103(5)	0.0690(2)	0.2209(2)	3.5(2)
C(7)	0.5861(5)	0.0144(2)	0.1701(3)	4.1(2)
C(8)	0.4884(6)	-0.0343(3)	0.2278(3)	5.1(2)
C(9)	0.6860(6)	0.3136(3)	0.1017(4)	5.3(3)
C(10)	0.5070(7)	0.2016(3)	-0.0025(3)	5.7(3)
C(11)	0.4667(5)	0.2261(3)	0.1855(3)	4.9(2)
C(12)	1.0674(9)	0.3327(3)	0.2953(5)	8.4(4)
C(13)	1.0332(5)	0.1587(2)	0.3625(2)	3.9(2)
C(14)	0.9712(6)	0.1256(3)	0.4365(3)	5.4(2)
C(15)	1.071(1)	0.0892(3)	0.5056(4)	8.0(4)
C(16)	1.229(1)	0.0841(4)	0.5010(5)	9.6(5)
C(17)	1.2924(7)	0.1156(4)	0.4281(5)	8.4(4)
C(18)	1.1957(6)	0.1535(3)	0.3597(3)	5.8(3)

Table 3-11. Selected Bond Distances (Å) and Bond Angles (°) for [R_{Co},R_P/S_{Co},S_P]-(η^5-C_5H_5)Co(C_3F_7)(PMe_3)(P(O)Ph(OMe)), **3-3bβ-1**.

	distance		angles
Co(1)-P(1)	2.208(1)	P(1)-Co(1)-P(2)	89.67(4)
Co(1)-P(2)	2.233(1)	P(1)-Co(1)-C(1)	104.6(1)
Co(1)-C(1)	2.116(4)	P(1)-Co(1)-C(2)	143.2(1)
Co(1)-C(2)	2.097(4)	P(1)-Co(1)-C(3)	148.1(2)
Co(1)-C(3)	2.078(4)	P(1)-Co(1)-C(4)	108.9(2)
Co(1)-C(4)	2.101(4)	P(1)-Co(1)-C(5)	88.4(1)
Co(1)-C(5)	2.122(4)	P(1)-Co(1)-C(6)	97.7(1)
Co(1)-C(6)	1.968(4)	P(2)-Co(1)-C(1)	157.6(1)
C(1)-C(2)	1.401(6)	P(2)-Co(1)-C(2)	126.2(2)
C(1)-C(5)	1.394(6)	P(2)-Co(1)-C(3)	93.4(1)
C(2)-C(3)	1.391(6)	P(2)-Co(1)-C(4)	94.4(1)
C(3)-C(4)	1.404(7)	P(2)-Co(1)-C(5)	127.3(1)
C(4)-C(5)	1.382(6)	P(2)-Co(1)-C(6)	91.3(1)
P(1)-C(9)	1.815(5)	C(1)-Co(1)-C(6)	103.5(2)
P(1)-C(10)	1.820(5)	C(2)-Co(1)-C(6)	90.3(2)
P(1)-C(11)	1.813(5)	C(3)-Co(1)-C(6)	114.0(9)
P(2)-O(1)	1.494(3)	C(4)-Co(1)-C(6)	152.8(2)
P(2)-O(2)	1.622(3)	C(5)-Co(1)-C(6)	141.0(2)
P(2)-C(13)	1.829(4)	Co(1)-P(2)-O(1)	118.9(1)
		Co(1)-P(2)-O(2)	103.3(1)
		Co(1)-P(2)-C(13)	113.7(1)
		O(1)-P(2)-O(2)	111.0(2)
		O(1)-P(2)-C(13)	107.2(2)
		O(2)-P(2)-C(13)	101.2(2)

3.2.3. NMR Spectroscopy of the Cobalt η^5-Cyclopentadienyl and η^5-Indenyl Phosphonate and Phosphinate Complexes. Complete ^1H, ^{31}P, ^{13}C and ^{19}F NMR parameters for the η^5-indenyl and η^5-cyclopentadienyl phosphonate and phosphinate complexes isolated in this study are given in Tables 3-12 - 3-14. ^{31}P NMR is an excellent diagnostic tool for the characterization of a phosphoryl group.[182] All phosphonate and phosphinate complexes **3-3** and **3-6** showed well resolved ^{31}P AX patterns (cf. Table 3-12). Coordinated $P(OMe)_3$ (δ=145 $\pm$ 2 ppm for neutral complexes **3-6a**α, **3-6'a**α, **3-3a**α) and $PPh(OMe)_2$ (δ=170$\pm$2 ppm for **3-6e**β) were considerably less shielded than $P(O)(OMe)_2$ (δ=73-93 ppm for **3-3a**α, **3-3b**α, **3-6a**α, **3-6'a**α, **3-6b**α and **3-6c**α) and P(O)Ph(OMe) (δ=97-112 ppm for **3-6b**β, **3-6c**β, **3-6d**β and **3-6e**β).

The most interesting features in the ^1H and ^{13}C NMR spectra of the phosphinate and phosphonate complexes derive from the presence of chiral P and/or Co centers which require that pairs of indenyl ring atoms (1,3; 4,7; 5,6; cf. Scheme 2-3 for numbering) as well as geminal substituents CX_2 (X = OMe, F) be diastereotopic. Large diastereotopic chemical shift differences of the indenyl ring and geminal phosphonate methoxyl resonances gave well-separated resonances in both the ^1H and ^{13}C NMR spectra. Intra-ring proton couplings were in general not resolved. Unequivocal ^1H and ^{13}C NMR assignments (cf. Tables 3-12 and 3-13) were possible on the basis of the ^1H nuclear Overhauser effect difference (nOed) spectra, which measured sequential nOe enhancements around the ring perimeter, and 2-D $^1H/^{13}C$

^1J heterocorrelation spectra as presented in Chapter 2. The ^{13}C chemical shift assignments permitted calculation of $\Delta\delta^{13}C_{3a,7a}$ distortion parameters (Table 3-15), which fell in the range -22 to -15 ppm for all π-indenyl complexes characterized in this study. Both solution NMR and solid state crystallographic evidence (*vide infra*) supported a moderately distorted η^5-indenyl coordination mode.[238, 279, 281, 282, 286, 299]

The perfluoropropyl C_α-C_γ ^{19}F NMR resonances (cf. Table 3-14) are well resolved in both the η^5-indenyl and the η^5-cyclopentadienyl series. Typically small vicinal couplings ($^3J_{FF}$=5-10 Hz) allow approximation of the ^{19}F spectra of the diastereotopic $C_\alpha F_2$ and $C_\beta F_2$ groups as isolated AB spin systems with $^2J_{FaFb}$ = 265-290 Hz.[208, 281, 282] The coupling constants $^2J_{FaFb}$ show a marked increase on passing from C_α to C_β but are relatively constant further along the perfluoroalkyl chain[281, 282] suggesting a weakening of the C_α-F bond[295] as discussed in Chapter 2. All complexes have larger diastereotopic chemical shift differences ($\Delta\delta(F_aF_b) = \delta(F_a)-\delta(F_b)$ (ppm)) for $C_\alpha F_aF_b$ than for $C_\beta F_aF_b$. Except for the diastereomeric pair **3-6bβ-1,2**, $\Delta\delta(F_aF_b)$ for C_α and C_β is larger in the high Rf complexes compared to the lower Rf complexes.

Table 3-12. ^{1}H and ^{31}P NMR for η^5-Cyclopentadienyl and η^5-Indenyl Co(III) Complexes[a,b]

Cpd	H_1	H_2	H_3	H_4	H_5	H_6	H_7	Cp	Me	C_6H_5	^{31}P
3-1b[c]								5.32	1.83 (d, 11.4)		16.38
3-1b'								5.46	1.70 (t,5.4)		14.83
3-3aα								5.23	3.76 (d, 10.9)[d] 3.66 (d, 10.7)[e] 3.67 (d, 10.9)[e]		146.12 (d, 173.7)[q] 73.00 (d, 173.7)[r]
3-3bα								5.10	1.58 (d, 11.1)[f] 3.66 (d, 10.9)[e] 3.67 (d, 9.6)[e]		22.71 (d, 123.8)[s] 92.29 (d, 123.8)[r]
3-5aα	6.10	5.71	6.10	[g]	[g]	[g]	[g]		3.75 (t, 5.4)		135.34
3-6aα	5.36	5.87 (m)[h]	5.79	7.39 (m)	7.30 (m)	7.30 (m)	7.46 (m)		3.62 (d, 10.4)[d] 3.63 (d, 10.7)[e] 3.65 (d, 10.3)[e]		144.70 (d, 163.6)[q] 85.44 (d, 163.6)[r]
3-6'aα	5.35	5.88 (m)[h]	5.79	7.39 (m)	7.31 (m)	7.31 (m)	7.45 (m)		3.62 (d, 10.4)[d] 3.64 (d, 10.7)[e] 3.66 (d, 10.2)[e]		144.45 (d, 165.7)[q] 84.94 (d, 165.7)[r]
3-6bα	5.07	5.97 (m)[h]	5.87	7.46 (m)	7.37 (m)	7.30 (m)	7.38 (m)		1.33 (d, 11.0)[f] 3.63 (d, 10.6)[e] 3.65 (d, 10.8)[e]		13.47 (d, 113.8)[s] 84.04 (d, 113.8)[r]
3-6cα	4.17	5.86	5.75	7.36 (m)	7.29 (m)	7.29 (m)	6.95 (m)		1.27 (d, 10.6)[f] 1.61 (d, 11.3)[f] 3.71 (d, 10.6)[e] 3.77 (d, 10.7)[e]	7.98(m,2H)[j], 7.55(m,3H)[j,k]	17.17 (d, 109.5)[s] 83.35 (d, 109.5)[r]
3-3bβ-1								5.04	1.65 (d,11.1)[f] 3.50 (d,10.9)[e]	7.68(m,2H)[j], 7.37(m,3H)[m,n]	22.5 (d,104.9)[s] 111.58 (d,104.9)[r]
3-3bβ-2								4.89	1.66 (d,11.1)[f] 3.39 (d,11.1)[e]	7.80(m,2H)[j], 7.42(m,3H)[m,n]	22.01 (d,110.8)[s] 105.63 (d,110.8)[r]
3-6bβ-1	5.39	5.72	5.67	7.35[o]	7.28	7.28	7.35[o]		1.28 (d,11.1)[f] 3.52 (d,10.7)[e]	7.72(m,2H)[j], 7.35(m,3H)[m,n]	13.82 (d,93.2)[s] 104.09 (d,93.2)[r]

Table 3-12. cont'd

3-6bβ-2	5.03	5.20 (m)	5.61 (m)	7.37 (m)	7.48 (m)[o]	7.37 (m)	7.37 (m)	1.42 (d,11.0)[f] 3.29 (d,11.4)[e]	7.86 (m,2H)[i], 7.48(m,2H)[m] 7.29 (m,1H)[n]	13.85 (d,105.1)[e] 100.74 (d,105.1)[r]
3-6cβ-1	4.70	6.08	5.49	7.30 (m)	7.13 (t,7.5)	6.97 (t,7.5)	6.64 (d,7.5)	1.38 (d,11.1)[f] 1.88 (d,11.1)[f] 3.50 (d,10.8)[e]	7.70 (m,4H)[j] 7.47 (m,3H),7.40 (m,3H)	17.79 (d,87.9)[e] 103.17 (d,87.9)[r]
3-6cβ-2	4.17	5.11	5.23	7.29 (m)	7.29 (m)	7.29 (m)	7.07 (m)	1.42 (d,10.5)[f] 1.81 (d,11.4)[f] 3.34 (d,11.4)[e]	8.26 (m,2H)[i], 7.96 (m,2H)[l] 7.55 (m,3H)[j,k] 7.49 (m,3H)[m,n]	15.89 (d,80.5)[e] 103.04 (d,80.5)[r]
3-6dβ-1	5.08	6.17 (m)	5.63	7.45 (m)	7.14 (t,7.7)	6.64 (t,7.7)	6.45 (d,7.7)	1.93 (dd,11.5,2.6)[f] 2.94 (d,10.9)[e]	7.92(m,2H)[i], 6.79(m,2H)[l] 7.53(m,2H)[j], 7.50(m,3H) 7.30(m,4H), 7.18(m,2H)	34.17 (d,96.3)[e] 98.70 (d,96.3)[r]
3-6dβ-2	4.79	5.45 (m)	5.39 (m)	7.56 (m)[o]	7.24 (t,7.9)	7.13 (t,7.9)	6.53 (d,7.9)	1.86 (d,10.2)[f] 2.91 (d,11.3)[e]	7.78(m,2H)[i], 7.72(m,4H)[l] 7.30-7.56(m,9H)	20.52 (d,101.4)[e] 97.71 (d,101.4)[r]
3-6eβ-1	4.87	6.13	5.90	7.35 (m)	7.18 (m)	7.18 (m)	7.05 (m)	3.27 (dd,10.6,1.8)[e] 3.42 (d,9.1)[d] 3.46 (d,8.9)[d]	8.15(m,2H)[i], 7.63(m,2H)[l] 7.52(m,3H)[j,k], 7.28(m,3H)[m,n]	106.71 (d,114.2)[r] 168.99 (d,114.2)[q]
3-6eβ-1	5.04	5.49	5.49	7.29 (m)	[p]	[p]	[p]	3.21 (d,11.2)[e] 3.52 (d,11.0)[d] 3.62 (d,10.7)[d]	7.76-7.90(m,4H)[j] 7.38-7.50(m,6H)	100.69 (d,111.1)[r] 172.23 (d,111.1)[q]

[a] ^{1}H (300.1 MHz) NMR chemical shifts in ppm relative to TMS; ^{31}P (121.5 MHz) NMR chemical shifts in ppm relative to external 85% H_3PO_4, J_{PP} in Hz are given in brackets, all peaks show further unresolved splitting.; Solvent = $CDCl_3$; m = multiplet; d = doublet; t = triplet; J values in Hz given in brackets. [b] All indenyl proton peaks show further small, unresolved coupling (0.3-1.5 Hz). [c] solvent = acetone-d_6. [d] PR(O*Me*)$_2$, $^3J_{PH}$. [e] P(O)R(O*Me*), $^3J_{PH}$. [f] P-*Me*, $^2J_{PH}$. [g] appear as a multiplet center at 7.54 ppm. [h] J = 3-5 Hz. [i] H_{ortho} of P-Ph. [j] H_{meta} of P-Ph. [k] H_{para} of P-Ph. [l] H_{ortho} of P(O)-Ph. [m] H_{meta} of P(O)-Ph. [n] H_{para} of P(O)-Ph. [o] overlapped with phenyl protons. [p] 7.10-7.23 (m, 3H). [q] *P*R(OMe)$_2$. [r] *P*(O)R(OMe). [s] *P*Ph$_n$Me$_{3-n}$.

Table 3-13. ^{13}C NMR for η^5-Cyclopentadienyl and η^5-Indenyl Co(III) Complexes[a].

Cpd	C_1	C_2	C_3	C_{3a}/C_{7a}	C_4	C_5	C_6	C_7	Cp	C_6H_5	Me
3-1b[b]									88.07		19.94 (d, 34.8)
3-1b'									90.88		22.15 (t, 16.0)
3-3aα									89.44		53.96 (d, 8.0)[c] 51.27 (d, 8.8)[d] 50.92 (d, 8.7)[d]
3-3bα									88.85		19.60 (d, 32.6)[e] 51.49 (d, 9.1)[d] 50.51 (d, 10.6)[d]
3-5aα	76.40	97.92	76.40	111.43	126.80	132.59	132.59	126.80			55.60 (d,4.5)
3-6aα	75.46	99.01	73.75 (t,5.0)	113.99, 110.81 (d,4.4)	126.24	129.25	128.51	126.07			53.77 (d,7.5)[c] 51.75 (d, 10.7)[d] 51.58 (d, 10.5)[d]
3-6'aα	75.50	99.14	73.95 (t, 5.0)	114.11, 110.77	126.35	129.29	128.56	126.10			53.84 (d, 8.7)[c] 51.83 (d, 8.7)[d] 51.64 (d, 8.7)[d]
3-6bα	74.60	100.43	72.53 (t,6.3)	113.74, 110.64 (d,4.8)	127.33 (d,4.5)	129.35	128.76	123.20			16.59 (d, 30.6)[e] 51.75 (d, 7.2)[d] 51.65 (d, 7.2)[d]
3-6cα	79.62	99.18	71.40	114.37(d,3.3), 109.19(d,8.7)	126.89 (d,5.0)	129.36	129.07	122.28		139.36(d,44.6)[f], 130.62[g] 130.51[g],129.98[h],128.42[i] 128.31[i]	10.94 (d, 26.7)[e] 17.81 (d, 28.3)[e] 51.89 (d, 11.1)[d]
3-3bβ-1									88.65	132.28(d,55.2)[f], 130.83[g] 130.69[g], 129.30[h], 127.60[i] 127.45[i]	19.34 (d,33.1)[e] 50.41 (d,8.7)[d]
3-3bβ-2									89.63	134.48(d,51.1)[f], 130.55[g] 130.40[g], 129.40[h], 127.89[i] 127.74[i]	19.63 (d,32.4)[e] 49.57 (d,12.5)[d]
3-6bβ-1	75.08	98.35	73.85	112.92, 112.86	126.04	129.43	128.90	125.46		142.11(d,53.9)[f], 130.96[g] 130.82[g], 128.85[h], 127.69[i] 127.56[i]	16.07 (d,32.3)[e] 50.79 (d,10.8)[d]

Table 3-13. cont'd

3-6bβ-2	75.34	100.96	71.83 (d, 4.0)	114.70, 111.70	126.60	129.67	128.93[j]	123.35	141.80(d,55.6)[f], 130.48[g] 130.35[g], 129.93[h], 128.02[i] 127.89[j]	16.50 (d,29.0)[e] 50.23 (d,11.8)[d]
3-6cβ-1	75.31	97.40	73.74	115.42, 113.11	127.19 (d,8.9)	129.97	128.49	121.89	138.58 (d,41.2)[f], 131.03[g] 130.90[g], 130.72[g], 130.62[g] 129.67[h], 129.54[h], 128.23[i] 128.11[j], 127.73[j], 127.60[j]	13.51 (d,27.7)[e] 16.81 (d,32.4)[e] 51.11 (d,10.5)[d]
3-6cβ-2	82.44	99.92	69.77 (t,6.1)	116.57, 109.06 (t,6.1)	125.92	129.85[h]	128.58	122.59	139.71 (d,45.5)[f], 132.59 (d,43.7)[f], 131.14[g] 131.04[g], 130.86[g], 130.73[g] 130.04[h], 129.85[h], 128.62[i] 128.44[j]	11.98 (d,26.2)[e] 17.18 (d,30.6)[e] 50.46 (d,13.2)[d]
3-6dβ-1	75.45	96.99	74.02	-	127.52	-	-	121.30	127.62-133.94	17.50 (d,25.5)[e] 51.01 (d,8.5)[d]
3-6dβ-2	77.50	98.34	70.74	-	-	-	-	120.45	126.80-134.75	16.86 (d,24.2)[e] 49.98 (d,10.3)[d]
3-6eβ-1	76.10	102.77	74.54 (t, 8.2)	113.00, 112.91	127.20 (d,8.5)	129.43	129.30	123.46	140.50(d,53.5)[f], 137.50(d,53.2)[f], 132.28[g] 132.17[g], 132.00[g], 131.83[g] 131.21[h], 128.74[h], 127.90[i] 127.77[j], 126.66[j], 126.51[j]	51.57 (d,11.6)[d] 53.94 (d,14.3)[c] 54.09 (d,8.8)[c]
3-6eβ-2	78.27	99.93	73.62	115.70, 111.61	125.89	129.52	128.71	124.63	142.40(d,54.3)[f], 135.73(d,53.5)[f], 132.09[g] 131.94[g], 130.89[g], 130.[illegible] 130.89[h], 129.52[h], 127.59[i] 127.71[j]	50.70 (d,11.4)[d] 54.77 (d,12.1)[c] 54.9 (d,14.9)[c]

[a] ^{13}C (75.47 MHz) NMR chemical shifts in ppm relative to solvent $CDCl_3$ = 77.00; d = doublet; J values in Hz given in brakets, J_{PC}; perfluoroalkyl carbons distributed in the chemical shift range of 105-140 ppm with very weak intensity. [b] solvent = acetone-d_6 (29.80, 206.00 ppm). [c] $PR(OMe)_2$. [d] P(O)R(OMe). [e] P-Me. [f] C_{ipso}. [g] C_{ortho}. [h] C_{para}. [i] C_{meta}. [j] overlapped with C_{para}.

Table 3-14. ^{19}F NMR for η^5-Cyclopentadienyl and η^5-Indenyl Co(III) Complexes[a].

Cpd	$C_\alpha F_2$ F_a, F_b	$C_\beta F_2$ F_a, F_b	CF_3
3-1b[b]	-60.90, -70.89 (d, 267.2)	-112.78, -113.29 (d, 282.1)	-78.20 (t, 11.9)
3-1b'	-66.28	-113.98	-78.98 (t, 11.5)
3-3aα	-61.51, -71.82 (d, 258.8)	-111.77, -115.92 (d, 281.35)	-79.33 (t, 12.7)
3-3bα	-65.91, -72.25 (d, 268.2)	-113.37, -115.05 (d, 280.9)	-78.99 (t, 12.8)
3-5aα	-60.62 (m)	-113.82	-79.43 (t, 10.7)
3-6aα	-71.49, -72.93 (d, 263.4)	-114.92	-79.19 (t, 10.5)
3-6'aα[c]	-70.42, -72.24 (d, 272.1)	-110.29, -111.07 (d, 291.0)	-81.36 (t, 8.7)
3-6bα	-73.28, -81.40 (d, 261.6)	-113.65, -115.96 (d, 282.2)	-79.17 (t, 11.0)
3-6cα	-73.78, -82.51 (d, 266.1)	-114.24, -115.92 (d, 282.7)	-79.22 (t, 12.8)
3-3bβ-1	-62.66, -77.70 (d, 269.3)	-112.34, -115.08 (d, 276.6)	-79.08 (t, 10.0)
3-3bβ-2	-63.08, -74.17 (d, 267.4)	-112.40, -114.50 (d, 279.2)	-79.00 (t, 9.8)
3-6bβ-1	-72.61	-114.02	-79.17 (t, 10.5)
3-6bβ-2	-73.72, -78.67 (d, 273.9)	-113.98	-79.26 (t, 10.7)
3-6cβ-1	-71.18, -79.96 (d, 278.7)	-112.80, -114.64 (d,277.4)	-79.16
3-6cβ-2	-76.16, -79.58 (d, 273.2)[d]	-113.24, -114.71 (d, 275.8)	-79.49
3-6dβ-1	-66.27, -81.04 (d, 290.02)	-112.76, -115.71 (d, 277.66)	-78.78
3-6dβ-2	-71.10, -74.76 (d, 275.0)	-113.51, -113.69	-79.29
3-6eβ-1	-67.06, -73.63 (d, 271.8)	-111.85, -115.23 (d, 280.5)[e]	-79.04 (t, 10.9)
3-6eβ-2	-70.77, -71.60 (d, 272.0)	-113.31, -113.91 (d, 277.1)	-79.43 (t, 11.0)

[a] 282.4 MHz, chemical shifts in ppm relative to $CFCl_3$; solvent = $CDCl_3$; $^2J_{FaFb}$, and $^3J_{FF}$ in the case of CF_3, in Hz given in brackets; all CF_2 peaks show further unresolved splitting by about 5-10 Hz (3 and more bond coupling). [b] solvent = acetone-d_6. [c] $C_\gamma F_2$: F_a, F_b=-121.10, -121.85, (d, 314.2); $C_\delta F_2$: Fa,F_b=-123.04; $C_\epsilon F_2$: F_a, F_b=-126.55. [d] $C_\alpha F_a$ shows further doublet with J = 39.0 Hz. [e] $C_\beta F_a$ shows further doublet with J = 9.8 Hz.

Table 3-15. Distortion Parameters in η^5-Indenyl Co(III) Complexes.

Cpd.	$\Delta\delta(C_{3a,7a})^a$ (Ave.)	Δ(M-C)^b (Å)	Hinge Angle^c (deg)	Fold Angle^d (deg)
3-5aα	-19.27	0.16(1)	5.8	11.0
3-6aα	-16.71, -19.89 (-18.30)			
3-6'aα	-16.59, -19.93 (-18.26)			
3-6bα	-16.96, -20.06 (-18.51)	0.153(4)	6.7	10.0
3-6cα	-16.33, -21.51 (-18.92)			
3-6bβ-1	-17.78, -17.84 (-17.81)	0.19(1)	7.3	11.4
3-6bβ-2	-16.00, -19.00 (-17.50)			
3-6cβ-1	-15.28, -17.59 (-16.44)			
3-6cβ-2	-14.13, -21.64 (-17.89)	0.16(1)	7.0	10.5
3-6eβ-1	-17.70, -17.79 (-17.75)			
3-6eβ-2	-15.00, -19.09 (-17.05)			

[a] $\Delta\delta(C_{3a,7a}) = \delta[C_{3a,7a}(\text{indenyl})] - \delta[C_{3a,7a}(Na^+\text{indenyl}^-)]$, $\delta[C_{3a,7a}(Na^+\text{indenyl}^-)] = 130.70$ ppm[236,279]. [b] Δ(M-C) = average of d(M-$C_{3a,7a}$) - average of d(M-$C_{1,3}$). [c] Hinge Angle = Dihedral Angle between the least-square planes C(1)-C(2)-C(3) and C(1)-C(3)-C(3a)-C(7a). [d] Fold Angle = Dihedral Angle between the least-square planes C(1)-C(2)-C(3) and C(3a)-C(4)-C(5)-C(6)-C(7)-C(7a).

3.2.4. Stereochemistry of the Cobalt η^5-Indenyl and η^5-Cyclopentadienyl Phosphinate Complexes. Assignments of relative configuration at Co and P for the diastereomeric pairs **3-6bβ-1**, **3-6cβ-2** and **3-3bβ-1**, necessary to establish the nature of the Co→P chiral induction, are based on crystallographic data. The

PLUTO molecular structure representation in Figure 3-5 and the modified Cahn-Ingold-Prelog[290-293] ligand priority series η^5-indenyl/η^5-Cp>P(O)Ph(OMe)>PMe_3>C_3F_7 and Co>OMe>O>Ph establish that cobalt and phosphorus have the same relative configuration ($S_{Co},S_P/R_{Co},R_P$) in the higher Rf diastereomer **3-6bβ-1** and therefore that the lower Rf diastereomer **3-6bβ-2** has the opposite relative configuration at cobalt and phosphorus ($S_{Co},R_P/R_{Co},S_P$). Similarly, the relative configuration of the lower Rf diastereomer **3-6cβ-2** (Figure 3-6) is $S_{Co},R_P/R_{Co},S_P$ and the higher Rf diastereomer, **3-6cβ-1**, is $S_{Co},S_P/R_{Co},R_P$. The relative configuration for the higher Rf diastereomer **3-3bβ-1** (Figure 3-7) and lower Rf diastereomer **3-3bβ-2** are $R_{Co},R_P/S_{Co},S_P$ and $R_{Co},S_P/S_{Co},R_P$, respectively, using the same procedure.

Relative configurations at Co and P for the diastereomeric pairs **3-6dβ-1,2** and **3-6eβ-1,2** were empirically determined by comparison of chromatographic Rf and NMR chemical shift parameters for the chiral phosphorus center. As summarized in Table 3-16, each pair of diastereomers shows the same NMR chemical shift pattern: δ(^{1}H, ^{13}C and $^{31}P_{(P(O)-OMe)}$(high Rf)) > δ(^{1}H, ^{13}C and $^{31}P_{(P(O)-OMe)}$(low Rf)). Accordingly, the relative configurations for the higher Rf diastereomers **3-6dβ-1** and **3-6eβ-1** can be assigned $S_{Co},S_P/R_{Co},R_P$, and the lower Rf diastereomers **3-6dβ-2** and **3-6eβ-2** are $S_{Co},R_P/R_{Co},S_P$. Interestingly, the direction of chiral induction in the reaction of **3-4c** and $PPh(OMe)_2$, which gives **3-6cβ-1,2** (cf. scheme 3-2), is opposite that found for the other cases examined in this study. The major product is low Rf $S_{Co},R_P/R_{Co},S_P$ **3-6cβ-2**, with the same relative configuration as the minor products for the remaining

examples in Schemes 3-1 and 3-2.

Table 3-16. Determination of the Relative Configuration for η^5-Indenyl and η^5-Cyclopentadienyl Phosphonate Cobalt complexes.[a]

Complex		$S_{Co}S_P/R_{Co}R_P$	$S_{Co}R_P/R_{Co}S_P$
	TLC	High Rf	Low Rf
$(\eta^5\text{-}C_9H_7)Co(C_3F_7)(PMe_3)(P(O)Ph(OMe))$		**3-6bβ-1**	**3-6bβ-2**
	^{1}H NMR	3.52	3.29
	^{13}C NMR	50.79	50.23
	^{31}P NMR	104.09	100.74
	X-ray	Yes	-
$(\eta^5\text{-}C_9H_7)Co(C_3F_7)(PPhMe_2)(P(O)Ph(OMe))$		**3-6cβ-1**	**3-6cβ-2**
	^{1}H NMR	3.50	3.34
	^{13}C NMR	51.11	50.46
	^{31}P NMR	103.17	103.04
	X-ray	-	Yes
$(\eta^5\text{-}C_9H_7)Co(C_3F_7)(PPh_2Me)(P(O)Ph(OMe))$		**3-6dβ-1**	**3-6dβ-2**
	^{1}H NMR	2.94	2.91
	^{13}C NMR	51.01	49.98
	^{31}P NMR	98.70	97.71
	X-ray	-	-
$(\eta^5\text{-}C_9H_7)Co(C_3F_7)(PPh(OMe)_2)(P(O)Ph(OMe))$		**3-6eβ-1**	**3-6eβ-2**
	^{1}H NMR	3.27	3.21
	^{13}C NMR	51.57	50.70
	^{31}P NMR	106.71	100.69
	X-ray	-	-
$(\eta^5\text{-}C_5H_5)Co(C_3F_7)(PMe_3)(P(O)Ph(OMe))$		**3-3bβ-1**	**3-3bβ-2**
	^{1}H NMR	3.50	3.39
	^{13}C NMR	50.41	49.57
	^{31}P NMR	111.58	105.63
	X-ray	Yes	-

[a] ^{1}H, ^{13}C NMR are the chemical shifts in ppm for P(O)Ph(O*Me*), ^{31}P NMR are the chemical shifts for *P*(O)Ph(OMe).

3.2.5. Conformational Analysis. The solution conformations of the phosphonate and phosphinate complexes were probed using ^{1}H nOed experiments. If the transition state for Arbuzov dealkylation (**3-2**→**3-3** and **3-5**→**3-6**) at prochiral phosphorus is product-like to a significant degree, restricted rotation about the Co-P(O) and Co-indenyl bonds in **3-3** and **3-6** would emerge as critical determinants for Co→P chiral transmission. Complexes **3-3bα**, **3-6bα**, **3-3bβ-1** and **3-6bβ-1** are illustrative.

Solution ^{1}H *nOed evidence* establishes the preferred conformation about the Co-indenyl bond for the π-indenyl complexes **3-6**. Partial saturation of P<u>Me</u>$_3$ in **3-6bα** results in strong enhancements to H_1 (4.2%) and H_7 (2.8%) but no enhancement to H_2 and H_3. Irradiation of the diastereotopic P-O<u>Me</u> signals shows specific enhancement (1.1%) to H_2. For **3-6bβ-1**, partial saturation of the indenyl H_1, H_2, and H_3 signals leads to 2.2%, 4.3%, and 0.3% enhancements to the H_{ortho} signals of P(O)<u>Ph</u>(OMe), respectively. The same relative enhancement order (5.1%, 6.9% and 1.2% enhancements to H_1, H_2, and H_3) was obtained on irradiation of the H_{ortho} signal of P(O)<u>Ph</u>(OMe). Taken together with the strong correlations to H_1 (3.5%) and H_7 (6.4%) when P<u>Me</u>$_3$ is irradiated, the nOed results are consistent with restricted rotation about the Co-indenyl bond and population of a major rotamer with P(O)$(OMe)_2$ or P(O)Ph(OMe) *trans* to the indenyl six-ring.

Figure 3-8 summarizes the nOed correlations measured for the indenyl phosphonate

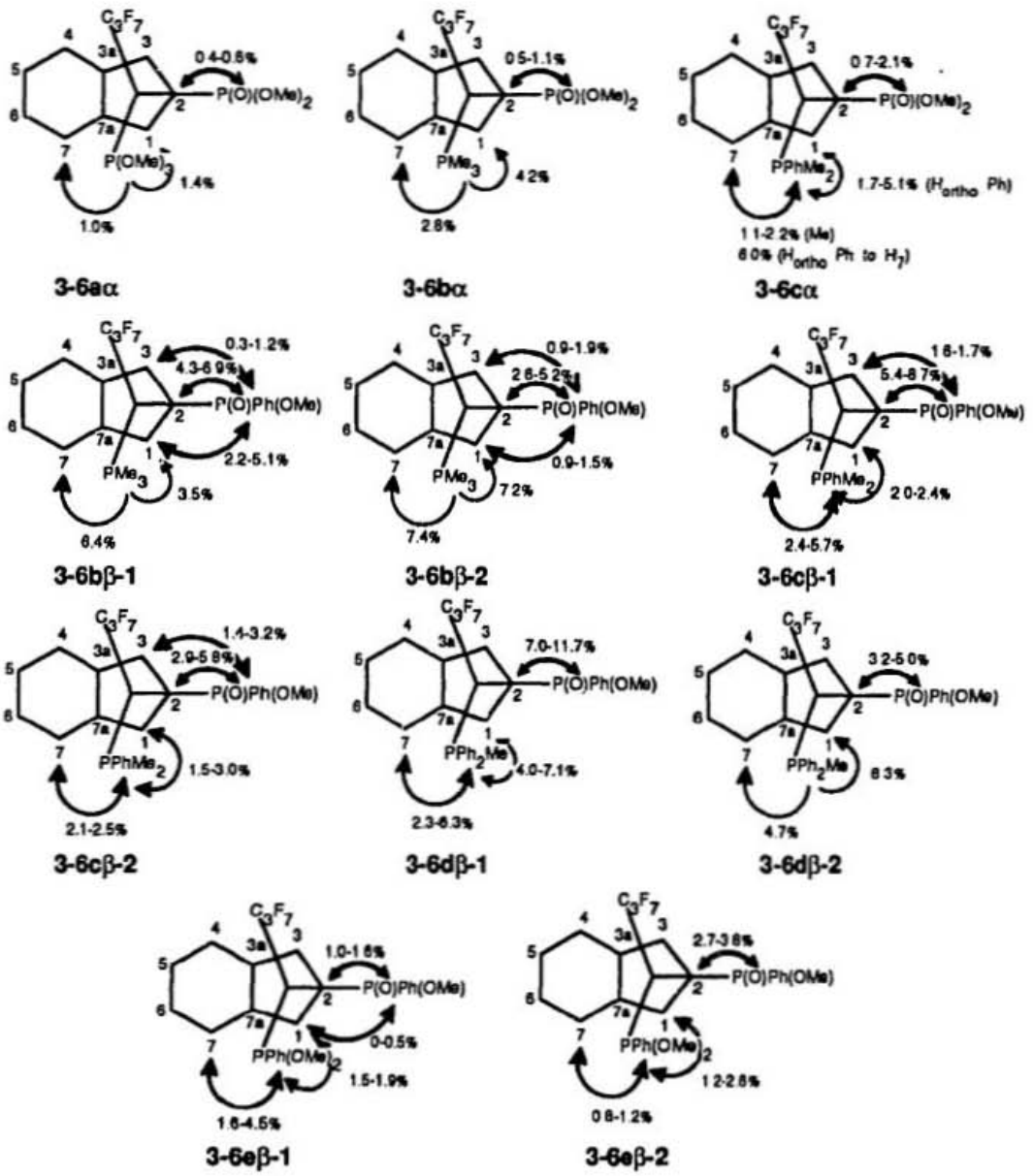

Figure 3-8. nOe Data and Solution Conformations.

and phosphinate complexes **3-6**. Both solid state and solution evidence concur that the dominant rotamer places phosphinate or phosphonate *anti* to the indenyl six-ring. Although steric effects are critical in substituted cyclopentadienyl 3-legged piano stools,[243, 310, 311] our results conclude that ligand steric requirements are not the

primary determinant of conformational preference about the Co-indenyl ring centroid bond. Arguments have been made[270, 300] which suggest that the ligand with the highest *trans* influence prefers the site *anti* to the indenyl six membered-ring in order to maximize aromatization. The *trans* influence order for the ligand set examined here can be estimated as P(O)R(OMe)>C_3F_7≥phosphine,[205, 312] which suggests that this interpretation has merit. However, this argument may not always be true. The conformational preference of η^5-indenyl complexes will be discussed in more detail in Chapter 4 on the basis of extended Hückel molecular orbital calculations.

Strong intramolecular hydrogen bonding (Scheme 1-50) in the aminophosphine-substituted phosphonate and phosphinate analogs studied previously constrained the Co-P(O) conformation by forcing L=$PPh_2NHCH(Me)Ph$ and P=O to be *syn*.[206-208, 217, 218] Since intramolecular hydrogen bonding is not possible for the phosphonates and phosphinates prepared in this study, it was of interest to examine conformation about the Co-P(O) bond. In the solid state, phosphonate **3-6bα** and both $S_{Co},S_P/R_{Co},R_P$ phosphinate complexes **3-6bβ-1** and **3-3bβ-1** adopt a staggered conformation similar to the aminophosphine deriatives of Scheme 1-50, in which the phosphoryl P=O double bond is aligned *anti* to the indenyl or cyclopentadienyl plane as shown in the Newman projections of Figure 3-9A,B,C. For **3-6bβ-1** and **3-3bβ-1** the P(O)Ph(OMe) phenyl group is *syn* and "edge-on" to the indenyl or cyclopentadienyl plane. The solid state conformation of $S_{Co},R_P/R_{Co},S_P$ **3-6cβ-2**, the major diastereomer for L=$PPhMe_2$, does not follow the pattern (cf. Figure 3-9D). However, a similar "edge

on" phenyl/indenyl interaction by placing the OMe group *anti* to the indenyl moiety is observed. The nOed evidence suggests that the solid state conformation about the Co-P(O) bond persists in solution. Partial saturation of either diastereotopic OMe resonance in **3-6bα** results in enhancement of the indenyl H_2 signal consistent with a conformation in which both methoxy groups are *syn* with respect to the indenyl ring. As described above for the case of **3-6bβ-1**, significant nOe enhancements were measured between the indenyl protons H_1, H_2 and H_3 and H_{ortho} of P(O)Ph(OMe), hence Ph is *syn* to the indenyl residue.

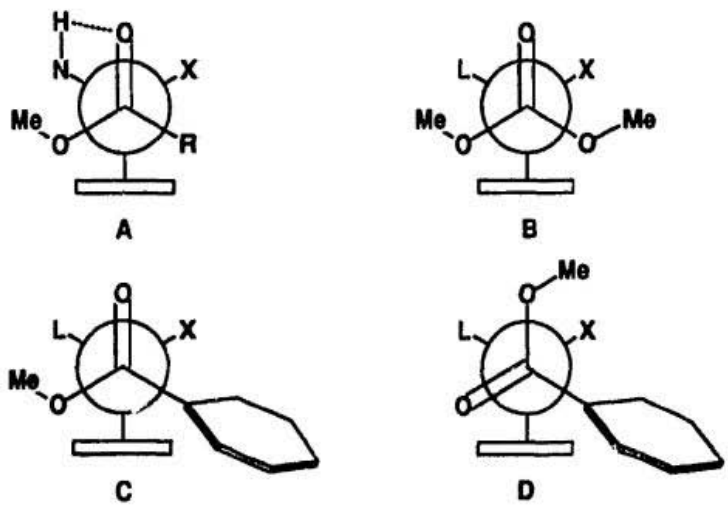

Figure 3-9. Newman Projections of the Phosphonate and Phosphinate Complexes along the P(O)-Co Bond.

Three-fold torsional barriers for rotation about M-ligar ' bonds in three-legged piano stool complexes have been discussed by several authors. [4, 142, 143, 313-315] The simple steric model favored by Davies[134] minimizes eclipsing interactions, and, as a

consequence of the near 90° interligand bond angles, it identifies the site *anti* to π-Cp' as the least sterically accessible. In agreement with results obtained for **3-6bα**, **3-6bβ-1** and **3-3bβ-1**, predictions based on a crude extension of the Davies model, which neglects stereoelectronic as well as dipole effects and assumes the steric sequence L>Cp or indenyl>R_t, predicts that the lowest energy rotamer will place the least sterically demanding phosphoryl oxygen *anti* to Cp or indenyl and, in the case of the phoshinates, the P(O)Ph(OMe) phenyl substituent *anti* to the largest Co-bound substituent, L (Figure 3-9). The major conformer adopted by **3-6cβ-2** is clearly not predicted from simple steric arguments since methoxy rather that oxygen occupies the least sterically accessible site. In this case, however, to force oxygen into the preferred site by rotation of 120° would incur an unfavorable *syn* interaction between the phenyl substituents of P(O)Ph)OMe) and L=$PPhMe_2$. The conformation found for **3-6cβ-2** reasonably represents the best compromise between constraints imposed by steric parameters and non-covalent (phenyl/Cp "edge-on") interactions.[316]

3.2.6. Optical Yields for Scheme 3-2. Nucleophilic attack of displaced iodide on the diastereotopic OMe groups of **3-2** and **3-5** proceeds with low to moderate $Co^{*}\rightarrow P$ chiral induction. Small but characteristic differences in the ^1H NMR η^5-Cp, η^5-indenyl, and methoxyl chemical shifts (^1H NMR: δ=3.2-3.5 ppm, $^3J_{PH}$ = 10±1 Hz) apparent for the diastereomeric phosphinate products were indispensable for measuring kinetic product distributions. ^1H NMR determination of product ratios

gave diastereotopic excesses of 4%, 27%, 48%, 46%, 35 % for **3-6bβ-1/3-6bβ-2**, **3-3bβ-1/3-3bβ-2**, **3-6cβ-2/3-6cβ-1**, **3-6dβ-1/3-6dβ-2** and **3-6eβ-1/3-6eβ-2**, respectively. Optical yields are lower than those observed in the reaction between aminophosphine-substituted iodo analogs $(\eta^5\text{-Cp})Co(PNH)(I)_2$ with $PPh(OMe)_2$ (80% de)[206] but, with the exception of **3-5bβ**, are comparable with the diastereoselectivity in the reaction between $(\eta^5\text{-Cp})Co(R_f)(PNH)(I)$ and $PPh(OMe)_2$ (R_f = CF_3, C_3F_7; 25-55% de).[217]

Several interesting features are evident from consideration of the optical yield data. It was anticipitated that removal of conformational restraints imposed by intramolecular hydrogen bonding (cf. Scheme 1-50) would result in reduced efficiency of chiral information transfer from cobalt to phosphorus. Although a nominal decrease was observed using the reaction of $(\eta^5\text{-Cp})Co(PNH)(I)_2$ with $PPh(OMe)_2$ as a reference,[206] no measurable decrease results with a reference reaction of $(\eta^5\text{-Cp})Co(R_f)(PNH)(I)$ and $PPh(OMe)_2$ (R_f = CF_3, C_3F_7).[217] Also surprising is the observation of a reversal in relative stereochemistry of the major diastereomer formed in the reaction of **3-4c** with $PPh(OMe)_2$. Detailed molecular mechanics[314, 317] calculations may be required to address the more subtle steric interactions implicit in this data. A convincing rationale for the direction of the reported optical inductions is not yet apparent.

3.3. Summary

Reactions of $(\eta^5\text{-Cp})Co(C_3F_7)(L)(I)$ (**3-1**, L = $P(OMe)_3$, PMe_3) and (η^5-indenyl)$Co(R_f)(L)(I)$ (**3-4**, R_f = C_3F_7, C_6F_{13}; L = $P(OMe)_3$, PMe_3, $PPhMe_2$, PPh_2Me, $PPh(OMe)_2$) with $PR(OMe)_2$ (R = OMe, Ph) initially afforded the corresponding labile ionic intermediates $[(\eta^5\text{-Cp})Co(C_3F_7)(L)(PR(OMe)_2)]^+$, **3-2**, and [($\eta^5$-indenyl)$Co(R_f)(L)(PR(OMe)_2)]^+$, **3-5**, respectively, which subsequently dealkylated with loss of MeI in benzene via an Arbuzov rearrangement to give the phosphonate and phosphinate complexes, $(\eta^5\text{-Cp})Co(C_3F_7)(L)(P(O)R(OMe))$ and (η^5-indenyl)$Co(R_f)(L)(P(O)R(OMe))$, **3-3** and **3-6** (R = OMe, Ph). In most cases intermediates **3-2** and **3-5** were directly observable by ^{1}H NMR in acetone-d_6. The solid state structure of $[(\eta^5\text{-indenyl})Co(C_3F_7)(P(OMe)_3)_2)]^+SbF_6^-$, **3-5aα,SbF$_6$**, was determined by X-ray diffraction. Crystal structures of several phosphonate and phosphinate derivatives established characteristic conformational preferences in the solid state which were domonstrated by ^{1}H nOed data to persist in solution. The dominant conformation places the highest *trans*-influence ligand, P(O)R(OMe), *anti* to the indenyl six-membered ring. Empirical correlations between chromatographic Rf values, NMR parameters and the relative configuration of the phosphinates, which provide a simple way to determine the stereochemistry of chiral cobaltophosphinates, were established. Decreased chiral induction from cobalt to phosphorus was observed using the reaction of $(\eta^5\text{-Cp})Co(PNH)(I)_2$ with $PPh(OMe)_2$ as a reference. However no measurable decrease results with a reference reaction of (η^5-Cp)$Co(R_f)(PNH)(I)$ and $PPh(OMe)_2$ (R_f = CF_3, C_3F_7).

3.4. Experimental Section

3.4.1. Reagents and Methods. All manipulations were performed under the same general conditions as described in Chapter 2. Spectral grade chloroform was used as received. Complexes **3-1a**, **3-4a-e**, and **3-4'a** were prepared as described in Chapter 2.

3.4.2. X-ray Crystallography. Crystal data for **3-5aα-SbF$_6$**, **3-6bα**, **3-6bβ-1**, **3-6cβ-2** and **3-3bβ-1** were collected at ambient temperature on a Rigaku AFC6S diffractometer with graphite monochromated Mo Kα radiation, λ=0.71069 Å, and a 2KW sealed tube generator using the ω-2θ scan technique to a maximum 2θ value of 50.0°. Space group assignments were based on systematic absences and on the successful solution and refinement of the structure. Weak reflections (I<10.0σ(I)) were rescanned (max 2) and the counts accumulated to assure good counting statistics. For **3-5aα-SbF$_6$**, **3-6bα**, **3-6bβ-1** and **3-3bβ-1** the intensities of three representative reflections measured after every 150 reflections remained constant throughout the data collection hence no decay corrections were applied. In the case of **3-6cβ-2** intensities of three representative reflections measured after every 150 reflections declined by 3.10% hence a linear correction factor was applied. The data were corrected for Lorentz and polarization effects. Structures were solved by direct methods,[305] using the Molecular Structure Corporation TEXSAN software. Non-hydrogen atoms were refined anisotropically. Idealized hydrogen atoms were included at the calculated positions but were not refined. Further details are given in Table

3-17.

3.4.3. Synthesis of Complexes.

3.4.3.1. Synthesis of [(η^5-C_9H_7)Co(C_3F_7)(P(OMe)$_3$)$_2$]$^+$$SbF_6^-$, 3-5aα. A solution prepared by dissolving 0.3952 g (1.150 mmol) of $AgSbF_6$ in 40 mL of acetone was slowly added via syringe into a stirred solution of **3-4a**, (η^5-C_9H_7)Co(C_3F_7)(I)(P(OMe)$_3$), (0.6610 g, 1.113 mmol) in 25 mL of acetone over a 30 minute period at room temperature. After stirring for an additional 30 minutes, the yellow AgI precipitate was filtered off through a 5 cm Celite pad in a Schlenk filter. P(OMe)$_3$ (0.1987 g, 1.601 mmol) was added to the filtrate by syringe, and the solution was stirred for 30 minutes. Removal of volatiles at aspirator followed by oil pump vacuum left an orange powder, which was dissolved in 5 mL of acetone and purified by thick layer radial chromatography eluting with acetone/hexane (7/5, v/v). Removal of the solvent from the first yellow band left **3-5a**α as an orange-yellow crystalline solid (0.8720 g, 95%). A crystalline specimen for X-ray characterization was prepared by slow diffusion of pentane into the CH_2Cl_2 solution of **3-5a**α at 0 °C.

3.4.3.2. Synthesis of (η^5-C_5H_5)Co(C_3F_7)(I)(PMe$_3$), 3-1b. PMe$_3$ (0.1714 g, 2.253 mmol) was added dropwise via syringe with stirring to a dark-green solution of (η^5-C_5H_5)Co(C_3F_7)(I)(CO), (0.9541 g, 2.130 mmol) in 25 mL of benzene at room temperature. After stirring for 5 minutes, a dark blue solution containing some

preciptate formed. Removal of the solvent at aspirator pressure left a dark blue powder. TLC analysis (benzene/hexane 2/1) showed dark blue (Rf=0.33) and yellow (Rf=0) products. The crude product was purified in several portions by thick layer radial chromatography eluting with benzene/hexane (5/1 v/v) collecting the initial dark blue band. Continued elution with acetone separated a yellow band. Removal of solvent from the combined dark blue eluates gave **3-1b** (0.7299 g, 69%) as a dark-blue powder. Removal of solvent from the combined yellow eluates gave a yellow powder (0.0862 g), which was crystallized by slow diffusion of hexane into an acetone solution and was identified as $[(\eta^5\text{-}C_5H_5)Co(C_3F_7)(PMe_3)_2]^+I^-$, **3-1b'**.

3.4.3.3. Synthesis of ***(η^5-Cp/η^5-C_9H_7)Co(R_I)(L)(P(O)(OMe)$_2$) (3-3aα, 3-3bα, 3-6aα, 3-6'aα, 3-6bα and 3-6cα).*** The phosphonate complexes were synthesized by adding a slight excess of $P(OMe)_3$ to the appropriate iodide (η^5-Cp/η^5-C_9H_7)Co(R_I)(L)(I) in benzene or acetone solution at room temperature and then heating. The reaction progress was followed by observing a color change to yellow (η^5-Cp) or red (η^5-indenyl) using a procedure similar to that described for **3-6a**α below.

$P(OMe)_3$ (0.0830 g, 0.669 mmol) was added via syringe with stirring to a solution of **3-4a** (0.2566 g, 0.4319 mmol) in 25 mL of benzene at ambient temperature. Heating the solution to reflux resulted in a color change from brown-red to red after *ca.* 0.5 h. Removal of the solvent at aspirator then oil pump vacuum left the product as a red paste. Crude **3-6a**α was dissolved in *ca.* 3 mL of acetone and purified by thick

layer radial chromatography eluting with acetone/methanol (20/1 v/v). Removal of the solvent from the last orange-yellow band at aspirator and then oil pump vacuum afforded **3-6aα** as a red powder (0.1941 g, 78%). Experimental parameters for the remaining phosphonate complexes are summarized in Table 3-18.

3.4.3.4. Synthesis of ***(η^5-C_9H_7)Co(C_3F_7)(PPhMe$_2$)(P(O)Ph(OMe)), 3-6cβ-1,2.***

PPh(OMe)$_2$ (0.0741 g, 0.436 mmol) was added slowly via syringe to a stirred solution of **3-4c**, (η^5-C_9H_7)Co(C_3F_7)(I)(PPhMe$_2$), (0.2170 g, 0.3568 mmol) in 20 mL of benzene at ambient temperature. Heating to 50 °C for about 5 h resulted in a color change from brown-red to red. TLC (ethyl acetate elution) of the crude reaction mixture showed four spots corresponding (in order of decreasing Rf value) to a low-yield, uncharacterized product, **3-6cβ-1**, **3-6cβ-2**, and the mixture of a disubstituted species (**3-6eβ**). Removal of the solvent by aspirator and then oil pump vacuum left a red paste, which was dissolved in 3 mL of ethyl acetate and separated chromatographically on a 2-mm radical silica gel plate. Ethyl acetate elution separated **3-6cβ-1** and **3-6cβ-2** as orange bands. Continued elution with ethyl acetate/methanol (20/1) separated yellow zones of the disubstituted byproducts. Removal of the solvent with water aspirator and then oil pump vacuum afforded **3-6cβ-1** (0.0328 g, 14%), **6cβ-2** (0.1058 g, 47%), **3-6eβ-1** (0.0098 g), and **3-6eβ-2** (0.0135 g) as red powders. Slow diffusion of hexane into a $CHCl_3$ solution of **3-6cβ-2** at room temperature gave **3-6cβ-2**•$CHCl_3$•2.85H_2O as red prismatic crystals for X-ray analysis.

3.4.3.5. Synthesis of $(\eta^5\text{-}C_9H_7)Co(C_3F_7)(PPh_2Me)(P(O)Ph(OMe))$, 3-6dβ-1,2. PPh_2Me (0.0594 g, 0.297 mmol) was added via syringe with stirring to a brown-red solution of **3-4e**, $(\eta^5\text{-}C_9H_7)Co(C_3F_7)(I)(PPh(OMe)_2)$, (0.1463 g, 0.2285 mmol) in 25 mL benzene and stirred for 14 hours at room temperature. TLC (ethyl acetate/dichloromethane 1:1) showed that **3-4e** was converted mainly into **3-4d**, **3-6eβ-1,2**, and uncharacterized Rf=0 material. Only very small amounts of **3-6dβ-1** and **3-6dβ-2** were detected. After removal of volatiles at aspirator pressure the residue was chromatographed on a 2 mm radial silica gel plate. Elution with ethyl acetate/dichloromethane (1:1) separated **3-6dβ-1,2** from **3-4d, 3-6eβ-1,2** and the decomposed material. Re-chromatographing the **3-6dβ-1,2** mixture with ethyl acetate/dichloromethane (1:1) as elutant gave **3-6dβ-1** (8.3 mg, 5%) and **3-6dβ-2** (3.0 mg, 2%) as red powders. Experimental parameters for the remaining phosphinate complexes are summarized in Table 3-18.

Table 3-17. Summary of Crystallographic Data.

	3-5aα,SbF$_6$	3-6bα	3-6bβ-1	3-6cβ-2	3-3bβ-1
formula	$C_{18}H_{25}O_6CoF_{13}P_2Sb$	$C_{17}H_{22}O_3CoF_7P_2$	$C_{22}H_{24}O_2CoF_7P_2$	$[C_{27}H_{26}O_2CoF_7P_2 \cdot CHCl_3]\cdot 2.85H_2O$	$C_{18}H_{22}O_2CoF_7P_2$
mol wt (g/mol)	827.00	528.23	574.30	807.09	524.24
color; habit	orange rect. plate	deep-red prism	red rect. plate	red prism	orange prism
cryst size (mm)	0.30x0.20x0.15	0.30x0.25x0.12	0.35x0.25x0.20	0.40x0.30x0.10	0.40x0.30x0.15
cryst syst	monoclinic	monoclinic	monoclinic	monoclinic	monoclinic
space group	$P2_1/c$ (#14)	$P2_1/c$ (#14)	$P2_1/c$ (#14)	C2/c (#15)	$P2_1/c$ (#14)
a (Å)	12.821(4)	8.235(2)	12.626(2)	21.794(8)	8.481(4)
b (Å)	12.057(3)	16.983(3)	14.017(7)	15.214(2)	17.916(3)
c (Å)	18.835(4)	15.795(2)	14.380(2)	21.115(3)	14.518(2)
β (deg)	99.74(2)	101.88(1)	107.46(1)	92.33(2)	97.31(2)
V (Å^3)	2609(1)	2161.6(7)	2428(1)	6995(3)	2188(1)
Z	4	4	4	8	4
D_{calcd} (g/cm^3)	1.914	1.623	1.571	1.533	1.591
F_{000}	1624	1072	1168	3284	1064
μ(MoKα)(cm^{-1})	17.48	10.10	9.04	8.80	9.95
Scan Width(deg)	1.31 + 0.30 tanθ	1.15+0.30 tanθ	1.26+0.30 tanθ	1.00+0.30 tanθ	1.26+0.30 tanθ
$2\theta_{max}$ (deg)	50.0	50.0	50.0	50.0	50.0
no. rflns measd					
Total	4524	4242	4675	6580	4269
Unique	4272	3952	4462	6398	3986
R_{int}	0.209	0.024	0.063	0.021	0.034
corrections[a]	Lorentz polarization absorbtion				
trans factors:	0.94-1.00	0.93-1.00	0.89-1.00	0.86-1.00	0.92-1.00
2° extn coefficient:	-	0.16748x10^{-6}	-	-	0.19909x10^{-6}
p-factor	0.01	0.01	0.01	0.00	0.01
no. obsd (I>3.00σ(I))	1913 (I>2.00σ(I))	2455	2158	3961 (I>2.00σ(I))	2780
no. variables	315	272	307	416	338
reflection/parameter	6.07	9.03	7.03	9.52	8.22
R[b]	0.055	0.038	0.051	0.052	0.036
R_w[c]	0.039	0.034	0.040	0.036	0.033
GOF[d]	1.81	1.76	1.85	2.60	1.83
Max Shift/Error in Final Cycle	0.00	0.00	0.02	0.00	0.03
Δρ final (max/min) (e$^-$/Å3)	0.51/-0.46	0.36/-0.22	0.74/-0.44	0.59/-0.48	0.41/-0.39

[a] cf. reference[305]. [b] $R=\Sigma||Fo|-|Fc||/\Sigma|Fo|$. [c] $R_w=[(\Sigma w(|Fo|-|Fc|)^2/\Sigma wFo^2)]^{1/2}$ [d] $GOF=(\Sigma(|Fo|-|Fc|)/\sigma)/(n-m))$ where n=#reflections, m=#variables, and σ^2=variance of (|Fo|-|Fc|); Function Minimized = $\Sigma w(|Fo|-|Fc|)^2$; least-squares weights: $4Fo^2/\sigma^2(Fo^2)$

Table 3-18. Prep. ..ative Parameters for the Reaction of **3-1** and **3-4** with $PR(OMe)_2$ (R=OMe, Ph)[a]

Cpd.	solvent	reaction temp/time	mole ratio ($PR(OMe)_2$/reactant)	chromatography solvent	% yield
3-3aα	benzene	reflux/15 h	1.42	acetone/methanol 10/1	87
3-3bα	acetone	50°C/10 h	1.29	-	96
3-6aα	benzene	reflux/0.5 h	1.55	acetone/mehanol 20/1	78
3-6'aα	benzene	reflux/0.5 h	1.55	acetone/methanol 20/1	85
3-6bα	benzene	50°C/4 h	1.09	acetone/methanol 20/1	90[b]
3-6cα	benzene	50°C/0.5 h	2.25	acetone	89[b]
3-3bβ-1,2	acetone	50°C/ 3 h	2.10	acetone/methanol 10/1	64,31[c]
3-6bβ-1,2	benzene	50°C/5 h	1.17	acetone	58,28
3-6cβ-1,2	benzene	50°C/5 h	1.22	ethyl acetate	14,47[d]
3-6eβ-1,2	benzene	22°C/14 h	1.35	ethyl acetate/methanol 20/1	35,27

[a] Crystal growth condition: slow diffusion of hexane into the solution of **3-6bα** (dichloromethane, room temp.), **3-6bβ-1** (dichloromethane, 0 °C), **3-6cβ-2** (chloroform, room temp.), and **3-3bβ-1** (acetone, 0 °C). [b] Minor amounts of **3-6aα** were also isolated in the lower Rf fractions. [c] **3-3eβ-1,2**[217] were detected in the crude product mixture. [d] Continued elution with ethyl acetate/methanol 20/1) separated **3-6eβ-1** (4 %) and **3-6eβ-2** (6 %).

Chapter 4

Distortion and Conformational Preferences of (η^5-indenyl)ML_n (n = 2,3) Complexes: An Extended Hückel Molecular Orbital (EHMO) Study.

4.1. Introduction

NMR spectroscopic and crystallographic results of the indenyl complexes discussed in Chapters 2 and 3 and reported in the literature reveal a propensity to distort.[238, 269, 270, 279-282, 286, 318] The distortion is described by several parameters: ring-slippage (Δ) of the metal atom away from the indenyl five-membered ring centroid toward C_2,

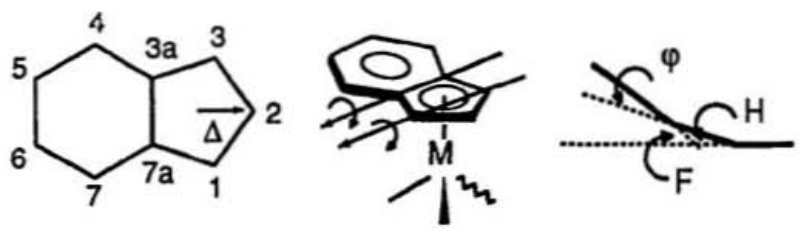

H (deg) = ∠plane C_1-C_2-C_3/plane C_1-C_3-C_{3a}-C_{7a}

φ (deg) = ∠plane C_1-C_3-C_{3a}-C_{7a}/plane C_4-C_5-C_6-C_7-C_{7a}-C_{3a}

F = H + φ

Scheme 4-1

indenyl ring puckering along the axes defined by C_3-C_1 and C_{3a}-C_{7a} resulting in a

hinge angle (H) between planes C_1-C_2-C_3 and C_1-C_3-C_{3a}-C_{7a}, and a fold angle (F) between planes C_1-C_2-C_3 and C_{3a}-C_4-C_5-C_6-C_7-C_{7a}, as shown in Scheme 4-1.

Indenyl ring distortions correlate well with the NMR parameters[225, 234, 238, 268, 271, 281, 282, 296-298, 318] and electron configuration of the metal.[279] Ring-slippage from η^5- toward η^3-indenyl is in accord with theoretical studies on (η^5-indenyl)$Cr(CO)_3$[319] and (η^5-indenyl)RhL_2 (L = CO, ethylene).[320, 321] In addition, the indenyl ring adopts a specific conformation with respect to ligands bonded to the metal center both in the solid state[219, 227, 229-232, 238, 243, 250, 264, 270, 271, 280-282, 286, 299, 318, 320-329] and in solution (cf. Table 4-1).[270, 271, 280-282, 299, 301, 318] Conformational preferences were attributed to the relative *trans*-influence of the ligands on the metal atom.[270, 281, 282, 318] The ligand with greatest *trans*-influence[312] is located *trans* to the indenyl six-membered ring, which was rationalized by postulating that greater aromatization of the benzene is aided by decreased C_{3a}-C_{7a} to metal interaction. This rationale, however, only partly explains the conformational preferences for three-legged indenyl transition metal complexes and is even less satisfactory for the rationalization of two-legged indenyl complexes (cf. Table 4-1).

The present chapter is directed at developing an understanding of indenyl ring distortions and the conformational preference with respect to a ML_n (n = 2, 3) fragment with the assistance of extended Hückel molecular orbital (EHMO) calculations. Although several EHMO calculations were performed to explain the

rotational barrier of (η^5-indenyl)RhL_2 (L = CO, ethylene)[320, 321] and to rationalize the photoelectron spectra of these two rhodium complexes[330] and several other η^5-indenyl metal complexes,[226, 228, 242, 330] no systematic theoretical study on the transition-metal indenyl complexes has been reported up to now. The important valence orbitals of the indenyl ring and ML_n fragments[331, 332] with different ligand combinations are constructed initially followed by the interaction of ML_n fragment orbitals with the indenyl orbitals at different orientations to explain the origin of ring distortion and of the conformational preferences. The indenyl ring rotational barrier will be briefly discussed.

Table 4-1. Summary of Distoration Parameters and Conformational Preferences for (η^5-Indenyl)ML_n (n = 2, 3) Complexes

Complex and Conformation	Δ_{M-C} (A)[a]	H (deg)[b]	F (deg)[c]	Ref.
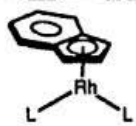		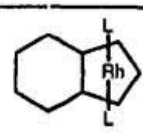		
L = CO	0.20	9.2	10.9	d
L = PMe_3	0.20	8.4	7.9	e
L = ethylene	0.16	8.1	7.4	e
	0.16	8.9	8.4	f
L = 	0.16	-	2.1	g
L_2 = 	0.15	8.9	7.4	h
	0.15	8.2	-	i
L_2 = 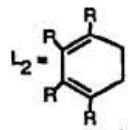 R = CF_3	0.14	-	-	j
L_2 = 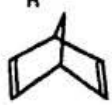	0.17	10.0	-	k
L_2 = 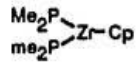	0.23	-	-	l
				
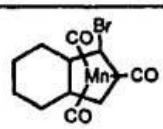	0.087	-	-	m

Table 4-1. cont'd

Complex and Conformation	Δ_{M-C} (Å)[a]	H (deg)[b]	F (deg)[c]	Ref.
				
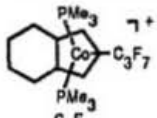	0.15	6.8	12.4	n
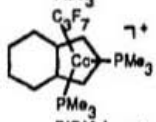	0.18	6.6	13.6	n
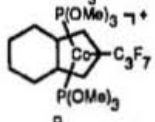	0.16	5.8	11.0	o
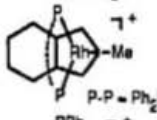	0.14	-	8.2	p
P-P = Ph_2P-CH(Me)CH_2-PPh_2	0.19	-	11.2	p
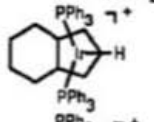	0.19	-	-	q
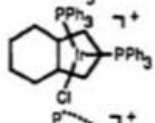	0.23	-	-	r
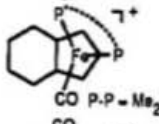	0.09	-	-	s
P-P = Me_2P-CH_2-PMe_2				
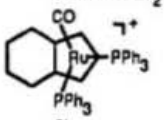	0.10	3.6	5.2	t
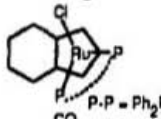	0.17	-	-	u
P-P = Ph_2P-CH(Me)CH(Me)-PPh_2				
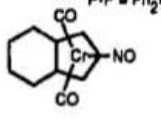	0.10	-	-	v

Table 4-1. cont'd

Complex and Conformation	Δ_{M-C} (A)[a]	H (deg)[b]	F (deg)[c]	Ref.
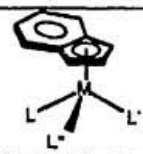				
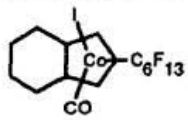	0.16	5.8	7.0	w
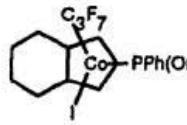	0.17	4.6	9.3	w
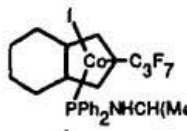	0.20	10.8	14.9	x
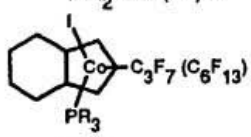	-	-	-	n, w
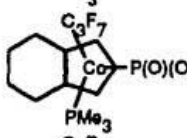	0.15	6.7	10.0	o
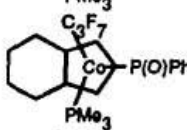	0.19	7.3	11.4	o
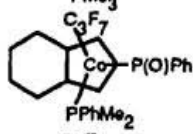	0.16	7.0	10.5	o
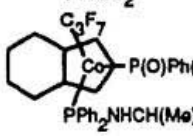	0.20	7.5	9.8	y

Table 4-1. cont'd

Complex and Conformation	$\Delta_{M\text{-}C}$ (A)[a]	H (deg)[b]	F (deg)[c]	Ref.
				
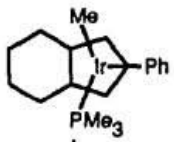	0.11	-	5.7	z
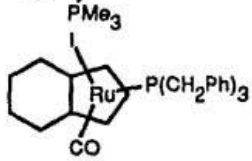	0.10	3.3	5.6	aa
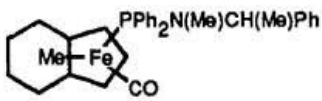	-	-	-	bb
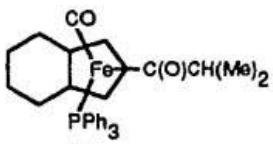	0.12	-	6.3	cc
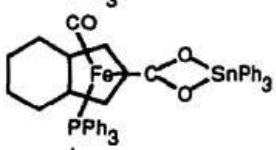	0.14	-	-	dd
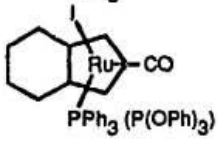	-	-	-	ee

a. $\Delta_{M\text{-}C}$ = average of d(M-$C_{3a,7a}$) - average of d(M-$C_{1,3}$). b. H (hingle angle in deg.) = angle between plane C_1-C_2-C_3 and plane C_1-C_3-C_{3a}-C_{7a} (cf. Scheme 1). c. F (fold angle in deg.) = angle between plane C_1-C_2-C_3 and plane C_{3a}-C_4-C_5-C_6-C_7-C_{7a} (cf. Scheme 1). d[227, 320]. e[299]. f[321]. g[229]. h[286]. i[322]. j[250, 323]. k[219]. l[238]. m[333]. n[282]. o[318]. p[232]. q[270]. r[271]. s[230]. t[325]. u[324]. v[326]. w[281]. x[280]. y[334]. z[327]. aa[243]. bb[328]. cc[231]. dd[329]. ee[298, 301].

4.2. Calculational Details

Extended Hückel molecular orbital (EHMO)[335-338] calculations, which have proved to be a reliable method for understanding the electronic structures and conformational preferences of transition-metal organometallic compounds,[157, 319, 339-351] were performed using the CACAO[352] program package on IBM-PC. The H_{ii}'s and orbital exponents are listed in Table 4-2, and were used as supplied by the program. Phosphorus d orbital parameters were not included in this calculation as normally suggested.[353] The structure parameters for the model complexes were derived from molecular structures of relevant complexes and are tabulated in Table 4-3. All (η^5-indenyl)ML_n (n = 2, 3) complexes were assumed to possess the ideal geometries shown in Scheme 4-2. Thus the ML_n fragment is initially connected to the indenyl five-membered ring centroid. All indenyl centroid-M-L angles were kept at 134° (M (d^8), L = CO), 132° (M (d^8), L = ethylene, PH_3) and 125° (M (d^6)), respectively, for (η^5-indenyl)ML_2 and (η^5-indenyl)ML_3, and the L-M-L angles in (η^5-indenyl)ML_3 were kept at 90° with pseudooctahedral geometry.

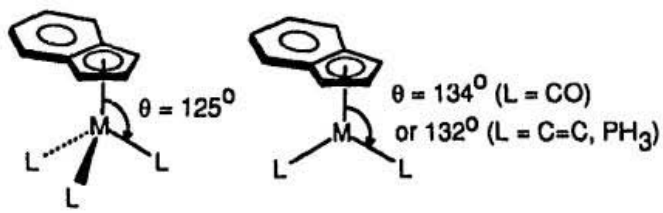

Scheme 4-2

As shown in Table 4-1, the conformational preferences of the indenyl ring with

respect to the ML_n fragment change greatly for different ligand combinations. In order to prove the validity of the theoretical results and to have a closer comparison with the experimental observations, EHMO calculations were performed on a series of d^8 ((η^5-indenyl)ML_2) and d^6 ((η^5-indenyl)ML_3) model complexes shown in Scheme 4-3.

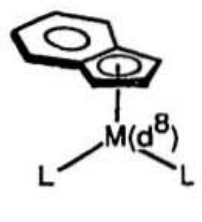

M = Co, Rh
L = CO, C≡C, PH_3

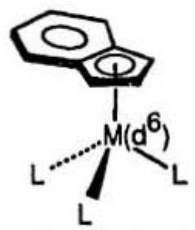

M = Co; L = CO, PH_3
M = Mn; L = CO

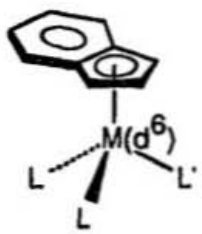

M = Co; L = PH_3; L' = Me, CF_3
M = Ir; L = PH_3; L' = H, Cl
M = Ru; L = PH_3; L' = CO
M = Cr; L = CO; L' = NO

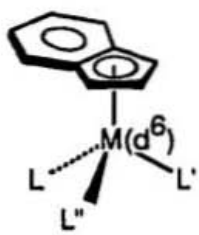

M = Co; L = Me; L' = I; L" = CO
M = Co; L = Me; L' = PH_3; L" = I
M = Co; L = Me; L' = PH_3; L" = $P(O)(OH)_2$
M = Fe; L = Me; L' = PH_3; L" = CO
M = Ru; L = PH_3; L' = I; L" = CO

Scheme 4-3

To assess ring distortion, Δ and H were varied simultaneously in initial geometry

searches. With the indenyl ring slipping away from the centroid toward C_2 (Δ), plane C_3-C_{3a}-C_4-C_5-C_6-C_7-C_{7a}-C_1 was allowed to pucker about the C_3-C_1 axis (H) to search for a geometry of minimum energy (cf. Scheme 4-1).

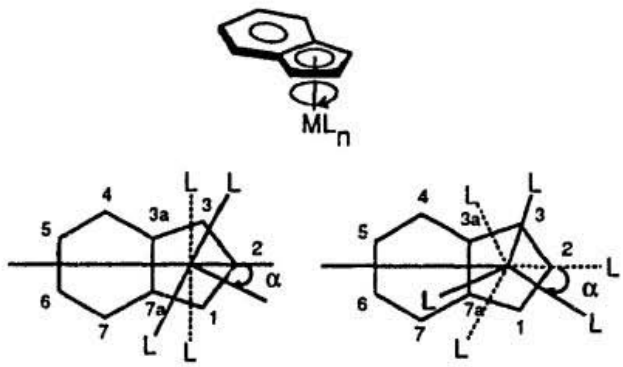

Scheme 4-4

The discussion below shows that, although the puckering of plane C_{7a}-C_{3a}-C_4-C_5-C_6-C_7 with respect to plane C_1-C_3-C_{3a}-C_{7a} (φ) is energetically favorable, the stabilization energy is much lower (even negligible, < 0.5 kJ/mol) compared to the ring slippage (Δ) and distortion about the C_3-C_1 axis (H). The distortion energy is dominated by Δ and H as shown in Scheme 4-1. Therefore, φ was obtained subsequent to minimization for Δ and H. ML_n (n = 2, 3) rotations (α) with respect to the metal-indenyl axis were carried out on geometries optimized for Δ, H, and φ to determine the low energy rotamer, as shown in Scheme 4-4.

Table 4-2. H_{ii} and Orbital Exponents Used in Extended Hückel Calculations

Orbital		H_{ii}	ζ_1	ζ_2	C_1[a]	C_2[a]
H	1s	-13.60	1.300			
C	2s	-21.40	1.625			
	2p	-11.40	1.625			
N	2s	-26.00	1.950			
	2p	-13.40	1.950			
O	2s	-32.30	2.275			
	2p	-14.80	2.275			
F	2s	-40.00	2.425			
	2p	-18.10	2.425			
P	3s	-18.60	1.600			
	3p	-14.00	1.600			
Cl	3s	-26.30	2.183			
	3p	-14.20	1.733			
I	5s	-18.00	2.679			
	5p	-12.70	2.322			
Cr	4s	-8.66	1.700			
	4p	-5.24	1.700			
	3d	-11.22	4.950	1.800	0.5058	0.6747
Mn	4s	-9.88	1.800			
	4p	-5.45	1.800			
	3d	-12.53	5.150	1.900	0.5311	0.6479
Fe	4s	-9.17	1.900			
	4p	-5.37	1.900			
	3d	-12.70	5.350	1.800	0.5366	0.6678
Co	4s	-9.21	2.000			
	4p	-5.29	2.000			
	3d	-13.18	5.550	2.100	0.5680	0.6060
Ru	5s	-8.00	2.078			
	5p	-4.30	2.043			
	4d	-12.20	4.210	1.950	0.5772	0.5692
Rh	5s	-8.09	2.135			
	5p	-4.57	2.100			
	4d	-12.50	4.290	1.970	0.5807	0.5685
Ir	6s	-11.36	2.500			
	6p	-4.50	2.200			
	5d	-12.17	5.796	2.557	0.6698	0.5860

[a] Contraction coefficients used in the double-ζ expansion.

Table 4-3. Structural Parameters Used in Extended Hückel Calculations

Distances (Å)			
Indenyl Centroid-M		Rh-CO	1.81
M = Cr	1.87	Rh-PH_3	2.21
Mn	1.78	Rh-ethylene centroid	2.03
Fe	1.80	Ir-PH_3	2.28
Co	1.80	Ir-Cl	2.39
Rh	1.95	Ir-H	1.50
Ir	1.94	Ir-Me	2.11
Ru	1.94	Ru-PH_3	2.35
Cr-CO	1.85	Ru-I	2.69
Cr-NO	1.73	Ru-CO	1.86
Mn-CO	1.80	C=C	1.40
Fe-CO	1.86	C-H	1.01
Fe-Me	1.98	C-F	1.36
Fe-PH_3	2.23	P=O	1.49
Co-CO	1.83	P-O	1.62
Co-ethylene centroid	2.01	P-H	1.40
Co-P	2.23	N-O (triple bond)	1.17
Co-C (Me, CF_3)	1.98	C-O (triple bond)	1.15
Co-I	2.57	O-H	0.96
Angles (deg.)			
Indenyl(centroid)-M(d^9)-CO	134.0	M-P=O	125.0
Indenyl(centroid)-M(d^8)-PH_3	132.0	M-P-O	103.5
Indenyl(centroid)-M(d^8)-ethylene	132.0	M-C-F	108.5
Indenyl(centroid)-M(d^6)-L	125.0	P-O-H	120.0
C-C-C (5-ring)	108.0	C-C-C (6-ring)	120.0

4.3. Results and Discussion

4.3.1. Indenyl Fragment Molecular Orbitals (FMO). As observed in many other η^n-polyene-transition metal complexes,[319, 339, 343, 344] the strongest bonding interactions between indenyl and ML_n originate from the indenyl frontier π orbitals and the valence, metal-centered orbitals of ML_n. The indenyl anion ($[C_9H_7]^-$) has nine π orbitals,[242, 319, 330] five of which are filled (cf. Figure 4-1). The HOMO (FMO 22 (π_5)) and NHOMO (FMO 23 (π_4)) are mainly localized on the indenyl five-membered ring and are energetically more accessible than the remaining filled orbitals to the symmetry adopted metal fragment orbitals. Therefore, these two FMO's are likely to have greater overlap with the metal orbitals if the metal is positioned to bond to the five-membered ring. Furthermore, the frontier π orbitals on the indenyl five-membered ring are not evenly distributed on all five carbons. In FMO 22 (π_5), the π orbital is localized mainly on C_1 and C_3, and in FMO 23 (π_4) on C_2 (major), C_{3a} and C_{7a}, respectively, which are of appropriate symmetry to interact with d_{yz} and d_{xz} descended orbitals in a ML_n fragment. It follows that these two FMO's also control the orientation of the ligand on ML_n with respect to the indenyl ring. Thus, the symmetry-adopted frontier fragment orbital interactions in both indenyl and ML_n play a key role in determining indenyl ring distortion and conformational preferences in η^5-indenyl transition-metal complexes.

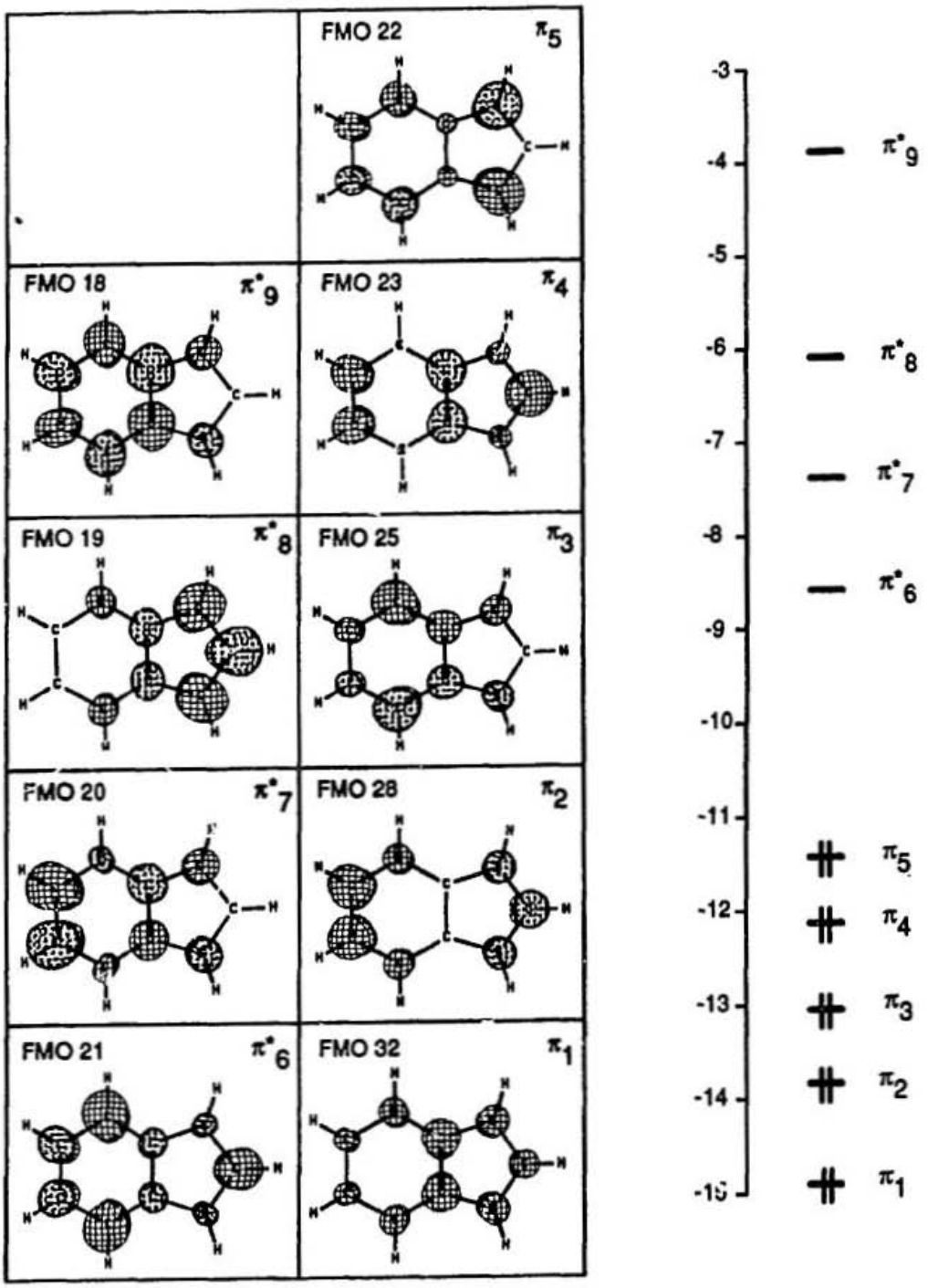

Figure 4-1. Indenyl Fragment π Orbitals.

4.3.2. (η^5-Indenyl)ML_2 Complexes (M (d^8) = Co, Rh, L = CO, PH_3, and ethylene (C=C)). Before discussion of the distortion and conformational preferences of these d^8 (η^5-Indenyl)ML_2 complexes, it is worthwhile to look into the orientation of important frontier fragment orbitals and their interactions with the indenyl frontier fragment orbitals. Figure 4-2 illustrates the fragment orbitals of CoL_2^+ (L = CO, C=C and PH_3). The FMO's for RhL_2^+ are almost the same as the corresponding FMO's of CoL_2^+ except for relatively small changes in the order of energy among the filled FMO's. Figure 4-2 clearly shows that all CoL_2^+ fragments possess essentially similar FMO's albeit with a small difference in their energies and energy orders. The low lying $1a_1$ (mainly d_{z2}) and high lying $3a_1$ resulting from the hybridization of s and p_z orbitals on CoL_2^+ have cylindrical symmetry around the z axis (the bonding axis) and interact primarily with the indenyl π_1 (FMO 32) and π_2 (FMO 28) orbitals. These interactions have almost no contribution to the distortion and conformational preferences of the resultant (η^5-indenyl)CoL_2 molecules. Neither do a_2 (mainly d_{xy}) and $2a_1$ (mainly d_{x2-y2}) orbitals of CoL_2^+ which have δ symmetry with respect to the indenyl ring and are essentially nonbonding (cf. Figure 4-3 to 4-5). In each CoL_2^+ fragment, the $1b_1$ and b_2 are crucial FMO's in determining the distortion of the indenyl ring and the conformational preference of CoL_2^+ about the indenyl fragment. The empty b_2 orbital resulting from the hybridization of the cobalt d_{yz} (major) and p_y (minor) orbitals lies on the yz plane and is of the correct symmetry for overlap with the filled indenyl π_5 (FMO 22) orbital. The strong interaction of these two orbitals generates a bonding 3a" and an antibonding 4a" MO (cf. Figure 4-3 to 4-5). The 3a" MO is filled and the

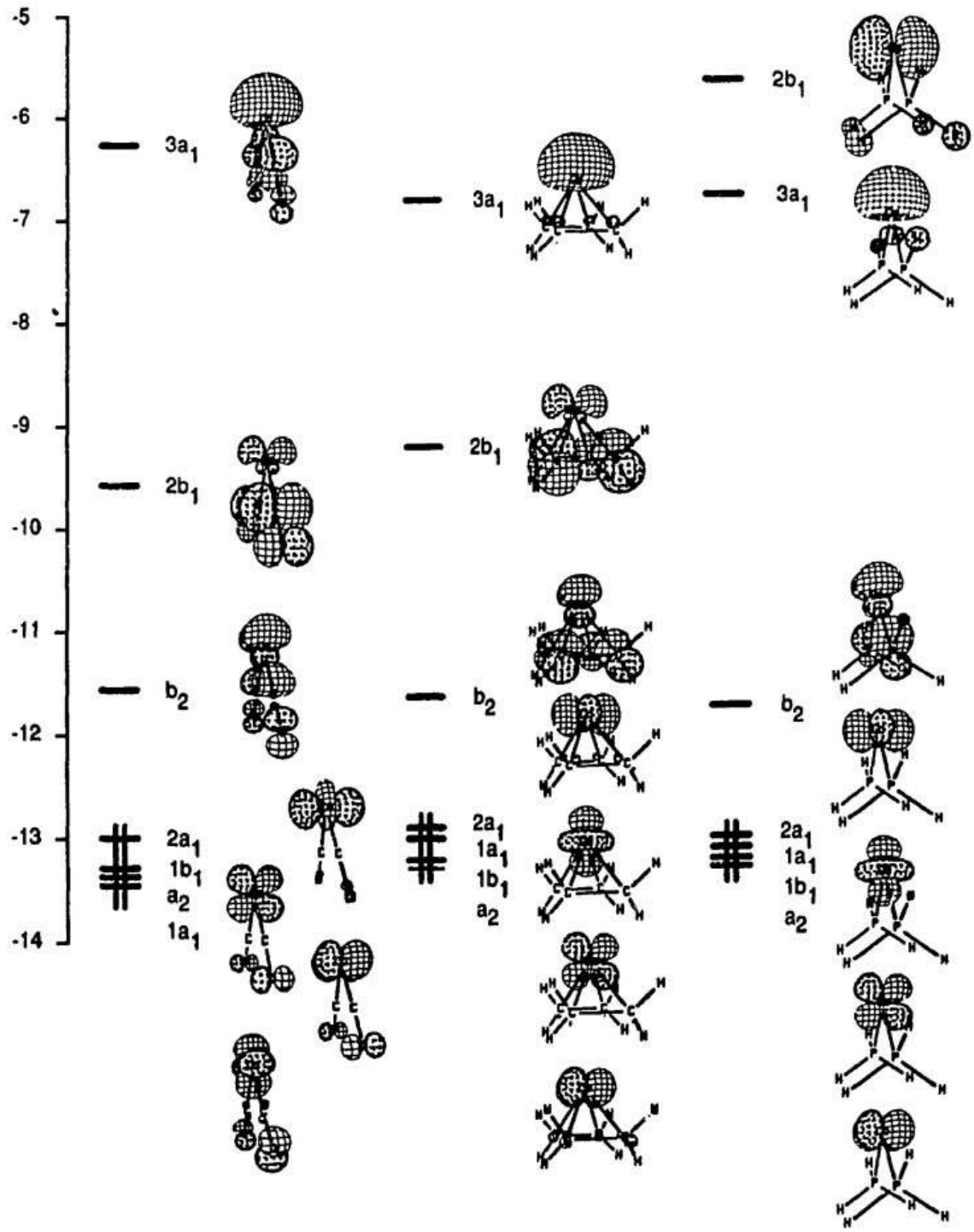

Figure 4-2. Important Fragment Molecule Orbitals of CoL_2

4a" is empty. The $1b_1$ FMO of CoL_2^+ (mainly d_{xz}) interacts primarily with the indenyl π_4 (FMO 23) orbital. Because both the metal $1b_1$ and indenyl π_4 are filled, the bonding 2a' (for L = CO) or 1a' (for L = C=C, PH_3) and the antibonding 4a' molecular orbitals are occupied (cf. Figures 4-3 to 4-5). Although the energy of the filled antibonding MO is lowered by a second-order mixing of $2b_1$ on CoL_2^+ into 4a', the resultant MO (4a') still lies at a moderately high energy level due to the d-indenyl π antibonding interaction, as shown in Scheme 4-5. This MO (4a') forms the HOMO in all (η^5-indenyl)ML_2 molecules. Any changes that diminish the antibonding interaction in the HOMO and strengthen the bonding interaction between indenyl and ML_2^+ fragments are energetically favorable.

The total energy change of (η^5-indenyl)ML_2 molecules as the indenyl ring distorts from η^5 toward η^3 coordination is shown in the lower part of Figures 4-3 to 4-5. An energy minimum with ΔE = 35.5 - 42.2 kJ/mol observed in each molecule at different Δ, H, and F, predicts that the indenyl ring distortion (ring slippage and puckering) is energetically favored by the (η^5-indenyl)ML_2 molecules. The calculations are consistent with experimental observations (cf. Table 4-1), as well as with theoretical calculations for η^5-Cp and other polyene-ML_2 complexes.[339, 345] The driving force for ML_2^+ shifting away from η^5-indenyl centroid toward C_2 and the 5-ring puckering about the C_3-C_1 axis (H increasing) may come from: i) the lowering of both HOMO (decrease of antibonding repulsion) and NHOMO (increase of bonding interaction) energy as shown in Figure 4-3 to 4-5; and ii) the increased aromatization of the indenyl six-membered ring which can be seen from the overlap population changes

among the indenyl six-membered ring carbons. The overlap populations between each pair of carbon atoms do show a tendency toward the average value. The overlap population between C_6-C_7 and C_4-C_5, which originally possesses more localized double bond character, decreases, and the overlap population between C_8-C_9, C_4-C_9, C_5-C_6 and C_7-C_8 increases, consistent with a conjugated aromatic ring (cf. Table 4-4).

The EHMO calculations showed that the stabilization energy of ring distortion mainly derives from Δ and H, *i.e.*, ring slippage from indenyl five-membered ring centroid toward C_2 and puckering of the indenyl ring along the C_3-C_1 axis. Puckering of the indenyl ring about axis C_{3a}-C_{7a} (φ) has small contribution to the distortion energy (cf. Table 4-5). For all (η^5-indenyl)ML_n (n = 2, 3) examined in this study, changing φ from -7.0 to 7.0° resulted in only < 0.5 kJ/mol change between the energy minimum and maximum. This result follows from inspection of the orbital interactions involved in this movement, since there is no obvious orbital interaction change by varying the φ. The φ values were determined on geometries minimized for Δ and H. Although the energy change is small, an energy minimum does exist at certain φ in all indenyl complexes. The indenyl six-membered ring in all (η^5-indenyl)ML_2 complexes prefers to bend down about the C_{3a}-C_{7a} axis toward the metal by about 1.0 to 2.0°, *i.e.*, φ = -1.0 to -2.0°.

Figure 4-6 illustrates the variation of the relative total energy (E_{total}) and HOMO energy (E_{HOMO}) for rotation (α = 0 - 360°) of the ML_2^+ fragment about the indenyl-

metal axis for (η^5-indenyl)ML_2 at the calculated low-energy geometry. The energy minima for rotation of ML_2* are located at 0, 180, and 360°, corresponding to a single low energy conformer with the ML_2 unit straddling the mirror plane of the (η^5-indenyl)ML_2 molecules (C_s point group) as found in their crystal structures. The rotational angle (α) dependence of the E_{HOMO} shows the same pattern as the variation of E_{total} and accounts for about 40-95% of the α dependence of E_{total}, which means that the HOMO in all (η^5-indenyl)ML_2 molecules plays an important role in determining their conformational preferences. As α increases, the antibonding repulsion between the metal centred orbital and the indenyl π orbitals increases. At α = 90° and 270° this interaction reaches a maximum, in which the orbital interactions between metal centred orbitals and the indenyl π orbitals switch hence the E_{HOMO} increases greatly. The resulting conformer with the ML_2 unit in the mirror plane of (η^5-indenyl)ML_2 molecules is predicted to be the most unstable and disfavored conformer as shown in Scheme 4-6.

It is likely that both ring distortion and rotational barriers are overestimated for these (η^5-indenyl)ML_2 molecules since no effort was made to optimize the geometry, which would undoubtedly lower the calculated distortion extent and rotational barriers. Nevertheless, the trends obtained are clear indicators for indenyl ring distortion and conformational preferences.

Calculations showed that the rotational barriers (ΔE_r) in all (η^5-indenyl)ML_2 molecules depend greatly on the extent of indenyl ring slippage (Δ) and hinge angle puckering

(H). Figure 4-7 shows the dependence of the rotational barrier (ΔE_r) with respect to Δ and H for (η^5-indenyl)$Co(CO)_2$. The greater the ring slippage, the higher the rotational barrier; and the larger the hinge angle the higher the rotational barrier.

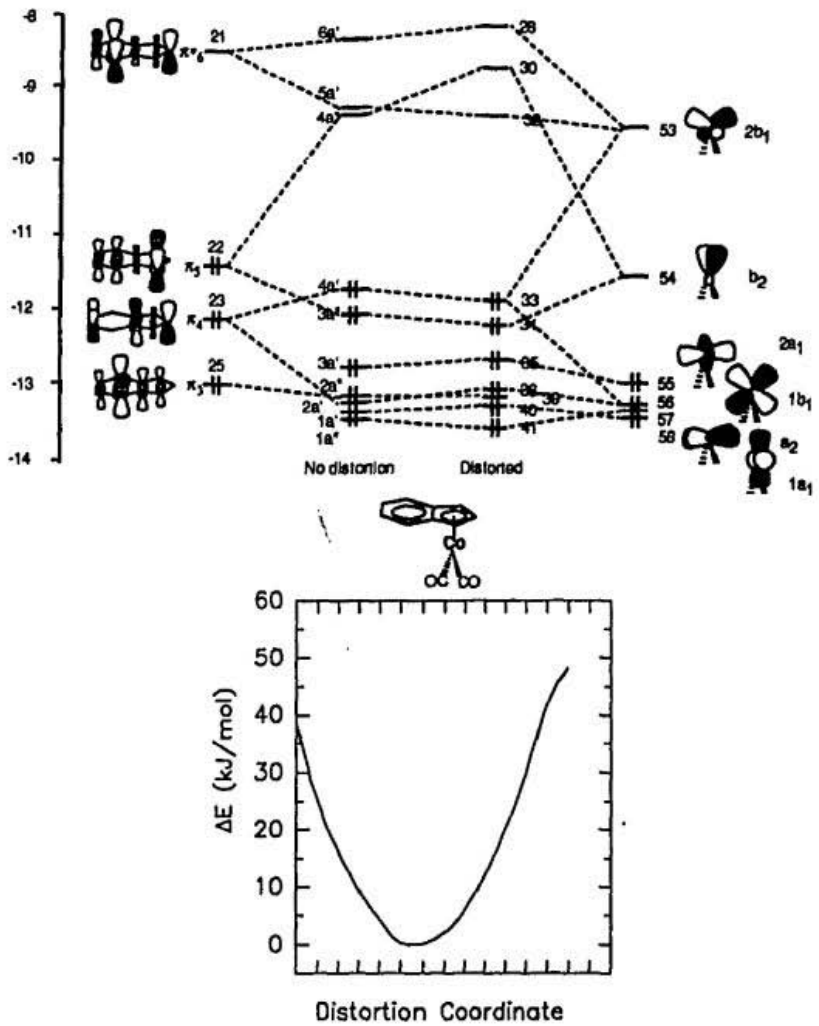

Figure 4-3. Interaction Diagram between Indenyl and $Co(CO)_2^+$ without and with Distortion (upper) and Total Energy Change as a Function of Indenyl Ring Distortion (cf. Table 4-5).

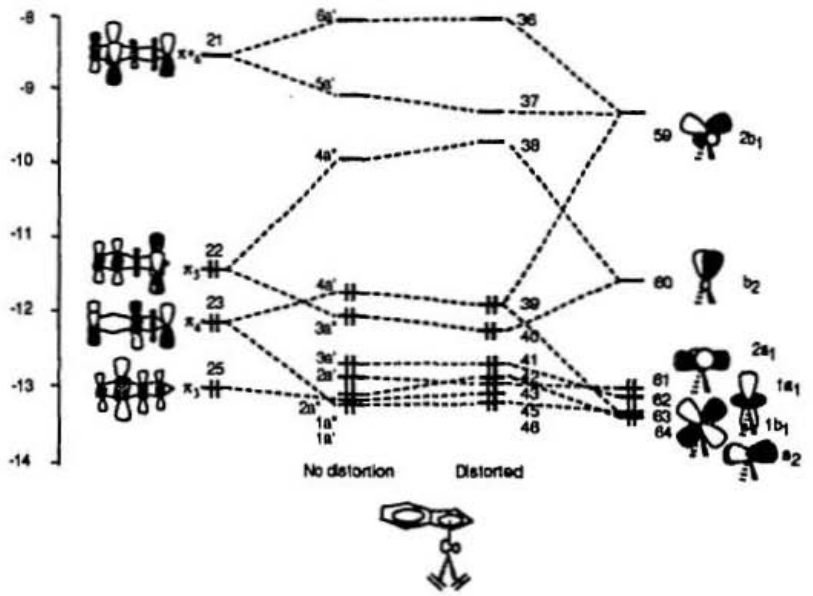

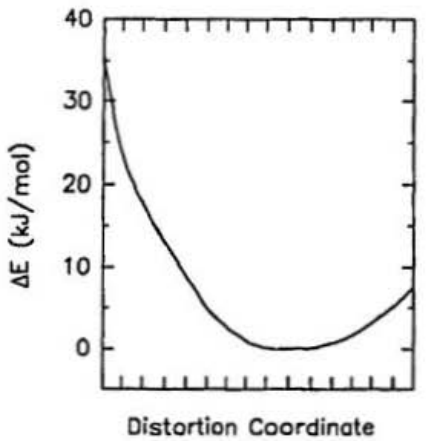

Figure 4-4. Interaction Diagram between Indenyl and Co(ethylene)$_2^+$ without and with Distortion (upper) and Total Energy Change as a Function of Indenyl Ring Distortion (cf. Table 4-5).

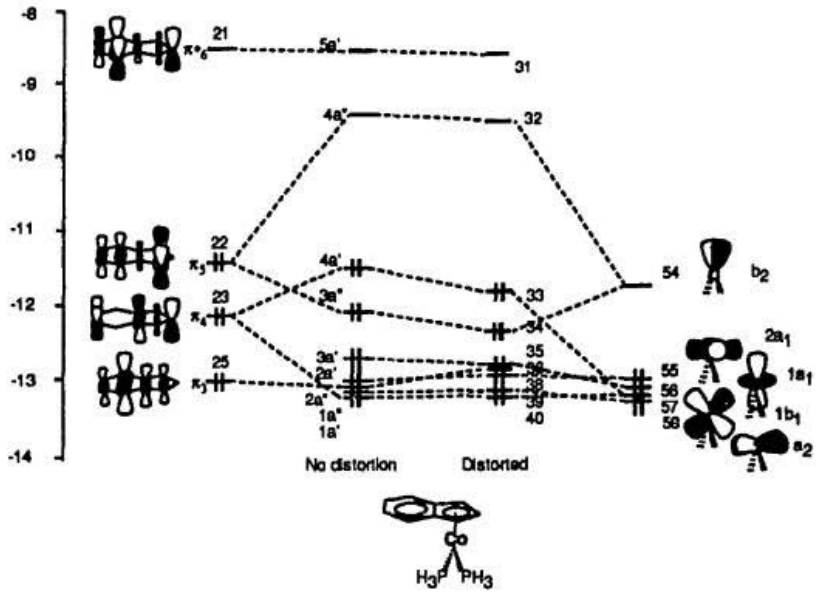

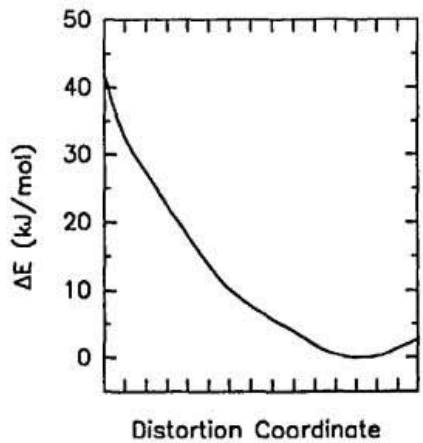

Figure 4-5. Interaction Diagram between Indenyl and $Co(PH_3)_2^+$ without and with Distortion (upper) and Total Energy Change as a Function of Indenyl Ring Distortion (cf. Table 4-5).

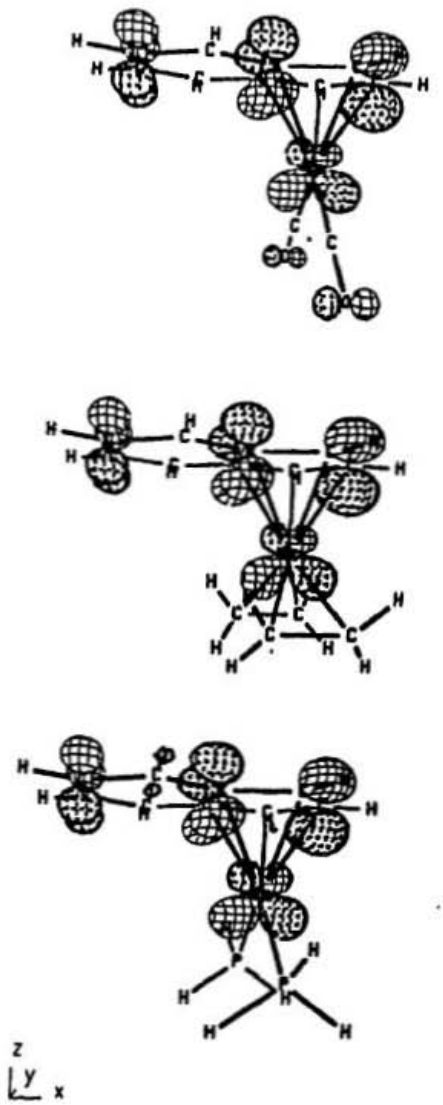

Scheme 4-5. The HOMO Showing Antibonding Repulsion in (η^5-Indenyl)ML_2 Molecules.

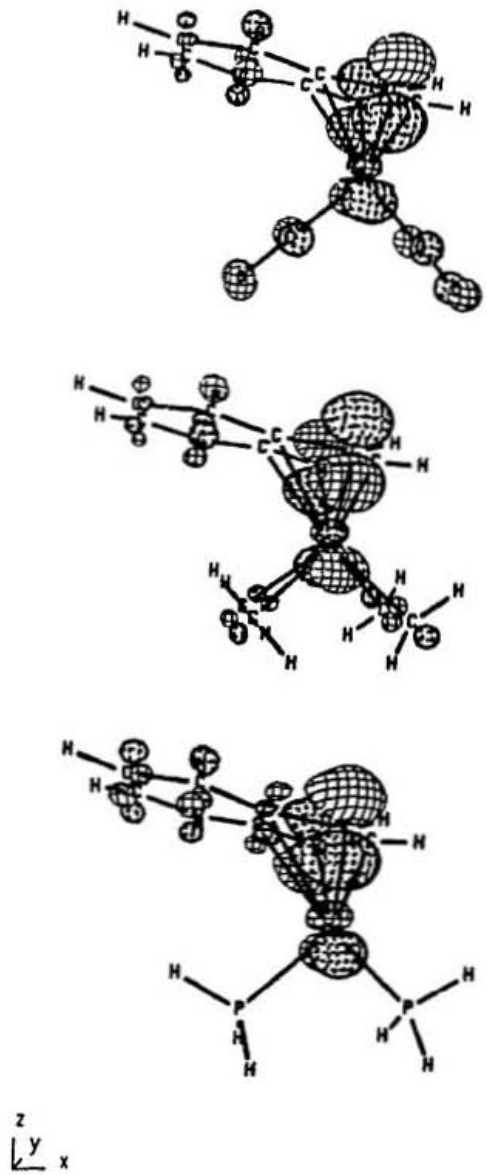

Scheme 4-6. The HOMO Showing Greater Antibonding Repulsion in (η^5-Indenyl)ML_2 Molecules after ML_2 Rotated 90°.

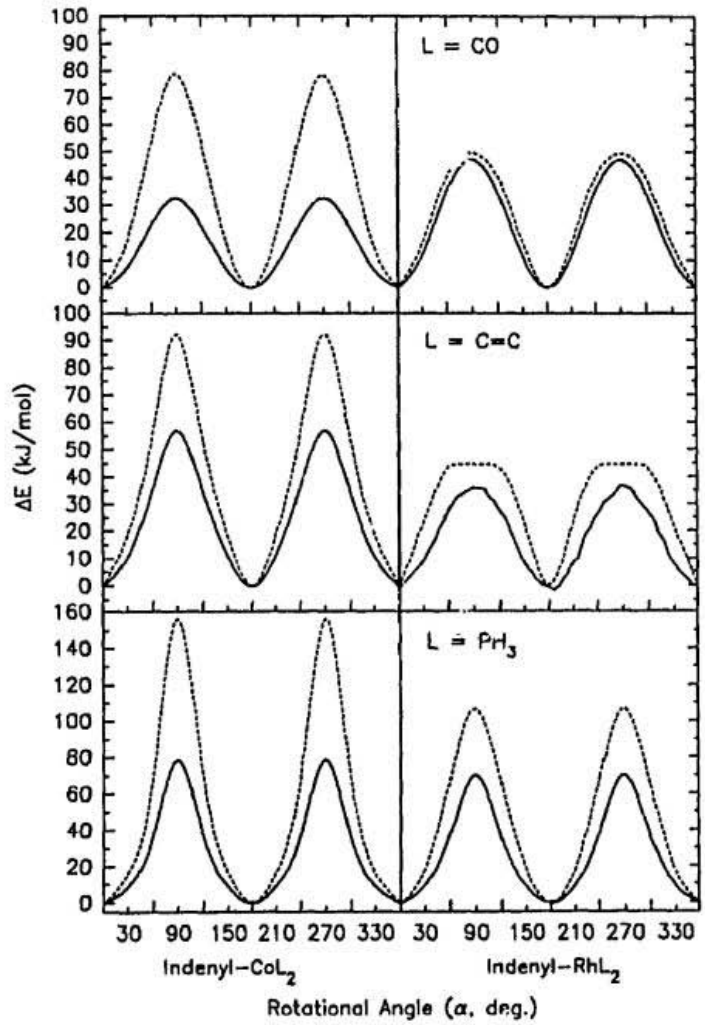

Figure 4-6. Total Energy (dashed line) and HOMO Energy (solid line) Changes for ML_2 Rotation about Indenyl-metal bonding axis for (η^5-indenyl)ML_2

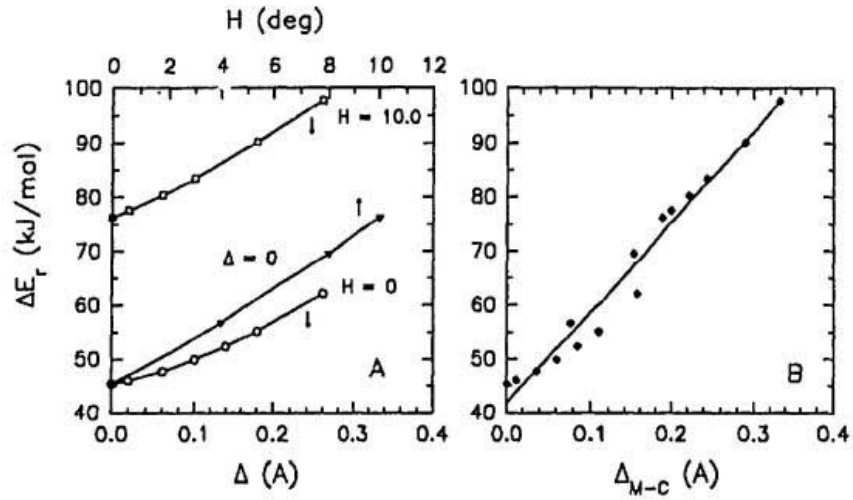

Figure 4-7. Dependence of Rotational Barrier (ΔE_r) on: (A) the Indenyl Ring Slippage (Δ), Hinge Angle Puckering (H); and (B) Overall Distortion (Δ_{M-C}) in (η^5-Indenyl)$Co(CO)_2$.

4.3.3. (η^5-Indenyl)ML_3 Complexes (M (d^6) = Co, L = CO, PH_3; M (d^6) = Mn, L = CO). The FMO's of d^6 ML_3 fragments, which are shown in Figure 4-8, are well-known.[319, 339, 340, 342-345] As with the a_1 FMO's in ML_2 fragments, the low lying $1a_1$ and high lying $2a_1$ and $3a_1$ in ML_3 interact mainly with the indenyl π_1 (FMO 32) and π_2 (FMO 28) FMO's, which make no contribution to the indenyl ring distortion and conformational preferences. Although the two filled 1e FMO's are tilted toward the indenyl π orbitals, the interactions between 1e and indenyl π_5 (FMO 22) and π_4 (FMO 23) are very weak since 1e results from the hybridization of d_{xy} and d_{yz} or d_{x2-y2} and d_{xz}, respectively. These two 1e orbitals are still mainly d_{xy} and d_{x2-y2} and hence are essentially non-bonding.

The two empty 2e FMO's in each ML_3 play the key role in controlling the distortion and conformational preference of (η^5-indenyl)ML_3 complexes. As shown in Figure 4-9, one of the 2e (FMO 57) resulting from the hybridization of the metal d_{yz} (major), d_{xy} and p_y orbitals is bisected by one ligand of ML_3 (cf. Scheme 4-7) and is of correct symmetry for overlap with the filled indenyl π_5 (FMO 22) orbital when ML_3 put its one ligand in the xz plane *trans* to the indenyl 6-ring. These two orbitals (FMO 57 and π_5) interact strongly affording bonding 3a" and antibonding 4a" MOs. The former is filled and the latter is empty. The other 2e orbital (FMO 58) derived from mixing of metal d_{xz} (major), d_{x2-y2} and p_x orbitals is in the xz plane and bisects the L-M-L angle, as shown in Scheme 4-7. This 2e (FMO 58) orbital interacts mainly with the indenyl π_4 (FMO 23) orbital giving a filled bonding orbital (3a') and an empty antibonding orbital (4a'). Unlike the b_2 FMO of ML_2, which is located in the yz plane, one component of 2e (FMO 57) tilts significantly toward the π_5 (FMO 22) orbital lobes localized mainly on indenyl C_1 and C_3. The other component of 2e (FMO 58) tilts toward the π_4 (FMO 23) orbital lobes localized mainly on indenyl C_2 , C_{3a} and C_{7a}. Much smaller indenyl ring distortion in (η^5-indenyl)ML_3 would be expected, compared to the corresponding (η^5-indenyl)ML_2 complexes, because of the easier interactions between the tilted 2e and π_5, π_4 FMOs in (η^5-indenyl)ML_3.

An energy minimum exists in each (η^5-indenyl)ML_3 molecule as the indenyl ring distorts from η^5 toward η^3 ... served in the (η^5-indenyl)ML_2 complexes. In accord with the prediction of FMO analysis, the calculated ring distortion in (η^5-indenyl)ML_3

is much smaller than that in (η^5-indenyl)ML_2 complexes (*cf.* Table 4-4). In addition, the calculated stabilization energy of distortion for all (η^5-indenyl)ML_3 complexes is much lower compared to the (η^5-indenyl)ML_2 cases.

Figure 4-10 shows the relative total energy and HOMO energy changes of (η^5-indenyl)ML_3 for rotation of the ML_3 fragment about the indenyl-metal bonding axis at the optimum distorted geometry. The preferred conformation has one ligand of ML_3 in the molecule mirror plane and *trans* to the indenyl 6-ring as predicted by the fragment orbital analysis and found experimentaly (cf. Table 4-1).[333] As α increases the bonding interaction between FMO 57 and π_5 weakens, resulting in the increase of the HOMO (3a") energy, which reaches a maximum at $\alpha = 60°$. The destabilization of the 3a" orbital is only partly cancelled by the strengthened bonding interaction between FMO 58 and π_4 resulting in the decrease of the orbital energy of the 3a' MO, whose α dependence is out of phase with respect to the HOMO energy change. Thus, the overall potential energy change as a function of α gives a relatively favored conformer (cf. Figure 4-10) even though the rotational barrier of ML_3 in (η^5-indenyl)ML_3 is very low compared to other molecules presented in this study. Consistent with the experimental observation[257,268] the preferred conformation for (η^3-indenyl)ML_3 (M = Fe (d^8), L = CO; M = Ir (d^8), L = PH_3) predicted by EHMO calculations places one ligand (L) in the molecular mirror plane underneath the indenyl six-membered ring.

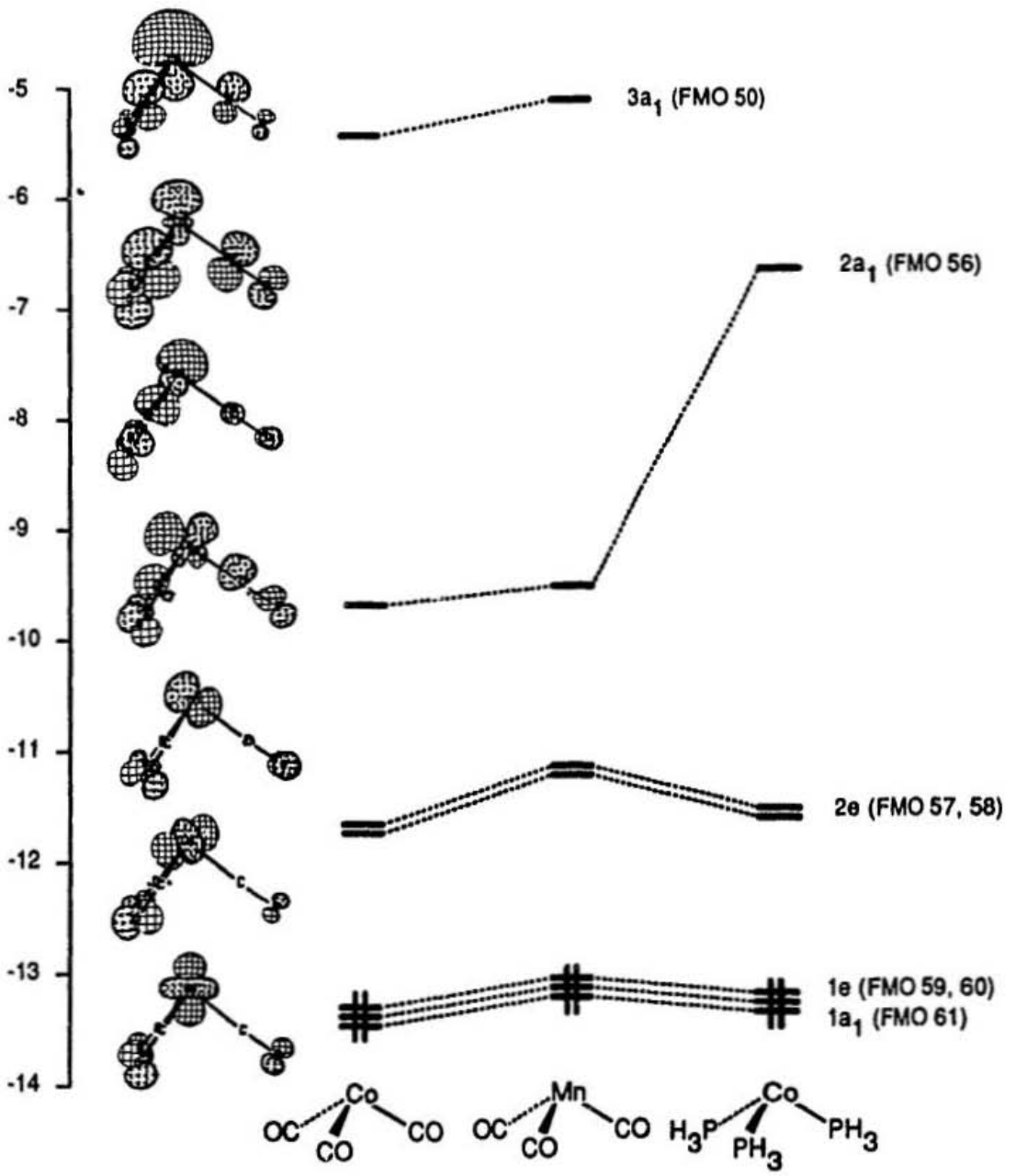

Figure 4-8. Important Fragment Molecular Orbitals of $Co(CO)_3^{3+}$ (the FMOs of $Mn(CO)_3^{+}$, and $Co(PH_3)_3^{3+}$ are similar to those of $Co(CO)_3^{3+}$, but have different energy).

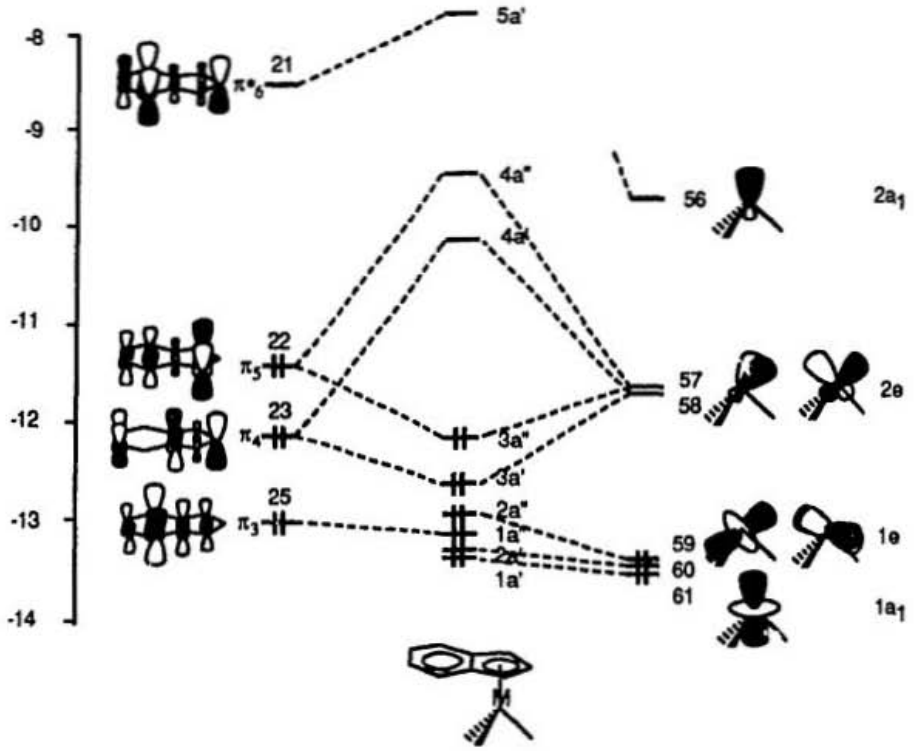

Figure 4-9. Interaction Diagram between Indenyl and ML_3 Fragments.

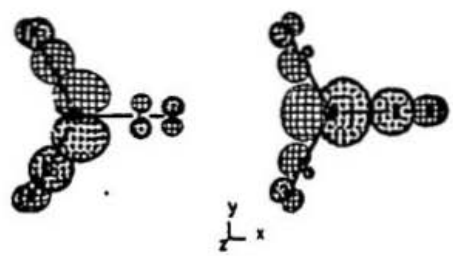

Scheme 4-7. Down Z-axis view of 2e Orbitals (FMO 57, FMO 58) of $Co(CO)_3^{3+}$ Fragment (orbitals for the remaining $M(d^6)L_3$ fragments are the same).

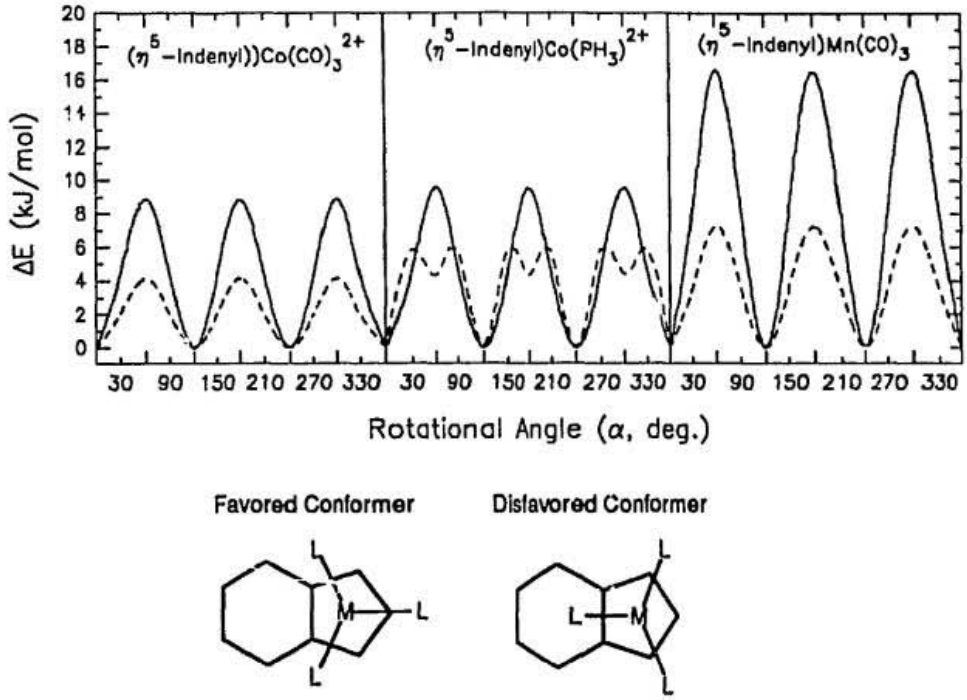

Figure 4-10. Total Energy (dashed line) and HOMO Energy (solid line) Changes as ML_3 Rotating about Indenyl-metal bonding Axis for (η^5-Indenyl)ML_3.

4.3.4. (η^5-Indenyl)ML_2L' Complexes (M (d^6) = Co, Ir, Ru, Cr; L = PH_3, CO; L' = Me, CF_3, H, Cl, CO, NO). As shown in Scheme 4-3, EHMO calculations of the six model complexes possessing the title formula were performed to investigate their distortion and conformational preferences. While fixing the L ligand in (η^5-Indenyl)ML_2L' as PH_3, the L' ligand was changed from σ-donor (Me, H), π-donor (Cl), to π-acceptor (CO), in order to provide some insight of the way different ligands direct conformational preferences in indenyl complexes.

As one ligand L in (η^5-Indenyl)ML_3 is substituted by L', the symmetry of the metal fragment changes from C_{3v} to C_s (ML_2L'), resulting in the loss of the degeneracy of the fragment MO's in Figure 4-8. The two filled 1e FMO's and the two empty 2e FMO's in the ML_3 fragment (cf. Figure 4-8) split into two filled a', a" FMO's and two empty a', a" in ML_2L' fragments as shown in Figure 4-11. Analogously to the FMO's discussed above, the two empty FMO's (2a" and 3a'), which are of appropriate symmetry for overlap with the two filled indenyl π_5 and π_4 orbitals, play a key role in determining the distortion and conformational preference of (η^5-indenyl)ML_2L' complexes. One common feature for the 2a" and 3a' FMO's in ML_2L' fragments is that the orbital lobes in 2a" are bisected by and tilted toward the L' ligand. The orbital lobes in 3a' are within the indenyl (centroid)-M-L' plane as shown in Figure 4-12.

4.3.4.1. [(η^5-Indenyl)Co(PH_3)$_2$(R)]$^+$ (R = Me, CF_3). Figure 4-13 shows the interaction diagram between indenyl π orbitals and the Co(PH_3)(Me)$^{2+}$ fragment MO's. The empty 2a" (FMO 58) orbital interacts strongly with the filled indenyl π_5 (FMO 22) orbital affording a filled bonding MO (3a") and an empty antibonding MO (4a"). The empty 3a' (FMO 57) orbital overlaps mainly with the filled indenyl π_4 (FMO 23) orbital to give an occupied 3a' MO and an unoccupied 4a' MO (cf. Figure 4-13). The two occupied frontier bonding molecular orbitals again dominate the indenyl ring distortion and the conformational preference. As the Co(PH_3)$_2$(Me)$^{2+}$ fragment moves away from the indenyl centroid toward C_2 and the indenyl 6-ring puckers along the C_3-C_1 and C_{7a}-C_{3a}

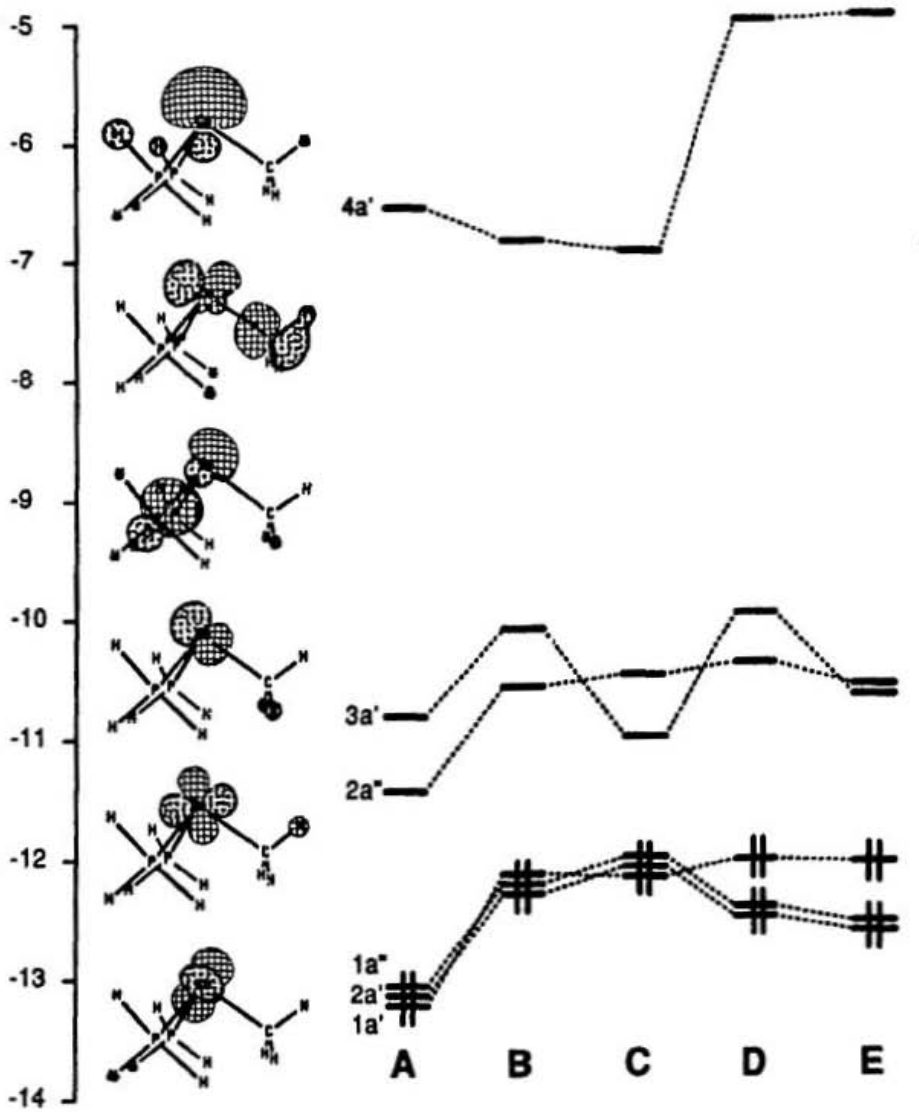

Figure 4-11. The Important Fragment Molecule Orbitals of $Co(PH_3)_2(Me)^{2+}$ (the FMOs of the remaining ML_2L' are similar to those of $Co(PH_3)_2(Me)^{2+}$, but have different energy. A: $Co(PH_3)_2(Me)^{2+}$, B: $Ir(PH_3)_2(H)^{2+}$, C: $Ir(PH_3)_2(Cl)^{2+}$, D: $Ru(PH_3)_2(CO)^{2+}$, E: $Cr(CO)_2(NO)^{+}$

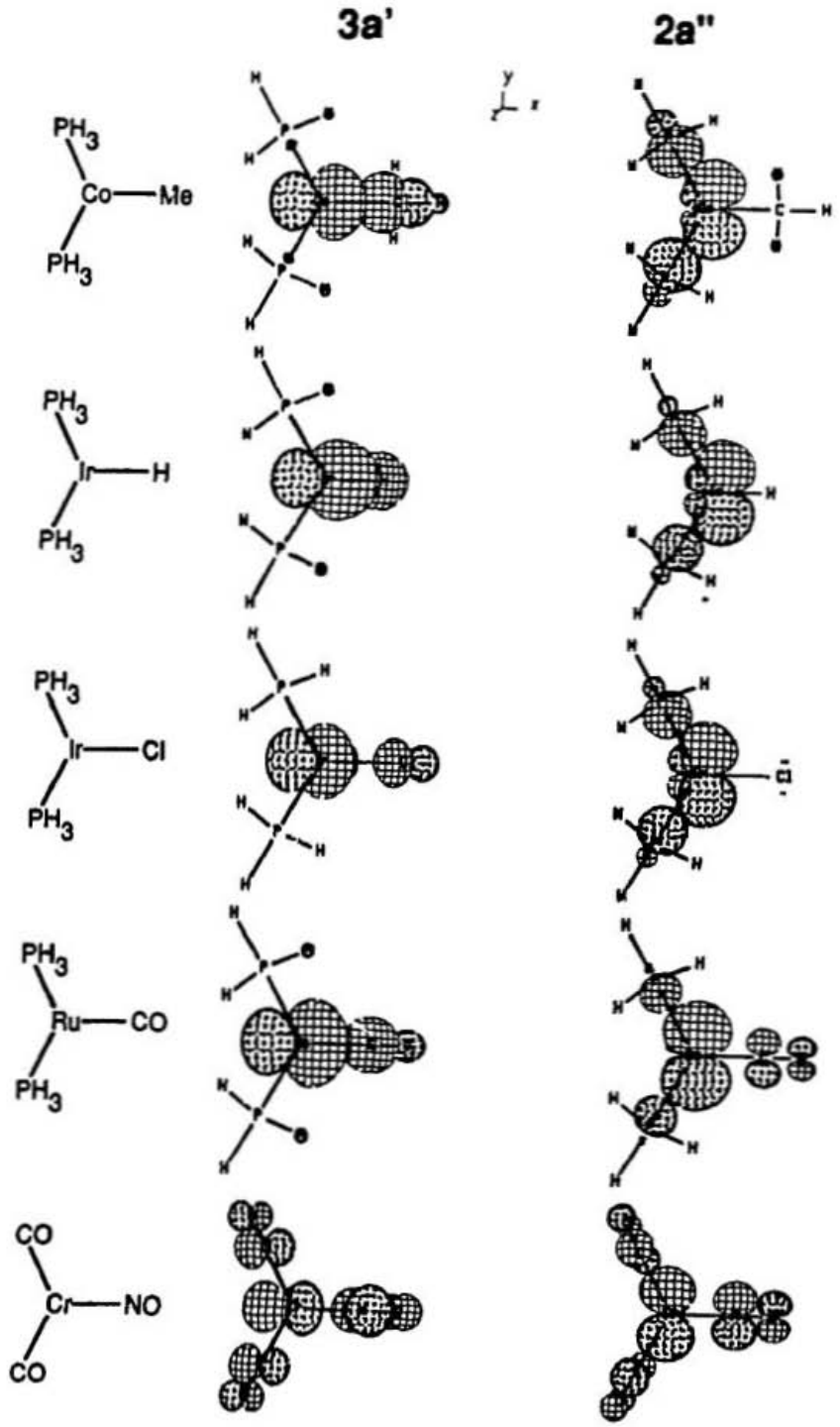

Figure 4-12. Down Z-Axis (Indenyl-Metal Bonding Axis) View of 2a" and 3a' FMOs of ML_2L'.

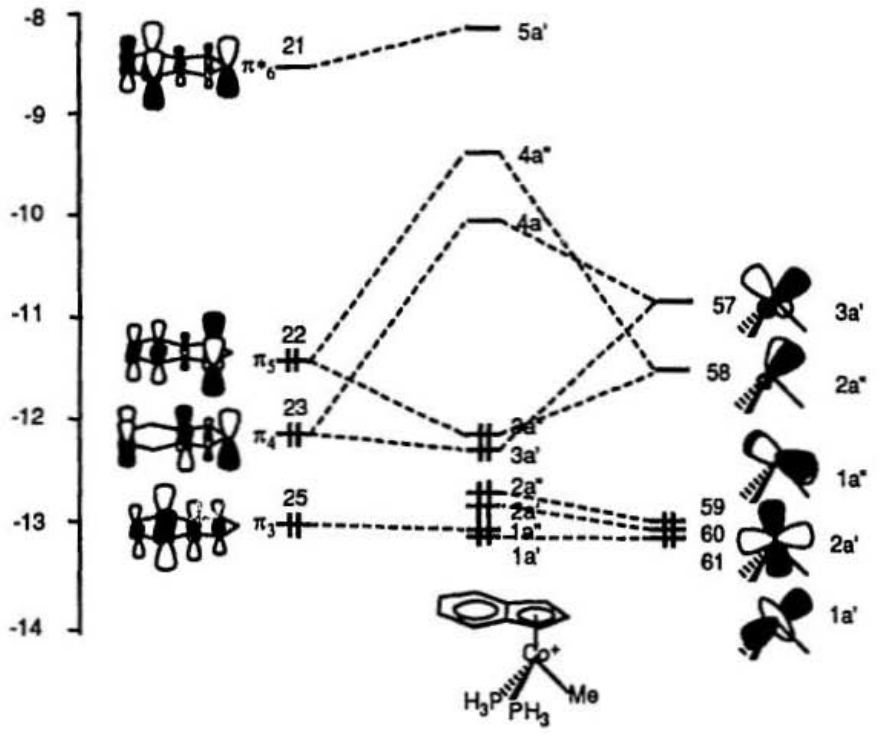

Figure 4-13. Interaction Diagram between Indenyl and $Co(PH_3)_2(Me)^{2+}$ Fragments.

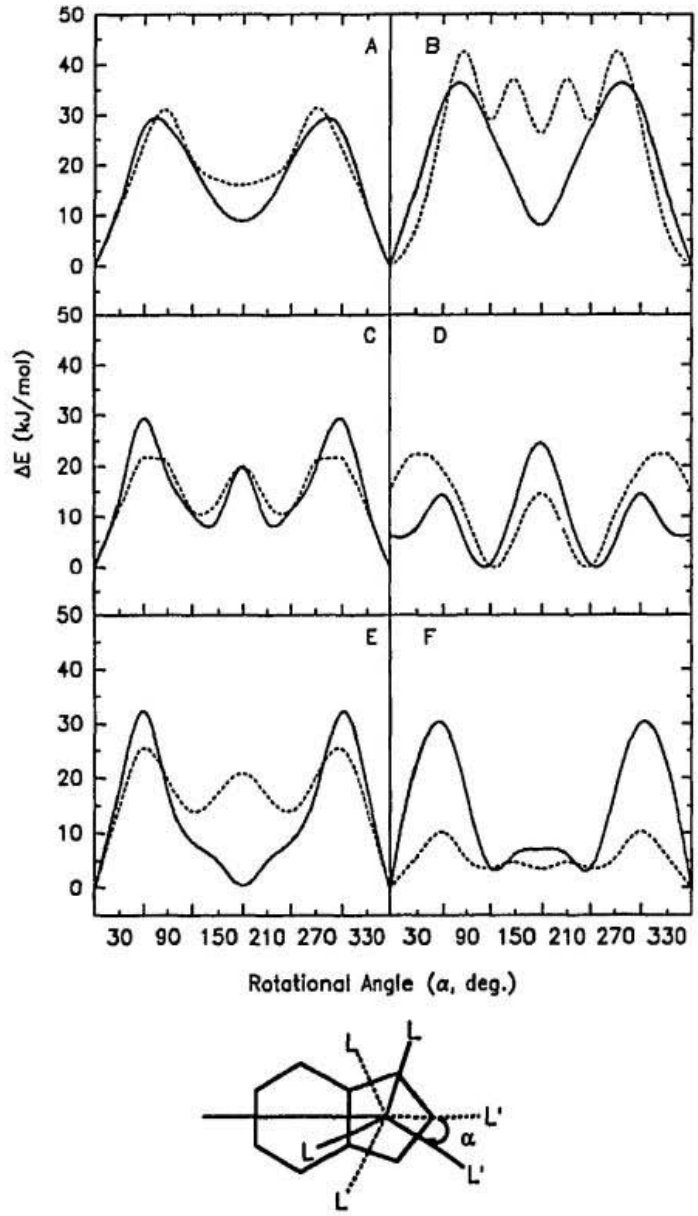

Figure 4-14. Total Energy (dashed line) and HOMO Energy (solid line) Changes for ML_2L' Rotation about the Indenyl-M Bonding Axis for (η^5-indenyl)ML_2L' with L' starting at $\alpha = 0$ (A: $Co(PH_3)_2(Me)^{2+}$, B: $Co(PH_3)_2(CF_3)^{2+}$, C: $Ir(PH_3)_2(H)^{2+}$, D: $Ir(PH_3)_2(Cl)^{2+}$, E: $Ru(PH_3)_2(CO)^{2+}$, F: $Cr(CO)_2(NO)^{+}$).

axes, the energies of both 3a" (HOMO) and 3a' (NHOMO) decrease, reaching a defined minimum. The total energy curve of $[(\eta^5\text{-indenyl})Co(PH_3)_2(Me)]^+$ shows an energy minimum at $\Delta_{M\text{-}C}$ = 0.24 Å, H = 8.0°, and F = 9.5°, as the indenyl ring distorts from the η^5 toward the η^3 coordination mode. The calculated distortional stabilization energy of 24.60 kJ/mol (cf. Table 4-5) agrees with the experimental results (cf. Table 4-1).[232, 282, 318] Increased conjugation of indenyl six-membered ring is also observed from the calculation result as shown in Table 4-4.

Figure 4-14A shows that the relative total energy and HOMO energy changes of $[(\eta^5\text{-indenyl})Co(PH_3)_2(Me)]^+$ possess two distinct energy minima for rotation of the $Co(PH_3)_2(Me)^{2+}$ fragment about the indenyl-metal bonding axis at the optimized distorted geometry. The lowest energy minimum at α = 0° corresponds to the conformation with Me group in the molecule mirror plane and trans to the indenyl six-membered ring as shown in Scheme 4-8A. The second energy minimum at α = 180° (ΔE = 16.03 kJ/mol) corresponds to the conformation with the Me ligand in the mirror plane and underneath the indenyl six-membered ring (cf. Scheme 4-8B). Replacement of Me by CF_3 results in similar distortion (cf. Tables 4-4 and 4-5) and potential energy - α pattern (cf. Figure 4-14B). However, there is one more metastable conformer with CF_3 at α = 120° and 240° as shown in Scheme 4-8B. As discussed above, in both $[(\eta^5\text{-Indenyl})Co(PH_3)_2(Me)]^+$ and $[(\eta^5\text{-Indenyl})Co(PH_3)_2(CF_3)]^+$ the morphology of total energy change/rotational angle α curve is dominated by the HOMO (MO 3a"). The NHOMO (MO 3a') energy curve is out of phase with respect to the HOMO (MO 3a") energy curve and determines the detailed shape of the total energy curve. Consistent with the EHMO predictions, the observed conformation

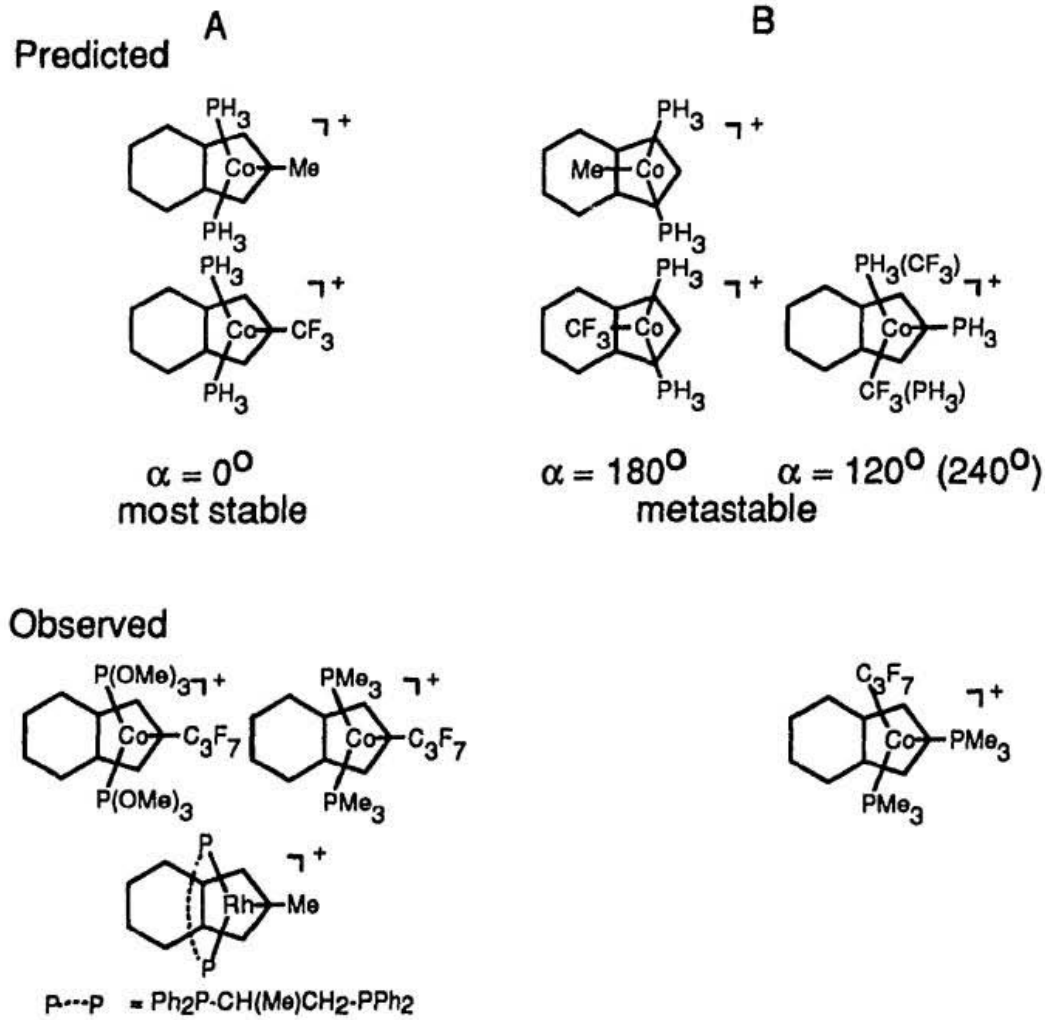

Scheme 4-8

adopted both in the solid state and in solution for $[(\eta^5\text{-indenyl})Co(PMe_3)_2(C_3F_7)]^+$,[282] $[(\eta^5\text{-indenyl})Co(P(OMe)_3)_2(C_3F_7)]^+$,[318] and $[(\eta^5\text{-indenyl})Rh(Ph_2P\text{-}CH(Me)CH_2\text{-}PPh_2)(Me)]^+$,[232] corresponds to the predicted lowest energy conformer with C_3F_7 or Me residing in the molecular mirror plane *trans* to the indenyl six-membered ring. Only in one example, $[(\eta^5\text{-indenyl})Co(PMe_3)_2(C_3F_7)]^+$,[282] are both the predicted most stable conformer and one of the metastable conformers with C_3F_7 at α = 240°

observed in the solid state (cf. Table 4-1 and Scheme 4-8).

4.3.4.2. [(η^5-Indenyl)Ir(PH_3)$_2$(R)]$^+$ (R = H, Cl) As shown in Figures 4-15 and 4-16, the interactions between indenyl π orbitals and the Ir(PH_3)$_2$(R)$^{2+}$ (R = H, Cl) fragment orbitals are similar to those between the indenyl π orbitals and Co(PH_3)$_2$(Me)$^{2+}$ fragment orbitals. However, there exists a second order mixing of metal 2a' (FMO 56) and 1a" (FMO 57) fragment orbitals into the filled 3a' and 3a" molecular orbitals as a result of energy increases of the these two fragment orbitals (2a' and 1a"). These second order interactions result in increases in energy of these two frontier orbitals (MO's 3a" and 3a'). The composition of MO's 3a" and 3a' change compared to those orbitals in [(η^5-indenyl)Co(PH_3)$_2$(Me)]$^+$, which may result in a potential energy change and in turn the change of conformational preferences as Ir(PH_3)$_2$(R)$^{2+}$ rotates about the indenyl-metal axis. Although the energy level of FMO's 2a" and 3a' in Ir(PH_3)$_2$(Cl)$^{2+}$ are interchanged and the energy of 3a' is decreased greatly compared to that in Ir(PH_3)$_2$(H)$^{2+}$, MO 3a", resulting from combination of FMO's 2a" and 1a" with the indenyl π_5 (FMO 22) orbital in both [(η^5-indenyl)Ir(PH_3)$_2$(H)]$^+$ and [(η^5-indenyl)Ir(PH_3)$_2$(Cl)]$^+$ forms the HOMO, which is important in determining the indenyl ring distortion and the conformational preferences.

The total energy curves of both [(η^5-indenyl)Ir(PH_3)$_2$(H)]$^+$ and [(η^5-indenyl)Ir(PH_3)$_2$(Cl)]$^+$ show energy minima at $\Delta_{M\text{-}C}$ = 0.15 Å, H = 5.0°, and F = 7.0°, or $\Delta_{M\text{-}C}$ = 0.12 Å, H = 4.0°, and F = 5.2°, respectively (cf. Table 4-5), as the Ir(PH_3)$_2$(R)$^{2+}$ moves away from the indenyl centroid towards C_2 and the indenyl six-membered ring puckers along the

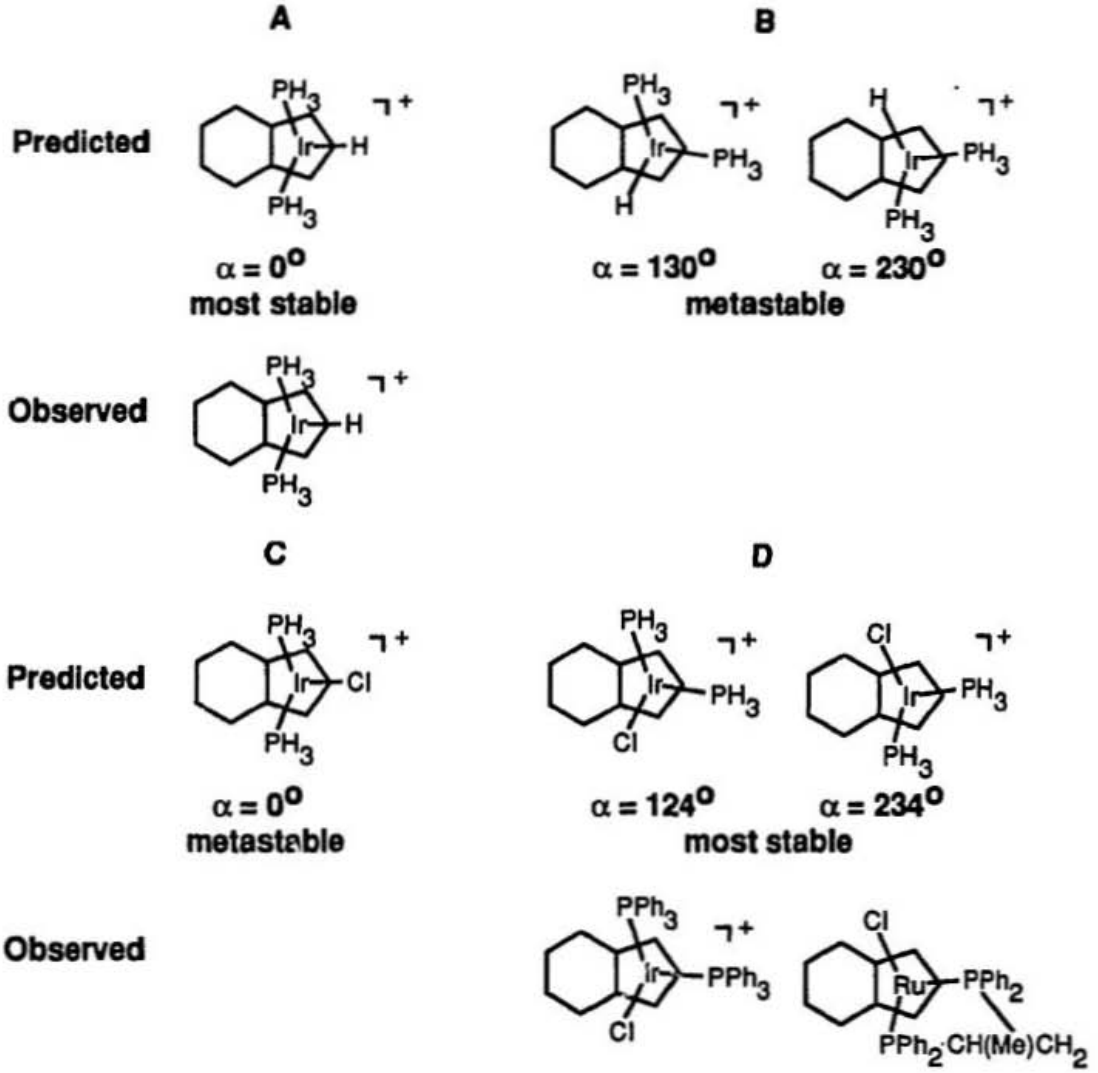

Scheme 4-9

C_3-C_1 and C_9-C_8 axes. Although increased conjugation of the indenyl six-membered ring is also observed (cf. Table 4-4) and the indenyl ring distortion from η^5 to η^3 is favored, the calculated stabilization energies for both $[(\eta^5\text{-indenyl})Ir(PH_3)_2(H)]^+$ and $[(\eta^5\text{-indenyl})Ir(PH_3)_2(Cl)]^+$ complexes are much lower than that for $[(\eta^5\text{-indenyl})Co(PH_3)_2(R)]^+$ (R = Me, CF_3; cf. Table 4-5).

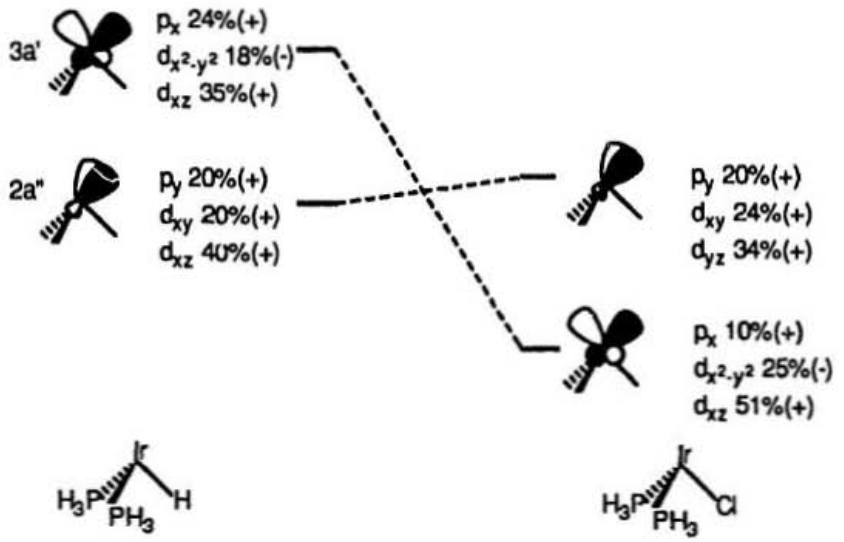

Scheme 4-10

Because of the variation in fragment orbital interactions and the composition changes of the frontier MOs (3a' and especially 3a" (HOMO)), the morphologies of the total energy and HOMO energy curves of $[(\eta^5\text{-indenyl})Ir(PH_3)_2(R)]^+$ (R = H, Cl) (cf. Figures 4-14C, D) show significant differences compared to those of $[(\eta^5\text{-indenyl})Co(PH_3)_2(R)]^+$ (R = Me, CF_3) (cf. Figures 4-14A, B). For $[(\eta^5\text{-indenyl})Ir(PH_3)_2(H)]^+$, there are three distinct energy minima as the $Ir(PH_3)_2(H)^{2+}$ rotates about the indenyl-metal axis from 0-360° (cf. Figure 4-14C). The lowest energy minimum at α = 0° corresponds to the crystallographically observed conformer[270] with H in the molecular mirror plane *trans* to the indenyl six-membered ring as shown in Scheme 4-9A. The second and the third energy minima (ΔE =

10.50 kJ/mol) at α = 130° and 230° correspond to the conformers shown in Scheme 4-9B. These two metastable conformers have not been observed so far.

For $[(\eta^5\text{-indenyl})Ir(PH_3)_2(Cl)]^+$, although there are also three energy minima in the ΔE-α curves as $Ir(PH_3)_2(Cl)^{2+}$ rotates about the indenyl-metal axis. The two lowest energy minima at α = 124° and 234° correspond to the conformers shown in Scheme 4-9D. The conformer with Cl at α = 0° (cf. Scheme 4-9C) now becomes metastable with 15.46 kJ/mol higher energy compared to the first two energy minima. The predicted lowest energy conformer is consistent with the crystallographically observed conformer[271, 324] as shown in Scheme 4-9D.

The difference in conformational preference of $[(\eta^5\text{-indenyl})Ir(PH_3)_2(H)]^+$ from that of $[(\eta^5\text{-indenyl})Ir(PH_3)_2(Cl)]^+$ may be explained on the basis of the energy and hybridization differences of the fragment orbitals of $Ir(PH_3)_2(H)^{2+}$ and $Ir(PH_3)_2(Cl)^{2+}$, especially FMOs 2a" and 3a'. Scheme 4-10 shows the relative energy and composition of 2a" and 3a' in $Ir(PH_3)_2(H)^{2+}$ and $Ir(PH_3)_2(Cl)^{2+}$ fragments. The component of d_{xz} in 3a' increases from 35% in $Ir(PH_3)_2(H)^{2+}$ to 51% in $Ir(PH_3)_2(Cl)^{2+}$, and the d_{yz} component in 2a" decreases from 40% in $Ir(PH_3)_2(H)^{2+}$ to 34% in $Ir(PH_3)_2(Cl)^{2+}$. The energy of 3a' in $Ir(PH_3)_2(Cl)^{2+}$ decreases greatly and is even lower than that of 2a". Therefore, the interaction between 3a' and indenyl π_4 in $[(\eta^5\text{-indenyl})Ir(PH_3)_2(Cl)]^+$ becomes more important in determining the conformational preference than that in $[(\eta^5\text{-indenyl})Ir(PH_3)_2(H)]^+$. The fragment orbital interactions of FMO 3a' with indenyl π_4 and FMO 2a" with indenyl π_5 reach a maximum at α = 115-

125° simultaneously in $[(\eta^5\text{-indenyl})Ir(PH_3)_2(Cl)]^+$, resulting in the preferred conformation shown in Scheme 4-9D.

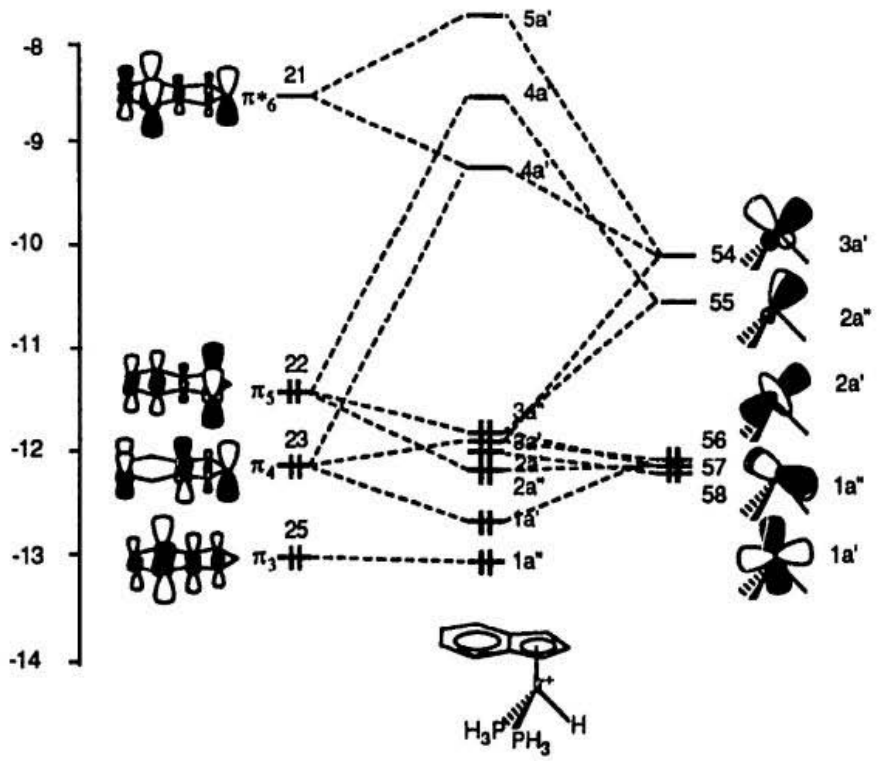

Figure 4-15. Interaction Diagram between Indenyl and $Ir(PH_3)_2(H)^{2+}$ Fragments.

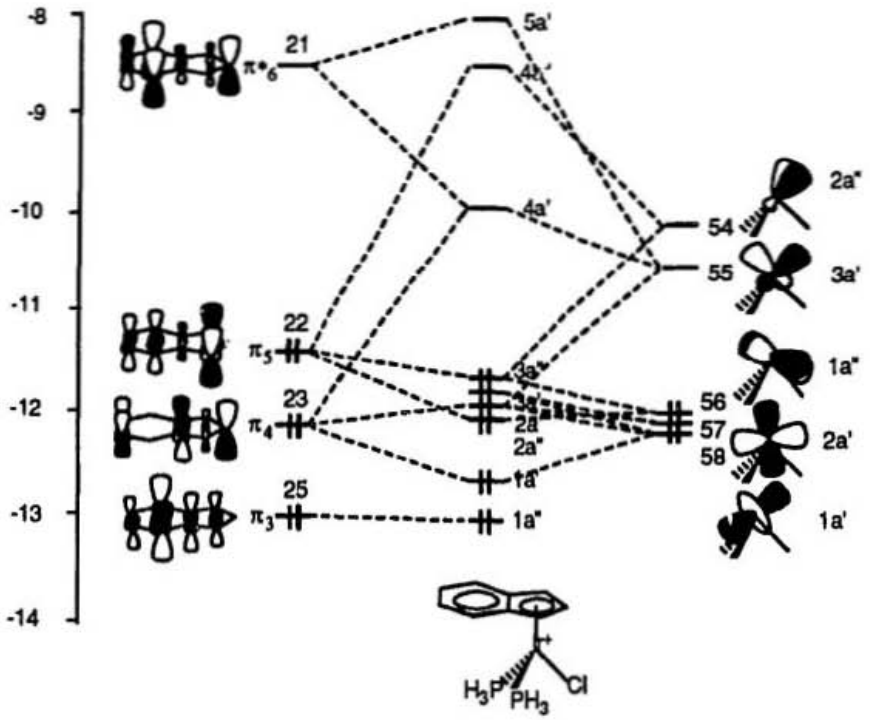

Figure 4-16. Interaction Diagram between Indenyl and $Ir(PH_3)_2(Cl)^{2+}$ Fragments.

4.3.4.3. [(η^5-Indenyl)Ru(PH_3)$_2$(CO)]$^+$ and (η^5-Indenyl)Cr(CO)$_2$(NO). Figure 4-17 illustrates the interaction diagram between the fragment molecular orbitals of $Ru(PH_3)(CO)^{2+}$ and the indenyl π orbitals. Since the d_{yz} component in FMO 2a" in $Ru(PH_3)(CO)^{2+}$ (50%) is higher than that in $Ir(PH_3)(H)^{2+}$ (40%), and the d_{xz} in FMO 3a' in $Ru(PH_3)(CO)^{2+}$ (27%) is lower than that in $Ir(PH_3)(H)^{2+}$ (34%), the overlap difference of FMO 2a" with indenyl π_5 from FMO 3a' with indenyl π_4 in [(η^5-indenyl)$Ru(PH_3)(CO)]^+$ is relatively larger than that in [(η^5-indenyl)$Ir(PH_3)(H)]^+$. In comparison with the interactions in [(η^5-indenyl)$Ir(PH_3)(H)]^+$ the interaction between FMO 2a" in $Ru(PH_3)(CO)^{2+}$ and indenyl π_5 is therefore much stronger than that

between FMO 3a' and indenyl π_4. In addition, a second order mixing of 2a' into the filled bonding orbital 3a' results in an energy increase. As a result, MO 3a' forms the HOMO and MO 3a" forms the NHOMO of $[(\eta^5\text{-indenyl})Ru(PH_3)(CO)]^+$ (cf. Figure 4-17). These two orbitals play a dominant role in controlling the distortion and the conformational preference of this complex.

The total energy curve of $[(\eta^5\text{-indenyl})Ru(PH_3)(CO)]^+$ shows an energy minimum at $\Delta_{M\text{-}C}$ = 0.15 Å, H = 5.0°, and F = 6.8° with a stabilization energy of ΔE = 9.65 kJ/mol (cf. Table V), as the $Ru(PH_3)_2(CO)^{2+}$ moves away from the indenyl centroid toward C_2 and the indenyl six-membered ring puckers along the C_3-C_1 and C_{7a}-C_{3a} axes. The indenyl 6-ring also shows increased conjugation as the indenyl ring distorts from η^5 toward η^3 coordination mode as shown in Table 4-4.

As the $Ru(PH_3)_2(CO)^{2+}$ fragment rotates from 0-360° about the indenyl-metal bonding axis at the optimum distorted low energy geometry, the energy curve of MO 3a' (HOMO) shows two minima at α = 0° and 180° (cf. Figure 4-14E). The energy curve of 3a" (NHOMO) remains almost unchanged in 240° < α < 120°. At α = 120° the energy begins to rise reaching a maximum at 180°. Combination of these two energy curves along with some minor modifications from the remaining orbitals gives the total energy/rotational angle (α) curve, shown in Figure 4-14E, containing three energy minima. The lowest energy minimum at α = 0° corresponds to the conformation with the CO ligand in the molecular mirror plane and *trans* to the indenyl six-membered ring, as shown in Scheme 4-11A. The second and the third

equal energy minima appear at α = 123° and 236° (ΔE = 13.99 kJ/mol) and correspond to the conformers shown in Scheme 4-11B. In this case, the crystallographically observed conformers[230, 325] are the predicted metastable conformers, rather than the lowest energy conformer.

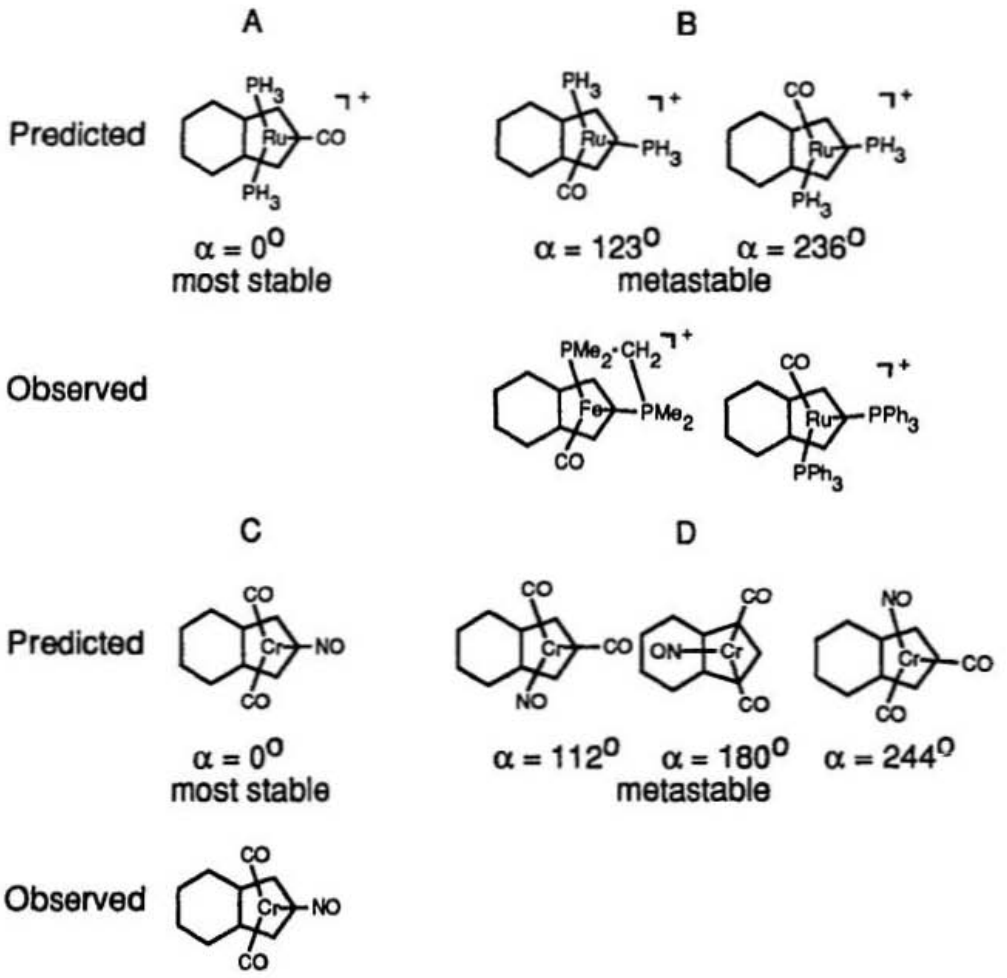

Scheme 4-11

The interaction between $Cr(CO)_2(NO)^+$ fragment orbitals and indenyl π orbitals is

more complicated compared to the remaining (η^5-indenyl)ML_2L' complexes. Figure 4-18 illustrates only the major interactions, which are similar to those of [(η^5-indenyl)$Ru(PH_3)_2(CO)]^+$. The metal-centred FMO 2a" is a combination of p_y (10%(+)) and d_{yz} (51%(+)) atomic orbitals which is different from the FMO 2a" in the other ML_2L' fragments. The MO 3a' resulting from the interaction between FMO 3a' and the indenyl π_4 forms the HOMO and the MO 3a" resulting from the overlap of FMO 2a" with indenyl π_5 forms the NHOMO. As shown in Table 4-5, the indenyl ring in (η^5-indenyl)$Cr(CO)_2(NO)$ also prefers to distort away from the ideal η^5 coordination mode, although the distortion stabilization energy is low (ΔE = 2.70 kJ/mol).

Rotation of the $Cr(CO)_2(NO)^+$ fragment about the indenyl-metal axis changes the HOMO (3a') energy significantly with an energy difference up to about 30 kJ/mol (cf. Figure 4-14F) as with that in other (η^5-indenyl)ML_2L' complexes. However, because the NHOMO (3a") energy - rotational angle (α) curve is exactly out of phase with the HOMO energy-α curve, the combination of these two curves results in the total energy-α curve having a very low rotational barrier (ΔE_r = 10.21 kJ/mol) as shown in Figure 4-14F. Nevertheless, there do exist several energy minima. The lowest energy minimum at α = 0° places NO in the molecular mirror plane *trans* to the indenyl six-membered ring (cf. Scheme 4-11C). The other three higher energy minima at α = 112°, 180° and 244° possess the same energy (ΔE = 3.55 kJ/mol) corresponding to the conformers shown in Scheme 4-11D. The predicted lowest energy conformer is the observed conformer in the solid state.[326]

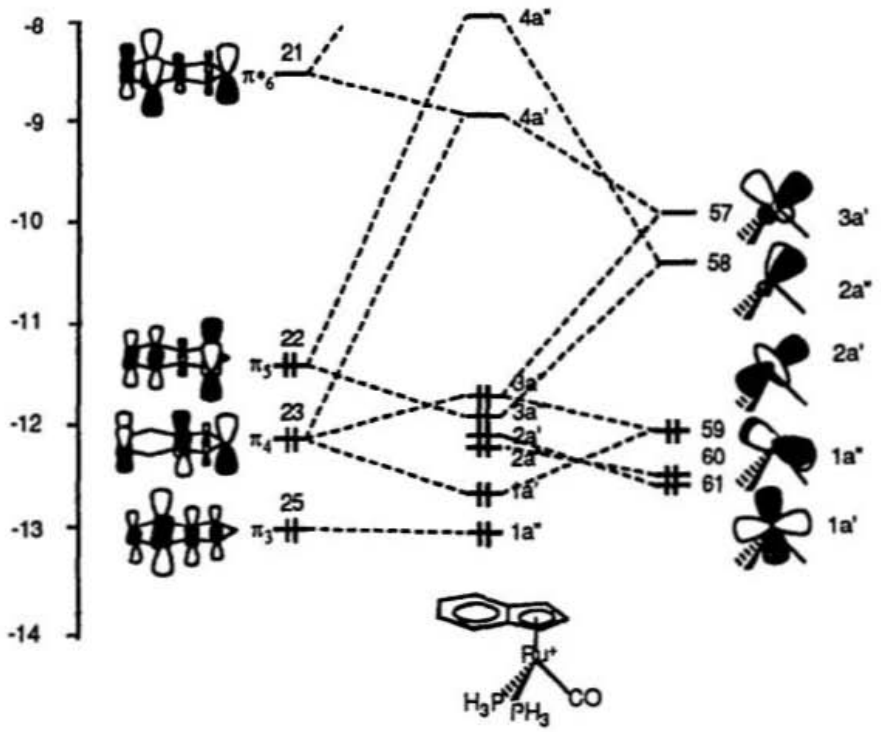

Figure 4-17. Interaction Diagram between Indenyl and $Ru(PH_3)_2(CO)^{2+}$ Fragments.

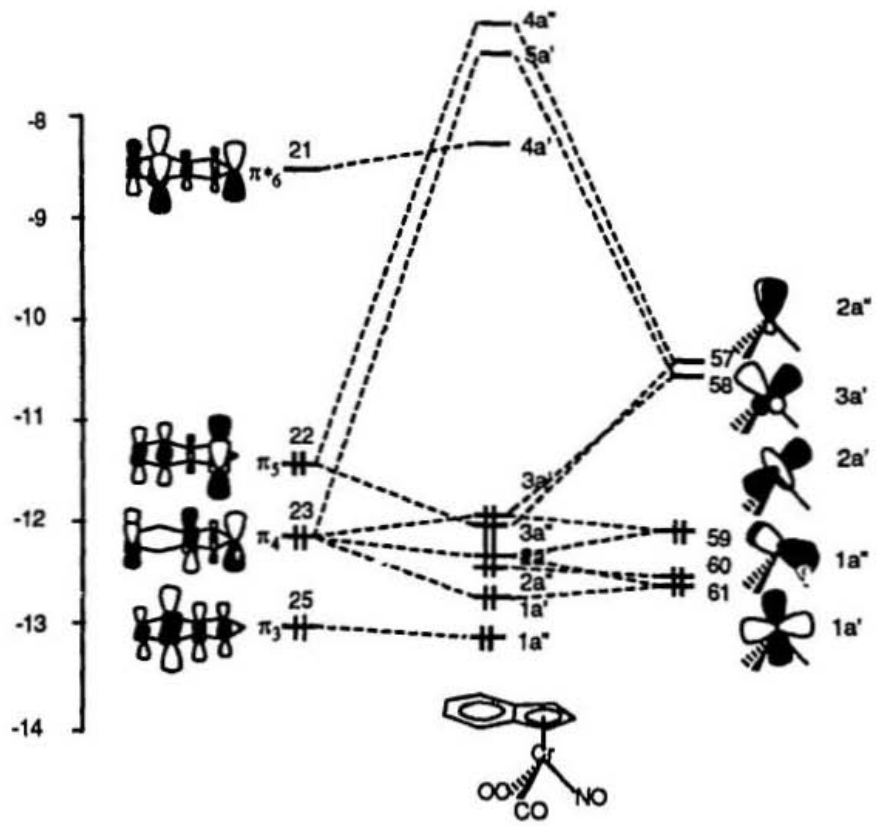

Figure 4-18. Interaction Diagram between Indenyl and $Cr(CO)_2(NO)^+$ Fragments.

4.3.5. (η^5-Indenyl) MLL'L" Complexes. Since these complexes possess three different ligands around the metal centre and η^5-indenyl can be considered to occupy the fourth coordination site, the metal atom is chiral. Due to the low symmetry of the MLL'L" fragments, the composition of the metal-centred fragment molecular orbitals becomes much more complicated. The resulting interaction diagrams between indenyl π orbitals and MLL'L" fragment orbitals for these (η^5-indenyl)MLL'L" complexes are more difficult to interpret. It is appropriate then to concentrate on the HOMO and the total energy curves in order to examine the conformational

preferences in these complexes.

The total energy curve of all the five chiral complexes examined in this study (cf. Scheme 4-3) shows an energy minimum (cf. Table 4-5), with the MLL'L" fragment moved away from the indenyl centroid toward C_2 and the indenyl six-membered ring puckered along the C_3-C_1 and C_{7a}-C_{3a} axis, corresponding to a moderate distortion of the indenyl ring from the η^5 toward the η^3 coordination mode as observed experimentally.[231, 243, 280, 281, 298, 301, 327-329, 334] Along with these distortions, enhanced conjugation of the indenyl six-membered ring is evident from the EHMO calculations (cf. Table 4-4).

Figure 4-19 illustrates the total energy and HOMO energy curves of (η^5-indenyl)MLL'L" complexes, as the MLL'L" fragment rotates about the indenyl-metal bonding axis. Except for (η^5-indenyl)Ru(CO)(I)(PH_3), the morphologies of the total energy-α curve and the HOMO energy-α curve match very well suggesting that the HOMO again dominates the conformational preference. The energy curves corresponding to one of the two enantiomers for each complex are shown. The energy curves for the other enantiomers are necessarily mirror images.

For (η^5-indenyl)Co(Me)(I)(CO), the total energy-α curve shows two energy minima (cf. Figure 4-19A). In agreement with the crystallographically observed conformer[281] the lowest energy conformer at $\alpha = 0°$ places the Me group *trans* to the indenyl six-membered ring as shown in Scheme 4-12A. The minimum (ΔE = 8.96 kJ/mol) at α = 125° corresponds to the conformer shown in Scheme 4-12B. Because the HOMO

of (η^5-indenyl)Co(Me)(I)(CO) results from the interaction between the indenyl π_5 and the metal-centred FMO 55 (the lowest empty FMO, cf. Scheme 4-13A), with lobes almost bisected by the Co-Mε bond and oriented toward the π_5 orbital centred on C_1 and C_3, the overlap of indenyl π_5 with FMO 55 reaches its maximum, providing a lowest energy minimum with the Me group at $\alpha = 0°$.

Similarly, the most stable conformer calculated for (η^5-indenyl)Co(Me)(I)(PH_3) (cf. Scheme 4-13B and Figure 4-19B) has its Me group at $\alpha = 0°$ *trans* to the indenyl six-membered ring as shown in Scheme 4-12C. The results are consistent with the observed conformational preferences for the series (η^5-indenyl)Co(R_f)(I)(PR_3) (R_f = C_3F_7, C_6F_{13}; PR_3 = PPh_3, $PPh_2NHCH(Me)Ph$, PPh_2Me, $PPh_2(OMe)$, $PPhMe_2$, $PPh(OMe)_2$, PMe_3, and $P(OMe)_3$) both in the solid state and in solution.[280-282] The case with PR_3 = $PPh(OMe)_2$ is an exception. Its solid state conformation is different from that in solution, which places the $PPh(OMe)_2$ ligand *trans* to the indenyl six-membered ring. The EHMO calculations predict another metastable conformer at α = 149° (ΔE = 14.39 kJ/mol) which is not experimentally observed (cf. Scheme 4-12D).

(η^5-Indenyl)Co($P(O)(OH)_2$)(PH_3)(Me) shows two energy minima with the $P(O)(OH)_2$ ligand at $\alpha = 0°$ and 135°, corresponding to the conformers shown in Scheme 4-12E, F. The HOMO for (η^5-indenyl)Co($P(O)(OH)_2$)(PH_3)(Me) complex is different from the composition of the HOMO in (η^5-indenyl)Co(Me)(I)(L) (L = CO, PH_3). Good overlap of indenyl π_5 with the metal-centred FMO 60 (the lowest empty FMO, cf. Scheme 4-13C) and the next lowest empty FMO 59 is possible, due to the different orientations

of these two fragment orbital lobes compared to those in (η^5-indenyl)Co(Me)(I)(L) (L = CO, PH_3) complexes. These bonding interactions reach their maxima at $\alpha = 0°$ and 135°, resulting in the preferred conformers shown in Scheme 4-12E, F. Experimentally, the rotamer with the P(O)(R')(OMe) at $\alpha = 0°$ is the only conformation observed so far both in the solid state and in solution (cf. Scheme 4-12E and Table 4-1).[318, 334]

Similarly, strong interactions of indenyl π_5 with the metal-centred lowest empty FMO 58 and the next lowest empty FMO 57 (cf. Scheme 4-13D) form the HOMO of (η^5-indenyl)Fe(CO)(Me)(PH_3) complex. Two energy minima at $\alpha = 0°$ and 235° result in the total energy-α curve. These minima correspond to the conformers with the CO ($\alpha = 0°$, Scheme 4-12G) and Me ($\alpha = 235°$, Scheme 4-12H) *trans* to the indenyl 6-ring. The latter is observed in the relevant complexes (cf. Scheme 4-12H),[231, 329] but the former has not been detected experimentally. An exception to the calculated result is that the conformation adopted by (η^5-indenyl)Fe(CO)(Me)(PPh_2N(Me)CH(Me)Ph) puts the Me underneath the indenyl six-membered ring (cf. Table 4-1), which is the computationally disfavored conformer. No reasonable rationale can be offered at this time. In addition there is one more energy minimum with higher energy (ΔE = 8.11 kJ/mol) at $\alpha = 104°$ (cf. Scheme 4-12I) in the total energy-α curve of (η^5-indenyl)Fe(CO)(Me)(PH_3) and no experimental example with this conformer exists.

The last example investigated in this study is (η^5-indenyl)Ru(CO)(I)(PH_3) complex.

The HOMO in this complex results from overlap of indenyl π_4 and the metal-centred next lowest empty FMO 54 (cf. Scheme 4-13E). Two minima with CO at $\alpha = 0°$ and 180° result in the E_{HOMO} - α curve. However, the energy minimum at $\alpha = 180°$ is largely cancelled by the energy maximum of the bonding orbital formed by the interaction between indenyl π_5 and the metal-centred lowest empty FMO 55 (cf. Scheme 4-13E), which shows minimum overlap as CO rotates to $\alpha = 180°$. The total energy-α curve, therefore shows three minima. The lowest energy minimum with CO at $\alpha = 0°$ corresponds to the conformer shown in Scheme 4-12J, which is the preferred conformation for several relevant complexes in solution.[298, 301] The second minimum with CO at $\alpha = 110°$ has higher energy (ΔE = 13.34 kJ/mol) and corresponds to the conformer shown in Scheme 4-12K, which is crystallographically observed.[243] No evidence for the predicted third higher energy conformer (ΔE = 18.58 kJ/mol, cf. Scheme 4-12M) with CO at $\alpha = 236°$ has been presented in the literature.

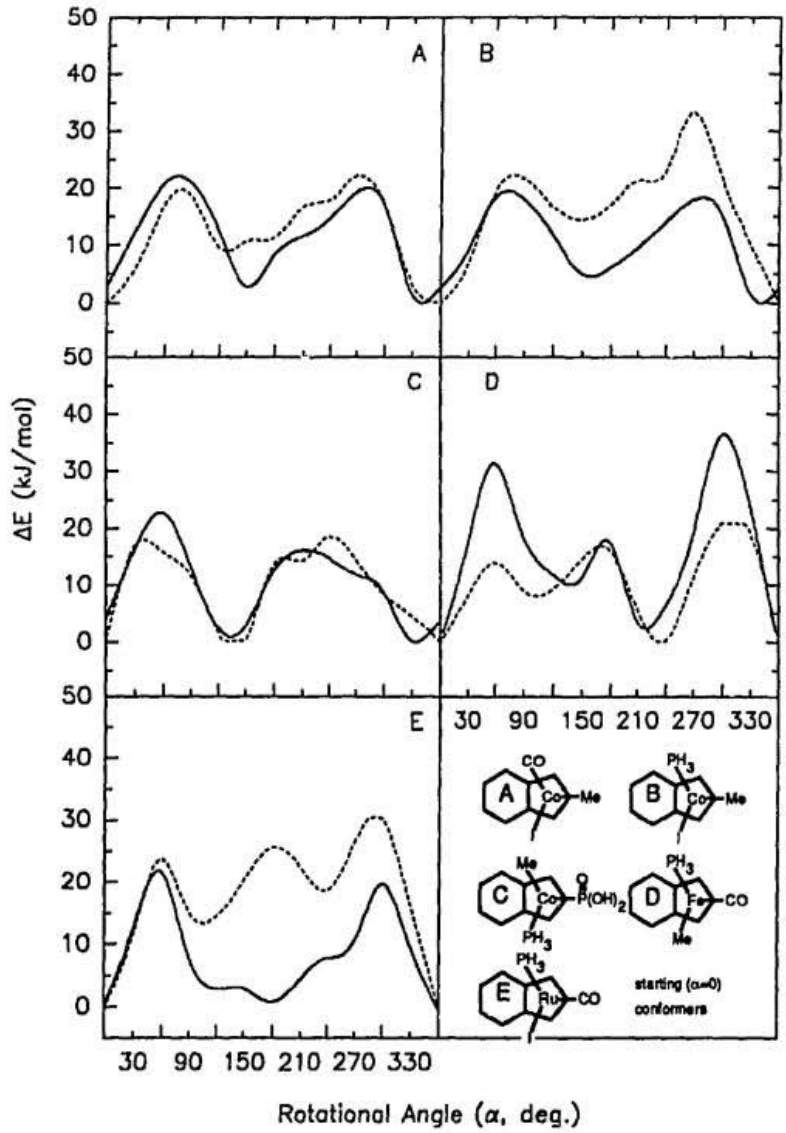

Figure 4-19. Total Energy (dashed line) and HOMO Energy (solid line) Changes for MLL'L" Rotation about the Indenyl-metal Bonding Axis for (η^5-indenyl)MLL'L".

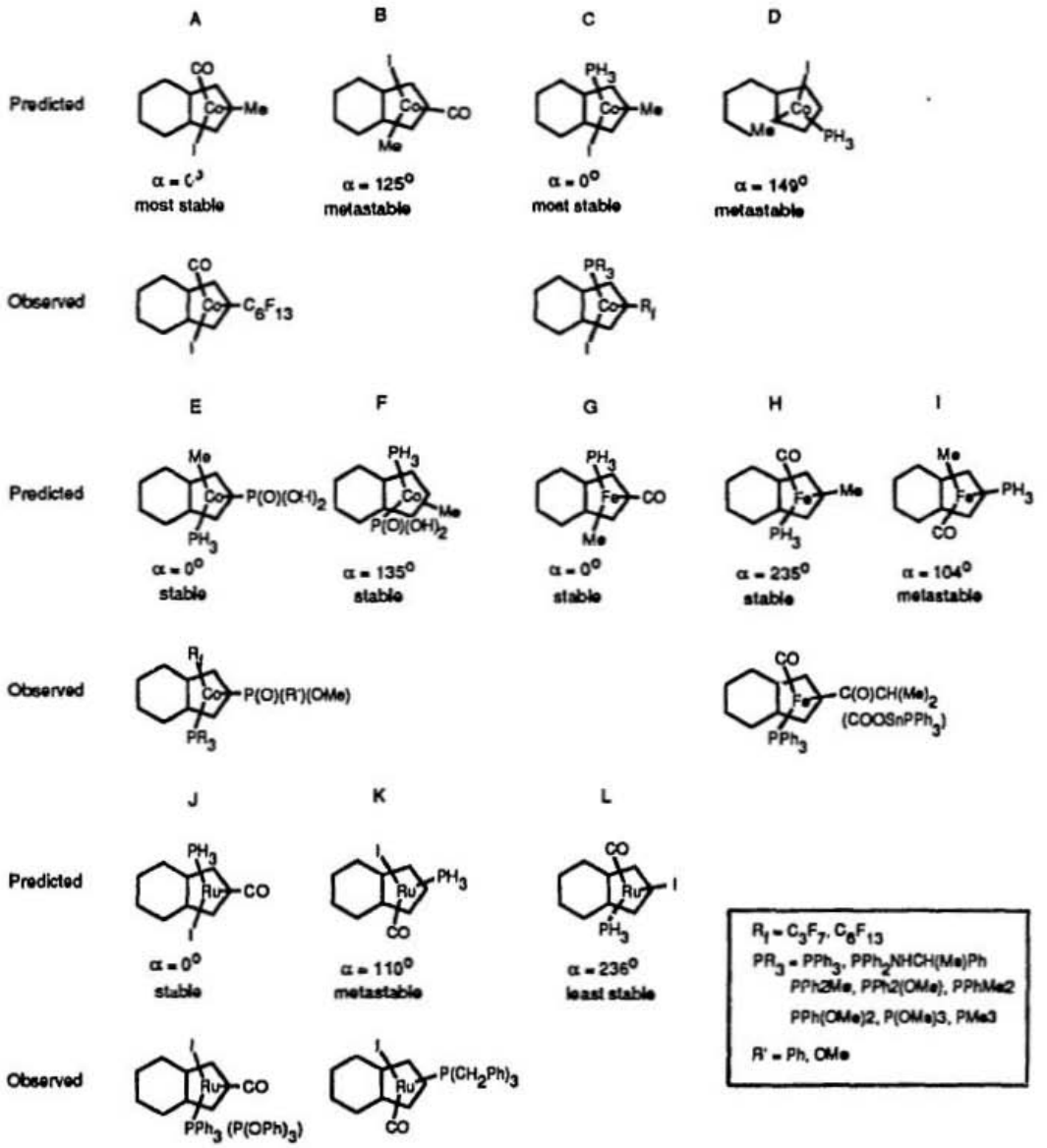
A
B
C
D
Predicted
α = 0°
most stable
α = 125°
metastable
α = 0°
most stable
α = 149°
metastable
Observed
E
F
G
H
I
Predicted
α = 0°
stable
α = 135°
stable
α = 0°
stable
α = 235°
stable
α = 104°
metastable
Observed
J
K
L
Predicted
α = 0°
stable
α = 110°
metastable
α = 236°
least stable
Observed
PPh3 (P(OPh)3)
P(CH2Ph)3
Rf = C3F7, C6F13
PR3 = PPh3, PPh2NHCH(Me)Ph
PPh2Me, PPh2(OMe), PPhMe2
PPh(OMe)2, P(OMe)3, PMe3
R' = Ph, OMe

Scheme 4-12

A: Co(Me)(I)(CO) (FMO 55)

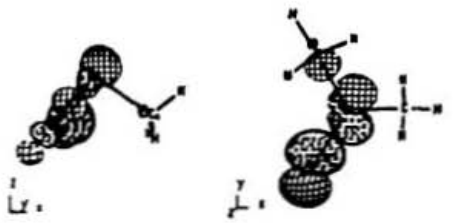

B: Co(Me)(I)(PH_3) (FMO 55)

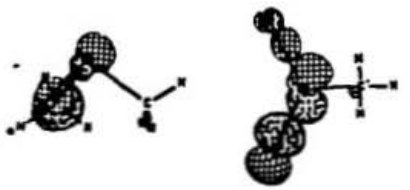

C: Co(P(O)$(OH)_2$(PH_3)(Me) (FMO 59 and FMO 60)

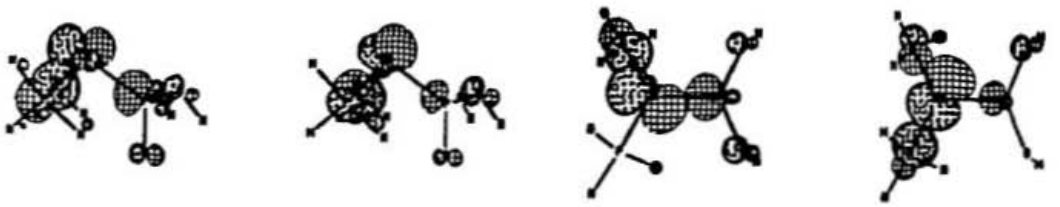

D: Fe(CO)(Me)(PH_3) (FMO 57 and FMO 58)

E: Ru(CO)(I)(PH_3) (FMO 54 and 55)

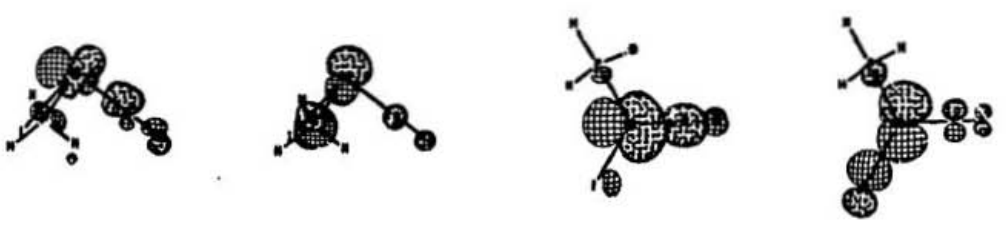

Scheme 4-13. Important Metal Centred Fragment Orbitals of MLL'L".

Table 4-4. Overlap Population Changes of Indenyl 6-ring in (η^5-indenyl)ML_n (n = 2, 3) Complexes.

(η^5-Indenyl)ML_n	distortion[a]	C_{3a}-C_{7a}	C_{3a}-C_4	C_4-C_5	C_5-C_6	C_6-C_7	C_7-C_{7a}
(η^5-Indenyl)Co$(CO)_2$	without	1.021	1.037	1.096	1.051	1.096	1.037
	with	1.042	1.051	1.087	1.059	1.087	1.051
(η^5-Indenyl)Co$(C{\equiv}C)_2$	without	1.022	1.041	1.093	1.054	1.093	1.041
	with	1.045	1.060	1.079	1.066	1.079	1.060
(η^5-Indenyl)Co$(PH_3)_2$	without	1.033	1.047	1.087	1.059	1.087	1.047
	with	1.054	1.069	1.072	1.074	1.072	1.069
(η^5-Indenyl)Rh$(CO)_2$	without	1.010	1.026	1.103	1.043	1.103	1.026
	with	1.032	1.041	1.093	1.053	1.093	1.041
(η^5-Indenyl)Rh$(C{\equiv}C)_2$	without	1.015	1.029	1.100	1.046	1.100	1.029
	with	1.029	1.037	1.094	1.051	1.094	1.037
(η^5-Indenyl)Rh$(PH_3)_2$	without	1.022	1.043	1.074	1.063	1.074	1.043
	with	1.037	1.056	1.070	1.069	1.071	1.056
[(η^5-Indenyl)Co$(CO)_3$]$^{2+}$	without	0.980	1.008	1.120	1.026	1.120	1.008
	with	0.983	1.012	1.118	1.027	1.118	1.012
[(η^5-Indenyl)Co$(PH_3)_3$]$^{2+}$	without	0.986	1.009	1.123	1.024	1.123	1.009
	with	0.998	1.021	1.113	1.030	1.113	1.021
(η^5-Indenyl)Mn$(CO)_3$	without	0.987	1.007	1.123	1.027	1.123	1.007
	with	0.993	1.012	1.119	1.029	1.119	1.012
[(η^5-Indenyl)Co$(PH_3)_2$(Me)]$^+$	without	1.002	1.019	1.115	1.033	1.115	1.019
	with	1.021	1.037	1.100	1.045	1.100	1.037
[(η^5-Indenyl)Co$(PH_3)_2(CF_3)$]$^+$	without	1.006	1.022	1.113	1.036	1.113	1.022
	with	1.026	1.041	1.096	1.049	1.096	1.041
[(η^5-Indenyl)Ir$(PH_3)_2$(H)]$^+$	without	1.010	1.023	1.113	1.037	1.113	1.023
	with	1.021	1.031	1.105	1.043	1.105	1.031
[(η^5-Indenyl)Co$(PH_3)_2$(Cl)]$^+$	without	1.003	1.020	1.115	1.036	1.113	1.020
	with	1.022	1.027	1.109	1.039	1.107	1.027
[(η^5-Indenyl)Ru$(PH_3)_2$(CO)]$^+$	without	1.008	1.019	1.113	1.037	1.113	1.019
	with	1.019	1.027	1.107	1.042	1.107	1.027
(η^5-Indenyl)Cr$(CO)_2$(NO)	without	1.002	1.016	1.116	1.034	1.116	1.016
	with	1.008	1.020	1.113	1.036	1.113	1.020

Table 4-4. cont'd

(η^5-Indenyl)Co(PH_3)(Me)(I)	without	1.002	1.021	1.113	1.035	1.111	1.023
	with	1.020	1.038	1.098	1.046	1.097	1.040
(η^5-Indenyl)Co(Me)(I)(CO)	without	0.998	1.018	1.112	1.035	1.111	1.023
	with	1.011	1.031	1.103	1.042	1.102	1.034
(η^5-Indenyl) Co(P(O)$(OH)_2$)(PH_3)(Me)	without	0.999	1.019	1.114	1.032	1.116	1.017
	with	1.013	1.030	1.105	1.040	1.105	1.030
(η^5-Indenyl)Fe(PH_3)(Me)(CO)	without	0.989	1.010	1.120	1.031	1.118	1.011
	with	1.005	1.021	1.111	1.037	1.111	1.021
(η^5-Indenyl)Ru(PH_3)(I)(CO)	without	1.009	1.020	1.112	1.038	1.111	1.021
	with	1.019	1.028	1.105	1.043	1.105	1.029

[a] Indenyl ring without distortion corresponds to the geometry with planar indenyl ring and the ML_n bonding to the indenyl centroid. The indenyl ring with distortion corresponds to the energy minimum geometry shown in Table 4-5.

Table 4-5. Ring Distortion Parameters for (η^5-indenyl)ML_n (n = 2, 3) Complexes.

(η^5-Indenyl)ML_n	Δ (Å)	H(°)	φ (°)	F (°)	Δ_{M-C}(Å)	ΔE(kJ/mol)[a]	ΔE_φ(kJ/mol)[b]
(η^5-Indenyl)Co$(CO)_2$	0.26	8.0	-1.5	6.5	0.30	38.88	0.10
(η^5-Indenyl)Co$(C{=}C)_2$	0.34	9.5	-1.5	8.0	0.37	35.60	0.17
(η^5-Indenyl)Co$(PH_3)_2$	0.44	13.0	-1.0	12.0	0.47	42.16	0.08
(η^5-Indenyl)Rh$(CO)_2$	0.14	10.0	-1.0	9.0	0.27	30.78	0.10
(η^5-Indenyl)Rh$(C{=}C)_2$	0.13	8.0	-1.0	7.0	0.23	39.85	0.10
(η^5-Indenyl)Rh$(PH_3)_2$	0.44	13.0	-1.0	12.0	0.47	37.82	0.10
$[(\eta^5$-Indenyl)Co$(CO)_3]^{2+}$	0.03	1.5	0.5	2.0	0.05	0.77	0.04
$[(\eta^5$-Indenyl)Co$(PH_3)_3]^{2+}$	0.12	5.5	2.5	8.0	0.18	15.63	0.50
(η^5-Indenyl)Mn$(CO)_3$	0.05	2.5	1.5	4.0	0.08	3.18	0.17
$[(\eta^5$-Indenyl)Co$(PH_3)_2$(Me)]$^+$	0.16	8.0	1.5	9.5	0.24	24.60	0.10
$[(\eta^5$-Indenyl)Co$(PH_3)_2(CF_3)]^+$	0.18	9.0	1.5	10.5	0.27	31.94	0.10
$[(\eta^5$-Indenyl)Ir$(PH_3)_2$(H)]$^+$	0.10	5.0	2.0	7.0	0.15	9.74	0.29
$[(\eta^5$-Indenyl)Ir$(PH_3)_2$(Cl)]$^+$	0.075	4.0	1.2	5.2	0.12	4.73	0.10
$[(\eta^5$-Indenyl)Ru$(PH_3)_2$(CO)]$^+$	0.10	5.0	1.8	6.8	0.15	9.65	0.29
(η^5-Indenyl)Cr$(CO)_2$(NO)	0.06	3.0	1.5	4.5	0.09	2.70	0.19
(η^5-Indenyl)Co(PH_3)(Me)(I)	0.17	7.5	1.0	8.5	0.24	20.17	0.04
(η^5-Indenyl)Co(Me)(I)(CO)	0.12	5.0	0.0	5.0	0.17	8.39	0.00
(η^5-Indenyl) Co$(P(O)(OH)_2(PH_3)$(Me)	0.12	6.0	1.5	7.5	0.19	12.83	0.19
(η^5-Indenyl)Fe(PH_3)(Me)(CO)	0.11	5.5	1.3	6.8	0.17	14.09	0.19
(η^5-Indenyl)Ru(PH_3)(I)(CO)	0.10	5.0	1.2	6.2	0.15	8.30	0.10

[a] $\Delta E = [E_{\text{without distortion}}\ (\Delta, H, \text{and } \varphi = 0)] - [E_{\text{with distortion}}\ (\Delta, H, \text{and } \varphi \neq 0)]$. [b] $\Delta E_\varphi = [E_{\Delta, H}\ (\varphi = 0)] - [E_{\Delta, H, \varphi}\ (\varphi \neq 0)]$

4.4. Summary

In this study, EHMO calculations have been performed for a series of (η^5-indenyl)M(d^8)L_2, (η^5-indenyl)M(d^6)L_3, (η^5-indenyl)M(d^6)L_2L', and (η^5-indenyl)M(d^6)LL'L" complexes. Indenyl ring distortion and conformational preferences have been examined on the basis of fragment molecular orbital analysis and compared with experimental observations. Several conclusions can be drawn from the results:

(i) The distortion and conformational preferences are dominated by the HOMO and NHOMO formed by overlap of the filled indenyl π orbitals (π_5 and π_4) and the symmetry-adopted metal-centred fragment MO's. The relative energy, orbital composition, and the orientation of the metal-centred fragment orbitals control the extent of indenyl ring distortion and the conformational preferences of the indenyl ring with respect to the ligands on the metal atom.

(ii) For all indenyl complexes investigated in this study, indenyl ring slippage (Δ) away from the indenyl centroid and puckering along C_3-C_1 and C_{3a}-C_{7a} axes are energetically favorable and are consistent with the experimental observations. The driving force for indenyl ring distortion from η^5 toward η^3-indenyl coordination derives from the lowering of both the HOMO and NHOMO energies of the η^5-indenyl complexes and the increased aromatization of the indenyl six-membered ring. In (η^5-indenyl)M(d^8)L_2 complexes indenyl ring distortions are required to diminish the antibonding interactions in the HOMO and strengthen the bonding interactions in the NHOMO. For all (η^5-indenyl)M(d^6)L_3, (η^5-indenyl)M(d^6)L_2L' and (η^5-indenyl)M(d^6)LL'L" complexes, indenyl ring distortions increase bonding interactions of both the filled indenyl π_5 and π_4 orbitals with the two lowest empty metal-centred fragment orbitals.

(iii) As shown in Figure 4-20, the EHMO predicted stable conformations are the preferred conformations observed experimentally both in the solid state and in solution for most complexes. (η^5-indenyl)Ru(PH_3)(CO) is an exception because the observed conformer is predicted to be a higher energy metastable conformer. In a few cases both the predicted stable and metastable conformers are observed experimentally. Two examples, (η^5-indenyl)Fe(CO)(Me)(PPh_2N(Me)CH(Me)Ph)) and (η^5-indenyl)Co(C_3F_7)(I)($PPh(OMe)_2$), whose solid state conformers do not correspond to either the predicted stable or metastable conformers, appear in the literature. However, the solution conformation of (η^5-indenyl)Co(C_3F_7)(I)($PPh(OMe)_2$) does correspond to the predicted stable conformer, possibly due to the influence of crystal packing forces, which vary the conformational preference of the indenyl ring.

(iv) The ML_2 fragment straddling the mirror plane in (η^5-indenyl)M(d^8)L_2 complexes is the highly preferred conformation. The (η^5-indenyl)M(d^6)L_3 complexes favor the conformation which places one ligand of ML_3 in the molecule mirror plane *trans* to the indenyl six-membered ring. For (η^5-indenyl)M(d^6)L_2L' and (η^5-indenyl)M(d^6)LL'L" complexes which contain different ligands, the ligand preference for occupancy of the position *trans* to the indenyl 6-ring decreases roughly in the following order: H ≈ Me ≈ CF_3 ≈ P(O)(R')(OR) > NO > CO ≈ PR_3 > I ≈ Cl. Figure 4-20 summarizes the success of the EHMO calculations carried out.

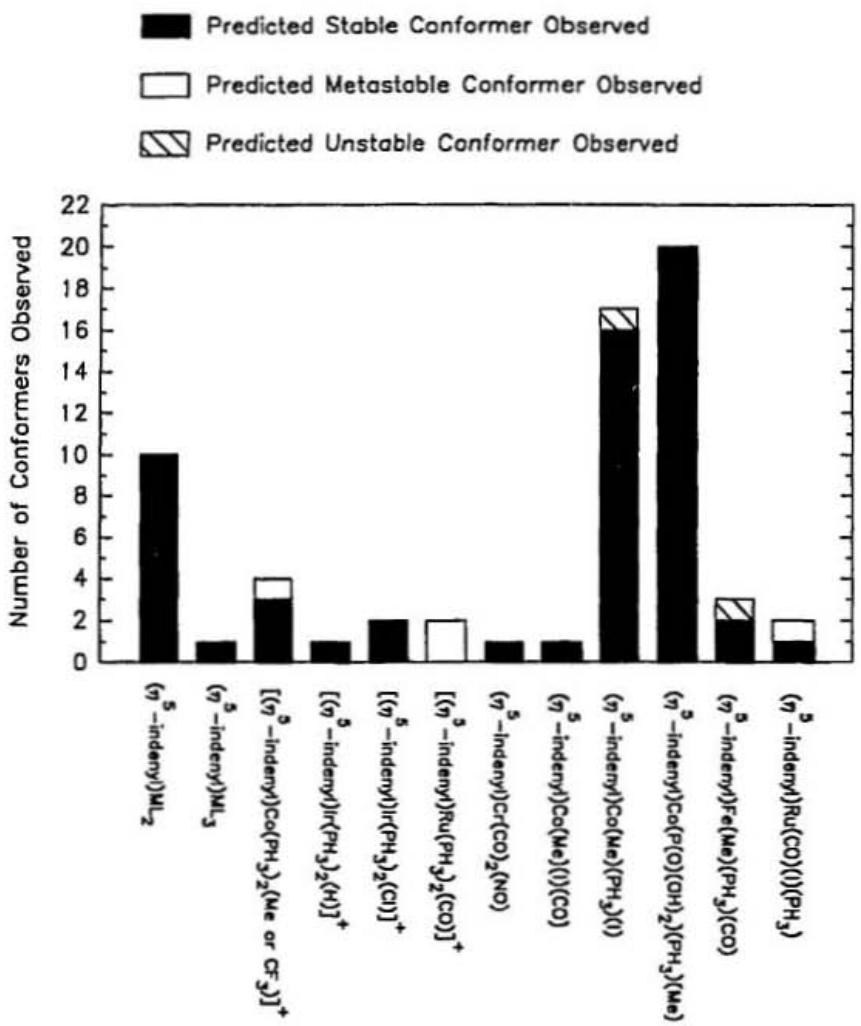

Figure 4-20. Correlation of Predicted and Observed Conformations of η^5-Indenyl Complexes.

Chapter 5

Synthesis, Structure, Absolute Configuration and Conformational Analysis of $(S_{Co},(S,R)_P,S_C)$-$(\eta^5$-Cp)Co(N-N*)(P(O)(Ph)(OMe)) and their Precursor, (S_{Co},S_C)-$[(\eta^5$-Cp)Co(N-N*)(PPh(OMe)$_2$)]$^+$I$^-$, (N-N* = Bidentate Schiff Base). Characterization of an Arbuzov Reaction Intermediate with a Strongly Nucleophilic Counterion.

5.1. Introduction

Chapter 3 discussed the Arbuzov-like dealkylation reactions of $P(OMe)_3$ and the prochiral phosphonite $PPh(OMe)_2$ mediated by the isostructural Co-chiral auxiliaries $[(\eta^5$-Cp)Co$(PMe_3)(C_3F_7)$-$]^+$ and $[(\eta^5$-indenyl)Co(L)(R_f)-$]^+$ (L = PPh_nMe_{3-n}, $PR(OMe)_2$ (R = OMe, Ph), R_f = C_3F_7, C_6F_{13}) which proceed via an ionic mechanism as observed in many other transition-metal-mediated Arbuzov reactions (cf. Chapter 1).[182, 184, 188, 192, 194-197, 199-201, 203-206, 209] This conclusion was made on the basis of direct NMR observations of the cationic intermediates in most of the reactions shown in Schemes 3-1 and 3-2 (cf. Figures 3-1 and 3-2) and the isolation of intermediate, $[(\eta^5$-indenyl)Co$(P(OMe)_3)_2(C_3F_7)]^+$, by halide abstraction (cf. Scheme 3-2 and Figure 3-

3).[318] It was anticipated that removal of conformational restraints imposed by intramolecular hydrogen bonding (cf. Scheme 1-51) would result in reduced efficiency of chiral information transfer from cobalt to phosphorus. Although a nominal decrease was observed using the reaction of $(\eta^5\text{-Cp})Co(PNH)(I)_2$ with $PPh(OMe)_2$ as a reference,[206] no measurable decrease results with a reference reaction of $(\eta^5\text{-Cp})Co(R_f)(PNH)(I)$ and $PPh(OMe)_2$ (R_f = CF_3, C_3F_7),[217] which suggests that the P=O•••H-N hydrogen bonding is only one of the factors, rather than the dominating factor, in determining the metal to phosphorus chiral induction.

In a search for alternative, non-hydrogen bonding supporting ligands several chiral, bidentate, uninegative Schiff-bases, $N^*\text{-}N^{1-}$, first reported by Brunner,[285] were examined. This chapter presents the resolution and X-ray crystallographic characterization of $(S_{Co},S_C)\text{-}[(\eta^5\text{-Cp})Co(N\text{-}N^*)(PPh(OMe)_2)]^+I^-$, **5-3a**, an example of an Arbuzov intermediate with a strongly nucleophilic counterion as well as its dealkylation to afford $(S_{Co},(S,R)_P,S_C)\text{-}(\eta^5\text{-Cp})Co(N\text{-}N^*)(P(O)(Ph)(OMe))$, **5-4a** and **5-4b**. The crystal structure of a model complex $(S_{Co},S_C)\text{-}[(\eta^5\text{-Cp})Co(N\text{-}N^*)(PPhMe_2)]^+I^-$, **5-5a**, prepared in order to establish the stereochemical stability of Arbuzov intermediates, is also described. The structure, absolute configuration and solution conformation of these complexes have been fully characterized using NMR, circular dichroism (CD), and crystallographic methods.

5.2. Results and Discussion

5.2.1. Synthesis and Characterization. The synthesis of the complexes used in this study is summarized in Scheme 5-1. Treatment of the diiodide **5-1** with N*-N (N*-N = *S*-Ph(Me)C*H-N=CH-$C_4H_3N^-$, $C_4H_3N^-$= pyrrolyl) in ether at room temperature[285] resulted in substitution of CO and I^- to afford a black, crystalline solid, ($(S,R)_{Co}$,S_C)-η^5-CpCo(N*-N)(I), **5-2a,b**, with a **5-2a/5-2b** ratio of 85/15 (determined by integration of the ^{1}H NMR Me doublets at 1.80 and 2.19 ppm) in a chemical yield of

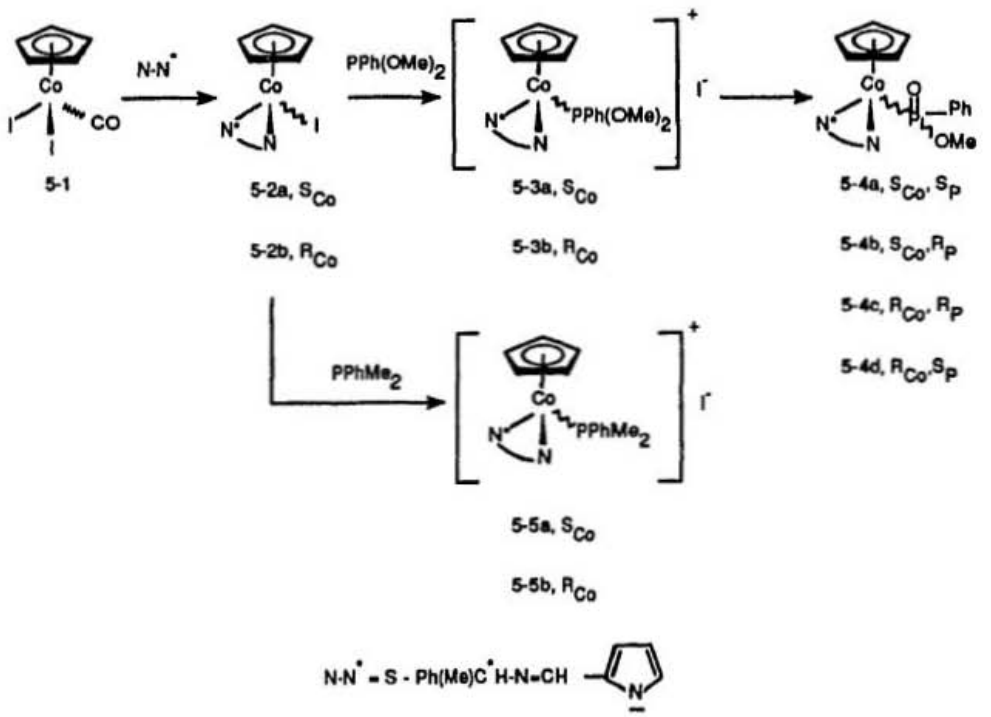

Scheme 5-1

92%. Addition of a slight excess of $PPh(OMe)_2$ to a dark blue, benzene solution of **5-2a,b** at room temperature resulted in the formation of an air-stable, deep red precipitate. Simple filtration afforded a *single* diastereomer, **5-3a**, (optical purity 98%) in 79% chemical yield. ^1H NMR analysis of the residue obtained by removing volatiles *in vacuo* from the filtrate showed six well-separated Cp singlets corresponding to both prochiral phosphonite iodide salts, $((S,R)_{Co})$-[(η^5-Cp)Co(N-N*)($PPh(OMe)_2$)]$^+I^-$, **5-3a** (5.40 ppm), **5-3b** (5.67 ppm) and four phosphinate products, $((S,R)_{Co},(S,R)_P)$-(η^5-Cp)Co(N-N*)(P(O)(Ph)(OMe)), **5-4a** (4.84 ppm), **5-4b** (4.71 ppm), **5-4c** (5.04 ppm), and **5-4d** (4.96 ppm).

The isolation of optically pure diastereomer, **5-3a**, an intermediate with a strongly nucleophilic I^- counterion, enabled us to investigate unambiguously Co*→P chiral induction in the ensuing Arbuzov dealkylation step. Complex **5-3a** is not air sensitive in the solid state or in solution. However, facile nucleophilic attack of I^- counterion on the coordinated $PPh(OMe)_2$ occurs in a variety of aprotic solvents such as benzene, hexane, dichloromethane, chloroform, acetone, and acetonitrile at ambient temperature to give two of the four possible diastereomeric Arbuzov products, **5-4a** and **5-4b**. The ion-pair **5-3a** is surprisingly stable in methanol (< 5% reaction after 24 h at 50 °C), presumably reflecting the reduced nucleophilicity of strongly solvated I^-. This result shows clearly that free halide ion is required for the dealkylation.

Heating a suspension of **5-3a** in benzene at 60 °C resulted in the loss of MeI and the

quantitative formation of two P-epimeric phosphinate products, **5-4a** and **5-4b**, with 36% de at phosphorus and complete retention of stereochemistry at Co. Retention at the chiral metal shows: (i) that substitution-resistant **5-3a**[206, 280, 285, 307, 354, 355] is configurationally stable at cobalt under Arbuzov reaction conditions, and (ii) that, in contrast with other transition-metal Arbuzov reactions,[182, 199, 201-203] substitution of $PPh(OMe)_2$ for I^- is *not* reversible under the reaction conditions. The P-epimeric diastereomers **5-4a** and **5-4b** were separated with difficulty as red, paste-like solids which are very stable both in the solid state and in solution, as observed for other metallophosphonate[197, 199, 208] and -phosphinate[356] complexes.

All complexes were characterized by ^1H, $^{31}P\{^1H\}$, and $^{13}C\{^1H\}$ NMR. ^{31}P NMR spectra (Table 5-1) showed characteristic singlets at 160.4 ppm (**5-3a**), 108.1 ppm (**5-4a**) and 101.6 ppm (**5-4b**) corresponding to coordinated phosphonite and phosphinate.[182] The ^1H NMR spectra of **5-3a**, **5-4a**, and **5-4b** (Table 5-1) showed distinct η^5-Cp, C*H, and C*-Me resonances typical for diastereomeric "piano-stool" complexes.[206-208, 355] The diastereotopic dimethyl phenylphosphonite OMe groups in **5-3a** appeared as two doublets at 4.05 ppm and 3.82 ppm with $^4J_{PH}$ = 11.4 Hz. The phosphinate OMe group appeared as a doublet at 3.55 ppm for **5-4a** and 3.45 ppm for **5-4b**.

The pyrrolyl ring protons, the *ortho*-protons of C*-Ph in **5-3a** and the *ortho*-, *meta*-, and *para*-protons of C*-Ph in **5-4a** were well resolved in all complexes and were assigned unambiguously on the basis of ^1H nOed spectra (*cf.* Figures. 5-1 and 5-2,

and Scheme 5-2). Spectra f, g, h in Figure 5-1 allow assignment of the pyrrolyl protons in **5-3a**. Irradiation of the multiplet of H_4 (6.35 ppm, Figure 5-1g) showed strong enhancements to the resonances at 6.72 ppm (8.1%) and 7.30 ppm (8.8%), and were confidently assigned to H_3 and H_5. Spectrum f (Figure 5-1f) correlated the Cp signal at 5.35 ppm with H_5 (8.4%), the proximal pyrrolyl proton, as shown in scheme 5-2, while spectrum h (Figure 5-1h) confirmed the assignments of H_3 and H_4. The multiplet centered at 7.06 ppm was assigned to H_{ortho} of C*-Ph based on spectra b and e (Figure 5-1b, e), which showed strong correlations between the H_{ortho} and C*-Me as well as the H_{ortho} and C*H.

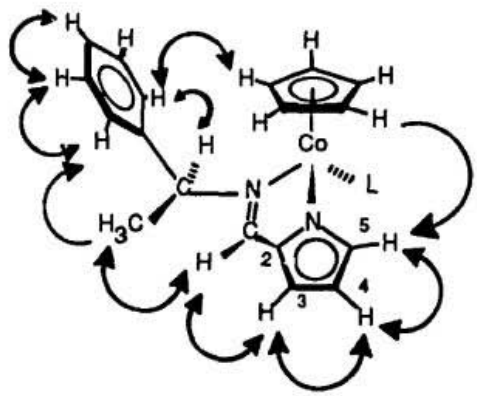

Scheme 5-2. Numbering Scheme and Major nOe Correlations

The well separated H_5/phenyl resonances (spectra e, f, j in Figure 5-2) allowed unambiguous assignment of the pyrrolyl protons in **5-4a**. Irradiation of the signal due to H_4 at 6.27 ppm (Figure 5-2e) resulted in a strong enhancement of H_3 (6.51 ppm, 4.2%) and H_5 (7.15 ppm, 3.2%). Irradiation of H_3 (Figure 5-2f) showed a 5.2% enhancement of H_4 but no enhancement of H_5, while irradiation of H_5 (Figure 5-2j)

showed 8.5% enhancement of H_4 but no enhancement of H_3.

^{1}H NMR assignments for **5-4b** were obtained by comparison with the spectra of **5-3a** and **5-4a**. In all complexes, as discussed above, the chemical shift of the pyrrolyl protons decreases in the order $H_5>H_3>H_4$, as found for other bidentate Schiff-base complexes.[285] The chemical shift assignments of the C*-Ph H_{ortho}, H_{meta}, and H_{para} in **5-4a** were based on spectra g', h', and j' in Figure 5-2. Irradiation of H_{meta} at 6.98 ppm (Figure 5-2h') showed a large enhancement of the resonances at 7.15 ppm (4.2%) and 6.78 ppm (4.8%), which were then assigned to H_{para} and H_{ortho}. The nOe correlation of the multiplet at 6.78 ppm with H_{meta} (5.3%) and C*H (1.5%) but not with the multiplet at 7.15 ppm allowed the assignment of 6.78 ppm multiplet to H_{ortho} on C*-Ph. Similarly the multiplet at 7.15 ppm can be assigned to H_{para} overlapped with H_5.

^{13}C NMR spectra (Table 5-2) were analyzed using 2-D ^{1}H/^{13}C ^{1}J heterocorrelation data which further confirm the ^{1}H NMR assignments. All carbon signals were resolved and showed characteristic spectroscopic patterns for chiral phosphonite or phosphinate cyclopentadienyl complexes.[206] The two diastereotopic dimethyl phenylphosphonite OMe groups of **5-3a** were easily assigned as a pair of doublets at 57.30 ppm and 57.12 ppm, respectively, with $^2J_{PC}$ = 13.2 Hz. The phosphinate OMe in **5-4a** and **5-4b** appeared as a doublet at 51.67 ppm ($^2J_{PC}$ = 10.9 Hz) and 50.99 ppm ($^2J_{PC}$ = 11.9 Hz), respectively. All phenyl and pyrrolyl carbons were

resolved and assigned unambiguously as shown in Table 5-2.

The model cationic phosphine complex, (S_{Co},S_C)-[(η^5-Cp)Co(N-N*)(PPhMe_2)]$^+I^-$, **5-5a**, originally isolated[285] as a Co-epimeric 88/12 **5-5a/5-5b** PF_6^- salt mixture, was prepared in order to demonstrate the configurational stability at the Co center of the isostructural phosphonite complex **5-3a**. Treatment of a dark blue solution of **5-2a,b** (**5-2a/5-2b** = 85/15) with excess P$PhMe_2$ following the procedure described for **5-3a** (Scheme 5-1) gave a deep-red precipitate of optically pure diastereomer, **5-5a**, with the same configuration at Co as **5-3a** in 75% chemical yield. Heating solutions of **5-5a** in $CDCl_3$ at 60 °C for 12 h resulted in no detectible Co epimerization, hence we infer a similar configurational stability for the isostructural intermediate **5-3a**. NMR spectra of **5-5a** and **5-3a** are very similar (cf. Tables 5-1 and 5-2). A ^{31}P singlet at 25.8 ppm for **5-5a** is characteristic for coordinated phosphine. ^1H NMR shows distinct C*H, C*-Me, P-Me, and pyrrolyl resonances similar to **5-3a**. All carbon signals (cf. Table 5-2) are well resolved and assigned clearly on the basis of ^1J $^1H/^{13}C$ heterocorrelation spectra as for **5-3a**. The isostructural complexes **5-3a** and **5-5a** adopt a similar solution conformations as discussed below.

Table 5-1. ^{1}H and ^{31}P NMR for $(\eta^5\text{-}C_p)Co(N\text{-}N^*)(L)$ Complexes[a].

No.	Cp	H_3	H_4	H_5	CH=N	C*H	POMe/PMe	C*Me	C*-Ph	P-Ph	^{31}P
5-3a	5.40 (s)	6.69 (m)	6.37 (dd, 4.0, 1.9)[d]	[b]	[c]	4.83 (q, 6.9)*	4.17(d,11.4)[f] 3.90(d,11.4)[f]	1.49 (d,6.9)*	7.05(m)[g] 7.29-7.49(m)	7.29-7.49(m)	160.4(s)
5-3a[h]	5.35 (s)	6.72 (dt, 4.0, 1.2)[i]	6.35 (dd, 4.0, 1.9)[d]	7.30[j]	7.52[j]	4.76 (q, 6.9)*	4.05(d,11.3)[f] 3.82(d,11.4)[f]	1.52 (d,6.9)*	7.06(m)[g] 7.29-7.55(m)	7.29-7.55(m)	
5-4a	4.84 (s)	6.51 (dt, 3.8, 0.6)[i]	6.27 (dd, 3.9, 1.8)[d]	7.15[k]	7.06 (d, 4.0)	5.20 (q, 6.9)*	3.55(d,11.0)[f]	1.45 (d,6.9)*	7.15(m)[l] 6.98(t)[m] 6.97(t)[m] 6.79(dd)[n] 6.76(dd)[n]	7.30-7.37(m)	108.1(s)
5-4b	4.70 (s)	6.72 (d, 3.8)[i]	6.29 (m)	7.02	7.47 (d, 3.6)	5.22 (m)	3.45(d,10.7)[f]	1.68 (d,6.9)*	7.20-7.44(m)	7.20-7.44(m)	101.6(s)
5-5a	5.29 (s)	6.88 (dt, 3.9, 1.0)[i]	6.47 (dd, 4.0, 1.9)[d]	7.20	7.56[j]	5.23 (q, 6.9)*	2.10(d,11.6)[o] 1.89(d,11.6)[o]	1.52 (d,6.9)*	7.35-7.54(m)	7.35-7.54(m)	25.8(s)

[a] ^{1}H (300.1 MHz) NMR chemical shifts in ppm relative to internal TMS; ^{31}P (121.5 MHz) NMR chemical shifts in ppm relative to external 85% H_3PO_4; Solvent = $CDCl_3$; m=multiplet; s=singlet; d=doublet; t=triplet; q=quartet; J values in Hz given in brackets. [b,c] overlapped with phenyl resonances. [d] ($^3J_{H3H4}$, $^3J_{H5H4}$). [e] $^3J_{HH}$. [f] $^3J_{PH}$. [g] H_{ortho} (2H). [h] Solvent = CD_3OD. [i] ($^3J_{H4H3}$, $^4J_{H5H3}$). [j] obtained from nOed spectra, overlapped with phenyl resonances. [k] overlapped with H_{para} on C*-Ph. [l] H_{para}. [m] H_{meta} ($^3J_{HH}$=7.6). [n] H_{ortho} ($^3J_{HH}$=8.4, $^4J_{HH}$=1.4). [o] $^2J_{PH}$.

Table 5-2. ^{13}C NMR for (η^5-C_p)Co(N-N*)(L) Complexes[a].

No	Cp	C_2	C_3	C_4	C_5	CH=N	C*H	POMe/PMe	Me	C*-Ph	P-Ph
5-3a	88.69	142.39	120.61	116.37	144.21	159.11	69.42	57.87(d,11.6)[b] 57.33(d,12.0)[b]	25.55	141.50[c] 132.51[d] 130.35[e] 130.19[e] 129.34[f]	136.60(d,55.4)[g] 128.87[e] 128.74[e] 128.35[d] 126.28[f]
5-3a[h]	89.83	144.49	121.88	117.05	145.27	162.20	71.10	57.30(d,13.2)[b] 57.12(d,13.2)[b]	25.81	143.58[c] 133.70[d] 131.78[e] 131.63[e] 130.42[f]	138.38(d,56.6)[g] 129.98[e] 129.84[e] 129.40[d] 127.71[f]
5-4a	87.64	144.21	117.90	114.02	142.98	157.11	67.50	51.67(d,10.9)[b]	25.29	141.81[c] 130.71[e] 130.57[e] 129.09[d] 126.94[f] 126.80[f]	135.33(d,49.7)[g] 128.76[e] 127.56[d] 126.38[f]
5-4b	87.81	144.16	117.27	113.72	143.00	157.81	68.05	50.99(d,11.9)[b]	25.36	142.01[c] 129.96[e] 129.82[e] 129.47[d] 127.51[f] 127.37[f]	135.60(d,50.4)[g] 128.79[e] 127.58[d] 126.39[f]
5-5a	88.13	142.54	119.98	116.39	143.11	158.89	69.10	15.42(d,31.2)[i] 14.66(d,30.5)[i]	25.75	141.58[c] 131.06[d] 129.78[e] 129.67[e] 129.08[f]	132.24(d,47.3)[g] 128.97[e] 128.83[e] 128.01[d] 126.10[f]

[a] ^{13}C (75.47 MHz) NMR chemical shifts in ppm relative to solvent $CDCl_3$=77.00; d=doublet; J values in Hz given in brackets. [b] $^2J_{PC}$. [c] C_{ipso}. [d] C_{para}. [e] C_{ortho}. [f] C_{meta}. [g] C_{ipso} ($^1J_{PC}$). [h] solvent = d_4-methanol (49.0 ppm). [i] $^1J_{PC}$.

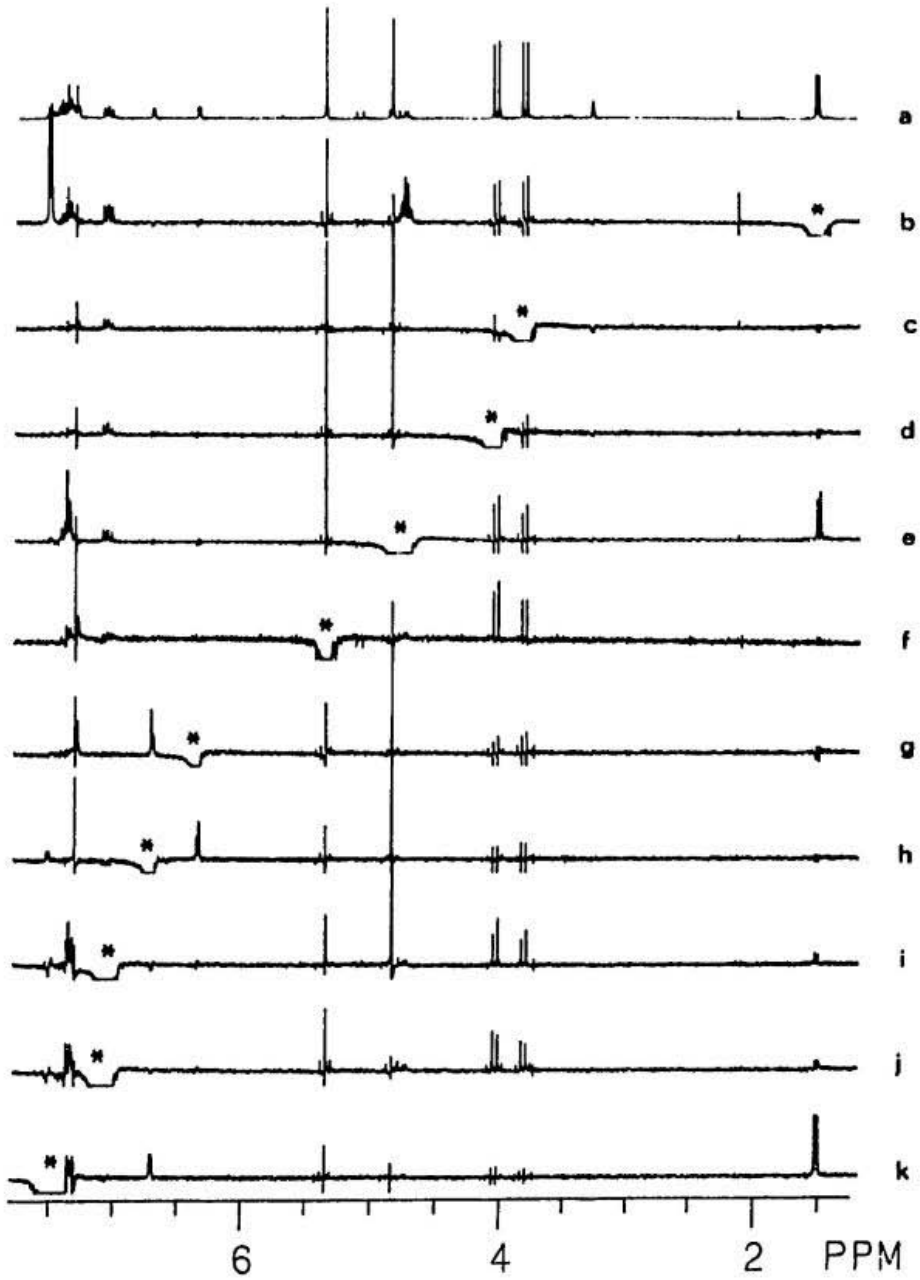

Figure 5-1. ^{1}H nOed spectra of **5-3a** in CD_3OD. (a) reference spectrum; (b-k) difference spectra (x 64) for irradiation at the indicated (*) frequency; (b) C*-Me; (c) & (d) P-OMe; (e) C*H; (f) Cp; (g) H_4; (h) H_3; (i) & (j) H_{ortho} of C*-Ph; (k) Ph & CH=N.

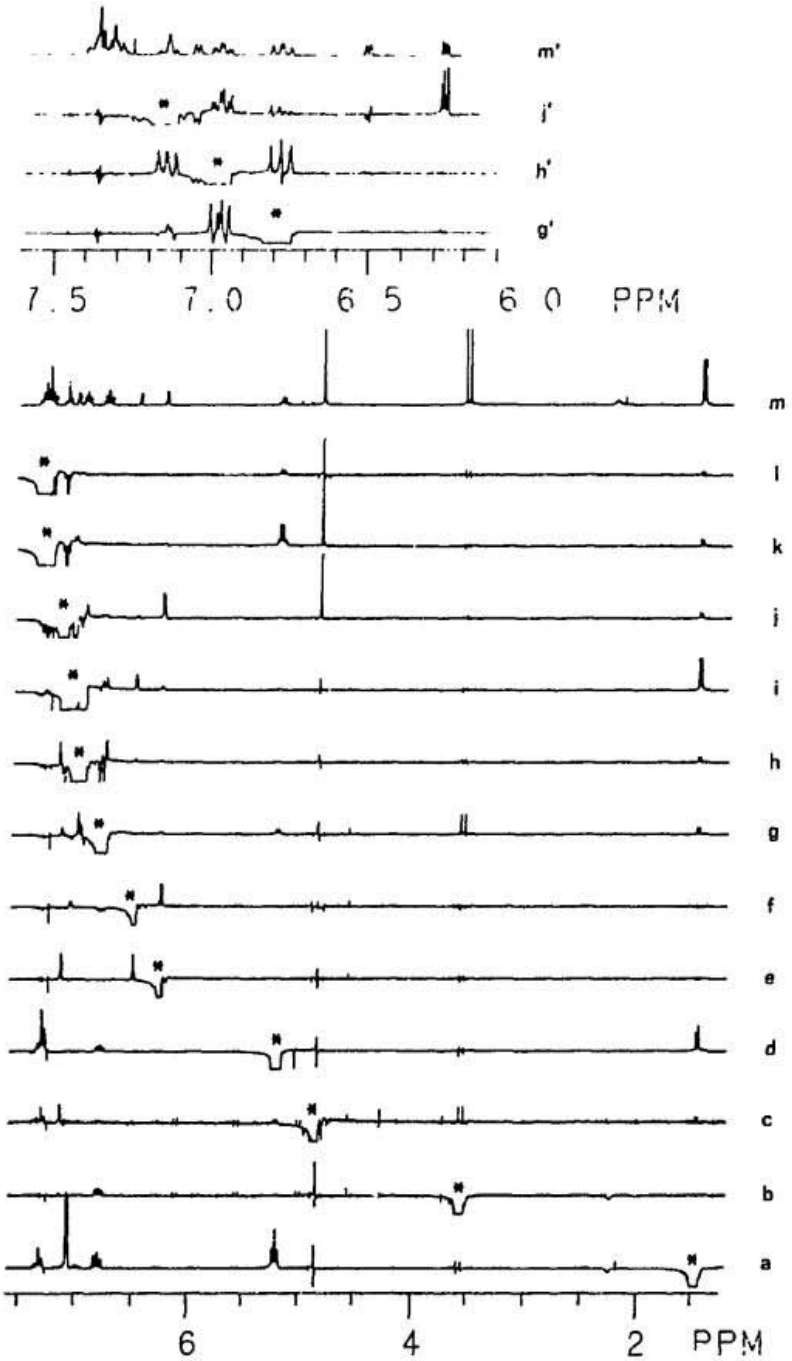

Figure 5-2. ^{1}H nOed spectra of **5-4a** in CD_3Cl. (m, m') reference spectrum; (a-l) difference spectra (x 32) for irradiation at the indicated (*) frequency; (a) C*-Me; (b) P-OMe; (c) Cp; (d) C*H; (e) H_4; (f) H_3; (g, g') H_{ortho} of C*-Ph; (h, h') H_{meta}; (i) CH=N; (j, j') H_5 & H_{para}; (k) &(l) P-Ph. (g', h', j' obtained with weaker decoupling power).

5.2.2. Crystal Structure and Absolute Configuration of 5-3a, 5-4a•2H$_2$O, and 5-5a. Absolute configurations of complexes **5-3a**, **5-4a•2H$_2$O**, and **5-5a** were assigned on the basis of crystallographic evidence. Crystallographic data are presented in Table 5-9. Compounds in this series have a propensity to form twinned crystals and such was the case for the specimen of **5-3a** selected for X-ray crystallographic analysis. Nevertheless, a well refined structure ($R_w = 0.041$) with correct assignment of the absolute configuration consistent with the known absolute configuration at carbon (S_C) proved possible. The η^5-Cp group in **5-3a** is rotationally disordered and refinement was carried out using a 55/45 occupancy model.

Refinement of the crystal structure of **5-4a** was complicated by the presence of disordered solvent in the unit cell. Attempts to grow a better quality crystal were not successful, however the overall structure and stereochemical assignments are consistent with spectroscopic parameters and the known absolute configuration of the internal reference S_C. The asymmetric unit contains two independent molecules (**5-4a**, **5-4a'**) each with one water molecule in close proximity as well as a more distant solvent cluster which was modelled as two water molecules with fractional occupancy. Thus, solid state samples of **5-4a** are formulated as a dihydrate, **4a•2H$_2$O** and **4a'•2H$_2$O**. The two crystallographically independent molecules have identical absolute configurations and differ only slightly in conformation (cf. Figure 5-5).

PLUTO representations of the structure of **5-3a**, **5-4a•2H$_2$O**, and **5-5a** are shown in Figures 5-3, 5-4, and 5-6, respectively. Coordinates, selected bond distances, and bond angles of **5-3a**, **5-4a•2H$_2$O**, **5-4a'•2H$_2$O** and **5-5a** are given in Tables 5-3 - 5-7. All of these molecules are pseudooctahedral, three-legged "piano-stools". The η^5-Cp moiety occupies three *facial* coordination sites with the P-donor and bidentate Schiff-base (N-N*) ligands completing the coordination sphere. Interligand bond angles (P-Co-N1 (pyrrolyl), P-Co-N2 (C*-N), N1-Co-N2) are approximately 90°. The coordinated Schiff-base is planar as a result of conjugation. All three molecules adopt a similar solid state conformation with C*-Ph *syn* and approximately edge-on and P-Ph *anti* to η^5-Cp. In each case the absolute configurations determined crystallographically were found to give the correct chirality at the known S_C center.

Consideration of these complexes as pseudotetrahedral cases with η^5-Cp effectively occupying one coordination site and use of the modified Cahn-Ingold-Prelog rules[290-293] with the ligand priority series Cp>P-donor>N-C*H(Me)Ph>N-pyrrolyl fixes the absolute configuration of **5-3a**, **5-4a•2H$_2$O**, and **5-5a**, as S_{Co},S_C. In the case of **5-4a•2H$_2$O**, the absolute configuration at P(O)(Ph)(OMe) with the priority series Co>OMe>O>Ph is S_P.

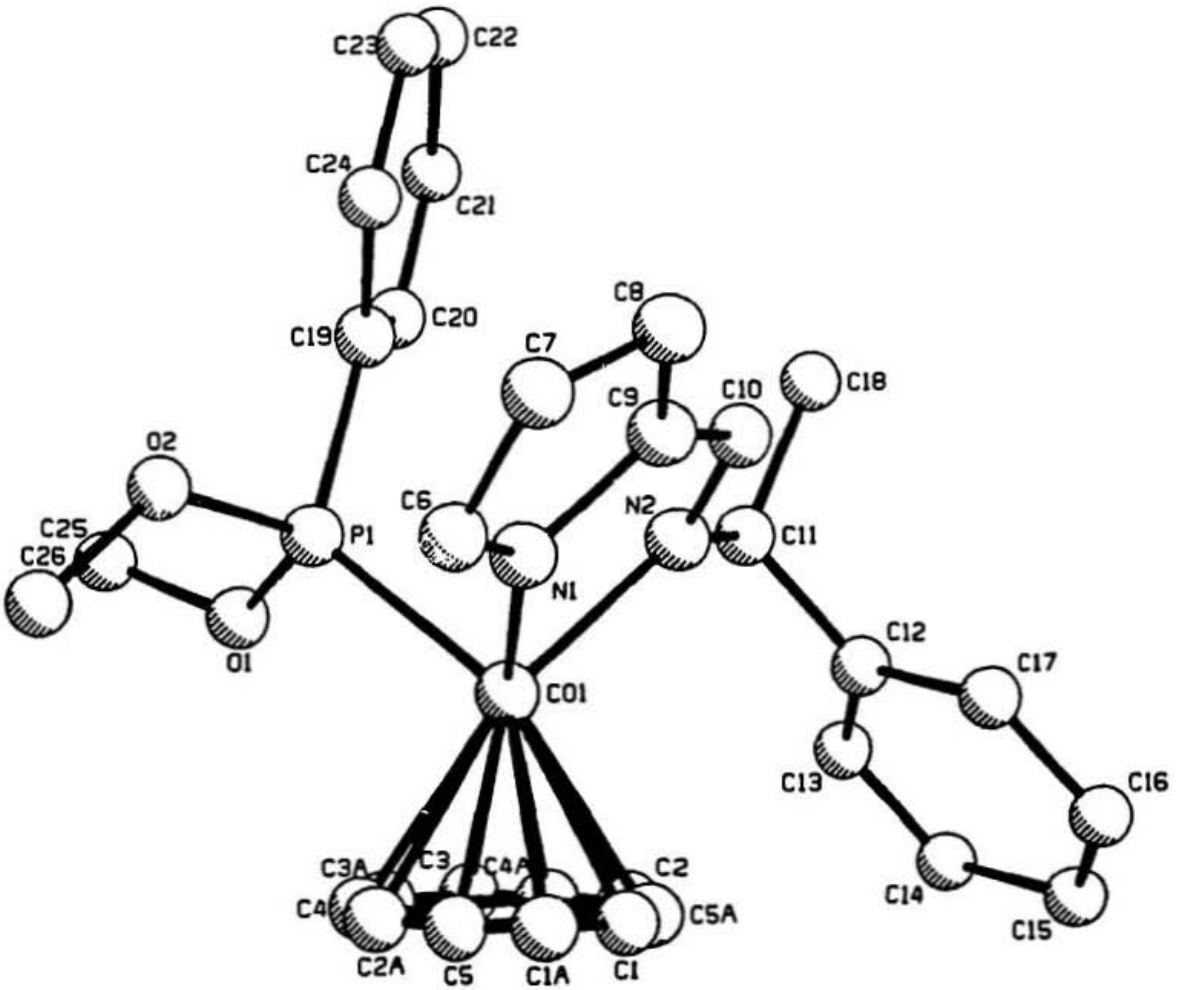

Figure 5-3. Molecular Structure of **5-3a** (I^- omitted for clarity).

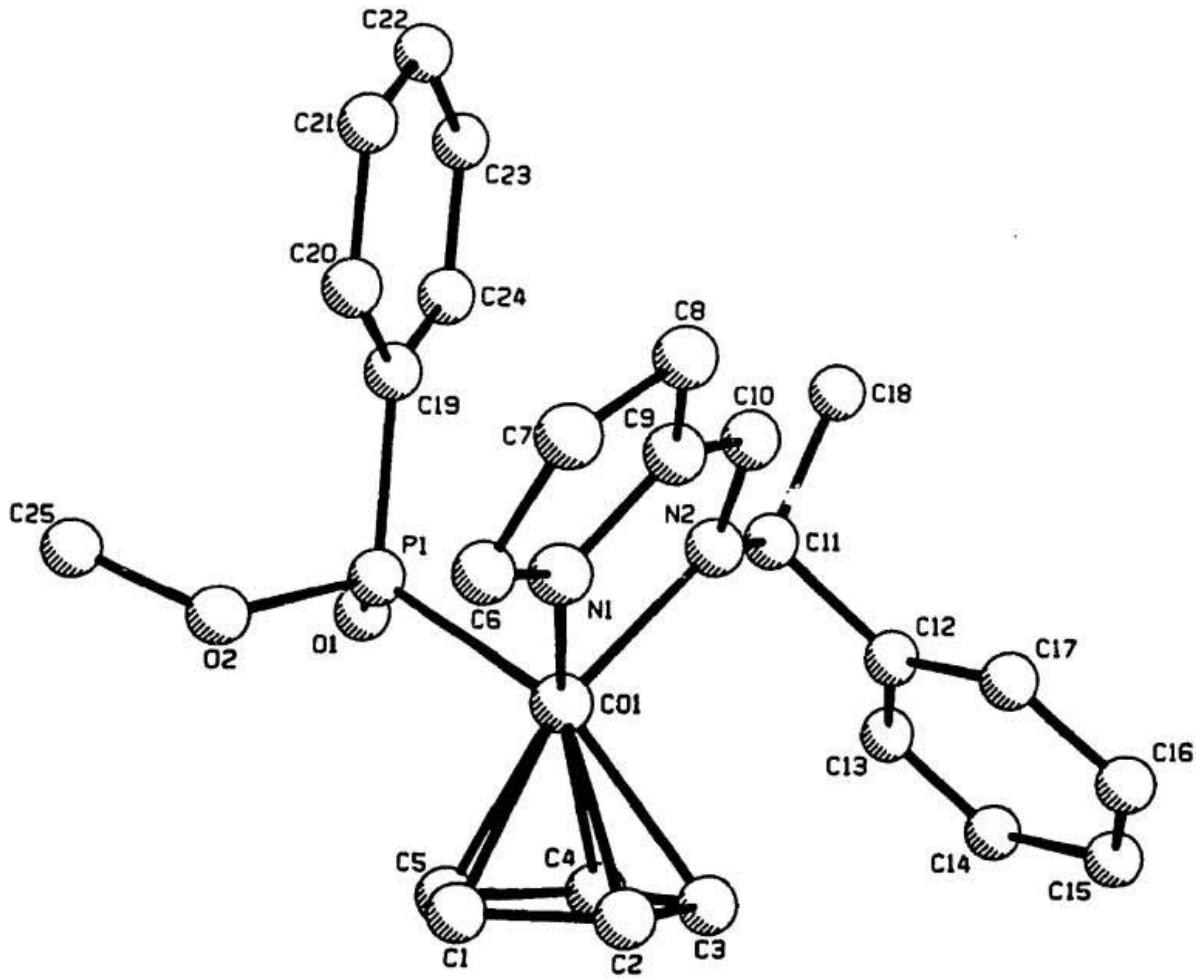

Figure 5-4. Molecular Structure of **5-4a**•H_2O (H_2O omitted for clarity).

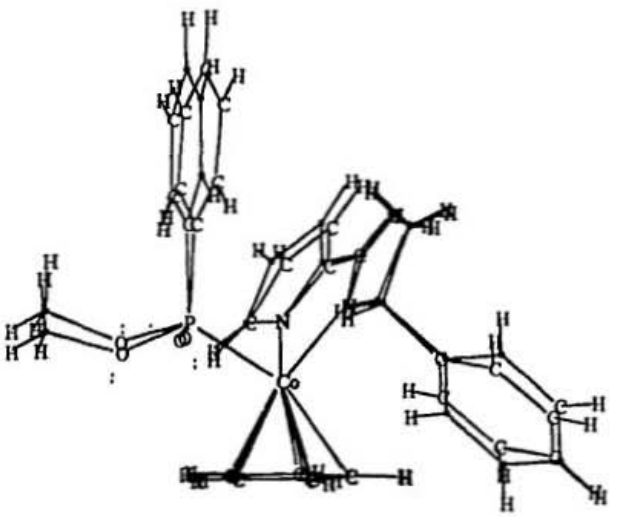

Figure 5-5. Structure Comparison of **5-4a**•H_2O and **5-4a'**•H_2O.

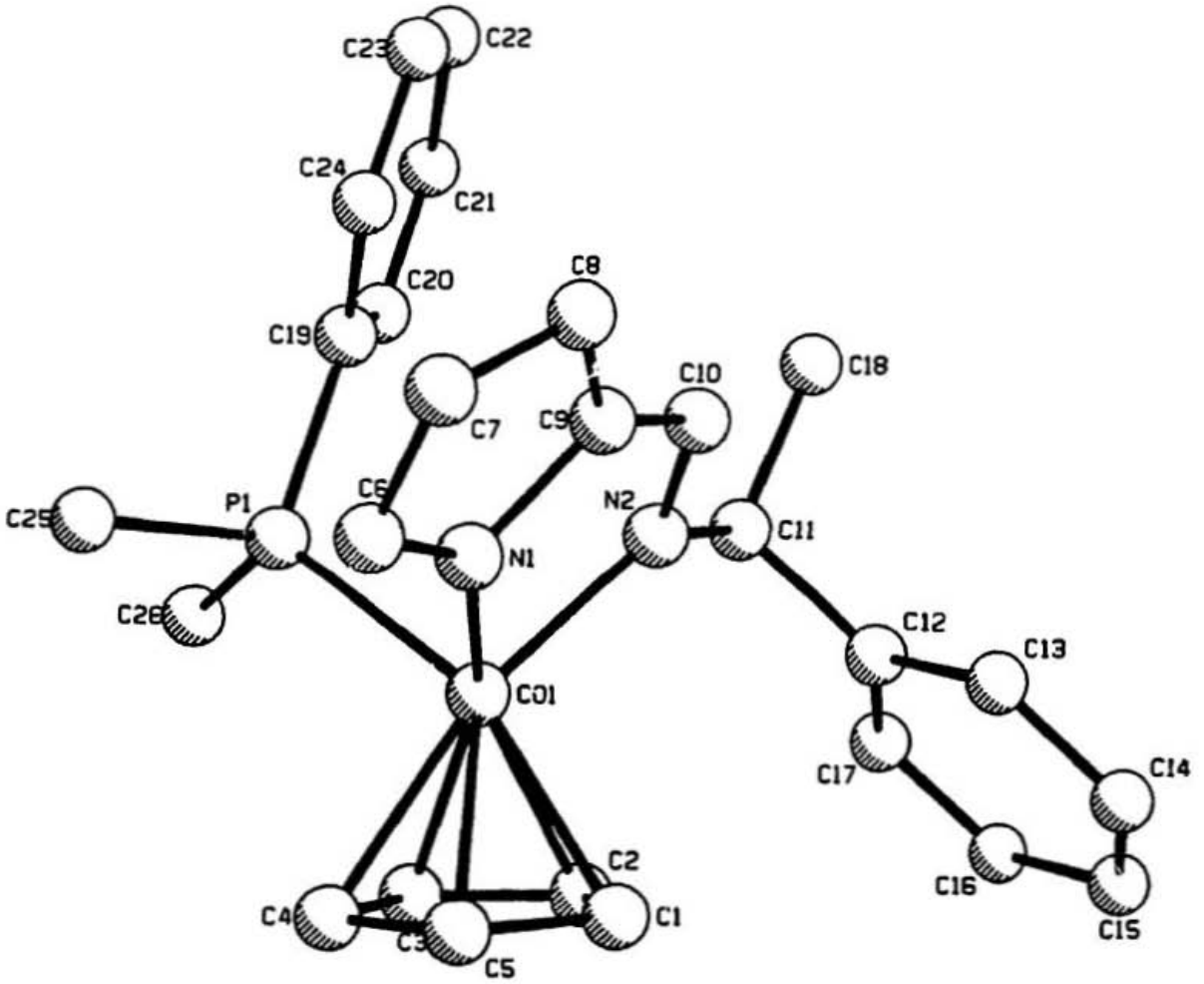

Figure 5-6. Molecular Structure of **5-5a** (I^- omitted for clarity)

Table 5-3. Atomic Coordinates for (S_{Co},S_C)-[$(\eta^5$-$C_p)$Co(N-N$^{\cdot}$)(PPh(OMe)$_2$)]$^+$ I$^-$, **5-3a**

atom	x	y	z	B(eq)	Occupancy
I(1)	0.60046(8)	0.02239(6)	0.2770(1)	6.92(7)	
Co(I)	0.5168(1)	0.0934(1)	0.7784(2)	3.7(1)	
P(1)	0.6279(3)	0.1570(2)	0.8736(4)	3.7(2)	
O(1)	0.6947(6)	0.1035(5)	0.9471(8)	3.9(5)	
O(2)	0.6938(7)	0.2077(5)	0.7917(9)	5.1(5)	
N(1)	0.4817(9)	0.1798(6)	0.687(1)	4.5(7)	
N(2)	0.4155(8)	0.1277(6)	0.8905(9)	3.9(6)	
C(6)	0.504(1)	0.2178(9)	0.581(1)	5.8(4)	
C(7)	0.444(1)	0.2768(8)	0.569(1)	5.3(4)	
C(8)	0.380(1)	0.2762(8)	0.661(1)	4.7(4)	
C(9)	0.400(1)	0.2144(7)	0.737(1)	4.2(3)	
C(10)	0.367(1)	0.1828(8)	0.849(1)	4.1(4)	
C(11)	0.386(1)	0.0960(7)	1.009(i)	3.9(3)	
C(18)	0.337(1)	0.1476(9)	1.099(1)	5.7(4)	
C(25)	0.779(1)	0.125(1)	1.008(1)	6.4(5)	
C(26)	0.754(1)	0.185(1)	0.692(2)	7.3(5)	
C(19)	0.5905(6)	0.2248(4)	0.9815(7)	3(1)	
C(20)	0.5874(6)	0.2059(4)	1.1060(8)	4(1)	
C(21)	0.5601(6)	0.2585(5)	1.1933(6)	6(1)	
C(22)	0.5359(6)	0.3301(5)	1.1561(8)	5(1)	
C(23)	0.5390(6)	0.3490(4)	1.0317(9)	6(1)	
C(24)	0.5663(6)	0.2963(5)	0.9444(6)	4(1)	
C(12)	0.3267(6)	0.0259(5)	0.9968(8)	4(2)	
C(13)	0.3501(5)	-0.0362(6)	1.0670(7)	6(2)	
C(14)	0.2943(7)	-0.1003(5)	1.0571(8)	6(2)	
C(15)	0.2152(6)	-0.1024(4)	0.9771(8)	6(2)	
C(16)	0.1917(5)	-0.0403(6)	0.9069(7)	6(2)	
C(17)	0.2475(7)	0.0239(5)	0.9168(7)	5(2)	
C(1)	0.459(1)	0.007(1)	0.673(2)	3.6(2)	0.550
C(2)	0.470(1)	-0.020(1)	0.793(2)	3.6(2)	0.550
C(3)	0.569(2)	-0.016(1)	0.824(1)	3.6(2)	0.550
C(4)	0.6187(8)	0.014(1)	0.723(2)	3.6(2)	0.550
C(5)	0.551(2)	0.028(1)	0.630(1)	3.6(2)	0.550
C(1A)	0.500(2)	0.026(2)	0.621(2)	4.0(3)	0.450
C(2A)	0.598(2)	0.031(2)	0.650(2)	4.0(3)	0.450
C(3A)	0.612(1)	0.002(2)	0.768(2)	4.0(3)	0.450
C(4A)	0.521(2)	-0.020(1)	0.813(2)	4.0(3)	0.450
C(5A)	0.452(1)	-0.006(2)	0.722(3)	4.0(3)	0.450

Table 5-4. Atomic Coordinates for (S_{Co},S_P,S_C)-(η^5-C_p)Co(N-N*)(P(O)(Ph)(OMe)), **5-4a•2H$_2$O**, **5-4a'•2H$_2$O**

atom	x	y	z	B(eq)	Occupancy
Co(1)	-0.0251(2)	0.0716(1)	-0.1302(3)	4.0(2)	
Co(1')	0.0770(2)	0.3466(1)	0.4561(3)	4.0(2)	
P(1)	0.1035(3)	0.0749(2)	-0.1721(5)	4.6(3)	
P(1')	-0.0493(3)	0.3603(2)	0.4069(5)	4.9(4)	
O(1)	0.1524(6)	0.0398(4)	-0.114(1)	5.5(3)	
O(1')	-0.0825(7)	0.3973(4)	0.488(1)	6.7(4)	
O(2)	0.1111(7)	0.0787(4)	-0.342(1)	6.1(3)	
O(2')	-0.0470(7)	0.3690(4)	0.238(1)	5.6(3)	
O(3)	0.1251(6)	-0.0214(3)	0.084(1)	5.4(3)	
O(4)	0.292(1)	-0.0011(6)	-0.171(2)	16.4(7)	
O(5)	-0.686(2)	0.083(1)	-0.719(3)	11(1)	0.500
O(6)	-0.613(4)	0.082(3)	-0.768(8)	15(1)	0.300
O(7)	-0.564(2)	0.073(2)	-0.791(6)	15(1)	0.400
O(8)	-0.596(3)	0.042(1)	-0.941(5)	15(1)	0.400
O(9)	-0.671(3)	0.024(1)	-0.887(5)	16(1)	0.400
N(1)	-0.0470(8)	0.1275(4)	-0.190(2)	4.2(4)	
N(1')	0.0730(8)	0.2923(4)	0.377(2)	5.1(4)	
N(2)	-0.0097(7)	0.0975(4)	0.056(1)	3.3(3)	
N(2')	0.0437(7)	0.3170(4)	0.625(1)	3.1(3)	
C(6)	-0.070(1)	0.1491(7)	-0.314(2)	6.6(5)	
C(6')	0.086(1)	0.2753(6)	0.246(2)	5.3(5)	
C(7)	-0.085(1)	0.1891(6)	-0.263(2)	5.7(5)	
C(7')	0.075(1)	0.2324(6)	0.261(2)	4.8(5)	
C(8)	-0.070(1)	0.1942(6)	-0.123(2)	6.4(5)	
C(8')	0.056(1)	0.2232(6)	0.401(2)	6.2(5)	
C(9)	-0.048(1)	0.1538(6)	-0.078(2)	5.0(5)	
C(9')	0.053(1)	0.2628(6)	0.469(2)	4.3(5)	
C(10)	-0.025(1)	0.1381(5)	0.053(2)	4.1(4)	
C(10')	0.036(1)	0.2779(6)	0.603(2)	4.4(5)	
C(11)	0.019(1)	0.0766(6)	0.183(2)	4.8(5)	
C(11')	0.026(1)	0.3373(5)	0.771(2)	4.1(5)	
C(18)	0.052(1)	0.1054(6)	0.300(2)	7.1(6)	
C(18')	-0.027(1)	0.3105(6)	0.866(2)	6.9(5)	
C(25)	0.190(1)	0.0807(7)	-0.405(2)	9.9(7)	
C(25')	-0.118(1)	0.3835(7)	0.170(2)	8.6(6)	
C(1)	-0.0748(9)	0.0404(4)	-0.302(1)	7.3(4)	
C(2)	-0.1370(6)	0.0497(3)	-0.207(1)	5.9(4)	
C(3)	-0.1197(7)	0.0307(4)	-0.077(1)	5.9(4)	
C(4)	-0.0469(7)	0.0096(3)	-0.091(1)	5.7(4)	

Table 5-4. cont'd

atom	x	y	z	B(eq)	Occupancy
C(5)	-0.0192(6)	0.0156(4)	-0.231(2)	6.9(4)	
C(1')	0.1403(8)	0.3782(4)	0.304(1)	6.6(4)	
C(2')	0.1964(6)	0.3574(3)	0.389(2)	6.0(4)	
C(3')	0.1880(6)	0.3717(3)	0.529(1)	5.2(4)	
C(4')	0.1268(7)	0.4013(3)	0.530(1)	5.8(4)	
C(5')	0.0973(5)	0.4053(3)	0.391(1)	4.8(4)	
C(19)	0.1508(7)	0.1215(3)	-0.108(2)	4.7(3)	
C(20)	0.1400(5)	0.1584(5)	-0.183(1)	6.5(3)	
C(21)	0.1754(8)	0.1948(3)	-0.134(1)	9.1(3)	
C(22)	0.2215(6)	0.1943(3)	-0.010(2)	6.6(3)	
C(23)	0.2324(5)	0.1574(5)	0.065(1)	9.1(3)	
C(24)	0.1970(8)	0.1210(3)	0.016(1)	6.2(3)	
C(19')	-0.1184(6)	0.3175(3)	0.424(2)	4.4(3)	
C(20')	-0.1744(8)	0.3174(3)	0.535(1)	6.7(3)	
C(21')	-0.2264(6)	0.2840(5)	0.551(1)	8.7(3)	
C(22')	-0.2224(7)	0.2506(3)	0.457(2)	7.7(3)	
C(23')	-0.1663(9)	0.2507(3)	0.347(1)	9.0(3)	
C(24')	-0.1144(6)	0.2842(5)	0.330(1)	6.7(3)	
C(12)	-0.0481(6)	0.0506(4)	0.254(1)	3.3(2)	
C(13)	-0.0304(5)	0.0111(4)	0.304(1)	4.6(2)	
C(14)	-0.0396(8)	-0.0123(2)	0.371(1)	5.1(2)	
C(15)	-0.1664(6)	0.0039(4)	0.389(1)	5.6(2)	
C(16)	-0.1841(5)	0.0435(4)	0.338(1)	5.6(2)	
C(17)	-0.1250(8)	0.0668(3)	0.271(1)	4.1(2)	
C(12')	0.1054(5)	0.3472(4)	0.842(1)	4.7(3)	
C(13')	0.1212(6)	0.3876(4)	0.885(1)	5.2(3)	
C(14')	0.1935(8)	0.3971(3)	0.952(1)	5.7(3)	
C(15')	0.2500(5)	0.3661(4)	0.976(1)	6.0(3)	
C(16')	0.2343(6)	0.3256(3)	0.932(1)	4.7(3)	
C(17')	0.1620(7)	0.3162(3)	0.865(1)	4.7(3)	

Table 5-5. Atomic Coordinates for (S_{Co},S_C)-[(η^5-Cp)Co(N-N$^{\bullet}$)(PPhMe$_2$)]$^{+}$I^{-}, **5-5a**

atom	x	y	z	B(eq)
I(1)	0.3991(1)	0.4840(1)	0.7197(2)	9.1(1)
Co(1)	0.9805(2)	0.0986(1)	0.7569(3)	3.0(1)
P(1)	0.8617(4)	0.1646(3)	0.6603(5)	4.1(3)
N(1)	1.025(1)	0.1851(8)	0.849(1)	4.1(4)
N(2)	1.087(1)	0.1296(7)	0.648(1)	2.6(3)
C(6)	1.001(2)	0.226(1)	0.953(2)	7.1(6)
C(7)	1.067(2)	0.284(1)	0.962(2)	5.7(6)
C(8)	1.131(1)	0.283(1)	0.867(2)	4.8(5)
C(9)	1.109(1)	0.221(1)	0.793(2)	4.6(5)
C(10)	1.138(1)	0.188(1)	0.683(2)	3.7(5)
C(11)	1.112(1)	0.0946(9)	0.524(2)	3.5(4)
C(18)	1.164(1)	0.147(1)	0.430(2)	5.6(5)
C(25)	0.787(1)	0.215(1)	0.771(2)	7.2(6)
C(26)	0.767(1)	0.113(1)	0.574(2)	5.1(5)
C(1)	1.0471(6)	0.0076(7)	0.845(1)	5.2(5)
C(2)	1.0008(8)	-0.0135(5)	0.734(1)	5.8(5)
C(3)	0.8982(7)	0.0028(6)	0.743(1)	4.9(4)
C(4)	0.8811(7)	0.0341(6)	0.860(1)	5.9(5)
C(5)	0.973(1)	0.0371(6)	0.9231(8)	5.8(5)
C(12)	1.1768(7)	0.0248(5)	0.540(1)	2.4(4)
C(13)	1.2589(8)	0.0236(6)	0.620(1)	4.7(5)
C(14)	1.3162(6)	-0.0409(7)	0.6327(8)	5.1(5)
C(15)	1.2914(8)	-0.1043(5)	0.565(1)	6.3(6)
C(16)	1.2093(9)	-0.1032(5)	0.484(1)	5.5(5)
C(17)	1.1520(6)	-0.0386(7)	0.4721(9)	4.8(5)
C(19)	0.9092(8)	0.2302(6)	0.550(1)	3.2(4)
C(20)	0.8999(7)	0.2126(5)	0.424(1)	4.1(4)
C(21)	0.9357(8)	0.2617(7)	0.3347(8)	5.9(6)
C(22)	0.9809(7)	0.3284(6)	0.370(1)	5.8(6)
C(23)	0.9902(7)	0.3460(5)	0.496(1)	5.1(5)
C(24)	0.9543(8)	0.2969(6)	0.5855(8)	4.6(5)

Table 5-6. Selected Bond Distances (Å) for **5-3a**, **5-4a**•$2H_2O$, **5-4a'**•$2H_2O$ and **5-5a**

	5-3a	**5-4a**•$2H_2O$	**5-4a'**•$2H_2O$	**5-5a**
Co(1)-P(1)	2.175(5)	2.186(5)	2.203(6)	2.236(6)
Co(1)-N(1)	1.92(1)	1.93(1)	1.91(1)	1.94(1)
Co(1)-N(2)	1.95(1)	1.95(1)	1.94(1)	1.93(1)
Co(1)-C(1)	2.09(2)	2.08(1)	2.05(1)	2.09(1)
Co(1)-C(2)	2.16(2)	2.12(1)	2.12(1)	2.05(1)
Co(1)-C(3)	2.16(2)	2.12(1)	2.13(1)	2.05(1)
Co(1)-C(4)	2.09(2)	2.07(1)	2.07(1)	2.08(1)
Co(1)-C(5)	2.05(2)	2.04(1)	2.02(1)	2.11(1)
Co(1)-C(1A)	2.12(2)			
Co(1)-C(2A)	2.12(2)			
Co(1)-C(3A)	2.10(3)			
Co(1)-C(4A)	2.09(3)			
Co(1)-C(5A)	2.10(3)			
P(1)-O(1)	1.556(9)	1.50(1)	1.52(1)	
P(1)-O(2)	1.57(1)	1.60(1)	1.61(1)	
P(1)-C(19)	1.772(9)	1.80(1)	1.81(1)	1.79(1)
N(1)-C(6)	1.37(2)	1.41(2)	1.37(2)	1.37(3)
N(1)-C(9)	1.40(2)	1.35(2)	1.33(2)	1.43(2)
N(2)-C(10)	1.28(2)	1.33(2)	1.29(2)	1.30(2)
N(2)-C(11)	1.47(2)	1.45(2)	1.54(2)	1.51(2)
C(6)-C(7)	1.35(2)	1.40(3)	1.41(3)	1.36(3)
C(7)-C(8)	1.34(2)	1.35(3)	1.38(3)	1.33(3)
C(8)-C(9)	1.42(2)	1.42(3)	1.43(3)	1.41(3)
C(9)-C(10)	1.42(2)	1.39(2)	1.38(3)	1.39(3)

Table 5-7. Selected Bond Angles (°) for **5-3a**, **5-4a·2H$_2$O**, **5-4a'·2H$_2$O** and **5-5a**

	5-3a	**5-4a·2H$_2$O**	**5-4a'·2H$_2$O**	**5-5a**
P(1)-Co(1)-N(1)	89.7(4)	95.1(4)	94.0(5)	91.5(4)
P(1)-Co(1)-N(2)	92.2(3)	90.6(4)	89.8(4)	94.8(4)
N(1)-Co(1)-N(2)	83.4(5)	83.3(6)	81.5(6)	81.8(6)
Co(1)-P(1)-O(1)	109.3(4)	115.7(5)	113.6(5)	110.5(7)[a]
Co(1)-P(1)-O(2)	116.5(4)	105.0(5)	102.6(5)	117.5(6)[b]
Co(1)-P(1)-C(19)	118.4(3)	114.2(5)	115.9(4)	114.2(4)
O(1)-P(1)-O(2)	108.1(5)	112.2(7)	111.4(7)	102.1(8)[c]
O(1)-P(1)-C(19)	105.2(5)	105.8(6)	108.9(7)	107.8(7)[d]
O(2)-P(1)-C(19)	98.0(5)	103.3(7)	103.8(7)	103.7(7)[e]
Co(1)-N(1)-C(6)	142(1)	139(1)	136(1)	141(1)
Co(1)-N(1)-C(9)	111.3(8)	111(1)	115(1)	112(1)
Co(1)-N(2)-C(10)	113.4(9)	112(1)	113(1)	116(1)
Co(1)-N(2)-C(11)	128.4(9)	125(1)	124.6(9)	125(2)
C(10)-N(2)-C(11)	118(1)	122(1)	123(1)	119(1)
N(1)-C(6)-C(7)	110(1)	103(2)	106(2)	109(2)
N(1)-C(9)-C(8)	106(1)	111(2)	110(2)	106(2)
N(1)-C(9)-C(10)	115(1)	117(2)	113(2)	113(2)
C(6)-C(7)-C(8)	108(1)	114(2)	110(2)	111(2)
C(7)-C(8)-C(9)	108(1)	103(2)	104(2)	108(2)
C(8)-C(9)-C(10)	139(1)	132(2)	137(2)	141(2)
N(2)-C(10)-C(9)	117(1)	115(2)	118(2)	117(2)
N(2)-C(11)-C(12)	114(1)	111(1)	108(1)	111(1)
N(2)-C(11)-C(18)	117(1)	115(1)	112(1)	115(1)

[a] Co(1)-P(1)-C(25). [b] Co(1)-P(1)-C(26). [c] C(25)-P(1)-C(26). [d] C(25)-P(1)-C(19). [e] C(26)-P(1)-C(19).

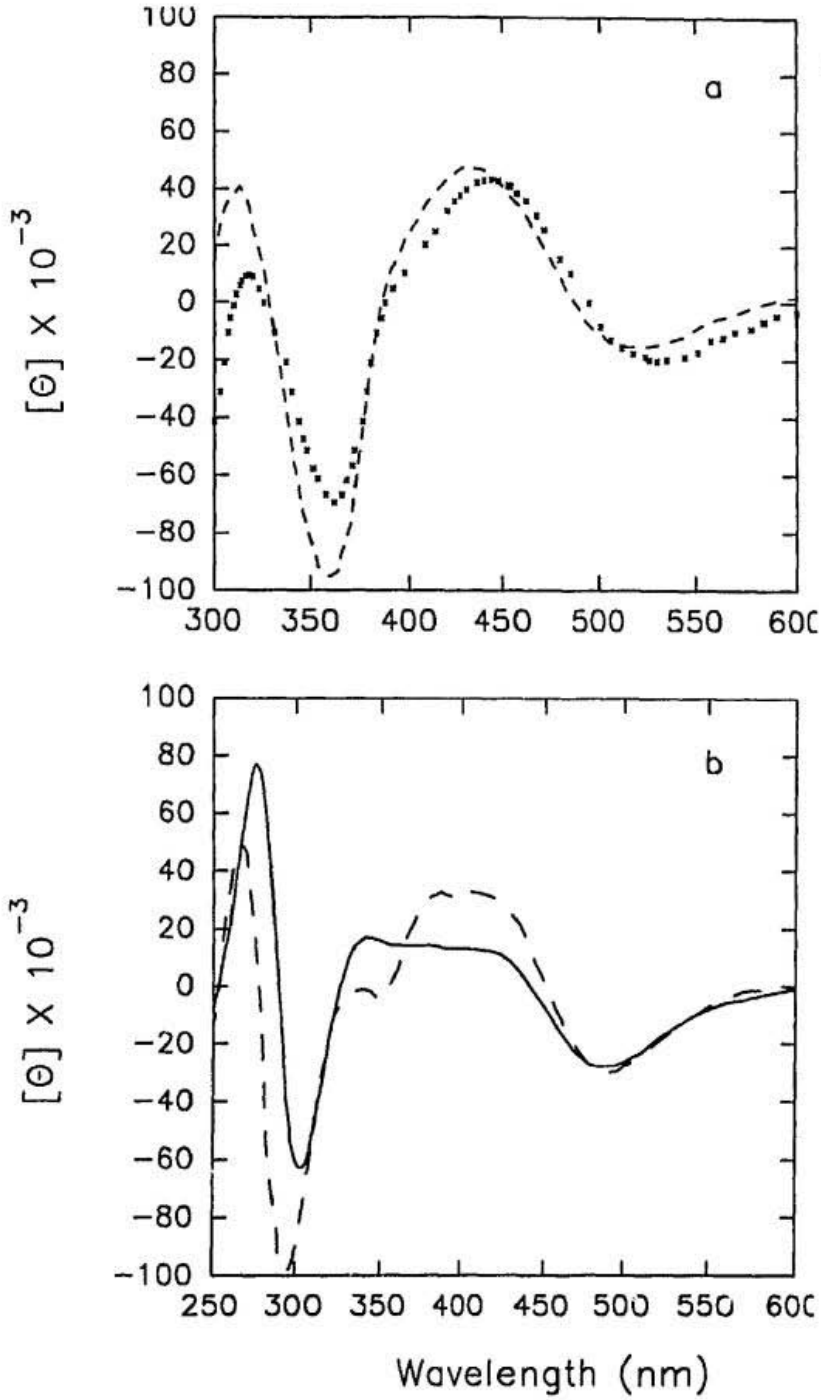

Figure 5-7. Circular Dichroism (CD) spectra of (a) **5-3a** (- - - -), **5-5a** (x x x x); (b) **5-4a** (— —), **4b** (——).

5.2.3. Chiroptical Properties and Absolute Configuration of 5-4b.

The isomorphous CD spectra of **5-3a, 5-4a, 5-5a** (Figure 5-7) are consistent with the same (S_{Co}) absolute configuration at cobalt as established by the x-ray crystal structure. Comparison of the CD spectra of the diastereomers **5-4a** and **5-4b** reveals a similar CD morphology congruent with an identical absolute configuration at cobalt (S_{Co}). The absolute configuration at phosphorus in **5-4b** must be R_P since **5-4a** and **5-4b** are the *only* products observed when ion pair **5-3a** collapses with retention at cobalt in solution.

5.2.4. Stereochemistry of the Arbuzov Dealkylation 5-3 → 5-4. There can be little question that simple halide substitution to give a cationic intermediate is the first step in the transition metal Arbuzov reaction.[182] Subsequent nucleophilic attack at carbon

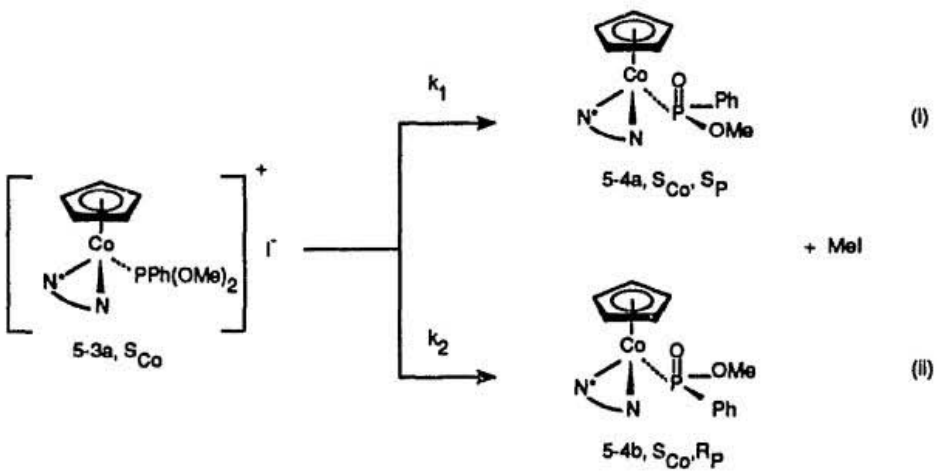

Scheme 5-3

on prochiral $P(OR)_2$ for the complexes examined in this study is diastereoselective, evolving under the influence of the chiral cobalt center. If we accept that configurationally stable **5-5a** is a good model for **5-3a**, comparison of the absolute stereochemistry of S_{Co}-**5-3a** and S_{Co}-**5-4a,b** establishes that Arbuzov dealkylation proceeds exclusively with retention at the metal center as required by Scheme 5-3. That the chiral induction in this reaction is similar to that for the reaction between (η^5-indenyl/η^5-Cp)Co(R_t)(L)(I) and $PPh(OMe)_2$ as presented in Chapter 3 is consistent with the importance of both the noncovalent P=O···HN hydrogen bonding and the stereochemical properties of the ligand sphere in chiral induction of Arbuzov dealkylation.

5.2.5. Solution Conformation. Proton nOed spectroscopy[206-208, 270, 280, 281, 285, 300, 357] was used to study the solution conformations of **5-3a**, **5-4a**, and **5-5a**. Comprehensive analysis showed that all three complexes adopt similar conformations both in solution and in the solid state. nOed spectra for **5-3a** showed that P-Ph and C*-Me are distal whereas C*-Ph and P-OMe are proximal to η^5-Cp. Irradiation of C*-Me at 1.52 ppm (Figure 5-1b) showed strong correlation to CH=N at 7.52 ppm (13.7%), H_{ortho} of C*-Ph (2.7%) and C*H (10.0%), indicating that C*-Me bond eclipses CH=N, as shown in Figure 5-3. This was consistent with the lack of enhancement of the CH=N resonance and small enhancements of Cp (0.6%), H_{ortho} of C*-Ph (1.3%), and C*-Me (1.4%) (Figure 5-1e), respectively, on irradiation of the C*H resonance at 4.76 ppm. The solid state, edge-on, syn C*-Ph/η^5-Cp, considered to

be the low energy conformation in similar cyclopentadienyl "piano stool" complexes,[285, 316] persisted in solution as indicated by irradiation of the Cp resonance at 5.35 ppm (Figure 5-1f), which gave a 0.8% enhancement of H_{ortho} of C*-Ph and a 1.5% enhancement of H_{meta} and H_{para} of C*-Ph, respectively. No correlation between Cp and P-Ph was observed when the Cp (Figure 5-1f) and P-Ph (Figure 5-1k) resonances were irradiated indicating that P-Ph is distal with respect to Cp. Irradiation of P-OMe signal at 3.82 ppm and 4.05 ppm gave small, positive enhancements (0.5% and 0.4%) of Cp signal (Figure 5-1c, d), respectively. Irradiation of the Cp resonance showed 1.7% and 1.4% enhancement to the diastereotopic $P(OMe)_2$ groups (Figure 5-1f). Similar nOed patterns were observed for **5-4a** and **5-5a** establishing that the solid state conformation is retained in solution for all three complexes.

5.2.6. Kinetic Studies. The isolation of the intermediate **5-3a** allowed investigation of not only the chiral induction from $Co^{\bullet} \rightarrow P$, but also direct measurement of the kinetics for the Arbuzov dealkylation step. NMR studies showed that two parallel dealkylation reactions occur when **5-3a** is dissolved as shown in Scheme 5-3. Kinetic data was analyzed by fitting integrated ^1H NMR time profiles for the appearance of **5-4a** and **5-4b** to the first order expression $A_t=A_{t\infty}(1-\exp(-k_1t))$ using an iterative, non-linear least squares procedure. Good fits over >2 half lives were obtained in methylene chloride and acetone. The reaction is significantly slower in acetonitrile but remains first order (0.2 half lives), and it does not proceed to a

significant extent under similar conditions in methanol. A representative set of experimental and calculated data for the disappearance of **5-3a** and appearance of **5-4a** and **5-4b** are shown in Figure 5-8.

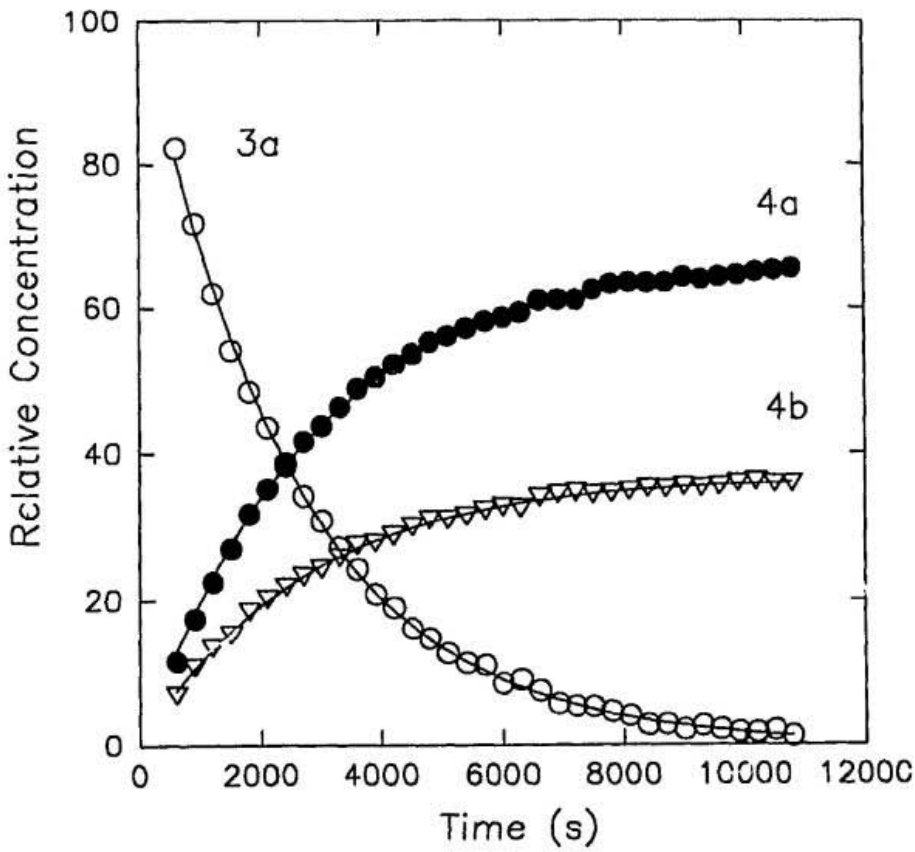

Figure 5-8. Representative Integrated Concentration vs. Time Profile of Experimental and Fitted Data for Scheme 5-3, Run 7 in Table 5-8.

A first order rate law follows from a kinetic model which assumes pre-equilibrium ion pair formation, **5-3a**$^+$ + I^- ↔ **5-3a**$^+$,I^-, with $\alpha<<1$ (where C is norminal concentration and α is tha degree of dissociation, α=[**5-3a**$^+$]/C(**5-3a**))[358] and a rate-determining conversion of the ion pair into products. Chiral induction in Scheme 5-3 depends on the ratio k_1/k_2 leading to S_{Co},S_P,S_C-**5-4a** and S_{Co},R_P,S_C-**5-4b**, respectively. The first order rate constants k_1 and k_2 for the reaction **5-3a**→**5-4a** and **5-3a**→**5-4b**, respectively, obtained as described above, are summarized in Table 5-8. Good agreement was obtained between the sum $k_1 + k_2$ and independently determined experimental values for the rate constant k_t for the first order consumption of **5-3a** verifying the rate law -d[**5-3a**]/dt = k_t[**5-3a**] = ($k_1 + k_2$)[**5-3a**] appropriate for product formation via two parallel first order reactions.

Several qualitative conclusions can be drawn from the kinetic data summarized in Table 5-8: (i) k_1 and k_2 are sensitive to solvent with $k_{dichloromethane} \approx k_{acetone} > k_{acetonitrile} >> k_{methanol}$. As is generally expected for cationic/anionic reactions involving charge destruction, reaction rate is inversely related to solvent dielectric.[359] Parker's critical analysis[360] reconciles the observation that reactions of the charge type shown in Scheme 5-3 are much slower in protic vs. aprotic dipolar solvents in terms of hydrogen bonding of the anion, X^-. Protic solvents are strong hydrogen bond donors and therefore solvate anions as reflected by the free energy of transfer of ions from a reference solvent,[361] ΔG_{tr}. With *N*,*N*-dimethylformamide (DMF) as a reference, $\Delta G_{tr}(I^-)$ becomes less favorable along the solvent series

methanol ($\Delta G_{tr}(I^-)$ = -10 kJ/mol) > acetonitrile ($\Delta G_{tr}(I^-)$ = -4 kJ/mol) > acetone ($\Delta G_{tr}(I^-)$ = +8 kJ/mol). Assuming that changes in anion solvation dominate, $\Delta G_{tr}(I^-)$ reflects the order of reaction rates measured for Scheme 5-3. Presumably the Arbuzov dealkylation of Scheme 5-3, which requires collapse of the ion pair via S_N2 attack of iodide on carbon, does not proceed in methanol since I^- is very strongly solvated compared to the case of aprotic dipolar solvents. In acetone, anion solvation is poor since hydrogen bonding cannot occur. The degree of dissociation α is very low and k_{obs} is large and insensitive to added halide. (ii) The kinetic product ratio k_1/k_2 is relatively independent of solvent as expected if $\Delta G_{tr}(I^-)$ dominates the solvent effect on reaction rate. k_1/k_2 = 1.6 in dichloromethane (ε=8.9), 1.8 in acetone (ε=20.7), and 1.5 in acetonitrile (ε=37.5) so that dealkylation favors the formation of $S_{Co}S_P,S_C$-**5-4a** with ca. 25(3)% de. It can be concluded that the reaction proceeds via collapse of a tight-ion pair in aprotic solvents.

Table 5-8. Kinetic Data for reaction **5-3a** → **5-4a** + **5-4b**.

No.	Solvent	ε	C_0 (**5-3a**) (mol•L^{-1})	C (Li^I) (mol•L^{-1})	T (K)	k_1 (s^{-1} x10^4)	k_2 (s^{-1} x10^4)
1	CD_2Cl_2	8.9	0.0167	0	298	2.1(±0.1)	1.3(±0.1)
2	CD_2Cl_2	"	0.0144	0	298	2.3(±0.1)	1.3(±0.1)
3	CD_2Cl_2	"	0.0185	0	298	2.0(±0.1)	1.1(±0.1)
4	Acetone-d_6	20.7	0.0153	0	298	2.3(±0.1)	1.3(±0.1)
5	Acetone-d_6	"	0.0137	0	308	5.6(±0.5)	2.9(±0.5)
6	Acetone-d_6	"	0.0230	0	318	20.(±3.5)	10.5(±3.5)
7	Acetone-d_6	"	0.0085	0.0572	298	2.3(±0.1)	1.3(±0.1)
8	Acetone-d_6	"	0.0105	0.187	298	2.7(±0.2)	1.6(±0.2)
9	CD_3OD	33.6	0.0130	0	298	No reaction after 24 h	
10	CD_3OD	"	0.0130	0	323	< 5% was converted in 24 h	
11	CD_3CN	36.8	0.0142	0	298	0.031(±0.001)	0.021(.001)

The activation parameters based on runs 4, 5, and 6 are: $\Delta H^{\neq}_1$ = 82.8(±1.2) kJ•mol^{-1}, $\Delta H^{\neq}_2$ = 79.2(±1.5) kJ•mol^{-1}, $\Delta S^{\neq}_1$ = -37.4(±3.9) J•K^{-1}•mol^{-1}, $\Delta S^{\neq}_2$ = -54.2(±4.9) J•K^{-1}•mol^{-1}.

5.3. Experimental Section

5.3.1. Reagents and Methods. All manipulations were performed under similar conditions as described in Chapters 2 and 3. In addition, pentane was distilled under nitrogen from blue solutions of sodium benzophenone ketyl. Optical rotation measurements were determined in dichloromethane (*ca.* 1 mg/mL) in a 1 cm path-length cell by using a Perkin-Elmer Model 141 polarimeter. Circular dichroism (CD) spectra were determined in dichloromethane (ca. 1 mg/mL) on a Jasco J 40 A apparatus using a 0.010 or 0.050 cm path-length cell. η^5-CpCo(CO)(I)$_2$ (**5-1**)[362, 363], and η^5-CpCo(N-N*)(I) (**5-2a,b**)[285] were prepared using the established procedures.

5.3.2. Crystal Structure Determinations. Crystal data were collected at ambient temperature on a Rigaku AFC6S diffractometer using the ω-2θ scan technique to maximum 2θ values of 45.1° (**5-3a**), 100.1° (**5-4a•2H$_2$O**), and 120.2° (**5-5a**), respectively. Structures were solved by direct methods[305] using the Molecular Structure Corporation TEXSAN software. The selected crystal for **5-3a** proved to be twinned showing broad, unsymmetrical peaks which occasionally revealed two distinct summits. However, the control program was able to center and refine during search and index. The space group $P2_12_12_1$ (#19) was assigned in all cases on the basis of systematic absences (h00: h ≠ 2n, 0k0: k ≠ 2n, and 00l: l ≠ 2n). All measurements were made with graphite monochromated Mo (**5-3a**) or Cu (**5-4a•2H$_2$O**, **5-5a**) Kα radiation and a 2 KW sealed tube generator. Weak reflections

($I < 10.0\sigma(I)$) were rescanned (max 2) and the counts accumulated to assure good counting statistics. For **5-4a•2H$_2$O** the intensities of three representative reflections, measured after every 150 reflections, declined by 11.00% hence a linear correction factor was applied to the data. The phenyl and the cyclopentadiene rings were refined as rigid groups. All non-hydrogen atoms were refined anisotropically. Idealized hydrogen atoms were included at the calculated positions but were not refined. A correction for secondary extinction was applied (coefficient = 0.87748 x 10^{-7}) in the case of **5-5a**. The absolute stereochemistry was confirmed in each case by refinement of the enantiomer to a higher R value and correct stereochemistry of the reference carbon known to be S_C. Further details are given in Table 5-9.

5.3.3. Kinetics for the Arbuzov Dealkylation Step. Kinetic studies of the Arbuzov dealkylation reaction were carried out in NMR tubes by dissolving solid **5-3a** in the required amount of solvent. Concentration/time data was obtained by integration of Cp and OMe ^{1}H NMR resonances of the reactant **5-3a** and the products **5-4a** and **5-4b**. In a typical experiment 6.61 mg of (0.0107 mmol) **5-3a** was dissolved in 0.70 mL of acetone-d_6 under nitrogen in a pre-weighed 5 mm NMR tube. The tube was closed with a screw-cap septum seal, the contents were mixed until homogenous using a vortex mixer, and the tube was transferred to a thermostatted NMR probe. Ten spectra were collected at time intervals of 300 s then the time intervals were increased to 600 s. The reactions were generally followed to completion. The first order rate constants k_1 and k_2 were obtained by nonlinear least-squares regression

analysis of the integrated concentration vs. time data.

5.3.4. Synthesis of Complexes.

5.3.4.1. Synthesis of Pyrrole-2-carboxald-(S)-(1-phenylethyl)iminate (N-N*). The Schiff base N-N* (N*-N = *S*-Ph(Me)C*H-N=CH-C_4H_3N, C_4H_3N= pyrrolyl) was prepared using a modification of the published procedure[285] which avoided the high temperature distillation step. Equimolar amounts of pyrrole-2-carboxaldehyde (5.444 g, 57.23 mmol) and (*S*)-phenylethylamine (6.988 g, 57.67 mmol) were dissolved in about 100 mL of benzene. p-Toluene sulfonic acid (10 mg) and 50 mL Molecular Sieves (activated type 4A, 4-8 mesh) were added, and the reaction mixture was stirred at room temperature. IR spectroscopy monitored the intensity decrease of $\nu_{C=O}$ at 1664 cm^{-1} and the intensity increase of $\nu_{C=N}$ at 1635 cm^{-1}. The reaction was generally complete after stirring for about 6 hours. The crude reaction mixture was filtered through a glass frit fitted with a Celite pad. The filtrate was collected, and the solvent removed at aspirator and then oil pump vacuum leaving the product as a pale yellow oil (10.306g, 91%), which was characterized by comparison of its NMR and IR data with the published data.[285] IR (neat, cm^{-1}): 1638 ($\nu_{C=N}$), 3417 (ν_{N-H}). ^{1}H NMR ($CDCl_3$, δppm): 1.54 (Me, d, 6.7 Hz), 4.46 (C*H, q, 6.7 Hz), 6.15 (H_4, m), 6.47 (H_3, m), 6.65 (H_5, m), 8.14 (CH=N, s), 9.75 (NH, broad), 7.14-7.33 (phenyl protons). ^{13}C NMR ($CDCl_3$, ppm): 24.32 (Me), 68.84 (C*H), 109.39 (C_4), 114.58 (C_3), 122.06 (C_5), 126.52, 126.71, 128.28 (C_{ortho}, C_{meta}, C_{para}), 129.99 (C_{ipso}), 144.74 (C_2), 150.74 ($C_{CH=N}$).

The N-N* anion was obtained as the sodium salt before the preparation of complex **5-2** by treatment with NaH.[285]

5.3.4.2. Synthesis of (S_{Co},S_C)-[(η^5-C_p)Co(N-N*)(PPh(OMe)$_2$)]*I, 5-3a. $PPh(OMe)_2$ (0.1906 g, 1.120 mmol) was added slowly via syringe with stirring to a dark blue solution of **5-2a,b** (**5-2a**/**5-2b** = 85/15, 0.4541 g, 1.013 mmol) in 30 mL of benzene at room temperature. A deep red precipitate immediately formed. After stirring for another 5 min the precipitate was collected on a glass frit, washed with cold benzene (5 x 5 mL), and then dried at room temperature under oil pump vacuum to afford the product as a deep red powder, 0.4950 g (79%). ^1H NMR (CD_3OD) showed the presence of a single diastereomer, **5-3a**. **5-3a** was dissolved in a small amount of CH_2Cl_2 and crystallized by slow diffusion of pentane at -20 °C to give deep red rectangular plates, mp 84-86 °C. $[\alpha]_{579}$ = -700. Due to low transmittance, optical rotations at other wavelengths were not measurable. Analysis (%): Calc. for $C_{26}H_{29}N_2O_2PICo$, C, 50.50; H, 4.73; N,4.53; Found, C, 50.14; H, 4.83; N, 4.40. ^1H NMR analysis of the residue obtained by removal of solvent from the filtrate under oil pump vacuum showed six Cp signals which correspond to **5-3a** (5.40 ppm), **5-3b** (5.67 ppm), **5-4a** (4.84 ppm), **5-4b** (4.71 ppm), **5-4c** (5.04 ppm), and **5-4d** (4.96 ppm).

5.3.4.3. Synthesis of $(S_{Co},(S,R_P),S_C)$-(η^5-C_p)Co(N-N*)(P(O)(Ph)(OMe)), 5-4a, b. A suspension of 0.4932 g (0.7976 mmol) **5-3a** in 50 mL of benzene was heated with

stirring at 60°C for 3 h. Removal of the solvent at aspirator then oil pump vacuum left a red, paste-like solid. ^{1}H NMR analysis of the crude product showed that the reaction is quantitative and that the two diastereomers **4a/4b** are formed with 36% de. Repeated chromatographic separation on 4 mm radial thick layer silica gel plates (Chromatotron) eluting with methanol/benzene (1:20 v/v) separated a faster moving orange-red zone of **5-4a**. Removal of the solvent gave a red paste-like solid, 0.1748g (46%). Red plates were obtained by slow diffusion of pentane at -20°C into a solution of **5-4a** in acetone, mp, 118-120 °C. $[\alpha]_{579}$ = -1292, $[\alpha]_{546}$ = -321 , $[\alpha]_{436}$ = +1693. Analysis (%) Calc. for $C_{25}H_{26}N_2O_2PCo{\bullet}2H_2O$, C, 58.60; H, 5.90; N, 5.47; Found, C, 57.19; H, 5.53; N, 5.17. A red, paste-like solid sample of low R_f **5-4b** was obtained by washing manually separated silica powder containing **5-4b** with methanol.

5.3.4.4. Synthesis of (S_{Co},S_P)-[(η^5-C_p)Co(N-N')($PPhMe_2$)]$^+$I$^-$, 5-5a. $PPhMe_2$ (0.1228 g, 0.8889 mmol) was added slowly via syringe with stirring to a dark blue solution of **5-2a,b** (**5-2a/5-2b** =85/15, 0.1603 g, 0.3577 mmol) in 10 mL of benzene at room temperature. A brown-red precipitate formed immediately. Stirring was continued for another 5 min, and then the precipitate was collected on a glass frit, washed with cold benzene (5 x 5 mL), and dried at room temperature at oil pump vacuum to give the title complex as a brown-red powder, 0.1564 g (75%). ^{1}H NMR analysis showed the presence of a single diastereomer, **5-5a**. The crude product was dissolved in a small amount of CH_2Cl_2 and crystallized by slow diffusion of hexane at -20 °C to

afford black rectangular plates, mp 154-156 °C. $[\alpha]_{579}$ = -580. Anal.(%): Calc. for $C_{26}H_{29}N_2PICo$, C, 53.26; H, 4.99; N, 4.78; Found, C, 53.20; H, 4.88; N, 4.89.

Table 5-9. Summary of Crystallographic Data for **5-3a**, **5-4a•2H$_2$O** and **5-5a**.

	3a	**4a•2H$_2$O**	**5a**
formula	$C_{26}H_{29}CoIN_2O_2P$	$C_{25}H_{30}CoN_2O_4P$	$C_{26}H_{29}CoIN_2P$
mol. wt.	618.34	512.43	586.34
cryst system	orthorhombic	orthorhombic	orthorhombic
cryst size (mm)	0.25x0.25x0.20	0.30x0.20x0.10	0.30x0.20x0.20
a (Å)	13.77(2)	16.692(5)	13.308(4)
b (Å)	18.08(1)	32.33(2)	17.977(4)
c (Å)	10.862(6)	9.379(6)	10.790(3)
V (Å^3)	2705(4)	5062(4)	2581(1)
Space Group	$P2_12_12_1$ (#19)	$P2_12_12_1$ (#19)	$P2_12_12_1$ (#19)
Z	4	8	4
D_{calc} (g cm^{-3})	1.518	1.345	1.509
F_{000}	1240	2144	1176
μ(cm^{-1})	18.44(MoKα)	64.38 (CuKα)	156.68 (CuKα)
scan type	ω-2θ	ω-2θ	ω-2θ
$2\theta_{max}$ (deg)	45.1	1000.1	120.2
Δ (deg)	1.78+0.30 tanθ	0.84+0.30 tanθ	1.15+0.30 tanθ
$2\theta_{max}$ (deg)	45.1	100.1	120.2
total data	7680	6002	4432
unique data	2052	3003	2216
R_{int}	0.072	0.156	0.164
no. obs data	962 (I>3.0σ(I))	1112 (I>3.0σ(I))	873 (I>3.0σ(I))
no. variables	138	231	111
Lorentz polarization			
trans factors[a]	0.91-1.00	0.61-1.00	0.71-1.14
R[b], R_w[c], GOF[d]	0.046,0.041,1.67	0.065,0.047,1.59	0.065,0.046,1.83
max/min resd density (e$^-$/Å^3)	0.53/-0.46	0.46/-0.48	0.81/-0.86

[a] Cf. reference[308]. [b] $R=\Sigma||Fo|-|Fc||/\Sigma|Fo|$.
[c] $R_w=[(\Sigma w(|Fo|-|Fc|)^2/\Sigma wFo^2)]^{1/2}$ [d] $GOF=(\Sigma(|Fo|-|Fc|)/\sigma)/(n-m))$ where n=#reflections, m=#variables, and σ^2=variance of (|Fo|-|Fc|)

Chapter 6

Synthesis, Structure, and Characterization of a series of Novel Cyclopentadienyl and Pentamethylcyclopentadienyl N-O Co(III) Complexes (N-O = 2-acylpyrrolyl): Arbuzov Reactions between $(C_5R_5)Co(R'C(O)-C_4H_3N)(I)$ and $PR''(OMe)_2$ (R, R' = H, Me; R'' = Ph, OMe).

6.1. Introduction

This chapter presents the synthesis, structure and characterization of a series of η^5-cyclopentadienyl and pentamethylcyclopentadienyl 2-acylpyrrolyl Co(III) complexes, their chiral induction in the Arbuzov reaction and the correlation of their structures and conformational preferences with ^{1}H NMR spectra. Since these complexes may have similar structures to the Schiff base complexes discussed in Chapter 5[308] and since the stereochemical difference between the two coordination sites is smaller for 2-acylpyrrolyl ligands, lower optical induction should be expected.

6.2. Results and Discussion

6.2.1. Synthesis and Characterization of $(\eta^5\text{-}C_5R_5)Co(R'C(O)\text{-}C_4H_3N)(I)$ (6-5 - 6-8).

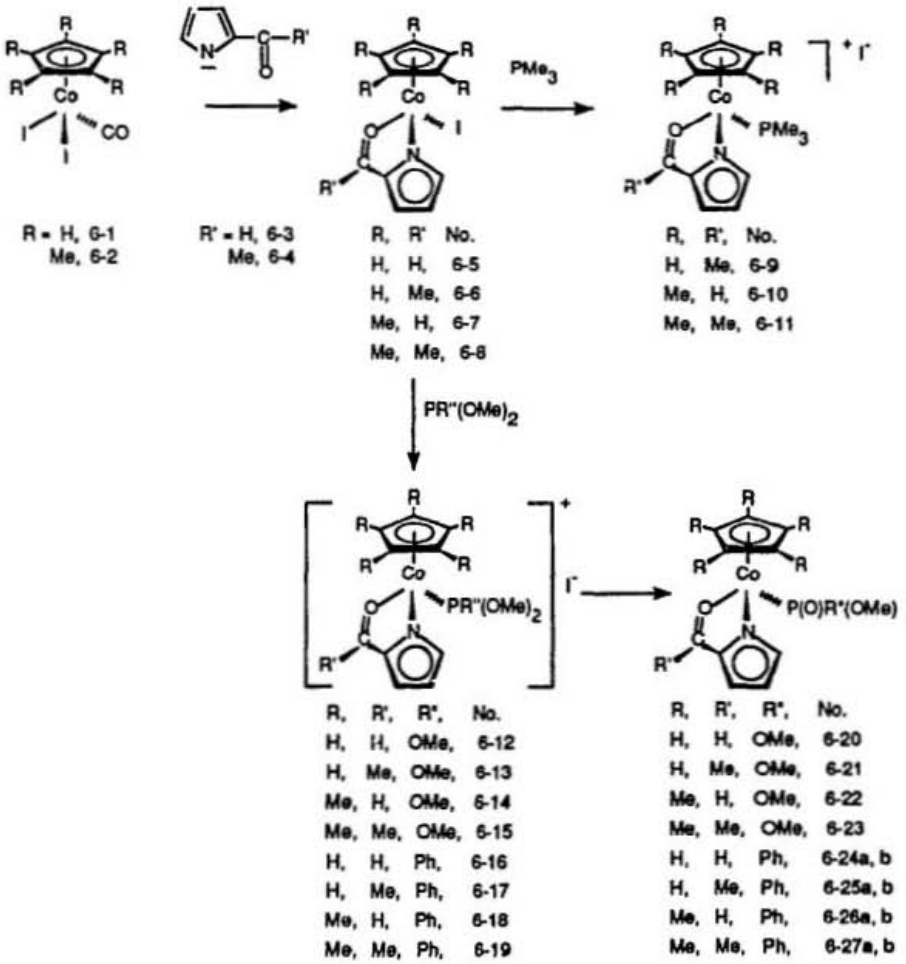

Scheme 6-1

As shown in Scheme 6-1, $(\eta^5\text{-}C_5R_5)Co(CO)(I)_2$ (R = H, **6-1**; R = Me, **6-2**) reacts with

2-acylpyrrolyl, R'C(O)-$C_4H_3N^-$ (R' = H, **6-3**; R' = Me, **6-4**) obtained *in situ* by treatment of 2-formylpyrrole or 2-acetylpyrrole with NaH in dry THF, to give the N,O-chelate products, (η^5-C_5R_5)Co(R'C(O)-C_4H_3N)(I) (**6-5 - 6-8**), as dark blue crystalline solids. These complexes are air stable in the solid state and in solution and are very soluble in benzene, dichloromethane, acetone, and methanol, but only slightly soluble in hexane. Their physical properties are tabulated in Table 6-1. Coordination to Co(III) lowers the $\nu_{C=O}$ of these complexes to 1549-1566 cm^{-1} compared to free C=O groups. Multinuclear NMR suggests that these complexes have piano-stool geometries, but cannot distinguish whether the C=O group coordinates to cobalt via the lone-pair on oxygen or via the π orbital. ^{1}H NMR data (Table 6-2) for complexes **6-5** and **6-6** show typical η^5-Cp resonances at 5.57 and 5.55 ppm, respectively, while the ^{1}H NMR of complexes **6-7** and **6-8** both consist of a singlet at 1.64 ppm for the Me on η^5-Cp*. The protons on the pyrrolyl ring in complexes **6-5 - 6-8** show well separated resonances with chemical shifts (cf. Scheme 6-2 for numbering): H_5 (7.6-8.0 ppm) > H_3 (7.0-7.2 ppm) > H_4 (6.5-6.6 ppm) as observed in other relevant complexes (cf. Chapter 5).[285, 308] The formyl proton in complexes **6-5** and **6-7** shows a doublet at about 8.0 ppm shifted *ca.* 1.5 ppm upfield compared to the uncoordinated CH=O (9.52 ppm) in 2-formylpyrrole. Their ^{13}C NMR (Table 6-3) resonances, assigned on the basis of 2-D ^{1}H/^{13}C ^{1}J heterocorrelation spectra, are well separated and also consistent with the piano-stool geometry.

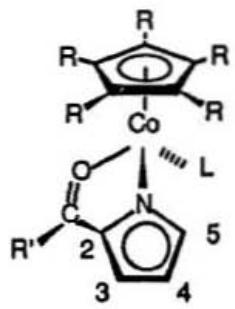

Scheme 6-2

6.2.2 Substitution Reactions of ***(η^5-C_5R_5)Co(R'C(O)-C_4H_3N)(I) with PMe_3.*** In order to test the lability of the 2-acylpyrrolyl iodide complexes, (η^5-C_5R_5)Co(R'C(O)-C_4H_3N)(I), complexes **6-6, 6-7**, and **6-8** were treated with PMe_3. Treatment of **6-6, 6-7**, or **6-8** with excess (x10) PMe_3 (cf. Scheme 6-1) both in refluxing benzene and at room temperature gave the monosubstituted cation, [(η^5-C_5R_5)Co(R'C(O)-C_4H_3N)(PMe_3)]$^+I^-$, **6-9, 6-10**, and **6-11** as the only products, respectively. These complexes are very stable both in the solid state and in solution. No reaction occurred when **6-9, 6-10** or **6-11** was treated with iodide in acetone-d_6 at room temperature and at 45 °C. NMR reactions of complexes **6-6, 6-7** or **6-8** in acetone-d_6 with excess (x10) PMe_3 at room temperature showed that complex **6-9, 6-10**, or **6-11** was also the only observed complex for several hours after the reactant complex **6-6, 6-7** or **6-8** disappeared. However, after overnight reaction at room temperature the N-O chelating ligand in these complexes was further substituted by excess PMe_3 to give a series of uncharacterized complexes. Thus, the N-O 2-acylpyrrolyl is a weakly coordinated ligand.

6.2.3. Arbuzov Dealkylation Reaction between (η^5-C_5R_5)Co(R'C(O)-C_4H_3N)(I) and $P(OMe)_3$: Correlation between the ^1H Chemical Shift Difference ($\Delta\delta_{OMe}$) of the Diastereotopic OMe in $P(O)(OMe)_2$ and the Molecular Structure and Conformational Preference. Experiments showed that reactions between (η^5-C_5H_5)Co(R'C(O)-C_4H_3N)(I) (**6-5, 6-6**) and $P(OMe)_3$ were much faster than those between (η^5-C_5Me_5)Co(R'C(O)-C_4H_3N)(I) (**6-7, 6-8**) and $P(OMe)_3$. Complexes **6-5** or

6-6 reacted readily with $P(OMe)_3$ in benzene at room temperature to give the cobaltophosphonates, $(\eta^5\text{-}C_5H_5)Co(R'C(O)\text{-}C_4H_3N)(P(O)(OMe)_2)$ (**6-20, 6-21**) as red solids (cf. Scheme 6-1). The cationic intermediates, $[(\eta^5\text{-}C_5H_5)Co(R'C(O)\text{-}C_4H_3N)(P(OMe)_3)]^+$ (**6-12, 6-13**), for these reactions in acetone-d_6 shown in Scheme 6-1 were observed by ^1H NMR spectroscopy (**6-12**, Cp: 5.81 ppm, $P(OMe)_3$: 3.80 ppm (d, 10.5 Hz); **6-13**, Cp: 5.80 ppm, $P(OMe)_3$: 3.77 ppm (d, 10.9 Hz)), which establishes that these Arbuzov reactions proceed via an ionic mechanism as reported previously.[182, 206, 208, 218, 308, 318]

Reactions of $(\eta^5\text{-}C_5Me_5)Co(R'C(O)\text{-}C_4H_3N)(I)$ (**6-7, 6-8**) with $P(OMe)_3$ proceeded with difficulty[207] and prolonged refluxing of complex **6-7** or **6-8** with $P(OMe)_3$ in benzene was required to form $(\eta^5\text{-}C_5Me_5)Co(R'C(O)\text{-}C_4H_3N)(P(O)(OMe)_2)$ (**6-22, or 6-23**). Physical properties and multinuclear NMR data are presented in Tables 6-1, 6-2, and 6-3. IR spectra show a coordination shift for $\nu_{C=O}$ to 1548-1566 cm^{-1}. A strong band characteristic of $\nu_{P=O}$ appears at 1149-1157 cm^{-1}.[186, 188, 206, 218] Well separated characteristic resonances for Cp/Cp* and the pyrrolyl protons similar to the relevant complexes **6-5 - 6-11** are observed in the ^1H NMR spectra (Table 6-2) of complexes **6-20 - 6-23**. The ^1H NMR spectra of complexes **6-20 - 6-23** show a pair of doublets ($^3J_{PH}$ = 11.0 ± 1.5) at 2.76-3.66 ppm assigned to the coordinated diastereotopic $P(O)(OMe)_2$.

Table 6-1. Physical Properties of (η^5-C_5R_5)Co(R'-C(O)-C_4H_3N)(L) Complexes.

No.	R	R'	L	Formula	Yield (%)	Appearance	m.p. (°C)	C,H,N% Calc'd (Found)	$\nu_{C=O}/\nu_{P=O}$ (cm^{-1})
6-5	H	H	I	$C_{10}H_9NOICo$	72	Dark blue crystalline	136-137	34.81, 2.63, 4.06 (34.80, 2.62, 4.02)	1566
6-6	H	Me	I	$C_{11}H_{11}NOICo$	78	Dark blue crystalline	160-161	36.80, 3.09, 3.90 (36.64, 3.03, 3.87)	1550
6-7	Me	H	I	$C_{15}H_{19}NOICo$	65	Dark blue crystalline	187-190	43.40, 4.61, 3.37 (43.33, 4.56, 3.39)	1566
6-8	Me	Me	I	$C_{16}H_{21}NOICo$	75	Dark blue prism crystal	205-208	44.78, 4.93, 3.26 (44.68, 4.89, 3.25)	1549
6-9	H	Me	PMe_3	$C_{14}H_{20}NOPICo$	95	Deep red powder	>110 dec.	38.64, 4.63, 3.22 (38.70, 4.64, 3.03)	1554
6-10	Me	H	PMe_3	$C_{18}H_{28}NOPICo$	86	Deep red powder	157-159	44.01, 5.74, 2.85 (44.35, 5.68, 2.85)	1564
6-11	Me	Me	PMe_3	$C_{19}H_{30}NOPICo$	99	Deep red powder	>130 dec.	45.17, 5.98, 2.77 (45.20, 6.16, 2.58)	1551
6-17	H	Me	$PPh(OMe)_2$	$C_{19}H_{22}NO_3PICo$	70	Deep red powder	75-77	43.12, 4.19, 2.65 (43.25, 4.15, 2.68)	1555
6-20	H	H	$P(O)(OMe)_2$	$C_{12}H_{15}NO_4PCo$	60	Red powder	95-97	-	1566/1157
6-21	H	Me	$P(O)(OMe)_2$	$C_{13}H_{17}NO_4PCo$	98	Red powder	99-101	45.76, 5.02, 4.11 (45.54, 4.90, 3.81)	1550/1156
6-22	Me	H	$P(O)(OMe)_2$	$C_{17}H_{25}NO_4PCo$	94	Red powder	81-83	51.39, 6.34, 3.53 (51.21, 6.45, 3.39)	1565/1149

Table 6-1. cont'd

6-23	Me	Me	$P(O)(OMe)_2$	$C_{18}H_{27}NO_4PCo$	93	Deep-red prism crystal	>130 dec.	52.56, 6.62, 3.41 (52.55, 6.56, 3.42)	1548/1152
6-24[c]	H	H	P(O)Ph(OMe)	$C_{17}H_{17}NO_3PCo$	71	Red crystalline	-	-	1548/1138
6-25[d]	H	Me	P(O)Ph(OMe)	$C_{18}H_{19}NO_3PCo$	95	Red crystalline	-	-	1550/1144
6-26[e]	Me	H	P(O)Ph(OMe)	$C_{22}H_{27}NO_3PCo$	92	Red crystalline	-	-	1564/1136
6-27[f]	Me	Me	P(O)Ph(OMe)	$C_{23}H_{29}NO_3PCo$	99	Red crystalline	-	60.40, 6.39, 3.06 (60.59, 6.45, 2.98)	1546/1135

[a] Isolated yield before crystallization. [b] Sealed (N_2) capillary. [c] mixture of two diastereomers a/b=57/43. [d] mixture of two diastereomers a/b=53/47. [e] mixture of two diastereomers a/b=51/49. [f] mixture of two diastereomers a/b=50/50.

Table 6-2. ^{1}H and ^{31}P NMR Data for $(\eta^5\text{-}C_5R_5)Co(R'\text{-}C(O)\text{-}C_4H_3N)(L)$ Complexes[a].

No.	R	R'	L	H_3	H_4	H_5	Cp-R	CR'=O	P-Me/P-OMe	^{31}P
6-5	H	H	I	7.12 (dd,4.2,0.8)[b]	6.56 (dd,4.4,1.4)[c]	7.62 (d,0.9)[d]	5.57 (s)	8.1 (d,1.0)[e]		
6-6	H	Me	I	7.01 (dd,4.2,1.0)[b]	6.52 (dd,4.2,1.5)[c]	8.00 (d,1.2)[d]	5.55 (s)	2.32 (s)		
6-7	Me	H	I	7.04 (dd,4.2,0.9)[b]	6.52 (dd,4.2,1.5)[c]	7.83 (dd,2.1,1.2)[f]	1.64 (s)	7.90 (d,0.9)[e]		
6-8	Me	Me	I	6.95 (dd,4.1,0.8)[b]	6.48 (dd,4.0,1.5)[c]	7.76 (d,1.2)[d]	1.64 (s)	2.32 (s)		
6-9	H	Me	PMe_3	7.16 (d,4.3)[g]	6.53 (dd,4.3,1.2)[c]	7.89 (s)	5.86 (s)	2.37 (s)	1.54 (d,12.6)[h]	26.33 (s)
6-10	Me	H	PMe_3	7.28 (dt,4.4,1.0)[i]	6.63 (dd,4.4,1.4)[c]	7.61 (s)	1.48 (d,1.8)[j]	8.22 (dd, 3.1,0.8)[k]	1.23 (d,11.1)[h]	15.20 (s)
6-11	Me	Me	PMe_3	7.16 (d,4.3)[g]	6.56 (dd,5.0,1.5)[c]	7.44 (d,0.6)[d]	1.48 (d,1.7)[j]	2.45 (s)	1.20 (d,11.0)[h]	16.95 (s)
6-17[l]	H	Me	$PPh(OMe)_2$	6.88 (d,4.4)[g]	6.42 (dd,4.3,1.6)[c]	7.87 (d,0.7)[d]	5.97 (s)	1.88 (s)	4.05 (d,12.1)[m] 3.96 (d,11.7)[m]	161.47 (s)
6-20	H	H	$P(O)(OMe)_2$	7.25 (d,4.2)[g]	6.47 (dd,4.4,1.4)[c]	7.60 (s)	5.35 (s)	7.90 (dd, 3.6,0.7)[k]	3.66 (d,11.1)[m] 2.97 (d,9.9)[m]	75.83 (s)
6-21	H	Me	$P(O)(OMe)_2$	7.14 (dd,4.2,0.5)[b]	6.41 (dd,4.2,1.4)[c]	7.50 (s)	5.33 (s)	2.33 (s)	3.65 (d,10.6)[m] 2.93 (d,9.4)[m]	77.34 (s)
6-22	Me	H	$P(O)(OMe)_2$	7.17 (d,4.2)[g]	6.47 (dd,4.2,1.3)[c]	7.46 (s)	1.47 (d,1.9)[j]	8.19 (dd,3.7,0.7)[k]	3.59 (d,10.8)[m] 2.76 (d,9.5)[m]	87.61 (s)
6-23	Me	Me	$P(O)(OMe)_2$	7.07 (dt,4.1,0.7)[f]	6.40 (dd,4.1,1.5)[c]	7.37 (d,1.1)[d]	1.47 (d,2.0)[j]	2.36 (s)	3.54 (d,10.6)[m] 2.77 (d,9.6)[m]	88.95 (s)

Table 6-2. cont'd

6-24a[n]	H	H	P(O)Ph(OMe)	6.91 (d,4.3)[g]	6.42 (dd,4.3,1.3)[c]	7.49 (s)	5.19 (s)	7.54 (d,2.9)[e]	3.31 (d,10.5)[m]	100.20 (s)
6-24b[n]	H	H	P(O)Ph(OMe)	6.71 (d,4.3)[g]	6.34 (dd,4.3,1.2)[c]	7.49 (s)	5.32 (s)	7.49[o]	3.77 (d,10.7)[m]	104.90 (s)
6-25a[p]	H	Me	P(O)Ph(OMe)	6.81 (dd,3.9,0.5)[b]	6.36 (dd,4.2,1.4)[c]	7.42 (s)	5.23 (s)	1.81 (s)	3.42 (d,10.5)[m]	104.74 (s)
6-25b[p]	H	Me	P(O)Ph(OMe)	6.60 (d,4.2)[g]	6.29 (dd,4.0,0.5)[c]	7.39 (s)	5.32 (s)	1.91 (s)	3.80 (d,11.5)[m]	107.55 (s)
6-26a[q]	Me	H	P(O)Ph(OMe)	6.78 (d,4.2)[g]	6.42 (dd,4.2,1.4)[c]	7.42 (t,0.9)[f]	1.41 (d,1.6)[j]	7.63 (dd,3.4,0.9)[k]	3.33 (d,10.4)[m]	108.76 (s)
6-26b[q]	Me	H	P(O)Ph(OMe)	6.55 (d,4.2)[g]	6.31 (dd,4.2,1.4)[c]	7.37 (t,0.9)[f]	1.48 (d,1.6)[j]	7.46 (dd,3.1,0.9)[k]	3.66 (d,10.6)[m]	110.88 (s)
6-27a[r]	Me	Me	P(O)Ph(OMe)	6.62 (d,4.1)[g]	6.34 (dd,4.1,1.4)[c]	7.32 (d,0.6)[d]	1.44 (d,1.6)[j]	1.83 (s)	3.43 (d,10.5)[m]	110.78 (s)
6-27b[r]	Me	Me	P(O)Ph(OMe)	6.44 (d,4.1)[g]	6.23 (dd,4.1,1.4)[c]	7.29 (d,0.9)[d]	1.48 (d,1.6)[j]	1.87 (s)	3.66 (d,10.5)[m]	112.41 (s)

[a] ^{1}H NMR (300.1 MHz) chemical shifts in ppm relative to internal TMS; ^{31}P NMR (121.5 MHz) chemical shifts in ppm relative to external 85% H_3PO_4; Solvent = $CDCl_3$; m = multiplet; s = singlet; t = triplet; dd = doublet of doublets; dt = doublet of triplets; J values in Hz given in brackets. [b] $^3J(H_3H_4)$, $^4J(H_3H_5)$. [c] $^3J(H_4H_3)$, $^3J(H_4H_5)$. [d] $^3J(H_5H_4)$. [e] $^3J(HH_3)$. [f] $^3J(H_5H_4)$, $^4J(H_5H_3)$. [g] $^3J(H_3H_4)$. [h] P-Me, $^2J(PH)$. [i] $^3J(HH)$, $^4J(HH)$. [j] $^4J(PH)$. [k] $^4J(PH)$, $^4J(HH)$. [l] Phenyl Protons: 7.49 (m, 1H, H_{ortho}); 7.38 (m, 2H, H_{ortho}/H_{para}); 7.17 (m, 2H, H_{meta}). [m] P-OMe, $^3J(PH)$. [n] a/b = 57/43, phenyl protons: 6.96-7.29 ppm. [o] overlaps with H_5. [p] a/b = 53/47, phenyl protons: 6.89-7.24 ppm. [q] a/b = 51/49, phenyl protons: 6.78-7.14 ppm. [r] a/b = 50/50 phenyl protons: 6.80-7.05 ppm.

Table 6-3. ^{13}C NMR Data for $(\eta^5\text{-}C_5R_5)Co(R'\text{-}C(O)\text{-}C_4H_3N)(L)$ Complexes[a].

No.	R	R'	L	C_2	C_3	C_4	C_5	C=O	C*R'*=O	Cp/Cp*	Cp-*R*	P-Me/P-OMe
6-5	H	H	I	145.98	125.15	119.68	149.21	181.68		83.03		
6-6	H	Me	I	144.22	122.90	118.04	147.00	193.34	21.38	82.88		
6-7	Me	H	I	145.43	123.87	118.70	144.70	179.38		91.24	10.41	
6-8	Me	Me	I	143.79	121.65	117.10	142.75	190.85	21.91	91.07	10.40	
6-9	H	Me	PMe_3	144.54	123.84	119.58	149.44	193.47	21.23	87.91		15.06 (d,29.1)[b]
6-10	Me	H	PMe_3	146.40	125.88	120.66	145.73	180.55		96.52	9.69	12.12 (d,29.6)[b]
6-11	Me	Me	PMe_3	144.26	123.59	119.04	143.30	192.44	22.23	96.27	9.56	12.06 (d,30.0)[b]
6-17[c]	H	Me	$PPh(OMe)_2$	147.33	123.92	119.65	150.23	192.94	20.64	89.00		57.26 (d,8.3)[d] 56.55 (d,9.4)[d]
6-20	H	H	$P(O)(OMe)_2$	146.55	123.95	118.36	150.13	182.40		86.91		51.50 (d,9.8)[d]
6-21	H	Me	$P(O)(OMe)_2$	144.69	121.54	116.61	147.99	194.09	21.19	86.77		51.39 (d,6.4)[d]
6-22	Me	H	$P(O)(OMe)_2$	145.97	122.90	117.56	144.78	180.51		95.10	8.84	50.37 (d,8.7)[d]
6-23	Me	Me	$P(O)(OMe)_2$	144.20	120.51	115.84	142.86	192.01	21.89	94.92	8.91	50.31 (d,7.7)[d]
6-24a[e]	H	H	P(O)Ph(OMe)	145.95	123.87	118.29	149.52	181.90		87.39		51.07 (d,9.1)[d]
6-24b[f]	H	H	P(O)Ph(OMe)	145.39	123.87	118.71	149.52	181.24		87.21		52.29 (d,12.2)[d]
6-25a[g]	H	Me	P(O)Ph(OMe)	144.57	121.47	116.62	147.28	193.29	20.73	87.20		51.10 (d,7.5)[d]
6-25b[g]	H	Me	P(O)Ph(OMe)	144.25	121.54	117.11	147.51	192.47	20.65	87.04		52.01 (d,7.3)[d]
6-26a[h]	Me	H	P(O)Ph(OMe)	145.95	123.06	117.64	144.08	179.74		94.81	8.69	50.35 (d,11.6)[d]
6-26b[i]	Me	H	P(O)Ph(OMe)	145.39	122.86	117.93	144.08	179.40		94.81	8.69	51.43 (d,11.5)[d]
6-27a[j]	Me	Me	P(O)Ph(OMe)	144.12	120.67	115.90	141.98	191.21	21.29	94.66	8.69	50.55 (d,11.6)[d]
6-27b[k]	Me	Me	P(O)Ph(OMe)	143.74	120.52	116.20	141.98	190.64	21.70	94.66	8.69	51.24 (d,11.9)[d]

[a] ^{13}C NMR (75.47 MHz) chemical shifts in ppm relative to solvent $CDCl_3$ = 77.00; d = doublet; J values in Hz given in brackets. [b] P-Me, $^1J(PC)$. [c] phenyl carbons: 147.49 (C_{ipso}); 132.64 (C_{para}); 130.35, 130.20 (C_{ortho}); 128.82, 128.66 (C_{meta}). [d] P-OMe, $^2J(PC)$. [e] phenyl carbons: 129.76 (C_{ortho}); 129.61 (C_{ortho} & C_{para}); 127.58, 127.44 (C_{meta}). [f] phenyl carbons: 130.30, 130.17 (C_{ortho}); 129.39 (C_{para}); 127.11, 126.98 (C_{meta}). [g] phenyl carbons: 127.35-129.79. [h] phenyl carbons: 137.03 (d, 40.7, C_{ipso}); 130.20, 130.05 (C_{ortho}); 128.40 (C_{para}); 126.45, 126.33 (C_{meta}). [i] phenyl carbons: 135.40 (d, 43.6, C_{ipso}); 130.20, 130.05 (C_{ortho}); 128.17 (C_{para}); 126.71, 126.61 (C_{meta}). [j] phenyl carbons: 137.07 (d, 39.8, C_{ipso}); 129.57, 129.41 (C_{ortho}); 128.03 (C_{para}); 126.49, 126.34 (C_{meta}). [k] phenyl carbons: 136.23 (d, 40.2, C_{ipso}); 129.88, 129.72 (C_{ortho}); 128.22 (C_{para}); 126.61, 126.49 (C_{meta}).

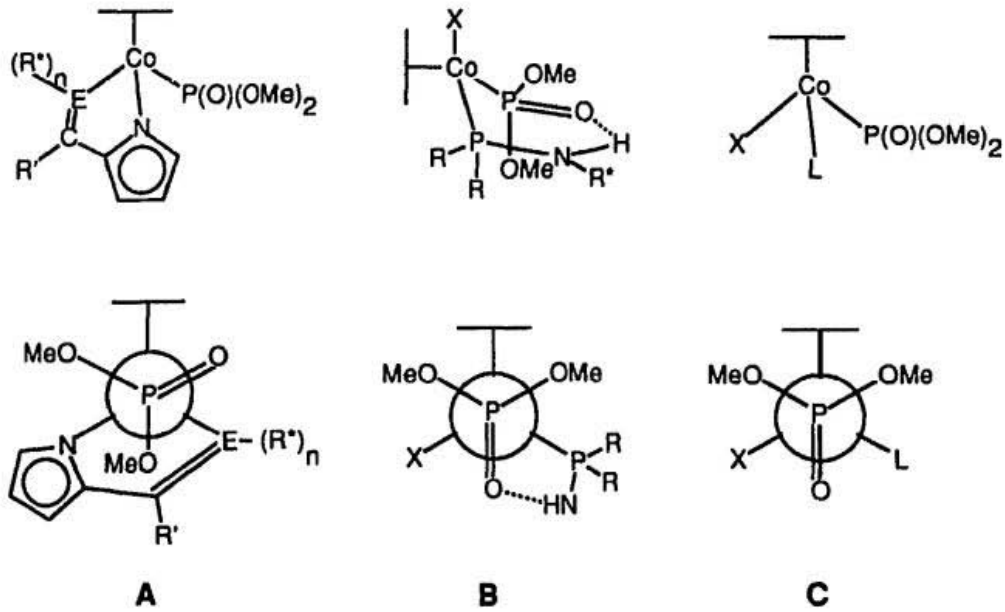

R = Ph, Et; R' = H, Me; R* = C*H(Me)Ph
E = O (n = 0), N (n = 1)
X = I, CF_3, C_3F_7; C_6F_{13}; $OCOCF_3$
L = PMe_3; $P(OMe)_3$; $PPhMe_2$
—— = C_5H_5; C_5Me_5; $C_5H_3(CHMe_2)$; C_9H_7

Scheme 6-4. Structure and Newman Projection along P(O)-Co Bond of Cobaltophosphonates.

Table 6-4 summarizes the ^1H NMR chemical shift difference ($\Delta\delta_{OMe} = \delta_{OMe}-\delta'_{OMe}$) for the diastereotopic P(O)(O<u>Me</u>)$_2$ groups in the chiral cobaltophosphonates. Examination of the diastereotopic chemical shift difference ($\Delta\delta_{OMe}$) suggests that $\Delta\delta_{OMe}$ may be a good diagnostic of the degree of asymmetry and for the solution conformation. The metallophosphonates can be divided into three groups with $\Delta\delta_{OMe}$ (Group A) >> $\Delta\delta_{OMe}$ (Group B) > $\Delta\delta_{OMe}$ (Group C) (cf. Table 6-4, Figure 6-1) according to their structures and their magnitudes of $\Delta\delta_{OMe}$. Group A consists of those complexes in which the

five-membered chelate ring and the pyrrolyl ring form a planar template and one of the OMe groups in $P(O)(OMe)_2$ is located over this plane (cf. Scheme 6-4A). As shown in the crystal structure of **6-23** (*vide infra*), one OMe group points toward the chelate plane, whereas the other points away from this plane. A significant population of this conformation establishes an anisotropic environment for the OMe's because of the ring current effect, which results in large $\Delta\delta_{OMe}$ values (111-249 Hz), as shown in Table 6-4 and Figure 6-1. Group B contains those complexes possessing an intramolecular P=O•••H bonding, which prevents rotation about the Co-P bond (cf. Scheme 6-4B). As a result, the OMe's sense a moderate anisotropic environment and have moderate $\Delta\delta_{OMe}$ values (15-45 Hz, Table 6-4 and Figure 6-1) compared to the group A complexes. Group C comprises those complexes in which all rotamers are significantly populated hence the diastereotopic OMe groups sense an average environment and have the smallest $\Delta\delta_{OMe}$ values. Note that almost all complexes in group C have $\Delta\delta_{OMe}$ less than 6 Hz, except for complexes (η^5-C_5Me_5)Co($P(OMe)_3$)(I)($P(O)(OMe)_2$) ($\Delta\delta_{OMe}$ = 12 Hz, entry C2 of Table 6-4), (η^5-$C_5H_3(CHMe_2)_2$)Co(PMe_3)($OCOCF_3$)($P(O)(OMe)_2$) ($\Delta\delta_{OMe}$ = 9 Hz, entry C3 of Table 6-4) and (η^5-C_9H_7)Co($PPhMe_2$)(C_3F_7)($P(O)(OMe)_2$) ($\Delta\delta_{OMe}$ = 18 Hz, entry C1 of Table 6-4). Because η^5-C_5Me_5 and η^5-$C_5H_3(CHMe_2)_2$ are bulkier than η^5-C_5H_5 and η^5-C_9H_7[310] and $PPhMe_2$ has a larger cone angle[302, 303] than the phosphines in the rest of the complexes in group C, the Co-$P(O)(OMe)_2$ rotamer populations are more skewed.

The conformational preferences for complexes **6-20 - 6-23** were studied using ^1H

nOed spectra (Table 6-5). When the two doublets of the methoxyl resonances on $P(O)(OMe)_2$ were irradiated separatedly, only the high field methoxyl group showed moderate enhancement of the pyrrolyl protons (H_5 and H_3). However, there was no enhancement observable of the pyrrolyl protons from the irradiation of the low field methoxyl group.

Table 6-4. Comparison of the ^{1}H NMR Difference for the Diastereotopic Methoxyl Group on $P(O)(OMe)_2$ in Cobaltophosponates.

Group	No.	Cobaltophosphonate L_n-Co-P(O)(OMe)$_2$		δ_{OMe} (ppm)	δ'_{OMe} (ppm)	$\Delta\delta_{OMe}$[a] (ppm)	(Hz)	ref
A	A1	**6-20**		3.66	2.97	0.69	207	b
	A2	**6-21**		3.65	2.93	0.72	216	b
	A3	**6-22**		3.59	2.76	0.83	249	b
	A4	**6-23**		3.54	2.77	0.77	231	b
	A5a	η^5-C_5H_5, N-N*[c]	S_{Co}	3.44	3.07	0.37	111	d
	A5b		R_{Co}	3.42	2.99	0.43	129	
	A6a	η^5-C_5Me_5, N-N*	S_{Co}	3.42	2.78	0.64	192	d
	A6b		R_{Co}	2.82	2.45	0.37	111	
B	B1a	η^5-C_5H_5, PNH*, I	S_{Co}	3.82	3.68	0.14	42	f
	B1b		R_{Co}	3.83	3.66	0.17	51	
	B2a	η^5-C_5Me_5, PNH, I	S_{Co}	3.79	3.70	0.09	27	g
	B2b		R_{Co}	3.77	3.64	0.13	39	
	B3a	η^5-C_5H_5, PNH, C_3F_7	R_{Co}	3.84	3.77	0.07	21	h
	B3b		S_{Co}	3.83	3.77	0.06	18	
	B4a	η^5-C_5H_5, PNH, CF_3	R_{Co}	3.82	3.77	0.05	15	h
	B4b		S_{Co}	3.82	3.77	0.05	15	
	B5a	η^5-C_9H_7, PNH, C_3F_7	R_{Co}	3.81	3.69	0.12	36	i
	B5b		S_{Co}	3.80	3.67	0.13	39	
	B6a	η^5-C_5H_5, PEtNH[j], C_3F_7	R_{Co}	3.75	3.60	0.15	45	i
	B6b		S_{Co}	3.76	3.68	0.08	24	
	B7a	η^5-C_9H_7, PEtNH, C_3F_7	R_{Co}	3.75	3.54	0.21	63	i
	B7b		S_{Co}	3.76	3.66	0.10	30	
	B8a	η^5-C_5H_5, PEtNH, I	S_{Co}	3.83	3.72	0.11	33	i
	B8b		R_{Co}	~84	3.72	0.12	36	
	B9a	η^5-C_5Me_5, PEtNH, I	S_{Co}	3.76	3.70	0.06	18	i
	B9b		R_{Co}	3.77	3.69	0.08	24	
C	C1	η^5-C_9H_7, $PPhMe_2$, C_3F_7		3.77	3.71	0.06	18	m
	C2	η^5-C_5Me_5, $P(OMe)_3$, I		3.68	3.64	0.04	12	k
	C3	η^5-$C_5H_3(CHMe_2)_2$, PMe_3, $OCOCF_3$		3.63	3.60	0.03	9	l
	C4	η^5-C_5H_5, $P(OMe)_3$, I		3.75	3.74	0.01	3	k
	C5	η^5-C_5H_5, $P(OMe)_3$, PMe_3		3.72	3.70	0.02	6	l
	C6	η^5-C_5H_5, $P(OMe)_3$, C_3F_7		3.67	3.66	0.01	3	m
	C7	η^5-C_5H_5, PMe_3, C_3F_7		3.67	3.66	0.01	3	m
	C8	η^5-C_9H_7, $P(OMe)_3$, C_3F_7		3.65	3.64	0.01	3	m
	C9	η^5-C_9H_7, $P(OMe)_3$, C_6F_{13}		3.66	3.64	0.02	6	m
	C10	η^5-C_9H_7, PMe_3, C_3F_7		3.65	3.63	0.02	6	m

[a] $\Delta\delta_{OMe} = \delta_{OMe} - \delta'_{OMe}$, operating frequency 300.1 MHz. [b] this work. [c] N-N* = (*S*)-C_4H_3N-C=N-CH(Me)Ph. d[264]. [e] PNH = (*S*)-PPh_2-NH-CH(Me)Ph. f[206]. g[207]. h[206]. [i] *cf.* Chapter 7. [j] PEtNH = (*S*)-PEt_2-NH-CH(Me)Ph. k[308]. l[306]. [m] *cf.* Chapter 3[315].

Table 6-5. Comparison of the ^1H nOed Data in $CDCl_3$ at 25 °C for Irradiating the Two Doublets on $P(O)(OMe)_2$.

Cpd	H_5	H_3	P-OMe (low field)	P-OMe (high field)
6-20	No enhancement	-	*	
6-20	1.1	0.8		*
6-21	No enhancement	-	*	
6-21	0.9	-		*
6-22	No enhancement	-	*	
6-22	0.9	0.9		*
6-23	No enhancement	-	*	
6-23	1.0	-		*

* The irradiated resonance.

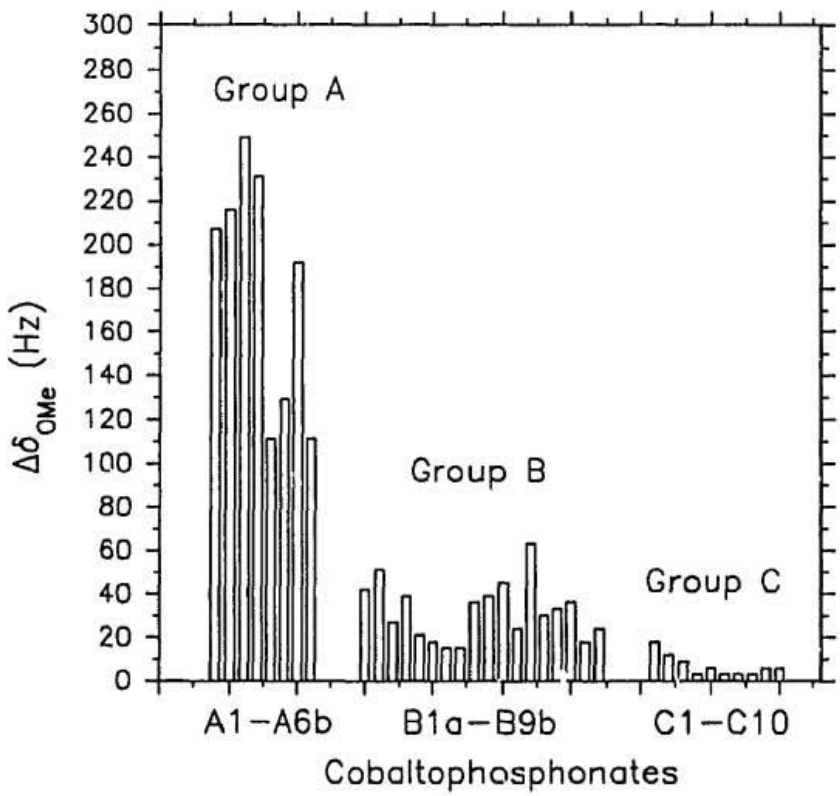

Figure 6-1. Bar Plot of the ^1H NMR Difference ($\Delta\delta_{OMe}$) for the Diastereotopic $P(O)(O\underline{Me})_2$ for Cobaltophosphonates (cf. Table 6-4).

6.2.4. Arbuzov Dealkylation Reaction between (η^5-C_5R_5)Co(R'C(O)-C_4H_3N)(I) and PPh(OMe)$_2$: Isolation of a Reaction Intermediate. As discussed above reactions between (η^5-C_5H_5)Co(R'C(O)-C_4H_3N)(I) (**6-5**, **6-6**) and PPh(OMe)$_2$ proceeded readily at room temperature to give cobaltophosphinates, (η^5-C_5H_5)Co(R'C(O)-C_4H_3N)(P(O)Ph(OMe)) (**6-24a,b; 6-25a,b**). The reaction proceeded via formation of a cationic intermediate followed by Arbuzov dealkylation. The cationic intermediates, [(η^5-C_5H_5)Co(R'C(O)-C_4H_3N)(PPh(OMe)$_2$)]$^+$ (**6-16, 6-17**), were detected by ^{1}H NMR in acetone-d_6 at room temperature (Scheme 6-1) (**6-16**, Cp: 5.94 ppm, PPh(OMe)$_2$: 4.02 ppm (d, 11.5 Hz), 3.94 ppm (d,11.0 Hz); **6-17**, Cp: 5.96 ppm, PPh(OMe)$_2$: 4.04 ppm (d,11.9 Hz), 3.96 ppm (d, 11.5 Hz)). Cation **6-17** was readily isolated from benzene at room temperature. Reactions between (η^5-C_5Me_5)Co(R'C(O)-C_4H_3N)(I) (**6-7, 6-8**) and PPh(OMe)$_2$ were very slow compared to the cyclopentadienyl substrates and extended reflux in benzene was necessary to obtain the pentamethylcyclopentadienyl cobaltophosphinates, (η^5-C_5Me_5)Co(R'C(O)-C_4H_3N)(P(O)Ph(OMe) (**6-26a,b; 6-27a,b**). Chiral induction from Co*→P was very low (0-14%) compared to other systems,[206, 217, 218, 308, 318] possibly because of the small asymmetry in the coordination sphere.

Chromatographic separation of diastereomers from the reactions between (η^5-C_5R_5)Co(R'C(O)-C_4H_3N)(I) (**6-5, 6-6, 6-7**, or **6-8**) and PPh(OMe)$_2$ was unsuccessful. However, these diastereomers can be distinguished easily by NMR spectroscopy. Complexes **6-24a,b, 6-25a,b, 6-26a,b,** and **6-27a,b** were characterized by IR, and

multinuclear NMR as diastereomeric mixtures. Their $\nu_{C=O}$ and $\nu_{P=O}$ (Table 6-1) appeared in the range of 1546-1564 cm^{-1} and 1135-1144 cm^{-1}, respectively, similar to those of the cobalophosphonates discussed above. ^1H NMR spectra (Table 6-2) of the individual diastereomers in the product mixtures were assigned using ^1H nOed spectra and confirmed by comparison with the spectra of other cobaltophosphinates.[308, 318] Their ^1H NMR spectra showed similar resonances for Cp/Cp* and the pyrrolyl protons as their reaction precursors (**6-5 - 6-8**) and relevant cobaltophosphonates (**6-20 - 6-23**). They also exibited a doublet assigned to the methoxyl group on P(O)Ph(OMe) in the range of 3.3-3.8 ppm ($^3J_{PH} = 11.0 \pm 0.5$). The ^{13}C NMR spectra were assigned on the basis of their 2-D $^1H/^{13}C$ ^1J heterocorrelation spectra, and the data are tabulated in Table 6-3, which shows characteristic resonances for the η^5-Cp/Cp* piano-stool cobaltophosphinates.[308, 318]

6.2.5. Crystal Structure of (η^5-C_5Me_5)Co(MeC(O)-C_4H_3N)(Y) (Y = I (6-8), P(O)(OMe)$_2$ (6-23)). In order to determine whether the C=O group is coordinated to cobalt in an η^1 or an η^2 fashion, X-ray crystal structures of complexes **6-8** and **6-23** were obtained. Both structures were solved using direct methods and refined using full-matrix least-squares method. The solution of the structure for complex **6-8** was complicated by two kinds of disorder in the crystal. First, the pentamethylcyclopentadienyl group appears to be freely rotating and some difficulties were encountered in positioning and subsequently refining the methyl groups. Second, the molecule is positioned on a glide plane with Co and I actually in the

plane and *both enantiomers* are able to occupy the same position, but not simultaneously, in the cell (Figure 6-2b). PLUTO representations for both **6-8** and **6-23** are shown in Figures 6-2 and 6-3. Selected bond distances, bond angles and atomic coordinates are given in Tables 6-5, 6-6, and 6-7. The coordination sphere of cobalt for both **6-8** and **6-23** is distorted octahedral with η^5-C_5Me_5 occupying three *fac* coordination sites. Interligand bond angles in both structures (I(1)-Co(1)-N(1), I(1)-Co(1)-O(1), O(1)-Co(1)-N(1) for complex **6-8** and P(1)-Co(1)-N(1), P(1)-Co(1)-O(4), O(4)-Co(1)-N(1) for complex **6-23**) are all close to 90°. The 2-acylpyrrolyl C=O group in both complexes is η^1 coordinated to cobalt. As a result, the chelate planes formed by Co(1)-O(1 or 4)-C(15)-C(14)-N(1) and the pyrrolyl ring in both complexes are coplanar as found in other similar complexes reported previously (cf. Chapter 5).[306, 316] The $P(O)(OMe)_2$ in complex **6-23** adopts the solid state conformation with the P=O bond gauche to the C_5Me_5 and one of the methoxyl groups pointing toward the pyrrolyl plane, as shown in Figure 6-3 and Scheme 6-4A.

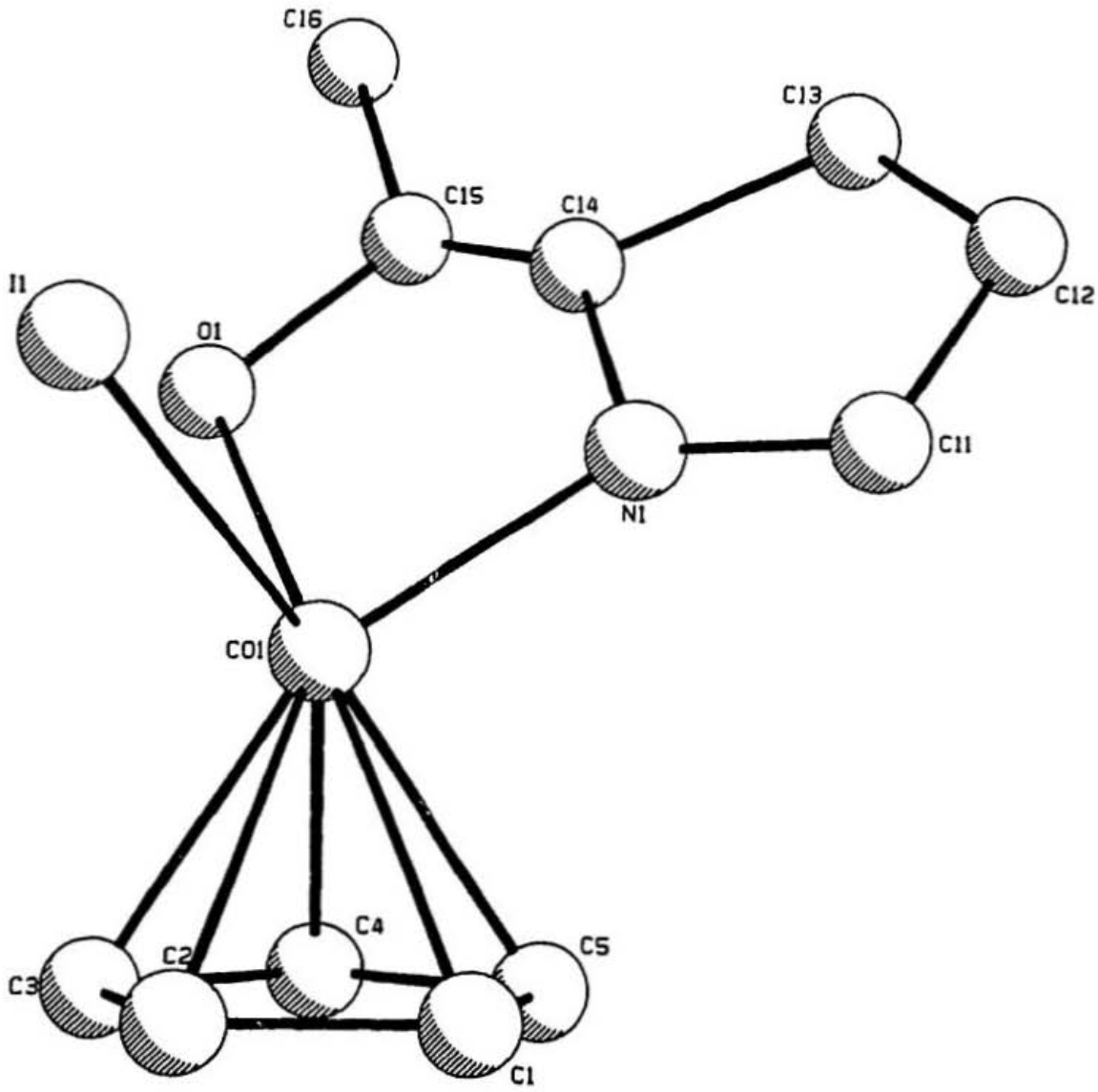

Figure 6-2a. Pluto Representation of (η^5-C_5Me_5)Co(MeC(O)-C_4H_3N)(I), **6-8** (Me Omitted and only One Cp ring shown).

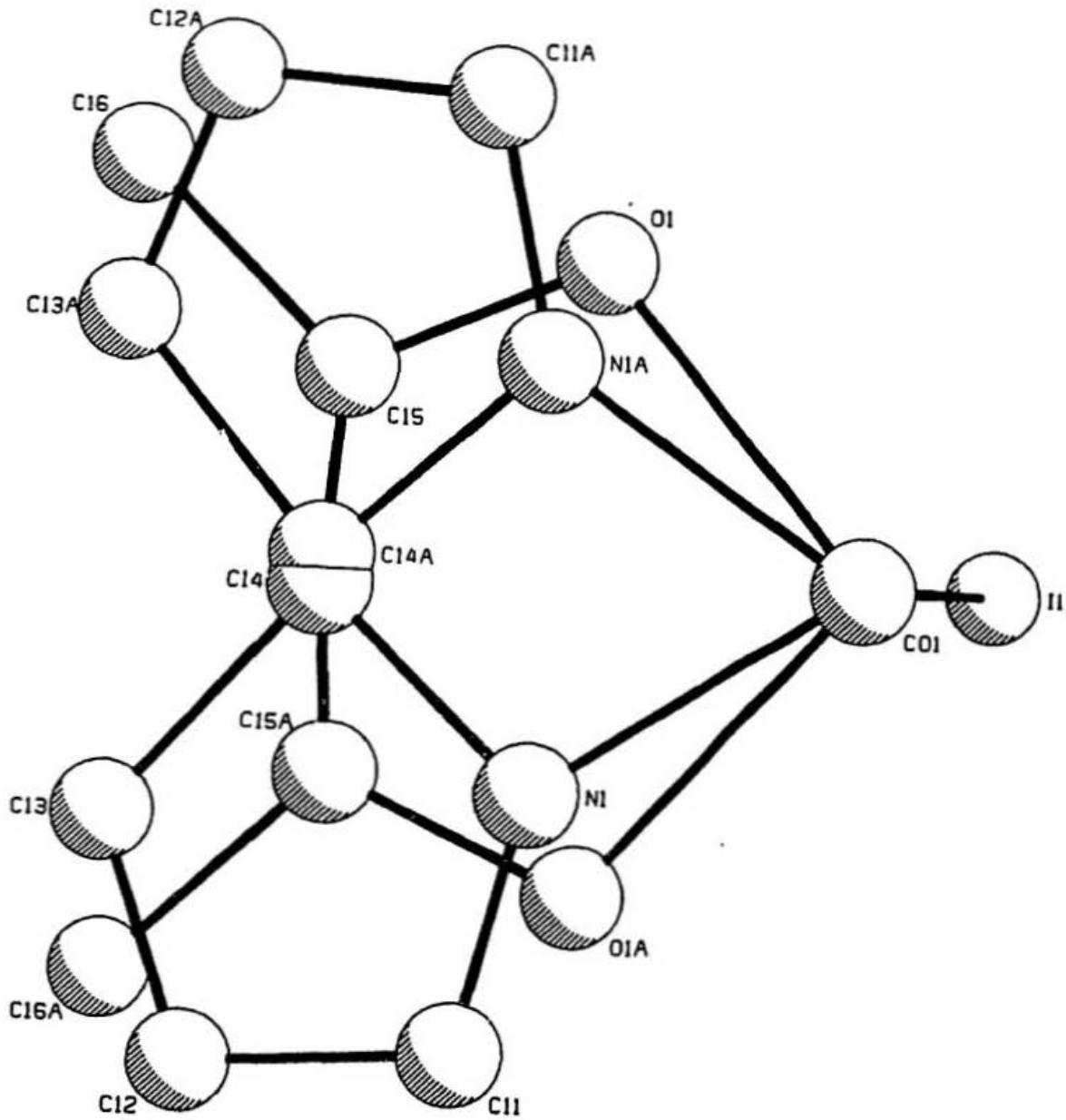

Figure 6-2b. Pluto Representation of the two enantiomers Occupying the Same Position in the Cell of (η^5-C_5Me_5)Co(MeC(O)-C_4H_3N)(I), **6-8** (C_5Me_5 Omitted for Clarity).

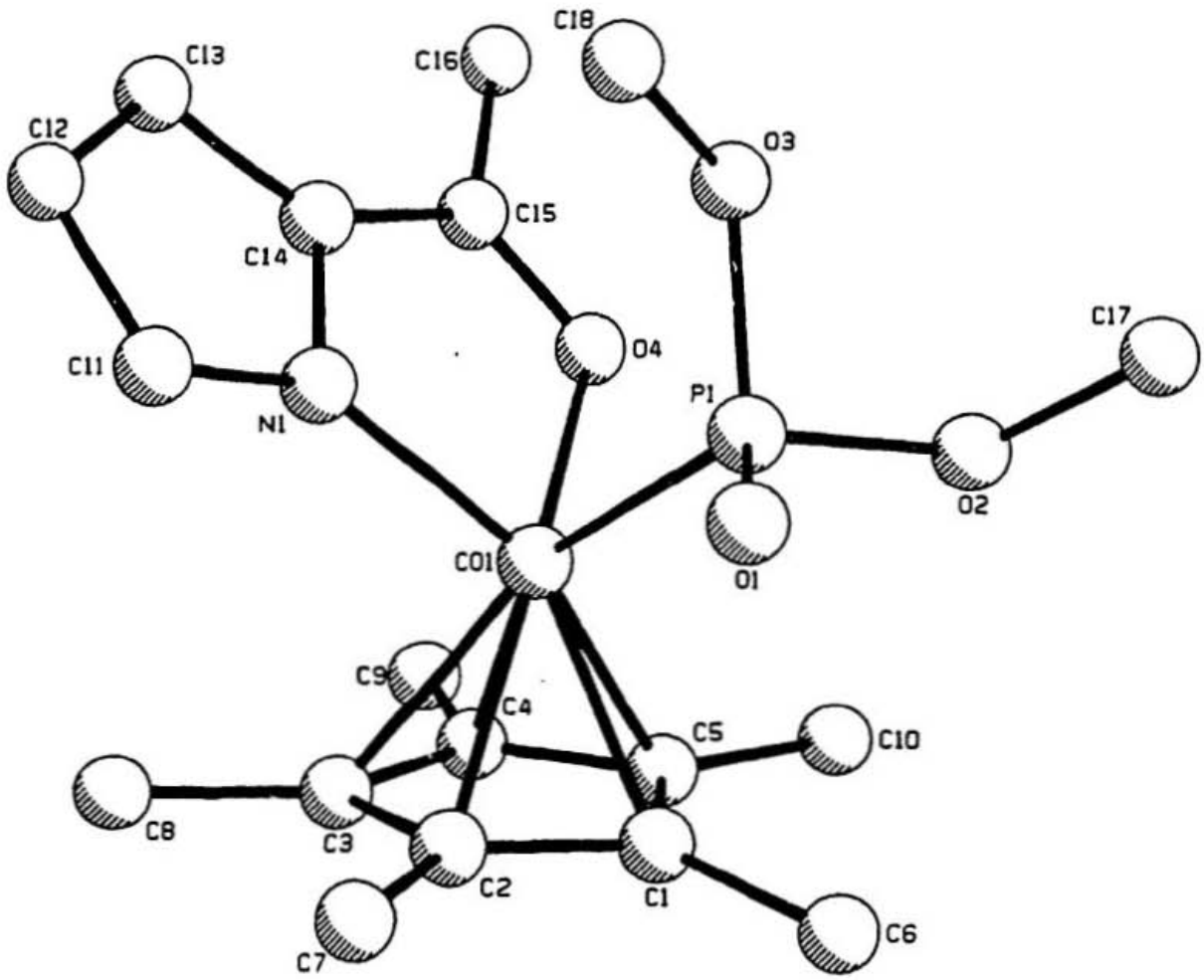

Figure 6-3. Pluto Representation of $(\eta^5\text{-}C_5Me_5)Co(MeC(O)\text{-}C_4H_3N)(P(O)(OMe)_2)$, **6-23**.

Table 6-6. Selected Bond Distances (Å) and Bond Angles (°) for Complexes **6-8** and **6-23**.

6-8		6-23	
	Bond Distances		
I(1)-Co(1)	2.563(1)	Co(1)-P(1)	2.195(1)
Co(1)-O(1)	2.07(2)	Co(1)-O(4)	1.970(2)
Co(1)-N(1)	1.89(3)	Co(1)-N(1)	1.928(3)
O(1)-C(15)	1.38(3)	Co(1)-C(1)	2.077(3)
N(1)-C(14)	1.48(7)	Co(1)-C(2)	2.039(3)
C(14)-C(15)	1.08(8)	Co(1)-C(3)	2.126(4)
C(15)-C(16)	1.57(5)	Co(1)-C(4)	2.110(4)
		Co(1)-C(5)	2.058(3)
		P(1)-O(1)	1.481(3)
		P(1)-O(2)	1.610(3)
		P(1)-O(3)	1.613(3)
		O(4)-C(15)	1.274(4)
		N(1)-C(14)	1.392(4)
		C(14)-C(15)	1.395(5)
		C(15)-C(16)	1.500(5)
	Bond Angles		
I(1)-Co(1)-O(1)	88.1(7)	P(1)-Co(1)-O(4)	92.34(8)
I(1)-Co(1)-N(1)	95.0(9)	P(1)-Co(1)-N(1)	90.37(9)
O(1)-Co(1)-N(1)	82(1)	O(4)-Co(1)-N(1)	83.1(1)
Co(1)-O(1)-C(15)	108(2)	Co(1)-P(1)-O(1)	118.3(1)
Co(1)-N(1)-C(11)	137(2)	Co(1)-P(1)-O(2)	104.6(1)
Co(1)-N(1)-C(14)	105(3)	Co(1)-P(1)-O(3)	110.5(1)
N(1)-C(14)-C(15)	129(4)	Co(1)-O(4)-C(15)	112.3(2)
O(1)-C(15)-C(14)	116(3)	Co(1)-N(1)-C(11)	142.1(3)
		Co(1)-N(1)-C(14)	111.4(2)
		N(1)-C(14)-C(15)	114.3(3)
		O(4)-C(15)-C(14)	118.7(3)

Table 6-7. Atomic Coordinates for (η^5-C_5Me_5)Co(Me-C(O)-C_4H_3N)(I), **6-8**.

Atom	x	y	z	B(eq)	Occupancy
I(1)	0.97715(3)	1/4	0.19808(8)	9.81(5)	1/2
Co(1)	1.05409(5)	1/4	-0.0956(1)	4.98(5)	1/2
O(1)	1.123(2)	0.362(2)	0.006(3)	6(1)	1/2
N(1)	1.139(2)	0.174(2)	-0.011(4)	5(1)	1/2
C(6)	1.154(1)	0.173(2)	-0.422(2)	12(1)	1/2
C(7)	1.099(1)	0.110(2)	-0.405(3)	14(2)	1/2
C(8)	1.022(2)	0.036(1)	-0.270(3)	15(2)	1/2
C(9)	0.929(2)	0.100(2)	-0.235(3)	15(2)	1/2
C(10)	0.872(1)	0.177(2)	-0.172(3)	16(2)	1/2
C(11)	1.156(1)	0.082(1)	0.002(2)	7(1)	1/2
C(12)	1.229(2)	0.073(3)	0.080(4)	9(2)	1/2
C(13)	1.254(2)	0.159(2)	0.125(4)	8(1)	1/2
C(14)	1.198(2)	0.246(6)	0.062(4)	10(1)	1/2
C(15)	1.192(1)	0.323(1)	0.072(2)	4.6(9)	1/2
C(16)	1.250(2)	0.399(4)	0.154(4)	9(2)	1/2
C(1)	0.998(2)	0.1449(8)	-0.268(3)	3.9(5)	1/4
C(2)	0.9465(7)	0.223(2)	-0.235(2)	3.7(6)	1/4
C(3)	0.985(2)	0.308(1)	-0.292(3)	2.9(4)	1/4
C(4)	1.059(1)	0.283(2)	-0.360(3)	5.5(7)	1/4
C(5)	1.067(1)	0.182(2)	-0.345(2)	3.6(6)	1/4
C(1A)	1.0806(7)	0.217(2)	-0.357(2)	3.3(6)	1/4
C(2A)	1.038(2)	0.3030(8)	-0.332(3)	4.1(6)	1/4
C(3A)	0.964(1)	0.279(2)	-0.259(3)	6.5(8)	1/4
C(4A)	0.961(1)	0.178(2)	-0.239(2)	3.5(4)	1/4
C(5A)	1.033(2)	0.1394(7)	-0.299(3)	4.0(4)	1/4

Table 6-8. Atomic Coordinates for (η^5-C_5Me_5)Co(Me-C(O)-C_4H_3N)(P(O)$(OMe)_2$), **6-23**.

Atom	x	y	z	B(eq)
Co(1)	0.28185(4)	0.01249(5)	0.28234(3)	2.35(2)
P(1)	0.16016(9)	0.1284(1)	0.18665(6)	3.26(4)
O(1)	0.2040(3)	0.2003(3)	0.1256(2)	5.1(1)
O(2)	0.0595(2)	0.0256(3)	0.1444(2)	4.7(1)
O(3)	0.0875(2)	0.2270(3)	0.2275(2)	4.1(1)
O(4)	0.1710(2)	-0.0095(2)	0.3464(1)	3.1(1)
N(1)	0.3241(2)	0.1691(3)	0.3492(2)	2.6(1)
C(1)	0.3215(3)	-0.1034(4)	0.1928(2)	3.0(2)
C(2)	0.4184(3)	-0.0289(4)	0.2394(2)	3.1(2)
C(3)	0.4474(3)	-0.0743(4)	0.3231(2)	3.1(2)
C(4)	0.3649(3)	-0.1661(4)	0.3295(2)	3.1(2)
C(5)	0.2847(3)	-0.1833(3)	0.2492(2)	3.1(2)
C(6)	0.2753(4)	-0.1073(5)	0.1002(2)	5.1(2)
C(7)	0.4836(4)	0.0702(4)	0.2047(3)	5.0(2)
C(8)	0.5501(4)	-0.0295(5)	0.3904(3)	5.4(2)
C(9)	0.3566(4)	-0.2336(4)	0.4071(3)	5.2(2)
C(10)	0.1835(4)	-0.2757(4)	0.2286(3)	5.4(2)
C(11)	0.3945(3)	0.2729(4)	0.3614(2)	3.6(2)
C(12)	0.3820(4)	0.3501(4)	0.4276(3)	4.1(2)
C(13)	0.3001(4)	0.2909(4)	0.4566(2)	3.8(2)
C(14)	0.2638(3)	0.1782(4)	0.4076(2)	2.9(1)
C(15)	0.1819(3)	0.0793(4)	0.4016(2)	3.3(2)
C(16)	0.1056(4)	0.0726(5)	0.4572(3)	5.6(2)
C(17)	-0.0425(4)	0.0719(6)	0.0856(3)	7.2(3)
C(18)	0.1129(4)	0.3655(5)	0.2360(3)	6.0(2)

6.3. Experimental Section

6.3.1. Reagents and Methods. All manipulations were performed under the similar conditions as described in the preceeding chapters. NaH (95%), 2-formylpyrrole (HC(O)-C_4H_3NH, **6-3**H) and 2-acetylpyrrole (Me-C(O)-C_4H_3NH, **6-4**H) were purchased from Aldrich and used as received. Complexes (η^5-C_5R_5)Co(CO)$(I)_2$ (R=H, **6-1**; R=Me, **6-2**)[362, 363] were prepared using the established procedures.

6.3.2. Crystal Structure Determination of (η^5-C_5Me_5)Co(Me-C(O)-C_4H_3N)(Y), (Y = I, 6-8; Y = P(O)(OMe)$_2$, 6-23). Crystal data collection, structure refinement are similar to those described in the preceeding chapters. The space groups Pnma (#62) (**6-8**) and $P2_1/c$ (#14) (**6-23**) were assigned on the basis of systematic absences (0k1: k+1 ≠ 2n and hk0: h ≠ 2n for **6-8**; h01: l ≠ 2n and 0k0: k≠2n for **6-23**) and on the successful solution and refinement of both structures. Further details are given in Table 6-9.

6.3.3. Synthesis of Complexes.

6.3.3.1. Synthesis of (η^5-C_5R_5)Co(R'-C(O)-C_4H_3N)(I), 6-5 - 6-8. As summarized in Table 6-10, complexes **6-5 - 6-8** used a similar procedure as for the synthesis of **6-5**. Excess NaH was added to a 100 mL of THF solution of 2-formylpyrrole (**6-3H**, 174.6 mg, 1.836 mmol) with stirring at room temperature. After evolution of hydrogen gas

ceased, the reaction was stirred for about 60 minutes. The solution was filtered through a glass frit fitted with a 2 cm plug of Celite and washed with THF (3x20 mL). The combined filtrate and washings (**6-3**) were dropped into a 100 mL of THF solution of $(\eta^5\text{-}C_5H_5)Co(CO)(I)_2$ (**6-1**, 731.7 mg, 1.803 mmol) with stirring at room temperature by means of a pressure equivalent dropping funnel over a 20 minute period. The solution color changed from purple to blue. After stirring for another 60 minutes the solvent was evaporated under vacuum. The resulting blue sticky residue was extracted with 50 mL of dichloromethane and passed through a glass frit fitted with a 10 cm silica gel (230-400 mesh) plug. Evaporation of the solvent left the crude product, which was purified by radial thick layer chromatography eluting with dichloromethane/benzene (4/1, v/v). Removal of the solvent from the first blue band left a dark blue crystalline solid (447.9 mg, 72%). Slow diffusion of hexane into the a dichloromethane solution of **6-8** afforded dark blue prisms suitable for X-ray structure determination.

6.3.3.2. Synthesis of $[(\eta^5\text{-}C_5R_5)Co(R'\text{-}C(O)\text{-}C_4H_3N)(PMe_3)]^+I^-$, 6-9 - 6-11. Preparation of complexes **6-9 - 6-11** used a procedure similar to that described for **6-9** (cf. Table 6-10). PMe_3 (14.9 mg, 0.196 mmol) was added via syringe to 15 mL of benzene solution of **6-6** (50.8 mg, 0.141 mmol) with stirring at room temperature. A deep red precipitate formed leaving a clear colorless solution. The precipitate was collected on a glass frit and washed with benzene (3x5 mL) and then pentane (3x5 mL). The product was dried in the air for several hours to give a deep red powder (58.5 mg,

95%).

6.3.3.3. Synthesis of [(η^5-C_5H_5)Co(Me-C(O)-C_4H_3N)(PPh(OMe)$_2$)]I, An Arbuzov reaction intermediate, 6-17. Excess PPh(OMe)$_2$ (96.0 mg, 0.564 mmol) was added quickly via syringe to a benzene (15 mL) solution of **6-6** (156.1 mg, 0.435 mmol) with stirring at room temperature. After stirring for about 10 minutes the solution color changed from blue to deep red, and some deep red precipitate formed. The precipitate was collected on a glass frit and washed with benzene (5x5 mL) and then pentane (5x5 mL). After drying in air for several hours a deep red powder was obtained (159.9 mg, 70%).

6.3.3.4. Synthesis of (η^5-C_5R_5)Co(R'-C(O)-C_4H_3N)(P(O)(OMe)$_2$), 6-20 - 6-23. The synthesis for complex **6-21** is representative. Details of the reaction conditions for other complexes are given in Table 6-10. Excess P(OMe)$_3$ (224.0 mg, 1.805 mmol) was added to a 30 mL benzene solution of **6-6** (358.3 mg, 0.9979 mmol) via syringe with stirring at room temperature. After stirring overnight volatiles were removed from the red solution at water aspirator pressure to leave a red sticky product. The crude product was purified by radial thick layer chromatography. Initial acetone elution removed a high Rf yellow band. Continued elution with acetone/methanol (10/1, v/v) separated a red band of the product. Removal of the solvent with water aspirator and then oil pump vacuum afforded a red solid (333.2 mg, 98%). Slow diffusion of hexane into a chloroform solution of **6-23** at room temperature afforded deep red prisms

suitable for X-ray structure determination.

6.3.3.5. Synthesis of ***(η^5-C_5R_5)Co(R'-C(O)-C_4H_3N)(P(O)Ph(OMe)), 6-24 - 6-27.*** The synthesis of **6-26** is typical. Similar procedures were used for complexes **6-24 - 6-27** (cf. Table 6-10). Excess $PPh(OMe)_2$ (65.0 mg, 0.382 mmol) was added to a benzene (20 mL) solution of **6-7** (72.0 mg, 0.173 mmol) via syringe with stirring at room temperature. Overnight reflux resulted in a color change from blue to red. TLC showed that the reaction was complete and the two diastereomers (distinguishable by NMR) could not be separated. Removal of volatiles at water aspirator pressure left a sticky residue which was chromatographed on a radial thick layer plate eluting with acetone/methanol (20/1, v/v). Removal of solvent from the first red band left a red solid (70.7 mg, 92%).

Table 6-9. Summary of Crystallographic Data for **6-8** and **6-23**.

	6-8	**6-23**
Formula	$C_{18}H_{21}ONICo$	$C_{18}H_{27}NO_4PCo$
F.W.(g/mol)	429.19	411.32
Crystal Habit	Dark-blue prism	Deep-red prism
Crystal Size (mm)	0.40x0.30x0.20	0.40x0.30x0.10
Crystal System	orthorhombic	monoclinic
No.Reflections used for unit cell determination(2θ range)	23 (24.4 - 43.3°)	25 (40.3 - 45.2°)
Omega Scan Peak Width at Half-height	0.32	0.33
Lattice Parameters		
a (Å)	16.809(3)	12.183(1)
b (Å)	13.755(5)	10.100(2)
c (Å)	7.535(2)	16.915(2)
β (°)	--	106.559(9)
V (Å^3)	1742(1)	1995.1(4)
Space Group	Pnma (#62)	$P2_1/c$ (#14)
Z	4	4
D_{calcd}(g/cm^3)	1.636	1.369
F_{000}	848	864
μ(MoKα)(cm^{-1})	27.33	9.56
Scan Width(°)	1.73 + 0.30 tanθ	1.10 + 0.30 tanθ
$2\theta_{max}$ (°)	50.0	50.0
No.Reflections Measured		
Total	1792	3911
Unique	--	3729
R_{int}	--	0.022
Corrections[a]	Lorentz-polarization Absorption	
trans.factors:	0.90-1.00	0.85-1.00
secondary extinction coeff.	0.19265x10^{-6}	--
Function Minimized	$\Sigma w(\|Fo\|-\|Fc\|)^2$	$\Sigma w(\|Fo\|-\|Fc\|)^2$
Least-squares weights	$4Fo^2/\sigma^2(Fo^2)$	$4Fo^2/\sigma^2(Fo^2)$
p-factor	0.01	0.01
Anomalous Dispersion	All non-hydrogen atoms	
No.Observations (I>3.00σ(I))	1096	2716
No.Variables	153	226
Reflection/Parameter Ratio	7.16	12.02
R[b]	0.038	0.036
R_w[c]	0.033	0.039
Goodness of Fit Indicator[d]	2.54	2.31
Max Shift/Error in Final Cycle	0.09	0.00
Maximum Peak in Final Diff. Map(e$^-$/Å^3)	0.58	0.30
Minimum Peak in Final Diff. Map(e$^-$/Å^3)	-0.57	0.33

[a] cf. *reference*[306]. [b] $R=\Sigma||Fo|-|Fc||/\Sigma|Fo|$.

[c] $R_w=[(\Sigma w(|Fo|-|Fc|)^2/\Sigma wFo^2)]^{1/2}$

[d] $GOF=(\Sigma(|Fo|-|Fc|)/\sigma)/(n-m))$ where n=#reflections, m=#variables, and σ^2=variance of (|Fo|-|Fc|)

Table 6-10. Reaction and Separation Condition for the Synthesis of $(\eta^5\text{-}C_5H_5)Co(R'\text{-}C(O)\text{-}C_4H_3N)(L)$ Complexes.

No.	R	R'	L	Amount of Reactants	Solvent	Temp. (°C)	Time (hr)	Purification	Amount of Product
6-5	H	H	I	**6-1**, 0.7317g (1.803 mmol) **6-3H**, 0.1746g (1.836 mmol)	THF (260 mL)	22	1.5	10 cm silica gel column (CH_2Cl_2), and then radial plate chromatography (CH_2Cl_2/benzene, 4/1)	0.4479g (72%)
6-6	H	Me	I	**6-1**, 1.0644g (2.623 mmol) **8-4H**, 0.2906g (2.663 mmol)	THF (300 mL)	22	1.0	10 cm silica gel column (CH_2Cl_2)	0.7338g (78%)
6-7	Me	H	I	**6-2**, 1.1747g (2.468 mmol) **6-3H**, 0.2395g (2.518 mmol)	THF (200 mL)	22	0.5	10 cm silica gel column (CH_2Cl_2)	0.6661g (65%)
6-8	Me	Me	I	**6-2**, 1.0252g (2.154 mmol) **6-4H**, 0.2430g (2.227 mmol)	THF (250 mL)	22	0.5	10 cm silica gel column (CH_2Cl_2)	0.6906g (75%)
6-9	H	Me	PMe_3	**6-6**, 0.0508g (0.141 mmol) PMe_3, 0.0149g (0.196 mmol)	benzene (15 mL)	22	0.2	filter with glass frit, wash with benzene (3x5 mL) & pentane (3x5 mL)	0.0585g (95%)
6-10	Me	H	PMe_3	**6-7**, 0.0660g (0.159 mmol) PMe_3, 0.0302g (0.397 mmol)	benzene (15 mL)	22	10	same as above	0.0672g (86%)
6-11	Me	Me	PMe_3	**6-8**, 0.0699g (0.163 mmol) PMe_3, 0.1000g (1.31 mmol)	benzene (15mL)	22	0.5	take off the volatiles with high vacuum	0.0815g (99%)
6-17	H	Me	$PPh(OMe)_2$	**6-6**, 0.1561g (0.435 mmol) $PPh(OMe)_2$, 0.0960g (0.564 mmol)	benzene (15 mL)	22	0.2	filter with glass frit, wash with benzene (5x5 mL) & pentane (5x5 mL)	0.1599g (70%)
6-20	H	H	$P(O)P(OMe)_2$	**6-5**, 0.0400g (0.116 mmol) $P(OMe)_3$, 0.0242g (0.195 mmol)	benzene (15 mL)	22	15	radial plate chromatography (acetone first, then methanol)	0.0226g (60%)

Table 6-10. contd.

6-21	H	Me	$P(O)P(OMe)_2$	**6-6**, 0.3583g (0.9979 mmol) $P(OMe)_3$, 0.2240g (1.805 mmol)	benzene (30 mL)	22	15	radial plate chromatography (acetone first, then acetone/methanol (10/1))	0.3332g (98%)
6-22	Me	H	$P(O)(OMe)_2$	**6-7**, 0.1083g (0.2610 mmol) $P(OMe)_3$, 0.0513g (0.413 mmol)	benzene (20 mL)	80	3	radial plate chromatography (acetone first, then methanol)	0.0977g (94%)
6-23	Me	Me	$P(O)(OMe)_2$	**6-8**, 0.1133g (0.2640 mmol) $P(OMe)_3$, 0.0484g (0.390 mmol)	benzene (20 mL)	80	6	radial plate chromatography (acetone first, then methanol)	0.1010g (93%)
6-24	H	H	P(O)Ph(OMe)	**6-5**, 0.0449g (0.130 mmol) $PPh(OMe)_2$, 0.0351g (0.206 mmol)	benzene (20 mL)	22	5.5	radial plate chromatography (acetone/methanol (25/3))	0.0342g (71%) a/b=57/43
6-25	H	Me	P(O)Ph(OMe)	**6-6**, 0.1538g (0.4281 mmol) $PPh(OMe)_2$, 0.0865g (0.508 mmol)	benzene/ CH_2Cl_2 (30/10 mL)	22	15	take off the volatiles with high vacuum	0.1576g (95%) a/b=53/47
6-26	Me	H	P(O)Ph(OMe)	**6-7**, 0.0720g (0.173 mmol) $PPh(OMe)_2$, 0.0650g (0.382 mmol)	benzene (20 mL)	80	15	radial plate chromatography (acetone/methanol (20/1))	0.0707g (92%) a/b=51/49
6-27	Me	Me	P(O)Ph(OMe)	**6-8**, 0.0742g (0.173 mmol) $PPh(OMe)_2$, 0.0650g (0.382 mmol)	benzene (20 mL)	80	15	radial plate chromatography (acetone/methanol (20/1))	0.0786g (99%) a/b=50/50

Chapter 7

Diastereomeric Cyclopentadienyl and Pentamethylcyclopentadienyl Cobaltophosphonates and Phosphinates: Arbuzov Reactions of $(\eta^5\text{-}C_5R_5)Co(X)(PEt_2NHC^*H(Me)Ph)(I)$ (X = I, C_3F_7) with $PR'(OMe)_2$ (R' = OMe, Ph).

7.1. Introduction

In order to investigate the steric effect of the spectator ligands on Co* → P chiral induction, a series of isostructural templates, $(\eta^5\text{-}C_5R_5)Co(X)(PEt_2NHC^*H(Me)Ph)(I)$ (X = I, C_3F_7) which give Arbuzov chemistry analogous to $(\eta^5\text{-}Cp)Co(X)(PPh_2NHC^*H(Me)Ph)(I)$ (R' = OMe, Ph),[206, 207, 217] were examined. In particular this chapter focuses on the "transmitter" effect of phenyl group by comparing the chemistry of $PPh_2NHC^*H(Me)Ph$ as ligand vs. $PEt_2NHC^*H(Me)Ph$ as ligand. Herein we present the synthesis, structure, absolute configuration and conformational analysis of the diastereomeric cyclopentadienyl cobaltophosphinates and their relevant derivative cobaltophosphonates.

7.2. Results and Discussion

7.2.1. Synthesis and Characterization of Cobaltophosphonates 7-12a,b, 7-13a,b and 7-14a,b. Facile substitution of CO in $(\eta^5\text{-}C_5R_5)Co(X)(I)(CO)$ (R = H, X = I, **7-1**; R = Me, X = I, **7-2**, and R = H, X = C_3F_7, **7-3**)[217, 362, 363] by S_C-$PEt_2NHC^*H(Me)Ph$ (PEtNH) proved to be a more convenient way[206-208, 217, 280-283, 285, 307, 308, 318] to the required substrate than oxidative addition of I_2 or C_3F_7I to the phosphine-substituted

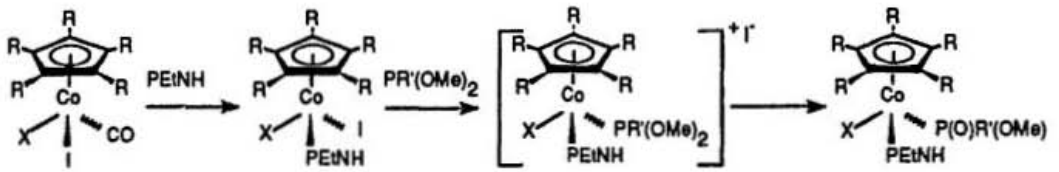

R	X	No.
H	I	7-1
Me	I	7-2
H	C_3F_7	7-3

R	X	No.
H	I	7-4
Me	I	7-5
H	C_3F_7	7-6a,b

R	X	R'	No.
H	I	OMe	7-7a,b
H	C_3F_7	OMe	7-8,a,b
Me	I	OMe	7-9a,b
H	I	Ph	7-10a,b
H	C_3F_7	Ph	7-11a,b

R	X	R'	No.
H	I	OMe	7-12a,b
H	C_3F_7	OMe	7-13a,b
Me	I	OMe	7-14a,b
H	I	Ph	7-15a,b,c,d
H	C_3F_7	Ph	7-16a,b,c,d

PEtNH = S_C-$PEt_2NHC^*H(Me)Ph$

Scheme 7-1

Co(I) complexes.[309] This afforded $(\eta^5\text{-}C_5R_5)Co(X)(PEt_2NHC^*H(Me)Ph)(I)$ as a purple (R = H, X = I, **7-4**), black (R = Me, X = I, **7-5**), or deep brown (R = H, X = C_3F_7, **7-6a,b**) powder, as shown in Scheme 7-1. Treatment of $(\eta^5\text{-}C_5H_5)Co(X)(PEt_2NHC^*H(Me)Ph)(I)$ (X = I, **7-4**; X = C_3F_7, **7-6a,b**) with $P(OMe)_3$ in benzene at room temperature afforded the corresponding phosphonates, $(\eta^5\text{-}C_5H_5)Co(PEt_2NHC^*H(Me)Ph)(X)(P(O)(OMe)_2)$ (X = I, **7-12a,b**, X = C_3F_7, **7-13a,b**), readily via Arbuzov dealkylation.[182, 184, 192, 196, 197, 206, 208, 217, 218, 308, 318] However, reaction

of $(\eta^5\text{-}C_5Me_5)Co(I)_2(PEt_2NHC^*H(Me)Ph)$, **7-5**, with $P(OMe)_3$ in benzene at ambient temperature was sluggish (cf. Chapter 6),[207] and required prolonged heating to give $(\eta^5\text{-}C_5Me_5)Co(PEt_2NHC^*H(Me)Ph)(I)(P(O)(OMe)_2)$, **7-14a,b** in low yield. The dark blue (X = I) or orange ($X = C_3F_7$) cobaltophosphonates **7-12a,b, 7-13a,b** and **7-14a,b** formed as about 50:50 mixtures of diastereomers differing only in the configuration at the cobalt center. Radial thick layer chromatographic separation of **7-12a,b, 7-13a,b** and **7-14a,b** gave the diastereomerically pure high Rf **7-12a, 7-13a, 7-14a** and the low Rf **7-12b, 7-13b, 7-14b** diastereomers, respectively. Co-epimeric diastereomers **7-12a, 7-12b, 7-14a** and **7-14b** with X = I are configurationally stable enough in solution for IR, NMR and circular dichroism characterization at ambient temperature. However, they epimerize slowly in solution to give diastereomeric mixtures. The perfluoroalkyl substituted diastereomers **7-13a** and **7-13b** are configurationally robust in solution. No detectable epimerization was observed after heating in benzene at 60 °C for several days in sealed NMR tubes.

Solution IR spectra of the phosphonates **7-12a,b** and **7-13a,b** in CH_2Cl_2 showed a strong P=O stretch at 1140 cm^{-1} (**7-12a** and **7-12b**), and 1128 cm^{-1} (**7-14a** and **7-14b**), respectively, at significantly lower frequencies[206, 207, 218] than that reported for related neutral dialkyl phosphonate iron[184] (1159-1180 cm^{-1}), nickel[186] (1150 cm^{-1}), rhodium[367] (1168 cm^{-1}) or cobalt (cf. Chapter 5)[365, 367] (1149-1157 cm^{-1}) complexes. The observed phosphoryl stretching frequencies were similar to metallophosphonate anions coordinated to cations.[195, 368, 369] The weakened P=O stretch expected for **7-**

13a,b was obscured by strong C-F absorptions.[206, 208] The decreased P=O force constant and the very large, concentration independent, bathochromic (red) shift for the N-H stretch in complexes **7-12a,b** (ν(N-H) = 3148, 3139 cm^{-1}), **7-13a,b** (ν(N-H) = 3194 cm^{-1}) and **7-14a,b** (ν(N-H) = 3149, 3145 cm^{-1}) compared to their parent complexes **7-4** to **7-6** (ν(N-H) = 3356 cm^{-1} for all) clearly indicated the presence of an intramolecular P=O•••H-N hydrogen bond in all diastereomers in solution,[206-208, 365] which was confirmed by ^1H NMR spectra and solid state structures. Large, concentration independent downfield ^1H NMR chemical shifts for the NH resonances in these phosphonate complexes **7-12a,b**, **7-13a,b** and **7-14a,b** were observed, compared to their parent complexes (cf. Table 7-1). The ^1H NMR resonances shifted downfield by 2.7-2.9 ppm (810-870 Hz) from those of the reactant precursors (η^5-C_5R_5)Co(X)($PEt_2NHC^*H(Me)Ph$)(I) (R = H, X = I, **7-4** (2.74 ppm); R = Me, X = I, **7-5** (2.72 ppm), R = H, X = C_3F_7, **7-6a,b** (2.68, 2.96 ppm)) to those of the cobaltophosphonates **7-12a** (5.46 ppm), **7-12b** (5.60 ppm), **7-14a** (5.61 ppm), **7-14b** (5.64 ppm), **7-13a** (5.50 ppm), and **7-13b** (5.66 ppm).

Each of the diastereomeric cobaltophosphonates **7-12a,b**, **7-13a,b** and **7-14a,b** displays distinct ^1H NMR resonances (Figure.7-1a). ^{13}C NMR resonances (Tables 7-1, 7-2) for η^5-Cp/Cp*, C*H, and C*Me groups are consistent with aminophosphine-coordinated piano-stool structures.[206, 208, 217, 355] ^{31}P NMR spectra (Table 7-1) of complexes **7-12a,b**, **7-13a,b** and **7-14a,b** contain pairs of AX doublets at 98.8(±2.0) and 82.9(±3.0) ppm, corresponding to the coordinated $P(O)(OMe)_2$ and

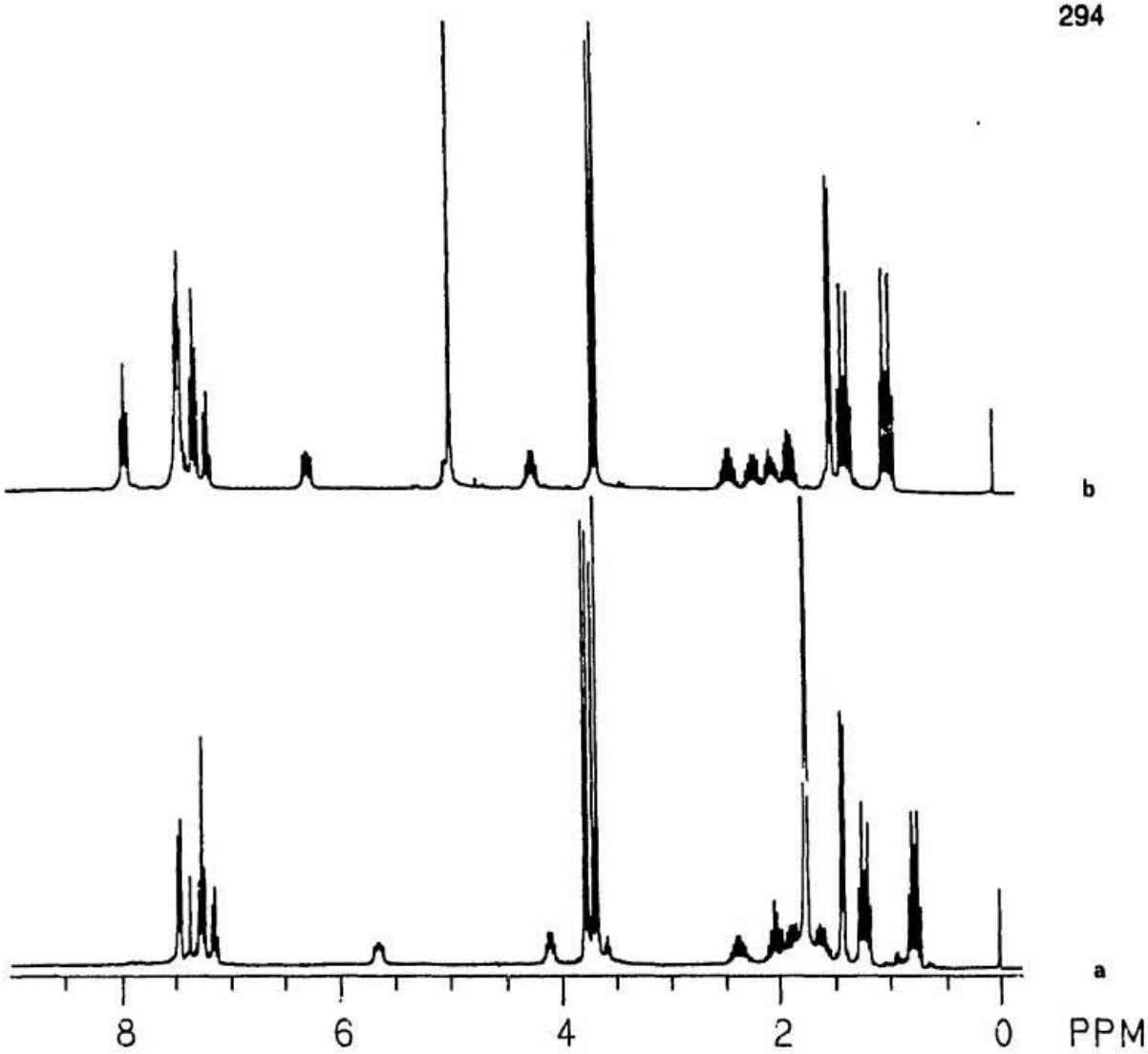

Figure 7-1. Representative ^{1}H NMR Spectra for (η^5-C_5R_5)Co($PEt_2NHC^*H(Me)(P(O)R'(OMe))$(I). (a. R = Me, R' = OMe, **7-14b**; b. R = H, R' = Ph, **7-15b**)

$PEt_2NHC^*H(Me)Ph$ respectively. The diastereotopic $P(O)(O\underline{Me})_2$, and $P(\underline{CH_2}CH_3)_2NHC^*H(Me)Ph$ show well separated resonances both in the ^{1}H and ^{13}C NMR spectra. Distinctive pairs of methoxy doublets are observed in the ^{1}H and ^{13}C NMR spectra for each diastereomer (Tables 7-1, 7-2). The diastereotopic P-

$(CH_2CH_3)_2$ appears approximately as two ABM_3X multiplets. Methylene multiplets (AB part of ABM_3X) appear in the region of 1.7-2.6 ppm for each complex, and the two diastereotopic methyl groups on P-$(CH_2\underline{Me})_2$ (M_3 part of ABM_3X) appear as a distinctive pair of double triplets at 0.87(±0.20) and 1.26(±0.20) ppm with $^2J_{PH}$ = 16.2(±2.0) Hz and $^3J_{HH}$ = 7.6(±0.2) Hz (Table 7-1), respectively. The ^{13}C NMR spectra of **7-12a,b**, **7-13a,b** and **7-14a,b** (Table 7-2) show pairs of well separated doublets at 19-29 ppm, corresponding to the two diastereotopic carbons of $P(\underline{C}H_2Me)_2$. The two diastereotopic carbons of $P(CH_2\underline{Me})_2$ appear as a pair of singlets, because $^2J_{PC}$ is small. The $PEt_2NHC^*H(\underline{C_6H_5})$ protons and carbons are also unambiguously assigned as three sets of well separated resonances at 7.40(±0.06), 7.28(±0.02), 7.17(±0.03) ppm corresponding to H_{ortho}, H_{meta} and H_{para}, respectively, in the ^1H NMR spectra (Table 7-1) and as four singlets at 147.91(±0.50), 128.14(±0.20), 126.34(±0.20), 126.06(±0.20) ppm in the ^{13}C NMR spectra assigned to C_{ipso}, C_{ortho}, C_{para} and C_{meta}, respectively. As shown in Table 7-3, the ^{19}F NMR spectra show well-resolved ^{19}F AB patterns[208, 281, 282, 318, 370] for the diastereotopic $C_\alpha F_2$ and $C_\beta F_2$ groups of n-C_3F_7 ligand, because of the typically small vicinal couplings ($^3J_{FF}$ = 5-10 Hz) compared to the large two bond F to F coupling. The coupling constants $^2J_{FaFb}$ show a marked increase on passing from C_α to C_β, as presented in the preceding chapters,[281, 282, 318] pointing to a weakening of the C_α-F bond.[295]

7.2.2. Preparation of $(\eta^5$-$C_5H_5)Co(C_3F_7)(PEt_2NHC^*H(Me)Ph)(I)$, 7-6a,b, an Easily Resolvable Chiral-at-metal Complex. Chapter 2 presented an example of a "self-resolved" chiral-at-metal complex, (η^5-indenyl)Co(C_3F_7)($PPh_2NHC^*H(Me)Ph$)(I), **2-**

8a,b. Similar behavior was found for complex **7-6a,b**. As shown in Scheme 7-1, facile substitution of CO in racemic $(\eta^5\text{-}C_5H_5)Co(C_3F_7)$-(CO)(I) (**7-3**)[371] by the chiral aminophosphine S_C-PEt_2NHC^*H-(Me)Ph (PEtNH) at room temperature in benzene solution afforded a 43:57 (**7-6b:7-6a**) Co-epimeric mixture of $((R,S)_{Co},S_C)$-$(\eta^5\text{-}C_5H_5)Co(C_3F_7)(PEt_2NHC^*H(Me)Ph)(I)$ (**7-6a,b**). TLC and ^1H NMR analysis of the crude product showed that the diastereomeric mixture **7-6a,b** in solution converts to a single diastereomer **7-6a** on removal of the solvent at room temperature/aspirator pressure or 0 °C/oil pump vacuum (0.1 Torr). "Self resolution" (second order asymmetric transformation) occurred during workup as reported previously.[280] Supporting evidence followed from the observation that: (i) NMR reaction at 25 °C in benzene-d_6 showed that the reaction of **7-3** with PEtNH was complete upon mixing to afford **7-6b:7-6a** in a kinetic product ratio of 43:57. (ii) Variable temperature epimerization experiments (Scheme 7-2) monitored by ^1H NMR spectroscopy in benzene-d_6 gave ΔH = 15.2(±0.5) kJ•mol^{-1} and ΔS = 48.0(±1.5) J•K^{-1}•mol^{-1} for Keq = **7-6b/7-6a** resulting in a calculated equilibrium ratio for **7-6b/7-6a** of 29:71 at 0 °C; (iii) Resolution/epimerization cycles were established by experiments involving repeated dissolving and removal of solvent from **7-6a,b**. Diastereomerically pure **7-6a** was dissolved in benzene-d_6 and epimerized to the mixture of **7-6a** and **7-6b**, which resolved again to a single

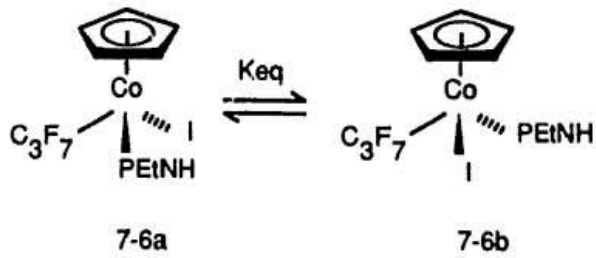

7-6a 7-6b

Scheme 7-2

diastereomer **7-6a** upon removal of solvent. (iv) Freezing an epimeric solution of **7-6a** and **7-6b** and low temperature (-12 °C) sublimation of the benzene to avoid formation of a liquid phase gave a 32:68 epimeric mixture of **7-6b/7-6a**. Therefore, the isolation of a single diastereomer by evaporation of solvent at room temperature or 0 °C was the result of a second-order asymmetric transformation[280, 284] which occurred during workup. As benzene was removed the less soluble diastereomer **7-6a** crystallizes out shifting the epimerization equilibrium **7-6b** ⇌ **7-6a** toward **7-6a** (Scheme 7-2).

Multinuclear NMR spectra establish that both **7-6a** and **7-6b** are η^5-Cp-coordinated piano-stool complexes with degenerate Cp singlets and distinguishable C*H, C*-Me, NH, and CH_2-Me resonances in their ^{1}H NMR spectra (Table 7-1). The ^{13}C spectrum of **7-6a** shows well separated resonances for the $PEt_2NHC^*H(Me)Ph$ ligand and η^5-Cp characteristic of diastereomeric aminophosphine complexes. The diastereotopic $C_\alpha F_2$, $C_\beta F_2$ fluorine atoms show the typical splitting patterns found in related perfluoroalkyl substituted chiral complexes.[280, 281, 306]

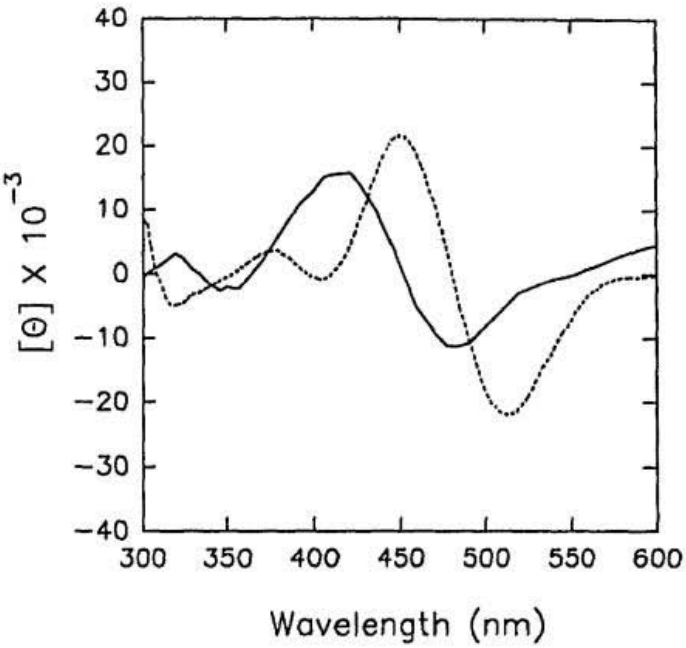

Figure 7-2. Circular Dichroism Spectra of **7-6a** (——) and S_{Co},S_C-(η^5-indenyl)Co(C_3F_7)($PPh_2NHC^*H(Me)Ph$)(I), **2-8a** (----).

The absolute configuration of the high Rf **7-6a** was determined by comparing its circular dichroism (CD) spectra to that of isostructural S_{Co},S_C-(η^5-indenyl)Co(C_3F_7)($PPh_2NHC^*H(Me)Ph$)(I) (high Rf **2-8a**, cf. Chapter 2.2.2)[280] Since these two complexes have the same relative Rf values (both high Rf) and possess similar CD morphology, as shown in Figure 7-2, they can be assigned the same absolute configuration at cobalt. Thus, the absolute configuration of **7-6a** is S_{Co},S_C on the basis of modified Cahn-Ingold-Prelog rules[290-293, 372] with the ligand priority series of I > η^5-Cp > (S_C)-$PEt_2NHC^*H(Me)Ph$ > C_3F_7.

7.2.3. Synthesis and Characterization of Cobaltophosphinates 7-15a,b,c,d and 7-16a,b,c,d. Reaction of **7-4** or **7-6a,b** with dimethyl phenylphosphonite, $PPh(OMe)_2$, in benzene or chloroform at room temperature afforded a dark blue or orange diastereomeric mixture of the phosphinates **7-15a,b,c,d** or **7-16a,b,c,d** via an Arbuzov dealkylation as shown in Scheme 7-1. A small amount of $(\eta^5\text{-}C_5H_5)Co(PPh(OMe)_2)(P(O)Ph(OMe))(X)$ (X = I, **7-17a,b**[206]; X = C_3F_7, **7-18a,b**[217]) was formed, presumably via the substitution of aminophosphine and iodide followed by an Arbuzov dealkylation (cf. Chapter 3).[217, 318] The observation (^1H NMR, $CDCl_3$) of ionic intermediates $[(\eta^5\text{-}C_5H_5)Co(PEt_2NHC^*H(Me)Ph)(PPh(OMe)_2)(I)]^+I^-$ (major, **7-10a,b:** δ(Cp) = 5.40, 5.47 ppm; **7a-10/7-10b** = 1:1) and $[(\eta^5\text{-}Cp)Co(PPh(OMe)_2)_2(I)]^+I^-$ (minor, δ(Cp) = 5.52 ppm)[206] proved that this assumption was correct. Diastereomeric **7-15a,b,c,d** and **7-16a,b,c,d** (in the order of decreasing Rf values) were separated as air stable solids by radial thick-layer chromatography, as shown in Scheme 7-3 and 7-4. The phosphinates with X = I (**7-15a**, **7-15b**, **7-15c**, and **7-15d**) are sufficiently stable to allow full characterization by ^1H, ^{13}C, and ^{31}P NMR and by circular dichroism spectroscopy. The phosphinates with X = C_3F_7 (**7-16a**, **7-16b**, **7-16c**, and **7-16d**) are more stable than the iodide analogs and no epimerization was detected after heating the phosphinates **7-16a**, **7-16b**, **7-16c**, or **7-16d** in benzene at 60 °C for several days in sealed NMR tubes.

Similar to the cobaltophosphonate derivatives, the solution IR spectra in CH_2Cl_2 for

each diastereomer shows a strong ν(P=O) resonance at 1128 cm^{-1} (**7-15a**), 1129 cm^{-1} (**7-15b**), 1125 cm^{-1} (**7-15c**), or 1124 cm^{-1} (**7-15d**). However, the expected ν(P=O) resonance in **7-16a,b,c,d** is obscured by strong C-F absorptions. The decreased stretching frequency compared to other alkyl arylphosphinate complexes (cf. Chapter 6)[184] can be attributed to a secondary P=O•••H-N hydrogen bonding interaction at the basic phosphoryl oxygen. Accordingly a large, but concentration independent, bathochromic (red) shift for the N-H stretch for **7-15a** (3115 cm^{-1}), **7-15b** (3115 cm^{-1}), **7-15c** (3120 cm^{-1}), **7-15d** (3120 cm^{-1}), **7-16a** (3139 cm^{-1}), **7-16b** (3139 cm^{-1}), **7-16c** (3140 cm^{-1}), **7-16d** (3147 cm^{-1}), compared to their parent complexes **7-4** and **7-6a,b** (3356 cm^{-1}) was observed in the IR spectra.

The presence of an intramolecular P=O•••H-N hydrogen bond was confirmed by ^{1}H NMR spectra and the solid state structures. As found in the phosphonate complexes, strong intramolecular P=O•••H-N hydrogen bonding in **7-15a,b,c,d** and **7-16a,b,c,d** considerably deshields the ^{1}H NMR N<u>H</u> resonance compared to that of **7-4** and **7-6a,b**. The proton chemical shift of N<u>H</u> in **7-15a** (6.10 ppm), **7-15b** (6.26 ppm), **7-15c** (5.59 ppm), **7-15d** (5.34 ppm), **7-16a** (5.98 ppm), **7-16b** (5.86 ppm), **7-16c** (5.99 ppm), and **7-16d** (5.75 ppm) shifted downfield about 2.6-3.5 ppm (780-1050 Hz) compared to the parent complex **7-4** (2.74 ppm) and **7-6a,b** (2.68, 2.96 ppm) (cf. Table 7-1). ^{31}P NMR spectra (Table 7-1) of each diastereomer show a pair of AX doublets at 115.0(±5.0) and 85.0(±5.0) ppm assigned to the coordinated P(O)Ph(OMe) and $PEt_2NHC^*H(Me)Ph$, respectively. The P(O)Ph(O<u>Me</u>) in these

diastereomers **7-15a,b,c,d** and **7-16a,b,c,d** appears as a doublet at about 3.52(±0.20) and 50.75(±0.75) ppm in the ^{1}H and ^{13}C NMR spectra respectively. The ^{1}H NMR resonance of H_{ortho} and the ^{13}C NMR resonance of P(O)-Ph can be clearly located for these complexes as shown in Figure 7-1b and Tables 7-1, 7-2. The ^{1}H, ^{13}C NMR resonances for the remaining groups and ^{19}F NMR are similar to those of the phosphonate complexes discussed above (Figure 7-1b and Tables 7-1, 7-2).

Table 7-1. ^{1}H and ^{31}P NMR for η^5-Cp/Cp* Co(III) Complexes[a]

Cpd	C_5H_5	C_5Me_5	C-C_6H_5	P-C_6H_5	C*H-Me	N-H/ P-OMe	CH_aH_bMe	^{31}P
7-4	5.13		7.37 (m)[c,d] 7.26 (m)[e]		4.52 (m)[f] 1.46 (d,6.7)[g]	2.74 (m)[h]	2.52 (m,2H)[i] 2.42 (m,1H)[i] 2.24 (m,1H)[i] 1.27 (dt, 16.1,7.7)[j] 1.10 (dt, 16.6,7.7)[j]	85.9
7-5		1.87 (d,1.3)	7.37 (m)[c,d] 7.26 (m)[e]		4.48 (m)[f] 1.51 (d,6.7)[g]	2.72 (m)[h]	2.48 (m,2H)[i] 2.23 (m,2H)[i] 1.23 (dt,14.9,7.6)[j] 0.93 (dt,15.4,7.7)[j]	82.8
7-6a	5.18		7.29 (m)[c,d,e]		4.37 (m)[f] 1.43 (d,6.6)[g]	2.68 (m)[h]	2.41 (m,1H)[i] 2.22 (m,1H)[i] 2.12 (m,1H)[i] 1.90 (m,1H)[i] 1.30 (dt, 15.8,7.8)[j] 1.00 (dt, 16.7,7.7)[j]	87.3
7-6a[b]	4.69		7.11 (m)[c,d,e]		4.05 (m)[f] 1.13 (d,6.6)[g]	2.77 (m)[h]	1.45-2.05 (m)[i] 0.96 (dt,15.6,7.6)[j] 0.59 (dt,16.8,7.7)[j]	
7-6b[b]	4.69		7.11 (m)[c,d,e]		3.95 (m)[f] 1.14 (d,6.6)[g]	3.11 (m)[h]	1.45-2.05 (m)[i] 0.82 (dt,15.6,7.8)[j] 0.69 (dt,16.7,7.6)[j]	
7-12a	5.09		7.39(d,7.3)[c] 7.30 (tt,7.3,1.6)[d] 7.20 (tt,7.3,1.6)[e]		4.21 (m)[f] 1.39 (d,6.7)[g]	5.46 (m)[h] 3.83 (d,10.1)[k] 3.72 (d,11.0)[k]	2.58 (m,1H)[i] 2.54 (m,1H)[i] 1.82 (m,2H)[i] 1.35 (dt,16.5,7.8)[j] 0.87 (dt,16.9,7.6)[j]	85.9 (d,134.7)[l] 97.6 (d,134.7)[m]

Table 7-1. cont'd

7-12b	5.13		7.38 (dd,7.6,1.6)[c] 7.27 (tt,7.6,1.6)[d] 7.16 (tt,7.6,1.6)[e]	4.20 (m)[f] 1.44 (d,6.7)[g]	5.60 (m)[h] 3.84 (d,10.1)[k] 3.72 (d,11.0)[k]	2.35 (m,1H)[i] 2.18 (m,1H)[i] 2.00 (m,1H)[i] 1.86 (m,1H)[i] 1.27 (dt,16.6,7.6)[j] 0.95 (dt,17.2,7.7)[j]	82.5 (d,133.0)[l] 96.9 (d,133.0)[m]
7-13a	5.10		7.39 (dt,7.9,1.4)[c] 7.29 (tt,7.9,1.4)[d] 7.19 (tt,7.9,1.4)[e]	4.15 (m)[f] 1.36 (d,6.7)[g]	5.50 (m)[h] 3.75 (d,10.5)[k] 3.60 (d,11.0)[k]	2.25 (m,1H)[i] 2.11 (m,1H)[i] 1.81 (m,2H)[i] 1.18 (dt,16.8,7.7)[j] 0.83 (dt,16.3,7.6)[j]	85.7 (d,120.8)[l] 99.8 (d,120.8)[m]
7-13b	5.12		7.26 (m)[c,d] 7.16 (m)[e]	4.14 (m)[f] 1.43 (d,6.6)[g]	5.66 (m)[h] 3.76 (d,10.6)[k] 3.68 (d,10.9)[k]	2.21 (m,1H)[i] 1.80 (m,1H)[i] 1.62 (m,2H)[i] 1.26 (dt,16.1,7.8)[j] 0.89 (dt,17.5,7.7)[j]	82.7 (d,118.1)[l] 100.4 (d,118.1)[m]
7-14a		1.74 (t,1.2)	7.38 (dt,7.1,1.5)[c] 7.28 (dt,7.1,1.5)[d] 7.17 (tt,7.1,1.5)[e]	4.15 (m)[f] 1.40 (d,6.9)[g]	5.61 (m)[h] 3.76 (d,9.6)[k] 3.70 (d,10.8)[k]	2.38 (m,1H)[i] 2.29 (m,1H)[i] 1.71 (m,1H)[i] 1.58 (m,1H)[i] 1.21 (dt,14.4,7.5)[j] 0.88 (dt,16.5,7.6)[j]	83.4 (d,135.9)[l] 100.8 (d,135.9)[m]
7-14b		1.75 (t,1.2)	7.46 (dd,7.3,1.4)[c] 7.26 (tt,7.3,1.4)[d] 7.14 (tt,7.3,1.4)[e]	4.11 (m)[f] 1.43 (d,6.7)[g]	5.64 (m)[h] 3.77 (d,9.6)[k] 3.69 (d,10.8)[k]	2.38 (m,1H)[i] 2.03 (m,1H)[i] 1.87 (m,1H)[i] 1.61 (m,1H)[i] 1.22 (dt,16.4,7.6)[j] 0.77 (dt,15.0,7.6)[j]	79.6 (d,135.3)[l] 99.8 (d,135.3)[m]

Table 7-1. cont'd

7-15a	4.94	7.45 (dd,7.6,1.4)[c] 7.30 (tt,7.6,1.4)[d] 7.20 (tt,7.6,1.4)[e]	7.91 (m)[c] 7.41 (m)[d,e]	4.23 (m)[f] 1.44 (d,6.6)[g]	6.10 (m)[h] 3.63 (d,10.7)[k]	2.52 (m,1H)[i] 2.22 (m,1H)[i] 1.88 (m,2H)[i] 1.35 (dt,16.1,7.9)[j] 0.93 (dt,16.8,7.6)[j]	84.7 (d,107.5)[l] 113.9 (d,107.5)[m]
7-15b	4.96	7.42 (m)[c] 7.29 (t,7.3)[d] 7.17 (tt,7.3,1.6)[e]	7.94 (m)[c] 7.42 (m)[d,e]	4.23 (m)[f] 1.48 (d,6.7)[g]	6.26 (m)[h] 3.65 (d,10.6)[k]	2.43 (m,1H)[i] 2.21 (m,1H)[i] 2.02 (m,1H)[i] 1.85 (m,1H)[i] 1.35 (dt,16.6,7.6)[j] 0.96 (dt,16.9,7.7)[j]	80.5 (d,103.5)[l] 112.6 (d,103.5)[m]
7-15c	4.73	7.48-7.22	8.20 (m)[c] 7.48-7.22[d,e]	4.44 (m)[f] 1.54 (d,6.7)[g]	5.59 (m)[h] 3.41 (d,11.1)[k]	2.44 (m,3H)[i] 1.68 (m,1H)[i] 1.27 (m,6H)[j]	83.1 (d,118.8)[l] 111.3 (d,118.8)[m]
7-15d	4.89	7.60-7.24	8.21 (m)[c] 7.60-7.24[d,e]	4.44 (m)[f] 1.47 (d,7.0)[g]	5.34 (m)[h] 3.39 (d,11.1)[k]	2.68 (m,1H)[i] 2.27 (m,2H)[i] 1.99 (m,1H)[i] 1.28 (dt,14.9,7.2)[j] 0.78 (dt,15.7,7.7)[j]	81.4 (d,118.2)[l] 111.0 (d,118.2)[m]
7-16a	5.03	7.41 (dt,7.2,1.4)[c] 7.31 (tt,7.2,1.4)[d] 7.21 (tt,7.2,1.4)[e]	7.70 (m)[c] 7.37 (m)[d,e]	4.17 (m)[f] 1.45 (d,6.6)[g]	5.98 (m)[h] 3.48 (d,11.0)[k]	2.26 (m,1H)[i] 1.97 (m,2H)[i] 1.71 (m,1H)[i] 1.10 (dt,15.6,7.5)[j] 1.00 (dt,16.4,7.6)[j]	89.6 (d,104.2)[l] 117.1 (d,104.2)[m]
7-16b	5.08	7.37 (m)[c] 7.29 (tt,7.1,1.5)[d] 7.19 (tt,7.1,1.5)[e]	7.70 (m)[c] 7.36 (m)[d,e]	4.26 (m)[f] 1.49 (d,6.7)[g]	5.86 (m)[h] 3.52 (d,10.9)[k]	2.22 (m,1H)[i] 2.06 (m,1H)[i] 1.82 (m,1H)[i] 1.69 (m,1H)[i] 1.32 (dt,16.2,7.9)[j] 0.91 (dt,16.4,7.9)[j]	83.3 (d,102.2)[l] 114.6 (d,102.2)[m]

Table 7-1. cont'd

7-16c	4.87	7.41 (dt,7.7,1.5)[c] 7.37 (m)[d] 7.25 (tt,7.7,1.5)[e]	7.78 (m)[c] 7.37 (m)[d,e]	4.31 (m)[f] 1.50 (d,6.7)[g]	5.99 (m)[h] 3.50 (d,11.1)[k]	2.38 (m,1H)[i] 1.99 (m,1H)[i] 1.92 (m,1H)[i] 1.69 (m,1H)[i] 1.24 (dt,15.9,7.8)[j] 0.96 (dt,16.2,7.8)[j]	83.8 (d,105.5)[l] 111.6 (d,105.5)[m]
7-16d	5.01	7.40 (d,7.0)[c] 7.28 (m)	7.84 (m)[c] 7.43[d,e]	4.34 (m)[f] 1.53 (d,6.7)[g]	5.75 (m)[h] 3.47 (d,11.2)[k]	2.08 (m,2H)[i] 1.96 (m,1H)[i] 1.57 (m,1H)[i] 1.15 (dt,15.8,7.8)[j] 0.84 (dt,16.4,7.9)[j]	81.8 (d,106.1)[l] 110.8 (d,106.1)[m]

[a] ^1H (300.1 MHz) NMR chemical shifts in ppm relative to TMS; ^{31}P (121.5 MHz) NMR chemical shifts in ppm relative to external 85% H_3PO_4; Solvent: $CDCl_3$; m = multiplet; d = doublet; t = triplet, q = quartet, dd = doublet of doublets, dt = doublet of triplets; J values in Hz given in brackets; Coupling constants of Cp-Me protons are $^4J_{PH}$. [b] Solvent: benzene, number obtained from the spectra after epimerization. [c] H_{ortho} (2H, J_{HH}). [d] H_{meta} (2H, J_{HH}). [e] H_{para} (1H, J_{HH}). [f] C*H ($^3J_{PH}$, $^3J_{HH}$, $^3J_{HH}$). [g] C*Me ($^3J_{HH}$). [h] N-H ($^2J_{PH}$, $^3J_{HH}$). [i] P-CH_aH_b- ($^2J_{PH}$, $^2J_{HH}$, $^3J_{HH}$). [j] P-CH_2-Me ($^3J_{PH}$, $^3J_{HH}$). [k] P(O)-OMe ($^3J_{PH}$). [l] $PEt_2NHCH(Me)Ph$ ($^2J_{PP}$). [m] P(O)(OMe) ($^2J_{PP}$).

Table 7-2. ^{13}C NMR for Ligand and η^5-Cp/Cp* Co(III) Complexes*.

Cpd	Cp/Cp*	Cp-Me	C-Ph ($C_{ipso,ortho,meta,para}$)	P-Ph ($C_{ortho,meta,para}$)	P-CH_2-Me	P-OMe	C*H-Me
7-4	85.53		146.71, 128.65, 125.64, 127.07		27.41 (d,34.2)[b] 26.54 (d,32.4)[b] 10.10[c], 9.81[c]		27.40 (d,5.0)[d] 54.04 (d,8.7)*
7-5	93.71	11.39	146.51, 128.52, 125.83, 126.94		25.13 (d,21.2)[b] 24.75 (d,23.2)[b] 10.57[c], 9.99[c]		27.39 (d,4.7)[d] 54.08 (d,11.4)*
7-6a	86.80		146.76, 128.56, 125.50, 126.98		25.95 (d,33.1)[b] 25.42 (d,29.6)[b] 9.43[c], 9.15[c]		27.54[d] 53.51 (d,12.0)*
7-12a	87.59		147.76, 128.31, 125.97, 126.43		27.32 (d,32.6)[b] 26.46 (d,34.5)[b] 10.46[c], 7.88[c]	53.37 (d,11.3)[f] 51.10 (d,8.9)[f]	27.35 (d, 5.6)[d] 54.70 (d,7.7)*
7-12b	87.62		147.43, 128.14, 125.90, 126.45		29.03 (d,37.1)[b] 24.09 (d,29.8)[b] 9.99[c], 7.86[c]	52.59 (d,11.4)[f] 51.15 (d,9.3)[f]	28.05 (d,6.0)[d] 54.83 (d,8.6)*
7-13a	88.10		147.41, 128.20, 126.08, 126.50		26.89 (d,36.9)[b] 24.50 (d,27.2)[b] 9.20[c], 7.43[c]	52.86 (d,9.5)[f] 50.47 (d,8.7)[f]	27.87[d] 52.39 (d,9.9)*
7-13b	88.08		147.64, 128.19, 125.74, 126.42		27.73 (d,30.3)[b] 24.30 (d,35.1)[b] 9.01[c], 7.50[c]	52.60 (d,11.4)[f] 50.64 (d,12.2)[f]	28.10 (d, 7.6)[d] 52.38 (d,9.7)*
7-14a	97.26	10.75	148.42, 128.16, 126.20, 126.31		24.51 (d,26.5)[b] 23.90 (d,32.0)[b] 11.73[c] 7.47[c]	54.30 (d,9.1)[f] 50.59 (d, 11.1)[f]	27.13 (d,8.2)[d] 53.77 (d,12.3)*
7-14b	97.33	10.61	148.01, 127.95, 126.16, 126.16		26.74 (d,35.5)[b] 19.49 (d,25.5)[b] 11.0[c], 7.61[c]	54.26 (d,9.1)[f] 50.73 (d,11.2)[f]	28.24 (d,6.3)[d] 52.89 (d,11.5)*

Table 7-2. cont'd

7-15a	87.55	148.06, 128.29, 126.09, 126.47	130.73/130.63, 127.51/127.39, 129.61	27.61 (d,39.0)[b] 26.85 (d,34.9)[b] 10.63[c], 7.85[c]	51.44 (d,9.9)[f]	27.39 (d,7.2)[d] 53.44 (d,9.4)[e]
7-15b	87.55	147.61, 128.12, 125.97, 126.40	130.63/130.48, 127.54/127.40, 129.59	29.60 (d,39.0)[b] 24.09 (d,31.2)[b] 10.19[c], 7.84[c]	51.45 (d,9.5)[f]	28.10 (d,8.0)[d] 52.45 (d,11.8)[e]
7-15c	89.43	147.90, 128.60, 125.60, 126.80	130.39/130.25, 127.98/127.85, 130.00	26.95 (d,30.1)[b] 23.57 (d,35.4)[b] 9.39[c], 9.19[c]	50.93 (d,11.6)[f]	27.15[d] 54.13 (d,11.0)[e]
7-15d	89.37	146.68, 128.30, 126.07, 126.51	130.53/130.37, 127.98/127.85, 130.01	26.76 (d,27.5)[b] 22.52 (d,35.8)[b] 9.16[c], 8.79[c]	50.79 (d,10.4)[f]	29.19 (d,6.6)[d] 53.67 (d,12.8)[e]
7-16a	88.19	148.15, 128.36, 126.10, 126.55	131.27/131.13, 127.51/127.40, 129.44	27.44 (d,33.8)[b] 23.76 (d,28.7)[b] 8.90[c], 8.00[c]	50.79 (d,11.0)[f]	27.44 (d,5.8)[d] 53.21 (d,9.6)[e]
7-16b	88.05	147.54, 128.21, 125.98, 126.48	131.22/131.06, 127.59/127.45, 129.39	26.29 (d,32.2)[b] 24.68 (d,31.3)[b] 8.80[c], 8.07[c]	50.61 (d, 11.1)[f]	28.16 (d,5.4)[d] 52.96 (d,10.3)[e]
7-16c	89.22	147.65, 128.56, 125.86, 126.74	130.56/130.40, 127.87/127.74, 129.55	25.33 (d,37.8)[b] 22.74 (d,24.6)[b] 8.60[c]	50.09 (d,14.53)[f]	27.39[d] 54.14 (d,10.7)[e]
7-16d	88.97	147.01, 128.25, 125.91, 126.51	131.90 (d,52.8)[g], 130.71/130.58, 127.90/127.76, 129.63	24.49 (d,34.7)[b] 24.39 (d,18.7)[b] 8.73[c], 8.52[c]	50.19 (d,11.0)[f]	28.75 (d,5.1)[d] 54.00 (d,12.3)[e]

[a] ^{13}C . 75.47 MHz) NMR chemical shifts in ppm relative to solvent $CDCl_3$ = 77.0; d = doublet; J values in Hz given in brackets. [b] P-CH_2- ($^1J_{PC}$). [c] P-CH_2-Me. [d] C*-Me ($^3J_{PC}$). [e] C*H ($^2J_{PC}$). [f] P-OMe ($^2J_{PC}$).

Table 7-3. ^{19}F NMR for η^5-Cp Co(III) Complexes[a].

Cpd	$C_\alpha F_2$	$C_\beta F_2$	CF_3
	F_a, F_b	F_a, F_b	
7-6a	-63.49, -66.63 (d, 260.5)	-111.22, -114.32 (d, 279.0)	-79.13 (t, 13.0)
7-6b	-65.40, -66.01 (d, 262.3)	-111.39, -114.53 (d, 279.1)	-79.18 (t, 13.5)
7-13a	-64.21, -75.00 (d, 266.6)	-115.39, -115.54 (d, 280.3)	-78.86 (t, 10.1)
7-13b	-63.91, -73.19 (d, 266.8)	-115.51, -115.90 (d, 280.3)	-78.89 (t, 10.3)
7-16a	-66.06, -71.06 (d, 272.8)	-113.41, -114.47 (d, 279.0)	-78.95 (t, 9.4)
7-16b	-67.02, -68.90 (d, 269.8)	-112.77, -114.32 (d, 277.6)	-78.99 (t, 10.3)
7-16c	-65.79, -68.94 (d, 269.2)	-112.91, -113.86 (d, 278.4)	-78.97 (t, 10.3)
7-16d	-65.74, -69.03 (d, 267.7)	-113.42, -114.16 (d, 278.8)	-78.95 (t, 10.2)

[a] 282.4 MHz, chemical shifts in ppm relative to $CFCl_3$; solvent = $CDCl_3$; $^2J_{F_aF_b}$, and $^3J_{FF}$ in the case of CF_3, in Hz given in brackets; all CF_2 peaks show further unresolved splitting by about 5-10 Hz due to $^3J_{FF}$.

7.2.4. Crystal Structures and Solid State Conformation of 7-12a, 7-13a, 7-15a, 7-16a and 7-16b. The X-ray crystal structures of two cobaltophosphonates **7-12a** and **7-13a** and three cobaltophosphinates **7-15a, 7-16a** and **7-16b** were obtained in order to confirm the structures and to establish the absolute configurations of the Arbuzov products. All structures were solved using direct methods. The hydrogen attached on the nitrogen atom in **7-12a, 7-13a, 7-15a** and **7-16b** was located in the difference maps, which allowed unambiguous identification of the intramolecular P=O•••H-N hydrogen bond. Atomic coordinates and selected bond distances and bond angles are given in Tables 7-4 - 7-13. Figures 7-3 - 7-7 show Pluto representations of complexes **7-12a, 7-13a, 7-15a, 7-16a** and **7-16b.** All complexes have typical piano-stool structures with the η^5-C_5H_5 occupying three *fac* coordination sites and the X (X = I, C_3F_7), $PEt_2NHC^*H(Me)Ph$, and $PR'(OMe)_2$ (R' = OMe, Ph) occupying the remaining three coordination sites. Interligand bond angles (I(1)-Co(1)-P(1), I(1)-Co(1)-P(2), P(1)-Co(1)-P(2) for **7-12a** and **7-15a**; C(6)-Co(1)-P(1), C(6)-Co(1)-P(2), P(1)-Co(1)-P(2) for **7-13a, 7-16a** and **7-16b**) in all complexes are close to 90° and are consistent with approximate octahedral geometry. Figure 7-8 shows that the two crystallographically independent molecules **7-16b** and **7-16b'** have identical absolute configurations and differ only slightly in conformation. For complexes **7-12a, 7-13a, 7-15a, 7-16a, 7-16b,** and **7-16b'** there is substantial double bond character in the phosphoryl bond as found in other related phosphonate and phosphinate complexes.[200, 206-208, 217, 218, 308, 318, 373, 374] Accordingly the P=O bond distances (1.486(4) Å (**7-12a**), 1.478(3) Å (**7-13a**), 1.497(6) Å (**7-15a**), 1.498(4) Å (**7-**

16a), 1.492(7) **Å** (**7-16b**) and 1.497(7) **Å** (**6-16b'**)) are considerably shorter than the P-OMe bond distance (1.615(5) **Å**) but within the range reported for the examples with[192, 196, 200, 206-208, 217, 218, 308, 318, 368, 375-380] or without[193, 204, 214, 373, 374, 381] secondary bonding interactions to electrophilic centers. The spectroscopically observed strong intramolecular P=O•••H-N hydrogen bonding in all complexes **7-12a**, **7-13a**, **7-15a**, **7-16a**, **7-16b** and **7-16b'** is confirmed by the proximity of the aminophosphine NH and the basic phosphoryl oxygen atom. The P=*O•••H*-N hydrogen bond distances for all complexes **7-12a** (O(1)-H(1N) = 1.98(5) **Å**), **7-13a** (O(1)-H(1N)) = 1.986 **Å**), **7-15a** (O(1)-H(1N) = 1.828 **Å**), **7-16a** (O(1)-H(1N) = 1.780 **Å**), **7-16b** (O(1)-H(1N)) = 1.851 **Å**) and **7-16b'** (O(1)-H(1N) = 1.889 **Å**)) are considerably shorter than the sum of the van der Waals' radii of O and H (2.60 **Å**) and are well within the range considered diagnostic for hydrogen bonded N-H•••O.[206-208, 217, 382, 383] The existence of the secondary hydrogen bonding interaction restricts the solid state conformations of **7-12a, 7-13a, 7-15a, 7-16a, 7-16b** and **7-16b'**, and results in a distorted six-membered Co-P-O•••H-N-P quasi-chair, as shown in Figure 7-9. The η^5-C_5H_5 group is pseudoequatorial and the iodide or perfluoropropyl is pseudoaxial as with the isostructural aminophosphine complexes.[206-208, 217, 382] The phosphoryl oxygen in all complexes adopts a conformation *anti* to the η^5-C_5H_5 plane placing the P-*R'* (R' = OMe, Ph), the P-*OMe* and the P-*Et*$_2$NHC*H(Me)Ph ethyl groups *gauche* to the η^5-C_5H_5, respectively, as a result of constraints due to strong hydrogen bonding (cf. Figure 7-9).

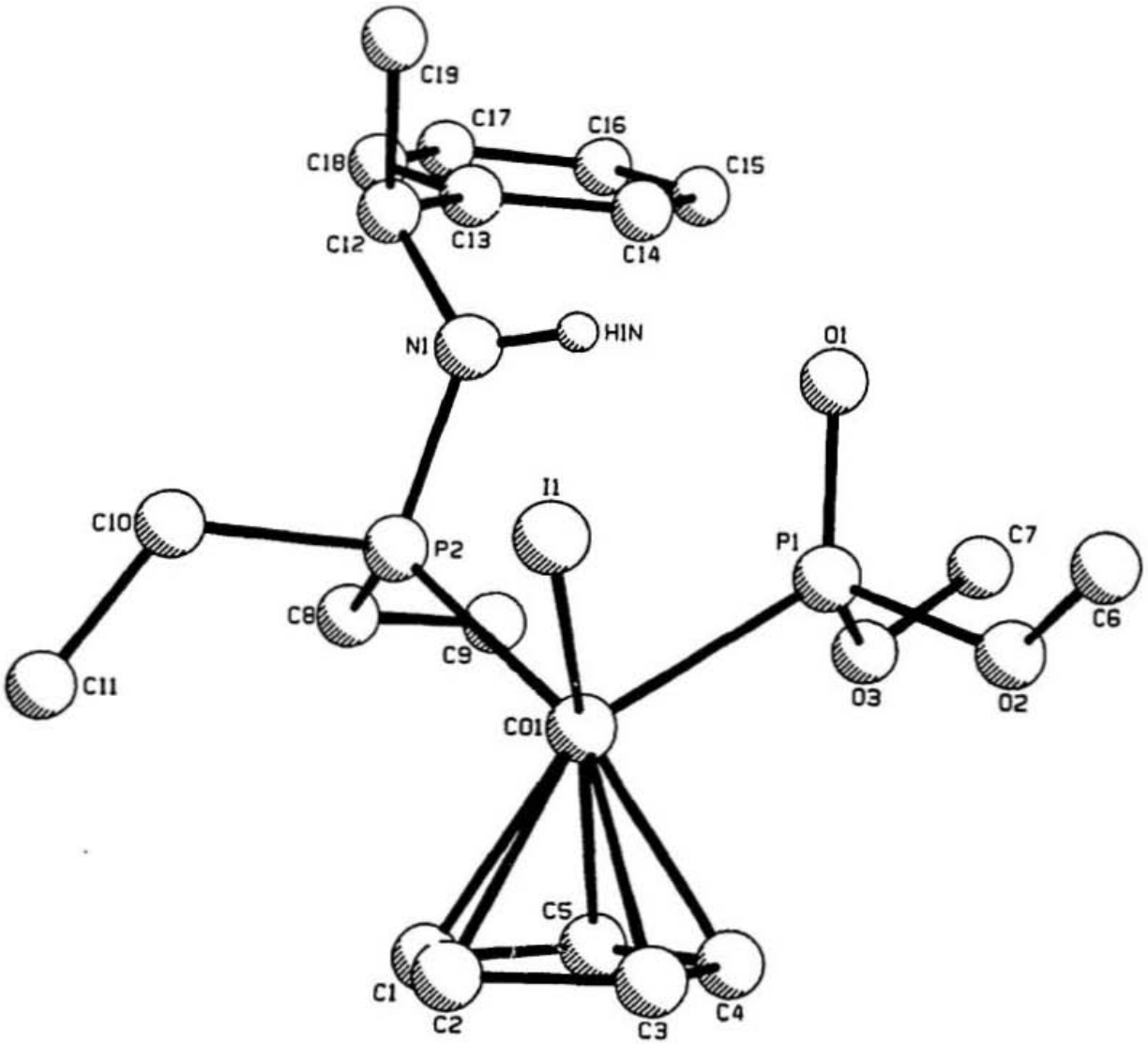

Figure 7-3. Molecular Structure of (S_{Co}, S_C)-(η^5-C_5H_5)Co(PEt_2NHC^*H)(Me)Ph)(P(O)($OMe)_2$)(I), **7-12a**.

Table 7-4. Atomic Coordinates for (S_{Co}, S_C)-(η^5-C_5H_5)Co($PEt_2NHC^*H(Me)Ph$)(P(O)$(OMe)_2$)(I), **7-12a**.

atom	x	y	z	B(eq)
I(1)	0.88181(3)	0.03531(2)	0.80140(4)	4.63(2)
Co(1)	0.91171(5)	-0.11303(5)	0.73255(7)	3.22(3)
P(I)	1.0008(1)	-0.14025(9)	0.8964(1)	3.43(7)
P(2)	1.0473(1)	-0.0776(1)	0.6238(1)	3.00(6)
O(1)	1.0869(3)	-0.0870(2)	0.9367(3)	3.8(2)
O(2)	0.9226(4)	-0.1544(2)	1.0066(4)	5.2(2)
O(3)	1.0400(3)	-0.2326(2)	0.8787(4)	4.9(2)
N(1)	1.1421(3)	-0.0384(3)	0.7036(4)	3.2(2)
C(1)	0.8407(7)	-0.1718(6)	0.5855(7)	6.7(5)
C(2)	0.7720(6)	-0.1190(5)	0.634(1)	6.9(5)
C(3)	0.7561(5)	-0.1437(5)	0.756(1)	6.6(5)
C(4)	0.8175(6)	-0.2106(4)	0.7763(7)	5.3(4)
C(5)	0.8717(6)	-0.2272(4)	0.6717(8)	5.9(4)
C(6)	0.9022(7)	-0.0977(4)	1.0943(7)	7.0(4)
C(7)	1.1183(6)	-0.2659(4)	0.9546(6)	5.7(4)
C(8)	1.1043(5)	-0.1590(4)	0.5320(5)	4.6(3)
C(9)	1.1472(5)	-0.2305(4)	0.6019(7)	4.9(3)
C(10)	1.0219(5)	0.0011(4)	0.5111(6)	4.4(3)
C(11)	0.9473(6)	-0.0154(5)	0.4116(7)	8.2(5)
C(12)	1.2442(5)	-0.0123(3)	0.6600(5)	3.4(3)
C(13)	1.3268(4)	-0.0757(3)	0.6834(5)	3.1(2)
C(14)	1.3282(4)	-0.1208(3)	0.7893(6)	3.8(3)
C(15)	1.4062(5)	-0.1791(4)	0.8069(6)	4.8(3)
C(16)	1.4817(5)	-0.1904(4)	0.7232(7)	5.1(4)
C(17)	1.4816(5)	-0.1440(4)	0.6200(7)	5.0(4)
C(18)	1.4045(5)	-0.0875(3)	0.5991(5)	3.9(3)
C(19)	1.2710(5)	0.0696(4)	0.7172(8)	6.0(4)
H(1N)	1.131(4)	-0.042(3)	0.780(4)	3.6

Table 7-5. Selected Bond Distances (Å) and Bond Angles (°) for (S_{Co},S_C)-$(\eta^5$-$C_5H_5)Co(PEt_2NHC^*H(Me)Ph)(P(O)(OMe)_2)(I)$, **7-12a**.

	Distances		Angles
I(1)-Co(1)	2.5778(9)	I(1)-Co(1)-P(1)	91.39(5)
Co(1)-P(1)	2.203(2)	I(1)-Co(1)-P(2)	91.96(5)
Co(1)-P(2)	2.211(2)	I(1)-Co(1)-C(1)	126.5(3)
Co(1)-C(1)	2.109(7)	I(1)-Co(1)-C(2)	93.9(3)
Co(1)-C(2)	2.117(7)	I(1)-Co(1)-C(3)	92.5(2)
Co(1)-C(3)	2.096(6)	I(1)-Co(1)-C(4)	124.7(2)
Co(1)-C(4)	2.070(6)	I(1)-Co(1)-C(5)	156.6(2)
Co(1)-C(5)	2.056(6)	P(1)-Co(1)-P(2)	95.05(7)
C(1)-C(2)	1.36(1)	Co(1)-P(1)-O(1)	121.6(2)
C(1)-C(5)	1.38(1)	Co(1)-P(1)-O(2)	109.2(2)
C(2)-C(3)	1.43(1)	Co(1)-P(1)-O(3)	104.8(2)
C(3)-C(4)	1.37(1)	O(1)-P(1)-O(2)	109.2(2)
C(4)-C(5)	1.39(1)	O(1)-P(1)-O(3)	110.6(2)
P(1)-O(1)	1.486(4)	O(2)-P(1)-O(3)	99.0(2)
P(1)-O(2)	1.608(4)	Co(1)-P(2)-N(1)	113.7(2)
P(1)-O(3)	1.609(4)	P(2)-N(1)-C(12)	127.4(4)
P(2)-N(1)	1.646(5)	P(2)-N(1)-H(1N)	112(4)
N(1)-H(1N)	0.86(5)	C(12)-N(1)-H(1N)	119(4)
O(1)-H(1N)	1.98(5)		

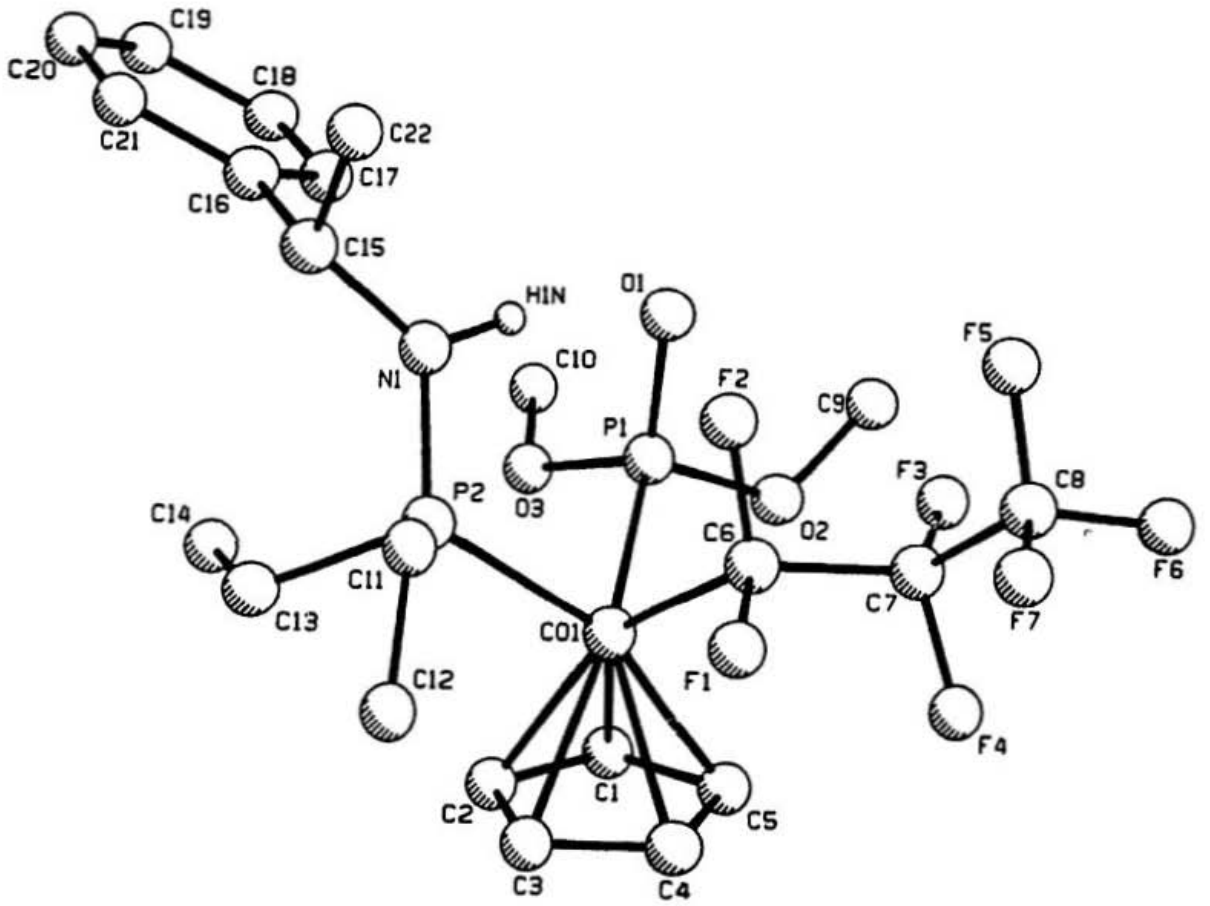

Figure 7-4. Molecular Structure of (R_{Co}, S_C)-(η^5-C_5H_5)Co(C_3F_7)($PEt_2NHCH(Me)Ph$)(P(O)($OMe)_2$), **7-13a**.

Table 7-6. Atomic Coordinates for (R_{Co}, S_C)-(η^5-C_5H_5)Co(C_3F_7)($PEt_2NHCH(Me)Ph$)(P(O)($OMe)_2$), **7-13a**.

atom	x	y	z	B(eq)
Co(1)	0.14130(6)	0.08181(2)	0.61478(7)	2.91(2)
P(1)	-0.0282(1)	0.11742(3)	0.7241(1)	2.81(5)
P(2)	0.2498(1)	0.13576(3)	0.5119(2)	3.36(5)
F(1)	0.1307(3)	0.05610(7)	0.2976(3)	4.7(1)
F(2)	-0.0068(3)	0.10751(6)	0.3376(3)	3.9(1)
F(3)	-0.1655(3)	0.0558(1)	0.5077(3)	6.5(2)
F(4)	-0.0481(3)	0.00623(7)	0.4433(4)	6.7(2)
F(5)	-0.2209(3)	0.0732(1)	0.1943(4)	7.8(2)
F(6)	-0.2710(4)	0.01362(9)	0.2592(4)	7.9(2)
F(7)	- 0.0850(3)	0.0262(1)	0.1294(4)	8.3(2)
O(1)	-0.1092(3)	0.14713(7)	0.6300(4)	3.7(1)
O(2)	-0.1353(3)	0.08724(8)	0.8138(3)	3.6(1)
O(3)	0.0461(3)	0.13925(8)	0.8740(4)	4.2(1)
N(1)	0.1518(4)	0.17619(8)	0.4999(4)	3.4(2)
C(1)	0.1630(6)	0.0556(1)	0.8415(6)	4.6(3)
C(2)	0.2945(6)	0.0688(1)	0.7879(8)	5.4(3)
C(3)	0.3283(5)	0.0482(2)	0.6480(8)	5.7(3)
C(4)	0.2177(6)	0.0222(1)	0.6138(7)	5.1(3)
C(5)	0.1137(5)	0.0271(1)	0.7330(7)	4.7(3)
C(6)	0.0397(5)	0.0726(1)	0.4108(5)	3.3(2)
C(7)	-0.0886(5)	0.0442(1)	0.4035(6)	4.1(2)
C(8)	-0.1655(6)	0.0393(2)	0.2429(6)	4.7(3)
C(9)	-0.2829(5)	0.0935(1)	0.8095(6)	5.2(3)
C(10)	-0.0400(6)	0.1608(1)	0.9861(7)	6.0(3)
C(11)	0.3226(5)	0.1293(1)	0.3098(6)	4.7(3)
C(12)	0.4343(5)	0.0971(1)	0.2843(8)	6.5(3)
C(13)	0.4072(5)	0.1517(1)	0.6193(8)	5.0(3)
C(14)	0.3834(6)	0.1722(1)	0.7791(7)	6.3(3)
C(15)	0.1968(4)	0.2170(1)	0.4538(6)	3.5(2)
C(16)	0.1668(4)	0.2484(1)	0.5829(5)	3.2(2)
C(17)	0.0783(5)	0.2416(1)	0.7101(6)	4.2(2)
C(18)	0.0556(5)	0.2709(1)	0.8259(6)	5.2(3)
C(19)	0.1217(6)	0.3078(1)	0.8135(6)	4.9(3)
C(20)	0.2090(5)	0.3150(1)	0.6864(7)	4.8(3)
C(21)	0.2313(5)	0.2860(1)	0.5704(6)	4.0(2)
C(22)	0.1346(6)	0.2296(1)	0.2929(6)	5.6(3)
H(1N)	0.0584	0.1700	0.5214	3.5

Table 7-7. Selected Bond Distances (Å) and Bond Angles (°) for (R_{Co},S_C)-(η^5-C_5H_5)Co(C_3F_7)($PEt_2NHCH(Me)Ph$)(P(O)($OMe)_2$), **7-13a**.

	Distances		Angles
Co(1)-P(1)	2.199(1)	P(1)-Co(1)-P(2)	93.85(5)
Co(1)-P(2)	2.240(1)	P(1)-Co(1)-C(1)	85.5(1)
Co(1)-C(1)	2.093(5)	P(1)-Co(1)-C(2)	109.6(2)
Co(1)-C(2)	2.099(5)	P(1)-Co(1)-C(3)	147.7(2)
Co(1)-C(3)	2.120(5)	P(1)-Co(1)-C(4)	139.4(2)
Co(1)-C(4)	2.111(4)	P(1)-Co(1)-C(5)	100.4(2)
Co(1)-C(5)	2.086(4)	P(1)-Co(1)-C(6)	94.6(1)
Co(1)-C(6)	1.982(4)	P(2)-Co(1)-C(6)	91.1(1)
C(1)-C(2)	1.400(7)	Co(1)-P(1)-O(1)	121.5(1)
C(1)-C(5)	1.393(6)	Co(1)-P(1)-O(2)	108.8(1)
C(2)-C(3)	1.391(7)	Co(1)-P(1)-O(3)	104.0(1)
C(3)-C(4)	1.392(6)	O(1)-P(1)-O(2)	109.3(2)
C(4)-C(5)	1.413(7)	O(1)-P(1)-O(3)	110.0(2)
F(1)-O(1)	1.478(3)	O(2)-P(1)-O(3)	101.4(2)
P(1)-O(2)	1.615(3)	Co(1)-P(2)-N(1)	114.6(1)
P(1)-O(3)	1.610(3)	P(2)-N(1)-C(15)	127.2(3)
P(2)-N(1)	1.639(3)	P(2)-N(1)-H(1N)	110.54
N(1)-H(1N)	0.930	C(15)-N(1)-H(1N)	122.21
O(1)-H(1N)	1.986		

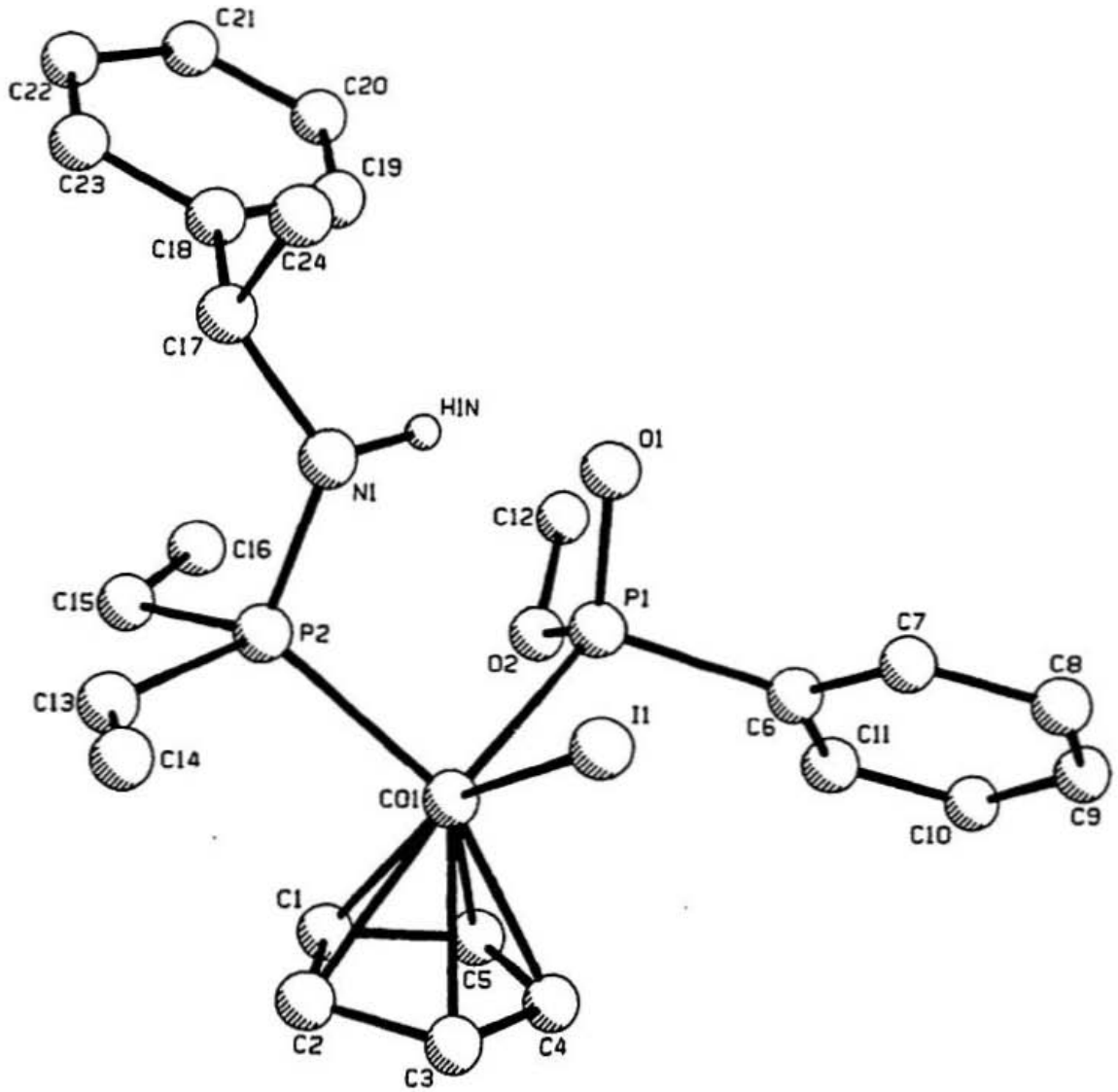

Figure 7-5. Molecular Structure of (S_{Co}, R_P, S_C)-$(\eta^5$-$C_5H_5)Co(PEt_2NHC^*H(Me)Ph)(P(O)Ph(OMe))(I)$, **7-15a**.

Table 7-8. Atomic Coordinates for (S_{Co}, R_P, S_C)-(η^5-C_5H_5)Co(PEt$_2$NHC*H(Me)Ph)(P(O)Ph(OMe))(I), **7-15a**.

atom	x	y	z	B(eq)
I(1)	1.11213(4)	0.19267(3)	0.81487(7)	4.86(3)
Co(1)	0.94089(7)	0.20183(5)	0.8791(1)	3.66(5)
P(1)	0.9089(1)	0.1997(1)	0.6214(2)	3.7(1)
P(2)	0.9445(2)	0.3040(1)	0.8943(3)	5.2(1)
O(1)	0.9534(4)	0.2453(2)	0.5120(6)	4.5(3)
O(2)	0.7989(3)	0.2049(3)	0.6142(6)	5.0(3)
N(1)	0.9969(4)	0.3360(3)	0.7417(8)	4.6(3)
C(1)	0.8308(6)	0.1910(5)	1.028(1)	5.8(5)
C(2)	0.9111(8)	0.1881(6)	1.123(1)	6.9(6)
C(3)	0.9606(8)	0.1377(7)	1.067(1)	7.7(7)
C(4)	0.913(1)	0.1112(5)	0.946(1)	7.5(8)
C(5)	0.8334(8)	0.1414(5)	0.919(1)	5.9(6)
C(6)	0.9296(7)	0.1225(4)	0.533(1)	4.6(5)
C(7)	1.0145(8)	0.1088(4)	0.472(1)	6.6(6)
C(8)	1.032(1)	0.0518(6)	0.396(1)	9.8(9)
C(9)	0.958(2)	0.0118(7)	0.384(2)	12(1)
C(10)	0.874(1)	0.0236(7)	0.444(2)	12(1)
C(11)	0.8596(8)	0.0797(5)	0.520(1)	7.7(7)
C(12)	0.7541(6)	0.2260(4)	0.472(1)	6.4(6)
C(13)	1.002(1)	0.3325(6)	1.075(2)	15(1)
C(14)	1.0788(8)	0.3202(7)	1.133(2)	15(1)
C(15)	0.8332(9)	0.3444(4)	0.923(1)	8.2(7)
C(16)	0.7619(8)	0.3347(5)	0.796(2)	9.1(8)
C(17)	1.0069(6)	0.4038(3)	0.713(1)	5.3(5)
C(18)	0.9336(5)	0.4318(3)	0.609(1)	4.2(4)
C(19)	0.8963(7)	0.4007(4)	0.480(1)	5.7(5)
C(20)	0.8303(7)	0.4283(4)	0.389(1)	6.5(6)
C(21)	0.8015(6)	0.4870(4)	0.420(1)	5.7(5)
C(22)	0.8381(7)	0.5186(4)	0.546(1)	5.7(5)
C(23)	0.9037(6)	0.4915(3)	0.639(1)	5.2(5)
C(24)	1.1034(6)	0.4135(4)	0.643(2)	8.8(7)
H(1N)	0.9687	0.3138	0.6363	5.6

Table 7-9. Selected Bond Distances (Å) and Bond Angles (°) for (S_{Co},R_P,S_C)-(η^5-C_5H_5)Co($PEt_2NHC^*H(Me)Ph$)(P(O)Ph(OMe))(I), **7-15a**.

	Distances		Angles
I(1)-Co(1)	2.562(1)	I(1)-Co(1)-P(1)	89.83(6)
Co(1)-P(1)	2.217(2)	I(1)-Co(1)-P(2)	93.80(8)
Co(1)-P(2)	2.217(3)	I(1)-Co(1)-C(1)	152.0(3)
Co(1)-C(1)	2.051(8)	I(1)-Co(1)-C(2)	113.2(3)
Co(1)-C(2)	2.115(8)	I(1)-Co(1)-C(3)	88.5(3)
Co(1)-C(3)	2.12(1)	I(1)-Co(1)-C(4)	100.1(4)
Co(1)-C(4)	2.08(1)	I(1)-Co(1)-C(5)	136.3(3)
Co(1)-C(5)	2.071(9)	P(1)-Co(1)-P(2)	94.71(9)
C(1)-C(2)	1.41(1)	Co(1)-P(1)-O(1)	119.9(2)
C(1)-C(5)	1.41(1)	Co(1)-P(1)-O(2)	104.2(2)
C(2)-C(3)	1.39(1)	Co(1)-P(1)-C(6)	112.1(3)
C(3)-C(4)	1.36(2)	O(1)-P(1)-O(2)	111.2(3)
C(4)-C(5)	1.35(1)	O(1)-P(1)-C(6)	106.2(4)
P(1)-O(1)	1.497(6)	O(2)-P(1)-C(6)	102.1(4)
P(1)-O(2)	1.610(5)	Co(1)-P(2)-N(1)	112.7(2)
P(1)-C(6)	1.855(8)	P(2)-N(1)-C(17)	125.8(6)
P(2)-N(1)	1.646(7)	P(2)-N(1)-H(1N)	105.82
N(1)-H(1N)	1.090	C(17)-N(1)-H(1N)	109.78
O(1)-H(1N)	1.828		

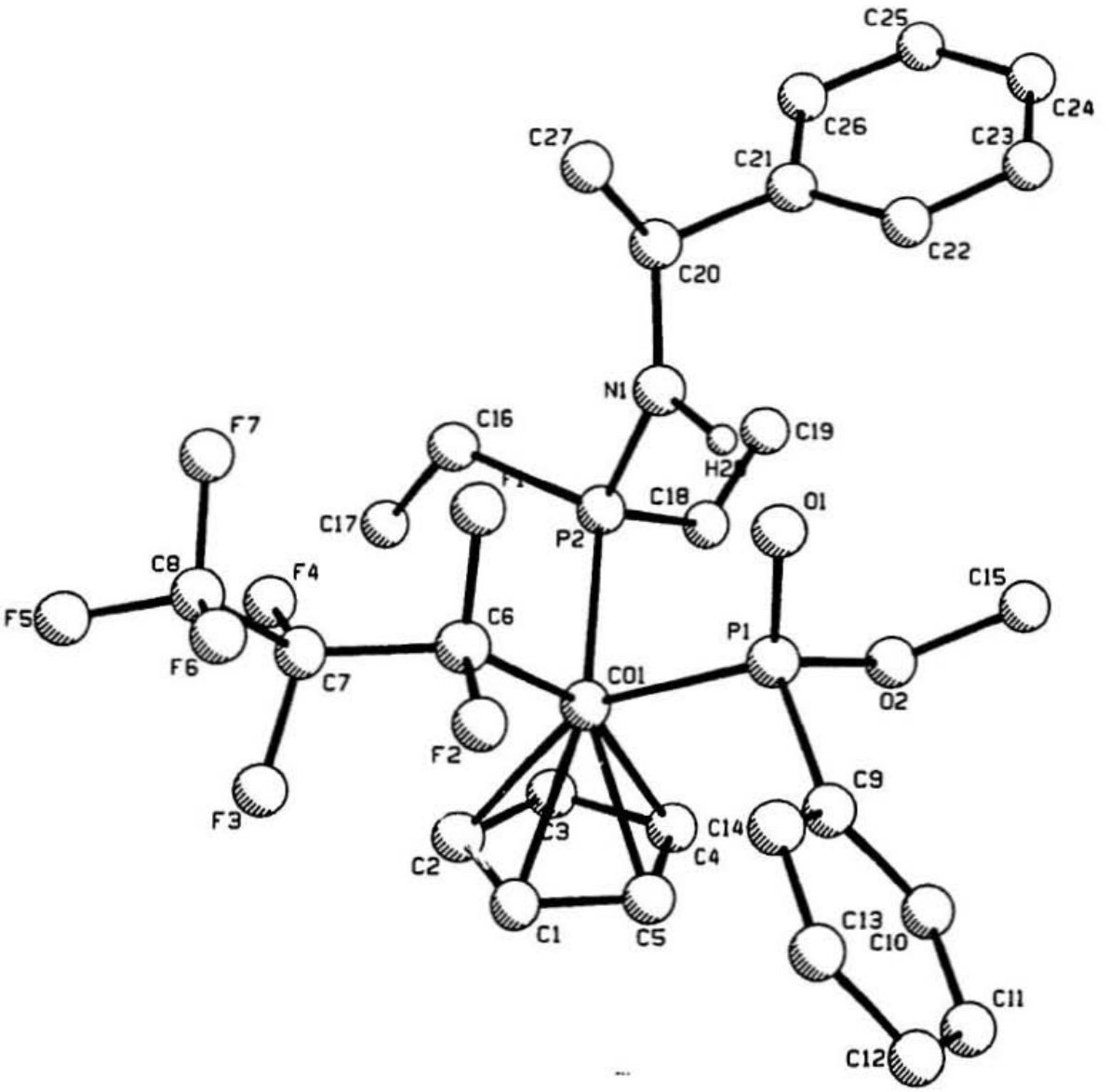

Figure 7-6. Molecular Structure of (R_{Co}, R_P, S_C)-(η^5-C_5H_5)Co(C_3F_7)($PEt_2NHCH(Me)Ph$)(P(O)Ph(OMe)), **7-16a**.

Table 7-10. Atomic Coordinates for (R_{Co}, R_P, S_C)-(η^5-C_5H_5)Co(C_3F_7)($PEt_2NHCH(Me)Ph$)(P(O)Ph(OMe)), **7-16a**.

atom	x	y	z	B(eq)
Co(1)	0.80182(7)	0.66857(3)	0.3822(1)	4.12(4)
P(1)	0.7743(1)	0.60308(7)	0.5580(3)	4.3(1)
P(2)	0.9521(1)	0.64656(7)	0.3510(3)	4.7(1)
F(1)	0.8928(3)	0.7005(1)	0.6926(5)	6.0(3)
F(2)	0.7438(3)	0.7147(2)	0.6887(6)	6.6(3)
F(3)	0.7633(4)	0.7934(2)	0.4920(7)	8.9(3)
F(4)	0.9081(4)	0.7781(2)	0.4419(7)	9.3(4)
F(5)	0.8717(5)	0.8506(2)	0.6758(7)	11.1(4)
F(6)	0.8052(5)	0.7986(2)	0.8401(7)	11.5(4)
F(7)	0.9454(4)	0.7917(2)	0.779(1)	12.7(5)
O(1)	0.8337(3)	0.5975(2)	0.7162(6)	4.6(2)
O(2)	0.7829(3)	0.5550(1)	0.4299(6)	5.4(3)
N(1)	0.9962(4)	0.6210(2)	0.5251(7)	4.9(3)
C(1)	0.6828(7)	0.7074(4)	0.297(1)	7.6(6)
C(2)	0.7567(7)	0.7220(3)	0.195(1)	5.9(5)
C(3)	0.7905(7)	0.6814(4)	0.112(1)	7.2(5)
C(4)	0.740(1)	0.6393(4)	0.157(1)	10.0(9)
C(5)	0.6732(8)	0.6569(5)	0.269(2)	9.3(8)
C(6)	0.8212(5)	0.7133(3)	0.579(1)	4.3(4)
C(7)	0.8424(6)	0.7708(3)	0.558(1)	5.3(5)
C(8)	0.8621(8)	0.8031(4)	0.718(1)	6.5(6)
C(9)	0.6513(5)	0.5986(3)	0.630(1)	4.5(4)
C(10)	0.5842(6)	0.5688(3)	0.543(1)	6.3(5)
C(11)	0.4926(6)	0.5671(4)	0.601(2)	7.7(7)
C(12)	0.4627(6)	0.5938(4)	0.741(1)	8.4(7)
C(13)	0.5289(6)	0.6217(3)	0.830(1)	7.1(6)
C(14)	0.6221(6)	0.6239(3)	0.774(1)	5.4(5)
C(15)	0.7912(6)	0.5049(3)	0.502(1)	7.7(5)
C(16)	1.0357(6)	0.6963(3)	0.293(1)	7.3(6)
C(17)	1.0210(6)	0.7260(3)	0.131(?)	8.1(6)
C(18)	0.9647(7)	0.6011(4)	0.175(1)	9.8(7)
C(19)	1.036(1)	0.5685(4)	0.159(2)	18(1)
C(20)	1.0967(5)	0.6118(3)	0.571(1)	5.0(4)
C(21)	1.1218(5)	0.5561(3)	0.579(1)	4.2(4)
C(22)	1.0618(5)	0.5209(3)	0.647(1)	5.3(4)
C(23)	1.0893(6)	0.4700(3)	0.649(1)	6.2(5)
C(24)	1.1735(6)	0.4550(3)	0.590(1)	6.4(5)
C(25)	1.2338(6)	0.4901(4)	0.523(1)	6.9(5)
C(26)	1.2095(5)	0.5401(3)	0.518(1)	6.1(5)
C(27)	1.1192(6)	0.6371(3)	0.742(1)	6.6(5)
H(28)	0.9362	0.6045	0.5864	5.6

Table 7-11. Selected Bond Distances (Å) and Bond Angles (°) for (R_{Co},R_P,S_C)-(η^5-C_5H_5)Co(C_3F_7)($PEt_2NHCH(Me)Ph$)(P(O)Ph(OMe)), **7-16a**.

	Distances		Angles
Co(1)-P(1)	2.243(2)	P(1)-Co(1)-P(2)	91.74(8)
Co(1)-P(2)	2.224(2)	P(1)-Co(1)-C(1)	115.7(4)
Co(1)-C(1)	2.084(8)	P(1)-Co(1)-C(2)	151.5(3)
Co(1)-C(2)	2.126(8)	P(1)-Co(1)-C(3)	135.3(3)
Co(1)-C(3)	2.131(9)	P(1)-Co(1)-C(4)	98.6(4)
Co(1)-C(4)	2.10(1)	P(1)-Co(1)-C(5)	89.4(3)
Co(1)-C(5)	2.05(1)	P(1)-Co(1)-C(6)	90.8(2)
Co(1)-C(6)	1.958(7)	P(2)-Co(1)-C(6)	96.3(2)
C(1)-C(2)	1.37(1)	Co(1)-P(1)-O(1)	118.6(2)
C(1)-C(5)	1.36(1)	Co(1)-P(1)-O(2)	102.7(2)
C(2)-C(3)	1.34(1)	Co(1)-P(1)-C(9)	113.6(2)
C(3)-C(4)	1.37(1)	O(1)-P(1)-O(2)	112.7(3)
C(4)-C(5)	1.37(1)	O(1)-P(1)-C(9)	106.2(3)
P(1)-O(1)	1.498(4)	O(2)-P(1)-C(9)	102.0(3)
P(1)-O(2)	1.621(5)	Co(1)-P(2)-N(1)	112.6(2)
P(1)-C(9)	1.836(7)	P(2)-N(1)-C(20)	129.1(5)
P(2)-N(1)	1.638(6)	P(2)-N(1)-H(28)	103.50
N(1)-H(28)	1.069	C(20)-N(1)-H(28)	126.09
O(1)-H(28)	1.780		

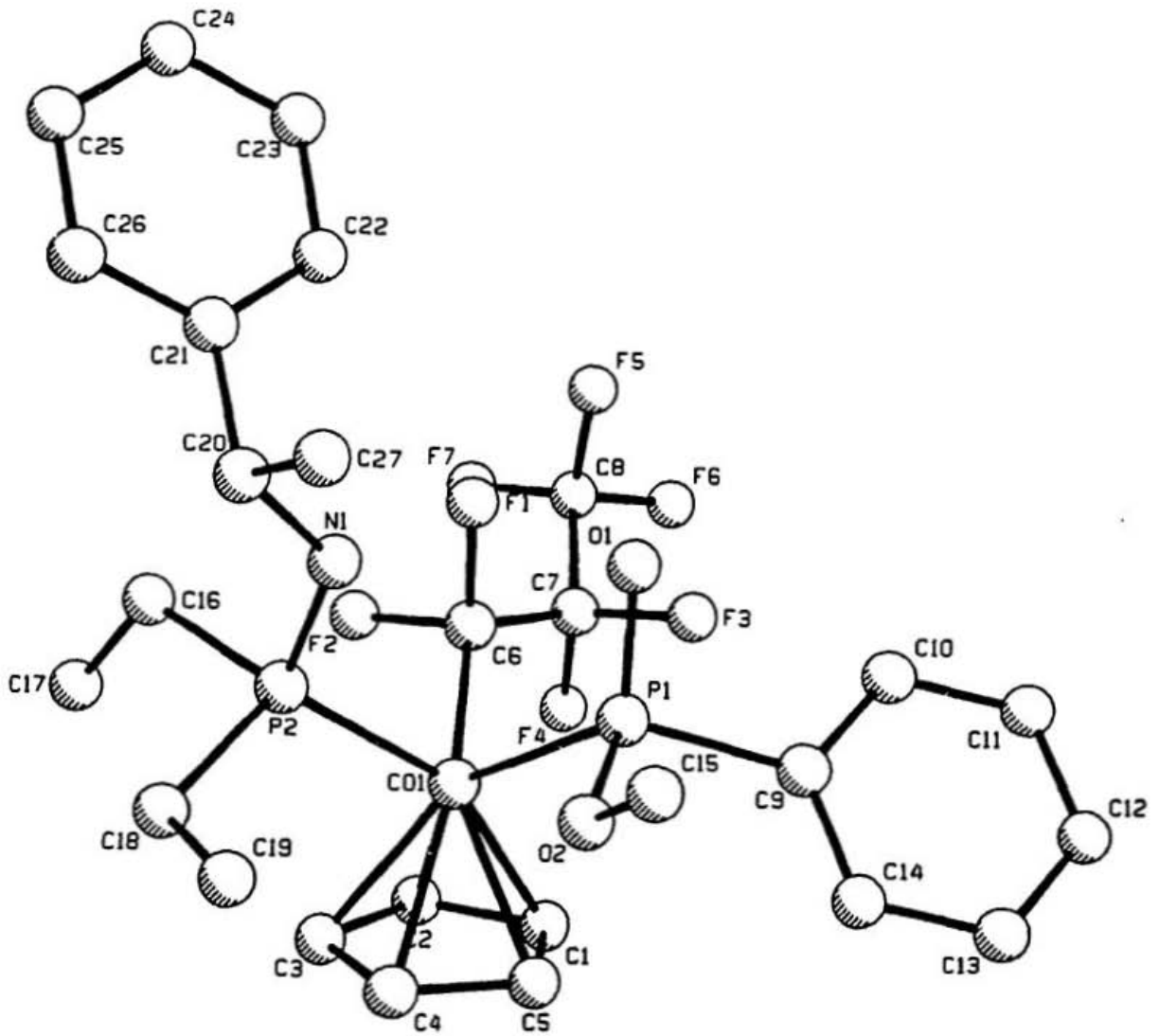

Figure 7-7. Molecular Structure of (S_{Co}, S_P, S_C)-$(\eta^5$-$C_5H_5)Co(C_3F_7)(PEt_2NHCH(Me)Ph)(P(O)Ph(OMe))$, **7-16b**.

Table 7-12. Atomic Coordinates for (S_{Co}, S_P, S_C)-(η^5-C_5H_5)Co(C_3F_7)($PEt_2NHCH(Me)Ph$)(P(O)Ph(OMe)), **7-16b** and **7-16b'**.

atom	x	y	z	B(eq)	Occupancy
Co(1)	0.26173(6)	0.09907(4)	0.7763(1)	3.57(6)	
P(1)	0.3129(1)	0.13826(9)	0.6239(2)	4.1(1)	
P(2)	0.2331(1)	0.16560(9)	0.8778(2)	3.9(1)	
F(1)	0.1188(3)	0.0805(2)	0.7825(6)	6.3(3)	
F(2)	0.1415(3)	0.1379(2)	0.6616(7)	6.6(4)	
F(3)	0.2020(4)	0.0708(3)	0.5016(6)	10.9(5)	
F(4)	0.1629(4)	0.0187(2)	0.6202(6)	8.9(5)	
F(5A)	0.0764(8)	0.0298(5)	0.454(2)	6.9(4)	0.550
F(5B)	0.036(1)	0.0768(8)	0.570(2)	8.3(5)	0.450
F(6A)	0.0365(7)	0.0424(5)	0.624(1)	7.8(3)	0.550
F(6B)	0.0986(9)	0.1051(6)	0.433(2)	8.7(4)	0.450
F(7A)	0.0514(7)	0.1012(4)	0.508(1)	6.8(3)	0.550
F(7B)	0.087(1)	0.0379(7)	0.412(2)	6.8(5)	0.450
O(1)	0.2722(4)	0.1768(2)	0.5648(6)	5.5(4)	
O(2)	0.3837(3)	0.1570(2)	0.6896(6)	5.3(4)	
N(1)	0.2275(4)	0.2122(2)	0.7866(6)	4.4(4)	
C(6)	0.1684(5)	0.0964(3)	0.699(1)	4.5(5)	
C(7)	0.1561(6)	0.0638(4)	0.585(1)	4.7(6)	
C(8)	0.083(1)	0.0633(6)	0.524(2)	10(1)	
C(15)	0.4210(6)	0.1941(4)	0.629(1)	8.4(8)	
C(16)	0.2915(6)	0.1842(4)	1.0017(9)	5.5(6)	
C(17)	0.3653(7)	0.1989(4)	0.966(1)	7.9(8)	
C(18)	0.1509(6)	0.1646(4)	0.960(1)	5.7(6)	
C(19)	0.1441(7)	0.1326(4)	1.072(1)	8.4(8)	
C(20)	0.2077(5)	0.2605(3)	0.8195(9)	4.9(5)	
C(27)	0.2617(6)	0.2935(3)	0.765(1)	7.6(7)	
H(1N)	0.2389	0.2069	0.7034	5.4	
Co(1')	0.68912(7)	0.11450(4)	0.6669(1)	3.97(6)	
P(1')	0.7029(1)	0.18666(9)	0.7460(2)	4.1(1)	
P(2')	0.7994(1)	0.0941(1)	0.7096(2)	4.2(1)	
F(1')	0.6938(3)	0.0946(2)	0.9225(5)	5.7(3)	
F(2')	0.6611(3)	0.0341(2)	0.8101(6)	6.3(3)	
F(3')	0.5648(3)	0.1337(2)	0.8762(7)	7.8(4)	
F(4')	0.5356(3)	0.0692(3)	0.7765(6)	7.8(4)	
F(5')	0.5918(3)	0.0782(2)	1.0753(6)	7.1(4)	
F(6')	0.4909(3)	0.0727(3)	1.0029(6)	8.1(4)	
F(7')	0.5656(4)	0.0168(2)	0.9757(7)	8.9(5)	
O(1')	0.7308(3)	0 1910(2)	0.8738(5)	4.6(3)	
O(2')	0.7551(4)	0.2095(2)	0.6472(6)	5.2(4)	
N(1')	0.8359(4)	0.1266(3)	0.8169(7)	4.6(4)	
C(6')	0.6543(5)	0.0842(4)	0.818(1)	4.4(5)	
C(7')	0.5796(6)	0.0879(4)	0.862(1)	5.7(7)	
C(8')	0.5571(6)	0.0617(5)	0.981(1)	5.5(7)	
C(15')	0.7912(6)	0.2524(4)	0.676(1)	7.2(7)	
C(16')	0.8138(6)	0.0339(4)	0.764(1)	6.0(6)	
C(17')	0.7914(7)	-0.0053(5)	0.681(1)	11(1)	

Table 7-12. contd.

C(18')	0.8608(5)	0.0952(4)	0.579(1)	6.0(6)
C(19')	0.8828(7)	0.1442(4)	0.534(1)	7.4(8)
C(20')	0.9078(5)	0.1232(4)	0.860(1)	5.6(6)
C(27')	0.9367(6)	0.1735(4)	0.874(1)	8.3(8)
H(1N')	0.8074	0.1499	0.8545	5.6
C(1)	0.3556(3)	0.0615(3)	0.8018(6)	5.4(2)
C(2)	0.3324(4)	0.0770(2)	0.9166(6)	5.7(3)
C(3)	0.2668(3)	0.0569(3)	0.9385(5)	5.7(2)
C(4)	0.2495(3)	0.0290(2)	0.8372(7)	5.9(3)
C(5)	0.3044(4)	0.0318(2)	0.7527(5)	5.9(2)
C(21)	0.1332(2)	0.2732(2)	0.7821(6)	4.1(2)
C(22)	0.0960(3)	0.2463(2)	0.6974(6)	4.9(2)
C(23)	0.0293(3)	0.2603(2)	0.6611(5)	5.6(3)
C(24)	-0.0002(3)	0.3011(2)	0.7095(7)	6.8(3)
C(25)	0.0371(4)	0.3279(2)	0.7942(6)	8.1(3)
C(26)	0.1038(3)	0.3140(2)	0.8305(5)	6.1(3)
C(9)	0.3517(3)	0.1046(2)	0.4966(5)	4.3(2)
C(10)	0.3205(3)	0.1098(2)	0.3818(6)	5.2(2)
C(11)	0.3500(3)	0.0884(2)	0.2791(5)	6.7(3)
C(12)	0.4109(3)	0.0618(2)	0.2912(6)	6.6(3)
C(13)	0.4421(3)	0.0566(2)	0.4060(7)	7.1(3)
C(14)	0.4125(3)	0.0780(2)	0.5087(5)	7.0(3)
C(1')	0.5973(3)	0.1182(3)	0.5636(6)	5.6(3)
C(2')	0.6217(4)	0.0719(2)	0.5610(7)	6.1(3)
C(3')	0.6877(4)	0.0719(2)	0.5058(7)	5.8(3)
C(4')	0.7041(3)	0.1183(3)	0.4742(6)	5.9(3)
C(5')	0.6483(4)	0.1469(2)	0.5100(7)	5.2(2)
C(9')	0.6292(3)	0.2282(2)	0.7412(7)	4.8(2)
C(10')	0.5859(4)	0.2328(2)	0.8434(6)	5.5(2)
C(11')	0.5323(3)	0.2660(3)	0.8433(6)	7.2(3)
C(12')	0.5220(3)	0.2946(2)	0.7410(8)	7.7(3)
C(13')	0.5653(4)	0.2900(2)	0.6388(6)	8.7(4)
C(14')	0.6189(3)	0.2569(3)	0.6389(6)	7.1(3)
C(21')	0.9139(4)	0.0973(2)	0.9828(6)	5.1(2)
C(22')	0.8625(3)	0.1026(2)	1.0723(8)	6.9(3)
C(23')	0.8717(4)	0.0827(3)	1.1882(7)	9.6(4)
C(24')	0.9325(5)	0.0577(3)	1.2146(6)	9.0(4)
C(25')	0.9840(3)	0.0524(2)	1.1252(8)	8.7(4)
C(26')	0.9747(3)	0.0722(3)	1.0092(7)	8.0(4)

Table 7-13. Selected Bond Distances (Å) and Bond Angles (°) for (R_{Co},R_P,S_C)-(η^5-C_5H_5)Co(C_3F_7)($PEt_2NHCH(Me)Ph$)(P(O)Ph(OMe)), **7-16b** and **7-16b'**.

	Distances			Angles	
	6b	**6b'**		**6b**	**6b'**
Co(1)-P(1)	2.228(3)	2.244(3)	P(1)-Co(1)-P(2)	93.0(1)	92.7(1)
Co(1)-P(2)	2.261(3)	2.240(3)	P(1)-Co(1)-C(1)	88.7(2)	105.0(2)
Co(1)-C(1)	2.111(6)	2.090(6)	P(1)-Co(1)-C(2)	113.7(2)	143.8(2)
Co(1)-C(2)	2.137(7)	2.115(7)	P(1)-Co(1)-C(3)	151.3(2)	146.9(2)
Co(1)-C(3)	2.139(7)	2.134(7)	P(1)-Co(1)-C(4)	139.0(2)	108.5(2)
Co(1)-C(4)	2.115(7)	2.123(7)	P(1)-Co(1)-C(5)	101.2(2)	87.4(2)
Co(1)-C(5)	2.098(7)	2.095(7)	P(1)-Co(1)-C(6)	95.6(3)	96.8(3)
Co(1)-C(6)	1.98(1)	1.98(1)	P(2)-Co(1)-C(6)	91.3(3)	91.8(3)
C(1)-C(2)	1.40(1)	1.40(1)	Co(1)-P(1)-O(1)	117.4(3)	118.4(3)
C(1)-C(5)	1.40(1)	1.400(9)	Co(1)-P(1)-O(2)	101.7(3)	100.7(3)
C(2)-C(3)	1.400(9)	1.40(1)	Co(1)-P(1)-C(9)	118.6(2)	119.2(2)
C(3)-C(4)	1.40(1)	1.400(9)	O(1)-P(1)-O(2)	112.6(4)	111.6(4)
C(4)-C(5)	1.40(1)	1.400(9)	O(1)-P(1)-C(9)	105.5(3)	104.3(4)
P(1)-O(1)	1.492(7)	1.497(7)	O(2)-P(1)-C(9)	99.6(3)	101.4(3)
P(1)-O(2)	1.623(7)	1.607(7)	Co(1)-P(2)-N(1)	113.0(3)	113.7(3)
P(1)-C(9)	1.834(6)	1.843(6)	P(2)-N(1)-C(20)	128.1(6)	126.5(7)
P(2)-N(1)	1.660(7)	1.646(8)	P(2)-N(1)-H(1N)	115.64	117.07
N(1)-H(1N)	0.944	0.952	C(20)-N(1)-H(1N)	116.28	116.47
O(1)-H(1N)	1.851	1.889			

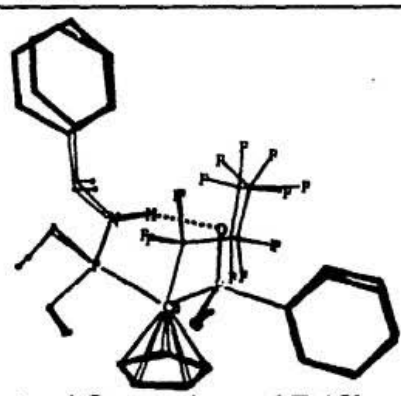

Figure 7-8. Structural Comparison of **7-16b** and **7-16b'**.

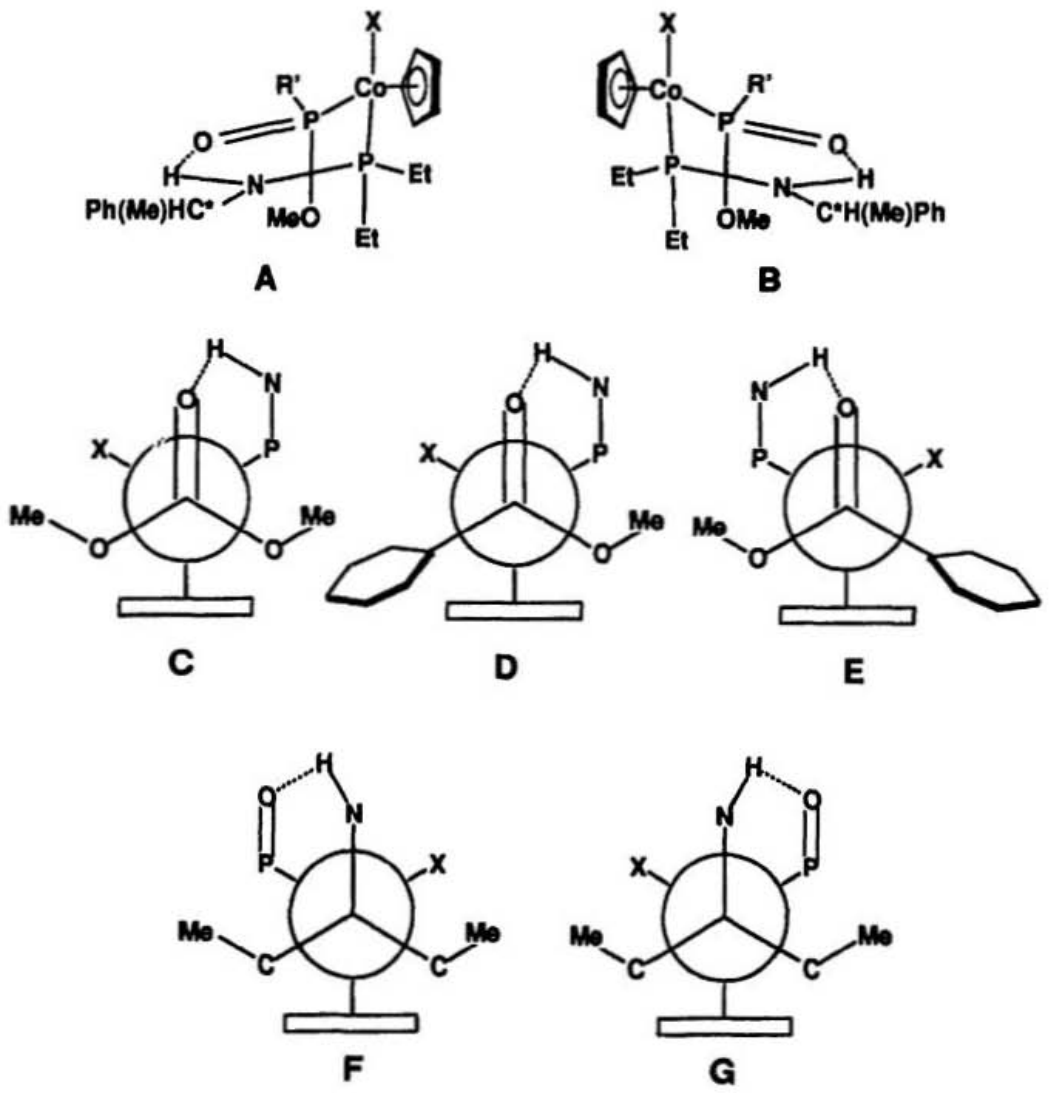

Figure 7-9. Solid State Conformations for **7-12a**, **7-13a**, **7-15a**, **7-16a** and **7-16b**. (A & B: Quasi-chair conformation for **7-12a** (A, R' = OMe, X = I), **7-13a** (A, R' = OMe, X = C_3F_7), **7-15a** (A, R' = Ph, X = I), **7-16a** (A, R' = Ph, X = C_3F_7), and **7-16b** (B, R' = Ph, X = C_3F_7); C, Dx& E: Newman Projection along P(O)-Co Bond for **7-12a** (C, X = I), **7-13a** (C, X = C_3F_7), **7-15a** (D, X = I), **7-16a** (D, X = C_3F_7), and **7-16b** (E, X = C_3F_7); F & G: Newman Projection along P(N)-Co Bond for **7-12a** (F, X = I), **7-13a** (F, X = C_3F_7), **7-15a** (F, X = I), **7-16a** (F, X = C_3F_7), and **7-16b** (G, X = C_3F_7).)

7.2.5. Absolute Configurations. The absolute configurations of the cobaltophosphonates **7-12a,b**, **7-13a,b**, **7-14a,b** and phosphinates **7-15a,b,c,d** and **7-16a,b,c,d** were determined by a combination of X-ray crystallography, circular dichroism (CD) spectra, chromatographic relative Rf values along with a comparison to the isostructural phosphonates of known configuration and confirmed by the epimerization circles in the cases with X = I (**7-15a,b,c,d**). The absolute configurations of **7-12a** (X = I) and **7-13a** (X = C_3F_7) were unequivocally assigned from the x-ray structures shown in Figures 7-3 and 7-4. The correct assignment of the absolute configurations of the chiral carbon, known to be *S* provided an internal reference for the assignment of the cobalt atom chirality. On the basis of the modified Cahn-Ingold-Prelog rules[290-293, 372] with the ligand priority series of I > η^5-C_5H_5 > P(O)$(OMe)_2$ > (S_C)-PEt_2NHC*H(Me)Ph (for **7-12a,b**) or η^5-C_5H_5 > P(O)$(OMe)_2$ > (S_C)-PEt_2NHC*H(Me)Ph > C_3F_7 (for **7-13a,b**) the absolute configurations of pseudotetrahedral complexes **7-12a** and **7-13a** were assigned as $S_{Co}S_C$ and $R_{Co}S_C$, respectively. Since the CD spectra of the high Rf **7-12a** and low Rf **7-12b** as well as the high Rf **7-13a** and the low Rf **7-13b** are quasi-mirror images (Figures 7-10a and 7-11a)[206, 208, 355, 365] and the morphology of the CD spectra is generally dominated by metal-centered electronic transitions,[384] **7-12a** and **7-12b** as well as **7-13a** and **7-13a** are epimeric at cobalt with absolute configurations $S_{Co}S_C$ (**7-12a**), $R_{Co}S_C$ (**7-12b**), $R_{Co}S_C$ (**7-13a**) and $S_{Co}S_C$ (**7-13b**), respectively. The assignments are consistent with reported results for isostructural (η^5-C_5H_5)Co(PPh_2NHC*H(Me)Ph)(P(O)$(OMe)_2$)(X) (X = I, **7-19a,b**[206]; X = C_3F_7, **7-20a,b**[208]). As shown in Figure 7-10a,c, the morphology

of the CD spectra for high Rf **7-12a** (Figure 7-10a) is similar to that of high Rf S_{Co},S_C-**7-19a** (Figure 7-10c).[206] Likewise the CD spectra relate the cobalt configurations of low Rf **7-12b** (Figure 7-10a) and low Rf R_{Co},S_C-**7-19b** (Figure 7-10c), high Rf **7-13a** (Figure 7-11a) and high Rf S_{Co},S_C-**7-20a** (Figure 7-11b),[208] and low Rf **7-13b** (Figure 7-11a) and low Rf R_{Co},S_C-**7-20b** (Figure 7-11b).[208] Although the absolute configurations of the high Rf **7-12a** and **7-13a** are different from each other because of the different CIP sequences, the high Rf isomers **7-12a** and **7-13a** possess the same relative stereochemistry. The same situation is true for the low Rf **7-12b** and **7-13b**.

Chromatographic relative Rf values and the CD spectra are reliable indicators of absolute configuration of the phosphonate complexes as demonstrated above and reported before,[208] and were used to establish the configurations of **7-14a** and **7-14b**. As shown in Figure 7-10b,d, the CD spectra of the high Rf **7-14a** and the low Rf **7-14b** are quasi-mirror images (Figure 7-10b) and are similar to the CD morphology (Figure 7-10d) of the isostructural phosphonates S_{Co},S_C-(high Rf)- and R_{Co},S_C-(low Rf)-(η^5-C_5Me_5)Co($PPh_2NHC^*H(Me)Ph$)(P(O)$(OMe)_2$)(I) (**7-21a,b**),[207] respectively. Accordingly, the absolute configurations of **7-14a** and **7-14b** are assigned as S_{Co},S_C and R_{Co},S_C, respectively, which are consistent with the assignments for the corresponding absolute configurations of **7-12a,b** and **19a,b**.

Similarly, the crystal structure of **7-15a** (Figure 7-5) fixes its absolute configuration

as S_{Co},R_P,S_C. Since the morphology of the CD spectra is dominated by the chiral metal center[384] and the chiral phosphorus center only displays a secondary effect,[206, 217, 365] the CD spectra (Figure 7-12a,b) along with the epimerization experiments allow determination of the absolute configurations for all four diastereomers **7-15a,b,c,d**. The similar CD morphology of **7-15a** (Figure 7-15a) and **7-15c** (Figure 7-12b) establishes that the absolute configurations at cobalt for **7-15a** and **7-15c** are identical (S_{Co}). Given that **7-15a** is S_{Co},R_P,S_C the diastereomeric relationship between **7-15a** and **7-15c** requires that they are epimeric at phosphorus. The absolute configuration of **7-15c** *must* therefore be S_{Co},S_P,S_C. Since the CD spectra of **7-15a** and **7-15b** (Figure 7-12a) as well as **7-15c** and **7-15d** (Figure 7-12b) are quasi-mirror images the absolute configurations of **7-15b** and **7-15d** can be assigned as R_{Co},S_P,S_C and R_{Co},R_P,S_C, respectively.

These assignments are confirmed by the specific interconversion of **7-15a** ↔ **7-15d** and **7-15b** ↔ **7-15c**. ^{1}H NMR spectra and TLC analysis showed that an identical mixture of **7-15a** and **7-15d** was formed on standing in $CDCl_3$ solution of diastereomerically pure **7-15a** or **7-15d**. Similarly, a diastereomerically pure $CDCl_3$ solution of **7-15b** or **7-15c** gave a mixture of **7-15b** and **7-15c**. If isomerization is a simple Co epimerization as the CD evidence suggests, the above interconversions require that the diastereomeric pairs **7-15a,d** and **7-15b,c** have identical configuration at phosphorus. Therefore, the absolute configurations of **7-15b** and **7-15d** are assigned as R_{Co},S_P,S_C and R_{Co},R_P,S_C, respectively. Further confirmation of these

assignments is made by comparison of the CD spectra of **7-15a,b,c,d** with those of the isostructural phosphinates (η^5-C_5H_5)Co(PPh_2NHC*H(Me)Ph)(P(O)R'(OMe))(I) (R' = Ph, **7-22a,b,c,d**[206]; R' = t-Bu, **7-23a,b,c,d**[218] and R' = Et, **7-24a,b,c,d**[218]) as well as by the consistent empirical correlation between the relative TLC Rf values and the absolute configurations. Complexes **7-15a,b,c,d** (Figure 7-12a,b) have similar CD morphology to complexes **7-22a,b,c,d** (Figure 7-12c,d).[206] In the order of decreasing Rf values, the absolute configurations of **7-22 - 7-24a,b,c,d** are S_{Co},R_P,S_C; R_{Co},S_P,S_C; S_{Co},S_P,S_C; and R_{Co},R_P,S_C, respectively. Hence, the assignments for the absolute configurations of **7-15a,b,c,d** , which follow the same pattern as **7-22 - 7-24a,b,c,d**, are correct.

The crystal structures of **7-16a** (Figure 7-6) and **7-16b** (Figure 7-7) unequivocally establish their absolute configurations as R_{Co},R_P,S_C and S_{Co},S_P,S_C, respectively, on the basis of modified Cahn-Ingold-Prelog rules[290-293, 372] with the ligand priority series of η^5-C_5H_5 > P(O)Ph(OMe) > (S_C)-PEt_2NHC*H(Me)Ph > C_3F_7. The similar CD morphology of **7-16a** (Figure 7-13a) and **7-16c** (Figure 7-13b) shows that the absolute configuration at cobalt for **7-16a** and **7-16c** is identical (R_{Co}). Given that **7-16a** has the absolute configuration of R_{Co},R_P,S_C, the diastereomeric relationship between **7-16a** and **7-16c** requires that they be epimeric at phosphorus, hence the absolute configuration of **7-16c** *must* be R_{Co},S_P,S_C. Accordingly, similar CD morphology of S_{Co},S_P,S_C-**7-16b** (Figure 7-13a) and **7-16d** (Figure 7-13b) establishes the absolute configuration of **7-16d** as S_{Co},R_P,S_C. The quasi-mirror image

relationships of the CD spectra for **7-16a/7-16b** and **7-16c/7-16d** confirm these assignments. Further confirmation derives from the consistent empirical correlation of chromatographic relative Rf values with the absolute configurations and by comparison of the CD spectra of **7-16a,b,c,d** with those of the isostructural phosphinates (η^5-C_5H_5)Co(C_nF_{2n+1})($PPh_2NHC^*H(Me)Ph$)(P(O)Ph(OMe)) (n = 1, **7-25a,b,c,d**; n = 2, **7-26a,b,c,d**[217]). Figure 7-13 shows that the CD spectra of complexes **7-16a,b,c,d** (Figure 7-13a,b) have morphologies similar to those of isostructural perfluoroalkyl phosphinates **7-26a,b,c,d** (Figure 7-13c,d).[217] In the order of decreasing Rf values, the absolute configurations of all isostructural perfluoroalkyl phosphinates are: $R_{Co}R_P,S_C$; $S_{Co}S_P,S_C$; $R_{Co}S_P,S_C$; and $S_{Co}R_P,S_C$, respectively.

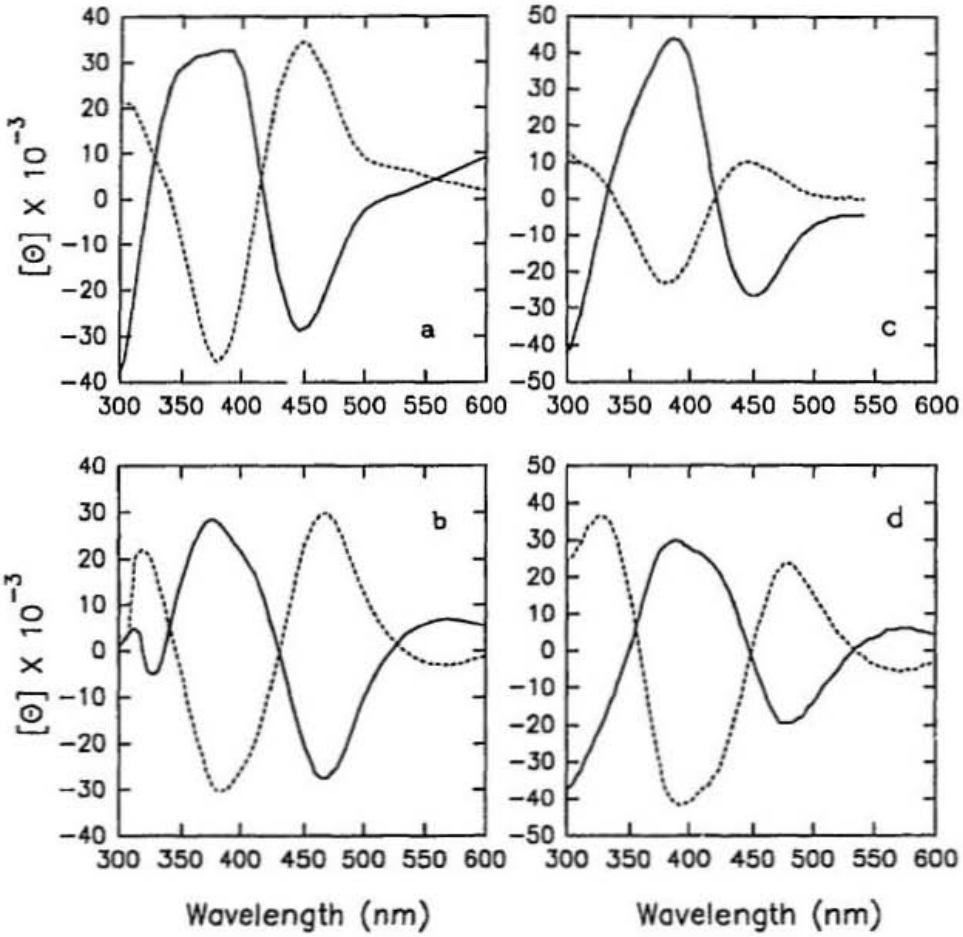

Figure 7-10. Circular Dichroism Spectra of (a) **7-12a** (——), **7-12b** (----); (b) **7-14a** (——), **7-14b** (----); (c) (η^5-C_5H_5)Co($PPh_2NHC^*H(Me)Ph$)(P(O)$(OMe)_2$)(I) , **7-19a,b**[206], S_{Co},S_C (—-—), R_{Co},S_C (----); (d) (η^5-C_5Me_5)Co($PPh_2NHC^*H(Me)Ph$)(P(O)$(OMe)_2$)(I), **7-21a,b**[207], S_{Co},S_C (——), R_{Co},S_C (----).

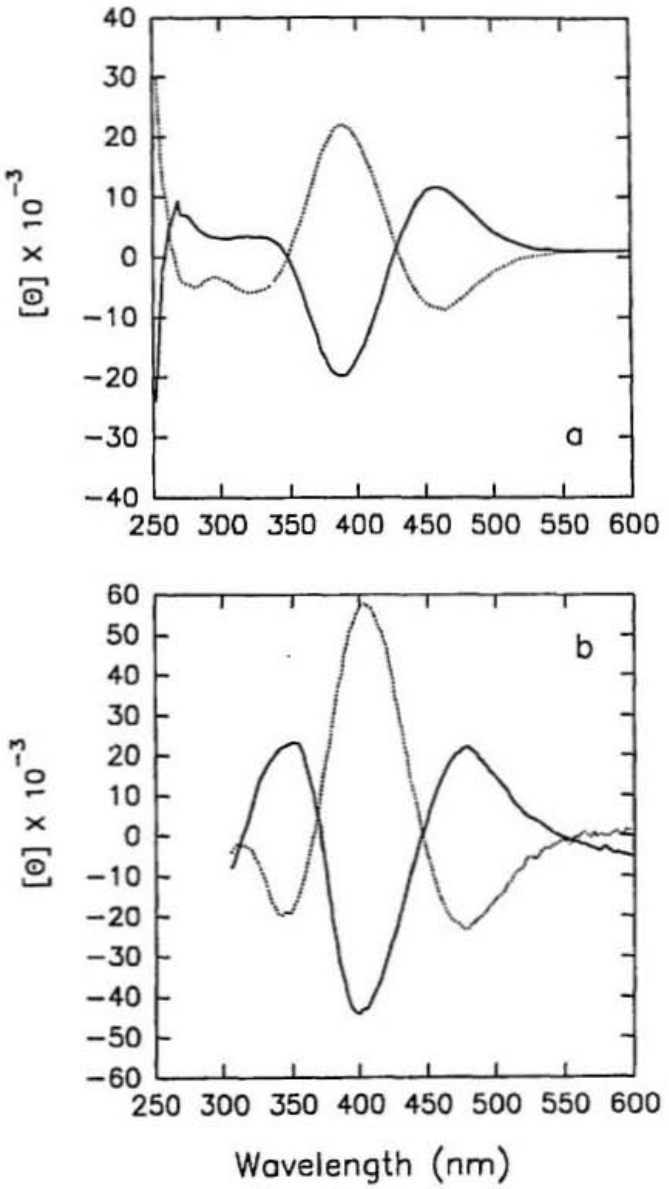

Figure 7-11. Circular Dichroism Spectra of (a) **7-13a** (——), **7-13b** (----); (b) (η^5-C_5H_5)Co($PPh_2NHC^*H(Me)Ph$)($P(O)(OMe)_2$)(C_3F_7), **7-20a,b**[208], $R_{Co}S_C$ (——), $S_{Co}S_C$ (----).

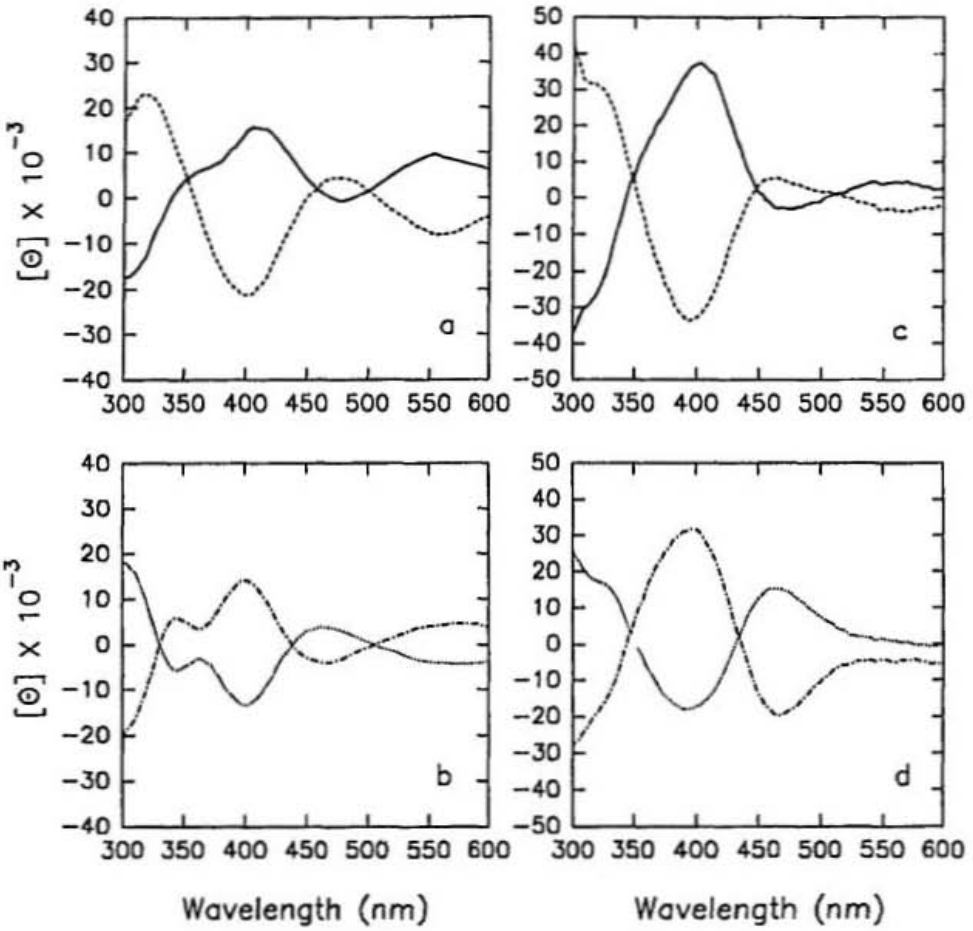

Figure 7-12. Circular dichroism spectra of (a) **7-15a** (——), **7-15b** (----); (b) **7-15c** (·· - · - · - · - ·), **7-15d** (· · · · · · · · ·). (c, d) (η^5-C_5H_5)Co(PPh_2NHC*H(Me)Ph)(P(O)Ph(OMe))(I), **7-22a,b,c,d**[206], $S_{Co}R_P,S_C$ (——), $R_{Co}S_P,S_C$ (----), $S_{Co}S_P,S_C$ (·· ·· ··), $R_{Co}R_P,S_C$ (· · · · ·).

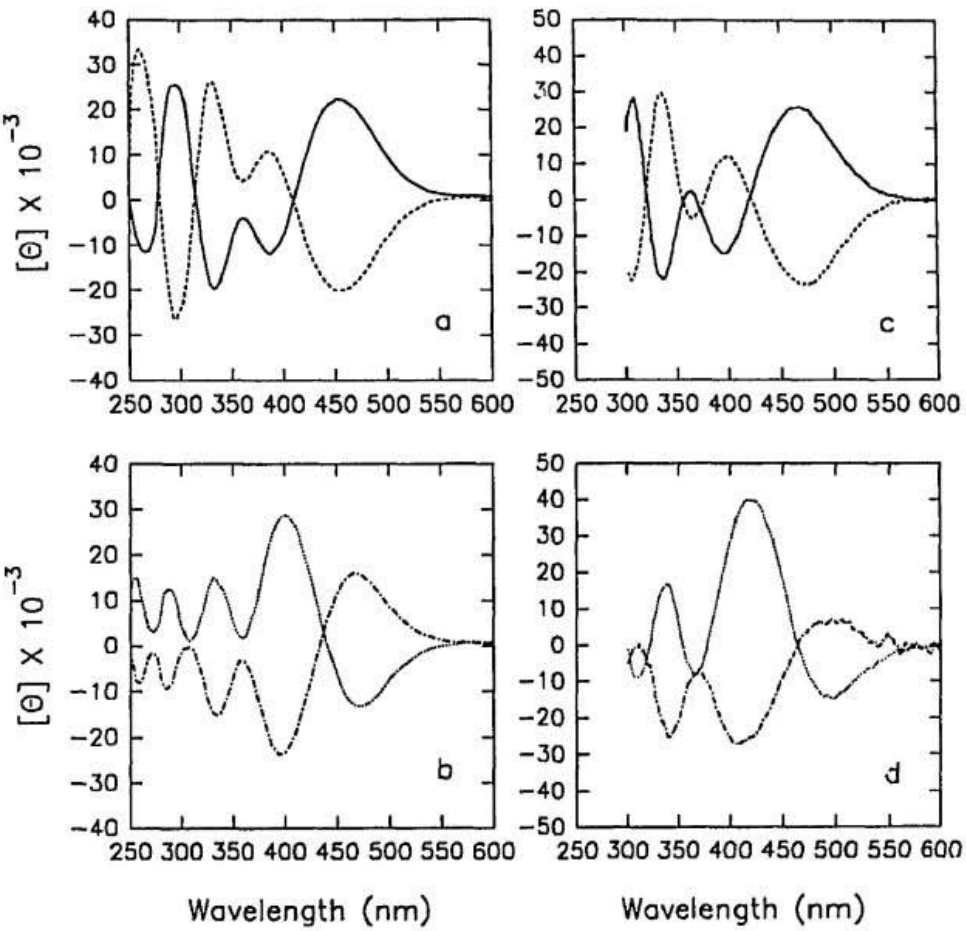

Figure 7-13. Circular dichroism spectra of (a) **7-16a** (——), **7-16b** (----); (b) **7-16c** (-· - · - ·), **7-16d** (· · · · ·). (c, d) (η^5-C_5H_5)Co($PPh_2NHC^*H(Me)Ph$)(P(O)Ph(OMe))(C_3F_7), **7-26a,b,c,d**[217], ***R**$_{Co}$**R**$_P$**S**$_C$* (——), ***S**$_{Co}$**S**$_P$**S**$_C$* (----), ***R**$_{Co}$**S**$_P$**S**$_C$* (-·-·), ***S**$_{Co}$**R**$_P$**S**$_C$* (····).

7.2.6. Solution Conformation. The ^{1}H nOed spectra (Figures 7-14, 7-15, 7-16) demonstrate that the solid state conformations of both cobaltophosphonates and cobaltophosphinates persist in solution. Intramolecular P=O•••H-N hydrogen bonding forces a quasi-chair conformation as shown in Figure 7-9. For the η^5-cyclopentadienyl and η^5-pentamethylcyclopentadienyl cobaltophosphonates **7-12a,b**, **7-13a,b** and **7-14a,b** the results strongly support the conformation with *equatorial* η^5-Cp/Cp* gauche with respect to an *axial/equatorial* pair of diastereotopic aminophosphine ethyl and phosphonate methoxy groups (cf. Figure 7-9).[206-208]

Using **7-14a** as an example (Figure 7-14C), irradiation of the Cp* resonance affords enhancements to the aminophosphine P-C<u>Ha</u>Hb- (4.2%), P-C'<u>Ha</u>Hb- (3.0%), P-CH_2-<u>Me</u> (3.1%), and P-C'H_2-<u>Me</u> (2.6%) as well as the phosphonate methoxy groups P-O<u>Me</u> (1.6%) and P-O<u>Me</u>' (1.6%), respectively. Partial saturation of the P-C'H_2-<u>Me</u> shows 0.9% enhancement specifically to the axial P-O<u>Me</u>. Similar NOE interactions are observed for the remaining phosphonate complexes **7-12a**, **7-12b**, **7-13a**, **7-13b**, **7-14b** (cf. Figures 7-14 and 7-15).

The conformational preferences for the two major diastereomers (**7-15a** and **7-15b**) of cobaltophosphinates **7-15a,b,c,d** (cf. Figure 7-14E,F) and the four isomers (**7-16a**, **7-16b**, **7-16c**, and **7-16d**) of the perfluoroalkyl cobaltophosphinates **7-16a,b,c,d** (cf. Figure 7-15C,D,E,F) are also evident from their nOed spectra. R_{Co},S_P,S_C-**7-15b** is representative (Figures 7-14F & 7-16). Irradiation of the Cp resonance (Figure 7-16c)

shows positive enhancements to the aminophosphine P-CHaHb- (1.6%), P-CH_2-Me (0.9%) and P-C'H_2-Me (0.8%) as well as the phosphinate P(O)-OMe (1.3%) and the H_{ortho} (2.1%) of P(O)-Ph, respectively. Reverse enhancement from the H_{ortho} of P(O)-Ph to Cp (1.6%) is observed with partial saturation of the H_{ortho} resonance of P(O)-Ph (Figure 7-16d). In accordance with the quasi-chair conformation, which places the P(O)-OMe and one P-Et in 1,3-*axial* positions, positive nOe enhancement to the *axial* P-CH_2-*Me* (0.9%) is observed specifically from the P(O)-OMe (but not from the H_{ortho} of the *equatorial* P(O)-Ph) when the P(O)-OMe (Figure 7-16b) and H_{ortho} of P(O)-Ph (Figure 7-16d) are irradiated. Therefore, the two major diastereomers, S_{Co},R_P,S_C-**7-15a** and R_{Co},S_P,S_C-**7-15b**, adopt conformations with 1,3-*diaxial* P(O)-OMe and the P-Et and *equatorial* P(O)-Ph, as shown in Figure 7-9. In contrast, the S_{Co},S_P,S_C-**7-15c** and R_{Co},R_P,S_C-**7-15d** diastereomers force the phenyl group of P(O)-Ph to occupy an unfavorable *axial* position.[206, 217, 218] Similarly, the two major diastereomers of perfluoroalkyl cobaltophosphinates R_{Co},R_P,S_C-**7-16a** and S_{Co},S_P,S_C-**7-16b** adopt a conformation with 1,3-*axial* P(O)-OMe and P-Et while the two minor diastereomers R_{Co},S_P,S_C-**7-16c** and S_{Co},R_P,S_C-**7-16d** would force the phenyl group of P(O)-Ph and P-Et into the unfavorable 1,3-*diaxial* position.[217]

Assumption of a product-like transition state[206, 217, 218] for the Arbuzov dealkylation of the prochiral phosphonite to phosphinate (Scheme 1-50) suggests that 1,3-diaxial steric interactions of the P(N) and P(O) substituents of the P=O•••H-N hydrogen bonded quasi-chair template control the product distribution. Scheme 1-50 predicts

diastereomers S_{Co},R_P and R_{Co},S_P (for X = I) and R_{Co},R_P and S_{Co},S_P (for X = C_3F_7) with minimum 1,3-diaxial interactions will be the major products. ^{1}H NMR reactions show that the kinetic product ratio for **7-4** → **7-15a,b,c,d** (Scheme 7-1) is 39/16/32/13 (**7-15a/7-15b/7-15c/7-15d**), which shows that the optical yields are very low compared to the isostructural $PPh_2NHC^*H(Me)Ph$[205,218] case. This is reasonable since the energy difference for ethyl/phenyl versus ethyl/methoxy 1,3-diaxial interactions in **7-15** is diminished compared to that for phenyl/phenyl versus phenyl/methoxy in **7-22**. Nevertheless, the absolute configuration of the major products is correctly predicted from the transition state placing Et/OMe in the favorable 1,3-*diaxial* positions. ^{1}H NMR showed that the optical yields are very low for the reaction from **7-6a,b** → **7-16a,b,c,d** (3.6 %de for R_{Co},R_P,S_C-**7-16a** versus R_{Co},S_P,S_C-**7-16c** and 3.2 %de for S_{Co},S_P,S_C-**7-16b** versus S_{Co},R_P,S_C-**7-16d**, cf. Scheme 7-1). The interpetation follows the above discussion for **7-4** → **7-15a,b,c,d**. These observations support the proposal that 1,3-diaxial interactions are the essential factor in the Co* → P chiral information transfer. When these steric interactions diminish the chiral induction decreases.

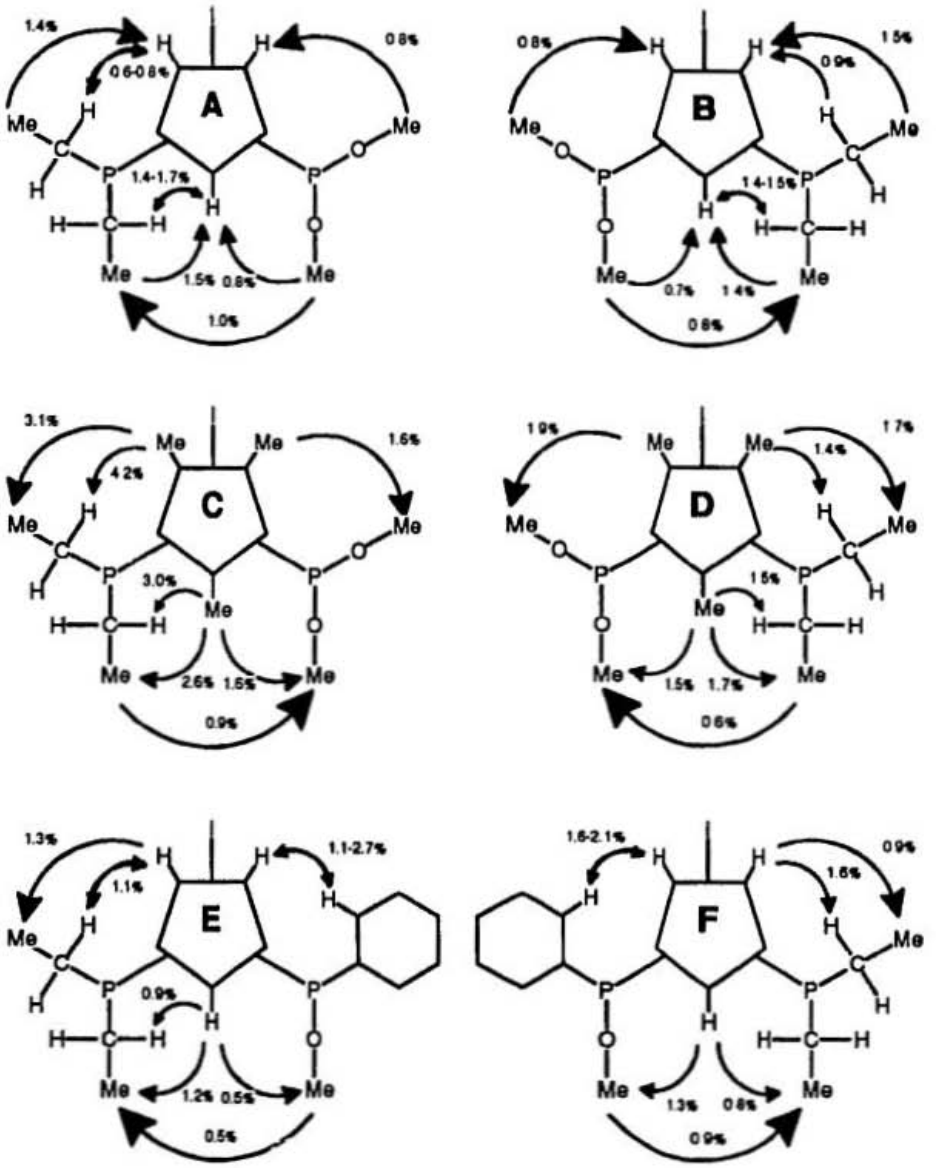

Figure 7-14. Major Nuclear Overhauser Effect Difference Data of Arbuzov Products with X = I. (A. $S_{Co}S_C$-**7-12a**; B. $R_{Co}S_C$-**7-12b**; C. $S_{Co}S_C$-**7-14a**; D. $R_{Co}S_C$-**7-14b**; E. $S_{Co}R_P S_C$-**7-15a**; F. $R_{Co}S_P S_C$-**7-15b**.)

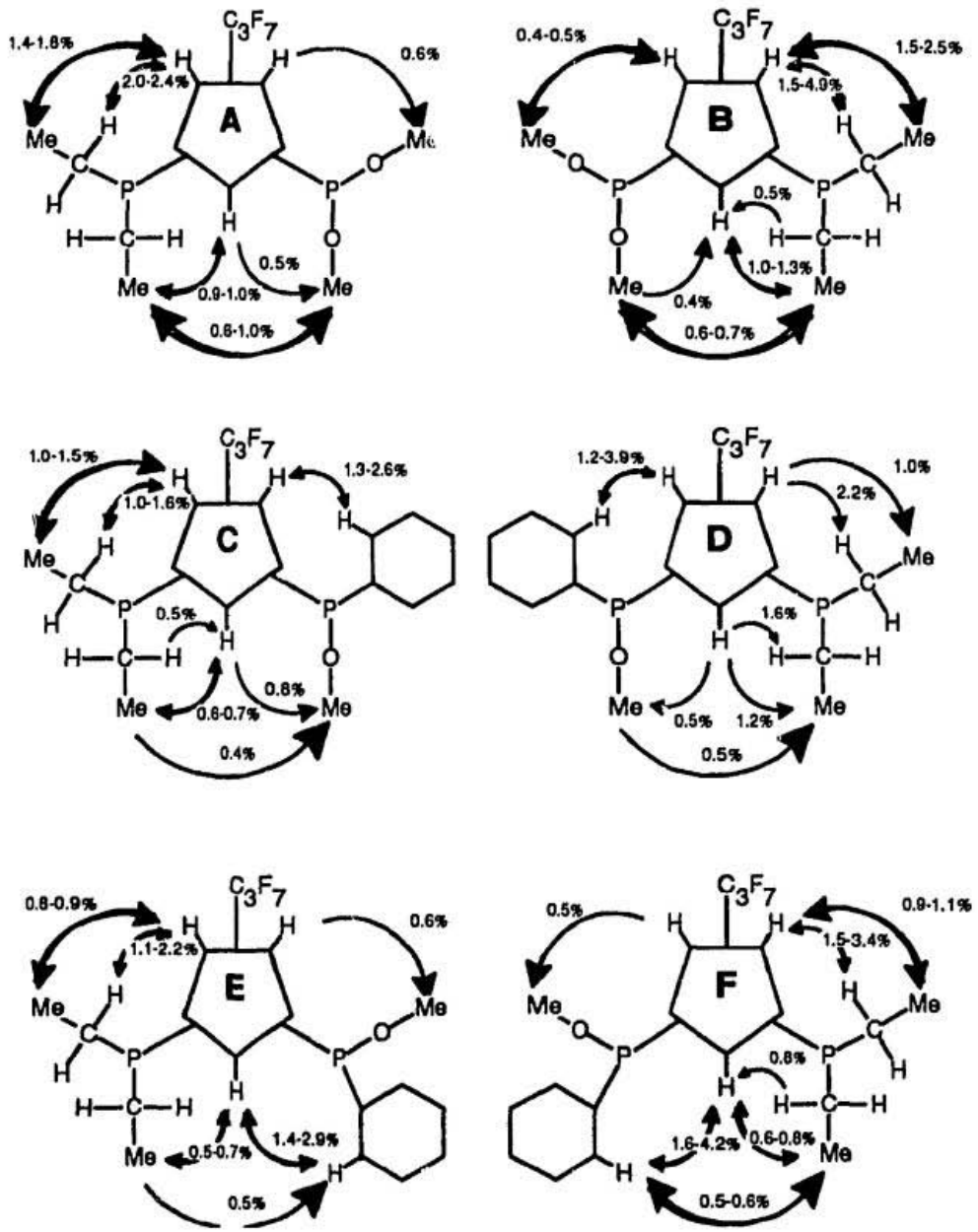

Figure 7-15. Major Nuclear Overhauser Effect Difference Data for Arbuzov Products with X = C_3F_7. (A. R_{Co},S_C-**7-13a**; B. S_{Co},S_C-**7-13b**; C. R_{Co},R_P,S_C-**7-16a**; D. S_{Co},S_P,S_C-**7-16b**; E. R_{Co},S_P,S_C-**7-16c**; F. S_{Co},R_P,S_C-**7-16d**.)

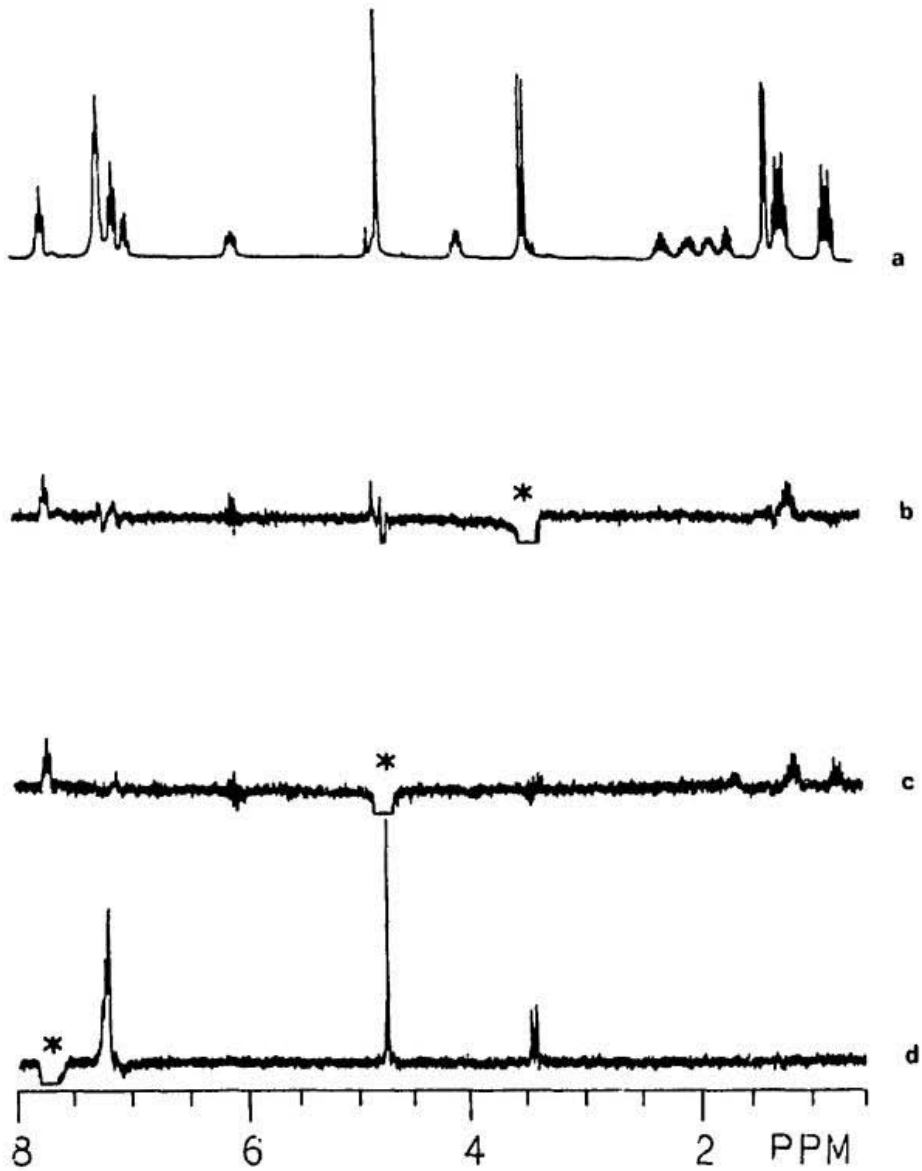

Figure 7-16. Representative Nuclear Overhauser Effect Difference Spectra for **7-15b**. (a) reference spectrum; (b-d) difference spectra (x32) for irradiation at the indicated (*) frequency; (b) P(O)-OMe; (c) η^5-Cp; (d) H_{ortho} of P(O)-Ph.

Table 7-14. Summary of Chiral Induction from Co* to P.

Without P=O...H-N Bonding			With P=O...H-N Bonding			
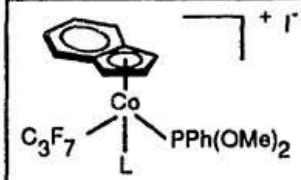		de %	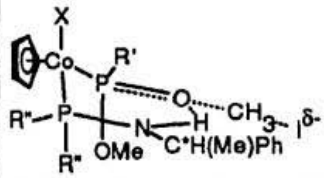			de %
L =	PMe_3	3	X	R'	R''	
	$PPh(OMe)_2$	35	I	Ph	t-Bu	100 [a]
	$PPhMe_2$	48	I	Ph	Ph	80 [b]
	PPh_2Me	46	I	Ph	Et	< 14 [a]
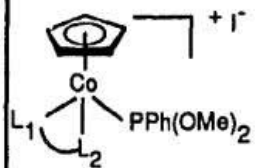			I	Et	Ph	10
			C_3F_7	Ph	Ph	45-55 [c]
			CF_3	Ph	Ph	25-30 [c]
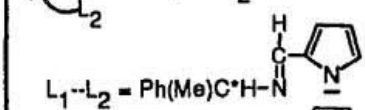		25-36	C_3F_7	Et	Ph	4
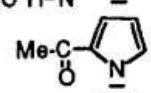		14				
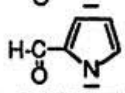		6				

[a] ref.[218]. [b] ref.[206]. [c] ref.[217]

This thesis has examined the stereochemistry of Abuzov reactions for three different kinds of templates with varying potential to form the intramolecular P=O•••H-N hydrogen bonding. Several interesting conclusions can be drawn from the discussion presented above and the data summarized in Table 7-14.[206, 217, 218] (i) The chiral metal center is essential for stereoselectivity. The chirality at phosphorus is dominated by

the chirality of the metal center. (ii) The size of the spectator ligands is crucial in determining the chiral induction. The bulkier the spectator ligands, the higher the chiral induction. (iii) The stereochemical properties of the entering phosphonites, $PR'(OMe)_2$,[218] are also important for high diastereoselectivity. Large substituent R' gives high diastereoselectivity. (iv) Intramolecular P=O•••H-N hydrogen bonding plays a significant role in controlling the stereoselectivity in the Arbuzov reaction by restricting the populations of solution conformations and maximizing the preference for one diastereomeric transition state.

7.3. Experimental Section

7.3.1. Reagents and Methods. All manipulations were performed under conditions similar to those described in the preceding chapters. Mass spectra were recorded on a MS'50 instrument in FAB operating mode with 3-nitrobenzyl alcohol as the matrix (UNB, New Brunswick). Complexes $(\eta^5\text{-}C_5R_5)Co(X)(CO)(I)$ (R = H, X = I, **7-1** [362]; R = Me, X = I, **7-2**[363]; R = H, X = C_3F_7, **7-3**[371]), were prepared as described previously.

7.3.2. Crystal Structure Determination of 7-12a, 7-13a, 7-15a, 7-16a and 7-16b.

Crystal data collection and structure refinement were similar to those described in the preceding chapters. The space group $P2_12_12_1$ (#19) was assigned in all cases on the basis of systematic absences (h00: $h \neq 2n$, 0k0: $k \neq 2n$ and 00l: $l \neq 2n$) and on the successful solution and refinement of all structures. Structures were solved by direct methods,[305] using the Molecular Structure Corporation TEXSAN software. In the case of **7-16b**, the asymmetric unit has two chemically identical but crystallographically distinguishable molecules (**7-16b** and **7-16b'**), one of which has a disordered CF_3 group which proved difficult to model. The cyclopentadienyl and phenyl moieties in **7-16b** and **7-16b'** were refined as rigid groups but the isotropic thermal parameters of constituent carbons were allowed to refine independently. Hydrogens in **7-16b** and **7-16b'** were introduced in calculated positions except the two NH's which were first assumed to be attached to trigonal nitrogen and then allowed to refine positionally for a round of least-squares refinement before being fixed. In the cases of **7-12a**, **7-13a**, **7-15a**, and **7-16a**, non-hydrogen atoms were refined anisotropically. The hydrogen attached to the nitrogen atom (H(1N)) was located in the difference map in all structures, however other hydrogens were placed in calculated positions with isotropic thermal parameters set to 20% greater than their bonding partners. H(1N) was refined with fixed thermal parameter. All other hydrogens were included but were not refined in the final rounds of least squares. The absolute stereochemistry for all structures was determined using the internal reference carbon known to be S_C. Further details are given in Table 7-15.

7.3.3. Synthesis of S_C-Et_2P-NH-CH(Me)Ph (PEtNH). $(Et)_2PCl$ (5.0 g, 0.040 mol) was added slowly into a solution of 12.5 g (0.103 mol) of S_C-Ph(Me)C*HNH_2 in 200 mL of benzene with stirring at 0 °C via syringe. The resulting wax-like solid was allowed to stand in an ice bath for an additional 5 h. The reaction mixture was then filtered through a glass frit and washed with benzene (3x50 mL). The combined filtrate was then passed through a basic alumina (10 cm) column and washed with 200 mL of benzene to remove unreacted free amine. The solvent was removed at water aspirator and then oil pump vacuum for 48 h to leave the product as a pale yellow oil (6.9 g, 82%). Anal., Calc. for $C_{12}H_{20}NP$ (Found), C, 68.87 (68.63), H, 9.63 (9.71), N, 6.69 (6.61). IR (pure oil), ν(N-H) = 3290 cm^{-1}. ^1H NMR ($CDCl_3$/TMS in ppm, 300.1 MHz), 4.12 (m, C*H), 1.41 (d, 6.7 Hz, C*-Me), 1.25-1.50 (m, P-(CH_2-)$_2$), 0.97 (dt, 14.7 Hz, 7.5 Hz, P-(CH_2-Me)$_2$); ^{13}C NMR ($CDCl_3$ in ppm, 75.47 MHz), 55.09 (d, 15.3 Hz, C*H), 26.46 (d, 5.3 Hz, C*-Me), 23.63 (d, 26.2 Hz, P-C_aH_2-), 23.48 (d, 26.2 Hz, P-C_bH_2-), 8.80 (d, 8.9 Hz, P-CH_2-Me), 8.63 (d, 5.8 Hz, P-CH_2-Me); ^{31}P NMR ($CDCl_3$/external 85% H_3PO_4 in ppm, 121.5 MHz), 44.5 (s).

7.3.4. Synthesis of Complexes.

7.3.4.1. Synthesis of (η^5-C_5R_5)Co(PEt_2NHC*H(Me)Ph)$(I)_2$, (R = H, 7-4; R = Me, 7-5). These two complexes were synthesized using the similar procedure for **7-4** described below. PEtNH (0.4957 g, 2.369 mmol) in 20 mL of benzene was dropped into a

stirred purple solution of **7-1** (0.9294 g, 2.290 mmol) in 20 mL of benzene over a 15 minute period at room temperature. The solution soon changed color from purple to black. After addition, the reaction mixture was stirred for another 2 h. Removal of solvent at water aspirator pressure left a black residue which was purified chromatographically with a 4 mm radial silica gel plate eluting with benzene/dichloromethane (2/1, v/v). The first dark purple band was collected. Removal of solvent at water aspirator pressure and then oil pump vacuum afforded a dark purple powder (0.8424 g, 63%). Anal., Calc. for $C_{17}H_{25}NPCoI_2$ (Found): C, 34.78 (35.21), H, 4.29 (4.36), N, 2.39 (2.35). m.p. 142-143 °C. IR (in CH_2Cl_2), ν(N-H) = 3356 cm^{-1}. **7-5** was obtained as a black powder in 70% yield. Anal. Calc. for $C_{22}H_{35}NPCoI_2$ (Found): C, 40.20 (40.29), H, 5.37 (5.21), N, 2.13 (2.07). m.p. 145-146 °C. IR (in CH_2Cl_2), ν(N-H) = 3356 cm^{-1}.

7.3.4.2. Synthesis of ***(η^5-C_5H_5)Co(C_3F_7)(PEt$_2$NHCH(Me)Ph)(I), 7-6a.*** A solution of 0.2316 g (1.107 mmol) of PEtNH in 20 mL of benzene was dropped into a stirred dark green solution of **7-3** (0.4121 g, 0.9199 mmol) in 20 mL of benzene over a 15 minute period at room temperature. After stirring overnight at room temperature, volatiles were removed at water aspirator pressure and the residue was chromatographed on a 2 mm radial silica gel plate eluting with benzene/hexane (2/1, v/v). The first deep-brown band was collected. Removal of the solvent at water aspirator and then oil pump vacuum at room temperature or 0 °C afforded the

product as a deep brown powder (0.5478 g, 95%). TLC and ^{1}H NMR analysis indicated the presence of a single isomer, which was shown to be **7-6a**. Anal., Calc. for $C_{20}H_{25}NPF_7ICo$ (Found): C, 38.18 (38.17), H, 4.00 (3.97), N, 2.23 (2.21). m.p. 113-114 °C. IR (in CH_2Cl_2), ν(N-H) = 3356 cm^{-1}. Polarimetric Data, **7-6a**: $[\alpha]_{579}$ = -1047, $[\alpha]_{546}$ = -449, $[\alpha]_{436}$ = -873.

7.3.4.3. Synthesis of ***(η^5-C_5H_5)Co(PEt$_2$NHC*H(Me)Ph)(P(O)(OMe)$_2$)(I), 7-12a, b.*** $P(OMe)_3$ (0.0564 g, 0.454 mmol) was added slowly via syringe with stirring to a solution of **7-4** (0.2342 g, 0.3989 mmol) in 35 mL of benzene at ambient temperature. The solution color changed from purple to bright brown. Stirring was continued for another 4 h and then volatiles were removed at water aspirator pressure. TLC (ethyl acetate) showed that the reaction mixture contained (in the order of decreasing R_f): reactant (**7-4**, purple), **7-12a, b** (dark blue), (η^5-C_5H_5)Co(P(OMe)$_3$(P(O)(OMe)$_2$)(I) (**7-27**, dark blue).[385] The crude reaction mixture was separated chromatographically on a 2 mm radial silica gel plate. Acetone elution separated a purple band reactant, **7-4**, followed by a dark blue band containing the product mixture, **7-12a, b**. Continued elution with acetone/methanol (10/4, v/v) separated a dark blue band which was characterized by ^{1}H NMR as (η^5-C_5H_5)Co(P(OMe)$_3$)(P(O)(OMe)$_2$)(I), **7-27**. Diastereomerically pure **7-12a** and **7-12b** were obtained by chromatographic separation of the **7-12a, b** mixture with ethyl acetate as eluent. Removal of the solvent with rotary evaporator followed by oil pump vacuum gave **7-4** (0.0105 g,), **7-**

27 (0.0150 g), **7-12a** (0.0964 g, 42%), and **7-12b** (0.0925 g, 41%). Slow diffusion of hexane into the dichloromethane solution of **7-12a** or **7-12b** at 0 °C gave **7-12a** and **7-12b** as black prisms. Anal., Calc. for $C_{19}H_{31}O_3NP_2ICo$: C, 40.09, H, 5.49, N, 2.46; Found: **7-12a**: C, 40.13, H, 5.31, N, 2.47; **7-12b**: C, 40.15, H, 5.36, N, 2.48. m.p., **7-12a**, 153-155 °C, **7-12b**, 162-163 °C. IR (in CH_2Cl_2), **7-12a**: ν(N-H) = 3148 cm^{-1}, ν(P=O) = 1140 cm^{-1}, ν(P-OMe) = 1040, 1014 cm^{-1}; **7-12b**: ν(N-H) = 3139 cm^{-1}, ν(P=O) = 1140 cm^{-1}, ν(P-OMe) = 1040, 1014 cm^{-1}. MS (FAB), m/z (ion, intensity), **7-12b**: 570 ($(M+H)^+$, 72%), 460 ($(M-P(O)(OMe)_2)^+$, 48%), 443 ($(M+H-I)^+$, 14%), 395 ($(M-P(O)(OMe)_2-Cp)^+$, 25%), 333 ($(M-I-P(O)(OMe)_2)^+$, 86%), 268 ($(M-I-P(O)(OMe)_2-Cp)^+$, 100%). Polarimetric Data, **7-12a**: $[\alpha]_{579}$ = -776, $[\alpha]_{546}$ = -592, $[\alpha]_{436}$ = -816; **7-12b**: $[\alpha]_{579}$ = +229, $[\alpha]_{546}$ = +584, $[\alpha]_{436}$ = +1917.

7.3.4.4. Synthesis of $(\eta^5\text{-}C_5H_5)Co(C_3F_7)(PEt_2NHC^*H(Me)Ph)(P(O)(OMe)_2)$, 7-13a,b. $P(OMe)_3$ (0.0641 g, 0.516 mmol) was added slowly via syringe with stirring to a solution of **7-6a,b** (0.1746 g, 0.2774 mmol) in 25 mL of benzene at ambient temperature. After stirring for about 6 h the solution color changed from deep brown to greenish yellow. Removal of the volatiles at water aspirator pressure gave a yellow powder, which was chromatographed on a 2 mm radial silica gel plate eluting with ethyl acetate/dichloromethane (2/1, v/v). Two orange bands (**7-13a** and **7-13b**) were collected, followed by a yellow band, eluted with acetone/methanol (10/1, v/v), which proved (^{1}H NMR) to be $(\eta^5\text{-}C_5H_5)Co(C_3F_7)(P(OMe)_3)(P(O)(OMe)_2)$ (**3-3aα**, cf. Chapter

3).[318] Removal of the solvent gave three orange crystalline solids: **7-13a** (0.0701 g, 41%), **7-13b** (0.0733 g, 43%), and **3-3aα** (0.0392 g). Slow diffusion of hexane into the solution of **7-13a** and **7-13b** in mixed dichloromethane and chloroform solvent at 0 °C gave **7-13a** as orange prisms and **7-13b** as orange columns. Anal., Calc. for $C_{22}H_{31}O_3NP_2F_7Co$: C, 43.22, H, 5.11, N, 2.29; Found: **7-13a**: C, 43.12, H, 5.08, N, 2.30; **7-13b**: C, 43.18, H, 5.04, N, 2.31. m.p., **7-13a**, 134-136 °C, **7-13b**, 152-153 °C. IR (in CH_2Cl_2), **7-13a**: ν(N-H) = 3194 cm^{-1}; **7-13b**: ν(N-H) = 3194 cm^{-1}. Polarimetric Data, **7-13a**: $[\alpha]_{579}$ = -300, $[\alpha]_{546}$ = +240, $[\alpha]_{436}$ = -3183; **7-13b**: $[\alpha]_{579}$ = -1419, $[\alpha]_{546}$ = 0, $[\alpha]_{436}$ = +2710.

7.3.4.5. Synthesis of (η^6-C_5Me_5)Co($PEt_2NHC^1H(Me)Ph$)(P(O)($OMe)_2$)(I), 7-14a,b. $P(OMe)_3$ (0.0428 g, 0.345 mmol) was added slowly via syringe with stirring to a solution of **7-5** (0.1879 g, 0.2859 mmol) in 35 mL of benzene at ambient temperature. No reaction was observed after stirring for about 24 h at room temperature. The reaction mixture was then heated to 60 °C and stirred for another 10 h. The solution color changed from black to dark blue. Removal of volatiles gave a dark blue residue which was chromatographed on a radial silica plate eluting with ethyl acetate/benzene (10/2, v/v). After elution of a dark blue band, which was not characterized, the second and third dark blue bands were collected. Removal of solvent at water aspirator followed by oil pump vacuum gave **7-14a** (0.0468 g, 27%), and **7-14b** (0.0545 g, 30%) as dark blue powders. Anal., Calc. for $C_{24}H_{41}O_3NP_2ICo$:

C, 45.09, H, 6.46, N, 2.19; Found: **7-14b**: C, 44.98, H, 6.49, N, 2.23. m.p., **7-14a**, 146-148 °C, **7-14b**, 155-157 °C. IR (in CH_2Cl_2), **7-14a**: ν(N-H) = 3149 cm^{-1}, ν(P=O) = 1128 cm^{-1}, ν(P-OMe) = 1043, 1016 cm^{-1}; **7-14b**: ν(N-H) = 3145 cm^{-1}, ν(P=O) = 1128 cm^{-1}, ν(P-OMe) = 1042, 1014 cm^{-1}. Polarimetric Data, **7-14a**: $[\alpha]_{579}$ = -363, $[\alpha]_{546}$ = -1287, $[\alpha]_{436}$ = -4092; **7-14b**: $[\alpha]_{579}$ = +677, $[\alpha]_{546}$ = +3613, $[\alpha]_{436}$ = +3129.

7.3.4.6. Synthesis of $(\eta^5\text{-}C_5H_5)Co(PEt_2NHC^*H(Me)Ph)(P(O)Ph(OMe))(I)$, 7-15a,b,c,d. $PPh(OMe)_2$ (0.1084 g, 0.6371 mmol) was added slowly to 0.2537 g (0.6024 mmol) of **7-4** in 40 mL of benzene with stirring via syringe at room temperature. As $PPh(OMe)_2$ was added, the solution color changed from purple to bright-brown. Stirring was continued for another 3 h and then volatiles were removed at water aspirator pressure. TLC (ethyl acetate/dichloromethane, 1:1) showed 6 spots corresponding to **7-4**, **7-15a**, **7-15b**, **7-15c**, **7-15d** and $(\eta^5\text{-}C_5H_5)Co(PPh(OMe)_2)(P(O)Ph(OMe))(I)$, **7-17a,b**,[206] respectively. Chromatography

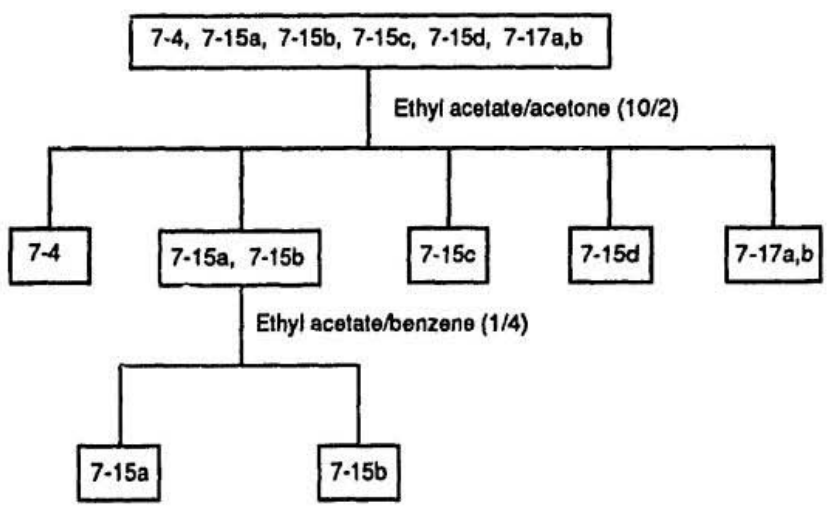

Scheme 7-3

as shown in Scheme 7-3 gave **7-15a** (45.4 mg, 12%), **7-15b** (39.8 mg, 11%), **7-15c** (55.7 mg, 15%), **7-15d** (51.8 mg, 14%), **7-4** (25.2 mg), and **7-17a,b** (12.5 mg). Slow diffusion of hexane into the dichloromethane and chloroform solution of **7-15a** gave black prisms which was used for structure determination. Anal., Calc. for $C_{24}H_{33}O_2NP_2ICo$: C, 46.85, H, 5.41, N, 2.28; Found, **7-15a**: C, 46.54, H, 5.26, N, 2.27; **7-15b**: C, 46.84, H, 5.34, N, 2.31. m.p. **7-15a**: 142-144 °C, **7-15b**: 145-148 °C, **7-15c**: 143-144 °C, **7-15d**: 134-136 °C. IR (in CH_2Cl_2), **7-15a**: ν(N-H) = 3115 cm^{-1}, ν(P=O) = 1128 cm^{-1}, ν(P-OMe) = 1012 cm^{-1}; **7-15b**: ν(N-H) = 3115 cm^{-1}, ν(P=O) = 1129 cm^{-1}, ν(P-OMe) = 1013 cm^{-1}. **7-15c**: ν(N-H) = 3120 cm^{-1}, ν(P=O) = 1125 cm^{-1}, ν(P-OMe) = 1015 cm^{-1}; **7-15d**: ν(N-H) = 3120 cm^{-1}, ν(P=O) = 1124 cm^{-1}, ν(P-OMe) = 1011 cm^{-1}. MS (FAB), m/z (ion, intensity), **7-15a**: 616 ($(M+H)^+$, 28%), 489 ($(M+H-I)^+$, 9%), 460 ($(M-P(O)Ph(OMe))^+$, 14%), 395 ($(M-P(O)Ph(OMe)-Cp)^+$, 19%), 333 ($(M-I-P(O)Ph(OMe))^+$, 98%), 268 ($(M-I-P(O)Ph(OMe)-Cp)^+$, 100%). Polarimetric data, **7-15a**: $[\alpha]_{579}$ = +1849, $[\alpha]_{546}$ = +224, $[\alpha]_{436}$ = +3585; **7-15b**: $[\alpha]_{579}$ = +226, $[\alpha]_{546}$ = +249; **7-15c**: $[\alpha]_{579}$ = -426, $[\alpha]_{546}$ = -266, $[\alpha]_{436}$ = -106; **7-15d**: $[\alpha]_{579}$ = -306, $[\alpha]_{546}$ = +500, $[\alpha]_{436}$ = -306.

7.3.4.7. Synthesis of $(\eta^5\text{-}C_5H_5)Co(C_3F_7)(PEt_2NHCH(Me)Ph)(P(O)Ph(OMe))$, 7-16a,b,c,d. $PPh(OMe)_2$ (0.0902 g, 0.530 mmol) was added slowly to 0.3290 g (0.5229 mmol) of **7-6a,b** in 45 mL of benzene with stirring via syringe at room temperature. After stirring overnight, TLC (benzene/ethyl acetate, 10/2) showed 8

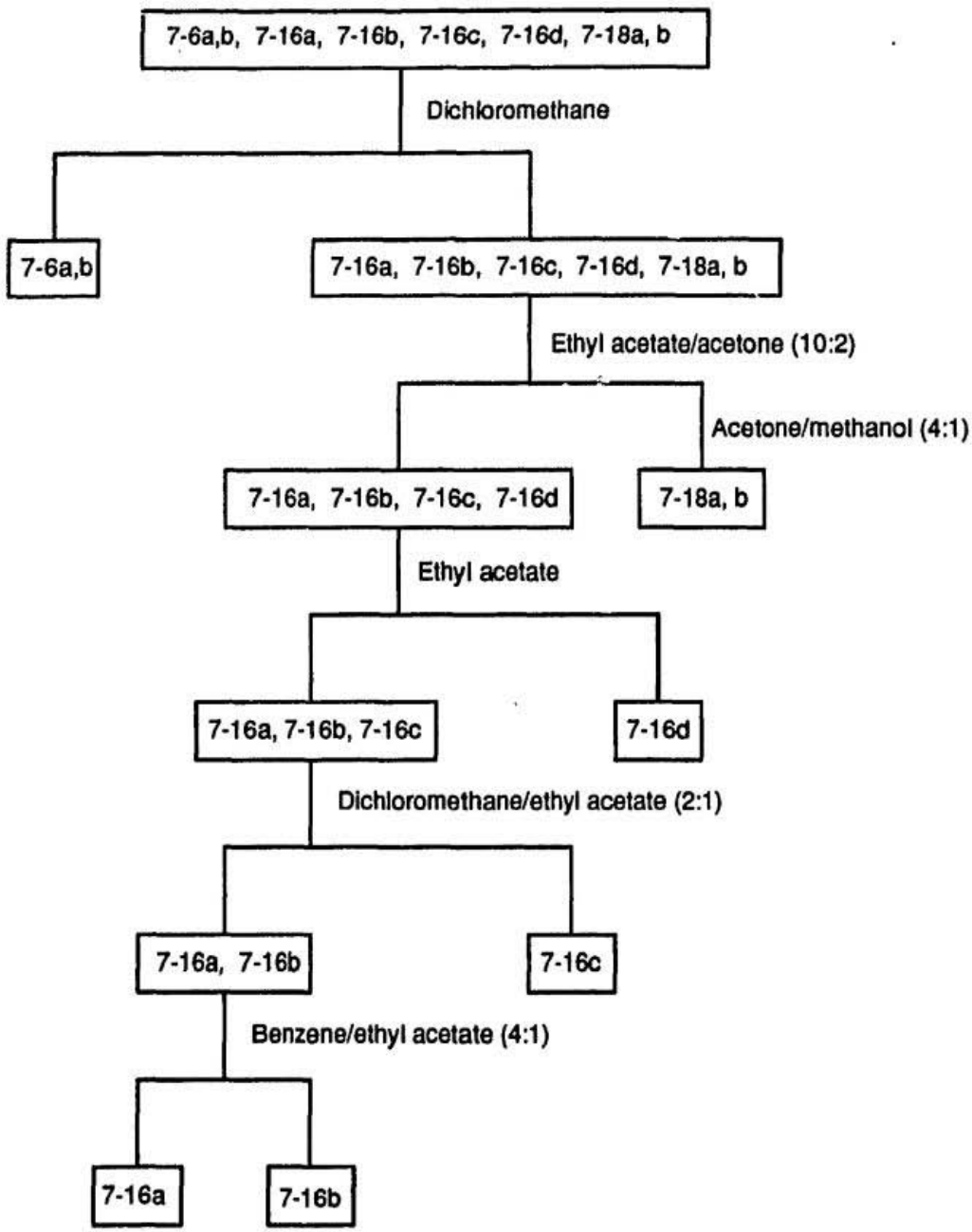

Scheme 7-4

spots corresponding to (in the order of decreasing R_f): **7-6a, 7-6b, 7-16a, 7-16b, 7-**

16c, **7-16d** and (η^5-C_5H_5)Co(C_3F_7)(PPh(OMe)$_2$)(P(O)Ph(OMe)) (**7-18a** and **7-18b**[217]), respectively. Volatiles were removed at water aspirator pressure and the residue was chromatographed stepwise as shown in Scheme 7-4 to give **7-16a** (35.4 mg, 10%), **7-16b** (32.9 mg, 10%), **7-16c** (45.8 mg, 13%), **7-16d** (42.5 mg, 12%) (**7-16a,b,c,d** as orange crystalline solid), **7-6a,b** (119.4 mg), and **7-18a,b** (58.1 mg), respectively. Slow diffusion of hexane into the solution of **7-16a** in the mixed ethyl acetate and dichloromethane solvent or **7-16b** in the mixed dichloromethne and chloroform solvent at room temperature gave **7-16a** as orange columns and **7-16b** as orange prisms. Anal., Calc. for $C_{27}H_{33}O_2NP_2F_7Co$: C, 49.33, H, 5.06, N, 2.13; Found, **7-16a**: C, 49.16, H, 5.02, N, 2.12; **7-16b**: C, 49.26, H, 4.97, N, 2.15; **7-16c**: C, 49.01, H, 5.00, N, 2.14; **7-16d**: C, 49.27, H, 4.98, N, 2.13. m.p. **7-16a**: 161-163 °C, **7-16b**: 115-117 °C, **7-16c**: 132-134 °C, **7-16d**: 155-156 °C. IR (in CH_2Cl_2), **7-16a**: ν(N-H) = 3139 cm^{-1}; **7-16b**: ν(N-H) = 3139 cm^{-1}; **7-16c**: ν(N-H) = 3140 cm^{-1}; **7-16d**: ν(N-H) = 3147 cm^{-1}. MS (FAB), m/z (ion, intensity), **7-16a**: 657 (M^+, 93%), 488 ($(M-C_3F_7)^+$, 36%), 437 ((M-Cp-P(O)Ph(OMe))$^+$, 13%), 436 ((M-Cp-P(O)Ph(OMe)-H)$^+$, 64%), 333 ((M-C_3F_7-P(O)Ph(OMe)), 66%), 268 ((M-C_3F_7-P(O)Ph(OMe)-Cp)$^+$, 100%). Polarimetric data, **7-16a**: $[\alpha]_{579}$ = +1208, $[\alpha]_{546}$ = +1030, $[\alpha]_{436}$ = +4920; **7-16b**: $[\alpha]_{579}$ = -710, $[\alpha]_{546}$ = -583, $[\alpha]_{436}$ = +1670; **7-16c**: $[\alpha]_{579}$ = -324, $[\alpha]_{546}$ = +588, $[\alpha]_{436}$ = -4147; **7-16d**: $[\alpha]_{579}$ = -728, $[\alpha]_{546}$ = -99, $[\alpha]_{436}$ = +3046.

Table 7-15. Summary of Crystallographic Data for **7-12a**, **7-13a**, **7-15a**, **7-16a** and **7-16b**.

	7-12a	**7-13a**	**7-15a**	**7-16a**	**7-16b**
Formula	$C_{19}H_{31}O_3NP_2ICo$	$C_{22}H_{31}O_3NP_2F_7Co$	$C_{24}H_{33}O_2NP_2ICo$	$C_{27}H_{33}O_2NP_2F_7Co$	$C_{27}H_{33}O_2NP_2F_7Co$
F.W.(g/mol)	569.24	611.36	615.32	657.43	657.43
Crystal Habit	Black prism	Orange prism	Black prism	Orange column	Orange prism
Crystal Size (mm)	0.40x0.30x0.15	0.30x0.20x0.20	0.35x0.25x0.20	0.40x0.20x0.20	0.40x0.20x0.18
Crystal System	orthorhombic	orthorhombic	orthorhombic	orthorhombic	orthorhombic
No.Rflns used for unit cell determ.(2θ range)	23 (37.3 - 42.7°)	23 (22.7 - 31.1°)	21 (27.2 - 34.3°)	20 (20.0 - 28.8°)	19 (20.6 - 24.5°)
Peak Width (Half-height)	0.32	0.32	0.32	0.32	0.32
a (Å)	12.968(4)	9.524(2)	14.580(2)	14.184(3)	19.152(8)
b (Å)	16.385(2)	33.223(4)	21.659(3)	26.487(3)	28.470(4)
c (Å)	11.119(3)	8.345(3)	8.407(4)	7.776(3)	10.900(3)
V (Å^3)	2362.6(9)	2640(1)	2655(1)	2921(1)	5944
Space Group	$P2_12_12_1$ (#19)	$P2_12_12_1$ (#19)	$P2_12_12_1$ (#19)	$P2_12_12_1$ (#19)	$P2_12_12_1$ (#19)
Z	4	4	4	4	8
D_{calcd}(g/cm^3)	1.600	1.538	1.539	1.495	1.469
F_{000}	1144	1256	1240	1352	2704
μ(MoKα)(cm^{-1})	21.69	8.39	19.34	7.61	7.49
Scan Width(°)	1.10 + 0.30 tanθ	0.88 + 0.30 tanθ	1.26 + 0.30 tanθ	0.88 + 0.30 tanθ	0.92 + 0.30 tanθ
$2\theta_{max}$ (°)	50.0	50.0	50.0	50.0	50.0
Total data	2391	2701	2688	2959	5821
Corrections[a]	Lorentz-polarization Absorption				
trans.factors:	0.91-1.00	0.96-1.00	0.87-1.00	0.96-1.00	0.91-1.00
Sec.Ext.Coeff.:	0.17884×10^{-5}	0.76317×10^{-6}	0.65868×10^{-6}	0.27535×10^{-6}	0.89136×10^{-7}
Funct.Minimized, Least-squares weights	$\Sigma w(\|Fo\|-\|Fc\|)^2$, $4Fo^2/\sigma^2(Fo^2)$				
p-factor	0.01	0.01	0.01	0.01	0.01
No.Obsd.(I>2.00σ(I))	2148	2227	2092	2024	3888
No.Variables	248	326	281	362	483
Reflection/Parameter	8.66	6.83	7.44	5.59	8.05
R[b]	0.026	0.030	0.034	0.044	0.057
R_w[c]	0.027	0.025	0.029	0.024	0.047
GOF[d]	1.81	1.36	1.55	1.78	2.06
Δρ(Max/min)(e$^-$/Å^3)	0.36/-0.46	0.22/-0.20	0.51/-0.53	0.26/-0.28	0.55/-0.34

[a] cf. reference[306]. [b] $R=\Sigma||Fo|-|Fc||/\Sigma|Fo|$.
[c] $R_w=[(\Sigma w(|Fo|-|Fc|)^2/\Sigma wFo^2)]^{1/2}$ [d] $GOF=(\Sigma(|Fo|-|Fc|)/\sigma)/(n-m))$ where n=#reflections, m=#variables, and σ^2=variance of (|Fo|-|Fc|)

References

1. Coppola, G. M.; Schuster, H. F. In *Asymmetric Synthesis - Construction of Chiral Molecules Using Amino Acids*; John Wiley & Sons: New York, 1987.

2. Mellin, G. W.; Katzenstein, M. *New Engl. J. Med.* **1962**, *267*, 1184.

3. Merck Chiralica (Catalog).

4. Crosby, J. In *Chirality in Industry: the Commercial Manufacture and Applications of Optically Active Compounds*; Collins, A. N.; Sheldrake, G. N.; Crosby, J., Eds.; John Wiley & Sons: Chichester, 1992; p1.

5. Morrison, J. D. In *Asymmetric Synthesis: Vol. 4. The Chiral Carbon Pool and Chirla S, N, P and Si Compcunds*; Academic Press: Orlando, 1984.

6. Blaser, H. U. *Chem. Rev.* **1992**, *92*, 935.

7. Allenmark, S. G. In *Chromatographic Enantioseparation: Methods and Applications*; Ellis Horwood: Chichester, 1988.

8. Kagan, H. B.; Fiaud, J. C. *Top. Stereochem.* **1988**, *18*, 249.

9. Parshall, G. W.; Ittel, S. D. In *Homogeneous Catalysis - The Application and Chemistry of Catalysis by Soluble Transition Metal Complexes*, 2nd; John Wiley & Sons: New York, 1992.

10. Ojima, I. In *Catalytic Asymmetric Synthesis*; VCH Publishers: New York, 1993.

11. Morrison, J. D. In *Asymmetric Synthesis - Vol 5. Chiral Catalysis*; Academic Press: Orlando, 1985.

12. Bosnich, B. In *Asymmetric Catalysis*; Martinus Nijhoff Publishers: Dordrecht, 1986.

13. Drayer, D. E. In *Drug Stereochemistry: Analytical Methods and Pharmacology*, 2nd; Wainer, I. W., Ed.; Marcel Dekker: New York, 1993; p1.

14. Blystone, S. I. *Chem. Rev.* **1989**, *89*, 1663.

15. Duthaler, R. O.; Hafner, A. *Chem. Rev.* **1992**, *92*, 807.

16. Fuji, K. *Chem. Rev.* **1993**, *93*, 2037.

17. Soai, K.; Niwa, S. *Chem. Rev.* **1992**, *92*, 833.

18. Davis, F. A.; Chen, B. C. *Chem. Rev.* **1992**, *92*, 919.

19. Chan, T. H.; Wang, D. *Chem. Rev.* **1992**, *92*, 995.

20. Kagan, H. B.; Riant, O. *Chem. Rev.* **1992**, *92*, 1007.

21. Collins, A. N.; Sheldrake, G. N.; Crosby, J. In *Chirality in Industry: The Commercial Manufacture and Applications of Optically Active Compounds*; John Wiley & Sons: Chichester, 1992.

22. Scott, J. W. *Top. Stereochem.* **1989**, *19*, 209.

23. Bosnich, B.; Fryzuk, M. D. *Top. Stereochem.* **1981**, *12*, 119.

24. Brunner, H. *Synthesis* **1988**, 645.

25. Brunner, H. *Top. Stereochem.* **1988**, *18*, 129.

26. Halpern, J. In *Asymmetric Synthesis: Vol. 5, Chiral Catalysis*; Morrison, J. D., Ed.; Academic Press: Orlando, 1985, p41.

27. Koenig, K. E. In *Asymmetric Synthesis: Vol. 5, Chiral Catalysis*; Morrison, J. D., Ed.; Academic Press: Orlando, 1985, p71.

28. Takaya, H.; Ohta, T. *J. Syn. Org. Chem. Japan* **1993**, *51*, 1013.

29. Takaya, H.; Ohta, T.; Noyori, R. In *Catalytic Asymmetric Synthesis*; Ojima, I., Ed.; V C H Publishers: New York, 1993; p1.

30. Noyori, R. *Science* **1990**, *248*, 1194.

31. Blyston, S. L. *Chem. Rev.* **1989**, *89*, 1663.

32. Kagan, H. B.; Sasaki, M. In *The Chemistry of Organophosphorous Compounds*; Hartley, F. R., Ed.; John Wiley & Sons: New York, 1990; Vol. 1, p53.

33. Noyori, R.; Takaya, H. *Acc. Chem. Res.* **1990**, *23*, 345.

34. Noyori, R. *Chemtech* **1992**, *22*, 360.

35. Kitamura, M.; Hsiao, Y.; Ohta, M.; Tsukamoto, M.; Ohta, T.; Takaya, H.; Noyori, R. *J. Org. Chem.* **1994**, *59*, 297.

36. Brunner, H.; Nishiyama, H.; Itoh, K. In *Catalytic Asymmetric Synthesis*; Ojima, I., Ed.; VCH Publishers: New York, 1993; p303.

37. Ojima, I.; Hirai, K. In *Asymmetric Synthesis: Vol. 5, Chiral Catalysis*; Morrison, J. D., Ed.; Academic Press: Orlando, 1985, p103.

38. Ojima, I.; Clos, N.; Bastos, C. *Tetrahedron* **1989**, *45*, 6901.

39. Gonsiglio, G. *Top. Curr. Chem.* **1982**, *105*, 77.

40. Consiglio, G. In *Catalytic Asymmetric Synthesis*; Ojima, I., Ed.; V C H Publishers: New York, 1993; p273.

41. Johnson, R. A.; Sharpless, K. B. In *Catalytic Asymmetric Synthesis*; Ojima, I., Ed.; VCH Publishers: New York, 1993; p103.

42. Finn, M. G.; Sharpless, K. B. In *Asymmetric Synthesis: Vol. 5, Chiral Catalysis*; Morrison, J. D., Ed.; Academic Publication: Orlando, 1985; p247.

43. Rossiter, B. E. In *Asymmetric Synthesis: Vol. 5, Chiral Catalysis*; Morrison, J. D., Ed.; Academic Press: Orlando, 1985; p193.

44. Bolm, C. *Angew. Chem., Int. Ed. Engl.* **1991**, *30*, 403.

45. Hanson, R. M. *Chem. Rev.* **1991**, *91*, 437.

46. Jacobsen, E. N. In *Catalytic Asymmetric Synthesis*; Ojima, I., Ed.; VCH Publishers: New York, 1993; p159.

47. Schurig, V.; Betschinger, F. *Chem. Rev.* **1992**, *92*, 873.

48. Doyle, M. P. In *Catalytic Asymmetric Synthesis*; Ojima, I., Ed.; V C H Publishers: New York, 1993; p63.

49. Doyle, M. P.; Protopopova, M. N.; Brandes, B. D.; Davies, H. M. L.; Huby, N. J. S.; Whitesell, J. K. *Synlett* **1993**, 151.

50. Hayashi, T. In *Catalytic Asymmetric Synthesis*; Ojima, I., Ed.; VCH Publishers: New York, 1993; p325.

51. Hayashi, T.; Kumada, M. In *Asymmetric Synthesis: Vol. 5, Chiral Catalysis*; Morrison, J. D., Ed.; Academic Press: Orlando, 1985; p147.

52. Horner, L.; Seigel, H.; Buthe, H. *Angew. Chem., Int. Ed. Engl.* **1968**, *7*, 942.

53. Knowles, W. S.; Sabacky, M. J. *J. Chem. Soc., Chem. Commun.* **1968**, 1445.

54. Knowles, W. S.; Sabacky, M. J.; Vineyard, B. D.; Weinkauff, D. J. *J. Am. Chem. Soc.* **1975**, *97*, 2567.

55. Markó, L.; Bakos, J. *Aspects of Homogeneous Catalysis* **1982**, *4*, 145.

56. Kagan, H. B. In *Asymmetric Synthesis, Vol. 5, Chiral Catalysis*; Morrison, J. D., Ed.; Academic Press: Orlando, 1985; p1.

57. Müller, D.; Umbricht, G.; Webber, B.; Pfaltz, A. *Helv. Chim. Acta* **1991**, *74*, 232.

58. Vonmatt, P.; Pfaltz, A. *Angew. Chem., Int. Ed. Engl.* **1993**, *32*, 566.

59. Bolm, C. *Angew. Chem., Int. Ed. Engl.* **1993**, *32*, 232.

60. Burk, M. J.; Feaster, J. E. *J. Am. Chem. Soc.* **1992**, *114*, 6266.

61. Halterman, R. L.; Volhardt, K. P. C.; Welker, M. E.; Bläser, D.; Boese, R. *J. Am. Chem. Soc.* **1987**, *109*, 8105.

62. Lubell, W. D.; Kitamura, M.; Noyori, R. *Tetrahedron: Asymmetry* **1991**, *2*, 543.

63. Willoughby, C. A.; Buchward, S. L. *J. Am. Chem. Soc.* **1992**, *114*, 7562.

64. Knowles, W. S. *Acc. Chem. Res.* **1983**, *16*, 106.

65. Tamao, K.; Kakui, T.; Kumada, M. *J. Am. Chem. Soc.* **1978**, *100*, 2268.

66. Tamao, K.; Ishida, N.; Tanaka, T.; Kumada, M. *Organometallics* **1983**, *2*, 1694.

67. Brunner, H. *Angew. Chem., Int. Ed. Engl.* **1983**, *22*, 897.

68. Brunner, H.; Obermann, U. *Chem. Ber.* **1989**, *122*, 499.

69. Brunner, H.; Becker, R.; Riepl, G. *Organometallics* **1984**, *3*, 1354.

70. Nishiyama, H.; Sakaguchi, H.; Nakamura, T.; Horihata, M.; Kondo, M.; Itoh, K. *Organometallics* **1989**, *8*, 846.

71. Nishiyama, H.; Kondo, M.; Nakamura, T.; Itoh, K. *Organometallics* **1991**, *10*, 500.

72. Hayashi, T.; Uozumi, Y. *J. Am. Chem. Soc.* **1991**, *113*, 9887.

73. Uozumi, Y.; Tanahashi, A.; Lee, S. Y.; Hayashi, T. *J. Org. Chem.* **1993**, *58*, 1945.

74. Parrinello, G.; Stille, J. K. *J. Am. Chem. Soc.* **1987**, *109*, 7122.

75. Kollar, L.; Bakos, J.; Toth, I.; Heil, B. *J. Organomet. Chem.* **1988**, *350*, 227.

76. Kollar, L.; Bakos, J.; Toth, I.; Heil, B. *J. Organomet. Chem.* **1989**, *370*, 257.

77. Stille, J. K.; Su, H.; Brechot, P.; Parrinello, G.; Hegedus, L. S. *Organometallics* **1991**, *10*, 1183.

78. Hanson, R. M.; Sharpless, K. B. *J. Org. Chem.* **1986**, *51*, 1922.

79. Gao, Y.; Hanson, R. M.; Klunder, J. M.; Ko, S. Y.; Masamune, H.; Sharpless, K. B. *J. Am. Chem. Soc.* **1987**, *109*, 5765.

80. Sharpless, K. B. *Chemtech* **1985**, *15*, 692.

81. News *C&EN* **1986**, *June 2*, 24.

82. Zhang, W.; Leibach, J. L.; Wilson, S. R.; Jacobsen, E. N. *J. Am. Chem. Soc.* **1990**, *112*, 2801.

83. Jacobsen, E. N.; Zhang, W.; Muci, A. R.; Ecker, J. R.; Deng, L. *J. Am. Chem. Soc.* **1991**, *113*, 7063.

84. Zhang, W.; Jacobsen, E. N. *J. Org. Chem.* **1991**, *56*, 2296.

85. Irie, R.; Noda, K.; Ito, Y.; Matsumoto, N.; Katsuki, T. *Tetrahedron Lett.* **1990**, *31*, 7345.

86. Irie, R.; Noda, K.; Ito, Y.; Katuski, T. *Tetrahedron Lett.* **1991**, *32*, 1055.

87. O'Connor, K. J.; Wey, S. J.; Burrows, C. J. *Tetrahedron Lett.* **1992**, *33*, 1001.

88. Reddy, D. R.; Thornton, E. R. *J. Chem. Soc., Chem. Commun.* **1992**, 172.

89. Lee, N. H.; Muci, A. R.; Jacobsen, E. N. *Tetrahedron Lett.* **1991**, *32*, 5055.

90. Lee, N. H.; Jacobsen, E. N. *Tetrahedron Lett.* **1991**, *32*, 6533.

91. Wang, L.; Sharpless, K. B. *J. Am. Chem. Soc.* **1992**, *114*, 7568.

92. Xu, D.; Crispino, G. A.; Sharpless, K. B. *J. Am. Chem. Soc.* **1992**, *114*, 7570.

93. Johnson, R. A.; Sharpless, K. B. In *Catalysis Asymmetric Synthesis*; Ojima, I., Ed.; VCH Publishers: New York, 1993; p227.

94. Sharpless, K. B.; Åmberg, W.; Bennani, Y. L.; Crispino, G. A.; Hartung, J.; Jeong, K. S.; Kwong, H.-L.; Morikawa, K.; Wang, Z.-M.; Xu, D.; Zhang, X.-L. *J. Org. Chem.* **1992**, *57*, 2768.

95. Oishi, T.; Iida, K.; Hirama, M. *Tetrahedron Lett.* **1993**, *34*, 3573.

96. Consiglio, G.; Waymouth, R. M. *Chem. Rev.* **1989**, *89*, 257.

97. Reiser, O. *Angew. Chem., Int. Ed. Engl.* **1993**, *32*, 547.

98. Davies, S. G. *Aldrichimica Acta* **1990**, *23*, 31.

99. Davies, S. G. *Pure Appl. Chem.* **1988**, *60*, 13.

100. Davies, S. G. *Chem. Br.* **1989**, *25*, 268.

101. Beckett, R. P.; Burgess, V. A.; Davies, S. G.; Whittaker, M. *Tetrahedron Lett.* **1993**, *34*, 3617.

102. Cooke, J. W. B.; Davies, S. G.; Naylor, A. *Tetrahedron* **1993**, *49*, 7955.

103. Bodwell, G. J.; Davies, S. G.; Mortlock, A. A. *Tetrahedron* **1991**, *47*, 10077.

104. Baker, T. M.; Bodwell, G. J.; Davies, S. G.; Edwards, A. J.; Metzler, M. R. *Tetrahedron* **1993**, *49*, 5635.

105. Broadley, K.; Davies, S. G. *Tetrahedron Lett.* **1984**, *25*, 1743.

106. Davies, S. G.; Seeman, J. I. *Tetrahedron Lett.* **1984**, *25*, 1845.

107. Davies, S. G.; Smallridge, A. J. *J. Organomet. Chem.* **1990**, *397*, C13.

108. Seeman, J. I.; Davies, S. G. *J. Am. Chem. Soc.* **1985**, *107*, 6522.

109. Aktogu, N.; Davies, S. G.; Dubac, J.; Mazerolles, P. *J. Organomet. Chem.* **1981**, *212*, C13.

110. Baird, G. J.; Davies, S. G. *J. Organomet. Chem.* **1983**, *248*, C1.

111. Baird, G. J.; Bandy, J. A.; Davies, S. G.; Prout, K. *J. Chem. Soc., Chem. Commun.* **1983**, 1202.

112. Aktogu, N.; Felkin, H.; Baird, G. J.; Davies, S. G.; Watts, O. *J. Organomet. Chem.* **1984**, *262*, 49.

113. Brown, S. L.; Davies, S. G.; Foster, D. F.; Seeman, J. I.; Warner, P. *Tetrahedron Lett.* **1986**, *27*, 623.

114. Davies, S. G.; Dordor, I. M.; Walker, J. C.; Warner, P. *Tetrahedron Lett.* **1984**, *25*, 2709.

115. Davies, S. G.; Dordor, I. M.; Warner, P. *J. Chem. Soc., Chem. Commun.* **1984**, 956.

116. Davies, S. G.; Dordor-Hedgecock, I. M.; Warner, P. *Tetrahedron Lett.* **1985**, *26*, 2125.

117. Ambler, P. W.; Davies, S. G. *Tetrahedron Lett.* **1985**, *26*, 2129.

118. Davies, S. G.; Dordor-Hedgecock, I. M.; Warner, P.; Jones, R. H.; Prout, K. *J. Organomet. Chem.* **1985**, *285*, 213.

119. Davies, S. G.; Walker, J. C. *J. Chem. Soc., Chem. Commun.* **1985**, 209.

120. Davies, S. G.; Walker, J. C. *J. Chem. Soc., Chem. Commun.* **1986**, 495.

121. Davies, S. G.; Easton, R. J. C.; Gonzalez, A.; Preston, S. C.; Sutton, K. H.; Walker, J. C. *Tetrahedron* **1986**, *42*, 3987.

122. Davies, S. G.; Dordor-Hedgecock, I. M.; Sutton, K. H.; Walker, J. C.; Jones, R. H.; Prout, K. *Tetrahedron* **1986**, *42*, 5123.

123. Davies, S. G.; Walker, J. C. *J. Chem. Soc., Chem. Commun.* **1986**, 609.

124. Liebeskind, L. S.; Welker, M. E. *Tetrahedron Lett.* **1984**, *25*, 4314.

125. Liebeskind, L. S.; Welker, M. E.; Goedkin, V. *J. Am. Chem. Soc.* **1984**, *106*, 441.

126. Liebeskind, L. S.; Welker, M. E. *Organometallics* **1983**, *2*, 194.

127. Liebeskind, L. S.; Welker, M. E.; Fengl, R. W. *J. Am. Chem. Soc.* **1986**, *108*, 6328.

128. Liebeskind, L. S.; Welker, M. E. *Tetrahedron Lett.* **1985**, *26*, 3079.

129. Aktogu, N.; Felkin, H.; Davies, S. G. *J. Chem. Soc., Chem. Commun.* **1982**, 1303.

130. Davies, S. G.; Dordor-Hedgecock, I. M.; Sutton, K. H.; Walker, J. C. *Tetrahedron Lett.* **1986**, *27*, 3787.

131. Brunner, H.; Schmidt, E. *J. Organomet. Chem.* **1970**, *21*, P53.

132. Brunner, H.; Schmidt, E. *J. Organomet. Chem.* **1973**, *50*, 219.

133. Baker, R. W.; Davies, S. G. *Tetrahedron: Asymmetry* **1993**, *4*, 1479.

134. Blackburn, B. K.; Davies, S. G.; Whittaker, M. In *Stereochemistry of Organometallic and Inorganic Compounds*; Bernal, I., Ed.; Elsevier: Amsterdam, 1989; Vol. 3, p141.

135. Blackburn, B. K.; Davies, S. G.; Sutton, K. H.; Whittaker, M. *Chem. Soc. Rev.* **1988**, *17*, 147.

136. Davies, S. G.; Derome, A. E.; McNally, J. P. *J. Am. Chem. Soc.* **1991**, *113*, 2854.

137. Davies, S. G.; Dordor-Hedgecock, I. M.; Sutton, K. H.; Whittaker, M. *J. Am. Chem. Soc.* **1987**, *109*, 5711.

138. Davies, S. G.; Dordor-Hedgecock, I. M.; Sutton, K. H.; Whittaker, M. *J. Organomet. Chem.* **1987**, *320*, C19.

139. Davies, S. G.; Seeman, J. I.; Williams, I. H. *Tetrahedron Lett.* **1986**, *27*, 619.

140. Seeman, J. I.; Davies, S. G. *J. Chem. Soc., Chem. Commun.* **1984**, 1019.

141. Blackburn, B. K.; Bromley, L.; Davies, S. G.; Whittaker, M.; Jones, R. H. *J. Chem. Soc., Perkin Trans.* **1989**, *2*, 1143.

142. Shambayati, S.; Crowe, W. E.; Schreiber, S. L. *Angew. Chem., Int. Ed. Engl.* **1990**, *29*, 256.

143. Crowe, W. E.; Schreiber, S. L. In *Advances in Metal-Organic Chemistry*;

Liebeskind, L., Ed.; JAI Press: London, 1991; Vol. 2, p247.

144. Bashiardes, G.; Davies, S. G. *Tetrahedron Lett.* **1987**, *28*, 5563.

145. Bashiardes, G.; Davies, S. G. *Tetrahedron Lett.* **1988**, *29*, 6509.

146. Casegreen, S. C.; Davies, S. G.; Hedgecock, C. J. R. *Synlett* **1991**, 779.

147. Wong, W.-K.; Tam, W.; Strouse, C. E.; Gladysz, J. A. *J. Chem. Soc., Chem. Commun.* **1979**, 530.

148. Smith, D. E.; Gladysz, J. A. *Organometallics* **1985**, *4*, 1480.

149. Heah, P. C.; Patton, A. T.; Gladysz, J. A. *J. Am. Chem. Soc.* **1986**, *108*, 1185.

150. Heah, P. C.; Gladysz, J. A. *J. Am. Chem. Soc.* **1984**, *106*, 7636.

151. Buhro, W. E.; Wong, A.; Merrifield, J. H.; Lin, G. Y.; Constable, A. G.; Gladysz, J. A. *Organometallics* **1983**, *2*, 1852.

152. Kiel, W. A.; Lin, G. Y.; Constable, A. G.; McCormick, F. B.; Strouse, C. E.; Eisenstein, O.; Gladysz, J. A. *J. Am. Chem. Soc.* **1982**, *104*, 4865.

153. Buhro, W. E.; Georgiou, S.; Fernandez, J. M.; Patton, A. T.; Strouse, C. E.; Gladysz, J. A. *Organometallics* **1986**, *5*, 956.

154. Kiel, W. A.; Buhro, W. E.; Gladysz, J. A. *Organometallics* **1984**, *3*, 879.

155. Bodner, G. S.; Smith, D. E.; Hatton, W. G.; Heah, P. C.; Georgiou, S.; Rheingold, A. L.; Geib, S. J.; Hutchinson, J. P.; Gladysz, J. A. *J. Am. Chem. Soc.* **1987**, *109*, 7688.

156. Hatton, W. G.; Gladysz, J. A. *J. Am. Chem. Soc.* **1983**, *105*, 6157.

157. Bodner, G. S.; Patton, A. T.; Smith, D. E.; Georgiou, S.; Tam, W.; Wong, W.-K.; Strouse, C. E.; Gladysz, J. A. *Organometallics* **1987**, *6*, 1954.

158. Merrifield, J. H.; Lin, G. Y.; Kiel, W. A.; Gladysz, J. A. *J. Am. Chem. Soc.* **1983**, *105(18)*, 5811.

159. Kiel, W. A.; Lin, G. Y.; Bodner, G. S.; Gladysz, J. A. *J. Am. Chem. Soc.* **1983**, *105*, 4958.

160. O'Connor, E. J.; Kobayashi, M.; Floss, H. G.; Gladysz, J. A. *J. Am. Chem.*

Soc. **1987**, *109*, 4837.

161. Fernandez, J. M.; Emerson, K.; Larsen, R. D.; Gladysz, J. A. *J. Chem. Soc., Chem. Commun.* **1988**, 37.

162. Dalton, D. M.; Fernandez, J. M.; Emerson, K.; Larsen, R. D.; Arif, A. M.; Gladysz, J. A. *J. Am. Chem. Soc.* **1990**, *112*, 9198.

163. Garner, C. M.; Quiros Mendez, N.; Kowalczyk, J. J.; Fernandez, J. M.; Emerson, K.; Larsen, R. D.; Gladysz, J. A. *J. Am. Chem. Soc.* **1990**, *112*, 5146.

164. Fernandez, J. M.; Emerson, K.; Larsen, R. H.; Gladysz, J. A. *J. Am. Chem. Soc.* **1986**, *108*, 8268.

165. Agbossou, F.; Ramsden, J. A.; Huang, Y. H.; Arif, A. M.; Gladysz, J. A. *Organometallics* **1992**, *11*, 693.

166. Pu, J. Q.; Peng, T. S.; Mayne, C. L.; Arif, A. M.; Gladysz, J. A. *Organometallics* **1993**, *12*, 2686.

167. Ramsden, J. A.; Weng, W. Q.; Arif, A. M.; Gladysz, J. A. *J. Am. Chem. Soc.* **1992**, *114*, 5890.

168. Ramsden, J. A.; Weng, W. Q.; Gladysz, J. A. *Organometallics* **1992**, *11*, 3635.

169. Adams, R. D.; Chodosh, D. F.; Faller, J. W.; Rosan, A. M. *J. Am. Chem. Soc.* **1979**, *101*, 2570.

170. Faller, J. W.; Chao, K. H. *J. Am. Chem. Soc.* **1983**, *105*, 3893.

171. Faller, J. W.; Chao, K. H. *Organometallics* **1984**, *3*, 927.

172. Faller, J. W.; Linebarrier, D. L. *J. Am. Chem. Soc.* **1989**, *111*, 1937.

173. Faller, J. W.; Linebarrier, D. L. *Organometallics* **1990**, *9*, 3182.

174. Faller, J. W.; John, J. A.; Mazzieri, M. R. *Tetrahedron Lett.* **1989**, *30*, 1769.

175. Faller, J. W.; Nguyen, J. T.; Ellis, W.; Mazzieri, M. R. *Organometallics* **1993**, *12*, 1434.

176. Faller, J. W.; Shvo, Y.; Chao, K. H.; Murray, H. H. *J. Organomet. Chem.* **1982**, *226*, 251.

177. Bhattacharya, A. K.; Thyagarajan, G. *Chem. Rev.* **1981**, *81*, 415.

178. Engel, R. In *Synthesis of Carbon-Phosphorus Bonds*; CRC Press: Boca Raton, Florida, 1988.

179. Hudson, H. R. *Top. Phos. Chem.* **1983**, *11*, 339.

180. Landauer, S. R.; Rydon, H. N. *J. Chem. Soc.* **1953**, 2224.

181. Worms, K. H.; Schmidt-Dunker, M. *Org. Phos. Comp.* **1976**, *7*, 24.

182. Brill, T. B.; Landon, S. J. *Chem. Rev.* **1984**, *84*, 577.

183. We have named the M-P(O)$(OR)_2$ (metallophosphonates) complexes as organometallic phosphonic acid esters (R'P(O)$(OR)_2$) and the M-P(O)R'(OR) (metallophosphinates) as organometallic 2°-phosphinic acid esters (R'_2P(O)(OR)).

184. Haines, R. J.; DuPreez, A. L.; Marais, L. L. *J. Organomet. Chem.* **1971**, *28*, 405.

185. Clemens, J.; Neukomm, H.; Werner, H. *Helv. Chim. Acta* **1974**, *57*, 2000.

186. Harder, V.; Werner, H. *Helv. Chim. Acta* **1973**, *56*, 1620.

187. Harder, V.; Dubler, E.; Werner, H. *J. Organomet. Chem.* **1974**, *71*, 427.

188. King, R. B.; Diefenbach, S. P. *Inorg. Chem.* **1979**, *18*, 63.

189. Newton, M. G.; Pantaleo, N. S.; King, R. B.; Diefenbach, S. P. *J. Chem. Soc., Chem. Commun.* **1979**, 55.

190. Shakir, R.; Atwood, J. L.; Janik, T. S.; Atwood, J. D. *J. Organomet. Chem.* **1980**, *190*, C14.

191. Bruce, M. I.; Shaw, G.; Stone, F. G. A. *J. Chem. Soc., Dalton Trans.* **1973**, 1667.

192. Schubert, U.; Werner, R.; Zinner, L.; Werner, H. *J. Organomet. Chem.* **1983**, *253*, 363.

193. Solar, J. M.; Rogers, R. D.; Mason, W. R. *Inorg. Chem.* **1984**, *23*, 373.

194. King, C.; Roundhill, D. M. *Inorg. Chem.* **1986**, *25*, 2271.

195. Klaeui, W.; Buchholz, E. *Inorg. Chem.* **1988**, *27*, 3500.

196. Nakazawa, H.; Kadoi, Y.; Mizuta, T.; Miyoshi, K.; Yoneda, H. *J. Organomet. Chem.* **1989**, *366*, 333.

197. Nakazawa, H.; Kadoi, Y.; Miyoshi, K. *Organometallics* **1989**, *8*, 2851.

198. Nakazawa, H.; Yamaguchi, M.; Kubo, K.; Miyoshi, K. *J. Organomet. Chem.* **1992**, *428*, 145.

199. Landon, S. J.; Brill, T. B. *J. Am. Chem. Soc.* **1982**, *104*, 6571.

200. Towle, D. K.; Landon, S. J.; Brill, T. B.; Tulip, T. H. *Organometallics* **1982**, *1*, 295.

201. Landon, S. J.; Brill, T. B. *Inorg. Chem.* **1984**, *23*, 4177.

202. Landon, S. J.; Brill, T. B. *Inorg. Chem.* **1985**, *24*, 2863.

203. Landon, S. J.; Brill, T. B. *Inorg. Chem.* **1984**, *23*, 1266.

204. Sullivan, R. J.; Bao, Q. B.; Landon, S. J.; Rheingold, A. L.; Brill, T. B. *Inorg. Chim. Acta* **1986**, *111*, 19.

205. Bao, Q. B.; Brill, T. B. *Inorg. Chem.* **1987**, *26*, 3447.

206. Brunner, H.; Jablonski, C. R.; Jones, P. G. *Organometallics* **1988**, *7*, 1283.

207. Jablonski, C. R.; Burrow, T.; Jones, P. G. *J. Organomet. Chem.* **1989**, *370*, 173.

208. Jablonski, C. R.; Ma, H. Z.; Hynes, R. C. *Organometallics* **1992**, *11*, 2796.

209. Neukomm, H.; Werner, H. *J. Organomet. Chem.* **1976**, *108*, C26.

210. Sweigart, D. A. *J. Chem. Soc., Chem. Commun.* **1980**, 1159.

211. Aradi, M. S.; Maisonnat, A.; Attali, S.; Poilblanc, R. *J. Organomet. Chem.* **1974**, *67*, 109.

212. Alex, R. F.; Pomeroy, R. K. *Organometallics* **1982**, *1*, 453.

213. Hartgerink, J.; Silavwe, N. D.; Alper, H. *Inorg. Chem.* **1980**, *19*, 2593.

214. Goh, L. Y.; D'aniello, M. J.; Slater, S.; Muetterties, E. L.; Tavanaiepour, I.; Chang, M. I.; Fredrich, M. F.; Day, V. W. *Inorg. Chem.* **1979**, *18*, 192.

215. Labinger, J. A. *J. Organomet. Chem.* **1977**, *136*, C31.

216. Fabian, B. D.; Labinger, J. A. *Organometallics* **1983**, *2*, 659.

217. Jablonski, C. R.; Ma, H. Z.; Chen, Z.; Hynes, R. C.; Bridson, J. N.; Bubenik, M. P. *Organometallics* **1993**, *12*, 917.

218. Boone, B. J.; Jablonski, C. R.; Jones, P. G.; Newlands, M. J.; Yu, Y. F. *Organometallics* **1993**, *12*, 3042.

219. Bonifaci, C.; Ceccon, A.; Gambaro, A.; Ganis, P.; Santi, S.; Valle, G.; Venzo, A. *Organometallics* **1993**, *12*, 4211.

220. Zhou, Y. L.; Dewey, M. A.; Gladysz, J. A. *Organometallics* **1993**, *12*, 3918.

221. Dewey, M. A.; Zhou, Y. L.; Liu, Y. M.; Gladysz, J. A. *Organometallics* **1993**, *12*, 3924.

222. Brammer, L.; Dunne, B. J.; Green, M.; Moran, G.; Orpen, A. G.; Reeve, C.; Schaverien, C. J. *J. Chem. Soc., Dalton Trans.* **1993**, 1747.

223. Lee, S. W.; Richmond, M. G. *Inorg. Chem.* **1991**, *30*, 2237.

224. Monti, D.; Bassetti, M. *J. Am. Chem. Soc.* **1993**, *115*, 4658.

225. Ceccon, A.; Elsevier, C. J.; Ernsting, J. M.; Gambaro, A.; Santi, S.; Venzo, A. *Inorg. Chim. Acta* **1993**, *204*, 15.

226. O'Hare, D.; Green, J. C.; Marder, T.; Collins, S.; Stringer, G.; Kakkar, A. K.; Kaltsoyannis, N.; Kuhn, A.; Lewis, R.; Mehnert, C.; Scott, P.; Kurmoo, M.; Pugh, S. *Organometallics* **1992**, *11*, 48.

227. Kakkar, A. K.; Taylor, N. J.; Marder, T. B.; Shen, J. K.; Hallinan, N.; Basolo, F. *Inorg. Chim. Acta* **1992**, *200*, 219.

228. O'Hare, D.; Murphy, V. J.; Kaltsoyannis, N. *J. Chem. Soc., Dalton Trans.* **1993**, 383.

229. Rau, D.; Behrens, U. *J. Organomet. Chem.* **1993**, *454*, 151.

230. Brown, D. A.; Fitzpatrick, N. J.; Glass, W. K.; Ahmed, H. A.; Cunningham, D.;

McArdle, P. *J. Organomet. Chem.* **1993**, *455*, 157.

231. Ambrosi, L.; Bassetti, M.; Buttiglieri, P.; Mannina, L.; Monti, D.; Bocelli, G. *J. Organomet. Chem.* **1993**, *455*, 167.

232. Morandini, F.; Pilloni, G.; Consiglio, G.; Sironi, A.; Moret, M. *Organometallics* **1993**, *12*, 3495.

233. Abel, E. W.; Moorhouse, S. *J. Chem. Soc., Dalton Trans.* **1973**, 1706.

234. Kohler, F. H. *Chem. Ber.* **1974**, *107*, 570.

235. Benn, R.; Cibura, K.; Hofmann, P.; Jonas, K.; Rufinska, A. *Organometallics* **1985**, *4*, 2214.

236. Smith, D. E.; Welch, A. J. *Organometallics* **1986**, *5*, 760.

237. Binger, P.; Milczarek, R.; Mynott, R.; Kruger, C.; Tsay, Y.-H.; Raabe, E.; Regitz, M. *Chem. Ber.* **1988**, *121*, 637.

238. Baker, R. T.; Tulip, T. H. *Organometallics* **1986**, *5*, 839.

239. Piccolrovazzi, N.; Pino, P.; Consiglio, G.; Sironi, A.; Moret, M. *Organometallics* **1990**, *9*, 3098.

240. Donovan, B. T.; Hughes, R. P.; Trujillo, H. A. *J. Am. Chem. Soc.* **1990**, *112*, 7076.

241. Donovan, B. T.; Hughes, R. P.; Trujillo, H. A.; Rheingold, A. L. *Organometallics* **1992**, *11*, 64.

242. Crossley, N. S.; Green, J. C.; Nagy, A.; Stringer, G. *J. Chem. Soc., Dalton Trans.* **1989**, 2139.

243. Loonat, M. S.; Carlton, L.; Boeyens, J. C. A.; Coville, N. J. *J. Chem. Soc., Dalton Trans.* **1989**, 2407.

244. Huffman, M. A.; Liebeskind, L. S. *J. Am. Chem. Soc.* **1990**, *112*, 8617.

245. Huffman, M. A.; Liebeskind, L. S.; Pennington, W. T. *Organometallics* **1992**, *11*, 255.

246. Green, M. L. H.; Hughes, A. K. *J. Chem. Soc., Dalton Trans.* **1992**, 527.

247. Hart-Davis, A. J.; Mawby, R. J. *J. Chem. Soc., (A)* **1969**, 2403.

248. Jones, D. J.; Mawby, R. J. *Inorg. Chim. Acta* **1972**, *6*, 157.

249. Caddy, P.; Green, M.; Howard, J. A. K.; Squire, J. M.; White, N. J. *J. Chem. Soc., Dalton Trans.* **1981**, 400.

250. Caddy, P.; Green, M.; O'Brien, E.; Smart, L. E.; Woodward, P. *J. Chem. Soc., Dalton Trans.* **1980**, 962.

251. Ji, L. N.; Rerek, M. E.; Basolo, F. *Organometallics* **1984**, *3*, 740.

252. Rerek, M. E.; Ji, L.-N.; Basolo, F. *J. Chem. Soc., Chem. Commun.* **1983**, 1208.

253. Casey, C. P.; O'Connor, J. M. *Organometallics* **1985**, *4*, 384.

254. Turaki, N. N.; Huggins, J. M.; Lebioda, L. *Inorg. Chem.* **1988**, *27*, 424.

255. Bang, H.; Lynch, T. J.; Basolo, F. *Organometallics* **1992**, *11*, 40.

256. Foo, T.; Bergman, R. G. *Organometallics* **1992**, *11*, 1811.

257. Forschner, T. C.; Cutler, A. R.; Kullnig, R. K. *Organometallics* **1987**, *6*, 889.

258. Forschner, T. C.; Cutler, A. R.; Kullnig, R. K. *J. Organomet. Chem.* **1988**, *356*, C12.

259. Forschner, T. C.; Cutler, A. R. *J. Organomet. Chem.* **1989**, *361*, C41.

260. Forschner, T. C.; Cutler, A. R. *Organometallics* **1985**, *4*, 1247.

261. Levitre, S. A.; Cutler, A. R.; Forschner, T. C. *Organometallics* **1989**, *8*, 1133.

262. Marder, T. B.; Roe, D. C.; Milstein, D. *Organometallics* **1988**, *7*, 1451.

263. Borrini, A.; Diversi, P.; Ingrosso, G.; Lucherini, A.; Serra, G. *J. Mol. Catal.* **1985**, *30*, 181.

264. Bonnemann, H.; Brijoux, W. *Aspects of Homogeneous Catalysis* **1984**, *5*, 75.

265. Bonnemann, H. *Angew. Chem., Int. Ed. Engl.* **1985**, *24*, 248.

266. O'Connor, J. M.; Casey, C. P. *Chem. Rev.* **1987**, *87*, 307.

267. Miller, G. A.; Therien, M. J.; Trogler, W. C. *J. Organomet. Chem.* **1990**, *383*, 271.

268. Merola, J. S.; Kacmarcik, R. T.; Engen, D. V. *J. Am. Chem. Soc.* **1986**, *108*, 329.

269. Kowaleski, R. M.; Rheingold, A. L.; Trogler, W., C; Basolo, F. *J. Am. Chem. Soc.* **1986**, *108*, 2460.

270. Faller, J. W.; Crabtree, R. H.; Habib, A. *Organometallics* **1985**, *4*, 929.

271. Habib, A.; Tanke, R. S.; Holt, E. M.; Crabtree, R. H. *Organometallics* **1989**, *8*, 1225.

272. Nesmeyanov, A. N.; Ustynyuk, N. A.; Makarova, L. G.; Andrianov, V. G.; Struchkov, Y. T.; Andrae, S.; Ustynyuk, Y. A.; Malyugina, S. G. *J. Organomet. Chem.* **1978**, *159*, 189.

273. Szajek, L. P.; Lawson, R. J.; Shapley, J. R. *Organometallics* **1991**, *10*, 357.

274. Ahmed, H.; Brown, D. A.; Fitzpatrick, N. J.; Glass, W. K. *J. Organomet. Chem.* **1991**, *418*, C14.

275. Salzer, A.; Taschler, C. *J. Organomet. Chem.* **1985**, *294*, 261.

276. Werner, H.; Mahr, J.; Hoerlin, G. *Z. Anorg. Allg. Chem.* **1989**, *577*, 283.

277. Diversi, P.; Giusti, A.; Ingrosso, G.; Lucherini, A. *J. Organomet. Chem.* **1981**, *205*, 239.

278. Fritz, H. P.; Kohler, F. H.; Schwarzhans, K. E. *J. Organomet. Chem.* **1969**, *16*, P14.

279. Westcott, S. A.; Kakkar, A. K.; Stringer, G.; Taylor, N. J.; Marder, T. B. *J. Organomet. Chem.* **1990**, *394*, 777.

280. Jablonski, C.; Zhou, Z.; Bridson, J. N. *J. Organomet. Chem.* **1992**, *429*, 379.

281. Jablonski, C. R.; Zhou, Z. *Can. J. Chem.* **1992**, *70*, 2544.

282. Zhou, Z.; Jablonski, C.; Bridson, J. *J. Organomet. Chem.* **1993**, *461*, 215.

283. Brunner, H.; Doppelberger, J.; Dreischl, P.; Moellenberg, T. *J. Organomet. Chem.* **1977**, *139*, 223.

284. Eliel, E. L. In *The Stereochemistry of Carbon Compounds*; McGraw-Hill: New York, 1962.

285. Brunner, H.; Riepl, G.; Benn, R.; Rufinska, A. *J. Organomet. Chem.* **1983**, *253*, 93.

286. Kakkar, A. K.; Jones, S. F.; Taylor, N. J.; Collins, S.; Marder, T. B. *J. Chem. Soc., Chem. Commun.* **1989**, 1454.

287. Dahl, T. *Acta Chem. Scand.* **1994**, *48*, 95.

288. Maddaluno, J. F.; Gresh, N.; Giessnerprettre, C. *J. Org. Chem.* **1994**, *59*, 793.

289. Mezrhab, B.; Dumas, F.; Dangelo, J.; Riche, C. *J. Org. Chem.* **1994**, *59*, 500.

290. Cahn, R. S.; Ingold, C.; Prelog, V. *Angew. Chem., Int. Ed. Engl.* **1966**, *5*, 385.

291. Stanley, K.; Baird, M. C. *J. Am. Chem. Soc.* **1975**, *97*, 6598.

292. Sloan, T. E. *Top. Stereochem.* **1981**, *12*, 1.

293. Mata, P.; Lobo, A. M.; Marshall, C.; Johnson, A. P. *Tetrahedron: Asymmetry* **1993**, *4*, 657.

294. Yoshikawa, K.; Yamamoto, N.; Murata, M.; Awano, K.; Morimoto, T.; Achiwa, K. *Tetrahedron: Asymmetry* **1992**, *3*, 13.

295. Karel, K. J.; Tulip, T. H.; Ittel, S. D. *Organometallics* **1990**, *9*, 1276.

296. Carlton, L.; Johnston, P.; Coville, N. J. *J. Organomet. Chem.* **1988**, *339*, 339.

297. Fritz, H. P.; Kreiter, C. G. *J. Organomet. Chem.* **1965**, *4*, 198.

298. Loonat, M. S.; Carlton, L.; Coville, N. J. *S. Afr. J. Chem.* **1988**, *41*, 72.

299. Marder, T. B.; Calabrese, J. C.; Roe, D. C.; Tulip, T. H. *Organometallics* **1987**, *6*, 2012.

300. Crabtree, R. H.; Parnell, C. P. *Organometallics* **1984**, *3*, 1727.

301. Johnston, P.; Loonat, M. S.; Ingham, W. L.; Carlton, L.; Coville, N. J. *Organometallics* **1987**, *6*, 2121.

302. Tolman, C. A. *Chem. Rev.* **1977**, *77*, 313.

303. Liu, Hong-Y.; Eriks, K.; Prock, A.; Giering, W. P. *Organometallics* **1990**, *9*, 1758.

304. Brunner, H.; Doppelberger, J. *Chem. Ber.* **1978**, *111*, 673.

305. Gilmore, C. J. *J. Appl. Cryst.* **1984**, *17*, 42.

306. Walker, N.; Stuart, D. *Acta Crystallogr., Sect. A: Found. Cryst.* **1983**, *A39*, 158.

307. Brunner, H.; Rambold, W. *J. Organomet. Chem.* **1974**, *64*, 373.

308. Zhou, Z.; Jablonski, C.; Bridson, J. *Organometallics* **1993**, *12*, 3677.

309. King, R. B. *Inorg. Chem.* **1965**, *1*, 82.

310. Coville, N. J.; Loonat, M. S.; White, D.; Carlton, L. *Organometallics* **1992**, *11*, 1082.

311. Du Plooy, K. E.; Marais, C. F.; Carlton, L.; Hunter, R.; Boeyens, J. C. A.; Coville, N. J. *Inorg. Chem.* **1989**, *28*, 3855.

312. Appleton, T. G.; Clark, H. C.; Manzer, L. E. *Coord. Chem. Rev.* **1973**, *10*, 335.

313. Mackie, S. C.; Park, Y. S.; Shurvell, H. F.; Baird, M. C. *Organometallics* **1991**, *10*, 2993.

314. Mackie, S. C.; Baird, M. C. *Organometallics* **1992**, *11*, 3712.

315. Garner, E.; Orpen, A. G. *J. Chem. Soc., Dalton Trans.* **1993**, 533.

316. Bernal, I.; Reisner, G. M.; Brunner, H.; Riepl, G. *J. Organomet. Chem.* **1985**, *284*, 115.

317. Polowin, J.; Mackie, S. C.; Baird, M. C. *Organometallics* **1992**, *11*, 3724.

318. Zhou, Z.; Jablonski, C.; Bridson, J. N. *Organometallics* **1994**, *13*, 781.

319. Albright, T. A.; Hofmann, P.; Hoffmann, R.; Lillya, C. P.; Dobosh, P. A. *J. Am. Chem. Soc.* **1983**, *105*, 3396.

320. Kakkar, A. K.; Taylor, N. J.; Calabrese, J. C.; Nugent, W. A.; Roe, D. C.; Connaway, E. A.; Marder, T. B. *J. Chem. Soc., Chem. Commun.* **1989**, 990.

321. Mlekuz, M.; Bougeard, P.; Sayer, B. G.; McGlinchey, M. J.; Rodger, C. A.; Churchill, M. R.; Ziller, J. W.; Kang, S. K.; Albright, T. A. *Organometallics* **1986**, *5*, 1656.

322. Ceccon, A.; Gambaro, A.; Santi, S.; Valle, G.; Venzo, A. *J. Chem. Soc., Chem. Commun.* **1989**, 51.

323. Caddy, P.; Green, M.; O'Brien, E.; Smart, L. E.; Woodward, P. *Angew. Chem., Int. Ed. Engl.* **1977**, *16*, 648.

324. Morandini, F.; Consiglio, G.; Sironi, A.; Moret, M. *J. Organomet. Chem.* **1989**, *370*, 305.

325. Oro, L. A.; Ciriano, M. A.; Campo, M.; Foces-Foces, C.; Cano, F. H. *J. Organomet. Chem.* **1985**, *289*, 117.

326. Shakir, R.; Atwood, J. L. *Acta Crystallogr., Sect. B: Struct. Sci.* **1981**, *B37*, 1656.

327. Foo, T.; Bergman, R. G. *Organometallics* **1992**, *11*, 1801.

328. Brunner, H.; Fisch, K.; Jones, P. G.; Salbeck, J. *Angew. Chem., Int. Ed. Engl.* **1989**, *28*, 1521.

329. Gibson, D. H.; Richardson, J. F.; Mbadike, O. P. *Acta Crystallogr., Sect. B: Struct. Sci.* **1993**, *49*, 784.

330. Frankcom, T. M.; Green, J. C.; Nagy, A.; Kakkar, A. K.; Marder, T. B. *Organometallics* **1993**, *12*, 3688.

331. Hoffmann, R. *Science* **1981**, *211*, 995.

332. Hoffmann, R. *Angew. Chem., Int. Ed. Engl.* **1982**, *21*, 711.

333. Honan, M. B.; Atwood, J. L.; Bernal, I.; Herrmann, W. A. *J. Organomet. Chem.* **1979**, *179*, 403.

334. Zhou, Z.; Jablonski, C. R. Manuscript in preparation (1994).

335. Hoffmann, R. *J. Chem. Phys.* **1963**, *39*, 1397.

336. Hoffmann, R. *J. Chem. Phys.* **1962**, *36*, 3179.

337. Hoffmann, R. *J. Chem. Phys.* **1962**, *36*, 3489.

338. Hoffmann, R. *J. Chem. Phys.* **1962**, *37*, 2872.

339. Albright, T. A.; Burdett, J. K.; Whangbo, M. H. In *Orbital Interactions in Chemistry*; John Wiley & Sons: New York, 1985.

340. Albright, T. A.; Hoffmann, R.; Hofmann, P. *Chem. Ber.* **1978**, *111*, 1591.

341. Schilling, G. E. R.; Hoffmann, R.; Faller, J. W. *J. Am. Chem. Soc.* **1979**, *101*, 592.

342. Hoffmann, R.; Hofmann, P. *J. Am. Chem. Soc.* **1976**, *98*, 598.

343. Anh, N. T.; Elian, M.; Hoffmann, R. *J. Am. Chem. Soc.* **1978**, *100*, 110.

344. Albright, T. A.; Hofmann, P.; Hoffmann, R. *J. Am. Chem. Soc.* **1977**, *99*, 7546.

345. Albright, T. A.; Hoffmann, R. *Chem. Ber.* **1978**, *111*, 1578.

346. Curtis, M. D.; Eisenstein, O. *Organometallics* **1984**, *3*, 887.

347. Piers, W. E.; Whittal, R. M.; Ferguson, G.; Gallagher, J. F.; Froese, R. D.; Stronks, H. J.; Krygsman, P. H. *Organometallics* **1992**, *11*, 4015.

348. Downton, P. A.; Sayer, B. G.; McGlinchey, M. J. *Organometallics* **1992**, *11*, 3281.

349. Decken, A.; Britten, J. F.; McGlinchey, M. J. *J. Am. Chem. Soc.* **1993**, *115*, 7275.

350. Esteruelas, M. A.; Lahuerta, O.; Modrego, J.; Nurnberg, O.; Ore, L. A.; Rodriguez, L.; Sola, E.; Werner, H. *Organometallics* **1993**, *12*, 266.

351. Ditchfield, R.; Hughes, R. P.; Tucker, D. S.; Bierwagen, E. P.; Robbins, J.; Robinson, D. J.; Zakutansky, J. A. *Organometallics* **1993**, *12*, 2258.

352. Mealli, C.; Proserpio, D. M. *J. Chem. Ed.* **1990**, *67*, 399.

353. Marynick, D. S. *J. Am. Chem. Soc.* **1984**, *106*, 4064.

354. Brunner, H. *Top. Curr. Chem.* **1975**, *56*, 67.

355. Brunner, H. *Adv. Organometal. Chem.* **1980**, *18*, 151.

356. Faure, B.; Archavlis, A.; Buono, G. *J. Chem. Soc., Chem. Commun.* **1989**,

805.

357. Sanders, J. K. M.; Mersh, J. D. *Prog. Nucl. Magn. Reson. Spectrosc.* **1983**, *15*, 353.

358. Moore, J. W.; Pearson, R. G. In *Kinetics and Mechanism*, 3rd; John Wiley and Sons: New York, 1981.

359. Amis, E. S. In *Solvent Effects on Reaction Rates and Mechanisms*; Academic Press: New York, 1966.

360. Parker, A. J. *Chem. Rev.* **1969**, *69*, 1.

361. Parker, A. J.; Mayer, U.; Schmid, R.; Gutmann, V. *J. Org. Chem.* **1978**, *43*, 1843.

362. King, R. B. *Inorg. Chem.* **1966**, *5*, 82.

363. Frith, S. A.; Spencer, J. L. *Inorg. Synth.* **1984**, *23*, 15.

364. Zhou, Z.; Jablonski, C. Unpublished results.

365. Zhou, Z.; Jablonski, C. R. Submitted for publication (1994).

366. Werner, H.; Hofmann, W. *Chem. Ber.* **1982**, *115*, 127.

367. Kläui, W.; Otto, H.; Eberspach, W.; Buchholz, E. *Chem. Ber.* **1982**, *115*, 1922.

368. Valderrama, M.; Scotti, M.; Campos, P.; Werner, H.; Mueller, G. *Chem. Ber.* **1990**, *123*, 1005.

369. Scotti, M.; Valderrama, M.; Campos, P.; Klaui, W. *Inorg. Chim. Acta* **1993**, *207*, 141.

370. Brunner, H.; Rambold, W. *J. Organomet. Chem.* **1973**, *60*, 351.

371. King, R. B.; Treichel, P. M.; Stone, F. G. A. *J. Am. Chem. Soc.* **1961**, *83*, 3593.

372. Lecomte, C.; Dusavsoy, Y.; Protas, J.; Tirouflet, J.; Dormand, A. *J. Organomet. Chem.* **1974**, *73*, 67.

373. Antonova, A. B.; Kovalenko, S., V; Korniets, E. D.; Ioganson, A. A.; Struchkov, Y. T.; Akhmedov, A. I.; Yanovskii, A. I. *J. Organomet. Chem.* **1983**, *244*, 35.

374. Day, V. W.; Tavanaiepour, I.; Abdel-Meguid, S. S.; Kimer, J. F.; Goh, L.-Y. *Inorg. Chem.* **1982**, *21*, 657.

375. Banbery, H. J.; Hussain, W.; Evans, I. G.; Hamor, T. A.; Jones, C. J.; McCleverty, J. A.; Schulte, Heinz-J.; Engles, B.; Klaui, W. *Polyhedron* **1990**, *9*, 2549.

376. Hitchcock, P. B.; Klein, S., I; Nixon, J. F. *J. Organomet. Chem.* **1983**, *241*, C9.

377. Buchholz, D.; Huttner, G.; Imhof, W. *J. Organomet. Chem.* **1989**, *388*, 307.

378. Liang, L.; Stevens, E. D.; Nolan, S. P. *Organometallics* **1992**, *11*, 3459.

379. Kläui, W.; Neukomm, H.; Werner, H.; Huttner, G. *Chem. Ber.* **1977**, *110*, 2283.

380. Bennett, J.; Pidcock, A.; Waterhouse, C. R.; Coggon, P.; McPhail, A. T. *J. Chem. Soc., (A)* **1970**, 2094.

381. Bao, Q.-B.; Geib, S. J.; Rheingold, A. L.; Brill, T. B. *Inorg. Chem.* **1987**, *26*, 3453.

382. Korp, J. D.; Bernal, I. *J. Organomet. Chem.* **1981**, *220*, 355.

383. Whuler, A.; Brouty, C.; Spinat, P. *Acta Crystallogr., Sect. B: Struct. Sci.* **1980**, *B36*, 1267.

384. Brunner, H. *Angew. Chem., Int. Ed. Engl.* **1971**, *10*, 249.

385. Kläui, W.; Neukomm, H. *Org. Magn. Reson.* **1977**, *10*, 126.

Appendix

The selected ^{1}H and ^{19}F NMR, $^{1}H/^{13}C$ HETCOR, ^{1}H nOed spectra, and sample input files for EHMO calculations are arranged according to the order in which they appear in the text. For experimental details see Experimental Sections in the corresponding chapters.

Figure A-1. ^1H NMR Spectra for (η^5-Indenyl)Co(C_6F_{13})(CO)(I) (**2-3**).

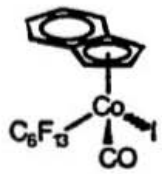

Figure A-2. ^{19}F NMR Spectra for (η^5-Indenyl)Co(C_6F_{13})(CO)(I) (2-3).

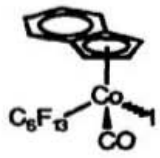

Figure A-3. $^{1}H/^{13}C$ HETCOR Spectra for (η^5-Indenyl)Co(C_6F_{13})(CO)(I) (**2-3**).

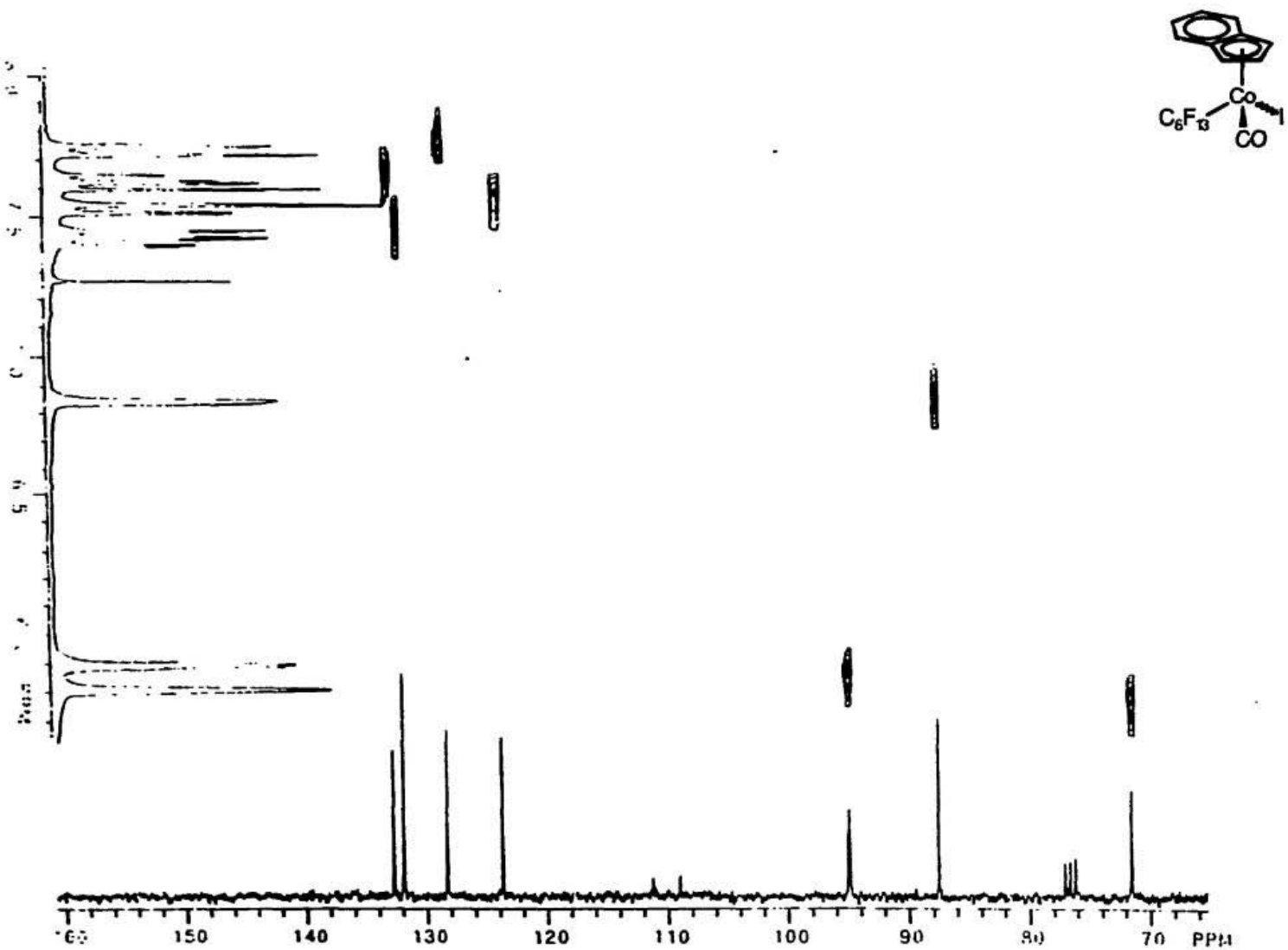

Figure A-4. ^{1}H NMR Spectra for (η^5-Indenyl)Co(C_6F_{13})(PPh_2Me)(I) (**2-15**).

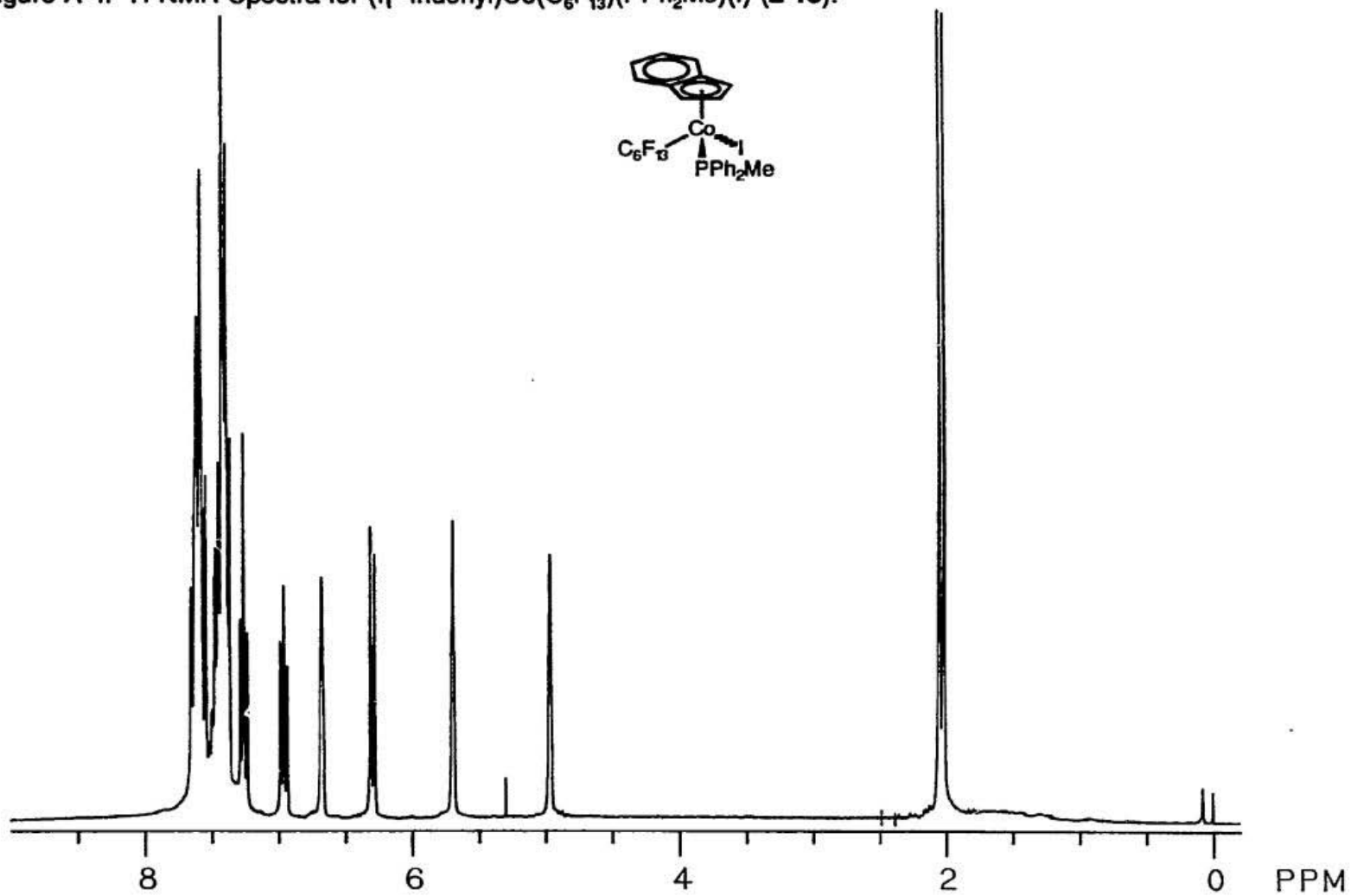

Figure A-5. ^{1}H NMR Spectra for $(\eta^5\text{-}C_5H_5)Co(C_3F_7)(P(OMe)_3)(P(O)(OMe)_2)$ (**3-3a**α).

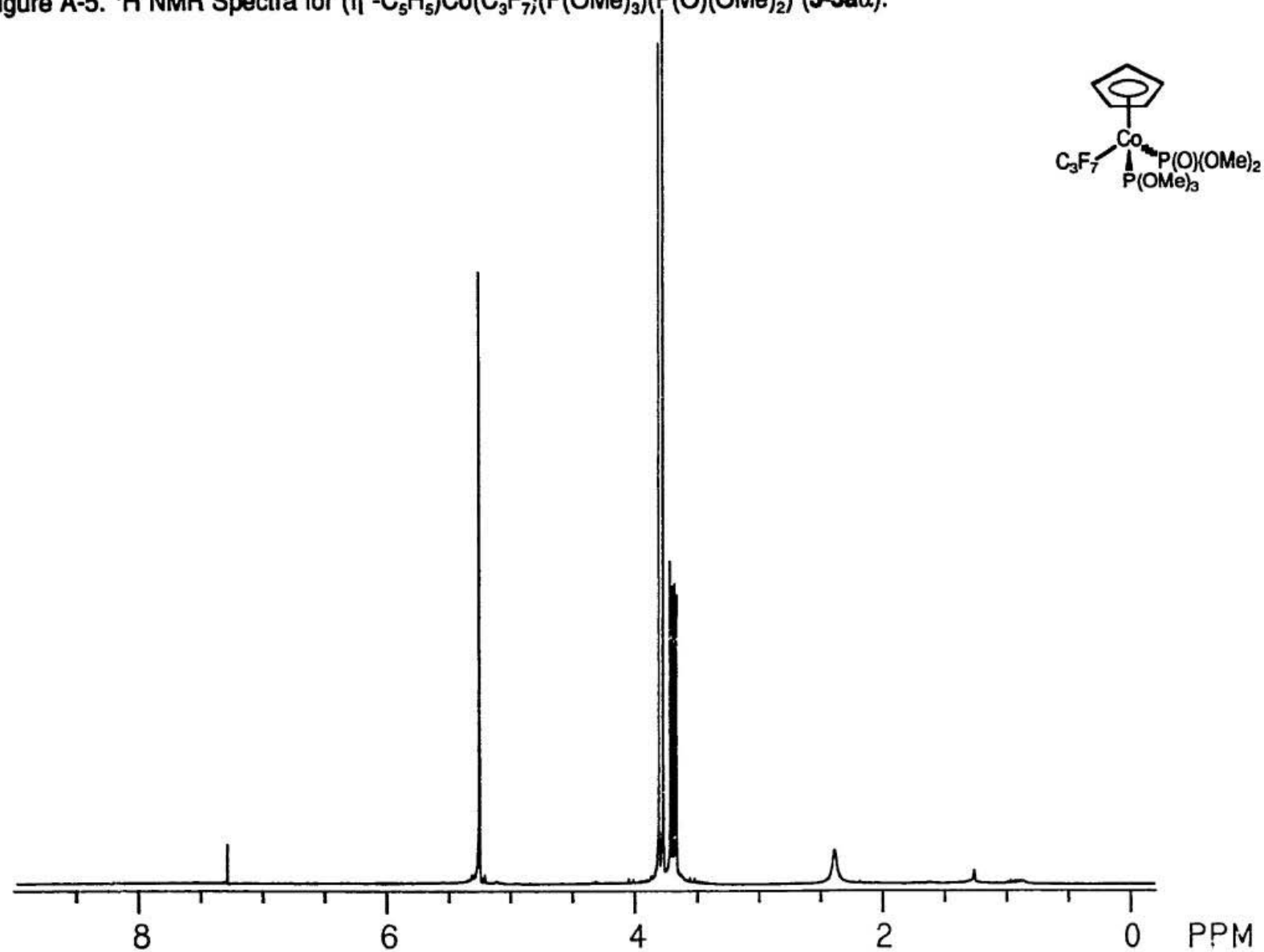

Figure A-6. ^{19}F NMR Spectra for $(\eta^5\text{-}C_5H_5)Co(C_3F_7)(P(OMe)_3)(P(O)(OMe)_2)$ (**3-3aα**).

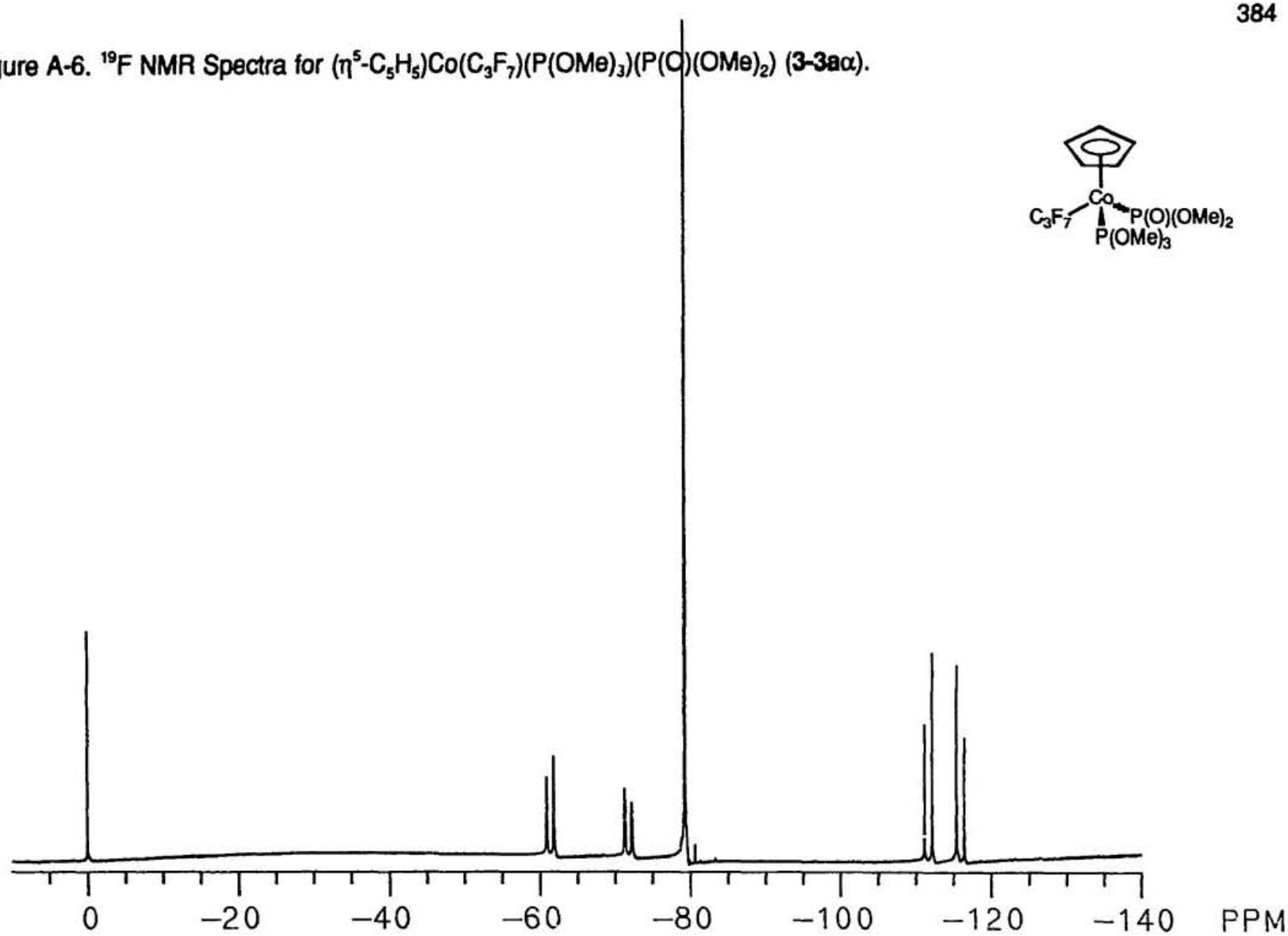

Figure A-7. ^{1}H NMR Spectra for [S_{Co},R_P/R_{Co},S_P]-[η^5-C_5H_5)Co(C_3F_7)(PMe_3)(P(O)Ph(OMe)) (**3-3bβ-2**).

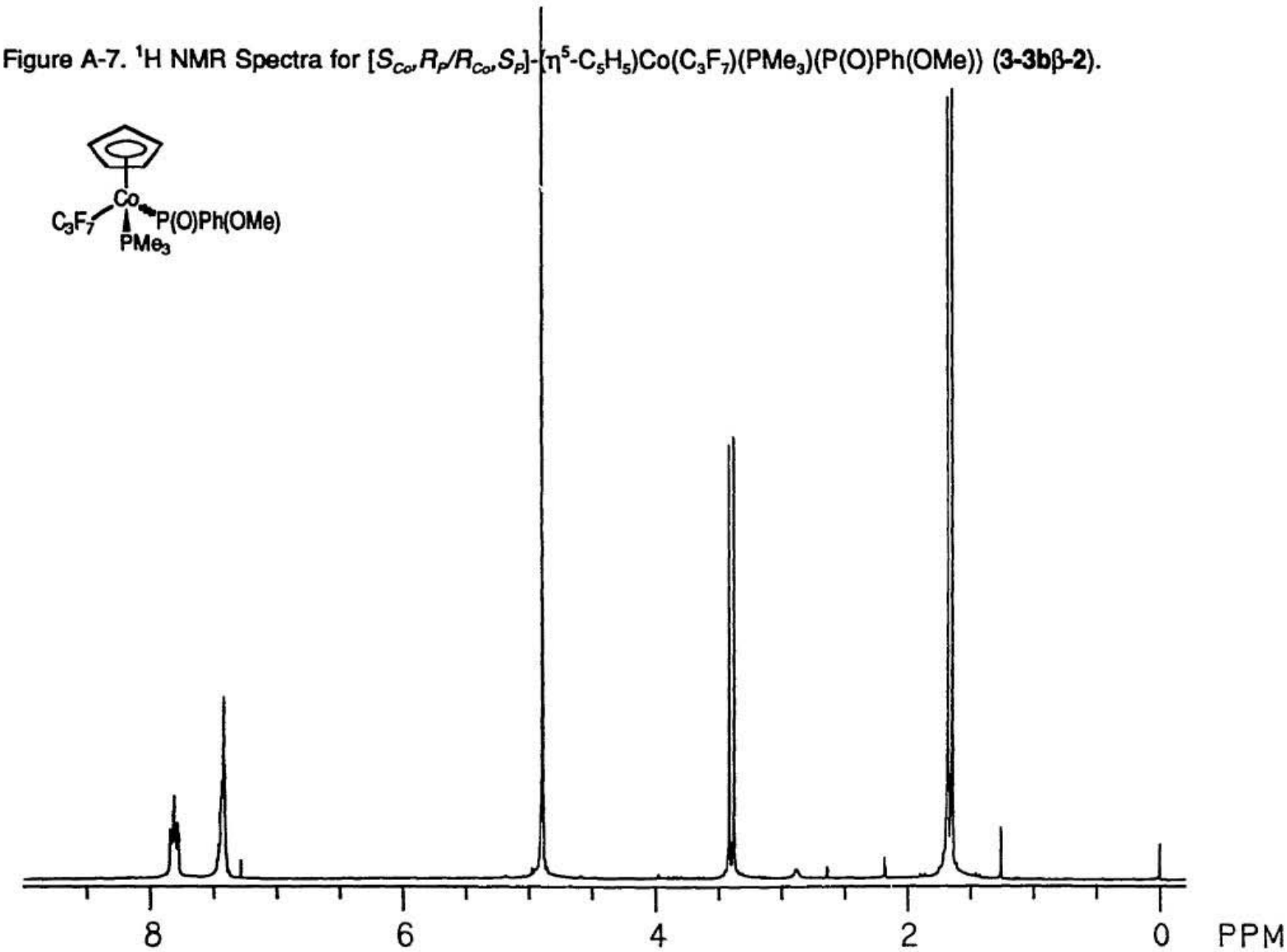

Figure A-8. ^{19}F NMR Spectra for [S_{Co},R_P/R_{Co},S_P]-(η^5-C_5H_5)Co(C_3F_7)(PMe_3)(P(O)Ph(OMe)) (**3-3bβ-2**).

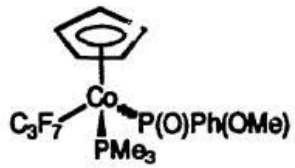

Figure A-9. ^{1}H NMR Spectra for [(η^5-Indenyl)Co(C_3F_7)($P(OMe)_3$)$_2$]$^+SbF_6^-$ (**3-5a**α).

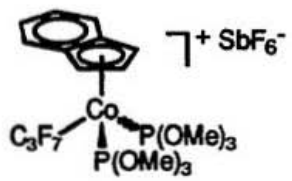

Figure A-10. ^{1}H NMR Spectra for (η^5-Indenyl)Co(C_6F_{13})($P(OMe)_3$)($P(O)(OMe)_2$) (**3-6'aα**).

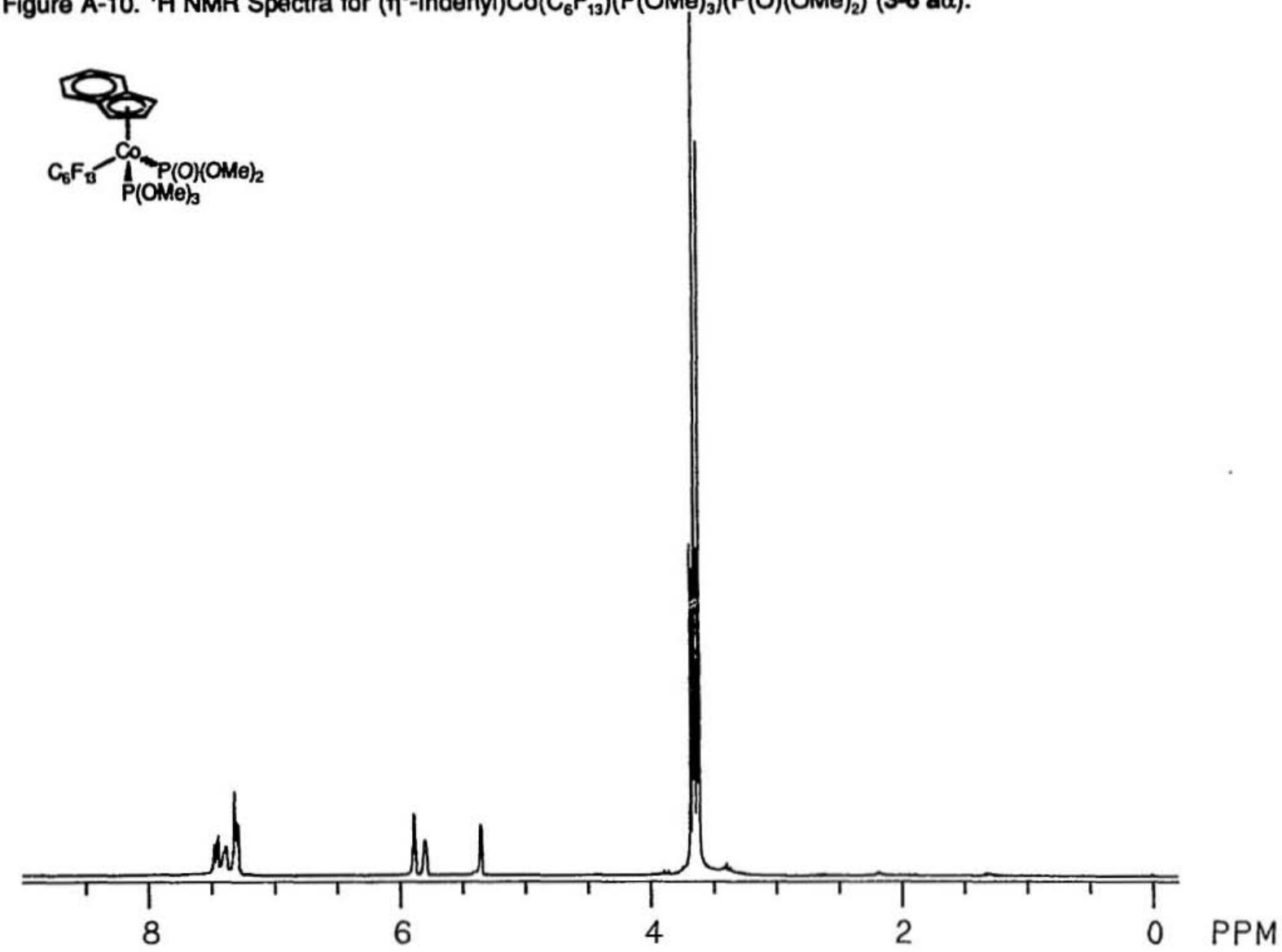

Figure A-11. ^{19}F NMR Spectra for (η^5-Indenyl)Co(C_6F_{13})($P(OMe)_3$)($P(O)(OMe)_2$) (**3-6'aα**).

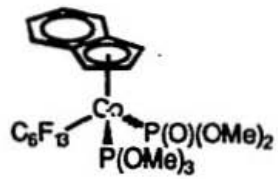

Figure A-12. ^{1}H NMR Spectra for (η^5-Indenyl)Co(C_3F_7)(PMe_3)(P(O)($OMe)_2$) (**3-6bα**).

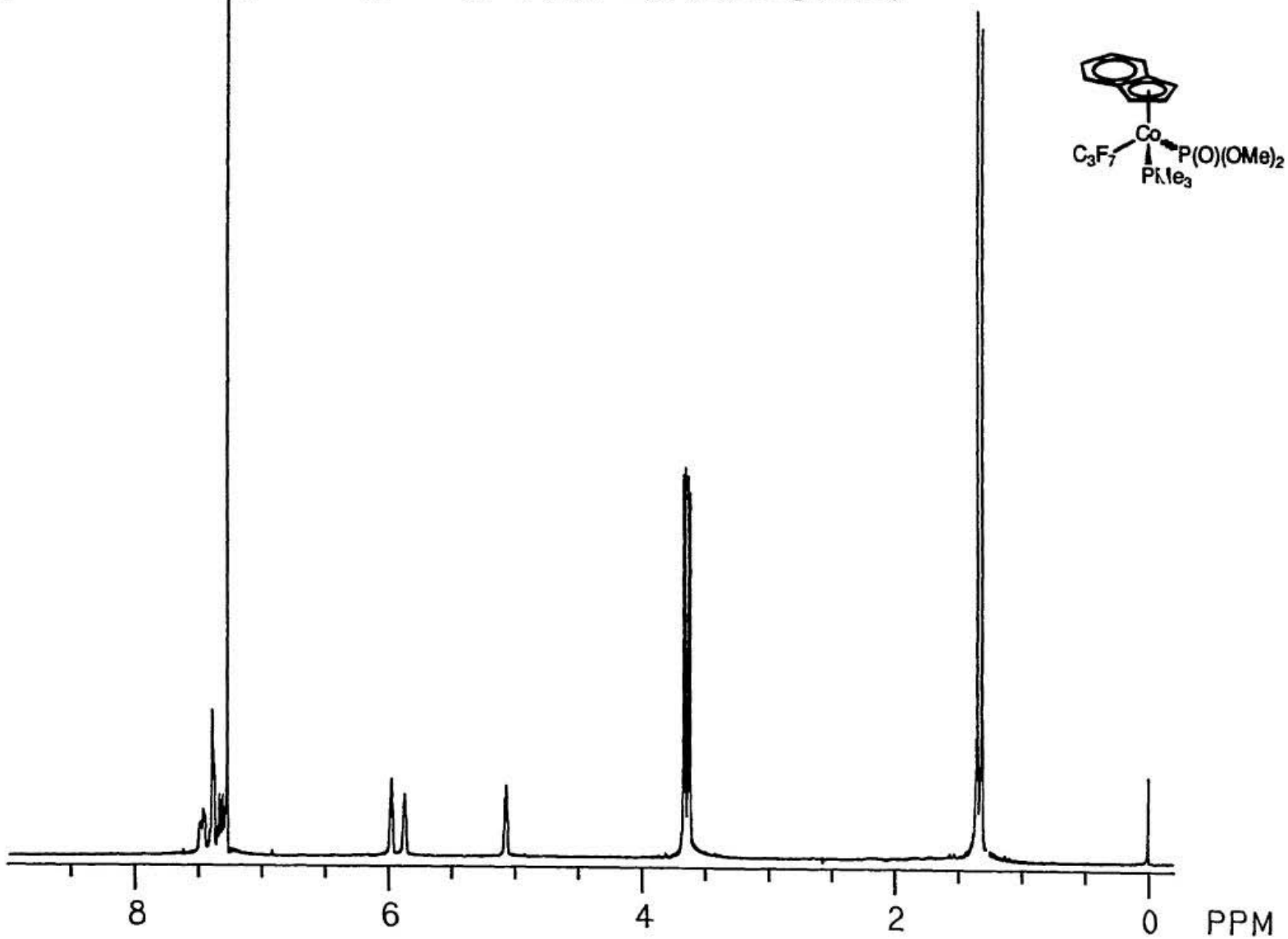

Figure A-13. ^{1}H NMR Spectra for (η^5-Indenyl)Co(C_3F_7)(PPhMe$_2$)(P(O)(OMe)$_2$) (**3-6cα**).

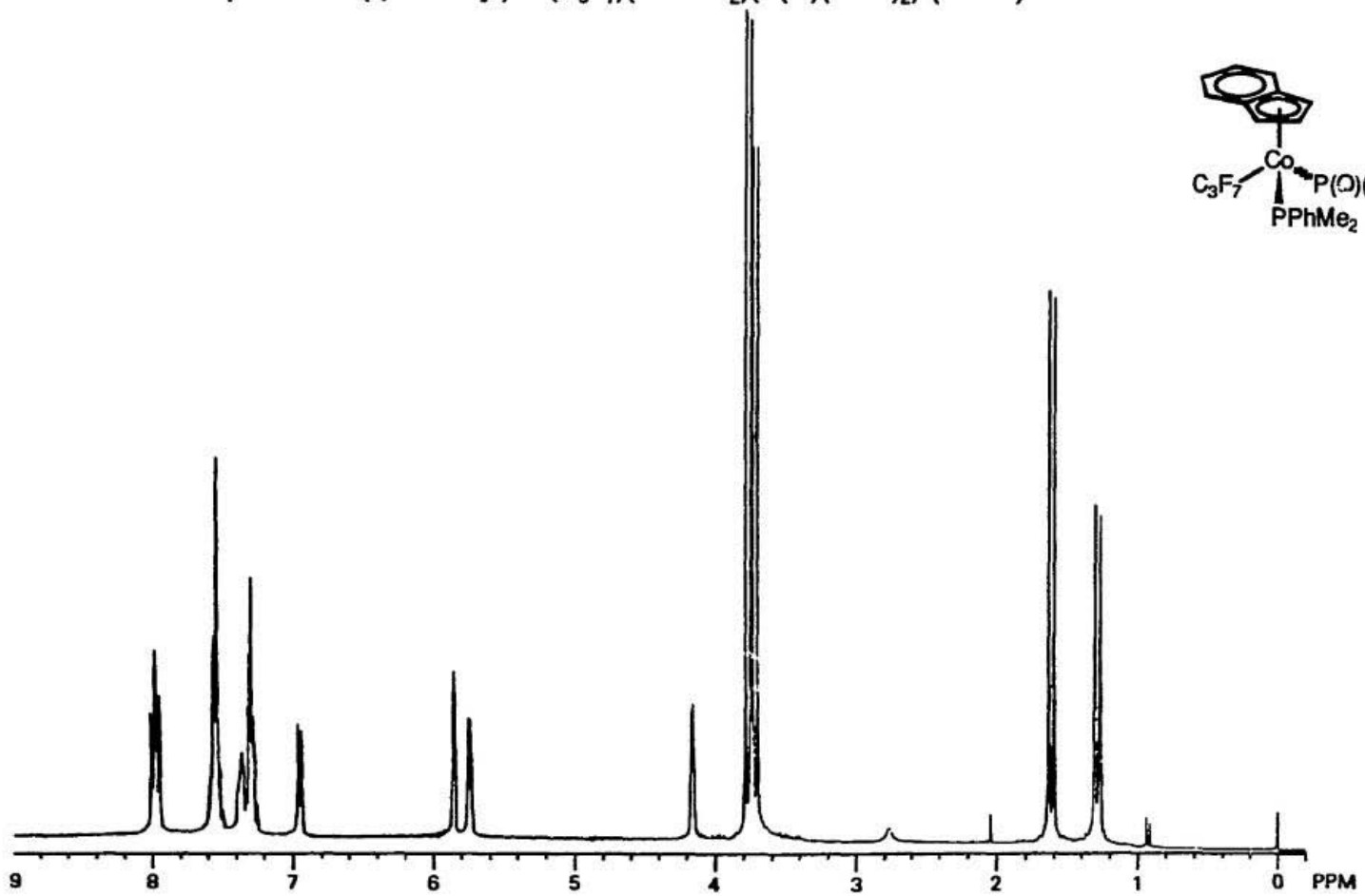

Figure A-14. ^{1}H NMR Spectra for [S_{Co},S_P/R_{Co},R_P]-(η^5-Indenyl)Co(C_3F_7)(PMe_3)(P(O)Ph(OMe)) (**3-6bβ-1**).

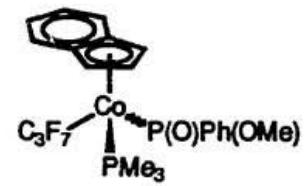

Figure A-15. ^{1}H NMR Spectra for [S_{Co},S_P/R_{Co},R_P]-(η^5-Indenyl)Co(C_3F_7)($PPhMe_2$)(P(O)Ph(OMe)) (**3-6cβ-1**).

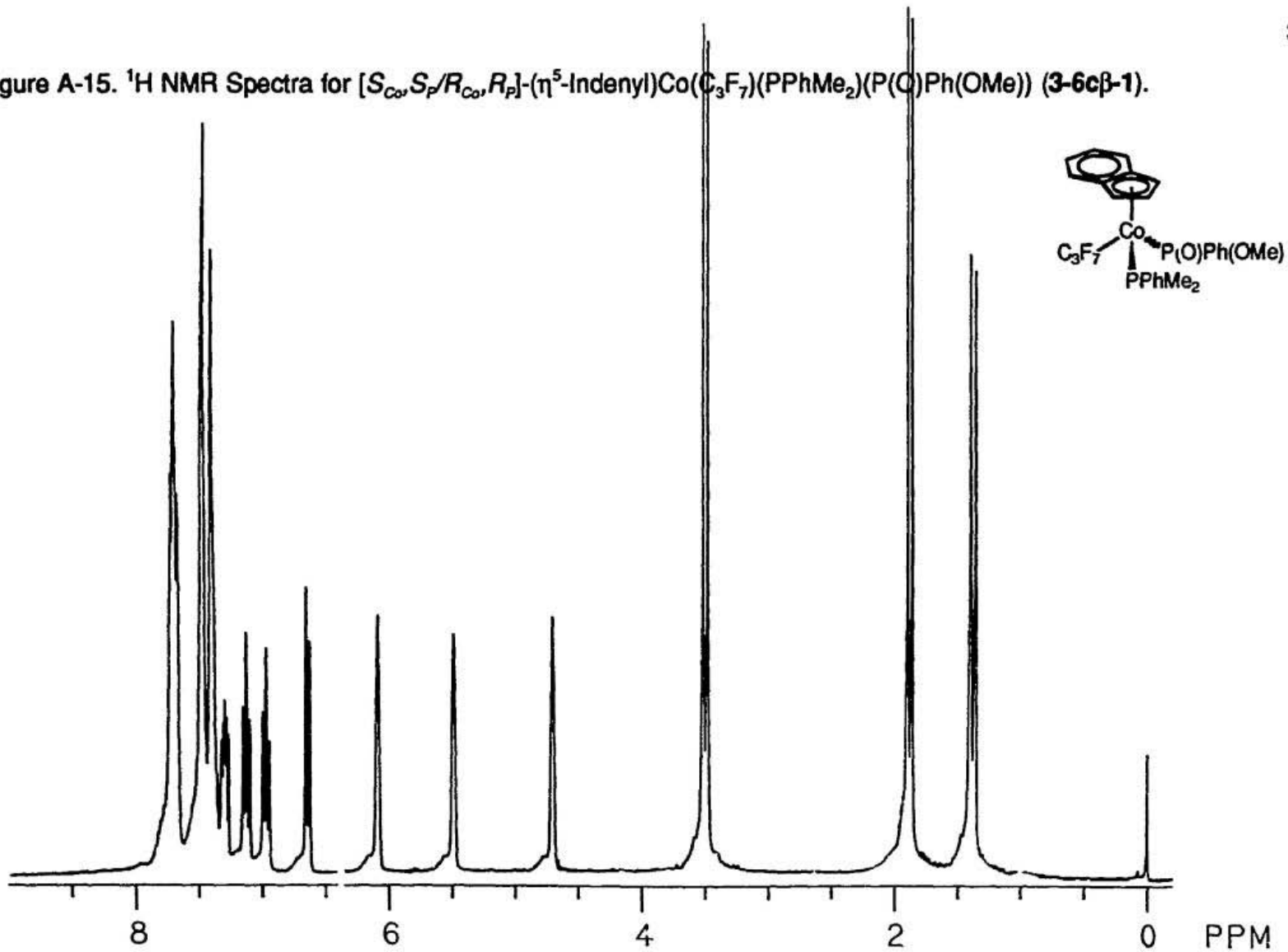

Figure A-16. ^{1}H NMR Spectra for [S_{Co},R_P/R_{Co},S_P]-(η^5-Indanyl)Co(C_3F_7)(PPh(OMe)$_2$)(P(O)Ph(OMe)) (**3-6eβ-2**).

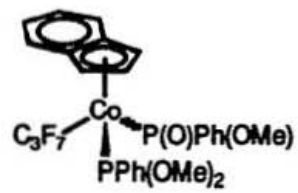

Table A-1. EHMO Input File for Searching the Energy Minimum for Indenyl Ring Distortion in (η^5-Indenyl)Co(PH_3)(I)(Me).

```
(Indenyl)Co(PH3)(I)(CH3) + H + slippage
 26  0DIST  0  2 13
0.01,0.04,0.06,0.08,0.10,0.12,0.14,0.16,0.18,0.20,0.24,0.26,0.28
0.,1.,2.,3.,4.,5.,6.,7.,8.,9.,10.,11.,12.
 EL RO
0.,0.,0.,DU
 -1  1 C 1.19,90.,288.
 -1  2 C 1.19,90.,0.
 -1  3 C 1.19,90.,72.
 -1  9 C 1.19,90.,144. ,1
 -1  8 C 1.19,90.,216. ,1
 -1 -2DU 2.18,90.,180.
 -2  4 C 1.40,90.,270. ,1 ,11
 -2  5 C 1.40,150.,270.,1 ,11
 -2  6 C 1.40,150.,90. ,1 ,11
 -2  7 C 1.40,90.,90.  ,1 ,11
  1 10 H 1.01,180.,0.
  2 11 H 1.01,180.,0.
  3 12 H 1.01,180.,0.
  4 13 H 1.01,180.,0.  ,1 ,11
  5 14 H 1.01,180.,0.  ,1 ,11
  6 15 H 1.01,180.,0.  ,1 ,11
  7 16 H 1.01,180.,0.  ,1 ,11
 -1 -3DU 1000.,90.,0.
 -3 17CO 1.80,90.,0.
 17 18ME 1.98,125.,180.
 17 22 I 2.57,125.,300.
 17 23FO 2.23,125.,60.
GR1  3  1  2000.
```

Table A-2. EHMO Input File for Indenyl Ring Rotation about Indenyl-Co Bond in (η^5-Indenyl)Co(PH_3)(I)(Me).

```
(Indenyl)Co(PH3)(I)(CH3) + H + F +SLIP +ROT ABOUT Co-IND
 26  0DIST  0  1 13
0.,30.,60.,90.,120.,150.,180.,210.,240.,270.,300.,330.,360.
 EL RO
0.,0.,0.,DU
 -1  1 C 1.19,90.,288.
 -1  2 C 1.19,90.,0.
 -1  3 C 1.19,90.,72.
 -1  9 C 1.19,90.,144. ,1
 -1  8 C 1.19,90.,216. ,1
 -1 -2DU 2.18,90.,180.
 -2  4 C 1.40,90.,270. ,1 ,11
 -2  5 C 1.40,150.,270.,1 ,11
 -2  6 C 1.40,150.,90. ,1 ,11
 -2  7 C 1.40,90.,90.  ,1 ,11
  1 10 H 1.01,180.,0.
  2 11 H 1.01,180.,0.
  3 12 H 1.01,180.,0.
  4 13 H 1.01,180.,0.  ,1 ,11
  5 14 H 1.01,180.,0.  ,1 ,11
  6 15 H 1.01,180.,0.  ,1 ,11
  7 16 H 1.01,180.,0.  ,1 ,11
 -1 -3DU 0.17,90.,0.
 -3 17CO 1.80,90.,0.    ,3
 17 18ME 1.98,125.,180. ,3
 17 22 I 2.57,125.,300. ,3
 17 23FO 2.23,125.,60.  ,3
GR1  3  1  7.5
GR1  9  8  1.
GR3 17 -3  1000.
```

Table A-3. EHMO Input File for Searching the Energy Minimum for Indenyl Ring Distortion in (η^5-Indenyl)Co(PH_3)(Me)(P(O)$(OH)_2$).

```
(Indenyl)Co(PH3)(P(O)(OH)2)(CH3) + H + slippage
 31   0DIST   0   2 13
0.01,0.02,0.04,0.06,0.08,0.10,0.12,0.14,0.16,0.18,0.20,0.24,0.26
0.,1.,2.,3.,4.,5.,6.,7.,8.,9.,10.,11.,12.
 EL RO
0.,0.,0.,DU
 -1   1 C 1.19,90.,288.
 -1   2 C 1.19,90.,0.
 -1   3 C 1.19,90.,72.
 -1   9 C 1.19,90.,144. ,1
 -1   8 C 1.19,90.,216. ,1
 -1 -2DU 2.18,90.,180.
 -2   4 C 1.40,90.,270. ,1 ,11
 -2   5 C 1.40,150.,270.,1 ,11
 -2   6 C 1.40,150.,90. ,1 ,11
 -2   7 C 1.40,90.,90.  ,1 ,11
  1  10 H 1.01,180.,0.
  2  11 H 1.01,180.,0.
  3  12 H 1.01,180.,0.
  4  13 H 1.01,180.,0.  ,1 ,11
  5  14 H 1.01,180.,0.  ,1 ,11
  6  15 H 1.01,180.,0.  ,1 ,11
  7  16 H 1.01,180.,0.  ,1 ,11
 -1 -3DU 1000.,90.,0.
 -3  17CO 1.80,90.,0.    ,3
 17  18  P 2.22,125.,180. ,3
 18  19  O 1.49,125.,180. ,3
 18  20  O 1.62,103.5,290.,3
 18  21  O 1.62,103.5,70. ,3
 20  22  H 0.96,120.,210. ,3
 21  23  H 0.96,120.,150. ,3
 17  24FO 2.23,125.,300. ,3
 17  28ME 1.98,125.,60. ,3
GR1   3   1   2000.
```

Table A-4. EHMO Input File for Indenyl Ring Rotation about Indenyl-Co bond in (η^5-Indenyl)Co(PH_3)(Me)(P(O)$(OH)_2$).

```
(Indenyl)Co(PH3)(P(O)(OH)2)(CH3) + H + F + slippage +ROTATION
 31   0DIST  0  1 13
0.,30.,60.,90.,120.,150.,180.,210.,240.,270.,300.,330.,360.
 EL RO
0.,0.,0.,DU
 -1   1 C 1.19,90.,288.
 -1   2 C 1.19,90.,0.
 -1   3 C 1.19,90.,72.
 -1   9 C 1.19,90.,144. ,1
 -1   8 C 1.19,90.,216. ,1
 -1 -2DU 2.18,90.,180.
 -2   4 C 1.40,90.,270. ,1 ,11
 -2   5 C 1.40,150.,270.,1 ,11
 -2   6 C 1.40,150.,90. ,1 ,11
 -2   7 C 1.40,90.,90.  ,1 ,11
  1  10 H 1.01,180.,0.
  2  11 H 1.01,180.,0.
  3  12 H 1.01,180.,0.
  4  13 H 1.01,180.,0.  ,1 ,11
  5  14 H 1.01,180.,0.  ,1 ,11
  6  15 H 1.01,180.,0.  ,1 ,11
  7  16 H 1.01,180.,0.  ,1 ,11
 -1 -3DU 0.12,90.,0.
 -3 17CO 1.80,90.,0.    ,3
 17  18 P 2.22,125.,180. ,3
 18  19 O 1.49,125.,180. ,3
 18  20 O 1.62,103.5,290.,3
 18  21 O 1.62,103.5,70. ,3
 20  22 H 0.96,120.,210. ,3
 21  23 H 0.96,120.,150. ,3
 17  24FO 2.23,125.,300. ,3
 17  28ME 1.98,125.,60.  ,3
GR1   3   1   6.
GR1   9   8   1.5
GR3  17  -3   1000.
```

Table A-5. EHMO Input File for Fragment Orbital Interactions in (η^5-Indenyl)Co(PH_3)(Me)(P(O)$(OH)_2$).

```
(Indenyl)Co(PH3)(P(O)(OH)2)(CH3) + H + F + slippage +INTERACTION
 31   0DIST  0   0   0
 EL RO
0.,0.,0.,DU
 -1   1 C 1.19,90.,288.
 -1   2 C 1.19,90.,0.
 -1   3 C 1.19,90.,72.
 -1   9 C 1.19,90.,144. ,1
 -1   8 C 1.19,90.,216. ,1
 -1 -2DU 2.18,90.,180.
 -2   4 C 1.40,90.,270. ,1 ,11
 -2   5 C 1.40,150.,270.,1 ,11
 -2   6 C 1.40,150.,90. ,1 ,11
 -2   7 C 1.40,90.,90.  ,1 ,11
  1 10 H 1.01,180.,0.
  2 11 H 1.01,180.,0.
  3 12 H 1.01,180.,0.
  4 13 H 1.01,180.,0.  ,1 ,11
  5 14 H 1.01,180.,0.  ,1 ,11
  6 15 H 1.01,180.,0.  ,1 ,11
  7 16 H 1.01,180.,0.  ,1 ,11
 -1 -3DU 0.12,90.,0.
 -3 17CO 1.80,90.,0.    ,3
 17 18 P 2.22,125.,180. ,3
 18 19 O 1.49,125.,180. ,3
 18 20 O 1.62,103.5,290.,3
 18 21 O 1.62,103.5,70. ,3
 20 22 H 0.96,120.,210. ,3
 21 23 H 0.96,120.,150. ,3
 17 24FO 2.23,125.,300. ,3
 17 28ME 1.98,125.,60.  ,3
GR1   3   1   6.
GR1   9   8   1.5
FMO
OP RO CM TO NC
2   16 15 -1   1
```

Figure A-17. ^{1}H NMR Spectra for [S_{Co},S_C]-[(η^5-C_5H_5)Co(N-N*)(PPh(OMe)$_2$)]$^+$I$^-$ (**5-3a**).

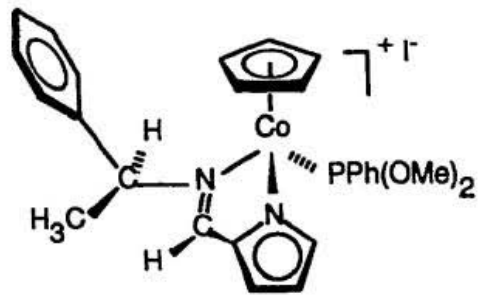

Figure A-18. ^{1}H NMR Spectra for [S_{Co},S_P,S_C]-(η^5-C_5H_5)Co(N-N*)(P(O)Ph(OMe)) (**5-4a**).

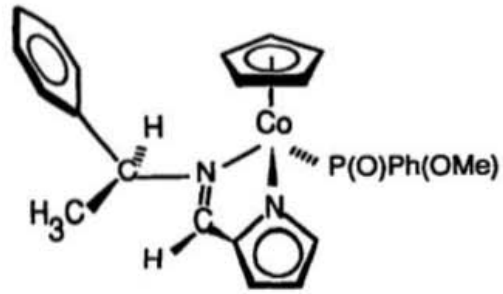

Figure A-19. ^{1}H NMR Spectra for $[S_{Co},S_C]$-[(η^5-C_5H_5)Co(N-N*)($PPhMe_2$)]$^+I^-$ (**5-5a**).

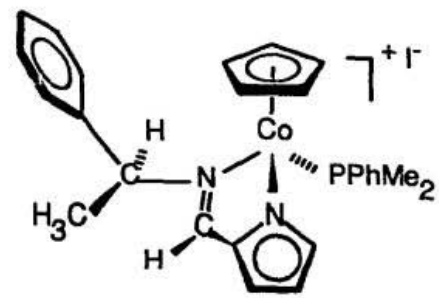

Figure A-20. ^{1}H NMR Spectra for (η^5-C_5H_5)Co(N-C(O)Me)(I) (**6-6**).

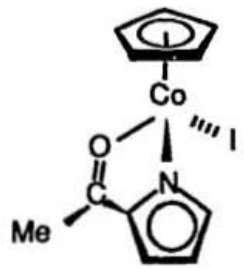

Figure A-21. ^{1}H NMR Spectra for (η^5-C_5Me_5)Co(N-C(O)H)(I) (**6-7**).

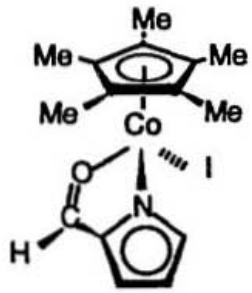

Figure A-22. ^{1}H NMR Spectra for $[(\eta^5\text{-}C_5Me_5)Co(N\text{-}C(O)H)(PMe_3)]^+I^-$ (**6-10**).

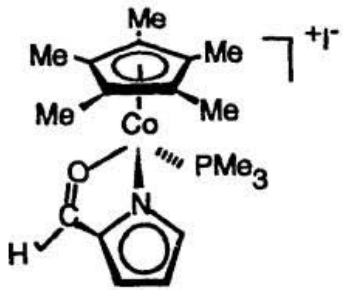

Figure A-23. ^1H NMR Spectra for $[(\eta^5\text{-}C_5H_5)Co(N\text{-}C(O)Me)(PPh(OMe)_2)]^+I^-$ (**6-17**).

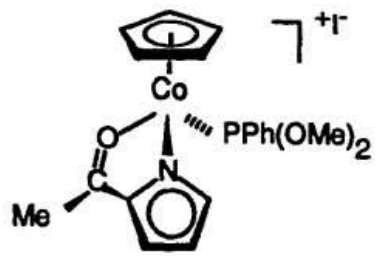

Figure A-24. ^{1}H NMR Spectra for (η^5-C_5Me_5)Co(N-C(O)H)(P(O)(OMe)$_2$) (**6-22**).

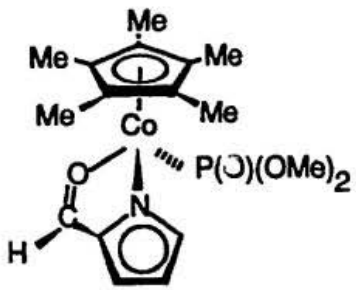

Figure A-25. ^{1}H NMR Spectra for (η^5-C_5H_5)Co(N-C(O)H)(P(O)Ph(OMe)) (**6-24a,b**).

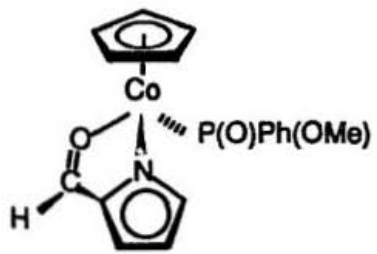

Figure A-26. ^{1}H NMR Spectra for (η^5-C_5Me_5)Co(N-C(O)H)(P(O)Ph(OMe)) (**6-26a,b**).

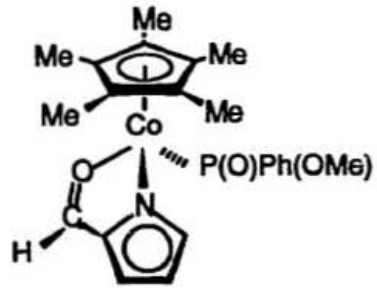

Figure A-27. ^{1}H NMR Spectra for [S_C]-PEt$_2$NH-C*H(Me)Ph (**PEtNH**).

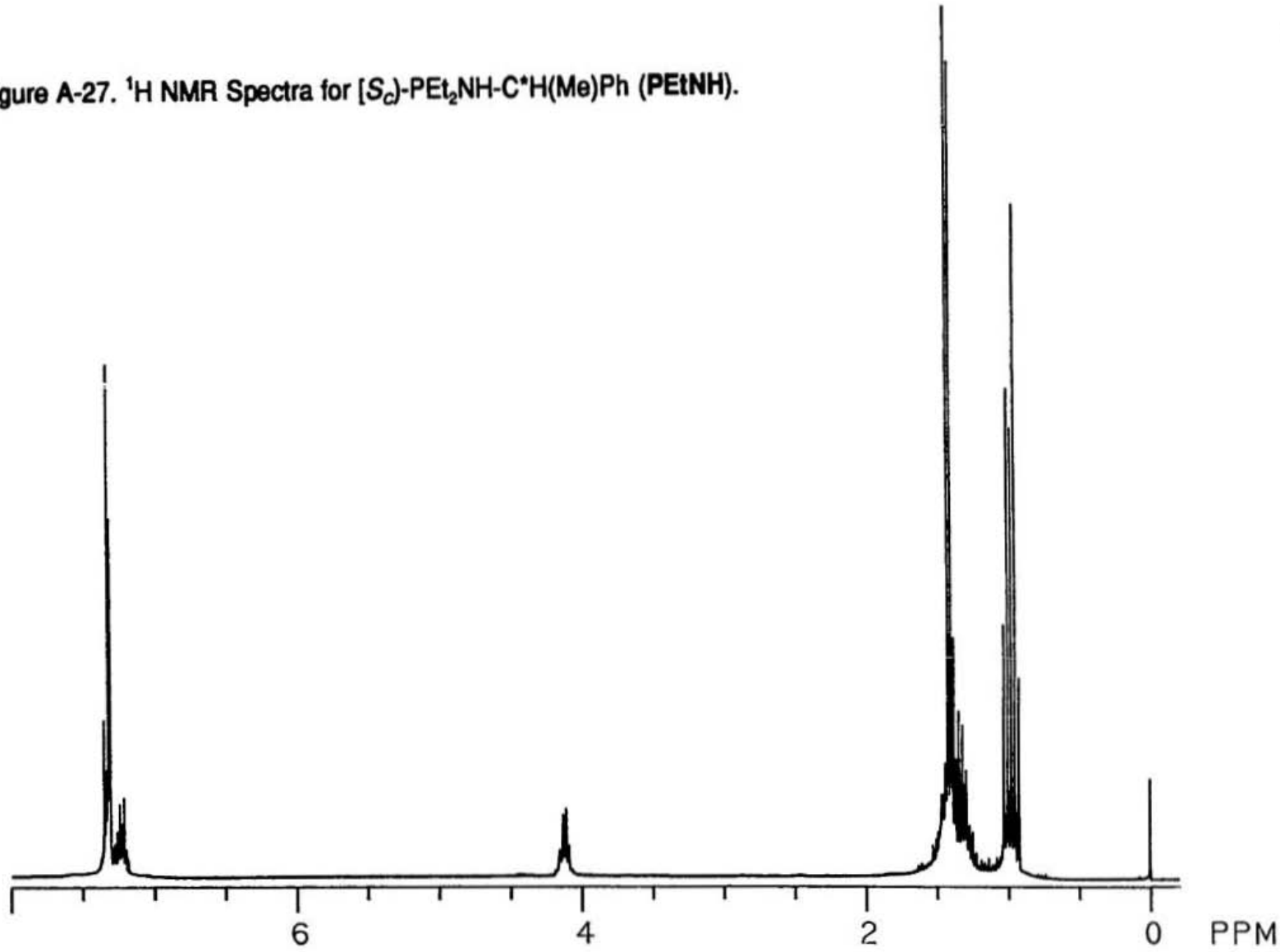

Figure A-28. ^{1}H NMR Spectra for (η^5-C_5H_5)Co(PEtNH)(I)$_2$) (**7-4**).

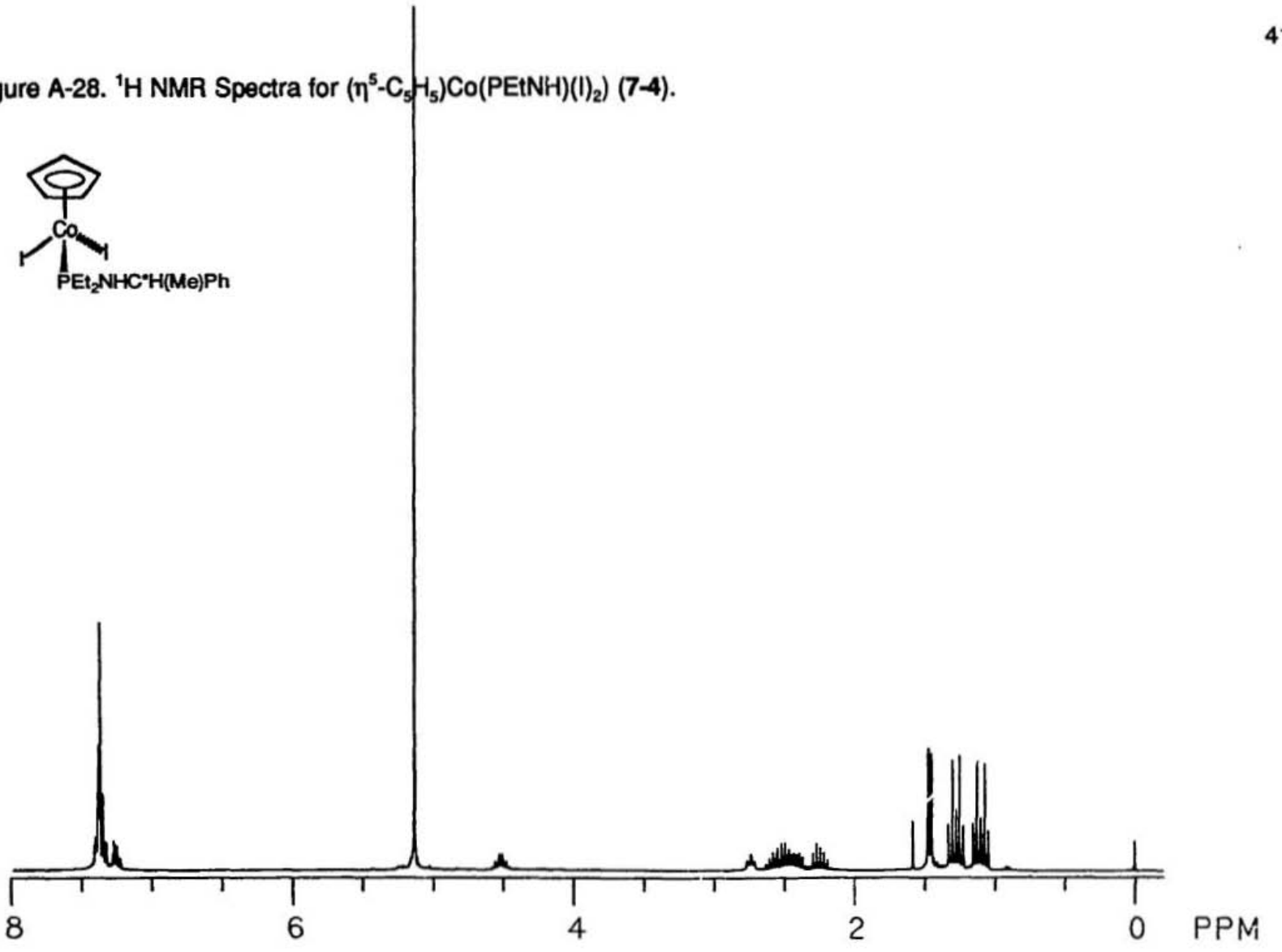

Figure A-29. ^{1}H NMR Spectra for $(\eta^5\text{-}C_5Me_5)Co(PEtNH)(I)_2$ **(7-5)**.

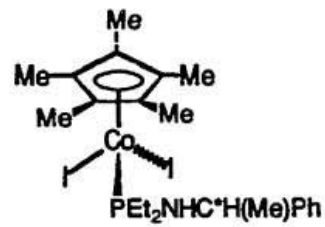

Figure A-30. ^{1}H NMR Spectra for [S_{Co},S_C]-(η^5-C_5H_5)Co(PEtNH)(C_3F_7)(I) (**7-6a**).

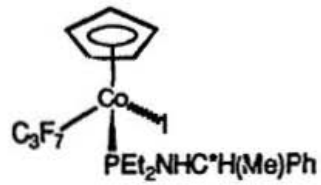

Figure A-31. ^{1}H NMR Spectra for [R_{Co},S_C]-(η^5-C_5H_5)Co(PEtNH)(C_3F_7)(P(O)(OMe)$_2$) (**7-13a**).

Figure A-32. ^{1}H NMR Spectra for [S_{Co},S_C]-(η^5-C_5H_5)Co(PEtNH)(C_3F_7)(P(O)(OMe)$_2$) (**7-13b**).

Figure A-33. ^{1}H NMR Spectra for [R_{Co},R_P,S_C]-(η^5-C_5H_5)Co(PEtNH)(C_3F_7)(P(O)Ph(OMe)) (**7-16a**).

Figure A-34. ^{1}H NMR Spectra for [R_{Co},S_P,S_C]-(η^5-C_5H_5)Co(PEtNH)(C_3F_7)(P(O)Ph(OMe)) (**7-16c**).

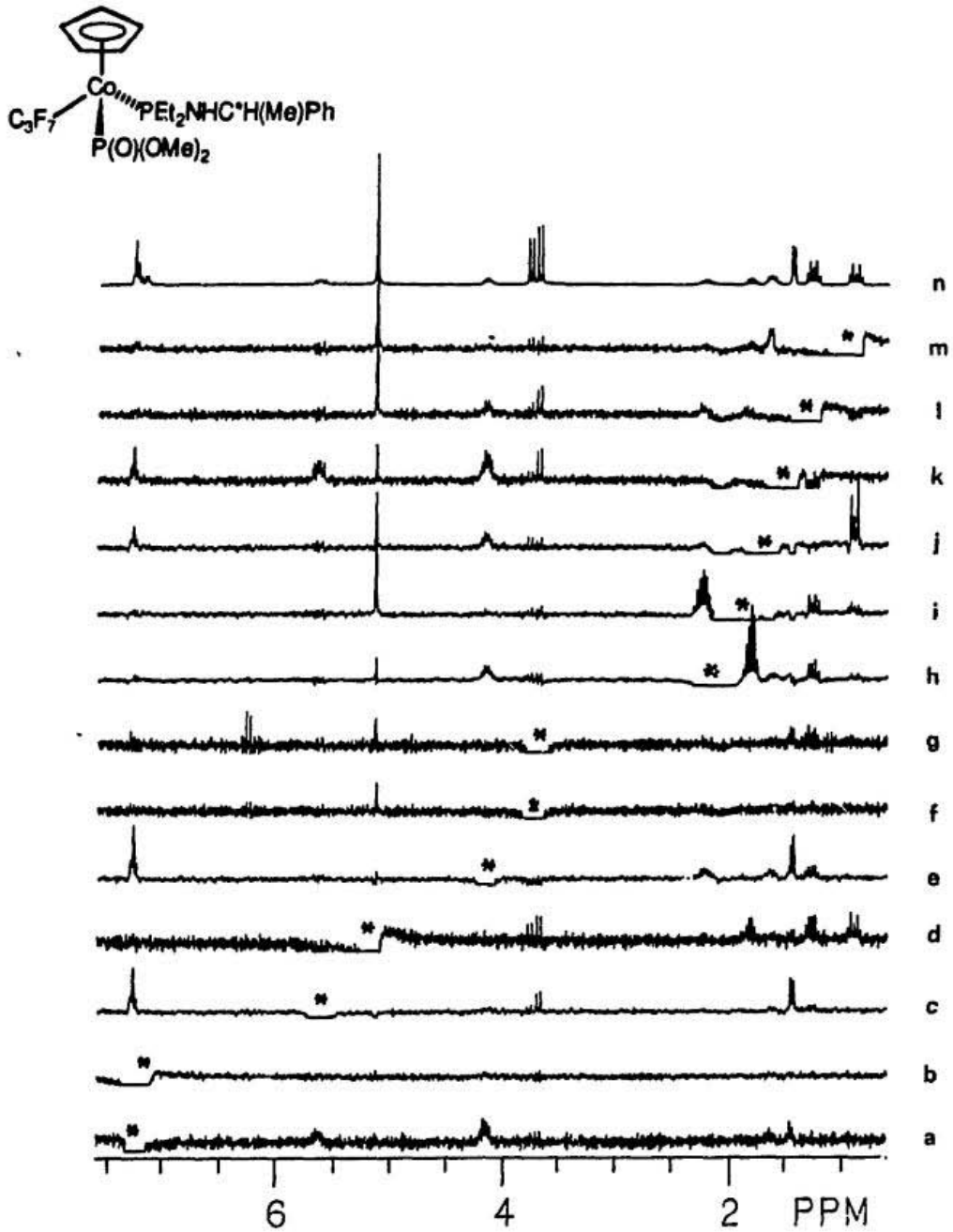

Figure A-35. ^{1}H nOed Spectra for [S_{Co},S_C]-(η^5-C_5H_5)Co(PEtNH)(C_3F_7)(P(O)(OMe)$_2$) (**7-13b**). (n) reference spectra; (a-m) difference spectra (x64) for irradiation at the indicated (*) frequency; (a) H_{ortho} of Ph; (b) H_{meta} & H_{para} of Ph; (c) N<u>H</u>; (d) η^5-C_5H_5; (e) C*<u>H</u>; (f & g) P(O)-O<u>Me</u>; (h, i & j) P-C<u>H$_2$</u>-; (k) C*-<u>Me</u>; (l & m) P-CH$_2$-<u>Me</u>.

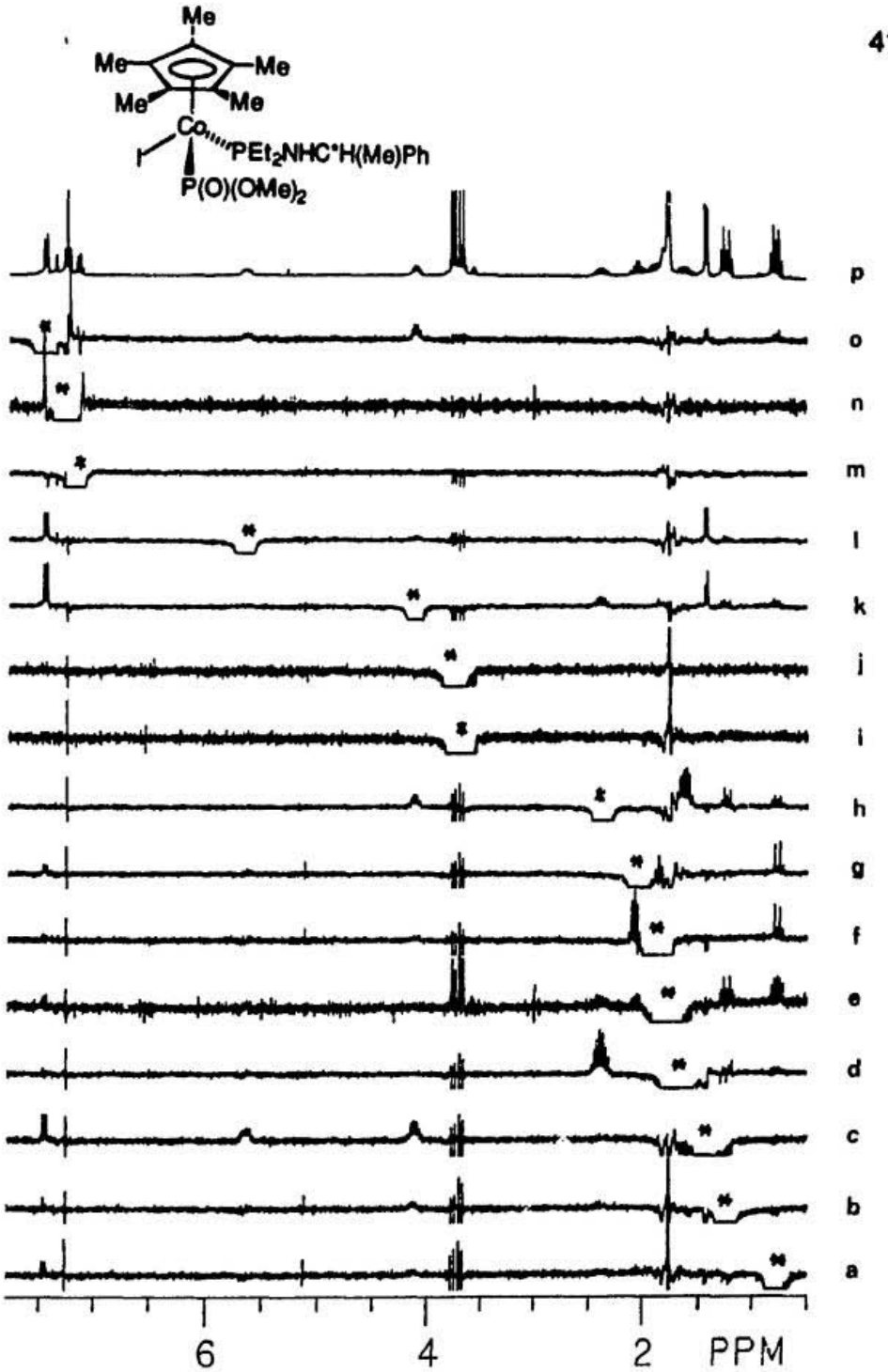

Figure A-36. ^{1}H nOed Spectra for [R_{Co},S_C]-(η^5-C_5Me_5)Co(PEtNH)(P(O)(OMe)$_2$)(I) (**7-14b**). (p) reference spectra; (a-o) difference spectra (x32) for irradiation at the indicated (*) frequency; (a & b) P-CH$_2$-Me; (c) C*-Me; (d, f, g & h) P-CH$_2$-; (e) η^5-C_5Me_5; (i & j) P(O)-OMe; (k) C*H; (l) NH; (m) H_{para} of Ph; (n) H_{meta} of Ph; (o) H_{ortho} of Ph.

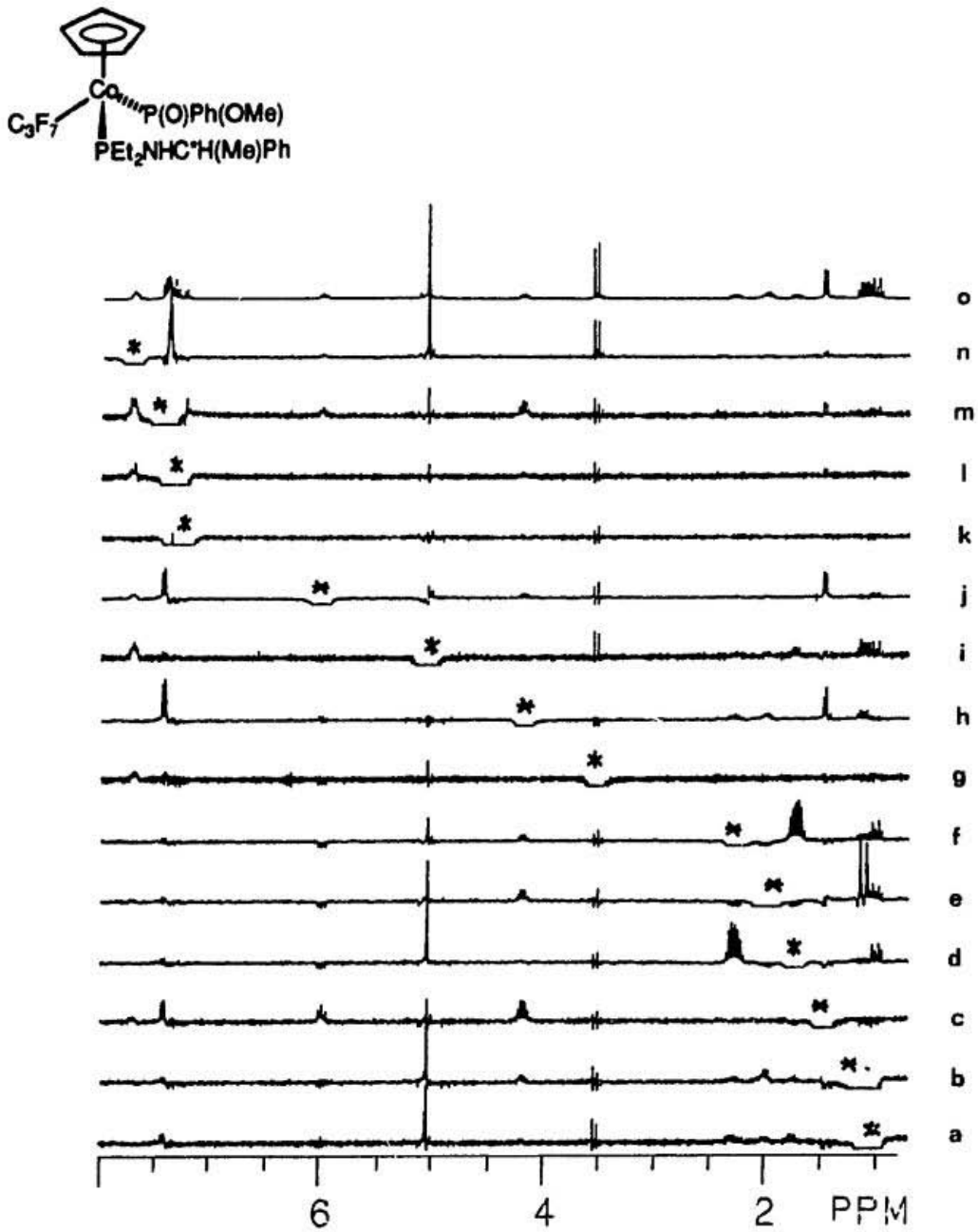

Figure A-37. ^{1}H nOed Spectra for [R_{Co},R_P,S_C]-(η^5-C_5H_5)Co(PEtNH)(C_3F_7)(P(O)Ph(OMe)) (**7-16a**). (o) reference spectra; (a-n) difference spectra (x64) for irradiation at the indicated (*) frequency; (a & b) P-CH_2-Me; (c) C*-Me; (d, e & f) P-CH_2-; (g) P(O)-OMe; (h) C*H; (i) η^5-C_5H_5; (j) NH; (k, l & m) H_{para} & H_{meta} of Ph; (n) H_{ortho} of Ph.

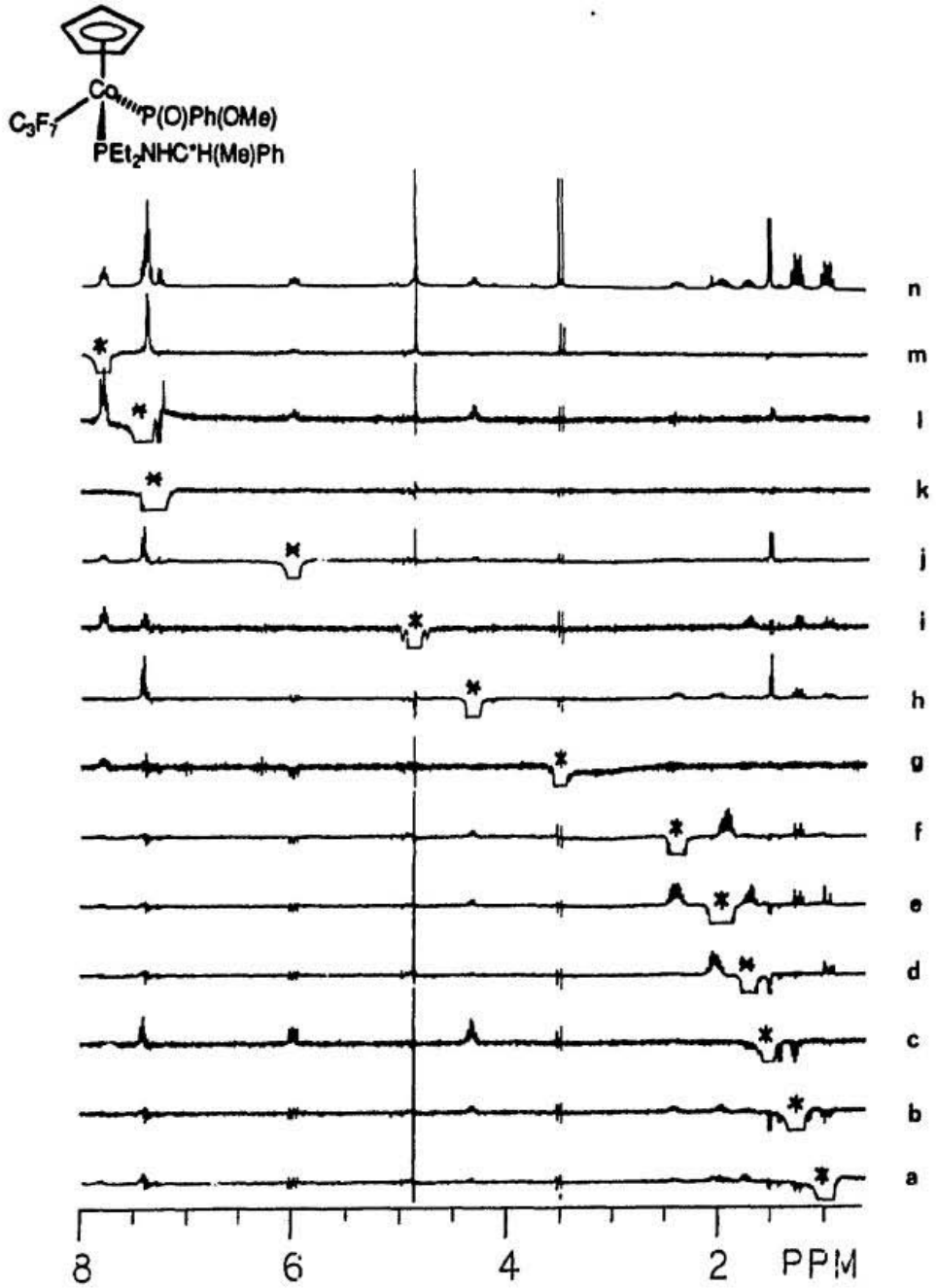

Figure A-38. ^{1}H nOed Spectra for [R_{Co},S_P,S_C]-(η^5-C_5H_5)Co(PEtNH)(C_3F_7)(P(O)Ph(OMe)) (**7-16c**). (n) reference spectra; (a-m) difference spectra (x32) for irradiation at the indicated (*) frequency; (a & b) P-CH_2-Me; (c) C*-Me; (d, e & f) P-CH_2-; (g) P(O)-OMe; (h) C*H; (i) η^5-C_5H_5; (j) NH; (k & l) H_{para} & H_{meta} of Ph; (m) H_{ortho} of Ph.